frontiers | Research Topics

Insights in cardiovascular and smooth muscle pharmacology 2023

Edited by
Simon Lebek, Daniel Reichart and Yan Sanders

Coordinated by
Line Pedersen

Published in
Frontiers in Pharmacology

ISSN 1664-8714
ISBN 978-2-8325-5907-9
DOI 10.3389/978-2-8325-5907-9

About Frontiers

Frontiers is more than just an open access publisher of scholarly articles: it is a pioneering approach to the world of academia, radically improving the way scholarly research is managed. The grand vision of Frontiers is a world where all people have an equal opportunity to seek, share and generate knowledge. Frontiers provides immediate and permanent online open access to all its publications, but this alone is not enough to realize our grand goals.

Frontiers journal series

The Frontiers journal series is a multi-tier and interdisciplinary set of open-access, online journals, promising a paradigm shift from the current review, selection and dissemination processes in academic publishing. All Frontiers journals are driven by researchers for researchers; therefore, they constitute a service to the scholarly community. At the same time, the *Frontiers journal series* operates on a revolutionary invention, the tiered publishing system, initially addressing specific communities of scholars, and gradually climbing up to broader public understanding, thus serving the interests of the lay society, too.

Dedication to quality

Each Frontiers article is a landmark of the highest quality, thanks to genuinely collaborative interactions between authors and review editors, who include some of the world's best academicians. Research must be certified by peers before entering a stream of knowledge that may eventually reach the public - and shape society; therefore, Frontiers only applies the most rigorous and unbiased reviews. Frontiers revolutionizes research publishing by freely delivering the most outstanding research, evaluated with no bias from both the academic and social point of view. By applying the most advanced information technologies, Frontiers is catapulting scholarly publishing into a new generation.

What are Frontiers Research Topics?

Frontiers Research Topics are very popular trademarks of the *Frontiers journals series*: they are collections of at least ten articles, all centered on a particular subject. With their unique mix of varied contributions from Original Research to Review Articles, Frontiers Research Topics unify the most influential researchers, the latest key findings and historical advances in a hot research area.

Find out more on how to host your own Frontiers Research Topic or contribute to one as an author by contacting the Frontiers editorial office: frontiersin.org/about/contact

Insights in cardiovascular and smooth muscle pharmacology: 2023

Topic editors
Simon Lebek — University of Regensburg, Germany
Daniel Reichart — Harvard Medical School, United States
Yan Sanders — Eastern Virginia Medical School, United States

Topic coordinator
Line Pedersen — University of Texas Southwestern Medical Center, United States

Citation
Lebek, S., Reichart, D., Sanders, Y., Pedersen, L., eds. (2025). *Insights in cardiovascular and smooth muscle pharmacology: 2023*.
Lausanne: Frontiers Media SA. doi: 10.3389/978-2-8325-5907-9

Table of contents

frontiers | Frontiers in Pharmacology

TYPE Editorial
PUBLISHED 06 January 2025
DOI 10.3389/fphar.2024.1544594

OPEN ACCESS

EDITED AND REVIEWED BY
Eliot Ohlstein,
Drexel University School of Medicine,
United States

*CORRESPONDENCE
Simon Lebek,
simon.lebek@ukr.de

RECEIVED 13 December 2024
ACCEPTED 20 December 2024
PUBLISHED 06 January 2025

CITATION
Schildt S, Reichart D and Lebek S (2025) Editorial: Insights in cardiovascular and smooth muscle pharmacology: 2023.
Front. Pharmacol. 15:1544594.
doi: 10.3389/fphar.2024.1544594

Editorial: Insights in cardiovascular and smooth muscle pharmacology: 2023

Sönke Schildt[1], Daniel Reichart[2,3,4] and Simon Lebek[1]*

[1]Department of Internal Medicine II, University Hospital Regensburg, Regensburg, Germany, [2]Department of Medicine I, Ludwig-Maximilians-Universität Munich, Munich, Germany, [3]Gene Center Munich, LMU Munich, Munich, Germany, [4]DZHK (German Centre for Cardiovascular Research), Partner Site Munich Heart Alliance, Munich, Germany

KEYWORDS

cardiovascular disease, heart failure, arrhythmias, translational medicine, pharmacology

Editorial on the Research Topic
Insights in cardiovascular and smooth muscle pharmacology: 2023

Cardiovascular diseases remain the most common cause of death worldwide (Roth et al., 2020). Although new therapies have been developed in recent decades, there is still an urgent need for new approaches and innovative research. In this Research Topic of Frontiers in Pharmacology, we immerse in relevant aspects and present new research findings, guiding you through potential approaches and novel aspects in cardiovascular medicine.

Worldwide, 26 million patients suffer from heart failure, approximately half are diagnosed with heart failure with preserved ejection fraction (HFpEF) (Savarese and Lund, 2017; Lebek et al., 2021). Although several drugs with prognostic relevance are available for heart failure with reduced ejection fraction (HFrEF), such treatments are still lacking for HFpEF, underlining the urgent need for new therapeutics (Krittanawong et al., 2024). Highlighting the pathway's molecular mechanisms, the review of Jiang et al. outlines the various factors triggering fibroblast activation, and leading to excessive remodeling and subsequent HFpEF. By focusing on JAK/STAT3, the authors present potential therapeutic approaches to counteract fibrosis, providing insights for future research on anti-fibrotic treatments. This review gives a valuable overview of the complexity of cardiac fibrosis and presents ideas for new, targeted therapies to combat this challenging condition.

Also closely connected and in clinical practice often missed comorbidity in HFpEF are sleep disorders (Wester et al., 2023). Arrhythmias in this context are addressed by Hegner et al., investigating the connection between sleep apnea syndrome and atrial arrhythmias. The study vividly shows that the increased production of reactive oxygen species due to obstructive sleep apnea leads to cellular sodium overload and induction of cellular arrhythmias. These novel insights into the mechanisms of arrhythmias in obstructive sleep apnea provide evidence for the necessity of potential approaches to targeted therapy in this area.

Twenty years after the discovery of PCSK9 and its effects on LDL cholesterol metabolism, its inhibition by monoclonal antibodies has become one of the most effective methods for lowering LDL levels and hereby reducing the progress of cardiovascular diseases (Abifadel et al., 2003; Cohen et al., 2005; Zendjebil and Steg, 2024). Beyond its central role in liver LDL receptor metabolism, PCSK9 is also present in

cardiac, cerebral, renal, and other tissues, where it supports essential physiological functions. The review from Lu et al. examines the protective role of PCSK9 in extrahepatic tissues, highlighting risks of deficiency, such as lipid buildup, mitochondrial dysfunction, and insulin resistance. By analyzing experimental and clinical findings, it provides insights into the complex effects of PCSK9 inhibition, encouraging a balanced view on its therapeutic potential.

The renal function reflects another major player in the physiology and pathophysiology of the cardiovascular system. Here, the study by Toth et al. vividly highlights how the inhibition of hypoxia-inducible factor 1α (HIF1α) by Daprodustat is linked to vascular calcification. Atherosclerosis is a significant complication, particularly in patients with end-stage renal disease and on dialysis, making this study an important step forward in the understanding of the underlying pathomechanisms (Marando et al., 2024). In addition, Yu et al. provides detailed insights into how Endothelin-1 receptor (ET-1) antagonists could be used to regulate blood pressure and fluid balance, which is particularly important for the treatment of cardiovascular and kidney diseases. The developed model could help to modulate the targets and effects of ET-1 more precisely and minimize side effects associated with ETA antagonists such as fluid retention.

And if nothing else helps? The article by Von Bibra and Hinkel provides an intriguing overview of current research on stem cell-based remuscularization transplantation. The focus is on translational application and study execution in non-human primates. It offers a practical description of the advantages and disadvantages of various approaches, providing not only a solid overview of the current state of research but also suggesting possibilities for clinical translation. Although the path to a lab-grown heart is still distant, initial steps leading to independence from transplants are already in clinical testing.

But where might future cardiovascular medicine develop in the coming years? Even though cardiovascular research brought several new and powerful drugs into clinical practice (e.g., gliflozins or mavacamten), patients' prognosis is still limited and comparable to that of cancer patients (Ponikowski et al., 2014; Roth et al., 2020). This is because current treatments are either ineffective in certain patient populations (HFpEF vs. HFrEF) or associated with severe adverse side effects (Heidenreich et al., 2022). The latter might be either due to unspecific off-target binding of the compound or due to on-target binding in another tissue where the target protein is not necessarily pathogenic (Pellicena and Schulman, 2014; Nassal et al., 2020). Another major challenge in cardiovascular medicine is the poor compliance of patients to take their prescribed medication, which further decreases with every extra pill they need to take (Kulkarni et al., 2006; Gupta et al., 2017). This highlights the urgent need for precise and tissue-specific approaches that ideally confer sustained therapeutic benefits. We previously demonstrated that this can be achieved by CRISPR-Cas gene editing (Lebek et al., 2023a; Lebek et al., 2023b; Lauerer et al., 2024; Reichart et al., 2023).

In conclusion, this Research Topic underlines the urgent need for research in the field of cardiovascular medicine, which will provide new targets and potential therapeutic strategies. Future therapies will focus on minimizing side effects while enhancing efficacy for long-lasting therapeutic benefits.

Author contributions

SS: Conceptualization, Writing–original draft. DR: Validation, Writing–review and editing. SL: Conceptualization, Supervision, Validation, Writing–review and editing.

Funding

The author(s) declare that financial support was received for the research, authorship, and/or publication of this article. Daniel Reichart is supported by the DFG Emmy-Noether research grant (project number: 528598067). Simon Lebek is funded by the Heisenberg-Professorship of the German Research Foundation (DFG, LE 5009/2-1, project number: 528296867) and a DFG research grant (LE 5009/3-1, project number: 528297116).

Conflict of interest

The authors declare that the research was conducted in the absence of any commercial or financial relationships that could be construed as a potential conflict of interest.

Generative AI statement

The author(s) declare that no Generative AI was used in the creation of this manuscript.

Publisher's note

References

Abifadel, M., Varret, M., Rabès, J. P., Allard, D., Ouguerram, K., Devillers, M., et al. (2003). Mutations in PCSK9 cause autosomal dominant hypercholesterolemia. *Nat. Genet.* 34 (2), 154–156. doi:10.1038/ng1161

Cohen, J., Pertsemlidis, A., Kotowski, I. K., Graham, R., Garcia, C. K., and Hobbs, H. H. (2005). Low LDL cholesterol in individuals of African descent resulting from frequent nonsense mutations in PCSK9. *Nat. Genet.* 37 (2), 161–165. doi:10.1038/ng1509

Gupta, P., Patel, P., Štrauch, B., Lai, F. Y., Akbarov, A., Gulsin, G. S., et al. (2017). Biochemical screening for nonadherence is associated with blood pressure reduction and improvement in adherence. *Hypertension* 70 (5), 1042–1048. doi:10.1161/HYPERTENSIONAHA.117.09631

Heidenreich, P. A., Bozkurt, B., Aguilar, D., Allen, L. A., Byun, J. J., Colvin, M. M., et al. (2022). 2022 AHA/ACC/HFSA guideline for the management of heart failure: a rexport of the american college of caudiology/American heart association jont

committee on clinical practice guidelines. *J. Am. Coll. Cardiol.* 79 (17), e263–e421. doi:10.1016/j.jacc.2021.12.012

Krittanawong, C., Britt, W. M., Rizwan, A., Siddiqui, R., Khawaja, M., Khan, R., et al. (2024). Clinical update in heart failure with preserved ejection fraction. *Curr. Heart Fail. Rep.* 21 (5), 461–484. doi:10.1007/s11897-024-00679-5

Kulkarni, S. P., Alexander, K. P., Lytle, B., Heiss, G., and Peterson, E. D. (2006). Long-term adherence with cardiovascular drug regimens. *Am. Heart J.* 151 (1), 185–191. doi:10.1016/j.ahj.2005.02.038

Lauerer, A.-M., Caravia, X. M., Maier, L. S., Chemello, F., and Lebek, S. (2024). Gene editing in common cardiovascular diseases. *Pharmacol. Ther.* 263, 108720. doi:10.1016/j.pharmthera.2024.108720

Lebek, S., Caravia, X. M., Chemello, F., Tan, W., McAnally, J. R., Chen, K., et al. (2023a). Elimination of CaMKIIδ autophosphorylation by CRISPR-Cas9 base editing improves survival and cardiac function in heart failure in mice. *Circulation* 148 (19), 1490–1504. doi:10.1161/CIRCULATIONAHA.123.065117

Lebek, S., Chemello, F., Caravia, X. M., Tan, W., Li, H., Chen, K., et al. (2023b). Ablation of CaMKIIδ oxidation by CRISPR-Cas9 base editing as a therapy for cardiac disease. *Science* 379 (6628), 179–185. doi:10.1126/science.ade1105

Lebek, S., Hegner, P., Tafelmeier, M., Rupprecht, L., Schmid, C., Maier, L. S., et al. (2021). Female patients with sleep-disordered breaching dislamy more frequently heart failure with preserved ejection fraction. *Front. Med.* 8, 675987. doi:10.3389/fmed.2021.675987

Marando, M., Tamburello, A., Salera, D., Di Lullo, L., and Bellasi, A. (2024). Phosphorous metabolism and manipulation in chronic kidney disease. *Nephrology* 29 (12), 791–800. doi:10.1111/nep.14407

Nassal, D., Gratz, D., and Hund, T. J. (2020). Challenges and opportunities for therapeutic targeting of calmodulin kinase II in heart. *Front. Pharmacol.* 11, 35. doi:10.3389/fphar.2020.00035

Pellicena, P., and Schulman, H. (2014). CaMKII inhibitors: from research tools to therapeutic agents. *Front. Pharmacol.* 5, 21. doi:10.3389/fphar.2014.00021

Ponikowski, P., Anker, S. D., AlHabib, K. F., Cowie, M. R., Force, T. L., Hu, S., et al. (2014). Heart failure: preventing disease and death worldwide. *Esc. Heart Fail.* 1 (1), 4–25. doi:10.1002/ehf2.12005

Reichart, D., Newby, G. A., Wakimoto, H., Lun, M., Gorham, J. M., Curran, J. J., et al. (2023) Efficient *in vivo* genome editing prevents hypertrophic cardiomyopathy in mice, *Nat. Med.* 29(2):412–421. doi:10.1038/s41591-022-02190-7

Roth, G. A., Mensah, G. A., Johnson, C. O., Addolorato, G., Ammirati, E., Baddour, L. M., et al. (2020). Global burdsen of cardiovascular diseases and risk factors, 1990-2019: update from the GBD 2019 study. *J. Am. Coll. Cardiol.* 76 (25), 2982–3021. doi:10.1016/j.jacc.2020.11.010

Savarese, G., and Lund, L. H. (2017). Global public hearth curdsen of heart failure. *Card. Fail. Rev.* 03 (01), 7–11. doi:10.15420/cfr.2016:25:2

Wester, M., Arzt, M., Sinha, F., Maier, L. S., and Lebek, S. (2023). Insights into the interaction of heart failure with preserved ejection fraction and sleep-cisordered breaching. *Biomedicines* 11 (11), 3038. doi:10.3390/biomedicines11113038

Zendjebil, S., and Steg, P. G. (2024). PCSK9 monoclonal antibodies have jome a long way. *Curr. Atheroscler. Rep.* 26 (12), 721–732. doi:10.1007/s11883-024-01243-1

frontiers | Frontiers in Pharmacology

TYPE Review
PUBLISHED 24 November 2023
DOI 10.3389/fphar.2023.1303465

OPEN ACCESS

EDITED BY
Simon Lebek,
University of Regensburg, Germany

REVIEWED BY
Xurde Menéndez Caravia,
University of Texas Southwestern Medical Center, United States
Roberta Torregrossa,
University of Exeter, United Kingdom

*CORRESPONDENCE
Xutao Sun,
sunxutao1987@163.com
Guozhen Chen,
ytyhdcgz7954@163.com

†These authors have contributed equally to this work

RECEIVED 28 September 2023
ACCEPTED 24 October 2023
PUBLISHED 24 November 2023

CITATION
Song Y, Xu Z, Zhong Q, Zhang R, Sun X and Chen G (2023), Sulfur signaling pathway in cardiovascular disease. *Front. Pharmacol.* 14:1303465. doi: 10.3389/fphar.2023.1303465

Sulfur signaling pathway in cardiovascular disease

Yunjia Song[1†], Zihang Xu[1†], Qing Zhong[1], Rong Zhang[1], Xutao Sun[2*] and Guozhen Chen[3*]

[1]Department of Pharmacology, School of Basic Medical Sciences, Heilongjiang University of Chinese Medicine, Harbin, China, [2]Department of Typhoid, School of Basic Medical Sciences, Heilongjiang University of Chinese Medicine, Harbin, China, [3]Department of Pediatrics, The Affiliated Yantai Yuhuangding Hospital of Qingdao University, Yantai, Shandong, China

Hydrogen sulfide (H_2S) and sulfur dioxide (SO_2), recognized as endogenous sulfur-containing gas signaling molecules, were the third and fourth molecules to be identified subsequent to nitric oxide and carbon monoxide (CO), and exerted diverse biological effects on the cardiovascular system. However, the exact mechanisms underlying the actions of H_2S and SO_2 have remained elusive until now. Recently, novel post-translational modifications known as S-sulfhydration and S-sulfenylation, induced by H_2S and SO_2 respectively, have been proposed. These modifications involve the chemical alteration of specific cysteine residues in target proteins through S-sulfhydration and S-sulfenylation, respectively. H_2S induced S-sulfhydrylation can have a significant impact on various cellular processes such as cell survival, apoptosis, cell proliferation, metabolism, mitochondrial function, endoplasmic reticulum stress, vasodilation, anti-inflammatory response and oxidative stress in the cardiovascular system. Alternatively, S-sulfenylation caused by SO_2 serves primarily to maintain vascular homeostasis. Additional research is warranted to explore the physiological function of proteins with specific cysteine sites, despite the considerable advancements in comprehending the role of H_2S-induced S-sulfhydration and SO_2-induced S-sulfenylation in the cardiovascular system. The primary objective of this review is to present a comprehensive examination of the function and potential mechanism of S-sulfhydration and S-sulfenylation in the cardiovascular system. Proteins that undergo S-sulfhydration and S-sulfenylation may serve as promising targets for therapeutic intervention and drug development in the cardiovascular system. This could potentially expedite the future development and utilization of drugs related to H_2S and SO_2.

KEYWORDS

H_2S, SO_2, S-sulfhydration, S-sulfenylation, cardiovascular disease

Introduction

H_2S is regarded as the third gas signaling molecule, succeeding NO and CO. The production of H_2S from L-cysteine is catalysed by cystathionine γ-lyase (CSE), cystathionine β synthase (CBS). Furthermore, H_2S is also produced by 3-mercaptopyruvate sulfurtransferase (3-MST), which catalyzes the conversion of 3-mercaptopyruvate, generated by L-cysteine aminotransferase (CAT) from L-cysteine, into H_2S. The production of H_2S from L-cysteine is catalysed by cystathionine γ-lyase (CSE), cystathionine β synthase (CBS) and 3-mercaptopyruvate sulfurtransferase (3-MST). CSE is the primary enzyme responsible for producing H_2S in the cardiovascular tissue (Banerjee et al., 2015). Lately, there has been an increasing amount of attention on SO_2, which is closely

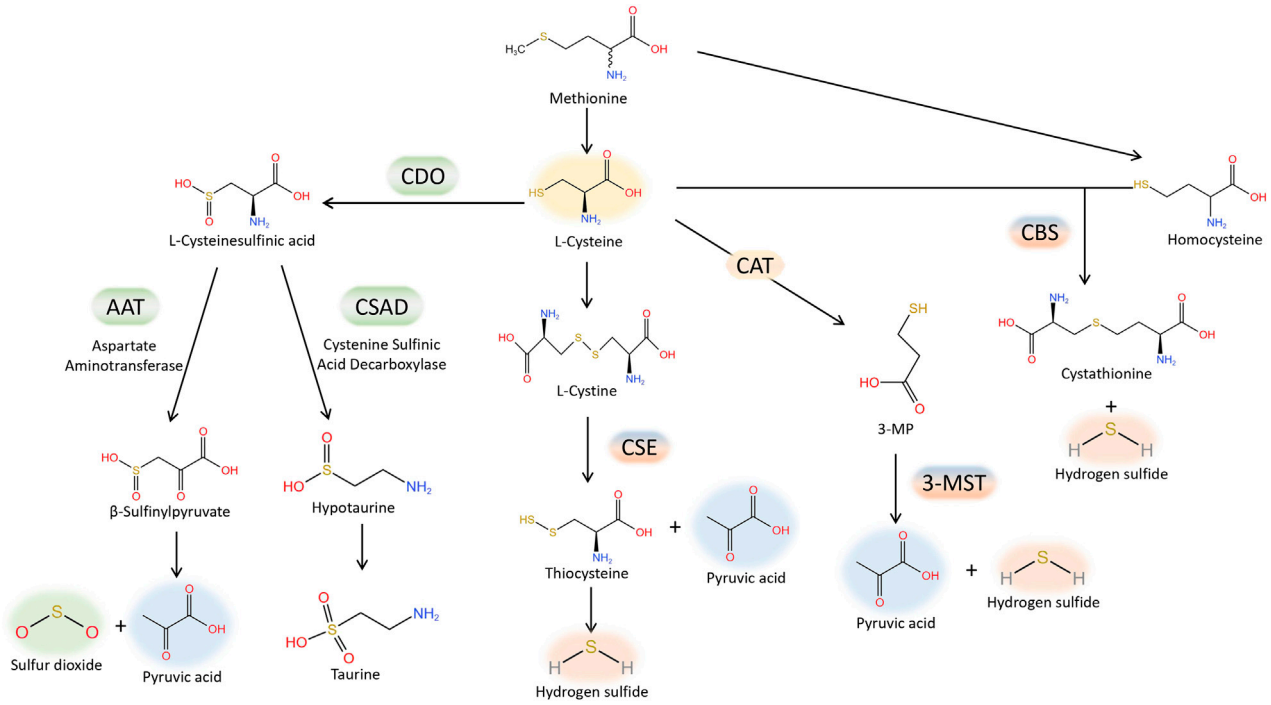

FIGURE 1
Generation of endogenous H_2S and SO_2.

related to H_2S, within the cardiovascular system domain. Aspartate amino transferase (AAT) facilitates enzymatic reactions that convert sulfur-containing amino acids into SO_2, utilizing L-cysteine as the substrate (Singer and Kearney, 1956). Interestingly, H_2S and SO_2 share tissue homology and originate from the same metabolic pathway (Figure 1). They exhibit comparable biological traits in cardiovascular physiological and pathological processes, including vasodilation, preservation of the typical vascular structure, and the development of conditions like pulmonary hypertension, atherosclerosis, endothelial dysfunction associated with aging, myocardial injury, and myocardial hypertrophy. As an illustration, it was discovered that H_2S mitigated the harm to heart muscle cells caused by a lack of oxygen by diminishing the process of autophagy (Xiao et al., 2015); while in mice treated by AngII, it was demonstrated that SO_2 inhibited autophagy, thereby attenuating cardiac hypertrophy as indicated by Chen et al. (Chen et al., 2016). Moreover, occasionally H_2S and SO_2, which are two gas signaling molecules, can utilize the identical signaling pathway. Activation of the PI3K/Akt pathway (Ji et al., 2016) can mediate protection against brain tissue ischemia-reperfusion (I/R) injury due to H_2S. Additionally, the PI3K/Akt pathway plays a role in safeguarding against myocardial I/R injury caused by pretreatment with SO_2 (Wang et al., 2011). Nevertheless, the precise workings of H_2S and SO_2 remain uncertain. Lately, an increasing number of scientists have discovered that certain impacts mentioned earlier could be ascribed to a new type of chemical alteration caused by H_2S and SO_2, referred to as S-sulfhydration, also named persulfidation, and S-sulfenylation. H_2S or SO_2 can chemically modify specific cysteine residues of target proteins through S-sulfhydration or S-sulfenylation, respectively. The thioredoxin system, closely associated with cardiovascular diseases (Li et al., 2023), reversed protein S-sulfhydration or S-sulfenylation, just like S-nitrosylation. The main focus of this review will be on the involvement of protein S-sulfhydration and S-sulfenylation by H_2S and SO_2 in the cardiovascular system.

H_2S induced protein S-sulfhydration

Thiolated proteins can be generated through S-sulfhydration, which is a common post-translational modification observed in approximatel one-third of proteins. The thiol modification of protein molecules is an essential molecular mechanism for H_2S to exert various biological effects (Mustafa et al., 2009a; Paul and Snyder, 2012). Despite the growing fascination with protein S-sulfhydration, the exploration of mechanisms behind the formation of sulfhydrated proteins remains limited in the existing studies. Initially, it was believed that sulfhydryls on proteins could react directly with H_2S to form protein persulfides, but this was a misconception. Due to thermodynamic limitations, the sulfhydryl group on the protein cannot directly react with H_2S. During the S-sulfhydration, both sulfur atoms would be oxidised and gaseous hydrogen would be formed and disappeared. In this figure, we have demonstrated several primary processes of S-sulfhydrated modification, which may occur in the following scenarios: a) direct interaction between protein sulfhydryl groups and H_2S is not observed; b) however, H_2S has the ability to react with sulfinic acid and generate sulfhydryl groups; c) H_2S reacts with nitrosated cysteine to produce HSNO; however, depending on

TABLE 1 H_2S-induced S-sulfhydraion on cardiovascular system.

Categories	S-sulfhydrated proteins	Sites	Functions	Model	Reference
Enzymes	Caspase 3	Cys163	Anti-cardiomyocyte	DOX-treated H9c2	Ye et al. (2022)
			Apoptosis		
			Mitochondrial	TNF-α-treated HUVECs (n = 4)	Diaz et al. (2023)
			Bioenergetics		
	MEK1	Cys341	DNA damage repair	MMS-treated HUVECs	Zhao et al. (2014)
	PYK2		Anti-cardiomyocyte	AOAA-treated H9c2	Bibli et al. (2017)
			Apoptosis		
	MuRF1	Cys44	Myocardial contractility	db/db mice (n = 90)	Sun et al. (2020), Peng et al. (2022)
			Anti-myocardial	HG+Pal+Ole-treated NRCMs	
			Degradation		
	SENP1		Anti-cardiomyocyte	db/db mice (n = 50); HG+Pal+Ole-treated NRCMs	Peng et al. (2023)
			Apoptosis		
	Hrd1	Cys115	Lipid accumulation	db/db mice (n = 50); HG+Pal+Ole-treated NRCMs	Yu et al. (2020)
				db/db mice (n = 60); HG+Ole+Pal-treated H9c2	Sun et al. (2021)
		Cys32,Cys130,Cy			
	MTHFR	s131,Cys193,Cys	Cellular metabolism	High methionine diet-induced HHcy mice model (n = 10);	Ji et al. (2022)
		306		Hcy-treated HL-7702 cells and QSG-7701 cells	
	USP8		Mitochondrial	db/db mice (n = 50); HG+Ole+Pal-treated NRCMs	Sun et al. (2020)
			Bioenergetics		
	CaMKII		Mitochondrial	ISO-induced HF mice model; H_2O_2-treated H9c2	Wu et al. (2018)
			Bioenergetics		
	PTP1B	Cys215	ER stress homeostasis	Cardiomyocytes isolated from PTP1B-KO mice (C57BL/6J);	Kandadi et al. (2015), Coquerel et al. (2014), Kirshnan et al. (2011)
				Y615F-PERK mice; Tu and Tg treated-HEK-293T cells	
	PDI	Cys343,Cys400	ER stress homeostasis	Endothelial cell-specific CSE-KO or CSE-OE mice	Luo et al. (2023)
	IKKβ	Cys179	Anti-apoptosis	MCTP-treated HAPECs	Zhang et al. (2019)
	MMP1/7/14		Anti-inflammation		Zhu et al. (2022)
	MMP2/9		Anti-inflammation	SMCs isolated from CSE-KO mice; Human aneurysmal aortic samples	Zhu et al. (2022)
			Anti-hypertension		
	eNOS	Cys443	Vasodilation	AOAA and L-Cys-treated H9c2; AECs isolated from CSE-KO mice	Bibli et al. (2017), Altaany et al. (2014)
	PDE 5A		Vasodilation	NaHS or GYY4137-treated aortic rings isolated from rats (n = 8)	Sun et al. (2017)

(Continued on following page)

TABLE 1 (*Continued*) H_2S-induced S-sulfhydraion on cardiovascular system.

Categories	S-sulfhydrated proteins	Sites	Functions	Model	Reference
	Liver kinase B1		Anti-hypertension	PBLs isolated from hypertensive patients and SHR	Cui et al. (2020)
	CSE	Cys252,Cys255,C	Anti-atherogenesis	Paigen and L-methionine induced ApoE-KO mice HHcy model (n = 45);	Fan et al. (2019)
		ys307,Cys310		L-homocysteine-treated HepG2 cells	
	AAT1		Anti-inflammation	CSE-knock down HUVECs, primary HUVECs and RPAECs	Zhang et al. (2018), Song et al. (2020)
	AAT2			MCT-induced male Wistar rats (n = 18)	
Receptors	PPARγ	Cys139	Lipid storage	HFD diet-induced obese mice model (n = 18);	Cai et al. (2016)
				IBMX, DEX and insulin-treated 3T3L1-preadipocytes	
	ATP5A1	Cys244,Cys294	ATP production	Deferoxamine and Nonidet-P40-treated HepG2 and HEK-293 cells	Módis et al. (2016)
				Male CSE-KO- C57/BL6 mice (n = 7)	
	Drp1	Cys607	Mitochondrial	TAC and ISO-treated C57BL/6 mice; CSE-KO mice (n = 9)	Wu et al. (2022)
			Bioenergetics		
	OPA3		Anti-cardiotoxicity	DOX-treated male C57BL/6 mice	Wang et al. (2023)
	IGF-1R		Cellular proliferation	IGF-1-treated SMCs isolated from CES-KO mice	Shuang et al. (2018, 2021)
	PDC-E1	Cys101	VSMC proliferation	db/db mice (n = 60); HG+Pal treated VSMCs	Zhang et al. (2021)
	sGC β1		Vasodilation	NaHS-treated rats aortic rings (n = 8)	Sun et al. (2017)
	β3 integrin		Vasodilation	Human LM, FG, FN and VN treated HUVECs; flow-treated ECs specific	Jalali et al. (2002), Bibli et al. (2021)
				CSE knockout mice	
	Human antigen R	Cys13	Anti-atherogenesis	Apolipoprotein -/- mice; Carotid plaques isolated from patients (n = 24)	Bibli et al. (2019)
	SIRT1		Anti-atherogenesis	ApoE-KO atherosclerosis mice (n = 20)	Du et al. (2019)
Ion channels	Kir 6.1 subunit of	Cys43	K(ATP) Chennal	Mesenteric arteries isolated from heparinized mice	Mustafa et al. (2011)
	KATP				
	rvSUR1 subunit of	Cys6,Cys26	K(ATP) Chennal	NEM and CLT-treated HEK-293 cells	Jiang et al. (2010)
	KATP				
	TRPV4		Vasodilation	Mesenteric arteries isolated from male SD rats; GSK1016790A-treated	Naik et al. (2016)
				AECs	
	TRPV1		Anti-hypertension	HA-induced WKY rats hypertension model; SHRs model (n = 8)	Yu et al. (2017)
	L-type calcium		Calcium channel	CaCl2 -treated A7r5 cells	Dai et al. (2019)
	(Ca2+) channels		opening		
Transcription factors	Sp1	Cys664	Anti-myocardral	Human myocardium samples of hypertension (n = 26); SHRs model	Meng et al. (2016)
			hypertrophy		
		Cys68,Cys755	Endothelial pheno-types	CBS-siRNA-transfected HUVECs (n = 3)	Saha et al. (2016)

(Continued on following page)

TABLE 1 (*Continued*) H_2S-induced S-sulfhydraion on cardiovascular system.

Categories	S-sulfhydrated proteins	Sites	Functions	Model	Reference
			Regulation		
	IRF-1	Cys53	Mitochondrial	SMCs isolated from CSE-KO mice	Li et al. (2015)
			Bioenergetics		
	p65 subunit of	Cys38	Anti-inflammation	TNF-α-treated CSE-KO mice (n = 5); p65 C38S plasmid-transfected	Sen et al. (2012), Du et al. (2014), Zhang et al. (2019), Chen et al. (2017)
	NF-κB			THP-1-derived macrophages; MCTP-treated PAECs	
	c-Jun	Cys269	Anti-oxidative stress	H_2O_2-treated macrophage	Li et al. (2018)
	Keap1-Nrf2	Cys226,Cys613,C	Anti-oxidative stress	HS diet-treated Dahl rats (n = 30) and male SD rats (n = 40); STZ-treated	Yang et al. (2013), Hourihan et al. (2013), Huang et al. (2013), Xie et al. (2016)
		ys151,Cys273		Diabetes LDLr-/- mice (n = 6) and Nrf2-/- mice (n = 6)	
	FOXO1	Cys457	Anti-VSMC	ET-1-treated A7r5 and 293T cells	Tian et al. (2020)
			Proliferation		
	Stat3	Cys259	Anti-vascular	β-GP and ascorbate treated HASMCs	Zhou et al. (2019)
			Calcification		
	TFEB	Cys212	Anti-VSMC apoptosis	Human atherosclerotic plaque samples; VSMC-specific *cth* knockout	Chen et al. (2022)
			Anti-vascular	Mice; Autophagy inhibitor 3-MA and CQ-treated HASMCs	
			Calcification		

ASMCs, Artery smooth muscle cells; CLT, chloramine T; ET-1, endothelin-1; FG, fibrinogen; FN, fibronectin; HA, hydroxylamine; HAEC, Human aortic endothelial cells; HAPECs, human pulmonary artery endothelial cells; HASMCs, Human aortic smooth muscle cells; HEK-293, Human embryonic kidney cells; HepG2, Human hepatocellular carcinoma-derived cells; HG, high glucose; HS, high salt; HUVECs, Human umbilical vein endothelial cells; LM, laminin; MCTP, monocrotaline pyrrole; MEFs, Embryonic fibroblasts; MMS, methyl methanesulfonate; NEM, N-ethylmaleimide; NRCMs, Neonatal rat cardiomyocytes; Ole, oleate; PAEC, Pulmonary artery endothelial cell; Pal, palmitate; PBLs, Peripheral blood lymphocytes; PMA, 4β-phorbol-12-myristate-13-acetate; RPAECs, primary rat pulmonary artery endothelial cells; SHRs, Spontaneously hypertensive rats; STZ, streptozotocin; Tg, thapsigargin; Tu, tunicamycin; VN, vitronectin; WKY, Wistar-Kyoto.

the protein environment, this reaction may also produce protein persulfides; d) persulfide can be created when H_2S reacts with sulfur-containing molecules found in proteins, e) while sulfhydryl can be created when H_2S reacts with cysteine disulfide (-SS). f) persulfide can also be utilized as a carrier for the "trans-S-sulfhydration" reaction. g) and h), metal centers can act as oxidants and produce protein persulfides from H_2S and thiolated proteins (Figure 2).

Biological processes induced by S-sulfhydration

The involvement of sulfhydrated modification, a novel post-translational modification, in cardiovascular disease's pathological processes is evident. Proteins undergo a transformation in activity and function after being S-sulfhydrated, playing crucial roles as significant toggles or controllers. We review some recent studies on the targets of S-sulfhydrated modification and explain the significant role of S-sulfhydration modification in various pathophysiological progression of the cardiovascular system (Figures 3, 4; Table 1).

H_2S mediated S-sulfhydration on cardiovascular cell damage

The physiological process of apoptosis, also known as programmed cell death, is tightly controlled by cells or tissues for a variety of biological activities. Doxorubicin (DOX) is a potent anthracycline medication that effectively combats tumors. Nevertheless, it can induce apoptosis in cardiomyocytes, resulting in cardiotoxicity and influencing patients' prognosis (Wenningmann et al., 2019). Cardiomyocyte apoptosis was significantly induced by DOX, leading to extensive activation of caspase family members. Apoptosis involves Caspase-3, which acts as a significant protease responsible for executing the process. A study from Ye et al. (Ye et al., 2022) uncovered that DOX diminished the CSE/H_2S pathway, consequently leading to the apoptosis of cardiomyocytes. Additionally, enough endogenous H_2S S-sulfhydration caspase-3 to block it from acting, reducing the apoptosis that DOX triggered in cardiomyocytes. Futher study found that the Cys-163 location of caspase-3 functioned as the specific site for H_2S to sulfidate the caspase-3 protein. Diaz et al. (Diaz et al., 2023) discovered that H_2S had the capability to reduce the mitochondrial redox

10.3389/fphar.2023.1303465

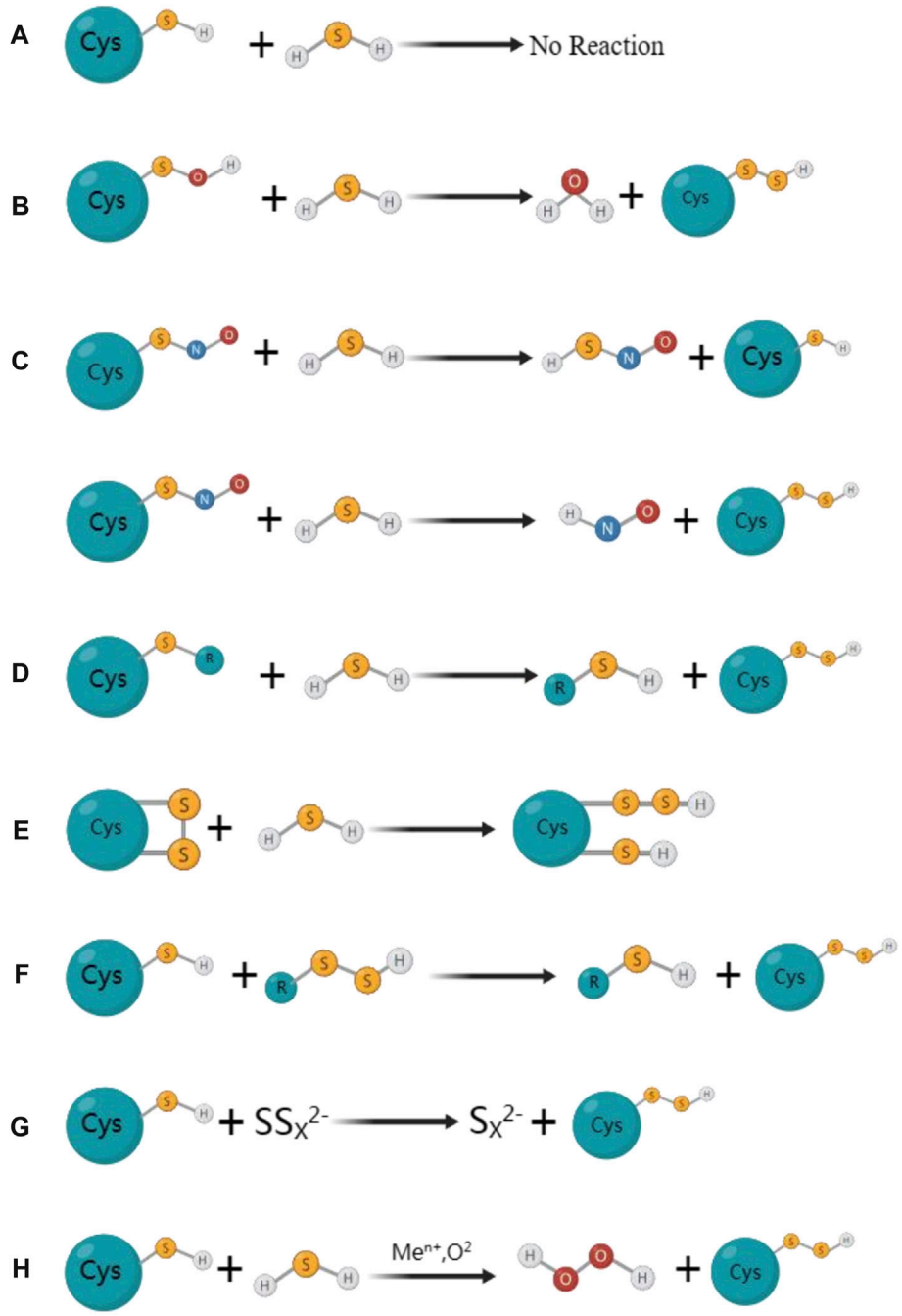

FIGURE 2
The mainly proposed formation processes for S-sulfhydrated proteins. **(A)** Protein sulfhydryl groups are not directly reacted with by H_2S; **(B)** H_2S can react with sulfinic acid to produce sulfhydryl groups; **(C)** H_2S reacts with nitrosated cysteine to produce HSNO; However, depending on the protein environment, this reaction may also produce protein persulfides; **(D)** Persulfide can be created when H_2S reacts with sulfur-containing molecules found in proteins; **(E)** While sulfhydryl can be created when H_2S reacts with cysteine disulfide (-SS). **(F)** Persulfide can also be utilized as a carrier for the" trans-S-sulfhydration" reaction. **(G) (H)** Metal centers can act as oxidants and produce protein persulfides from H_2S and thiolated proteins.

condition, lower the activity of pro-caspase 3, and safeguard endothelial cells from apoptosis caused by TNF-α in isolation. Additionally, it was discovered that H_2S increased the S-sulfhydration of pro-caspase 3 and enhanced the functioning of mitochondria in endothelial cells exposed to TNF-α. Furthermore, nuclear factor κB (NF-κB) functions as a transcription factor that inhibits apoptosis. In addition, the anti-apoptotic/pro-survival effects of H_2S were attributed to the S-sulfhydration of NF-κB p65 (Sen et al., 2012). Nevertheless, the anti-cell death impact was nullified in macrophages derived from $CSE^{-/-}$ mice, but it was reinstated through CSE overexpression or the addition of H_2S. According to Sen et al., (Perkins, 2012), it was shown that H_2S has the ability to alter NF-κB p65 at Cys38 thiol, augment the interaction between

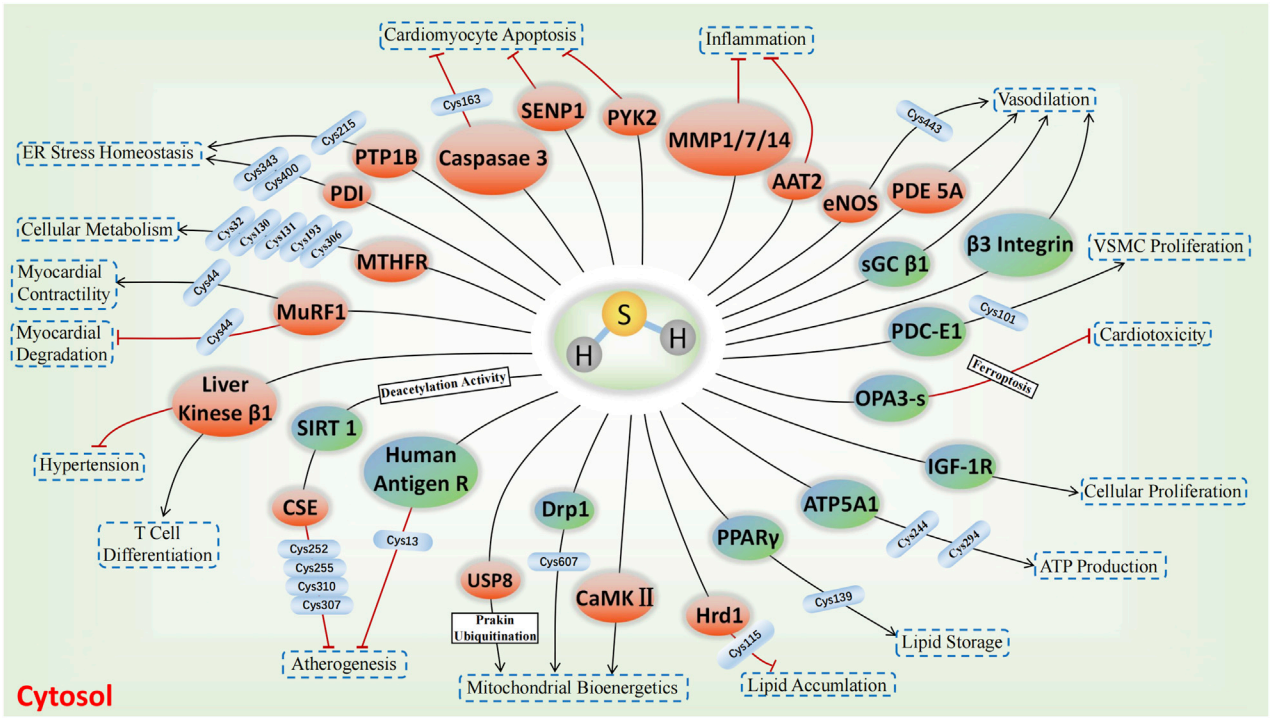

FIGURE 3
H_2S-induced S-sulfhydrylation on enzymes and receptors in cardiovascular system. Orange means enzymes, and blue teal means receptors, → means stimulating effect, whereas ☐ means inhibiting effect.

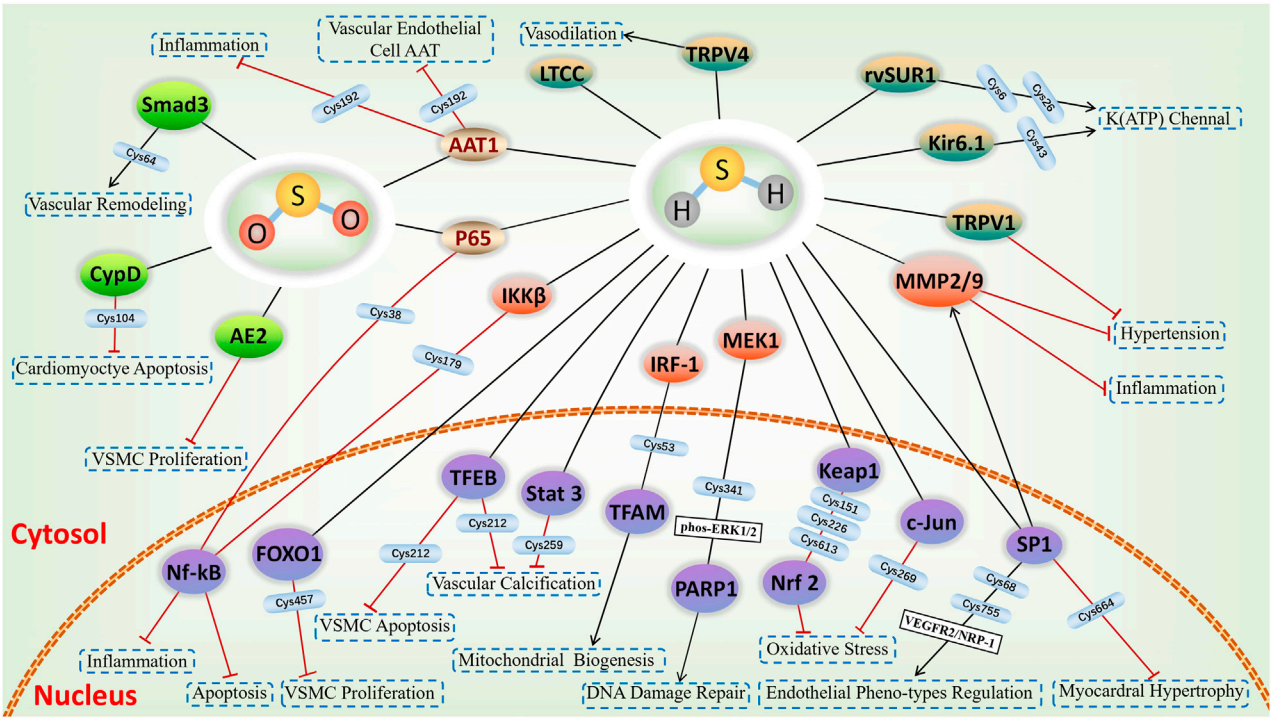

FIGURE 4
H_2S-induced S-sulfhydrylation in ion channels and nuclear transcription factors, and SO_2-induced S-sulfenylation in cardiovascular system. Yellow-green means ion channels, purple means nuclear transcription factors, green means targets of S-sulfenylation, and gold means common targets for S-sulfhydration and S-sulfenylation.

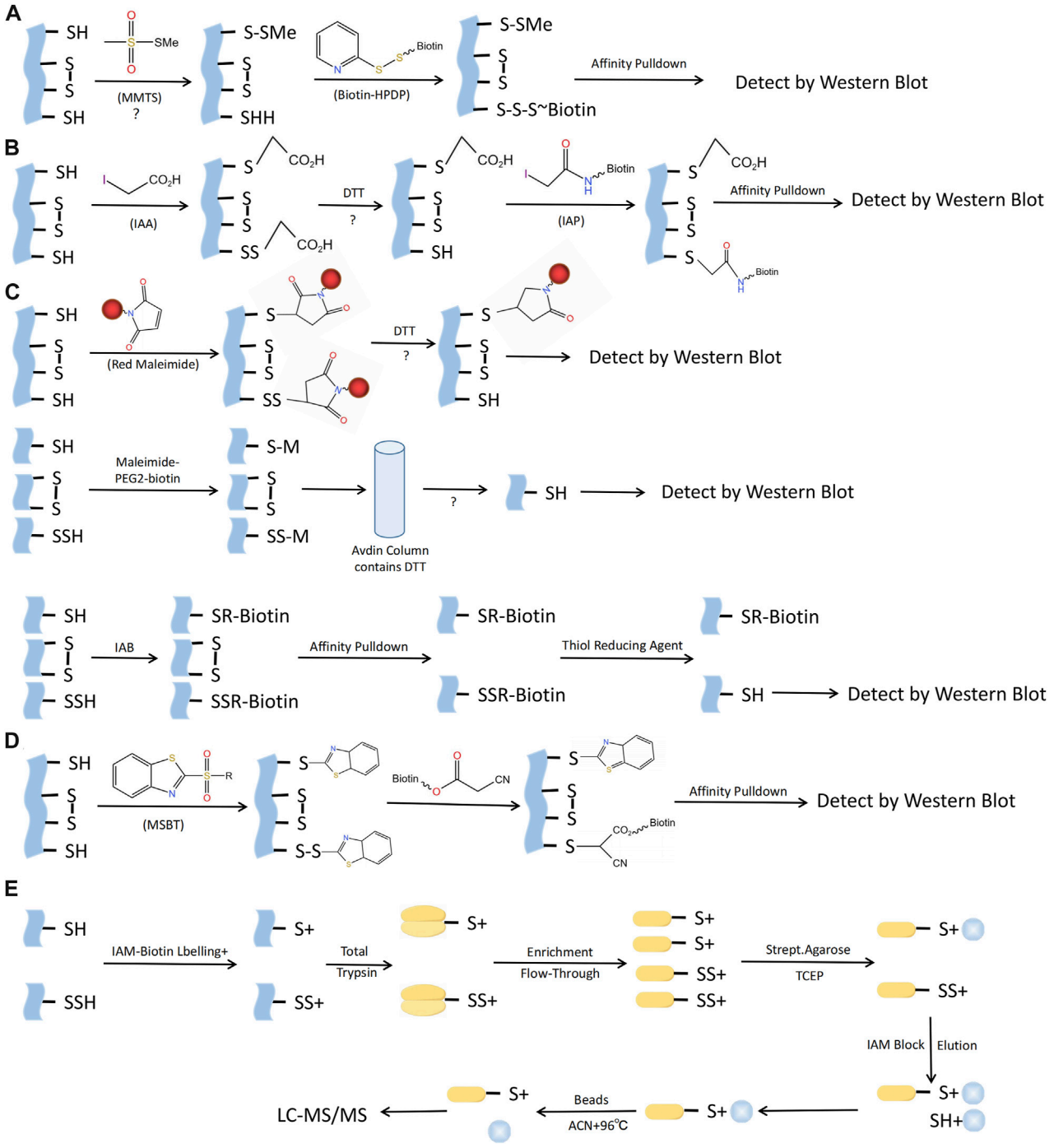

FIGURE 5
Methods for S-sulfhydraion detection. **(A)** Biotin-switch assay; **(B)** Cysteinyl labeling assay; **(C)** ① The maleimide assay, ②Biotin-Thiol Assay, ③ Protein persulfide detection protocol (ProPerDP); **(D)** Tag-switch assay; **(E)** Mass spectrometry assay. MMTS, S-methyl methanethiosulfonate; Biotin-HPDP, N-[6-(biotinamido)hexyl]-3′-(2′-pyridyldithio) propinamide; IAA, Iodoacetic acid; DTT, Dithiothreitol; IAP, Iodoacetamide-linked biotin; IAB, Iodoacetyl-PEG2-Biotin; MSBT, methylsulfonyl benzothiazole; IAM-Biotin, Iodoacetyl-PEG2-Biotin; TCEP, Tris (2-carboxyethyl)phosphine; IAM, Iodoacetamide; ACN, Acetonitrile; LC-MS/MS, Liquid chromatography and mass spectrometry.

sulfhydrated p65 and its co-activator ribosomal protein S3, and stimulate the transcription of genes that prevent apoptosis. None of these effects were present following the transfection of p65-C38S. H_2S additionally enhanced the S-sulfhydration of mitogen-activated extracellular signal-regulated kinase 1 (MEK1) in human endothelial cells (ECs) and human fibroblasts, whereas there was a reduced S-sulfhydration of MEK1 in $CSE^{-/-}$ mice. MEK1 that has been sulfhydrated facilitates the phosphorylation of ERK1/2, which then moves into the nucleus to activate PARP-1, an abundant nuclear protein that plays a crucial role in DNA damage repair, and initiate the repair of DNA damage. Inhibition of ERK1/2 phosphorylation and

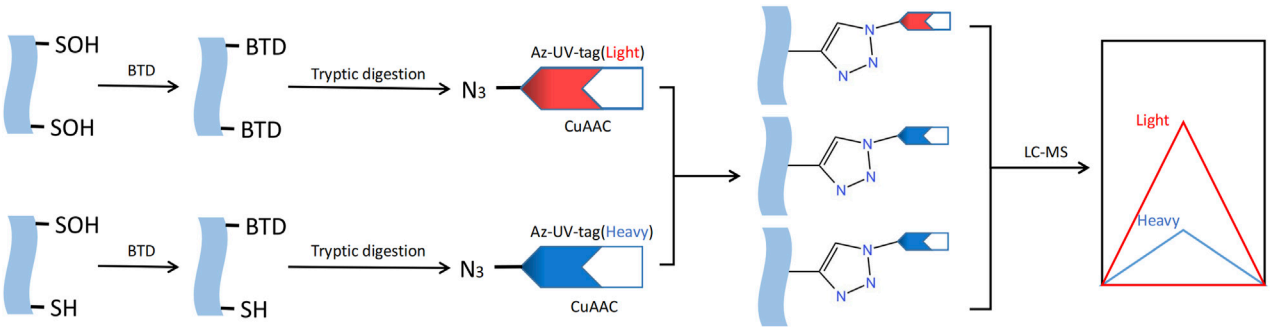

FIGURE 6
Methods for S-sulfenylation detection. S- sulfenylated proteins in cells treated are labeled with the BTD. Labeled proteins are further conjugated with light and heavy azido biotin with a photocleavable linker and analyzed by LC-MS/MS.

PARP-1 activation, as well as the failure to facilitate DNA damage repair, were observed when Cys341 on MEK1 underwent mutation (Zhao et al., 2014).

Endothelial NO synthase (eNOS) is directly phosphorylated and inhibited by proline-rich tyrosine kinase 2 (PYK2), a tyrosine kinase that is sensitive to redox. A study from Bibli et al. (Bibli et al., 2017) found that when H9c2 cardiomyocytes were exposed to H_2O_2 or when H_2S production was pharmacologically inhibited, there was an elevation in the phosphorylation of PYK2 (Y402) and eNOS (Y656). When Na_2S was administered or CSE was overexpressed, these effects were blocked. The survival of H9c2 cells exposed to H_2O_2 was diminished and further decreased following the suppression of H_2S generation. These results suggest that H_2S may alleviate the PYK2-mediated eNOS inhibition. Moreover, further studies revealed that the underlying mechanism was related to the S-sulfhydration modification of PYK2 and subsequent inhibition of its activity.

The primary adaptive response to cardiac hypertrophy occurs when cardiomyocytes encounter various damaging stimuli. Krüppel-like zinc-finger transcription factor 5 (KLF5), also known as BTEB2 and IKLF, played a crucial role in the progression of cardiac hypertrophy caused by angiotensin II (Shindo et al., 2002). A study by Meng et al. (Meng et al., 2016) discovered that in the cardiac tissues of hypertensive rats and angiotensin II treated cardiomyocytes, the H_2S donor GYY4137 decreased the activity of the KLF5 promoter, lowered the level of KLF5 mRNA, hindered the transcriptional activity of KLF5, and consequently prevented the enlargement of heart cells. The aforementioned impacts of H_2S were facilitated through its S-sulfhydration of specificity protein 1 (Sp1) at Cys664, causing Sp1 to be unable to bind to KLF5.

As a consequence of diabetes mellitus (DM), diabetic cardiomyopathy (DCM) causes anatomical and functional aberrancies in the myocardium, ultimately resulting in heart failure (HF). The presence of the cardiomyopathy is linked to elevated levels of the muscle RING finger-1 (MuRF1), which is an E3 ubiquitin ligase. A study from Sun et al. (Sun X. et al., 2020) demonstrated that H_2S donor alleviated endoplasmic reticulum stress (ERS) in db/db mice, including the restoration of cardiomyocyte activity and structural repair. Additionally, H_2S donor has the ability to inhibit the ubiquitination of myosin heavy chain 6 (MHC6) and myosin light chain 2 (MLC2) in the myocardial tissues of db/db mice. Subsequent investigation revealed that H_2S S-sulfhydrated MuRF1 at Cys44 to diminish its association between and MHC6 and MLC2, preventing myocardial degradation in the db/db mice. As a crucial calcium transport enzyme in the ER, SERCA2a has an impact on the relaxation and contraction of the myocardium. A study from Peng et al. (Peng et al., 2022) demonstrated that H_2S donor effectively increased SERCA2a protein levels and activity, while decreasing its ubiquitination levels, as well as MuRF1 expression and cytosolic calcium concentrations in comparison to the db/db mice. Additional research revealed that the administration of NaHS increased the S-sulfhydration of MuRF1, subsequently boosting SERCA2a activity and expression. While, MuRF1-Cys44 mutant plasmid deteriorated H_2S-mediated S-sulfhydration of MuRF1. The results indicated that H_2S influences the ubiquitination of SERCA2a by S-sulfhydrating MuRF1 at Cys44, thereby preventing a decrease in myocardial contractility caused by elevated cytosolic calcium levels. Moreover, Peng et al. (2023) found that exogenous H_2S suppresses SENP1s by S-sulfhydrating SENP1s at C683 site, which subsequently increases SERCA2asumo orylation, improves myocardial contractile-diastolic function, and reduces cardiomyocytes apoptosis in DCM.

H_2S mediated S-sulfhydration on cardiovascular cellular metabolism

Hyperhomocysteinemia (HHcy), an abnormal elevation of homocysteine in the plasma, hyperglycemia, and hyperlipidemia are recognized as risk factors resulting in various complications related to the cardiovascular diseases. The importance of H_2S in regulating homocysteine, lipid, and glucose metabolism has been confirmed in numerous studies. CSE-H_2S enhanced the nuclear accumulation of peroxisome proliferator activated receptor γ (PPARγ), its activity to bind DNA, and the expression of genes related to adipogenesis through directly S-sulfhydrating PPARγ at Cys139, resulting in the conversion of glucose into triglyceride storage within adipocytes. Based on what we know so far, PPAR has an important role in regulating blood lipid and glucose levels. Thereby, PPARγ S-sulfhydration could potentially serve as a new

focus for addressing diabetes, obesity, hyperlipidemia, and associated cardiovascular complications (Cai et al., 2016).

HMG-CoA reductase degradation protein (Hrd1), an E3 ubiquitin ligase responsible for transiting protein. In the models of high glucose-treated db/db mice and neonatal rat cardiomyocytes, it was discovered that the levels of CSE and Hrd1 expression were reduced compared to the control mice, while CD36 and VAMP3 level was elevated. Further study found that administration of NaHS decreased the accumulation of lipids, restored the expression of Hrd1 as well as reduced the expression of VAMP3 and facilitated its ubiquitylation. The underlying mechanism is that H_2S S-sulfhydrated Hrd1 at Cys115 to regulate VAMP3 ubiquitylation and prevent CD36 translocation in diabetic cardiomyopathy (Yu et al., 2020). Additionally, a study by Sun et al. (2021) demonstrated that the H_2S donor could boost Hrd1 expression, as well as enhance DGAT 1 and 2 ubiquitination level in the myocardium of db/db mice. The underlying mechanism was associated with H_2S-induced S-sulfhydration Hrd1 at Cys115, which boosted the connection between Hrd1 and DGAT1 and 2, ultimately preventing the development of liposome in the myocardial tissues of db/db mice.

The investigation of the key enzymes involved in Hcy metabolism is crucial as HHcy has been regarded as a contributing factor to cardiovascular disease. Methylenetetrahydrofolate reductase (MTHFR) is a pivotal enzyme controlling the Hcy metabolism within cells. A study from Ji et al. (2022) found that the bioactivity of MTHFR was decreased in HHcy of both vivo and vitro studies. The deficiency of H_2S led to a further decrease in MTHFR activity and worsened HHcy. However, the decreased bioactivity of MTHFR in HHcy was reversed by H_2S donors, resulting in a reduction of the excessive Hcy level. Furthermore, MTHFR undergoes H_2S-mediated S-sulfhydration at Cys32, Cys130, Cys131, Cys193, and Cys306 in normal conditions, and the level of S-sulfhydration is directly linked to the bioactivity of MTHFR. The findings of this research indicated that H_2S has the potential to enhance the bioactivity of MTHFR through S-sulfhydration, offering a potential therapeutic approach for HHcy.

H_2S mediated S-sulfhydration on cardiovascular mitochondrial bioenergetics

Over the past few years, mounting proof has indicated that H_2S has the ability to preserve the structure of mitochondria, decrease the emission of signals indicating mitochondrial death, and mitigate cell death reactions regulated by mitochondria in different forms, thereby providing protection in the cardiovascular system (Szczesny et al., 2014). Under physiological conditions, H_2S can cause a S-sulfydration of the α subunit of ATP synthase (ATP5A1) at Cys244 and Cys294. This process helps to sustain the activation of ATP synthase, thereby supporting mitochondrial bioenergetics (Módis et al., 2016). A study from Li and Yang, (2015) validated the significance of H_2S in upholding the replication of mitochondrial DNA and the expression of genes that serve as markers for mitochondria. According to their findings, interferon regulatory factor 1 (IRF-1) was sulfhydrated at Cys 53 by H_2S, which increased its affinity for the Dnmt3a promoter. This led to a decrease in DNA methyltransferase 3a (Dnmt3a) expression and the demethylation of the mitochondrial transcription factor A promoter, ultimately facilitating mitochondrial DNA replication. In addition, Wu et al. (2022) discovered that the CSE/H_2S pathway regulates the activity and translocation of dynamin related protein 1 (Drp1), thereby influencing cardiac function and mitochondrial morphology. In terms of mechanism, H_2S-mediated Drp1 S-sulfhydration at Cys607 caused a decrease in phosphorylation, oligomerization, and GTPase activity of Drp1, and directly competed with NO-mediated S-nitrosylation. This research revealed that H_2S suppressed Drp1 activity through S-sulfhydrating Drp1 at Cys607, thereby protecting against HF.

DOX-induced cardiotoxicity is primarily attributed to ferroptosis a new type of cell death accompanied with an excessive amount of iron accumulation (Dixon et al., 2012). H_2S had a defensive impact on DOX-triggered ferroptosis in cardiomyocytes according to the study from Wang et al. (2023). This effect was achieved through the involvement of optic atrophy 3 (OPA3), a crucial protein in the mitochondrial membrane. DOX caused a decrease in OPA3 levels, but exogenous H_2S was able to restore them. OPA3 participates in the control of ferroptosis through its interaction with NFS1, resulting in the inhibition of ferroptosis. Exogenous H_2S counteracted the ubiquitination of OPA3 induced by DOX through the promotion of OPA3 S-sulfhydration. These results indicated that H_2S safeguards cardiomyocytes from DOX-induced ferroptosis by S-sulfhydrating OPA3, inhibiting the ubiquitination of OPA3 and enhances the expression of cysteine desulfurase (NFS1).

Mitochondrial injury caused by the excessive generation of reactive oxygen species (ROS) leads to myocardial injury in diabetic condition. A research by Sun Y. et al. (2020) discovered that H_2S donor enhanced heart functions, decreased levels of reactive ROS, facilitated the movement of parkin into mitochondria, and stimulated the formation of mitophagy in the hearts of db/db mice. The aforementioned effects of H_2S were associated with the rise in S-sulfhydration of USP8, resulting in the augmentation of parkin deubiquitination process by attracting parkin to mitochondria.

The involvement of Ca^{2+}/calmodulin-dependent protein kinase II (CaMKII) is crucial in the progression of HF and the initiation of damage to myocardial mitochondria. In CSE knockout mouse models, it was discovered that administering H_2S donor resulted in the mitigation of HF, decrease of lipid peroxidation, maintenance of mitochondrial function, and inhibition of CaMKII phosphorylation. And the potential mechanism could be associated with the S-sulfhydration of CaMKII by H_2S, resulting in the inhibition of CAMKII activity and the maintenance of cardiovascular homeostasis (Wu et al., 2018).

H_2S induced S-sulfhydration on endoplasmic reticulum stress (ERS) in the cardiovascular system

The endoplasmic reticulum (ER) consists of a eukaryotic cell membrane and serves as a crucial organelle for the synthesis, folding, and secretion of proteins. ERS can be caused by changes

in the external or internal environment. Numerous studies have shown that ERS is closely related to the onset and progress of various cardiovascular ailments. Protein tyrosine phosphatase 1B (PTP1B), a crucial player in ERS, is considered a promising candidate for therapeutic intervention in cardiovascular dysfunction caused by obesity and septic shock (Coquerel et al., 2014; Kandadi et al., 2015). Krishnan et al. (2011) discovered that H_2S caused S-sulfhydration of PTP1B at Cys215, leading to the inhibition of its function. This inhibition, in turn, facilitated the phosphorylation and activation of protein kinase-like ER kinase, ultimately promoting the restoration of ER homeostasis. None of these effects were present in HeLa cells with CSE deletion. These results imply that H_2S controls endoplasmic ERS by S-sulfhydration, leading to the deactivation of PTP1B. This could potentially serve as a new mechanism for the beneficial impact of H_2S on the cardiovascular system.

Aortic aneurysm and aortic dissection (AAD) are serious conditions affecting blood vessels, where the primary focus of treatment for AAD is the endothelium. According to a research conducted by Luo et al. (2023), it was discovered that the deletion of CSE specifically in ECs worsened, while the overexpression of CSE specifically in ECs improved the advancement of AAD. During AAD, there was a decrease in S-sulfhydration of proteins in the endothelium, with protein disulfide isomerase (PDI) being the primary focus. Enhancing PDI activity and alleviating ERS was achieved through S-sulfhydration of PDI at Cys343 and Cys400. This data indicates that H_2S mitigated the advancement of AAD by boosting the activity of protein PDI through the regulation of S-sulfhydration at Cys343 and Cys400 of PDI.

H_2S mediated S-sulfhydration on cardiovascular cellular inflammation

The connection between H_2S and inflammation within the cardiovascular system is intricate. A study from Du et al. (Du et al., 2014) discovered that H_2S suppressed the inflammation of macrophages caused by oxidized low-density lipoprotein through sulfhydrating NF-κB p65 at Cys38, which consequently inhibited the its phosphorylation, nuclear translocation and DNA binding activity. Furthermore, it was discovered that H_2S suppressed macrophage inflammation caused by H_2O_2 through reducing the activation of the NLRP3 inflammasome, which resulted in the activation of caspase-1, ultimately decreasing the production of mitochondrial ROS (mtROS). The underlying mechanism is that H_2S-induced S-sulfhydration of c-Jun increased transcriptional activity of SIRT3 and p62, leading to a reduction in mtROS production. Additional discoveries indicated that mutation of c-Jun Cys269 diminished the protection effects of H_2S-induced c-Jun S-sulfhydration. To summarize, these findings indicate that H_2S alleviates oxidative stress-mediated generation of ROS and the activation of the NLRP3 inflammasome in mitochondria through S-sulfhydration of c-Jun at Cys269 (Lin et al., 2018).

Inflammation of the ECs in the pulmonary artery is a crucial occurrence in the progression of pulmonary arterial hypertension (PAH). A study by Zhang et al. (Zhang et al., 2018) showed that in monocrotaline (MCT)-induced pulmonary vascular inflammation and CSE knockdown-induced ECs inflammation, H_2S level was decrcased while SO_2 level was increased. The underlying mechanism was related to the S-sulfhydration of AAT1/2 by H_2S to inhibite the activity of AAT, leading to the reduction of endogenous SO_2 generation. Additionally, the rise in endogenous SO_2 production could potentially act as a compensative mechanism when the H_2S/CSE pathway was suppressed, thus exerting protection against endothelial inflammatory responses. Furthermore, they showed that endogenous H_2S effectively deactivated IKKβ by sulfhydrating Cys179 of IKKβ to suppress NF-κB pathway activation, ultimately attenuating pulmonary artery ECs inflammation in PAH (Zhang et al., 2019).

H_2S mediated S-sulfhydration on cardiovascular cellular oxidative stress

Oxidative stress is closely related to cardiovascular diseases. Several experimental findings indicate Keap1 and Nrf2 have a strong correlation with oxidative stress damage and antioxidant response. Nrf2 serves as a chief controller of the antioxidant reaction, while Keap1 functions as a suppressor of Nrf2 (Uesugi et al., 2017; Wasik et al., 2017). It was confirmed (Yang et al., 2013) that Keap1 underwent S-sulfhydration in embryonic fibroblasts obtained from mice with the WT genotype, whereas this modification was not observed in CSE knockout mice. In mouse embryonic fibroblasts, NaHS-induced S-sulfhydration of Keap1 at Cys151 to control Nrf2 expression, positioning and function. Possibly, this could be an innovative approach to hinder cellular aging through the S-sulfhydration of Keap1 mediated by H_2S. Moreover, Hourihan et al. (Hourihan et al., 2013) additionally found that H_2S deactivated Keap1 through the S-sulfhydration of Keap1 at the Cys226 and Cys613 location to upregulate the expression of Nrf 2, which subsequently protects cells from oxidative stress.

According to recent studies, H_2S increased the S-sulfhydration of Keap1, leading to a decrease in the connection between Keap1 and Nrf2 in high-salt treated rat, which subsequently followed by a reduction in blood pressure, collagen buildup, and oxidative stress (Huang et al., 2016). The findings from aforementioned indicate that targeting H_2S-induced S-sulfhydration of Keap1 could potentially help reduce oxidative stress and associated cardiovascular diseases.

H_2S induced S-sulfhydration on vascular structure

The excessive growth of vascular smooth muscle cells (VSMCs) serves as a crucial physiological and pathological foundation for numerous cardiovascular disorders. And H_2S is discovered to maintain the structure of blood vessels by suppressing the proliferation of VSMCs. The receptor of insulin-like growth factor-1 (IGF-1), known as IGF-1R, has various effects on the vasculature, including promoting the growth and movement of VSMCs, as well as preventing the death of VSMCs both in normal and abnormal conditions. Studies from Shuang et al. found that H_2S effectively reduces the levels of IGF-1R expression and promotes IGF-1R S-sulfhydration to weaken the interaction between IGF-1 and IGF-1R, elucidating the mechanism by which H_2S inhibits VSMCs proliferation (Shuang et al., 2018; Shuang et al., 2021). Further study

showed that H_2S S-sulfhydrates IGF-1R to decrease formation of IGF-1R/ER-α hybrid, preventing estrogen-induced VSMCs proliferation (Shuang et al., 2021). In addition, a study from Tian et al. (Tian et al., 2020) found that the stimulation of ET-1 led to an augmentation in the proliferation of VSMC A7R5 cells, along with the phosphorylation of transcription factor forkhead box transcription factor 1 (FOXO1) and its subsequent relocation from the nucleus to the cytoplasm in the A7R5 cells. Nevertheless, administration of NaHS effectively nullified the aforementioned results induced by ET-1. Additionally, further study found that H_2S hinders the phosphorylation of FOXO1 at Ser256 by S-sulfhydrating FOXO1 at Cys457. As a result, this action maintains the nuclear positioning and stimulation of FOXO1 while restraining VSMCs proliferation.

The proliferation of VSMCs induced by hyperglycaemia and hyperlipidaemia is inhibited by H_2S. A study by Zhang et al. (Zhang et al., 2021) demonstrated that mitochondrial pyruvate dehydrogenase complex-E1 (PDC-E1) significantly translocated to the nucleus in VSMCs after high glucose and palmitate treatment. Further study found that H_2S hindered the translocation of PDC-E1 through S-sulfhydration. Furthermore, PDC-E1 with a mutation at Cys101 abolished the inhibitory effect of H_2S on the proliferation of VSMCs. These findings indicated that H_2S prevented the translocation of PDC-E1 by S-sulfhydrating PDC-E1 at Cys101, subsequently inhibiting the proliferation of VSMCs treated with diabetic.

Insufficient growth of ECs is a crucial characteristic of endothelial dysfunction, leading to diseases related to vascular injury. The study according to Saha et al. (Saha et al., 2016) discovered that H_2S derived from CBS preserved the cellular response dependent on VEGF, which includes proliferation induced by VEGF due to the upregulation of VEGFR-2 and neuropilin-1 in ECs. And the underlying mechanism was that H_2S S-sulfhydrated the transcription factor Sp1 on Cys68 and Cys755 residues to enhance Sp1 binding to VEGFR-2, consequently boosting the proliferation and migration of ECs.

Maintaining elastin homeostasis is a crucial function of the CSE/H_2S system. It was discovered that older CSE knockout mice experienced significant expansion of the aorta and deterioration of elasticity in the abdominal aorta, and exhibited heightened susceptibility to aortic elastic degradation induced by angiotensin II. While NaHS safeguarded against angiotensin II-induced aortic medial degeneration in old mice. Furthermore, application of NaHS or overexpression of CSE reduced the hyperactivity of MMP2/9 and elastolysis in TNFα-induced SMCs; however, CSE-deficiency worsened these effects. Additionally study discovered that H_2S hindered the transcription of MMP2 through S-sulfhydrating Sp1. And H_2S as well straightly inhibited excessive MMP activity through the S-sulfhydration of MMP1, MMP2, MMP7, MMP9, and MMP14. In sum, these results indicated that the CSE/H_2S-induced S-sulfhydration, resulting in the inactivation of MMPs, contributes to the development of aortic elastolysis and medial degeneration (Zhu et al., 2022). This suggests that targeting the CSE/H_2S system could be a potential treatment for aortic aneurysm.

Hyperglycemia can increase vascular calcification. The depletion of elastin in the tunica media encourages the SMCs to undergo an osteogenic transformation, leading to the calcification of arterial medial, which condition is linked to a significant cardiovascular risk in individuals diagnosed with type 2 diabetes. A study conducted by Zhou et al. (Zhou Y. B. et al., 2019) demonstrated that NaHS reduced the calcification of HASMCs exposed to high glucose by lowering levels of calcium and phosphorus, inhibiting calcium deposition and alkaline phosphatase (ALP) activity. Additionally, H_2S hindered HASMCs osteogenic transformation by increasing the expression of SMα-actin and SM22α, which are two characteristic markers of smooth muscle cells, while decreasing the protein expression of core binding factor α-1 (Cbfα-1), a crucial factor in bone formation. Furthermore, the administration of NaHS suppressed the activation of Stat3, as well as the activity and expression of cathepsin S (CAS), while simultaneously elevating the elastin protein level. Further study found that inhibiting the activity or silencing the gene of Stat3 not only reversed the loss of elastin, but also reduced the expression of CAS. Elastin loss was alleviated by inhibiting CAS, whereas CAS overexpression worsened it. Additional research revealed that NaHS triggered S-sulfhydration in the wild type, but had no effect on the C259S Stat3 mutant. In conclusion, these findings indicate that H_2S may directly S-sulfhydrated Stat3 at Cys259 and then inhibited Stat3/CAS signaling to upregulate elastin level, resulting in the attenuation of vascular calcification.

H_2S induced S-sulfhydration on vasorelaxtion

Vasorelaxation of H_2S and its processes have been thoroughly researched as one of the significant physiologic activities caused by H_2S. With the establishment of S-sulfhydration, a significant amount of knowledge has been gained regarding the molecular mechanisms underlying vasodilation induced by H_2S.

H_2S plays as a vasodilation by S-sulfhydration various KATP channels subunit. S-sulfhydration of Kir6.1, a component of the KATP channels, was observed upon overexpression of CSE, and this phenomenon was not observed in the absence or mutation of CSE. An additional investigation verified that S-sulfhydrated Kir6.1 at Cys43 reduced ATP synthesis while increasing the interaction between phosphatidylinositol 4,5-bisphosphate and Kir6.1, thereby enhancing KATP channel function and enhancing vasodilation. Furthermore, the Kir6.1-Cys43 mutants exhibited a reduction in both in S-sulfhydration and vasodilatation induced by H_2S. Possibly, this could be the primary mechanism through which H_2S functions as a relaxing factor derived from ECs (Mustafa et al., 2011). Furthermore, it was found that H_2S-induced S-sulfhydration targeted Cys6 and Cys26 in rvSUR1, which is a subunit of the extracellular loop KATP channel complex in rats. The KATP channel was activated by H_2S, leading to S-sulfhydration and subsequent relaxation of the blood vessels (Jiang et al., 2010). Additionally, Kang et al. (Kang et al., 2015) discovered that H_2S S-sulfhydrated sulphonylurea 2B (SUR2B) at Cys24 and Cys1455, which are both part of the KATP channels complex, resulting in the recovery of smooth muscle contraction.

In previous studies, ECs are shown to produce endogenous H_2S and to cause dilation in response to H_2S. A study by Naik et al. (Naik et al., 2016) discovered that upon inhibiting TRPV4, the dilation of vessels caused by H_2S-induced influx of Ca^{2+} and K^+ was prevented. Furthermore, the S-sulfhydration of TRPV4 was increased following the administration of Na_2S in aortic ECs. This implies that TRPV4 is triggered following S-sulfhydration, potentially serving as the crucial element in vasodilation. In addition, it was showed that the ability of the carotid sinus baroreceptor to regulate blood pressure was enhanced through the S-sulfhydration of TRPV1 by H_2S derived from CBS, as

indicated by Yu et al. (Yu et al., 2017). Additionaly, Dai et al. (Dai et al., 2019) discovered that NaHS decreased the level of intracellular Ca^{2+} by sulfhydrating L-type Ca^{2+} channels in VSMCs, thereby impacting the PKC/ERK pathway downstream and preventing the constriction of VSMCs.

The eNOS, an enzyme that produces NO, is a protein targeted by H_2S, leading to vasodilation. A Study by Altaany et al. (Altaany et al., 2014) discovered that H_2S enhances the activity of eNOS by causing the S-sulfhydration of eNOS at Cys443, which results in the promotion of eNOS phosphorylation and inhibition of its S-nitrosylation, ultimately leading to vasodilation. The soluble guanylatecyclase β1 (sGC β1), one of the subunits of the sGC protein, plays a crucial role as an enzyme in the process of catalyzing the synthesis of cGMP; on the other hand, phosphodiesterase (PDE) facilitates the breakdown of cGMP. And the sGC β1/PDE/cGMP is a signal transduction pathway associated with vascular relaxation. A study from Sun et al. (Sun et al., 2017) found that H_2S increased cGMP synthesis by S-sulfhydrating sGC β1 and inhibited the degradation of cGMP by S-sulfhydrating PDE 5A to exert vasorelaxant effect in vascular tissues.

Integrins have been related to the detection of flow in ECs. The activation of β3 integrin occurred when shear stress was applied to ECs, causing a change in conformation (Jalali et al., 2002). A study from Bibli et al. (Bibli et al., 2021) discovered that the absence of S-sulfhydration hindered the connections between β3 integrin and Gα13, leading to the constant activation of RhoA and hindering the realignment of ECs caused by flow. Furthermore, there was a correlation between endothelial function and reduced H_2S production, compromised dilation caused by flow, and the inability to detect β3 integrin S-sulfhydration. However, all of these results were restored when H_2S supplement was administered. This study suggests that vascular illness is linked to significant alterations in the S-sulfhydration of proteins found in ECs, which play a role in facilitating responses to fluid movement. Enhancing vascular reactivity in humans was observed with the temporary addition of H_2S, indicating the possibility of utilizing this pathway for the treatment of vascular disease.

Endogenous CSE/H_2S in $CD4^+$ T-cells plays an important role in the development of hypertension. In the case of hypertensive patients or spontaneously hypertensive rats, it was discovered that CSE/H_2S in the isolated peripheral blood lymphocytes reacted to alterations in blood pressure. This was confirmed by variations in lymphocyte CSE protein and a negative association between H_2S production and systolic and diastolic blood pressure. However, there was a positive association between H_2S production and the interleukin 10 level of serum, which is an anti-inflammatory cytokine. The activation of liver kinase B1 by H_2S derived from CSE, through constitutive S-sulfhydration, triggers the activation of its target kinase, AMP-activated protein kinase. This activation promotes the differentiation and proliferation of Treg cells, which helps to reduce immune-inflammation in the vascular and renal systems, ultimately preventing hypertension (Bibli et al., 2021).

H_2S induced S-sulfhydration on atherosclerotic

The presence of intimal plaques and cholesterol buildup in the arterial walls defines atherosclerosis, which is a primarily contributor to global mortality due to the susceptibility of plaque rupture. H_2S, primarily produced by CSE in cardiovascular organs, serves as a safeguarding gasotransmitter in atherosclerosis (Zhang et al., 2013). A study from Chen et al. (Chen et al., 2022) found that CSE-H_2S significantly decreased in ACTA2-positive cells within plaques from patients, atherosclerotic mice, or VSMCs stimulated with ox-LDL. And the H_2S donor supplementation partially rescued the exacerbation of plaque size and reduction of autophagy, resulting from the deletion of CSE in VSMCs, thereby lowering plaque stability. In terms of mechanism, the S-sulfhydration of TFEB at the Cys212 site by CSE-H_2S facilitates its translocation to the nucleus, subsequently enhancing VSMCs autophagy. This process promotes the secretion of collagen and suppresses apoptosis, ultimately reducing the progression of atherosclerosis and the vulnerability of plaques. Moreover, a study from Xie et al. (Xie et al., 2016) discovered that GYY4137 reduced the development of atherosclerotic plaques in the aorta and lowered levels of ROS in streptozotocin-induced LDL receptor knockout mice ($LDLr^{-/-}$). However, this effect was not observed in mice with double knockout of $LDLr^{-/-}$ and $Nrf2^{-/-}$. GYY4137 additionally reduced foam cell development and oxidative stress in peritoneal macrophages obtained from wild type mice, while having no effect on $Nrf2^{-/-}$ mice, implying that H_2S mitigates the progression of atherosclerosis in diabetes through a mechanism that relies on Nrf2. Additional research revealed that GYY4137 facilitated the separation of Keap1 from Nrf2 in ECs stimulated by ox-LDL and high-glucose, potentially due to the S-sulfhydration of Keap1 at Cys151 and Cys273 sites. In the meantime, the Keap1 mutation at position C151A eliminated the dissociation of Keap1/Nrf2, the translocation of Nrf2 into the nucleus, and the inhibition of ROS induced by the administration of GYY4137. Therefore, it is suggested that the S-sulfhydration of proteins by H_2S could serve as a new therapeutic objective for the prevention of atherosclerosis accelerated by diabetes. In addition, it was discovered that CSE specifically deficiency in ECs resulted in an increase in the expression of CD62E, which is associated with the activation of ECs and the development of atherosclerosis, and led to an elevated adherence of monocytes even without an inflammatory trigger, along with also accelerated the progression of endothelial dysfunction and atherosclerosis; but these effects were restored when treated with H_2S donor. Mechanistically, the prevention of homodimerization and activity of human antigen R is achieved through the CSE-H_2S induced S-sulfhydration at Cys13, leading to the attenuation of CD62E target protein expression (Bibli et al., 2019).

SIRT1, a crucial gene for promoting longevity, acts as a histone deacetylase and controls the acetylation of certain functional proteins, thereby exerting an anti-atherogenic impact. In atherosclerosis mice lacking ApoE, the administration of H_2S donor, NaHS or GYY4137, resulted in decreased area of atherosclerotic plaque, infiltration of macrophages, inflammation in the aorta, and levels of lipids in the bloodstream. Treatment with H_2S enhanced the expression of SIRT1 mRNA in the aorta and liver, as well as promoted SIRT1 deacetylation in ECs and macrophages, subsequently resulting in the reduction of inflammation in ECs and macrophages. Mechanismly, the direct S-sulfhydration of H_2S on SIRT1 enhanced the binding of SIRT1 to zinc ion, subsequently boosting its deacetylation function and stability, ultimately reducing the formation of atherosclerotic plaques (Du et al., 2019).

Elevated levels of homocysteine can lead to various effects including dysfunction of the endothelium, heightened risk of blood clot formation, faster proliferation and movement of VSMCs, and hindered cholesterol

transportation by monocytes and macrophages. These factors collectively contribute to the development of atherosclerosis (Thambyrajah and Townend, 2000; Lai and Kan, 2015). In the mice with atherosclerosis and hyperhomocysteinemia, it was discovered that the serum homocysteine level increased. Additionally, the mRNA, protein levels and catalytic activity of CSE, which is a crucial enzyme responsible for homocysteine trans-sulfuration, were reduced due to hyperhomocysteinemia; while the administration of H_2S donor reversed all of these effects. In terms of mechanism, hyperhomocysteinemia caused S-nitrosylation of CSE, while H_2S S-sulfhydrated CSE at the identical cysteine sites. Additional research revealed that the catalytic and binding capabilities of CSE towards L-homocysteine were reduced with S-nitrosylated CSE, while they were enhanced with S-sulfhydrated CSE. The alteration of Cys252, Cys255, Cys307, and Cys310 sites in CSE eliminated the S-nitrosylation or S-sulfhydration of CSE and hindered its interaction with L-homocysteine. To sum up, the administration of H_2S donor improved the S-sulfhydration of CSE, leading to a reduction in serum levels of L-homocysteine. This, in turn, played a role in the beneficial effects against atherosclerosis observed in ApoE-knockout mice with hyperhomocysteinemia (Fan et al., 2019).

SO_2-induced S-sulfenylation on cardiovascular biological effects

Protein S-sulfenylation, also known as the oxidation of cysteine thiol to sulfenic acid (Cys-SOH), is a reversible post-translational modification, playing a pivotal role of SO_2 in the modulation of the cardiovascular system (Figure 4). Following CO, NO, and H_2S, endogenous SO_2 has emerged as a new gas signalling molecule implicated in cardiovascular diseases. Hence, ensuring a consistent and appropriate production of endogenous SO_2 is a crucial subject when it comes to maintaining cardiovascular balance. A study from Song et al. (Song et al., 2020) demonstrated that within vascular ECs, SO_2 regulates its own production by employing negative feedback inhibition of AAT1 function through S-sulfenylation of Cys192 on AAT1. The discovery will significantly enhance the comprehension of regulatory mechanisms in maintaining cardiovascular balance.

According to recent research, it has been indicated that internal SO_2 has the ability to alter different biological processes, including inflammation, apoptosis, as well as vascular remodeling. Moreover, it is suggested to have a therapeutic effect through S-sulfenylation. For example, SO_2 induced S-sulfenylation of NF-κB p65 at Cys38, which resulted in the inhibition of NF-κB nuclear translocation and DNA binding activity. As a result, the NF-κB signaling pathway caused inflammation was inhibited, leading to a curative effect on oleic acid-induced acute lung injury (Chen et al., 2017).

The growth of cells relies on the pH level within the cells, known as intracellular pH (pHi). The alteration of cysteine in the transmembrane region of the Na^+-independent Cl^-/HCO_3^-exchanger, also known as anion exchanger (AE), has an impact on pHi. According to research conducted by Wang et al. (Wang et al., 2019) demonstrated that SO_2 decreased the pHi and strongly activated AE. Conversely, the AE inhibitor greatly reduced the impact of SO_2 on pHi in VSMCs. AE2 S-sulfenylation was associated with the impact of SO_2. Moreover, the AE blocker abolished the inhibitory effect of SO_2 on the proliferation of VSMCs stimulated by platelet-derived growth factor-BB (PDGF-BB). To summarize, this research showed that SO_2 hinders the growth of VSMCs by directly activating the AE through posttranslational S-sulfenylation and causing intracellular acidification.

Another study by Huang et al. (Huang et al., 2021) determined SO_2-induced S-sulfenylation proteomics through chemoproteomics in angiotensin II-treated VSMCs, which identified a total of 1137 S-sulfenylated cysteine residues in 658 proteins. Interestingly, 42% of these residues were found to be influenced by SO_2. Among these, an increase in S-sulfenylation was detected in Cys64 of Smad3, resulting in a decrease in the ability to bind to DNA. Ultimately, the collagen protein levels were considerably inhibited, resulting in a reduction in angiotensin II-mediated vascular remodeling and abnormality.

Extended activation of mitochondrial permeability transition pore (mPTP) may result in impairment of mitochondrial energy, enlargement, breakage, programmed cell death, and necrosis (Zhou B. et al., 2019). Cyclophilin-D (CypD) serves as a significant controller in the modulation of mPTP opening (Sun et al., 2019). A study from Lv et al. (Lv et al., 2022) demonstrated that the SO_2-induced S-sulfenylation of CypD at Cys104 leaded to the inhibition of mPTP opening, safeguarding cardiomyocyte against apoptosis.

Detection of S-sulfhydration

There are several techniques for identifying S-sulfhydration, such as the altered biotin switch test, cysteinyl labeling test, maleimide test using fluorescent thiol modifying agents, tag-switch approach, and mass spectrometry (Figure 5). Nevertheless, currently there is no perfect technique for identifying S-sulfhydration due to the presence of inaccurate indications or inadequate sensitivity in the aforementioned methods. There is an urgent need for more specific methods to identify S-sulfhydration uniquely. An example of an original assay for detecting protein S-sulfhydration is the Biotin-Switch method (Mustafa et al., 2009b). The thiol in proteins was blocked by S-methyl methanethiosulfonate (MMTS), an alkylating agent. Subsequently, Biotin-HPDP was conjugated with the persulfides group. Nevertheless, this approach facilitated the concurrent labeling of S-sulfhydration and S-nitrosylation, resulting in poor selectivity. The cysteine labeling method uses IAA as a blocking agent, and IAP is used to label the persulfide modified proteins (Krishnan et al., 2011). One concern with this approach is its inability to differentiate persulfides from intramolecular, intermolecular, and S-nitrosothiols, all of which will also be broken down by DTT. The maleimide test relies on the chemical properties of N-ethyl maleimide, a reagent that blocks both free thiol and persulfide groups (Sen et al., 2012). A drawback of this fluorescence technique is its limited applicability for proteomic analysis. The Biotin-Thiol-Assay can employ NM-Biotin or IAB to alkylate both thiol and persulfide functional groups (Gao et al., 2015; Dóka et al., 2016), but this approach may result in inaccurate negative signals.

Considering the aforementioned issues with the Biotin-Switch technique and maleimide approach, Zhang et al. proposed the tag-switch assay to detect S-sulfhydration modification, the core of which is the use of two different reagents to label supersulfide. Currently, the eligible thiol sealers are methansulfonyl benzothiazole (methylsulfonylbenzothiazole, MSBT) and methyl cyanoacetate (Park et al., 2015; Wedmann et al., 2016). Furthermore, the analysis of protein S-sulfhydration also involved the utilization of mass spectrometry (MS). By obstructing sulfol groups in the proteins using MSBT, the biotin-

labeled proteins were subsequently separated into polypeptides in order to detect persulfated modified proteins and their respective locations. Nonetheless, this method presents an equal challenge in fully obstructing protein samples and, as a result, can easily produce inaccurate positive outcomes (Park et al., 2015).

To summarize, the exploration of S-sulfhydration alteration is still in its early stages, and the criticality of choosing exceptionally precise detection agents cannot be overstated in advancing this domain. Furthermore, the integration of the aforementioned testing technique with mass spectrometry can effectively prevent inaccurate positive outcomes. In addition, the development of fluorescent probes that detect S-Sulfhydrylation protein imaging, even commercially available ones, is also worthwhile. In short, the exploration of the detection methods for S-sulfhydration modification will provide an insight into the biological significance of this post-translational modification.

Detection of S-sulfenylation

S-sulfenylation, a post-translational modification that can be reversed, is crucial for regulating protein activity through redox control in numerous biological processes. The detection and study of protein S-sulfenylation is not possible directly because it is inherently unstable. Over the last few decades, different dimedones (aka dicarbonyl) are now more readily available for the specific identification and detection of cysteine S-sulfenylation (Furdui and Poole, 2014). For instance, Western blotting with the appropriate antibody can be employed to detect cysteine S-sulfenylation labeled with dimedone (Seo and Carroll, 2009). Dimedone analogs containing fluorescent or biotin reporter groups can be used to visualize and enhance S-sulfenylated proteins (Charles et al., 2007). Carroll Lab created the initial DAz-1 probe for detecting sulfenic acid in its natural environment. This compound is dimedone that has been chemically modified with an azide group, enabling its selective recognition by phosphine reagents through the Staudinger ligation method. This technique is used for the detection, enrichment, and visualization of altered proteins (Reddie and Carroll, 2008). In 2012, the Carroll laboratory developed DYn-2, a novel dimedone analog labeled with alkyne that had superior stability and efficiency compared to previous probes based on dimedone for labeling Cys-SOH *in situ* (Paulsen et al., 2011). The use of dimedone-based probes has greatly expanded the number of S-sulfenylated proteins and their corresponding sites. Several other chemical compounds, apart from dimedone, have been extensively studied for the specific labeling of S-sulfenic acids (Qian et al., 2012; Poole et al., 2014; McGarry et al., 2016; Alcock et al., 2018). In order to develop the next iteration of chemoproteomic probe for the worldwide exploration of S-sulfenylome, Carroll Lab initially constructed an innovative collection of 100 cyclic carbon-nucleophiles that selectively interact with Cys-SOH (Gupta and Carroll, 2016). Expanding on this source, they additionally created four novel alkyne-labeled probes, namely, TD, PYD, PRD, and BTD, for the specific marking of protein S-sulfenic acids. Due to its exceptional response rate towards Cys-SOH, BTD displayed the utmost degree of reactivity towards S-sulfenylome (Gupta et al., 2017). And BTD has demonstrated a strong compatibility with chemoproteomic platforms that focus on specific sites. Hence, the novel BTD probe (Fu et al., 2019) can be utilized to achieve a more efficient approach in mapping and quantifying cysteine S-sulfenylation in intricate proteomes (Figure 6).

Conclusion

Despite the notable advancements in drug treatment and clinical guidance for cardiovascular diseases, the prevalence and fatality rates of such conditions persist at elevated levels due to the aging population and escalating risk factors. Consequently, there is an urgent demand for novel therapeutic concepts and strategies to address cardiovascular diseases. In this context, the discovery of H_2S and SO_2 as gas signaling molecules in recent years has emerged as a significant development, as they exhibit crucial protective effects within the cardiovascular system. Currently, there is ongoing development of various H_2S and SO_2 donors or targeted prodrugs. In recent years, different types of SO_2 donors and prodrugs with distinct triggering mechanisms have been designed, including thiol-activated SO_2 prodrugs (Zhang et al., 2023), thermally-activated SO_2 prodrugs (Li et al., 2019), hydrolysis-based SO_2 prodrugs (Day et al., 2016), glutathione-responsive SO_2 prodrugs (Xia et al., 2022), and esterase-sensitive SO_2 prodrugs (Wang and Wang, 2017). Additionally, H_2S donors such as CySSPe (Tocmo and Parkin, 2019) and Diallyl trisulfide (Qiao et al., 2018), and the mitochondrial targeting of H_2S prodrugs AP39 and RT01 (Magierowska et al., 2022), as well as photothermal therapy-triggered H_2S prodrugs (Chen et al., 2015), have emerged as novel strategies for the treatment of cardiovascular diseases. Over the last decade, an increasing number of studies have elucidated the diverse biological regulatory functions of H_2S and SO_2, specifically through the direct S-sulfhydration and S-sulfenylation of target proteins. These modifications have been shown to effectively and promptly regulate cell signal transmission. Notably, significant progress has been made in comprehending the role of protein S-sulfhydration and S-sulfenylation mediated by H_2S and SO_2 in the cardiovascular system. It is undeniable that research on protein S-sulfhydration and S-sulfenylation is being increasingly suggested as a prospective avenue for future investigations in the realm of gas signaling molecules. Consequently, the exploration and creation of cardiovascular protective medications that target S-sulfhydration and S-sulfenylation may represent a novel path for clinical drug treatment of cardiovascular injury diseases. In light of this, it is imperative to collaborate with the fields of drug research and development and pharmacology research to facilitate the translation of fundamental research into clinical applications.

However, there exist numerous significant concerns pertaining to the utilization of H_2S-induced S-sulfhydration and SO_2-induced S-sulfenylation in drug development, which necessitate attention for their prospective clinical application. (1) During the protein S-sulfhydration process, the generation of both small-molecule based persulfides and protein persulfides occurs, resulting in highly reactive species. The metabolic regulation of these species remains largely unexplored. (2) it is intriguing to investigate the distinct utilization of H_2S and SO_2 by cardiovascular cells at specific temporal intervals. (3) There is an urgent requirement for improved scientific techniques that possess greater sensitivity and specificity in order to identify S-sulfhydration. (4) Further research is required to

explore additional proteins and thoroughly examine the specific cysteine sites associated with S-sulfhydration and S-sulfenylation within the cardiovascular system. (5) Nevertheless, not every protein that undergoes S-sulfhydration and S-sulfenylation experiences a modified spatial arrangement and functionality. The determination of this could depend on the positioning of the cysteines that are S-sulfhydrated/S-sulfenylated. Protein function and signal transduction will be altered if S-sulfhydrated/S-sulfenylated cysteines are found in the crucial domain, which is essential for maintaining the structure and activity of the protein. Put simply, there could be no notable distinction following S-sulfhydration and S-sulfenylation, commonly referred to as 'ineffective S-sulfhydration and S-sulfenylation'. (6) Furthermore, further studies will explore the importance of S-sulfhydration/S-sulfenylation in the cardiovascular system, including but not limited to target gene transcription, enzymatic activity, and ion channel permeability. (7) The thioredoxin system regulates the levels of S-sulfhydration and S-sulfenylation, indicating that modifying the activity or expression of thioredoxin may play a role in controlling the intracellular levels of the two modifications and the biological and pharmacological effects mediated by H_2S and SO_2. (8) Further investigation is warranted to explore the potential interactions between S-sulfhydration and S-sulfenylation and other post-translational modifications, with the aim of expediting the advancement of cardiovascular disease treatment. (9) A comprehensive examination is necessary to thoroughly explore the clinical significance of S-sulfhydration and S-sulfenylation in cardiovascular disorders. (10) Additionally, it is important to acknowledge that proteins modified through S-sulfhydration and S-sulfenylation may elicit biological effects by activating downstream components of the target protein. For instance, the anti-oxidation effect of Keap1 modified by H_2S can be observed in the activation of Nrf2 in the Keap1-Nrf2 pathway, leading to the activation of downstream anti-oxidation genes. However, it is important to note that the activation of Nrf2 is not solely regulated by Keap1, and excessive Nrf2 activation can result in bodily abnormalities. Therefore, the control of drug release is crucial in minimizing adverse reactions.

Protein S-sulfhydration or S-sulfenylation, a crucial post-translational modification induced by H_2S or SO_2, may potentially function as a molecular mechanism underlying the effects of H_2S or SO_2. Further exploration is necessary to determine the clinical significance of S-sulfhydration and S-sulfenylation in cardiovascular disorders. Acquiring additional knowledge concerning S-sulfhydration and S-sulfenylation will augment our understanding of the beneficial influence that these modifications can exert on specific cysteines in various cardiovascular conditions. Furthermore, the proteins that are S-sulfhydrated and S-sulfenylated could serve as promising new targets for therapeutic intervention and drug development in the cardiovascular system. This, in turn, could expedite the advancement and utilization of drugs associated with H_2S or SO_2 in the coming years.

Author contributions

YS: Writing–original draft. ZX: Writing–original draft. QZ: Writing–original draft. RZ: Writing–original draft. XS: Writing–review and editing. GC: Writing–review and editing.

Funding

The author(s) declare financial support was received for the research, authorship, and/or publication of this article. This study was supported by National Natural Science Foundation of China (82204792), China Postdoctoral Science Foundation (2022M711089), Heilongjiang Provincial Natural Science Foundation (YQ 2022H020), Postdoctoral Fund of Heilongjiang Province (LBH-Z21080) and (LBH-Z19035), Heilongjiang Provincial Health Commission Fund (20210202010178), and Doctor Innovation Fund of Heilongjiang University of Traditional Chinese Medicine (2019BS06).

Conflict of interest

The authors declare that the research was conducted in the absence of any commercial or financial relationships that could be construed as a potential conflict of interest.

Publisher's note

References

Alcock, L. J., Perkins, M. V., and Chalker, J. M. (2018). Chemical methods for mapping cysteine oxidation. *Chem. Soc. Rev.* 47 (1), 231–268. doi:10.1039/c7cs00607a

Altaany, Z., Ju, Y., Yang, G., and Wang, R. (2014). The coordination of S-sulfhydration, S-nitrosylation, and phosphorylation of endothelial nitric oxide synthase by hydrogen sulfide. *Sci. Signal.* 7 (342), ra87. doi:10.1126/scisignal.2005478

Banerjee, R., Chiku, T., Kabil, O., Libiad, M., Motl, N., and Yadav, P. K. (2015). Assay methods for H2S biogenesis and catabolism enzymes. *Methods. Enzymol.* 554, 189–200. doi:10.1016/bs.mie.2014.11.016

Bibli, S. I., Hu, J., Looso, M., Weigert, A., Ratiu, C., Wittig, J., et al. (2021). Mapping the endothelial cell *S*-sulfhydrome highlights the crucial role of integrin sulfhydration in vascular function. *Circulation* 143 (9), 935–948. doi:10.1161/CIRCULATIONAHA.120.051877

Bibli, S. I., Hu, J., Sigala, F., Wittig, I., Heidler, J., Zukunft, S., et al. (2019). Cystathionine γ lyase sulfhydrates the RNA binding protein human antigen R to preserve endothelial cell function and delay atherogenesis. *Circulation* 139 (1), 101–114. doi:10.1161/CIRCULATIONAHA.118.034757

Bibli, S. I., Szabo, C., Chatzianastasiou, A., Luck, B., Zukunft, S., Fleming, I., et al. (2017). Hydrogen sulfide preserves endothelial nitric oxide synthase function by inhibiting proline-rich kinase 2: implications for cardiomyocyte survival and cardioprotection. *Mol. Pharmacol.* 92 (6), 718–730. doi:10.1124/mol.117.109645

Cai, J., Shi, X., Wang, H., Fan, J., Feng, Y., Lin, X., et al. (2016). Cystathionine γ lyase-hydrogen sulfide increases peroxisome proliferator-activated receptor γ activity by sulfhydration at C139 site thereby promoting glucose uptake and lipid storage in adipocytes. *Biochim. Biophys. Acta.* 1861 (5), 419–429. doi:10.1016/j.bbalip.2016.03.001

Charles, R. L., Schröder, E., May, G., Free, P., Gaffney, P. R., Wait, R., et al. (2007). Protein sulfenation as a redox sensor: proteomics studies using a novel biotinylated dimedone analogue. *Mol. Cell. Proteomics.* 6 (9), 1473–1484. doi:10.1074/mcp.M700065-MCP200

Chen, Q., Zhang, L., Chen, S., Huang, Y., Li, K., Yu, X., et al. (2016). Downregulated endogenous sulfur dioxide/aspartate aminotransferase pathway is involved in angiotensin II-stimulated cardiomyocyte autophagy and myocardial hypertrophy in mice. *Int. J. Cardiol.* 225, 392–401. doi:10.1016/j.ijcard.2016.09.111

Chen, S., Huang, Y., Liu, Z., Yu, W., Zhang, H., Li, K., et al. (2017). Sulphur dioxide suppresses inflammatory response by sulphenylating NF-κB p65 at Cys38 in a rat model of acute lung injury. *Clin. Sci. (Lond).* 131 (21), 2655–2670. doi:10.1042/CS20170274

Chen, W., Chen, M., Zang, Q., Wang, L., Tang, F., Han, Y., et al. (2015). NIR light controlled release of caged hydrogen sulfide based on upconversion nanoparticles. *Chem. Commun. (Camb)* 51 (44), 9193–9196. doi:10.1039/c5cc02508g

Chen, Z., Ouyang, C., Zhang, H., Gu, Y., Deng, Y., Du, C., et al. (2022). Vascular smooth muscle cell-derived hydrogen sulfide promotes atherosclerotic plaque stability via TFEB (transcription factor EB)-mediated autophagy. *Autophagy* 18 (10), 2270–2287. doi:10.1080/15548627.2022.2026097

Coquerel, D., Neviere, R., Delile, E., Mulder, P., Marechal, X., Montaigne, D., et al. (2014). Gene deletion of protein tyrosine phosphatase 1B protects against sepsis-induced cardiovascular dysfunction and mortality. *Arterioscler. Thromb. Vasc. Biol.* 34 (5), 1032–1044. doi:10.1161/ATVBAHA.114.303450

Dai, L., Qian, Y., Zhou, J., Zhu, C., Jin, L., and Li, S. (2019). Hydrogen sulfide inhibited L-type calcium channels (CaV1.2) via up-regulation of the channel sulfhydration in vascular smooth muscle cells. *Eur. J. Pharmacol.* 858, 172455. doi:10.1016/j.ejphar.2019.172455

Day, J. J., Yang, Z., Chen, W., Pacheco, A., and Xian, M. (2016). BenzothiazoleSulfinate: A water-soluble and slow-releasing sulfur dioxide donor. *ACS Chem. Biol.* 11 (6), 1647–1651. doi:10.1021/acschembio.6b00106

Diaz, S. L., Sanchez-Aranguren, L., Wang, K., Spickett, C. M., Griffiths, H. R., and Dias, I. H. K. (2023). TNF-α-Mediated endothelial cell apoptosis is rescued by hydrogen sulfide. *Antioxidants. (Basel)* 12 (3), 734. doi:10.3390/antiox12030734

Dixon, S. J., Lemberg, K. M., Lamprecht, M. R., Skouta, R., Zaitsev, E. M., Gleason, C. E., et al. (2012). Ferroptosis: An iron-dependent form of nonapoptotic cell death. *Cell.* 149 (5), 1060–1072. doi:10.1016/j.cell.2012.03.042

Dóka, É., Pader, I., Bíró, A., Johansson, K., Cheng, Q., Ballagó, K., et al. (2016). A novel persulfide detection method reveals protein persulfide- and polysulfide-reducing functions of thioredoxin and glutathione systems. *Sci. Adv.* 2 (1), e1500968. doi:10.1126/sciadv.1500968

Du, C., Lin, X., Xu, W., Zheng, F., Cai, J., Yang, J., et al. (2019). Sulfhydrated sirtuin-1 increasing its deacetylation activity is an essential epigenetics mechanism of anti-atherogenesis by hydrogen sulfide. *Antioxid. Redox. Signal.* 30 (2), 184–197. doi:10.1089/ars.2017.7195

Du, J., Huang, Y., Yan, H., Zhang, Q., Zhao, M., Zhu, M., et al. (2014). Hydrogen sulfide suppresses oxidized low-density lipoprotein (ox-LDL)-stimulated monocyte chemoattractant protein 1 generation from macrophages via the nuclear factor κB (NF-κB) pathway. *J. Biol. Chem.* 289 (14), 9741–9753. doi:10.1074/jbc.M113.517995

Fan, J., Zheng, F., Li, S., Cui, C., Jiang, S., Zhang, J., et al. (2019). Hydrogen sulfide lowers hyperhomocysteinemia dependent on cystathionine γ lyase S-sulfhydration in ApoE-knockout atherosclerotic mice. *Br. J. Pharmacol.* 176 (17), 3180–3192. doi:10.1111/bph.14719

Fu, L., Liu, K., Ferreira, R. B., Carroll, K. S., and Yang, J. (2019). Proteome-wide analysis of cysteine S-sulfenylation using a benzothiazine-based probe. *Curr. Protoc. Protein. Sci.* 95 (1), e76. doi:10.1002/cpps.76

Furdui, C. M., and Poole, L. B. (2014). Chemical approaches to detect and analyze protein sulfenic acids. *Mass. Spectrom. Rev.* 33 (2), 126–146. doi:10.1002/mas.21384

Gao, X. H., Krokowski, D., Guan, B. J., Bederman, I., Majumder, M., Parisien, M., et al. (2015). Quantitative H2S-mediated protein sulfhydration reveals metabolic reprogramming during the integrated stress response. *Elife* 4, e10067. doi:10.7554/eLife.10067

Gupta, V., and Carroll, K. S. (2016). Profiling the reactivity of cyclic C-nucleophiles towards electrophilic sulfur in cysteine sulfenic acid. *Chem. Sci.* 7 (1), 400–415. doi:10.1039/C5SC02569A

Gupta, V., Yang, J., Liebler, D. C., and Carroll, K. S. (2017). Diverse redoxome reactivity profiles of carbon nucleophiles. *J. Am. Chem. Soc.* 139 (15), 5588–5595. doi:10.1021/jacs.7b01791

Hourihan, J. M., Kenna, J. G., and Hayes, J. D. (2013). The gasotransmitter hydrogen sulfide induces nrf2-target genes by inactivating the keap1 ubiquitin ligase substrate adaptor through formation of a disulfide bond between cys-226 and cys-613. *Antioxid. Redox. Signal.* 19 (5), 465–481. doi:10.1089/ars.2012.4944

Huang, P., Shen, Z., Liu, J., Huang, Y., Chen, S., Yu, W., et al. (2016). Hydrogen sulfide inhibits high-salt diet-induced renal oxidative stress and kidney injury in dahl rats. *Oxid. Med. Cell. Longev.* 2016, 2807490. doi:10.1155/2016/2807490

Huang, Y., Li, Z., Zhang, L., Tang, H., Zhang, H., Wang, C., et al. (2021). Endogenous SO2-dependent Smad3 redox modification controls vascular remodeling. *Redox. Biol.* 41, 101898. doi:10.1016/j.redox.2021.101898

Jalali, S., Pozo, M. A., Chen, K., Miao, H., Li, Y., Schwartz, M. A., et al. (2002). Integrin-mediated mechanotransduction requires its dynamic interaction with specific extracellular matrix (ECM) ligands. *Proc. Natl. Acad. Sci. U. S. A.* 98 (3), 1042–1046. doi:10.1073/pnas.031562998

Ji, D., Luo, C., Liu, J., Cao, Y., Wu, J., Yan, W., et al. (2022). Insufficient S-sulfhydration of methylenetetrahydrofolate reductase contributes to the progress of hyperhomocysteinemia. *Antioxid. Redox. Signal.* 36 (1-3), 1–14. doi:10.1089/ars.2021.0029

Ji, K., Xue, L., Cheng, J., and Bai, Y. (2016). Preconditioning of H2S inhalation protects against cerebral ischemia/reperfusion injury by induction of HSP70 through PI3K/Akt/Nrf2 pathway. *Brain. Res. Bull.* 121, 68–74. doi:10.1016/j.brainresbull.2015.12.007

Jiang, B., Tang, G., Cao, K., Wu, L., and Wang, R. (2010). Molecular mechanism for H(2)S-induced activation of K(ATP) channels. *Antioxid. Redox. Signal.* 12 (10), 1167–1178. doi:10.1089/ars.2009.2894

Kandadi, M. R., Panzhinskiy, E., Roe, N. D., Nair, S., Hu, D., and Sun, A. (2015). Deletion of protein tyrosine phosphatase 1B rescues against myocardial anomalies in high fat diet-induced obesity: role of AMPK-dependent autophagy. *Biochim. Biophys. Acta.* 1852 (2), 299–309. doi:10.1016/j.bbadis.2014.07.004

Kang, M., Hashimoto, A., Gade, A., and Akbarali, H. I. (2015). Interaction between hydrogen sulfide-induced sulfhydration and tyrosine nitration in the KATP channel complex. *Am. J. Physiol. Gastrointest. Liver. Physiol.* 308 (6), G532–G539. doi:10.1152/ajpgi.00281.2014

Krishnan, N., Fu, C., Pappin, D. J., and Tonks, N. K. (2011). H2S-Induced sulfhydration of the phosphatase PTP1B and its role in the endoplasmic reticulum stress response. *Sci. Signal.* 4 (203), ra86. doi:10.1126/scisignal.2002329

Lai, W. K., and Kan, M. Y. (2015). Homocysteine-induced endothelial dysfunction. *Ann. Nutr. Metab.* 67 (1), 1–12. doi:10.1159/000437098

Li, S., Liu, R., Jiang, X., Qiu, Y., Song, X., Huang, G., et al. (2019). Near-infrared light-triggered sulfur dioxide gas therapy of cancer. *ACS Nano.* 13 (2), 2103–2113. doi:10.1021/acsnano.8b08700

Li, S., and Yang, G. (2015). Hydrogen sulfide maintains mitochondrial DNA replication via demethylation of TFAM. *Antioxid. Redox. Signal.* 23 (7), 630–642. doi:10.1089/ars.2014.6186

Li, Z., Huang, Y., Lv, B., Du, J., Yang, J., Fu, L., et al. (2023). Gasotransmitter-mediated cysteinome oxidative posttranslational modifications: formation, biological effects, and detection. *Antioxid. Redox. Signal* 2023. doi:10.1089/ars.2023.0407

Lin, Z., Altaf, N., Li, C., Chen, M., Pan, L., Wang, D., et al. (2018). Hydrogen sulfide attenuates oxidative stress-induced NLRP3 inflammasome activation via S-sulfhydrating c-Jun at Cys269 in macrophages. *Biochim. Biophys. Acta. Mol. Basis. Dis.* 1864 (9), 2890–2900. doi:10.1016/j.bbadis.2018.05.023

Luo, S., Kong, C., Zhao, S., Tang, X., Wang, Y., Zhou, X., et al. (2023). Endothelial HDAC1-ZEB2-NuRD complex drives aortic aneurysm and dissection through regulation of protein S-sulfhydration. *Circulation* 147 (18), 1382–1403. doi:10.1161/CIRCULATIONAHA.122.062743

Lv, B., Peng, H., Qiu, B., Zhang, L., Ge, M., Bu, D., et al. (2022). Sulphenylation of CypD at cysteine 104: a novel mechanism by which SO2 inhibits cardiomyocyte apoptosis. *Front. Cell. Dev. Biol.* 9, 784799. doi:10.3389/fcell.2021.784799

Magierowska, K., Korbut, E., Wójcik-Grzybek, D., Bakalarz, D., Sliwowski, Z., Cieszkowski, J., et al. (2022). Mitochondria-targeted hydrogen sulfide donors versus acute oxidative gastric mucosal injury. *J. Control. Release.* 348, 321–334. doi:10.1016/j.jconrel.2022.05.051

McGarry, D. J., Shchepinova, M. M., Lilla, S., Hartley, R. C., and Olson, M. F. (2016). A cell-permeable biscyclooctyne as a novel probe for the identification of protein sulfenic acids. *Acs. Chem. Biol.* 11 (12), 3300–3304. doi:10.1021/acschembio.6b00742

Meng, G., Xiao, Y., Ma, Y., Tang, X., Xie, L., Liu, J., et al. (2016). Hydrogen sulfide regulates krüppel-like factor 5 transcription activity via specificity protein 1 S-sulfhydration at Cys664 to prevent myocardial hypertrophy. *J. Am. Heart. Assoc.* 5 (9), e004160. doi:10.1161/JAHA.116.004160

Módis, K., Ju, Y., Ahmad, A., Untereiner, A. A., Altaany, Z., Wu, L., et al. (2016). S-Sulfhydration of ATP synthase by hydrogen sulfide stimulates mitochondrial bioenergetics. *Pharmacol. Res.* 113, 116–124. doi:10.1016/j.phrs.2016.08.023

Mustafa, A. K., Gadalla, M. M., Sen, N., Kim, S., Mu, W., Gazi, S. K., et al. (2009a). H2S signals through protein S-sulfhydration. *Sci. Signal.* 2 (96), ra72. doi:10.1126/scisignal.2000464

Mustafa, A. K., Gadalla, M. M., and Snyder, S. H. (2009b). Signaling by gasotransmitters. *Sci. Signal.* 2 (68), re2. doi:10.1126/scisignal.268re2

Mustafa, A. K., Sikka, G., Gazi, S. K., Steppan, J., Jung, S. M., Bhunia, A. K., et al. (2011). Hydrogen sulfide as endothelium-derived hyperpolarizing factor sulfhydrates potassium channels. *Circ. Res.* 109 (11), 1259–1268. doi:10.1161/CIRCRESAHA.111.240242

Naik, J. S., Osmond, J. M., Walker, B. R., and Kanagy, N. L. (2016). Hydrogen sulfide-induced vasodilation mediated by endothelial TRPV4 channels. *Am. J. Physiol. Heart. Circ. Physiol.* 311 (6), H1437–H1444. doi:10.1152/ajpheart.00465.2016

Park, C. M., Macinkovic, I., Filipovic, M. R., and Xian, M. (2015). Use of the "tag-switch" method for the detection of protein S-sulfhydration. *Methods. Enzymol.* 555, 39–56. doi:10.1016/bs.mie.2014.11.033

Paul, B. D., and Snyder, S. H. (2012). H_2S signalling through protein sulfhydration and beyond. *Nat. Rev. Mol. Cell. Biol.* 13 (8), 499–507. doi:10.1038/nrm3391

Paulsen, C. E., Truong, T. H., Garcia, F. J., Homann, A., Gupta, V., Leonard, S. E., et al. (2011). Peroxide-dependent sulfenylation of the EGFR catalytic site enhances kinase activity. *Nat. Chem. Biol.* 8 (1), 57–64. doi:10.1038/nchembio.736

Peng, S., Wang, M., Zhang, S., Liu, N., Li, Q., Kang, J., et al. (2023). Hydrogen sulfide regulates SERCA2a SUMOylation by S-Sulfhydration of SENP1 to ameliorate cardiac systole-diastole function in diabetic cardiomyopathy. *Biomed. Pharmacother.* 160, 114200. doi:10.1016/j.biopha.2022.114200

Peng, S., Zhao, D., Li, Q., Wang, M., Zhang, S., Pang, K., et al. (2022). Hydrogen sulfide regulates SERCA2a ubiquitylation via muscle RING finger-1 S-sulfhydration to affect cardiac contractility in db/db mice. *Cells* 11 (21), 3465. doi:10.3390/cells11213465

Perkins, N. D. (2012). Cysteine 38 holds the key to NF-κB activation. *Mol. Cell.* 45 (1), 1–3. doi:10.1016/j.molcel.2011.12.023

Poole, T. H., Reisz, J. A., Zhao, W., Poole, L. B., Furdui, C. M., and King, S. B. (2014). Strained cycloalkynes as new protein sulfenic acid traps. *J. Am. Chem. Soc.* 136 (17), 6167–6170. doi:10.1021/ja500364r

Qian, J., Wani, R., Klomsiri, C., Poole, L. B., Tsang, A. W., and Furdui, C. M. (2012). A simple and effective strategy for labeling cysteine sulfenic acid in proteins by utilization of β-ketoesters as cleavable probes. *Chem. Commun. (Camb).* 48 (34), 4091–4093. doi:10.1039/c2cc17868k

Qiao, J., Yongyan, D., Fan, J., Zhe, T., and Jian, J. (2018). Gas therapy: An emerging "green" strategy for anticancer therapeutics. *Appl. Ther.* 1 (6), 1800084. doi:10.1002/adtp.201800084

Reddie, K. G., and Carroll, K. S. (2008). Expanding the functional diversity of proteins through cysteine oxidation. *Curr. Opin. Chem. Biol.* 12 (6), 746–754. doi:10.1016/j.cbpa.2008.07.028

Saha, S., Chakraborty, P. K., Xiong, X., Dwivedi, S. K., Mustafi, S. B., Leigh, N. R., et al. (2016). Cystathionine β-synthase regulates endothelial function via protein S-sulfhydration. *Faseb. J.* 30 (1), 441–456. doi:10.1096/fj.15-278648

Sen, N., Paul, B. D., Gadalla, M. M., Mustafa, A. K., Sen, T., Xu, R., et al. (2012). Hydrogen sulfide-linked sulfhydration of NF-κB mediates its antiapoptotic actions. *Mol. Cell.* 45 (1), 13–24. doi:10.1016/j.molcel.2011.10.021

Seo, Y. H., and Carroll, K. S. (2009). Profiling protein thiol oxidation in tumor cells using sulfenic acid-specific antibodies. *Proc. Natl. Acad. Sci. U. S. A.* 106 (38), 16163–16168. doi:10.1073/pnas.0903015106

Shindo, T., Manabe, I., Fukushima, Y., Tobe, K., Aizawa, K., Miyamoto, S., et al. (2002). Krüppel-like zinc-finger transcription factor KLF5/BTEB2 is a target for angiotensin II signaling and an essential regulator of cardiovascular remodeling. *Nat. Med.* 8 (8), 856–863. doi:10.1038/nm738

Shuang, T., Fu, M., Yang, G., Huang, Y., Qian, Z., Wu, L., et al. (2021). Interaction among estrogen, IGF-1, and H2S on smooth muscle cell proliferation. *J. Endocrinol.* 248 (1), 17–30. doi:10.1530/JOE-20-0190

Shuang, T., Fu, M., Yang, G., Wu, L., and Wang, R. (2018). The interaction of IGF-1/IGF-1R and hydrogen sulfide on the proliferation of mouse primary vascular smooth muscle cells. *Biochem. Pharmacol.* 149, 143–152. doi:10.1016/j.bcp.2017.12.009

Singer, T. P., and Kearney, E. B. (1956). Intermediary metabolism of L-cysteinesulfinic acid in animal tissues. *Arch. Biochem. Biophys.* 61 (2), 397–409. doi:10.1016/0003-9861(56)90363-0

Song, Y., Peng, H., Bu, D., Ding, X., Yang, F., Zhu, Z., et al. (2020). Negative auto-regulation of sulfur dioxide generation in vascular endothelial cells: AAT1 S-sulfenylation. *Biochem. Biophys. Res. Commun.* S0006-291X (20), 231–237. doi:10.1016/j.bbrc.2020.02.040

Sun, T., Ding, W., Xu, T., Ao, X., Yu, T., Li, M., et al. (2019). Parkin regulates programmed necrosis and myocardial ischemia/reperfusion injury by targeting cyclophilin-D. *Antioxid. Redox. Signal.* 31 (16), 1177–1193. doi:10.1089/ars.2019.7734

Sun, X., Zhao, D., Lu, F., Peng, S., Yu, M., Liu, N., et al. (2020a). Hydrogen sulfide regulates muscle RING finger-1 protein S-sulfhydration at Cys44 to prevent cardiac structural damage in diabetic cardiomyopathy. *Br. J. Pharmacol.* 177 (4), 836–856. doi:10.1111/bph.14601

Sun, Y., Huang, Y., Yu, W., Chen, S., Yao, Q., Zhang, C., et al. (2017). Sulfhydration-associated phosphodiesterase 5A dimerization mediates vasorelaxant effect of hydrogen sulfide. *Oncotarget* 8 (19), 31888–31900. doi:10.18632/oncotarget.16649

Sun, Y., Lu, F., Yu, X., Wang, B., Chen, J., Lu, F., et al. (2020b). Exogenous H2S promoted USP8 sulfhydration to regulate mitophagy in the hearts of db/db mice. *Aging. Dis.* 11 (2), 269–285. doi:10.14336/AD.2019.0524

Sun, Y., Zhang, L., Lu, B., Wen, J., Wang, M., Zhang, S., et al. (2021). Hydrogen sulphide reduced the accumulation of lipid droplets in cardiac tissues of db/db mice via Hrd1 S-sulfhydration. *J. Cell. Mol. Med.* 25 (19), 9154–9167. doi:10.1111/jcmm.16781

Szczesny, B., Módis, K., Yanagi, K., Coletta, C., Le, T. S., Perry, A., et al. (2014). AP39, a novel mitochondria-targeted hydrogen sulfide donor, stimulates cellular bioenergetics, exerts cytoprotective effects and protects against the loss of mitochondrial DNA integrity in oxidatively stressed endothelial cells *in vitro*. *Nitric. Oxide* 41, 120–130. doi:10.1016/j.niox.2014.04.008

Thambyrajah, J., and Townend, J. N. (2000). Homocysteine and atherothrombosis--mechanisms for injury. *Eur. Heart. J.* 21 (12), 967–974. doi:10.1053/euhj.1999.1914

Tian, X., Zhou, D., Zhang, Y., Song, Y., Zhang, Q., Bu, D., et al. (2020). Persulfidation of transcription factor FOXO1 at cysteine 457: a novel mechanism by which H2S inhibits vascular smooth muscle cell proliferation. *J. Adv. Res.* 27, 155–164. doi:10.1016/j.jare.2020.06.023

Tocmo, R., and Parkin, K. (2019). S-1-propenylmercaptocysteine protects murine hepatocytes against oxidative stress via persulfidation of Keap1 and activation of Nrf2. *Free. Radic. Biol. Med.* 143, 164–175. doi:10.1016/j.freeradbiomed.2019.07.022

Uesugi, S., Muroi, M., Kondoh, Y., Shiono, Y., Osada, H., and Kimura, K. I. (2017). Allantopyrone A activates Keap1-Nrf2 pathway and protects PC12 cells from oxidative stress-induced cell death. *J. Antibiot. (Tokyo).* 70 (4), 429–434. doi:10.1038/ja.2016.99

Wang, W., and Wang, B. (2017). Esterase-sensitive sulfur dioxide prodrugs inspired by modified Julia olefination. *Chem. Commun. (Camb)* 53 (73), 10124–10127. doi:10.1039/c7cc05392d

Wang, X. B., Huang, X. M., Ochs, T., Li, X. Y., Jin, H. F., Tang, C. S., et al. (2011). Effect of sulfur dioxide preconditioning on rat myocardial ischemia/reperfusion injury by inducing endoplasmic reticulum stress. *Basic. Res. Cardiol.* 106 (5), 865–878. doi:10.1007/s00395-011-0176-x

Wang, Y., Wang, X., Chen, S., Tian, X., Zhang, L., Huang, Y., et al. (2019). Sulfur dioxide activates Cl-/HCO3- exchanger via sulphenylating AE2 to reduce intracellular pH in vascular smooth muscle cells. *Front. Pharmacol.* 10, 313. doi:10.3389/fphar.2019.00313

Wang, Y., Ying, X., Wang, Y., Zou, Z., Yuan, A., Xiao, Z., et al. (2023). Hydrogen sulfide alleviates mitochondrial damage and ferroptosis by regulating OPA3-NFS1 axis in doxorubicin-induced cardiotoxicity. *Cell. Signal.* 107, 110655. doi:10.1016/j.cellsig.2023.110655

Wasik, U., Milkiewicz, M., Kempinska-Podhorodecka, A., and Milkiewicz, P. (2017). Protection against oxidative stress mediated by the Nrf2/Keap1 axis is impaired in Primary Biliary Cholangitis. *Sci. Rep.* 7, 44769. doi:10.1038/srep44769

Wedmann, R., Onderka, C., Wei, S., Szijártó, I. A., Miljkovic, J. L., Mitrovic, A., et al. (2016). Improved tag-switch method reveals that thioredoxin acts as depersulfidase and controls the intracellular levels of protein persulfidation. *Chem. Sci.* 7 (5), 3414–3426. doi:10.1039/c5sc04818d

Wenningmann, N., Knapp, M., Ande, A., Vaidya, T. R., and Ait-Oudhia, S. (2019). Insights into doxorubicin-induced cardiotoxicity: molecular mechanisms, preventive strategies, and early monitoring. *Mol. Pharmacol.* 96 (2), 219–232. doi:10.1124/mol.119.115725

Wu, D., Hu, Q., Tan, B., Ros, e P., Zhu, D., and Zhu, Y. Z. (2018). Amelioration of mitochondrial dysfunction in heart failure through S-sulfhydration of Ca2+/calmodulin-dependent protein kinase II. *Redox. Biol.* 19, 250–262. doi:10.1016/j.redox.2018.08.008

Wu, D., Tan, B., Sun, Y., and Hu, Q. (2022). Cystathionine γ lyase S-sulfhydrates Drp1 to ameliorate heart dysfunction. *Redox. Biol.* 58, 102519. doi:10.1016/j.redox.2022.102519

Xia, M., Guo, Z., Liu, X., Wang, Y., and Xiao, C. (2022). A glutathione-responsive sulfur dioxide polymer prodrug selectively induces ferroptosis in gastric cancer therapy. *Biomater. Sci.* 10 (15), 4184–4192. doi:10.1039/d2bm00678b

Xiao, J., Zhu, X., Kang, B., Xu, J., Wu, L., Hong, J., et al. (2015). Hydrogen sulfide attenuates myocardial hypoxia-reoxygenation injury by inhibiting autophagy via mTOR activation. *Cell. Physiol. biochem.* 37 (6), 2444–2453. doi:10.1159/000438597

Xie, L., Gu, Y., Wen, M., Zhao, S., Wang, W., Ma, Y., et al. (2016). Hydrogen sulfide induces keap1 S-sulfhydration and suppresses diabetes-accelerated atherosclerosis via Nrf2 activation. *Diabetes* 65 (10), 3171–3184. doi:10.2337/db16-0020

Yang, G., Zhao, K., Ju, Y., Mani, S., Cao, Q., Puukila, S., et al. (2013). Hydrogen sulfide protects against cellular senescence via S-sulfhydration of Keap1 and activation of Nrf2. *Antioxid. Redox. Signal.* 18 (15), 1906–1919. doi:10.1089/ars.2012.4645

Ye, X., Li, Y., Lv, B., Qiu, B., Zhang, S., Peng, H., et al. (2022). Endogenous hydrogen sulfide persulfidates caspase-3 at cysteine 163 to inhibit doxorubicin-induced cardiomyocyte apoptosis. *Oxid. Med. Cell Longev.* 2022, 6153772. doi:10.1155/2022/6153772

Yu, M., Du, H., Wang, B., Chen, J., Lu, F., Peng, S., et al. (2020). Exogenous H2S induces Hrd1 S-sulfhydration and prevents CD36 translocation via VAMP3 ubiquitylation in diabetic hearts. *Aging. Dis.* 11 (2), 286–300. doi:10.14336/AD.2019.0530

Yu, W., Liao, Y., Huang, Y., Chen, S. Y., Sun, Y., Sun, C., et al. (2017). Endogenous hydrogen sulfide enhances carotid sinus baroreceptor sensitivity by activating the transient receptor potential cation channel subfamily V member 1 (TRPV1) channel. *J. Am. Heart. Assoc.* 6 (5), e004971. doi:10.1161/JAHA.116.004971

Zhang, D., Wang, X., Chen, S., Chen, S., Yu, W., Liu, X., et al. (2019). Endogenous hydrogen sulfide sulfhydrates IKKβ at cysteine 179 to control pulmonary artery endothelial cell inflammation. *Clin. Sci. (Lond).* 133 (20), 2045–2059. doi:10.1042/CS20190514

Zhang, D., Wang, X., Tian, X., Zhang, L., Yang, G., Tao, Y., et al. (2018). The increased endogenous sulfur dioxide acts as a compensatory mechanism for the downregulated endogenous hydrogen sulfide pathway in the endothelial cell inflammation. *Front. Immunol.* 9, 882. doi:10.3389/fimmu.2018.00882

Zhang, L., Jiang, X., Liu, N., Li, M., Kang, J., Chen, L., et al. (2021). Exogenous H2 S prevents the nuclear translocation of PDC-E1 and inhibits vascular smooth muscle cell proliferation in the diabetic state. *J. Cell. Mol. Med.* 25 (17), 8201–8214. doi:10.1111/jcmm.16688

Zhang, Y., Liu, X., He, P., Tang, B., Xiao, C., Chen, X., et al. (2023). Thiol-responsive polypeptide sulfur dioxide prodrug nanoparticles for effective tumor inhibition. *Biomacromolecules.* 24 (9), 4316–4327. doi:10.1021/acs.biomac.3c00767

Zhang, Y., Tang, Z. H., Ren, Z., Qu, S. L., Liu, M. H., Liu, L. S., et al. (2013). Hydrogen sulfide, the next potent preventive and therapeutic agent in aging and age-associated diseases. *Mol. Cell. Biol.* 33 (6), 1104–1113. doi:10.1128/MCB.01215-12

Zhao, K., Ju, Y., Li, S., Altaany, Z., Wang, R., and Yang, G. (2014). S-sulfhydration of MEK1 leads to PARP-1 activation and DNA damage repair. *EMBO. Rep.* 15 (7), 792–800. doi:10.1002/embr.201338213

Zhou, B., Kreuzer, J., Kumsta, C., Wu, L., Kamer, K. J., Cedillo, L., et al. (2019b). Mitochondrial permeability uncouples elevated autophagy and lifespan extension. *Cell* 177 (2), 299–314. doi:10.1016/j.cell.2019.02.013

Zhou, Y. B., Zhou, H., Li, L., Kang, Y., Cao, X., Wu, Z. Y., et al. (2019a). Hydrogen sulfide prevents elastin loss and attenuates calcification induced by high glucose in smooth muscle cells through suppression of stat3/cathepsin S signaling pathway. *Int. J. Mol. Sci.* 20 (17), 4202. doi:10.3390/ijms20174202

Zhu, J., Wang, Y., Rivett, A., Li, H., Wu, L., Wang, R., et al. (2022). Deficiency of cystathionine gamma-lyase promotes aortic elastolysis and medial degeneration in aged mice. *J. Mol. Cell. Cardiol.* 171, 30–44. doi:10.1016/j.yjmcc.2022.06.011

frontiers | Frontiers in Pharmacology

TYPE Review
PUBLISHED 02 February 2024
DOI 10.3389/fphar.2024.1334218

OPEN ACCESS

EDITED BY
Yan Sanders,
Eastern Virginia Medical School, United States

REVIEWED BY
Michael H. Baumann,
National Institute on Drug Abuse (NIH), United States
Marco Niello,
Italian Institute of Technology (IIT), Italy

*CORRESPONDENCE
Joachim Neumann,
joachim.neumann@medizin.uni-halle.de

RECEIVED 06 November 2023
ACCEPTED 10 January 2024
PUBLISHED 02 February 2024

CITATION
Neumann J, Dhein S, Kirchhefer U, Hofmann B and Gergs U (2024), Effects of hallucinogenic drugs on the human heart.
Front. Pharmacol. 15:1334218.
doi: 10.3389/fphar.2024.1334218

Effects of hallucinogenic drugs on the human heart

Joachim Neumann[1]*, Stefan Dhein[2], Uwe Kirchhefer[3], Britt Hofmann[4] and Ulrich Gergs[1]

[1]Institut für Pharmakologie und Toxikologie, Medizinische Fakultät, Martin-Luther-Universität Halle-Wittenberg, Halle, Germany, [2]Rudolf-Boehm Institut für Pharmakologie und Toxikologie, Universität Leipzig, Leipzig, Germany, [3]Institut für Pharmakologie und Toxikologie, Medizinische Fakultät, Universität Münster, Münster, Germany, [4]Cardiac Surgery, Medizinische Fakultät, Martin-Luther-Universität Halle-Wittenberg, Halle, Germany

Hallucinogenic drugs are used because they have effects on the central nervous system. Their hallucinogenic effects probably occur via stimulation of serotonin receptors, namely, 5-HT_{2A}-serotonin receptors in the brain. However, a close study reveals that they also act on the heart, possibly increasing the force of contraction and beating rate and may lead to arrhythmias. Here, we will review the inotropic and chronotropic actions of bufotenin, psilocin, psilocybin, lysergic acid diethylamide (LSD), ergotamine, ergometrine, N,N-dimethyltryptamine, and 5-methoxy-N,N-dimethyltryptamine in the human heart.

KEYWORDS

bufotenin, psilocin, psilocybin, LSD, ergotamine, ergometrine, N,N-dimethyltryptamine

Introduction

In this review, "drugs of interest" include the following organic molecules: bufotenin, psilocin, psilocybin, lysergic acid diethylamide (LSD), ergotamine, ergometrine, N,N-dimethyl-tryptamine and 5-methoxy-N,N-dimethyltryptamine. These drugs of interest (Figure 1A) are referred to as tryptamine derivatives. These drugs of interest are thus structurally similar to 5-hydroxyl-tryptamine (serotonin, 5-HT), the physiological agonist at serotonin receptors. Unlike indirect sympathomimetic drugs (e.g., metamphetamine, amphetamine), these compounds probably do not act solely or mainly as releasers of noradrenaline from storage sites in the human heart (Neumann et al., 2023a; Neumann et al., 2023b). In contrast, they are directly activate serotonin receptors in the heart (e.g., Jacob et al., 2023a). However, at least *in vitro* these tryptamines or related tiophene analogs may also act as monoamine transport releasers (Blough et al., 2014; Rudin et al., 2022). The hallucinogenic effects of these compounds are explained by the stimulation of 5-HT_{2A}-serotonin receptors in the brain. In the heart, these drugs of interest can activate serotonin receptors. However, serotonin increases the force of contraction and beating rate in the human heart via 5-HT_4-serotonin receptors and not via 5-HT_{2A}-serotonin receptor (Neumann et al., 2017; Neumann et al., 2023a). In contrast to other species 5-HT_{2A}-(rat) or 5-HT_3-(guinea pig) serotonin receptors do not increase force in the human heart (Kaumann et al., 1990, reviews; Neumann et al., 2017; Neumann et al., 2023a). In order to provide a small animal model for human 5-HT_4 serotonin receptors in the heart, we have generated transgenic mice that overexpress the human 5-HT_4-serotonin receptor in the heart (5-HT_4-TG). In cardiac preparations from 5-HT_4 TG, serotonin increased the force of contraction (Gergs et al., 2010). Serotonin does not increase the force of contraction in isolated mouse cardiac preparations from wild-type mice (Gergs et al., 2010).

10.3389/fphar.2024.1334218

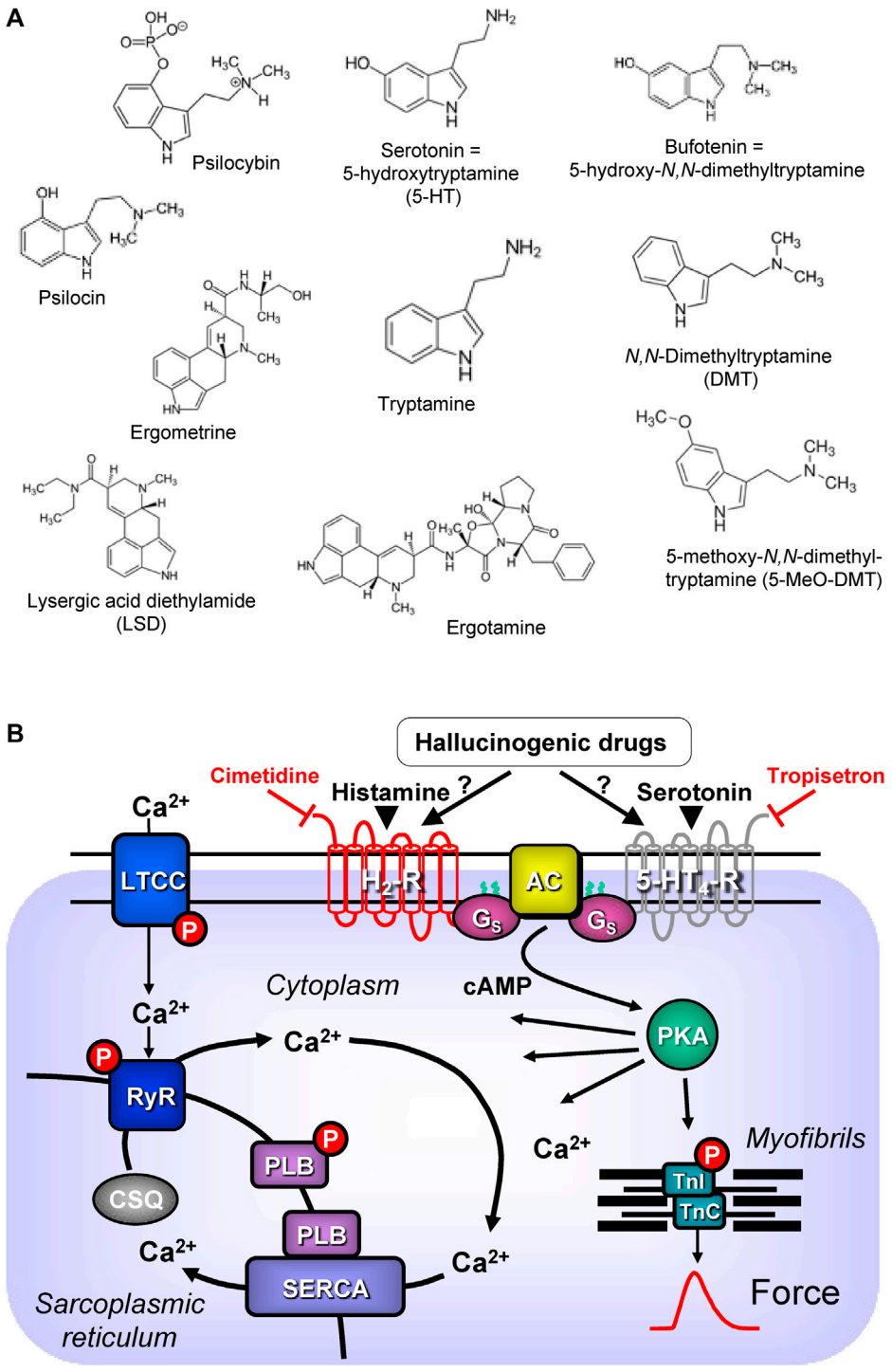

FIGURE 1
(A) Structural formulae of tryptamine derived hallucinogenic compounds. **(B)** Schematic drawing of the proposed signalling of hallucinogenic compounds in cardiac myocytes. Ca^{2+} enters the mammalian heart cell via the L-type Ca^{2+} channel (LTCC). This process can be enhanced by hallucinogenic compounds via a cascade starting in the sarcolemma via stimulation of Gs-protein (G_s)-coupled 5-HT_4 serotonin or H_2 histamine receptors. Activation of adenylyl cyclase (AC) elevates subsequent production of cAMP and thereby activates cAMP-dependent protein kinase (PKA). PKA increases cardiac force generation and relaxation by increasing the phosphorylation state (P) of the L-type calcium channel (LTCC), of phospholamban (PLB) and of the inhibitory subunit of troponin (TnI). Trigger Ca^{2+} initiates release of Ca^{2+} from the sarcoplasmic reticulum via ryanodine receptors (RYR) into the cytosol. There, Ca^{2+} activates myofilaments and this activation leads to increased inotropy. In diastole, Ca^{2+} is taken up into the sarcoplasmic reticulum via a sarcoplasmic reticulum Ca^{2+}-ATPase (SERCA), the activity of which is enhanced due to an increased phosphorylation state of PLB.

TABLE 1 Sources of the hallucinogenic drug.

	Source	References
Bufotenin	[1]Toad skin	[1]Handovsky (1920)
	[2]Brosimum acutifolium	[2]Moretti et al. (2006)
	[3]Anandenanthera peregrina	[3]Ott (2001)
	[4]Human body	[4]Forsström et al. (2001)
Ergometrine	Fungi: Claviceps purpurea	Dudley and Moir (1935)
Ergotamine	Fungi: Claviceps purpurea	Stange et al. (1998)
LSD: Lysergic acid diethylamide	Chemical laboratory	Hofmann (1959)
DMT: N,N-dimethyl-tryptamine	[1]Diplopterys cabreana	[1,2]McKenna et al. (1984a)
	[2]Banisteriopsis caapi	[3,4]Brito-da Costa et al. (2020)
	[3]Psychotria viridis	
	[4]Human brain	
5-methoxy-N,N-dimethyltryptamine	[1]Toad skin	[1]Araujo et al. (2015)
	[2]Banisteriopsis caapi	[2]McKenna et al. (1984b)
Psilocin	Fungi: psilocybe	Hofmann (1958), Hofmann (1959)
Psilocybin	Fungi: psilocybe	Hofmann (1958), Hofmann (1959)

Interestingly, some of these drugs of interest (e.g., LSD) also activate histamine receptors, namely, H_2-histamine receptors in the human heart. In the human heart, unlike in some animal hearts, H_2-histamine receptors primarily mediate the positive inotropic or positive chronotropic effects of exogenous or endogenous histamine (reviews: Neumann et al., 2021a; Neumann et al., 2022; Neumann et al., 2023d). To study human H_2-histamine receptors in a small animal model, we generated transgenic mice that overexpress the H_2-histamine receptors in the heart (H_2-TG), wherein histamine increased the force of contraction (Gergs et al., 2020; Neumann et al., 2021b; Neumann et al. 2021c; Neumann et al. 2021d; Neumann et al. 2021e; Gergs et al., 2021). Similar to serotonin, histamine does not increase the force of contraction in isolated cardiac preparations from wild type mice (Gergs et al., 2019).

5-HT_4-serotonin and H_2-histamine receptors share a common signal transduction system (Figure 1B). Both receptors are located on the outside of sarcolemma in cardiomyocytes and they couple to stimulatory G-proteins. Thereby they increase the activity of the adenylyl cyclases in the sarcolemma. Finally, both receptors lead to increased production of 3′, 5′-cyclic adenosine monophosphate (cAMP). This cAMP activates cAMP-dependent protein kinases in the cytosol of the cardiomyocytes. The cAMP is eventually degraded and inactivated by the action of phosphodiesterases. After stimulation of 5-HT_4-serotonin and H_2-histamine receptors, several target proteins in many compartments of the cardiomyocyte are phosphorylated and usually activated. A key role is played by the phosphorylation of the L-type Ca^{2+} channel (LTCC) in the sarcolemma. This leads to increased entering of trigger Ca^{2+} into the cardiomyocytes. This trigger Ca^{2+} then releases Ca^{2+} from intracellular stores in the sarcoplasmic reticulum (SR) and this Ca^{2+} activates the myofilaments. At the same time phosphorylation of phospholamban in the SR comes about. This mechanism increases the uptake rate of Ca^{2+} into the SR and this enhances relaxation of the heart muscle but also leads to higher filling of Ca^{2+} into the SR (Figure 1B). Thus, the next heart beat can be more vigorous because more Ca^{2+} can be released by trigger Ca^{2+} from the SR (Neumann et al., 2017; Neumann et al., 2022; Neumann et al., 2023c).

Except for LSD, all the drugs of interest occur naturally (Table 1). They are found mainly in plants or moulds. Some hallucinogenic compounds are present in high concentrations in animals, such as frogs or even in humans. The present review of the effects of the drugs of interest is limited to the mammalian heart, more specifically the human heart.

The clinical use of this review will facilitate the safe usage of the drugs of interest. This knowledge is essential because nearly all drugs of interest have the potential to treat psychiatric diseases. In addition, during “recreational use”, overdoses of hallucinogenic drugs can occur. Then, it is helpful to have guidance on what antidotes might make sense from a pharmacological point of view.

Bufotenin

Exogenous or endogenous serotonin (5-hydroxytryptamine, 5-HT) induces a positive inotropic effect, a relaxant effect, a positive dromotropic effect, and a positive chronotropic effect in the human heart via human 5-HT_4-serotonin receptors (for reviews: Kaumann and Levy, 2006; Neumann et al., 2017; Neumann et al., 2023a). Studies on isolated porcine heart preparations have found that 5-HT can increase force and frequency via porcine 5-HT_4-serotonin receptors (Kaumann, 1990; Villalón et al., 1990). In humans and porcine but not in other mammalian hearts like mice, cats, rats, dogs, or rabbits, 5-HT can augment force and beating rate via 5-HT_4-serotonin receptors (Kaumann and Levy, 2006; Neumann et al., 2017; Neumann et al., 2023c; Neumann et al., 2023d).

Bufotenin (5-hydroxy-dimethyltryptamine) is structurally related to serotonin; it is a dimethylated (on the primary amine atom) form of serotonin (Figure 1). Hence, it is not surprising that, based on this similarity, bufotenin can bind to serotonin receptors and activate them. Indeed, *in vitro* bufotenin binds to 5-HT_{2A}- and 5-HT_{2C}- serotonin receptors (Almaula et al., 1996). Agonist binding to 5-HT_{2A}-serotonin receptors might explain the hallucinogenic effects of bufotenin (Titeler et al., 1988). Moreover, bufotenin binds potently to 5-HT_{1A}-, 5-HT_{1B}- 5-HT_{1D}-serotonin receptors (Dumuis et al., 1988).

In this context of affinities to various serotonin receptors, it seems necessary to discuss the possible detrimental effects of 5-HT_{2B}- serotonin receptor stimulation for the heart. There is convincing evidence from cell culture work, animal studies, clinical retrospective and case control studies that in principle stimulation of 5-HT_{2B}- serotonin receptor can induce proliferation of fibroblasts in the mammalian heart. This proliferation leads to abnormal thickening of leaflets of valves and can take place. This thickening can occur in the mitral leaflets, in tricuspid leaflets or on aortic cusps (Cosyns et al., 2013). This alteration in the anatomy of valves in the human heart can induce mitral insufficiency, tricuspid insufficiency or aortic insufficiency. This drug-induced valvular thickening is diagnosed by exclusion of other underlying pathologies (e.g., genetic defects or infections) and anamnesis of drug treatment by using echocardiography. Such alterations of the mitral valve and/or the aortic valve in the left heart are a burden to cardiac function and can lead to congestive heart failure. Similar damage to the tricuspid valves in the right heart will lead to pulmonary hypertension, like left ventricular heart failure a potentially deadly disease. In principle, any drug that stimulates 5-HT_{2B} -serotonin receptors can have such deadly consequences by the pathological pathway just mentioned because the 5-HT_{2B}- serotonin receptor in the leaflets can lead to proliferation of local fibroblasts. Hence, bufotenin might damage the function of cardiac valves. On the other hand, stimulation of 5-HT_{2B}- serotonin receptor probably has to be present for a prolonged period of time and with a sufficiently high occupancy of the 5-HT_{2B}-serotonin receptor. Hence, if it were sufficient to treat patients for a short period of (e.g., every 3 months) with small doses of hallucinogenic drugs like bufotenine (smaller than 100 mg per os or 10 mg parenterally: Ott, 2001), then the harm for the cardiac valves could be acceptable (discussed in: McIntyre, 2023).

In this context, one should also mention effects of 5-HT on human coronary arteries, and human pulmonary arteries, because they may complicate therapy with hallucinogenic drugs. In brief, there is convincing evidence that serotonin can lead to vasoconstriction in coronary vessels (McFadden et al., 1991). This can lead to or at least may worsen ischemic heart disease because constriction of coronary arteries. This vasocontraction can occur via stimulation of 5-HT_{2A}-serotonin receptors (Kaumann et al., 1994; Nilsson et al., 1999) and/or 5-HT_{1B}-serotonin receptors (van den Broek et al., 2002) will lead to less perfusion of the heart. Likewise, pulmonary hypertension can be caused or aggravated if drugs stimulate 5-HT_{2A}- or 5-HT_{1B} serotonin receptors in human pulmonary arteries (Cortijo et al., 1997). Indeed, bufotenin and most hallucinogenic drugs can activate to 5-HT_{2A}-serotonin receptors and/or 5-HT_{1B}-serotonin receptors (Dumuis et al., 1988; Almaula et al., 1996) and thus they may cause vasoconstriction. Whether this vasoconstriction occurs with bufotenin in humans is unclear and might be worth further studies.

Bufotenin exerted positive chronotropic effects in isolated spontaneously beating right atrial preparations from pigs, mediated by porcine 5-HT_4-serotonin receptors (Medhurst and Kaumann, 1993). As far as we could find out, there are in the literature no binding data of bufotenin to 5-HT_4-serotonin receptors. An interaction of bufotenin to 5-HT_4-serotonin receptors is likely from the following experiments: bufotenin increased force of contraction and beating rate only in isolated left or right atrial preparations, respectively, of transgenic mice where the human 5-HT_4-receptor was overexpressed in the heart (5-HT_4-TG, Neumann et al., 2023e; Table 4). These effects were antagonized by 5-HT_4 serotonin receptor antagonists (Neumann et al., 2023e). Moreover, in isolated human right atrial strips, which were paced to induce contraction, bufotenin likewise increased force of contraction and these effects were antagonized in transgenic mice by 5-HT_4 serotonin antagonists (Neumann et al., 2023e; Table 4).

Bufotenin was first isolated to purity in Prague from toad skin (in Latin, *Bufo* means toad, Handovsky, 1920). The correct structural formula (they called it "5-Oxy-indolyl-äthyl-dimethylamin") was found later in Munich and confirmed by synthesis (Wieland et al., 1934; Hoshino and Shimodaira, 1935, review; Chilton et al., 1979).

Bufotenin occurs not only in animals like toads but also in plants. Shamans in French Guiana used latex from Brosimum acutifolium to obtain hallucinogenic mixtures containing bufotenin (Moretti et al., 2006). Interestingly, bufotenin has been found in toads and the human body (Forsström et al., 2001). It might be formed enzymatically using a methyltransferase from serotonin (Figure 1) in human neuronal cells (Kärkkäinen et al., 2005). Bufotenin may underlie the fairy tale of the *Frog Prince* by the Grimm brothers (Siegel and McDaniel, 1991). In the fairy tale, kissing frogs may have released bufotenin from the frog's skin (probably a toad). This bufotenin may have entered the human brain and led to hallucinations. Under these conditions, one might have confused the frog with a prince (Siegel and McDaniel, 1991).

Recently, a novel indolethylamine-N-methyltransferase in the skin and parotid glands of some toad species has been cloned (Chen et al., 2023). This enzyme probably underlies the production of bufotenin in the skin of particular toad species (e.g., *Bufo marinus*, *Bufo Bufo*) that are known to be used as sources of bufotenin (Chen et al., 2023). This novel enzyme is absent in common frogs (Chen et al., 2023). In toads, biosynthesis starts with tryptophan, which is hydroxylated to 5-hydroxytryptophan and then decarboxylated, leading to serotonin. The primary amine in serotonin is first methylated to monomethylserotonin. This secondary amine is then methylated again to the tertiary amine N,N-dimethylserotonin (bufotenin, Chen et al., 2023).

In the first paper on pure bufotenin, bufotenin was studied for its cardiac effects. While bufotenin (at high doses) did not alter the force of contraction in the isolated frog heart, it reduced the heart rate (Handovsky, 1920). Intravenous injection of bufotenin in dogs, cats, or rabbits increased blood pressure, but shortly after the injection, the animals died (Handovsky, 1920). However, these data are questionable. As noted above, no functional cardiac 5-HT_4 serotonin receptors were present in these animals (dog: Chiba, 1977, cat and rabbit; Trendelenburg, 1960). The increase in blood

TABLE 2 Clinical studies and tested indications of the hallucinogenic drug.

	Clinical studies in "ClinicalTrials.gov"	Some tested indications for the drugs in "ClinicalTrials.gov"	Remarks	"Pubmed" hits
Bufotenin	5 (as metabolite of 5-Me-DMT)	Pharmacokinetics, Depression, Autism	Studied in depression Uthaug et al. (2019)	634
Ergometrine	9	Postpartum hemorrhage		2,781
Ergotamine	0		migraine	13,369
LSD: Lysergic acid diethylamide	8	Pharmacokinetics, Cluster headache, Palliative care	Studied in alcoholism, depression Passie et al. (2008); Bogenschutz et al. (2013)	5,638
DMT: N,N-dimethyl-tryptamine	0		Religious ceremonies Brito-da Costa (2020)	42
5-methoxy-N,N-dimethyltryptamine	10	Pharmacokinetics, Depression	Religious ceremonies Brito-da Costa (2020)	578
Psilocin	1	Comparison with psilocybin	Depression: Ross et al. (2016)	275
Psilocybin	130	Pharmacokinetics, depression, terminal illness, concussion headache, migraine, phantom limb pain, treatment of cocaine addiction, alcoholism, smoke cessation, interaction with serotonin reuptake inhibitors in depression, anorexia nervosa, post traumatic stress, binge eating, Morbus Alzheimer, burn out	Depression: Ross et al. (2016)	1834

pressure is likely not due to an increase in cardiac output, but probably due to peripheral vasoconstriction following stimulation of vascular arterial smooth muscle 5-HT_{2A}-serotonin receptors in these animals.

Moreover, bufotenin can raise the phosphorylation state of phospholamban (Neumann et al., 2023e). Increased phosphorylation of phospholamban (Tada et al., 1976) leads to reduced time to relaxation and an increased rate of tension relaxation in atrial and ventricular preparations from 5-HT_4-TG mice. Phosphorylated phospholamban de-inhibits the activity of the Ca^{2+} pump (Figure 1B) in the sarcoplasmic reticulum, thus increasing the rate at which calcium cations are pumped from the cytosol into the sarcoplasmic reticulum; fewer calcium cations bind to the myofilaments, and myofilaments relax faster (Hamstra et al., 2020).

This cardiac effect of bufotenin might play a clinical role (Table 2). Bufotenin can be taken orally to induce hallucinogenic effects, but perorally, high doses of bufotenin must be given in humans, because bufotenin seems to undergo a strong first-pass effect. Indeed, much higher peroral doses (100 mg) of bufotenin than parenteral doses (10 mg) are needed in humans to bring about hallucinogenic effects (self-experimentation: Ott, 2001).

In humans, bufotenin can be found physiologically in plasma. One might ask whether this bufotenin is clinically relevant. Indeed, plasma levels of bufotenin were elevated in patients with autism and schizophrenia (Emanuele et al., 2010; Table 3). On the one hand, one might hypothesise that these high levels of bufotenin might explain some of the hallucinations accompanying psychiatric diseases. On the other hand, elevated levels of bufotenin may lead to tachycardia in untreated patients. If that were the case, one could reduce the bufotenin-induced tachycardia with 5-HT_4-serotonin receptor antagonists such as tropisetron or piboserod.

Bufotenin has some beneficial effects on depressive patients (Uthaug et al., 2019). However, there is currently no accepted clinical indication for bufotenin. Over several decades, bufotenin and frog skins or plants containing bufotenin have sometimes been used as "recreational drugs" and have led to intoxication (Chamakura, 1994; Shen et al., 2010; Davis et al., 2018).

Bufotenin is an important active metabolite of the hallucinogenic compound 5-methoxy N,N-dimethyltryptamine (found in plants, *vide infra*). Bufotenin might be formed by metabolism in humans taking 5-methoxy N,N-dimethyltryptamine (Shen et al., 2010). One could treat severely ill patients with tropisetron, typically regarded as a 5-HT_3-serotonin receptor antagonist. However, the tropisetron also blocks human 5-HT_4-serotonin receptors (Kaumann et al., 1990) and is approved for use in humans in many countries. Alternatively, one can use the specific 5-HT_4-serotonin receptor antagonist piboserod (Kjekshus et al., 2009), which has been used in at least one heart failure study in humans; thus, it might be used off-label, should the need arise in the patient.

Lysergic acid diethylamide

Lysergic acid diethylamide (in the original publications in German: Lysergsäurediäthylamid: thence LSD) (LSD, Figure 1A) is an ergot derivative developed as an analeptic agent (review: Nichols, 2018). However, LSD turned out to be a hallucinogenic drug when Albert Hoffmann, the chemist at the Sandoz pharmaceutical company in Basel, Switzerland, who had synthesised LSD in 1938 AD, inadvertently ingested around 10–30 µg of LSD in 1943 (review: Nichols, 2018). At that time, LSD was the most potent hallucinogenic drug. LSD was first

TABLE 3 "Therapeutic" and toxic plasma concentrations of the hallucinogenic drug in humans.

	Therapeutic	Toxic	References
Bufotenin	8–16 nM	Active metabolite of 5-Me DMT	Emanuele et al. (2010) (endogenous concentrations)
Ergometrine	4 nM		de Groot et al. (1993)
Ergotamine	0.69 nM[1]	15 nM[2]	[1]Sanders et al. (1986)
			[2]Stange et al. (1998)
LSD: Lysergic acid diethylamide	[1]3–9 nM	[2]33 μM	[1]Holze et al. (2020)
			[2]Mardal et al. (2017)
DMT: N,N-dimethyl-tryptamine	[1]0.38 μM		[1]Strassman et al. (1994)
	[2]0.3 nM		[2]Good et al. (2023)
5-Me DMT: 5-methoxy N,N-dimethyltrypta-mine	4 nM		Reckweg et al. (2021)
Psilocin	1 0.1 μM	[2]0.15 μM	[1]Madsen et al. (2019)
			[2]Lim et al. (2012)

published in a scientific journal in 1947 (Nichols, 2018). Sandoz produced and gave LSD out to psychiatrists in Europe and the United States of America to look for potential clinical applications (Nichols, 2018). LSD (Delysid®) was studied in the 1960s in psychiatry with the hope of better understanding the molecular mechanisms of how psychosis is caused and to help with a psychotherapeutic approach to the patient (Nichols, 2018). However, from that time on, LSD was primarily used in illicit ways and, therefore, was practically removed from the legitimate drug market worldwide (Nichols, 2018). Currently, there is renewed interest in psychiatry in studying LSD in some contexts. The hallucinogenic effects of LSD are thought to be caused by the activation of 5-HT_{2A}-serotonin receptors in the brain (Preller et al., 2017; review; Liechti et al., 2017), as with the other drugs of interest in this review.

In ligand binding studies, LSD had the following rank or of potencies: 5-HT_{1A}- >5-HT_{2A}- >5-HT_{2C}- >5-HT_{2B}- serotonin receptors. This rank order should be a little bit more specified: by far the highest affinity was displayed by LSD to 5-H_{1A}-serotonin receptors and also the affinity at 5-HT_{2A}-serotonin receptors and 5-HT_{2C}- serotonin receptors is in the nanomolar concentration range. In contrast, the affinity for the 5-HT_{2B}- serotonin receptor is much lower with about 10 μM (Rickli et al., 2016). Recent data also noted that LSD has an affinity for 5-HT_4-serotonin receptors and H_2-histamine receptors (around 10 μM for these receptors: Lewis et al., 2023). From these binding data at 5-HT_{2B}-serotonin receptors one would assume that LSD can activate this receptor in the patient. This might lead valvular heart disease (*vide supra*). However, others claimed that any proofs for valvular damage through LSD from clinical studies is currently lacking (Tagen et al., 2023). However, this valvular side effect should be looked for in prospective clinical trials.

In isolated cardiac preparations, LSD was found to be a partial agonist at cardiac H_2-histamine receptors in rabbit and guinea pig cardiac preparations (Angus and Black, 1980; Table 4). This conclusion was based on the following findings: LSD at low concentrations increased and at high concentrations reduced the beating rate in isolated right atrial preparations from rabbits in a cimetidine (a H_2-histamine receptor antagonist)-sensitive fashion (Angus and Black, 1980). Moreover, LSD antagonised the positive inotropic effect of histamine in isolated guinea pig papillary muscles (Angus and Black, 1980). Currently, LSD is used primarily for "recreational" and "personal" purposes (Araújo et al., 2015), while some medical studies on its use in the treatment of alcoholism and depression are on record (Bogenschutz, 2003; Passie et al., 2008). Also, in Basel, Switzerland, from 2021 to 2023, a trial was recruited to test LSD versus placebo for the treatment of cluster headache pain (ClinicalTrials.gov Identifier: NCT03781128, Table 2).

Low doses of LSD, given through the mouth in a solution of 0.5 mL volume (up to 26 μg) in healthy volunteers (male and female) led to a significant increase in systolic blood pressure, but not in heart rate or diastolic blood pressure. The missing effect of LSD in diastolic blood pressure and heart rate (mean values were higher) could be due to the low dosage of LSD. Indeed, in another study with more LSD, heart rate and diastolic blood pressure was found to be elevated: In this clinical study 200 μg LSD, given as an oral solution, increased systolic and diastolic blood pressure and heart rate in healthy subjects (male and female). These effects peaked at about 1 hour after drug application and returned to initial values within about 12 h (Holze et al., 2022). Under these conditions the peak plasma concentration of LSD was given as 25 ng/mL (Holze et al., 2022). In another clinical study from Switzerland, 100 μg of LSD was taken orally, there was an increase in body temperature, blood pressure, and heart rate compared to a placebo (Holze et al., 2020). In these probands, peak plasma concentrations of LSD ranged between 0.99 and 2.9 ng/mL (3.06–8.9 nM: Holze et al., 2020). In another study, the proportionality of plasma concentrations and doses taken per os for LSD was reported; a plasma half-life of 2.6 h for LSD and a first-order elimination pharmacokinetic behaviour of LSD were detected (Dolder et al., 2017). The use of nuclear magnetic imaging in the brain has deepened our understanding of the molecular actions of LSD in the human brain (Kaelen et al., 2016). Evidence for the binding of LSD to 5-HT_{2A}-serotonin receptors may result this work (Kaelen et al., 2016).

TABLE 4 Cardiac effects in animal and human cardiac preparations of the drugs of interest.

	Animal studies	Human studies	References
Bufotenin	Positive chronotropic effect in isolated porcine atrial preparations via 5-HT_4 receptors[1], increase in force of contraction and in beating rate via 5-HT_4 receptors in pigs[2] and 5-HT_4-TG[3]	Increase in force of contraction in isolated human right atrial preparations via 5-HT_4 receptors[3]	[1]Medhurst and Kaumann (1993) [2]Villalon et al. (1990) [3]Neumann et al. (2023e)
Ergometrine	Increase in left ventricular force of contraction in isolated perfused guinea pig heart via H_2 receptors[1], increase in force of contraction and beating rate in atrial preparations only via H_2 receptors (H_2-TG)[2]	Increase in force of contraction in isolated human right atrial preparations only via H_2 receptors[2]	[1] Bongrani et al. (1979) [2] Jacob et al. (2023a)
Ergotamine	Increase in force of contraction and beating rate in atrial preparations via both H_2- and 5-HT_4-receptors (H_2-TG, 5-HT_4-TG)	Increase in force of contraction in isolated human right atrial preparations only via H_2-receptors	Jacob et al. (2023b)
LSD: Lysergic acid diethylamide	Increase in force of contraction in guinea pig and rabbit ventricular preparations via H_2 receptors[1], increase in force of contraction and in beating rate in atrial preparations via both H_2- and 5-HT_4-receptors (H_2-TG, 5-HT_4-TG)[2]	Increase in force of contraction in isolated human right atrial preparations via both 5-HT_4-receptors and H_2 receptors[2]	[1]Angus and Black (1980) [2]Gergs et al. (2023)
DMT: N,N-dimethyl-tryptamine	Increase in force of contraction and beating rate in atrial preparations via 5-HT_4 receptors (5-HT_4-TG)	Increase in force of contraction in isolated human right atrial preparations via 5-HT_4 receptors	Dietrich et al. (2023)
5-methoxy-N,N-dimethyltryptamine	Positive chronotropic effect in isolated porcine right atrial preparations via 5-HT_4 receptors[1], increase in force of contraction and beating rate in atrial preparations via 5-HT_4 receptors (5-HT_4-TG)[2]	Increase in force of contraction in isolated human right atrial preparations via 5-HT_4-receptors[2]	[1]Medhurst and Kaumann (1993) [2] Dietrich et al. (2023)
Psilocin	Increase in force of contraction and beating rate in atrial preparations via 5-HT_4 receptors (5-HT_4-TG)	Increase in force of contraction in isolated human right atrial preparations via 5-HT_4 receptors	Dimov et al. (2023)
Psilocybin	Increase in force of contraction and beating rate in atrial preparations via 5-HT_4 receptors (5-HT_4-TG)	Increase in force of contraction in isolated human right atrial preparations via 5-HT_4 receptors	Dimov et al. (2023)

At the time of this review, 122 studies of LSD had started, were ongoing or were going to be started (clinical.trials.gov, Table 2). In some of these studies, LSD was tested for the treatment of cluster headaches or depression. Hence, it might be of clinical interest that LSD can stimulate human H_2-histamine receptors in the heart. A resultant tachycardia would be detrimental, especially by reducing the oxygen supply to the heart. These effects are even more overt in the presence of phosphodiesterase (PDE) inhibitors. In everyday life, PDEs can be inhibited by theophylline (in tea) or caffeine (in coffee beverages or power drinks). In patients, PDEs are inhibited when taking milrinone or levosimendan for heart failure or rolipram for asthma treatment. In such patients, special caution with LSD is warranted. One would recommend H_2-histamine receptors and 5-HT_4-serotonin receptor antagonists to treat tachycardia. Conceivably, prophylactic treatment, at least in patients suffering from angina pectoris with cimetidine, is indicated. This would not block the potential therapeutic agonist action of LSD on 5-HT_{2A} serotonin receptors or other serotonin receptors in the brain.

Intoxications with LSD are still being recorded (Liakoni et al., 2015; Li et al., 2019). In one series, the highest plasma concentration of LSD during intoxication amounted to 5.9 nM (McCarron et al., 1990). Brain tissue concentrations of up to 33 µM LSD (and metabolites) have been reported (Mardal et al., 2017), which are well in the range of the concentrations needed to elicit contractile effects in isolated cardiac preparations from H_2-TG or the isolated human atrium (Gergs et al., 2023). Cardiovascular alterations during LSD intoxication include sinus tachycardia and hypertension (Blaho et al., 1997). One can probably recommend that the treatment of LSD intoxication should include an intravenously applied H_2-histamine receptor antagonist, such as cimetidine or ranitidine.

LSD binds to many receptors (e.g., several isoforms 5-HT-receptors) (Roth et al., 2002). Notably, LSD binds as an agonist to 5-HT_{2A}- and 5-HT_{2B}- serotonin receptors and the crystal structure of LSD bound to 5-HT_{2B}- serotonin receptors is now known (Wacker et al., 2017). LSD led to tachycardia in users (e.g., Holze et al., 2020). Indeed, we noted contractile effects in atrial and ventricular preparations of LSD in H_2-TG and 5-HT_4-TG (Gergs et al., 2023). In isolated human right atrial preparations, LSD increased the force of contraction via H_2- and 5-HT_4-serotonin receptors (Gergs et al., 2023). However, it is currently not known whether LSD increases ventricular function in the human heart. This is an interesting question to study. In the ventricles of humans, H_2-histamine receptors are present and functional in failing human hearts (Bristow et al., 1982; Baumann et al., 1983; Matsuda et al., 2004). 5-HT_4 serotonin receptors are likewise expressed in the human ventricle. However, 5-HT increased force only in isolated failing human ventricles, but not in isolated non-failing ventricles (review: Neumann et al., 2023c). In non-failing ventricular human preparations, serotonin only increased the force of contraction when initially a phosphodiesterase inhibitor was given (Neumann et al., 2023c; Table 4).

Hence, it is likely that LSD stimulates force in the ventricle, but this remains a hypothesis. In the absence of a PDE inhibitor, LSD concentration dependently reduced the force of contraction (Jacob et al., 2024). These effects may be due to the antiadrenergic effects of LSD. Indeed, early binding data have reported an affinity of LSD to

β-adrenergic receptors (Dolphin et al., 1978). It was noted that after pretreatment with the β-adrenoceptor agonist isoprenaline, LSD concentration dependently reduced the force of contraction in the isolated human atrium (Jacob et al., 2024). Similarly, Angus and Black (1980) found that in guinea pig papillary muscles, LSD antagonised the positive inotropic effects of histamine. Likewise LSD inhibited cAMP formation that was stimulated by histamine (Green et al., 1977). Consistent with the general concept that LSD is a partial agonist at serotonin receptors, after prestimulation with serotonin, LSD exerts a concentration-dependent negative inotropic effect in human right atrial preparations (Jacob et al., 2024). In summary, LSD behaves as a partial agonist in histamine and serotonin receptors and as an antagonist at β-adrenergic receptors in the human isolated atrium. The clinical consequences of this warrant further investigation.

Ergotamine

Ergotamine and LSD share the lysergic acid moiety (Figure 1A). Hence, it may not be surprising that ergotamine, like LSD, can bind to 5-HT_{2A}-serotonin receptors in the brain. As with LSD, ergotamine can lead to hallucinations (Gulbranson et al., 2002; Silberstein and McCrory, 2003). Ergotamine can also stimulate peripheral 5-HT_{2A}-serotonin receptors but also, as a partial agonist, vasoconstrictory α_1-adrenoceptors (review: Silberstein and McCrory, 2003). Ergotamine is found in fungi like Claviceps purpurea that grow on cereals and still causes arterial constrictions, but possibly also hallucinations in consumers of cereals (e.g., Stange et al., 1998; Liegl and McGrath, 2016; Cervellin et al., 2020; Huybrechts et al., 2021). Moreover, ergotamine is also degraded by the cytochrome CYP2D6; some cases of ergotamine intoxication have been reported when patients are additionally treated with drugs that are inhibitors of CYP2D6 (Mohamedi et al., 2021).

Ergotamine is also binding to 5-HT_{2B}- serotonin receptors (Fitzgerald et al., 2000). This binding to and activation of 5-HT_{2B}- serotonin receptors may explain why ergotamine was the first drug reported to lead to valvular heart disease (review: Ledwos et al., 2022). One has argued the ergotamine was given in these cases continuously over a long time, e.g., to migraine patients. This long lasting stimulation of 5-HT_{2B}-serotonin receptors for the reasons discussed above (section on bufotenin) may explain these detrimental effects of ergotamine (Ledwos et al., 2022).

Ergotamine is formed in fungi from lysergic acid to which alanine, proline and phenylalanine are covalently linked (Jamieson et al., 2021). No inotropic effect of ergotamine was found in isolated paced cat papillary muscles (Rabinowitz et al., 1975). However, this is a species problem because H_2-histamine receptors and 5-HT_4-serotonin receptors are functionally absent in the cat heart (Laher and McNeill, 1980, review; Neumann et al., 2021a). In contrast, a close derivative of ergotamine, called ergometrine (Figure 1), has been shown to elicit an increase in force in the guinea pig heart, which contains functional H_2-histamine receptors (review: Neumann et al., 2021a). In intoxications (Table 3), much high plasma levels of ergotamine, such as 0.015 μM, have been reported (Stange et al., 1998), which could be agonistic in cardiac preparations.

Interestingly, ergotamine was an agonist at the human H_2-histamine and serotonin 5-HT_4-receptors in the transgenic mouse atrium (Jacob et al., 2023b; Table 4). This is not without precedence. Ergotamine acts on many G-protein coupled receptors (Silberstein and McCrory, 2003). However, In isolated human right atrial preparations ergotamine increased force of contraction only via H_2-histamine receptors (Jacob et al., 2023b). As with LSD, one noted with ergotamine alone a time- and concentration-dependent negative inotropic effect. This negative inotropic effect of ergotamine is not due to the blocking of β-adrenergic receptors (Jacob et al., 2024).

Ergometrine (ergobasine, ergonovine and ergotocine)

Ergometrine is on the list of essential drugs of the World Health Organisation (WHO, 2021). Like ergotamine, ergometrine is closely related to LSD (Figure 1). In LSD, the primary lysergic acid molecule contains two diethyl substituents in the amino group of its amide derivative (Meneghetti et al., 2020). In the molecule of ergometrine, there is at this position only one substituent, namely, an isopropanolol group (lysergic acid beta-propanolamine: Stoll, 1936; Stoll and Burckhardt, 1935; Thomson, 1935).

As mentioned above, in the ergoline ring that is part of the lysergic acid structure, one can discern structural elements of at least four neurotransmitters: serotonin, dopamine, noradrenaline and histamine (Figure 1A). Hence, the agonistic or antagonistic action of ergometrine on the receptors of these four neurotransmitters can be predicted. These four neurotransmitters use more than one receptor. As a result, a broad spectrum of action via diverse receptors is expected with ergometrine and is indeed a clinical and experimental observation. Ergometrine can stimulate α_1-and α_2-adrenoceptors, leading to vasoconstriction in rats (Kalkman et al., 1982). Moreover, ergometrine stimulates 5-HT_1-serotonin receptors, which can induce vasoconstriction (Bai et al., 2004). Ergometrine can also act as a partial agonist at 5-HT_{2A} serotonin receptors (Hollingsworth 1988. Stimulation of these HT_{2A} serotonin receptors in humans can lead to vasoconstriction (Kaumann et al., 1994; van den Broek et al., 2002). If resistance vessels in the periphery constrict, hypertension would follow. If vasoconstriction via HT_{2A} serotonin receptors occurs in the coronary arteries, angina pectoris can follow (Kaumann and Levy, 2006). Hence, several serotonin receptors alone or combined could explain why ergometrine can cause vasoconstriction.

Peripheral vasoconstriction due to ergometrine has probably been noted since the Middle Ages in Europe (review: Grzybowski et al., 2021). Ergometrine constricts the arteries of the legs, arms, and coronary arteries in susceptible patients. This detrimental effect is sometimes used for diagnostic purposes in cardiology. In some countries, ergometrine is given to intentionally induce contraction of the coronary arteries. In this way, patients with variant angina or "Prinzmetal angina" can be better diagnosed (Romagnoli et al., 2005; Koizumi et al., 2006; Sueda et al., 2017; Picard et al., 2019).

Interestingly, there are cases in which ergometrine has probably induced atrial fibrillation in postpartum women (Birch et al., 2019). These arrhythmias could be due to the stimulation of receptors, as

ergometrine binds to and stimulates human H_2-histamine and 5-HT_4-serotonin receptors (Jacob et al., 2023a) and because H_2-histamine and 5-HT_4-serotonin receptors can cause cardiac arrhythmias (review: Neumann et al., 2021a; Neumann et al., 2023c).

As mentioned above, ergometrine is agonistic at 5-HT_{2A} serotonin receptors (Hollingsworth et al., 1988). This interaction in the brain may lead to hallucinations (animal studies: Balsara et al., 1986, humans; Ott and Neely, 1980). In patients, intoxication with ergometrine is rare. However, there are case reports that imply the misuse of ergometrine-containing plants. Seeds of the Hawaiian baby woodrose (argyreia nervosa) led to hallucinations in humans (Klinke et al., 2010).

Ergometrine stimulates H_2-histamine receptors in guinea pig perfused hearts (Bongrani et al., 1979; Table 4). Moreover, ergometrine increased force of contraction and beating rate in left or right atrial preparations from H_2-TG and from 5-HT_4-TG via human H2-histamine receptors and 5-HT4-serotonin receptors (Jacob et al., 2023a). However, ergometrine was more effective via H_2-histamine receptors than via 5-HT_4-serotonin receptors (Jacob et al., 2023a). In addition, ergometrine via H_2-histamine receptors can increase the force of contraction in isolated human right atrial preparations if a phosphodiesterase inhibitor is present but only via H_2-histamine receptors and not via 5-HT_4-serotonin receptors (Jacob et al., 2023a). Like ergotamine and LSD, ergometrine induced (in the absence of a phosphodiesterase inhibitor) a negative inotropic effect (Jacob al. 2023a).

Phosphodiesterases degrade cAMP and thus inactivate cAMP. The most relevant phosphodiesterase in the human heart is called phosphodiesterase III (Kamel et al., 2023). If this phosphodiesterase III is inhibited by milrinone or cilostamide, then the effect of cAMP producing pathways is amplified because less cAMP is inactivated and thus more cAMP is functional to lead to positive inotropic effects (Feldman et al., 1987). Thus, inhibition of phosphodiesterases is sometimes used to amplify receptor mediated positive inotropic effects in human cardiac preparations.

We noted that this negative inotropic effect of ergometrine is similar to that of LSD and due to antagonistic action at β-adrenoceptors (Jacob et al., 2024). Moreover, normal therapeutic peak plasma concentrations of ergometrine (used in gynaecology) are 4 nM (Table 3) and are thus too low to affect contractile functions (Jacob et al., 2023a). In cases of intoxication with ergometrine or ergometrine-containing extracts, higher ergometrine concentrations might be active on the heart.

N,N-dimethyltryptamine (DMT)

N,N-dimethyltryptamine is structurally related to serotonin (5-hydroxytryptamine) because it is a substituted tryptamine derivative with methyl moieties at the aliphatic amino group. Hence, it is not surprising that, based on this similarity to serotonin, N,N-dimethyltryptamine can bind to serotonin receptors. Agonist binding to 5-HT_{2A}-serotonin receptors is thought to explain the hallucinogenic effects of N,N-dimethyltryptamine (Titeler et al., 1988). N,N-dimethyltryptamine exerted positive chronotropic effects in isolated spontaneously beating hearts from rabbits (Fozard and Ali, 1978). However, the contractile effects of 5-HT in rabbit atria are not mediated by 5-HT_4-serotonin receptors but by the release of noradrenaline (Trendelenburg, 1960). Hence, the effects of DMT in rabbit hearts were not 5-HT_4-serotonin receptor-mediated.

N,N-dimethyltryptamine occurs in many plants (Rätsch, 2015) and is used as a recreational psychedelic drug (global prevalence studied by Winstock et al., 2014) and even for ritual or religious purposes (McKenna et al., 1984a, review; Gable, 2007). DMT was found in the leaves of the plant Diplopterys cabrerana in Ecuador and Colombia (Ott, 1999; Brito-da Costa et al., 2020). However, DMT is also synthesised in the human brain and may be a neurotransmitter in humans (review: Carbonaro and Gatch, 2016). DMT was initially synthesised out of sheer chemical curiosity without studying biological responses in humans (Manske, 1931). In some species of toads, DMT was also detected. As in other animals, tryptophan is decarboxylated to tryptamine in toads. The decisive next step is catalysed by the high turnover rates of a particular enzyme in some species of toads (as mentioned above for bufotenin). Tryptamine is then sequentially methylated via monomethyltryptamine to DMT via a newly cloned indolethylamine methylase found, especially in *Bufo marinus* (Chen et al., 2023).

The leaves of the *Psychotria viridis* bush contain DMT. The bark of a plant (*Banisteriopsis caapi* vine) and contains harmala alkaloids which can inhibit the activity enzyme monoamine oxidase A (MAO-A) (Brito-da-Costa et al., 2020). This mixture, called ayahuasca, has been used since pre-Columbian times by indigenous tribes of the Amazon Basin (Gable, 2007). Ayahuasca is used for medical purposes (Brito-da-Costa et al., 2020). However, if extracts containing only DMT were drunk, the DMT would be rapidly inactivated by the MAO-A in the stomach lining. Therefore, users included plant extracts (here: harmala alkaloids) that contain MAO-A inhibitors (which at higher concentrations also inhibit monoamine oxidase B (MAO-B) (reviewed in: Callaway et al., 1999) when they used ayahuasca (McKenna et al., 1984a).

As with ayahuasca, pure DMT applied perorally alone does not lead to hallucinations due to the strong first-pass effect. DMT is metabolised in the gut and liver (McKenna et al., 1984a; Ott, 1999) like perorally applied serotonin. However, MAO activity (an example of a first-pass effect) of the gastrointestinal tract is anatomically avoided, such as when smoking or via injection of DMT or insufflation of DMT. In this case, DMT is active (Gable, 2007). Moreover, if the metabolism of DMT is impaired by drugs, hallucinogenic effects will occur.

In many countries, DMT use is restricted out of fear of misuse. One can argue that the beneficial effects of DMT, for instance, in psychiatric patients, might be considerable because the toxicity of DMT is low, and few deaths from DMT have been reported (Brito-da-Costa et al., 2020). The DMT content in *Psychotria viridis* bush and of β-carboline alkaloids in *Banisteriopsis caapi* vine ranges from 3–9.5 or 0.05%–1.95% mg/g dry weight, respectively, indicating high variability of doses taken and thus of pharmacological outcome (McKenna et al., 1984a; Callaway et al., 1996; Callaway et al., 1999; Callaway et al., 2005). Ayahuasca contains 0.14–0.6 mg/mL, equal to a total daily dose of 33–36 mg (Gable, 2007). As expected, injection of DMT leads to cognitive effects faster than taking ayahuasca (10 min versus 60 min), and the psychological effects are more potent due to a higher peak plasma concentration of DMT after injection of the same dose (Riba et al., 2015). Interestingly, some

species of nutmeg, namely, Virola (Myristicaceae), contain high concentrations of DMT and at least minute amounts of MAO-inhibitory β-carbolines (McKenna et al., 1984b). A resin prepared from the bark of Virola is used by autochthonous Amazon tribes for hallucinogenic purposes (Plotkin and Schultes, 1990).

There is some debate as to the toxicity of DMT (Cameron et al., 2018) The lethal dose of DMT in mice is around 47 mg/kg if given intraperitoneally (Gable, 2007). Based on rodent studies, the dose where half of the patient would die (LD_{50}) of DMT in men is estimated at 1.6 mg/kg given intravenously (Gable, 2007). There have not been recorded deaths due to ayahuasca, but when polypharmacy is used and pure 5-methoxy-DMT is added, at least one human death is found in the literature (Sklerov et al., 2005).

In ligand binding studies, DMT had the following rank or of potencies: 5-HT_{1A}- >5-HT_{2A}- > 5-HT_{2C}- > 5-HT_{2B} (3.4 μM) serotonin receptors. The highest affinity was displayed by DMT to 5-H_{1A}-serotonin receptors with 75 nM. The affinity for 5-HT_{2C}-serotonin is much lower, about 420 nM (Rickli et al., 2016). DMT inhibited transporters with most potent inhibition for serotonin-transporter, then noradrenaline-transporter and lowest at dopamine-transporter (52 μM, Rickli et al., 2016). For adrenergic and dopaminergic receptors the rank order of affinity of DMT was: α_1-adrenoceptor > α_2-adrenoceptor > D_2-dopamine receptor > D_1-dopamine receptor (Rickli et al., 2016). From these binding data at 5-HT_{2B}-serotonin receptors, one would assume that DMT can activate this 5-HT_{2B}-serotonin receptor in the patient only under certain conditions. This might lead valvular heart disease (*vide supra*). However, others claimed that any proofs from clinical studies is currently lacking for valvular damage by DMT (Tagen et al., 2023). However, this side effect should be looked for in prospective clinical trials.

Initial studies of pure DMT administered intramuscularly in normal volunteers (0.7–1.1 mg/kg body weight) led to rapid (5–10 min) brief (1 h) visual hallucinations, euphoria, mydriasis, and an increase in blood pressure (Szára, 1956). In a placebo-controlled study in humans, intravenous application of 0.3 mg/kg DMT led to peak DMT plasma levels (at about 5 min after injection) of 70 ng/mL (about 0.38 μM, Table 3) and increased heart rate and blood pressure. Additional results included increased temperature, adrenocorticotropic hormone, prolactin, and cortisol levels in plasma (Strassman et al., 1994). Similarly, using ayahuasca preparations from the Amazon Basin in human volunteers, the half-life of DMT was reported as about 260 min, with a volume of distribution of about 55 L per kilogram. Temperature, heart rate, blood pressure, pupil diameter, and breathing rate increased (Callaway et al., 1999). The plasma concentration of harmine, another tryptamine derivative, and MAO inhibitor peaked when drunk with ayahuasca brew at about the same time as DMT, with a similar volume of distribution (Callaway et al., 1996; Callaway et al., 1999). These findings may mean that the plant contains not only the hallucinogenic compound but also some other related ingredient that improves the bioavailability of the hallucinogenic compound, at least in part. DMT binds to 5-$HT_{1A, 1B, 1D}$, - and 5-HT_{2A}, 5-HT_{2B}, 5-HT_{2C}, 5-HT_6 - and 5-HT_7 -serotonin receptors (Deliganis et al., 1991; Brito-da-Costa, 2020). Binding to 5-HT_4 serotonin receptors has never been reported to the best of our knowledge.

5-methoxy-N,N,-dimethyltryptamine (5-Me-DMT)

5-methoxy-N,N-dimethyltryptamine is also structurally related to serotonin (5-hydroxytryptamine) because it is a substituted tryptamine derivative (Figure 1). The molecule 5-methoxy-N,N-dimethyltryptamine is found in plants and animals (Ott, 2001; Araújo et al., 2015). Perorally given alone, 5-methoxy-N,N-dimethyltryptamine is rapidly metabolised by monoamine oxidases in the gastrointestinal tract to inactive metabolites (Shen et al., 2010). Hence, it is used parenterally or in combination with inhibitors of the enzymatic activity of monoamine oxidases (Shen et al., 2010). These inhibitors could be antidepressant drugs, such as tranylcypromine. There are also reports in the literature that pure 5-methoxy-N,N-dimethyltryptamine was mixed with plant extracts containing the natural monoamino oxidase inhibitor harmaline, which eventually brought the user to the intensive care unit because he was intoxicated (Brush et al., 2004).

In anaesthetised rats, 5-methoxy-N,N-dimethyltryptamine reduced heart rate and blood pressure (Dabiré et al., 1987). These effects have been suggested to be due to the stimulation of 5-HT_1 serotonin receptors (Dabiré et al., 1987). The interpretation of the data in rat might be made complicated because Dabiré et al., 1987 used anaesthesia during their experiments. The anaesthesia might have exerted powerful modulatory effects on cardiac responsiveness. In contrast, we reported that 5-HT increased the force of contraction in isolated rat hearts via 5-HT_{2A} serotonin receptors (Läer et al., 1998).

In pithed rats, 5-methoxy-N,N-dimethyltryptamine failed to affect the beating rate of the heart (Dabiré et al., 1992). Surprisingly, the rat heart contains inotropically functional 5-HT_{2A} serotonin receptors (Läer et al., 1998). The beating rate in narcotised rats or neonatal rat cardiomyocytes could be increased by serotonin (Higgins et al., 1981; Torres et al., 1996). In the isolated blood-perfused rat heart, minor positive chronotropic effects but significant inotropic effects of 5-HT were observed (Sakai and Akima, 1979). These divergent findings might result from methodological differences.

5-methoxy-N,N-dimethyltryptamine is found in plants and toads. It is often prepared from the Sonoran Desert toad (a toad with very high concentrations of 5-methoxy-N,N-dimethyltryptamine in the parotids and the skin) in the southern United States of America and Central and South America for ritual or recreational purposes (Araújo et al., 2015). 5-methoxy-N,N-dimethyltryptamine is a substrate for CYP2D6. CYP2D6 converts 5-methoxy-N,N-dimethyltryptamine to bufotenin (5-hydroxy-N,N-dimethyltryptamine, see above), also a naturally occurring (in toad skin or toad venom) hallucinogenic compound (review: Eichelbaum, 2003; Shen et al., 2010, *vide supra*). The expression of CYP2D6 is genetically regulated. Thus, slow and fast metabolisers are expected to experience longer or slower responses to 5-methoxy-N,N-dimethyltryptamine (review: Eichelbaum, 2003; Shen et al., 2010). Inhibitors of CYP2D6 are expected to prolong the hallucinogenic effects of 5-methoxy-N,N-dimethyltryptamine, but this has not yet been reported in patients.

One could speculate that the hallucinogenic effects of 5-methoxy-N,N-dimethyltryptamine result, at least in part, from bufotenine which is an active metabolite of 5-methoxy-N,N-

dimethyltryptamine (Figure 1A). High concentrations of 5-methoxy-N,N-dimethyltryptamine are found in the bark and leaves of some species of the Virola plant (Myristicaceae, nutmeg) in the federal state Amazonas of the Union of Brazil (review: Ott, 2001). Extracts of the aforementioned plants were used as snuffs in shamanic ceremonies in South America dating back to pre-Columbian times (Ott, 2001). Preparations from species of Virola contained varying amounts of 5-methoxy-N,N-dimethyltryptamine (ranging from 0.017% to 1.57% of weight), sometimes together with smaller amounts of DMT. Hence, 5-methoxy-N,N-dimethyl-tryptamine is currently thought to be the main hallucinogenic principle of Virola extracts or Virola-containing pasts (Ott, 2001).

5-methoxy-N,N-dimethyltryptamine is psychoactive in various routes of application: 5-methoxy-N,N-dimethyltryptamine can be injected intravenously, can be breathed as a vapour, used as a snuff or as an errhine. In addition 5-methoxy-N,N-dimethyltryptamine can be given intranasally or sublingually, but also perorally in humans (Ott, 2001; Table 3). Typically, 10 mg (0.14 mg(kg) of chemical pure 5-methoxy-N,N,-dimethyltryptamine induced (in all the galenic forms mentioned) a hallucinogenic effect in humans (self-experiments: Ott, 2001). The addition of MAO inhibitors (harmaline 3.7 mg and a higher free base) potentiated the hallucinogenic effect of 5-methoxy-N,N-dimethyltryptamine, at least when using them nasally, sublingually, and perorally in humans (self-experiments: Ott, 2001). On the other hand, this seems to imply that it is active on its own, regardless of the additional presence of an MAO inhibitor, in contrast to DMT. In the human heart, 5-methoxy-N,N-dimethyltryptamine is more potent and effective than DMT in raising the force of contraction, at least in isolated human atrial preparations (Dietrich et al., 2023; Table 4).

Recreational drugs like N,N-dimethyltryptamine and 5-methoxy-N,N-dimethyltryptamine have led to intoxications (Brush et al., 2004). Our data might argue that these intoxications can involve the heart and that cardiac side effects could be treated by 5-HT_4 receptor antagonists (Dietrich et al., 2023; Table 4). From a practical point of view, one could treat severely ill patients with tropisetron. Our data indicate that tropisetron can reduce the cardiac effects of 5-methoxy-N,N-dimethyltryptamine on human 5-HT_4 serotonin receptors. Currently, there are 14 studies of N,N-dimethyltryptamine and two of 5-methoxy-N,N-dimethyltryptamine (clinical trials.gov, Table 2). The main indication in these clinical trials was depression. 5-methoxy-N,N-dimethyltryptamine is metabolised by CYP2D6 (Shen et al., 2010). The potency of 5-methoxy-N,N-dimethyltryptamine to increase the force of contraction could be increased by pretreatment of human atrial preparations from 5-HT_4-TG in combination with the phosphodiesterase inhibitor cilostamide (Dietrich et al., 2023). As already mentioned above, In everyday life, PDEs can be inhibited by theophylline (in tea) or caffeine (in coffee beverages or power drinks). In patients, PDEs are inhibited when taking milrinone or levosimendan for heart failure or rolipram for asthma treatment. In such patients, special caution is warranted with 5-methoxy-N,N-dimethyltryptamine, based on our data (Dietrich et al., 2023; Table 4).

Psilocin

Psilocin (Table 1A) is chemically related to serotonin (Hofmann et al., 1958; Hofmann et al., 1959). Psilocin and its precursor, psilocybin, can be described as substituted indole derivatives, namely, [3-(2-dimethylaminoethyl)-1H-indol-4-yl] dihydrogen phosphate and 4-hydroxy-N,N-dimethyltryptamine, respectively (Hofmann et al., 1958; Hofmann et al., 1959; Figure 1A). Psilocin has a high affinity to many receptors, mainly 5-$HT_{2A,B,C}$ (pdsp.unc.edu., Halberstadt and Geyer, 2011), but its affinity to 5-HT_4 serotonin receptors has not yet been reported (McKenna et al., 1990). The Food and Drug Administration (FDA) in the United States of America has since given psilocybin a fast-track designation for depression (Hesselgrave et al., 2021). Clinical studies have found that psilocybin might be useful in treating alcoholism, tobacco addiction, depression, and anxiety in cancer patients (discussed in Geiger et al., 2018).

In ligand binding studies, psilocin had the following rank or of potencies: 5-HT_{2A}- >5-HT_{2C}- >5-HT_{1A}-serotonin-receptors (Rickli et al., 2016). It has been recently suggested that psilocybin might be chemically modified such that a derivate still acts as an antidepressant but is devoid of unwanted hallucinogenic effects which are currently thought to result from binding of psilocin to 5-HT_{2A}-serotonin receptors (Hesselgrave et al., 2021). There was practically no affinity of psilocin for the 5-HT_{2B}-serotonin receptor (larger than 20 μM, Rickli et al., 2016). From these binding data of psilocin at 5-HT_{2B}-serotonin receptors, one would assume that psilocin cannot activate this receptor in the normal client or patient. Likewise, there is not any proof from clinical studies for valvular damage due to psilocin (Tagen et al., 2023). However, this side effect should be looked for in prospective clinical trials. The affinity of psilocin at others receptors probably does not play a clinical role. For instance, the affinity at the most sensitive adrenergic receptor, the α_2-adrenoceptor amounts to 2.1 μM (Rickli et al., 2016). Likewise, psilocin probably does not act clinically via inhibition of the serotonin transporter (SERT) activity because its affinity for SERT is too low. For instance, a Ki value of 3.8 μM (Poulie et al., 2019) at SERT was reported. Such a high concentration is not reached with therapeutic dosage of psilocin (e.g., 0.1 μM plasma concentration of psilocin. Madsen et al., 2019).

Comparing the structural formulae of 5-HT and psilocin, it is obvious that psilocin is different in two regards: 1) psilocin contains hydroxyl-moiety at C4, not C5 of the indole ring, and 2) the amine function is doubly methylated (Figure 1A). Psilocybin is dephosphorylated to psilocin by alkaline phosphatases that occur in the blood and in many tissues (*in vitro* dephosphorylation of psilocybin: Horita and Weber, 1962; *in vivo* dephosphorylation of psilocybin in humans; Hasler et al., 1997). Psilocin is a structural isomer of bufotenin, chemically 5-hydroxy-N,N-dimethyltryptamine, and is hallucinogenic (*vide supra*, Figure 1A). Psilocybin is regarded as a prodrug, and the active metabolite formed in humans is psilocin (Hasler et al., 1997). Psilocybin and psilocin are found in many fungi from the genus Psilocybe (review: Nichols, 2020). The name was coined using ancient Greek, from the appearance of the fungi to botanists: psilos (ψιλος, naked) kube (κυβη, head) (Rätsch, 2015). These fungi have been used in religious ceremonies since prehistoric times in some parts of the world (Geiger et al., 2018). They have been

called "magic mushrooms" because they can cause mind-altering experiences like hallucinations. The active ingredients of the fungi are, therefore, often classified as hallucinogenic drugs. The active ingredients were identified by Albert Hofmann, a Swiss organic chemist known as the inventor of LSD, in mushrooms from Central Mexico; he also synthesised psilocin and psilocybin *in vitro* (Hofmann et al., 1958; Hofmann et al., 1959).

These magic mushrooms and their ingredients are popular recreational drugs in the United States of America. Moreover, psilocybin was detected in several other fungi or moulds, namely, Conocybe spp. Galerina steglichii, Inocybe spp. and Pluteus spp. (Rätsch, 2015). Psilocybin is not produced in human cells, but more generally in mammals, conceivably because crucial synthetic enzymes are lacking in animals that are present in fungi. The synthesis of psilocybin in fungi and the enzymes involved its synthesis in fungi have been presented by others (Geiger et al., 2018). In brief, in fungi, psilocybin is formed from L-tryptophan, which is decarboxylated to tryptamine; the next steps are hydroxylation, phosphorylation, and methylation, ending with psilocybin (Fricke et al., 2017). Psilocin can be metabolised via side-chain oxidation and the formation of glucuronides, and it has a half-life of about 3 hours in humans (Geiger et al., 2018). The enzymes involved have not yet been clearly described. However, if they are the typical cytochromes described above, drugs that inhibit cytochromes are predicted to prolong the half-life and, thus, the pharmacological action of psilocin (Geiger et al., 2018). Not only psilocybin but also MAO inhibitors, such as harmine, were formed at the same time. This is relevant because psilocin is metabolised by MAO-A to the inactive derivative 4-hydroxyindol-3-yl-acetaldedyde (Blei et al., 2020). It has been speculated that for better protection against predators, some fungi produce both hallucinogen (e.g., psilocybin) and compounds that prolong hallucinogenic (e.g., harmine) effects because inactivation is impaired (Blei et al., 2020).

In Europe and the United States of America, several attempts were made in the 1960s to use psilocin in psychiatry. The Swiss pharmaceutical company Sandoz supplied for these studies psilocybin under the trade name Indocybin®. In such studies therapeutic applications of psilocybin were sought after. For instance, one asked whether psilocybin might be an appropriate tool to explore traits of personality or might help in understanding the mechanisms of a psychosis (Aldahaff, 1963; Charalampous et al., 1963; Leary et al., 1963). These studies were regarded as failures (review: Studerus et al., 2011) and psilocybin fell into disuse and was removed from the legitimate market. In recent years, a renaissance of psilocybin has occurred in terminally ill cancer patients and people suffering from depression (Ross et al., 2016). In these later studies, the effects of psilocybin on cardiovascular parameters in patients were reported. They noted tachycardia (Ross et al., 2016). However, the receptor mechanism has not been studied (Ross et al., 2016). There are scarce data from the older literature on the cardiac effects of psilocybin in animals. We found that both psilocin and psilocybin exerted a positive inotropic effect in isolated human atrial preparations (Dimov et al., 2023; Table 4). Hence, the proarrhythmic effects reported in clinical studies of psilocin and psilocybin might be due, in part, to their cyclic adenosine monophosphate (cAMP)-increasing effects on the heart.

The so-called "magic mushrooms" contain psilocin and its prodrug psilocybin; they are heat stable, meaning that they cannot be inactivated by heating extracts of the mushrooms. Psilocybin contains a phosphate at the phenolic part of the molecule, in contrast to its less polar metabolite, hallucinogenic psilocin (Figure 1). Therefore, psilocybin is more polar and thus soluble in water than psilocin, which requires organic solvents. Unexpectedly, we noted that psilocybin, usually regarded as an inactive precursor of psilocin, was active in isolated human atrial preparations to raise force of contraction (Dimov et al., 2023; Table 2). Hence, one may argue that the 5-HT_4 serotonin receptor binding part of both compounds resides in the amino moiety of the drugs and not in the phenolic ring. However, this speculation needs to be confirmed by direct analysis of the crystal structure of psilocin and psilocybin bound to the recombinant human 5-HT_4 serotonin receptor in the future.

The hallucinogenic effects of psilocin are usually explained by its agonistic potency (81 nM = Ki) at 5-HT_{2A} serotonin receptors, which is less than the potency of LSD at this receptor (Nichols, 2020). Moreover, psilocin binds to 5-HT_{2C} serotonin receptors (140 nM, Nichols, 2020). A complete list of the affinities of psilocin for 5-HT receptors was found in Geiger et al. (2018). From a cardiovascular point of view, the agonistic effect of psilocin on cardiac 5-HT_{2A} - and 5-HT_1 serotonin receptors in the coronaries might cause harmful vasoconstriction. Stimulation of 5-HT_2 serotonin receptors might lead to cuspid leaf defects. Binding to 5-HT_4 serotonin receptors has never been reported (Geiger et al., 2018). It might be relevant that psilocin binds to H_1 histamine receptors (Geiger et al., 2018). In the human heart, H_1-histamine receptors induce bradycardia, have a negative dromotropic effect and might alter the force of contraction (review: Neumann et al., 2023c). This indicates a pleiotropic action of psilocin, possibly explaining its broad spectrum of effects on perception and awareness (Nichols, 2018).

Psilocybin undergoes a first-pass effect by metabolism in the liver by an alkaline phosphatase that can be inhibited by β-glycerolphosphate (Horita, 1963). 25% of perorally taken psilocin in rats is excreted unmetabolised (Kalberer et al., 1962). The fact that tropisetron antagonised the positive inotropic effect and positive chronotropic effect of psilocin and psilocybin is essential for two reasons (Dimov et al., 2023). This corroborates the conclusion that psilocin and psilocybin act via 5-HT_4-serotonin receptors. Moreover, these findings suggest that one could treat magic-mushroom-intoxications with an approved drug, tropisetron. One could also use a more selective and potent 5-HT_4 antagonist like piboserod which is however not readily available anymore (Kjekshus et al., 2009).

The potency of psilocin to increase the force of contraction could be increased by pretreatment of atrial preparations from 5-HT_4-TG with a combination of the phosphodiesterase inhibitors cilostamide (1 μM) and rolipram (0.1 μM). This is consistent with our previous studies; cilostamide is a PDE III inhibitor, and rolipram is a PDE IV inhibitor (Neumann et al., 2019). We have previously used the concentrations of these drugs to potentiate the PIE of 5-HT in atrial preparations of 5-HT_4-TG (Neumann et al., 2019). These findings support our conclusion that psilocin acts via the generation of cAMP. If the degradation of cAMP is reduced by reducing PDE activity, the agonist at the 5-HT_4 serotonin receptor can lead to higher cAMP levels and, thus, higher force generation and elevated heart beating rate (compare Figure 1).

Extracts from the genus Psilocybe have been used at least as early as AD 300 in shamanic rites as hallucinogenic products in Middle America (Nichols, 2020). Psilocybe, however, is naturally occurring

worldwide and, hence, has probably been used by people in many places (Nichols, 2020). Psilocin in mushrooms might have been used in Africa in the Sahara Desert, ancient Egypt and prehistoric caves in Spain (Geiger et al., 2018). In healthy volunteers, hallucinogenic doses (up to 30 mg per os) of psilocybin increased blood pressure (Hasler et al., 2004). For instance, 30 mg of psilocybin led to peak plasma levels of about 0.1 μM of psilocin and about 50% occupation of 5-HT_{2A} serotonin receptors in the brain, as measured by positron emission tomography (Madsen et al., 2019).

Psilocin and psilocybin could directly lead to tachycardia in users by stimulating 5-HT_4 serotonin receptors in the sinus node. Tachycardia is a problem in patients with coronary heart disease because the oxygen supply of the heart might be reduced, and angina and myocardial infarction might occur. This tachycardia might be prevented or treated with tropisetron because tropisetron blocks (not only but also) 5-HT_4-serotonin receptors. If one wants to treat depressive patients (there are currently 66 studies for psilocybin on file at clinical trials.gov, Table 2) with psilocybin, it might be useful to give an additional β-adrenoceptor antagonist to reduce the heart rate. Alternatively, one could prescribe, in addition to psilocin, a 5-HT_4 antagonist that does not pass the blood–brain barrier (tropisetron easily passes the blood–brain barrier: Wolf, 2000). However, such drugs are currently regrettably not yet available.

Moreover, in normal dosing, one can question whether psilocin plasma levels are high enough to stimulate cardiac 5-HT_4 serotonin receptors. As mentioned above, 0.1 μM of psilocin was measured under therapeutic conditions below any contractile effect. However, phosphodiesterase inhibitors (clinically used as levosimendan, milrinone, roflumilast, theophylline or caffeine) potentiate the contractile effects of 5-HT. We would argue that phosphodiesterase inhibitors would also potentiate the effects of psilocin. Finally, if depressive patients used an MAO inhibitor such as moclobemide, tranylcypromine, or deprenyl, the degradation of psilocin would be impaired, and higher plasma concentrations of psilocin might be reached; this could induce rapid heartbeat by simulating the cardiac 5-HT_4 serotonin receptors. It has been reported that taking mushrooms led to cardiac death, probably via cardiac arrhythmia, in a patient 10 years after her heart transplant. The postmortal psilocin concentration in her plasma was 30 μg/L (0.15 μM, Lim et al., 2012; Table 3).

When giving increasing dosage of psilocybin to healthy volunteers, one did not notice even at the highest dosage (315 μg per kilogram body weight) changes in surface electrocardiograms or increased incidences of supraventricular or ventricular arrhythmias nor increases in heart rate (Hasler et al., 2004). However, at this dosing they noted an increase in blood pressure (Hasler et al., 2004). However, the study recruited only eight male and female volunteers with an age range of 22–44 years, so larger studies seem to be needed (Hasler et al., 2004). In a later clinical study on twelve healthy volunteers (gender and age were not reported), 0.6 mg per kilo Gram body weight was given (Dahmane et al., 2021). Under these conditions psilocybin, probably through its metabolite psilocin, increased the heart rate in these volunteers and tended to prolong the heart rate corrected QT interval. Hence, at high dosages psilocybin may cause detrimental torsade de pointes, a cardiac arrhythmia (Dahmane et al., 2021). The authors however, argued that the therapeutic dosing would be lower and therefore arrhythmias might not occur (Dahmane et al., 2021). In a third study, 32 volunteers were given 20 mg psilocybin through the mouth. The only cardiovascular alteration the authors reported was an increase in diastolic blood pressure (Ley et al., 2023). No other cardiovascular effects like arrhythmias were reported (Ley et al., 2023).

Outlook

Hallucinogenic compounds are undergoing renewed interest in psychiatry. It remains to be seen how effective and safe they will be in the clinical routine treatment of psychiatric patients. Moreover, people will continue to take hallucinogenic drugs for thought-altering or recreational purposes. Hence, side effects remain a concern. This review provides a detailed oversight of the known cardiac effects in humans and how they can be predicted with some certainty, based on studies in experimental animals. One can summarize our review in the following way for inotropy in the human atrium: ergometrine is solely an agonist at H_2-histamine receptors. Psilocin, psilocybin, DMT and 5-Me-DMT are solely agonists at 5-HT_4-serotonin receptors. Finally, LSD is a dual agonist at H_2-receptors and at 5-HT_4-receptors. At least proarrhythmic side effects should be considered and treated using approved drugs that are antagonistic to the 5-HT_4-serotonin or H_2-histamine receptors. Controlled clinical trials should be initiated to make the therapeutic use of hallucinogenic drugs safer.

Author contributions

JN: Conceptualization, Writing–original draft. SD: Writing–review and editing. UK: Writing–review and editing. BH: Resources, Writing–review and editing. UG: Funding acquisition, Writing–original draft.

Funding

The author(s) declare financial support was received for the research, authorship, and/or publication of this article. This work was supported by the Deutsche Forschungsgemeinschaft (German research foundation) with grant number 510383218.

Conflict of interest

The authors declare that the research was conducted in the absence of any commercial or financial relationships that could be construed as a potential conflict of interest.

Publisher's note

References

Almaula, N., Ebersole, B. J., Ballesteros, J. A., Weinstein, H., and Sealfon, S. C. (1996). Contribution of a helix 5 locus to selectivity of hallucinogenic and nonhallucinogenic ligands for the human 5-hydroxytryptamine2A and 5-hydroxytryptamine2C receptors: direct and indirect effects on ligand affinity mediated by the same locus. *Mol. Pharmacol.* 50 (1), 34–42.

Angus, J. A., and Black, J. W. (1980). Pharmacological assay of cardiac H2-receptor blockade by amitriptyline and lysergic acid diethylamide. *Circ. Res.* 46, I64–I69.

Araújo, A. M., Carvalho, F., Bastos Mde, L., Guedes de Pinho, P., and Carvalho, M. (2015). The hallucinogenic world of tryptamines: an updated review. *Arch. Toxicol.* 89 (8), 1151–1173. doi:10.1007/s00204-015-1513-x

Bai, F., Yin, T., Johnstone, E. M., Su, C., Varga, G., Little, S. P., et al. (2004). Molecular cloning and pharmacological characterization of the Guinea pig 5-HT1E receptor. *Eur. J. Pharmacol.* 484 (2-3), 127–139. doi:10.1016/j.ejphar.2003.11.019

Balsara, J. J., Bapat, T. R., Nandal, N. V., Gada, V. P., and Chandorkar, A. G. (1986). Head-twitch response induced by ergometrine in mice: behavioural evidence for direct stimulation of central 5-hydroxytryptamine receptors by ergometrine. *Psychopharmacol. Berl.* 88 (3), 275–278. doi:10.1007/BF00180824

Baumann, G., Mercader, D., Busch, U., Felix, S. B., Loher, U., Ludwig, L., et al. (1983). Effects of the H2-receptor agonist impromidine in human myocardium from patients with heart failure due to mitral and aortic valve disease. *J. Cardiovasc Pharmacol.* 5 (4), 618–625. doi:10.1097/00005344-198307000-00017

Birch, S., and Lu, C. (2019). Ergometrine-induced atrial fibrillation at caesarean section. *BMJ Case Rep.* 12 (2), e226747. doi:10.1136/bcr-2018-226747

Blaho, K., Merigian, K., Winbery, S., Geraci, S. A., and Smartt, C. (1997). Clinical pharmacology of lysergic acid diethylamide: case reports and review of the treatment of intoxication. *Am. J. Ther.* 4 (5-6), 211–221. doi:10.1097/00045391-199705000-00008

Blei, F., Dörner, S., Fricke, J., Baldeweg, F., Trottmann, F., Komor, A., et al. (2020). Simultaneous production of psilocybin and a cocktail of β-carboline monoamine oxidase inhibitors in "magic" mushrooms. *Chemistry* 26 (3), 729–734. doi:10.1002/chem.201904363

Blough, B. E., Landavazo, A., Decker, A. M., Partilla, J. S., Baumann, M. H., and Rothman, R. B. (2014). Interaction of psychoactive tryptamines with biogenic amine transporters and serotonin receptor subtypes. *Psychopharmacol. Berl.* 231 (21), 4135–4144. doi:10.1007/s00213-014-3557-7

Bogenschutz, M. P. (2013). Studying the effects of classic hallucinogens in the treatment of alcoholism: rationale, methodology, and current research with psilocybin. *Curr. Drug Abuse Rev.* 6 (1), 17–29. doi:10.2174/15733998113099990002

Bongrani, S., Di Donato, M., Visioli, O., and Mantovani, P. (1979). Effect of ergometrine on contractile force of Guinea-pig isolated heart: antagonism by cimetidine. *Agents Actions* 9 (1), 15–17. doi:10.1007/BF02024090

Bristow, M. R., Cubicciotti, R., Ginsburg, R., Stinson, E. B., and Johnson, C. (1982). Histamine-mediated adenylate cyclase stimulation in human myocardium. *Mol. Pharmacol.* 21 (3), 671–679.

Brito-da-Costa, A. M., Dias-da-Silva, D., Gomes, N. G. M., Dinis-Oliveira, R. J., and Madureira-Carvalho, Á. (2020). Toxicokinetics and toxicodynamics of ayahuasca alkaloids N,N-dimethyltryptamine (DMT), harmine, harmaline and tetrahydroharmine: clinical and forensic impact. *Pharm. (Basel)* 13 (11), 334. doi:10.3390/ph13110334

Brush, D. E., Bird, S. B., and Boyer, E. W. (2004). Monoamine oxidase inhibitor poisoning resulting from Internet misinformation on illicit substances. *J. Toxicol. Clin. Toxicol.* 42 (2), 191–195. doi:10.1081/clt-120030949

Callaway, J. C., Brito, G. S., and Neves, E. S. (2005). Phytochemical analyses of Banisteriopsis caapi and Psychotria viridis. *J. Psychoact. Drugs* 37 (2), 145–150. doi:10.1080/02791072.2005.10399795

Callaway, J. C., McKenna, D. J., Grob, C. S., Brito, G. S., Raymon, L. P., Poland, R. E., et al. (1999). Pharmacokinetics of Hoasca alkaloids in healthy humans. *J. Ethnopharmacol.* 65 (3), 243–256. doi:10.1016/s0378-8741(98)00168-8

Callaway, J. C., Raymon, L. P., Hearn, W. L., McKenna, D. J., Grob, C. S., Brito, G. S., et al. (1996). Quantitation of N,N-dimethyltryptamine and harmala alkaloids in human plasma after oral dosing with ayahuasca. *J. Anal. Toxicol.* 20 (6), 492–497. doi:10.1093/jat/20.6.492

Cameron, L. P., and Olson, D. E. (2018). Dark classics in chemical neuroscience: N, N-dimethyltryptamine (DMT). *ACS Chem. Neurosci.* 9 (10), 2344–2357. doi:10.1021/acschemneuro.8b00101

Carbonaro, T. M., and Gatch, M. B. (2016). Neuropharmacology of N,N-dimethyltryptamine. *Brain Res. Bull.* 126, 74–88. doi:10.1016/j.brainresbull.2016.04.016

Cervellin, G., Longobardi, U., and Lippi, G. (2020). One holy man, one eponym, three distinct diseases. St. Anthony's fire revisited. *Acta Biomed.* 92 (1), e2021008. doi:10.23750/abm.v92i1.9015

Chamakura, R. P. (1994). Bufotenine - a hallucinogen in ancient snuff powders of South America and a drug of abuse on the streets of New York city. *Forensic Sci. Rev.* 6 (1), 1–18.

Charalampous, K. D., and Kinross-Wright, J. (1963). Hallucinogens. Tools for research and therapeutic agents. *Tex State J. Med.* 59, 848–852.

Chen, X., Li, J., Yu, L., Maule, F., Chang, L., Gallant, J., et al. (2023). A cane toad (Rhinella marina) N-methyltransferase converts primary indolethylamines to tertiary psychedelic amines. *J. Biol. Chem.* 299, 105231. doi:10.1016/j.jbc.2023.105231

Chiba, S. (1977). Pharmacologic analysis of chronotropic and inotropic responses to 5-hydroxytryptamine in the dog heart. *Jpn. J. Pharmacol.* 27 (5), 727–734. doi:10.1254/jjp.27.727

Chilton, W. S., Bigwood, J., and Jensen, R. E. (1979). Psilocin, bufotenine and serotonin: historical and biosynthetic observations. *J. Psychedelic Drugs* 11 (1-2), 61–69. doi:10.1080/02791072.1979.10472093

Cortijo, J., Martí-Cabrera, M., Bernabeu, E., Domènech, T., Bou, J., Fernández, A. G., et al. (1997). Characterization of 5-HT receptors on human pulmonary artery and vein: functional and binding studies. *Br. J. Pharmacol.* 122 (7), 1455–1463. doi:10.1038/sj.bjp.0701509

Cosyns, B., Droogmans, S., Rosenhek, R., and Lancellotti, P. (2013). Drug-induced valvular heart disease. *Heart* 99 (1), 7–12. doi:10.1136/heartjnl-2012-302239

Dabiré, H., Chaouche-Teyara, K., Cherqui, C., Fournier, B., and Schmitt, H. (1992). Pharmacological analysis of the cardiac effects of 5-HT and some 5-HT receptor agonists in the pithed rat. *Fundam. Clin. Pharmacol.* 6 (6), 237–245. doi:10.1111/j.1472-8206.1992.tb00116.x

Dabiré, H., Cherqui, C., Fournier, B., and Schmitt, H. (1987). Comparison of effects of some 5-HT1 agonists on blood pressure and heart rate of normotensive anaesthetized rats. *Eur. J. Pharmacol.* 140 (3), 259–266. doi:10.1016/0014-2999(87)90282-2

Dahmane, E., Hutson, P. R., and Gobburu, J. V. S. (2021). Exposure-Response analysis to assess the concentration-QTc relationship of psilocybin/psilocin. *Clin. Pharmacol. Drug Dev.* 10 (1), 78–85. doi:10.1002/cpdd.796

Davis, A. K., Barsuglia, J. P., Lancelotta, R., Grant, R. M., and Renn, E. (2018). The epidemiology of 5-methoxy- N, N-dimethyltryptamine (5-MeO-DMT) use: benefits, consequences, patterns of use, subjective effects, and reasons for consumption. *J. Psychopharmacol.* 32 (7), 779–792. doi:10.1177/0269881118769063

Deliganis, A. V., Pierce, P. A., and Peroutka, S. J. (1991). Differential interactions of dimethyltryptamine (DMT) with 5-HT1A and 5-HT2 receptors. *Biochem. Pharmacol.* 41 (11), 1739–1744. doi:10.1016/0006-2952(91)90178-8

de Groot, A. N., Vree, T. B., Hekster, Y. A., Baars, A. M., van den Biggelaar-Martea, M., and van Dongen, P. W. (1993). High-performance liquid chromatography of ergometrine and preliminary pharmacokinetics in plasma of men. *J. Chromatogr.* 613 (1), 158–161. doi:10.1016/0378-4347(93)80210-u

Dietrich, T., Gergs, U., Hoffmann, B., Höhm, C., and Neumann, J. (2023). Cardiac effects of 5-methoxydimethyltryptamine and dimethyltryptamine. *Naunyn-Schmiedeberg's. Arch. Pharmacol.* 396, S44. doi:10.1007/s00210-023-02397-6 Suppl1.

Dimov, K., Gergs, U., Hoffmann, B., and Neumann, J. (2023). Atrial effects of psilocin and psilocybin. *Naunyn-Schmiedeb. Arch. Pharmacol.* 396, S44–S45. doi:10.1007/s00210-023-02397-6 Suppl1.

Dolder, P. C., Schmid, Y., Steuer, A. E., Kraemer, T., Rentsch, K. M., Hammann, F., et al. (2017). Pharmacokinetics and pharmacodynamics of lysergic acid diethylamide in healthy subjects. *Clin. Pharmacokinet.* 56 (10), 1219–1230. doi:10.1007/s40262-017-0513-9

Dolphin, A., Enjalbert, A., Tassin, J. P., Lucas, M., and Bockaert, J. (1978). Direct interaction of LSD with central "beta"-adrenergic receptors. *Life Sci.* 22 (4), 345–352. doi:10.1016/0024-3205(78)90142-x

Dudley, H. W., and Moir, J. C. (1935). The substance responsible for the traditional clinical effect of ergot. *Br. Med. J.* 1, 520–523. doi:10.1136/bmj.1.3871.520

Dumuis, A., Sebben, M., and Bockaert, J. (1988). Pharmacology of 5-hydroxytryptamine-1A receptors which inhibit cAMP production in hippocampal and cortical neurons in primary culture. *Mol. Pharmacol.* 33 (2), 178–186.

Eichelbaum, M. (2003). In search of endogenous CYP2D6 substrates. *Pharmacogenetics* 13 (6), 305–306. doi:10.1097/00008571-200306000-00001

Emanuele, E., Colombo, R., Martinelli, V., Brondino, N., Marini, M., Boso, M., et al. (2010). Elevated urine levels of bufotenine in patients with autistic spectrum disorders and schizophrenia. *Neuro Endocrinol. Lett.* 31 (1), 117–121.

Feldman, M. D., Copelas, L., Gwathmey, J. K., Phillips, P., Warren, S. E., Schoen, F. J., et al. (1987). Deficient production of cyclic AMP: pharmacologic evidence of an important cause of contractile dysfunction in patients with end-stage heart failure. *Circulation* 75 (2), 331–339. doi:10.1161/01.cir.75.2.331

Fitzgerald, L. W., Burn, T. C., Brown, B. S., Patterson, J. P., Corjay, M. H., Valentine, P. A., et al. (2000). Possible role of valvular serotonin 5-HT(2B) receptors in the cardiopathy associated with fenfluramine. *Mol. Pharmacol.* 57 (1), 75–81.

Forsström, T., Tuominen, J., and Karkkäinen, J. (2001). Determination of potentially hallucinogenic N-dimethylated indoleamines in human urine by HPLC/ESI-MS-MS. *Scand. J. Clin. Lab. Invest.* 61 (7), 547–556. doi:10.1080/00365510175321831 9

Fozard, J. R., and Ali, A. T. (1978). Receptors for 5-hydroxytryptamine on the sympathetic nerves of the rabbit heart. *Naunyn Schmiedeb. Arch. Pharmacol.* 301 (3), 223–235. doi:10.1007/BF00507041

Fricke, J., Blei, F., and Hoffmeister, D. (2017). Enzymatic synthesis of psilocybin. *Angew. Chem. Int. Ed. Engl.* 56 (40), 12352–12355. doi:10.1002/anie.201705489

Gable, R. S. (2007). Risk assessment of ritual use of oral dimethyltryptamine (DMT) and harmala alkaloids. *Addiction* 102 (1), 24–34. doi:10.1111/j.1360-0443.2006.01652.x

Geiger, H. A., Wurst, M. G., and Daniels, R. N. (2018). DARK classics in chemical neuroscience: psilocybin. *ACS Chem. Neurosci.* 9 (10), 2438–2447. doi:10.1021/acschemneuro.8b00186

Gergs, U., Baumann, M., Böckler, A., Buchwalow, I. B., Ebelt, H., Fabritz, L., et al. (2010). Cardiac overexpression of the human 5-HT4-receptor in mice. *Am. J. Physiol. Heart Circ. Physiol.* 299 (3), H788–H798. doi:10.1152/ajpheart.00691.2009

Gergs, U., Bernhardt, G., Buchwalow, I. B., Edler, H., Fröba, J., Keller, M., et al. (2019). Initial characterization of transgenic mice overexpressing human histamine H2 receptors. *J. Pharmacol. Exp. Ther.* 369, 129–141. doi:10.1124/jpet.118.255711

Gergs, U., Böckler, A., Ebelt, H., Hauptmann, S., Keller, N., Otto, V., et al. (2013). Human 5-HT$_4$receptor stimulation in atria of transgenic mice. *Naunyn Schmiedeb. Arch. Pharmacol.* 386 (5), 357–367. doi:10.1007/s00210-013-0831-x

Gergs, U., Jacob, H., Braekow, P., Hofmann, B., Pockes, S., Humphrys, L. J., et al. (2023). Lysergic acid diethylamide stimulates cardiac human H_2-histamine receptors and cardiac human 5-HT_4 serotonin receptors. *Schmiedeb. Arch. Pharmacol.* 397, 221–236. doi:10.1007/s00210-023-02591-6

Gergs, U., Kirchhefer, U., Bergmann, F., Künstler, B., Mißlinger, N., Au, B., et al. (2020). Characterization of stressed transgenic mice overexpressing H2-histamine receptors in the heart. *J. Pharmacol. Exp. Ther.* 374 (3), 479–488. doi:10.1124/jpet.120.000063

Gergs, U., Weisgut, J., Griethe, K., Mißlinger, N., Kirchhefer, U., and Neumann, J. (2021). Human histamine H2 receptors can initiate cardiac arrhythmias in a transgenic mouse. *Naunyn Schmiedeb. Arch. Pharmacol.* 394 (9), 1963–1973. doi:10.1007/s00210-021-02098-y

Good, M., Joel, Z., Benway, T., Routledge, C., Timmermann, C., Erritzoe, D., et al. (2023). Pharmacokinetics of N,N-dimethyltryptamine in humans. *Eur. J. Drug Metab. Pharmacokinet.* 48 (3), 311–327. doi:10.1007/s13318-023-00822-y

Green, J. P., Johnson, C. L., Weinstein, H., and Maayani, S. (1977). Antagonism of histamine-activated adenylate cyclase in brain by D-lysergic acid diethylamide. *Proc. Natl. Acad. Sci. U. S. A.* 74 (12), 5697–5701. doi:10.1073/pnas.74.12.5697

Grzybowski, A., Pawlikowska-Łagód, K., and Polak, A. (2021). Ergotism and saint anthony's fire. *Clin. Dermatol* 39 (6), 1088–1094. doi:10.1016/j.clindermatol.2021.07.009

Gulbranson, S. H., Mock, R. E., and Wolfrey, J. D. (2002). Possible ergotamine-caffeine-associated delirium. *Pharmacotherapy* 22 (1), 126–129. doi:10.1592/phco.22.1.126.33500

Halberstadt, A. L., and Geyer, M. A. (2011). Multiple receptors contribute to the behavioral effects of indoleamine hallucinogens. *Neuropharmacology* 61 (3), 364–381. doi:10.1016/j.neuropharm.2011.01.017

Hamstra, S. I., Whitley, K. C., Baranowski, R. W., Kurgan, N., Braun, J. L., Messner, H. N., et al. (2020). The role of phospholamban and GSK3 in regulating rodent cardiac SERCA function. *Am. J. Physiol. Cell Physiol.* 319 (4), C694–C699. doi:10.1152/ajpcell.00318.2020

Handovsky, H. (1920). Ein Alkaloid im Gifte von Bufo vulgaris. *Arch. F. Exp. Pathol. U. Pharmakol.* 86, 138–158. doi:10.1007/BF01864237

Hasler, F., Bourquin, D., Brenneisen, R., Bär, T., and Vollenweider, F. X. (1997). Determination of psilocin and 4-hydroxyindole-3-acetic acid in plasma by HPLC-ECD and pharmacokinetic profiles of oral and intravenous psilocybin in man. *Pharm. Acta Helv.* 72 (3), 175–184. doi:10.1016/s0031-6865(97)00014-9

Hasler, F., Grimberg, U., Benz, M. A., Huber, T., and Vollenweider, F. X. (2004). Acute psychological and physiological effects of psilocybin in healthy humans: a double-blind, placebo-controlled dose-effect study. *Psychopharmacol. Berl.* 172 (2), 145–156. doi:10.1007/s00213-003-1640-6

Hesselgrave, N., Troppoli, T. A., Wulff, A. B., Cole, A. B., and Thompson, S. M. (2021). Harnessing psilocybin: antidepressant-like behavioral and synaptic actions of psilocybin are independent of 5-HT2R activation in mice. *Proc. Natl. Acad. Sci. U. S. A.* 118 (17), e2022489118. doi:10.1073/pnas.2022489118

Higgins, T. J., Bailey, P. J., and Allsopp, D. (1981). Mechanism of stimulation of cardiac myocyte beating rate by 5-hydroxytryptamine. *Life Sci.* 28 (9), 999–1005. doi:10.1016/0024-3205(81)90745-1

Hofmann, A., Heim, R., Brack, A., and Kobel, H. (1958). Psilocybin, ein psychotroper Wirkstoff aus dem mexikanischen Rauschpilz Psilocybe mexicana Heim. *Experientia* 14, 107–109. doi:10.1007/BF02159243

Hofmann, A., Heim, R., Brack, A., Kobel, H., Frey, A., Ott, H., et al. (1959). Psilocybin und Psilocin, zwei psychotrope Wirkstoffe aus mexikanischen Rauschpilzen. *Helvetica Chim. Acta* 42, 1557–1572. doi:10.1002/hlca.19590420518

Hollingsworth, M., Edwards, D., and Miller, M. (1988). Ergometrine--a partial agonist at 5-HT receptors in the uterus isolated from the oestrogen-primed rat. *Eur. J. Pharmacol.* 158 (1-2), 79–84. doi:10.1016/0014-2999(88)90255-5

Holze, F., Ley, L., Müller, F., Becker, A. M., Straumann, I., Vizeli, P., et al. (2022). Direct comparison of the acute effects of lysergic acid diethylamide and psilocybin in a double-blind placebo-controlled study in healthy subjects. *Neuropsychopharmacology* 47 (6), 1180–1187. doi:10.1038/s41386-022-01297-2

Holze, F., Vizeli, P., Müller, F., Ley, L., Duerig, R., Varghese, N., et al. (2020). Distinct acute effects of LSD, MDMA, and D-amphetamine in healthy subjects. *Neuropsychopharmacology* 45 (3), 462–471. doi:10.1038/s41386-019-0569-3

Horita, A. (1963). Some biochemical studies on psilocybin and psilogin. *J. Neuropsychiatr.* 4, 270–273.

Horita, A., and Weber, L. J. (1962). Dephosphorylation of psilocybin in the intact mouse. *Toxicol. Appl. Pharmacol.* 4, 730–737. doi:10.1016/0041-008x(62)90102-3

Hoshino, T., and Shimodaira, K. (1935). Synthese des Bufotenins und über 3-Methyl-3-β-oxyäthyl-indolenin. Synthesen in der Indol-Gruppe. XIV. *Justus Liebigs Ann. Chem.* 520 (1), 19–30. doi:10.1002/jlac.19355200104

Huybrechts, B., Malysheva, S. V., and Masquelier, J. (2021). A targeted UHPLC-MS/MS method validated for the quantification of ergot alkaloids in cereal-based baby food from the Belgian market. *Toxins (Basel)* 13 (8), 531. doi:10.3390/toxins13080531

Jacob, H., Braekow, P., Hofmann, B., Kirchhefer, U., Forster, L., Mönnich, D., et al. (2023a). Ergometrine stimulates histamine H2 receptors in the isolated human atrium. *Naunyn Schmiedeb. Arch. Pharmacol.* 396 (12), 3809–3822. doi:10.1007/s00210-023-02573-8

Jacob, H., Braekow, P., Schwarz, R., Höhm, C., Kirchhefer, U., Hofmann, B., et al. (2023b). Ergotamine stimulates human 5-HT4-serotonin receptors and human H2-histamine receptors in the heart. *Int. J. Mol. Sci.* 24, 4749. doi:10.3390/ijms24054749

Jacob, H., Gergs, U., Hofmann, B., and Neumann, J. (2024). Lysergic acid diethylamide (LSD) has β-anti-adrenergic effects in the isolated human atrium. *Schmiedeb. Arch. Pharmacol.* (Abstract, in press).

Jamieson, C. S., Misa, J., Tang, Y., and Billingsley, J. M. (2021). Biosynthesis and synthetic biology of psychoactive natural products. *Chem. Soc. Rev.* 50 (12), 6950–7008. doi:10.1039/d1cs00065a

Kaelen, M., Roseman, L., Kahan, J., Santos-Ribeiro, A., Orban, C., Lorenz, R., et al. (2016). LSD modulates music-induced imagery via changes in parahippocampal connectivity. *Eur. Neuropsychopharmacol.* 26 (7), 1099–1109. doi:10.1016/j.euroneuro.2016.03.018

Kalberer, F., Kreis, W., and Rutschmann, J. (1962). The fate of psilocin in the rat. *Biochem. Pharmacol.* 11, 261–269. doi:10.1016/0006-2952(62)90050-3

Kalkman, H. O., Van Gelderen, E. M., Timmermans, P. B., and Van Zwieten, P. A. (1982). Involvement of alpha 1- and alpha 2-adrenoceptors in the vasoconstriction caused by ergometrine. *Eur. J. Pharmacol.* 78 (1), 107–111. doi:10.1016/0014-2999(82)90377-6

Kamel, R., Leroy, J., Vandecasteele, G., and Fischmeister, R. (2023). Cyclic nucleotide phosphodiesterases as therapeutic targets in cardiac hypertrophy and heart failure. *Nat. Rev. Cardiol.* 20 (2), 90–108. doi:10.1038/s41569-022-00756-z

Kärkkäinen, J., Forsström, T., Tornaeus, J., Wähälä, K., Kiuru, P., Honkanen, A., et al. (2005). Potentially hallucinogenic 5-hydroxytryptamine receptor ligands bufotenine and dimethyltryptamine in blood and tissues. *Scand. J. Clin. Lab. Invest.* 65 (3), 189–199. doi:10.1080/00365510510013604

Kaumann, A. J. (1990). Piglet sinoatrial 5-HT receptors resemble human atrial 5-HT4-like receptors. *Naunyn Schmiedebergs Arch. Pharmacol.* 342 (5), 619–622. doi:10.1007/BF00169055

Kaumann, A. J., Frenken, M., Posival, H., and Brown, A. M. (1994). Variable participation of 5-HT1-like receptors and 5-HT2 receptors in serotonin-induced contraction of human isolated coronary arteries. 5-HT1-like receptors resemble cloned 5-HT1D beta receptors. *Circulation* 90 (3), 1141–1153. doi:10.1161/01.cir.90.3.1141

Kaumann, A. J., and Levy, F. O. (2006). 5-hydroxytryptamine receptors in the human cardiovascular system. *Pharmacol. Ther.* 111 (3), 674–706. doi:10.1016/j.pharmthera.2005.12.004

Kaumann, A. J., Sanders, L., Brown, A. M., Murray, K. J., and Brown, M. J. (1990). A 5-hydroxytryptamine receptor in human atrium. *Br. J. Pharmacol.* 100 (4), 879–885. doi:10.1111/j.1476-5381.1990.tb14108.x

Kjekshus, J. K., Torp-Pedersen, C., Gullestad, L., Køber, L., Edvardsen, T., Olsen, I. C., et al. (2009). Effect of piboserod, a 5-HT4-serotonin receptor antagonist, on left ventricular function in patients with symptomatic heart failure. *Eur. J. Heart Fail* 11 (8), 771–778. doi:10.1093/eurjhf/hfp087

Klinke, H. B., Müller, I. B., Steffenrud, S., and Dahl-Sørensen, R. (2010). Two cases of lysergamide intoxication by ingestion of seeds from Hawaiian Baby Woodrose. *Forensic Sci. Int.* 197 (1-3), e1–e5. doi:10.1016/j.forsciint.2009.11.017

Koizumi, T., Yokoyama, M., Namikawa, S., Kuriyama, N., Nameki, M., Nakayama, T., et al. (2006). Location of focal vasospasm provoked by ergonovine maleate within coronary arteries in patients with vasospastic angina pectoris. *Am. J. Cardiol.* 97 (9), 1322–1325. doi:10.1016/j.amjcard.2005.11.073

Läer, S., Remmers, F., Scholz, H., Stein, B., Müller, F. U., and Neumann, J. (1998). Receptor mechanisms involved in the 5-HT-induced inotropic action in the rat isolated atrium. *Br. J. Pharmacol.* 123 (6), 1182–1188. doi:10.1038/sj.bjp.0701702

Laher, I., and McNeill, J. H. (1980). Effects of histamine in the isolated kitten heart. *Can. J. Physiol. Pharmacol.* 58 (11), 1256–1261. doi:10.1139/y80-192

Leary, T., Litwin, G. H., and Metzner, R. (1963). Reactions to psilocybin administered in a supportive environment. *J. Nerv. Ment. Dis.* 137, 561–573. doi:10.1097/00005053-196312000-00007

Ledwos, N., Rosenblat, J. D., Blumberger, D. M., Castle, D. J., McIntyre, R. S., Mulsant, B. H., et al. (2022). A critical appraisal of evidence on the efficacy and safety of serotonergic psychedelic drugs as emerging antidepressants: mind the evidence gap. *J. Clin. Psychopharmacol.* 42 (6), 581–588. doi:10.1097/JCP.0000000000001608

Lewis, V., Bonniwell, E. M., Lanham, J. K., Ghaffari, A., Sheshbaradaran, H., Cao, A. B., et al. (2023). A non-hallucinogenic LSD analog with therapeutic potential for mood disorders. *Cell Rep.* 42 (3), 112203. doi:10.1016/j.celrep.2023.112203

Ley, L., Holze, F., Arikci, D., Becker, A. M., Straumann, I., Klaiber, A., et al. (2023). Comparative acute effects of mescaline, lysergic acid diethylamide, and psilocybin in a randomized, double-blind, placebo-controlled cross-over study in healthy participants. *Neuropsychopharmacology* 48 (11), 1659–1667. doi:10.1038/s41386-023-01607-2

Li, C., Tang, M. H. Y., Chong, Y. K., Chan, T. Y. C., and Mak, T. W. L. (2019). Lysergic acid diethylamide-associated intoxication in Hong Kong: a case series. *Hong Kong Med. J.* 25 (4), 323–325. doi:10.12809/hkmj197942

Liakoni, E., Dolder, P. C., Rentsch, K., and Liechti, M. E. (2015). Acute health problems due to recreational drug use in patients presenting to an urban emergency department in Switzerland. *Swiss Med. Wkly.* 145, w14166. doi:10.4414/smw.2015.14166

Liechti, M. E. (2017). Modern clinical research on LSD. *Neuropsychopharmacology* 42, 2114–2127. doi:10.1038/npp.2017.86

Liegl, C. A., and McGrath, M. A. (2016). Ergotism: case report and review of the literature. *Int. J. Angiol.* 25 (5), e8–e11. doi:10.1055/s-0034-1376397

Lim, T. H., Wasywich, C. A., and Ruygrok, P. N. (2012). A fatal case of 'magic mushroom' ingestion in a heart transplant recipient. *Intern Med. J.* 42 (11), 1268–1269. doi:10.1111/j.1445-5994.2012.02955.x

Madsen, M. K., Fisher, P. M., Burmester, D., Dyssegaard, A., Stenbæk, D. S., Kristiansen, S., et al. (2019). Psychedelic effects of psilocybin correlate with serotonin 2A receptor occupancy and plasma psilocin levels. *Neuropsychopharmacology* 44 (7), 1328–1334. doi:10.1038/s41386-019-0324-9

Manske, R. H. F. (1931). A synthesis of the methyltryptamines and some derivatives. *Can. J. Res.* 5, 592–600. doi:10.1139/cjr31-097

Mardal, M., Johansen, S. S., Thomsen, R., and Linnet, K. (2017). Advantages of analyzing postmortem brain samples in routine forensic drug screening-Case series of three non-natural deaths tested positive for lysergic acid diethylamide (LSD). *Forensic Sci. Int.* 278, e14–e18. doi:10.1016/j.forsciint.2017.07.025

Matsuda, N., Jesmin, S., Takahashi, Y., Hatta, E., Kobayashi, M., Matsuyama, K., et al. (2004). Histamine H1 and H2 receptor gene and protein levels are differentially expressed in the hearts of rodents and humans. *J. Pharmacol. Exp. Ther.* 309 (2), 786–795. doi:10.1124/jpet.103.063065

McCarron, M. M., Walberg, C. B., and Baselt, R. C. (1990). Confirmation of LSD intoxication by analysis of serum and urine. *J. Anal. Toxicol.* 14 (3), 165–167. doi:10.1093/jat/14.3.165

McFadden, E. P., Clarke, J. G., Davies, G. J., Kaski, J. C., Haider, A. W., and Maseri, A. (1991). Effect of intracoronary serotonin on coronary vessels in patients with stable angina and patients with variant angina. *N. Engl. J. Med.* 324 (10), 648–654. doi:10.1056/NEJM199103073241002

McIntyre, R. S. (2023). Serotonin 5-HT_{2B} receptor agonism and valvular heart disease: implications for the development of psilocybin and related agents. *Expert Opin. Drug Saf.* 22 (10), 881–883. doi:10.1080/14740338.2023.2248883

McKenna, D. J., Repke, D. B., Lo, L., and Peroutka, S. J. (1990). Differential interactions of indolealkylamines with 5-hydroxytryptamine receptor subtypes. *Neuropharmacology* 29 (3), 193–198. doi:10.1016/0028-3908(90)90001-8

McKenna, D. J., Towers, G. H., and Abbott, F. (1984a). Monoamine oxidase inhibitors in South American hallucinogenic plants: tryptamine and beta-carboline constituents of ayahuasca. *J. Ethnopharmacol.* 10 (2), 195–223. doi:10.1016/0378-8741(84)90003-5

McKenna, D. J., Towers, G. H., and Abbott, F. S. (1984b). Monoamine oxidase inhibitors in South American hallucinogenic plants Part 2: constituents of orally-active Myristicaceous hallucinogens. *J. Ethnopharmacol.* 12 (2), 179–211. doi:10.1016/0378-8741(84)90048-5

Medhurst, A. D., and Kaumann, A. J. (1993). Characterization of the 5-HT4 receptor mediating tachycardia in piglet isolated right atrium. *Br. J. Pharmacol.* 110 (3), 1023–1030. doi:10.1111/j.1476-5381.1993.tb13916.x

Meneghetti, F., Ferraboschi, P., Grisenti, P., Reza Elahi, S., Mori, M., and Ciceri, S. (2020). Crystallographic and NMR investigation of ergometrine and methylergometrine, two alkaloids from Claviceps purpurea. *Molecules* 25 (2), 331. doi:10.3390/molecules25020331

Mohamedi, N., Mirault, T., Durivage, A., Di Primio, M., Khider, L., Detriche, G., et al. (2021). Ergotism with acute limb ischemia, provoked by HIV protease inhibitors interaction with ergotamine, rescued by multisite transluminal balloon angioplasty. *J. Med. Vasc.* 46 (1), 13–21. doi:10.1016/j.jdmv.2020.12.002

Moretti, C., Gaillard, Y., Grenand, P., Bévalot, F., and Prévosto, J. M. (2006). Identification of 5-hydroxy-tryptamine (bufotenine) in takini (Brosimumacutifolium Huber subsp. acutifolium C.C. Berg, Moraceae), a shamanic potion used in the Guiana Plateau. *J. Ethnopharmacol.* 106 (2), 198–202. doi:10.1016/j.jep.2005.12.022

Neumann, J., Hofmann, B., and Gergs, U. (2017). "Production and function of serotonin in cardiac cells," in *Serotonin - a chemical messenger between all types of living cells chapter 13*. Editor S. Kaneez Fatima, 271–305.

Neumann, J., Käufler, B., and Gergs, U. (2019). Which phosphodiesterase can decrease cardiac effects of 5-HT4 receptor activation in transgenic mice? *Naunyn Schmiedeb. Arch. Pharmacol.* 392 (8), 991–1004. doi:10.1007/s00210-019-01653-y

Neumann, J., Kirchhefer, U., Dhein, S., Hofmann, B., and Gergs, U. (2021a). Role of cardiovascular H_2-histamine receptors under normal and pathophysiological conditions. *Front. Pharmacol.* 12, 732842. doi:10.3389/fphar.2021.732842

Neumann, J., Voss, R., Laufs, U., Werner, C., and Gergs, U. (2021b). Phosphodiesterases 2, 3 and 4 can decrease cardiac effects of H2-histamine-receptor activation in isolated atria of transgenic mice. *Naunyn Schmiedeb. Arch. Pharmacol.* 394 (6), 1215–1229. doi:10.1007/s00210-021-02052-y

Neumann, J., Binter, M. B., Fehse, C., Marušáková, M., Büxel, M. L., Kirchhefer, U., et al. (2021c). Amitriptyline functionally antagonizes cardiac H_2 histamine receptors in transgenic mice and human atria. *Naunyn Schmiedeb. Arch. Pharmacol.* 394 (6), 1251–1262. doi:10.1007/s00210-021-02065-7

Neumann, J., Grobe, J. M., Weisgut, J., Schwelberger, H. G., Fogel, W. A., Marušáková, M., et al. (2021d). Histamine can be formed and degraded in the human and mouse heart. *Front. Pharmacol.* 12, 582916. doi:10.3389/fphar.2021.582916

Neumann, J., Schwarzer, D., Fehse, C., Schwarz, R., Marusakova, M., Kirchhefer, U., et al. (2021e). Functional interaction of H2-receptors and 5HT4-receptors in atrial tissues isolated from double transgenic mice and from human patients. *Naunyn Schmiedeb. Arch. Pharmacol.* 394 (12), 2401–2418. doi:10.1007/s00210-021-02145-8

Neumann, J., Seidler, T., Fehse, C., Marušáková, M., Hofmann, B., and Gergs, U. (2021f). Cardiovascular effects of metoclopramide and domperidone on human 5-HT4-serotonin-receptors in transgenic mice and in human atrial preparations. *Eur. J. Pharmacol.* 901, 174074. doi:10.1016/j.ejphar.2021.174074

Neumann, J., Kirchhefer, U., Dhein, S., Hofmann, B., and Gergs, U. (2022). "Cardiac role of histamine and histamine receptors," in *Horizons in world cardiovascular research 22* (New York, United States: Nova Science Publishers). doi:10.52305/VGWV3099

Neumann, J., Hofmann, B., Dhein, S., and Gergs, U. (2023a). Cardiac roles of serotonin (5-HT) and 5-HT-receptors in health and disease. *Int. J. Mol. Sci.* 24 (5), 4765. doi:10.3390/ijms24054765

Neumann, J., Hofmann, B., Dhein, S., and Gergs, U. (2023b). Role of Dopamine in the Heart in Health and Disease. *Int. J. Mol. Sci.* 24 (5), 5042. doi:10.3390/ijms24055042

Neumann, J., Hofmann, B., Kirchhefer, U., Dhein, S., and Gergs, U. (2023c). Function and role of histamine H1 receptor in the mammalian heart. *Pharm. (Basel)* 16 (5), 734. doi:10.3390/ph16050734

Neumann, J., Hußler, W., Azatsian, K., Hofmann, B., and Gergs, U. (2023d). Methamphetamine increases force of contraction in isolated human atrial preparations through the release of noradrenaline. *Toxicol. Lett.* 383, 112–120. doi:10.1016/j.toxlet.2023.06.012

Neumann, J., Hußler, W., Hofmann, B., and Gergs, U. (2023e). Contractile effects of amphetamine, pseudoephedrine, nor-pseudoephedrine (cathine) and cathinone on atrial preparations of mice and humans. *J. Cardiovasc Pharmacol.* (in press). doi:10.1097/FJC.0000000000001536

Neumann, J., Schulz, N., Fehse, C., Azatsian, K., Čináková, A., Marušáková, M., et al. (2023f). Cardiovascular effects of bufotenin on human 5-HT4 serotonin receptors in cardiac preparations of transgenic mice and in human atrial preparations. *Naunyn Schmiedeb. Arch. Pharmacol.* 396 (7), 1471–1485. doi:10.1007/s00210-023-02414-8

Nichols, D. E. (2018). Dark classics in chemical neuroscience: lysergic acid diethylamide (LSD). *ACS Chem. Neurosci.* 9 (10), 2331–2343. doi:10.1021/acschemneuro.8b00043

Nichols, D. E. (2020). Psilocybin: from ancient magic to modern medicine. *J. Antibiot. (Tokyo)* 73 (10), 679–686. doi:10.1038/s41429-020-0311-8

Nilsson, T., Longmore, J., Shaw, D., Pantev, E., Bard, J. A., Branchek, T., et al. (1999). Characterisation of 5-HT receptors in human coronary arteries by molecular and pharmacological techniques. *Eur. J. Pharmacol.* 372 (1), 49–56. doi:10.1016/s0014-2999(99)00114-4

Ott, J. (1999). Pharmahuasca: human pharmacology of oral DMT plus harmine. *J. Psychoact. Drugs* 31 (2), 171–177. doi:10.1080/02791072.1999.10471741

Ott, J. (2001). Pharmañopo-psychonautics: human intranasal, sublingual, intrarectal, pulmonary and oral pharmacology of bufotenine. *J. Psychoact. Drugs* 33 (3), 273–281. doi:10.1080/02791072.2001.10400574

Ott, J., and Neely, P. (1980). Entheogenic (hallucinogenic) effects of methylergonovine. *J. Psychedelic Drugs* 12 (2), 165–166. doi:10.1080/02791072.1980.10471568

Passie, T., Halpern, J. H., Stichtenoth, D. O., Emrich, H. M., and Hintzen, A. (2008). The pharmacology of lysergic acid diethylamide: a review. *CNS Neurosci. Ther.* 14 (4), 295–314. doi:10.1111/j.1755-5949.2008.00059.x

Picard, F., Sayah, N., Spagnoli, V., Adjedj, J., and Varenne, O. (2019). Vasospastic angina: a literature review of current evidence. *Arch. Cardiovasc Dis.* 112 (1), 44–55. doi:10.1016/j.acvd.2018.08.002

Plotkin, M. J., and Schultes, R. E. (1990). Virola: a promising genus for ethnopharmacological investigation. *J. Psychoact. Drugs* 22 (3), 357–361. doi:10.1080/02791072.1990.10472561

Poulie, C. B. M., Jensen, A. A., Halberstadt, A. L., and Kristensen, J. L. (2019). DARK classics in chemical neuroscience: NBOMes. *ACS Chem. Neurosci.* 11, 3860–3869. doi:10.1021/acschemneuro.9b00528

Preller, K. H., Herdener, M., Pokorny, T., Planzer, A., Kraehenmann, R., Stämpfli, P., et al. (2017). The fabric of meaning and subjective effects in LSD-induced states depend on serotonin 2A receptor activation. *Curr. Biol.* 27 (3), 451–457. doi:10.1016/j.cub.2016.12.030

Rabinowitz, B., Chuck, L., Kligerman, M., and Parmley, W. W. (1975). Positive inotropic effects of methoxamine: evidence for alpha-adrenergic receptors in ventricular myocardium. *Am. J. Physiol.* 229 (3), 582–585. doi:10.1152/ajplegacy.1975.229.3.582

Rätsch, C. (2015). *Enzyklopädie der psychoaktiven Substanzen*. 12. Aarau, Switzerland: AT Verlag.

Reckweg, J., Mason, N. L., van Leeuwen, C., Toennes, S. W., Terwey, T. H., Ramaekers, J. G., et al. (2021). A phase 1, dose-ranging study to assess safety and psychoactive effects of a vaporized 5-methoxy-N, N-dimethyltryptamine formulation (GH001) in healthy volunteers. *Front. Pharmacol.* 12, 760671. doi:10.3389/fphar.2021.760671

Riba, J., McIlhenny, E. H., Bouso, J. C., and Barker, S. A. (2015). Metabolism and urinary disposition of N,N-dimethyltryptamine after oral and smoked administration: a comparative study. *Drug Test. Anal.* 7 (5), 401–406. doi:10.1002/dta.1685

Rickli, A., Moning, O. D., Hoener, M. C., and Liechti, M. E. (2016). Receptor interaction profiles of novel psychoactive tryptamines compared with classic hallucinogens. *Eur. Neuropsychopharmacol.* 26 (8), 1327–1337. doi:10.1016/j.euroneuro.2016.05.001

Romagnoli, E., Niccoli, G., and Crea, F. (2005). Images in cardiology: a coronary organic stenosis distal to severe, ergonovine induced spasm: decision making. *Heart* 91 (10), 1310. doi:10.1136/hrt.2004.058560

Ross, S., Bossis, A., Guss, J., Agin-Liebes, G., Malone, T., Cohen, B., et al. (2016). Rapid and sustained symptom reduction following psilocybin treatment for anxiety and depression in patients with life-threatening cancer: a randomized controlled trial. *J. Psychopharmacol.* 30 (12), 1165–1180. doi:10.1177/0269881116675512

Roth, B. L., Baner, K., Westkaemper, R., Siebert, D., Rice, K. C., Steinberg, S., et al. (2002). Salvinorin A: a potent naturally occurring nonnitrogenous kappa opioid selective agonist. *Proc. Natl. Acad. Sci. U. S. A.* 99 (18), 11934–11939. doi:10.1073/pnas.182234399

Rudin, D., McCorvy, J. D., Glatfelter, G. C., Luethi, D., Szöllősi, D., Ljubišić, T., et al. (2022). (2-Aminopropyl)benzo[β]thiophenes (APBTs) are novel monoamine transporter ligands that lack stimulant effects but display psychedelic-like activity in mice. *Neuropsychopharmacology* 47 (4), 914–923. doi:10.1038/s41386-021-01221-0

Sakai, K., and Akima, M. (1979). An analysis of the stimulant effects of 5-hydroxytryptamine on isolated, blood-perfused rat heart. *Eur. J. Pharmacol.* 55 (4), 421–424. doi:10.1016/0014-2999(79)90119-5

Sanders, S. W., Haering, N., Mosberg, H., and Jaeger, H. (1986). Pharmacokinetics of ergotamine in healthy volunteers following oral and rectal dosing. *Eur. J. Clin. Pharmacol.* 30 (3), 331–334. doi:10.1007/BF00541538

Shen, H. W., Jiang, X. L., Winter, J. C., and Yu, A. M. (2010). Psychedelic 5-methoxy-N,N-dimethyltryptamine: metabolism, pharmacokinetics, drug interactions, and pharmacological actions. *Curr. Drug Metab.* 11 (8), 659–666. doi:10.2174/138920010794233495

Siegel, D. M., and McDaniel, S. H. (1991). The frog prince: tale and toxicology. *Am. J. Orthopsychiatry* 61 (4), 558–562. doi:10.1037/h0079283

Silberstein, S. D., and McCrory, D. C. (2003). Ergotamine and dihydroergotamine: history, pharmacology, and efficacy. *Headache* 43 (2), 144–166. doi:10.1046/j.1526-4610.2003.03034.x

Sklerov, J., Levine, B., Moore, K. A., King, T., and Fowler, D. (2005). A fatal intoxication following the ingestion of 5-methoxy-N,N-dimethyltryptamine in an ayahuasca preparation. *J. Anal. Toxicol.* 29 (8), 838–841. doi:10.1093/jat/29.8.838

Stange, K., Pohlmeier, H., Lübbesmeyer, A., Gumbinger, G., Schmitz, W., and Baumgart, P. (1998). Vascular ergotism through inhalation of grain dust. *Dtsch. Med. Wochenschr* 123 (51-52), 1547–1550. doi:10.1055/s-2007-1024221

Stoll, A. (1936). The new ergot alkaloid. *Science* 82, 415–417. doi:10.1126/science.82.2131.415-b

Stoll, A., and Burckhardt, E. (1935). L'ergobasine, un nouvel alcoloíde de l´ergot de seigle, soluble dans l'eau (The new water-soluble ergotalkaloid, ergobasine). *Bull. Sei Pharm.* 42, 257–266.

Strassman, R. J., and Qualls, C. R. (1994). Dose-response study of N,N-dimethyltryptamine in humans. I. Neuroendocrine, autonomic, and cardiovascular effects. *Arch. Gen. Psychiatry* 51 (2), 85–97. doi:10.1001/archpsyc.1994.03950020009001

Studerus, E., Kometer, M., Hasler, F., and Vollenweider, F. X. (2011). Acute, subacute and long-term subjective effects of psilocybin in healthy humans: a pooled analysis of experimental studies. *J. Psychopharmacol.* 25 (11), 1434–1452. doi:10.1177/0269881110382466

Sueda, S., Kohno, H., Ochi, T., Uraoka, T., and Tsunemitsu, K. (2017). Overview of the pharmacological spasm provocation test: comparisons between acetylcholine and ergonovine. *J. Cardiol.* 69 (1), 57–65. doi:10.1016/j.jjcc.2016.09.012

Szára, S. (1956). Dimethyltryptamin: its metabolism in man; the relation to its psychotic effect to the serotonin metabolism. *Experientia* 12 (11), 441–442. doi:10.1007/BF02157378

Tada, M., Kirchberger, M. A., and Katz, A. M. (1976). Regulation of calcium transport in cardiac sarcoplasmic reticulum by cyclic AMP-dependent protein kinase. *Recent Adv. Stud. Card. Struct. Metab.* 9, 225–239.

Tagen, M., Mantuani, D., van Heerden, L., Holstein, A., Klumpers, L. E., and Knowles, R. (2023). The risk of chronic psychedelic and MDMA microdosing for valvular heart disease. *J. Psychopharmacol.* 37 (9), 876–890. doi:10.1177/02698811231190865

Thompson, M. R. (1935). The active constituents of ergot. A pharmacological and chemical study. *J. Am. Pharm. Assoc.* 24, 24–38. doi:10.1002/jps.3080240111

Thoren, F. B., Aurelius, J., and Martner, A. (2011). Antitumor properties of histamine *in vivo*. *Nat. Med.* 17 (5), 537–538. author reply 537-8. doi:10.1038/nm0511-537a

Titeler, M., Lyon, R. A., and Glennon, R. A. (1988). Radioligand binding evidence implicates the brain 5-HT2 receptor as a site of action for LSD and phenylisopropylamine hallucinogens. *Psychopharmacol. Berl.* 94 (2), 213–216. doi:10.1007/BF00176847

Torres, A., Davila, D. F., Gottberg, C. F., Donis, J. H., Holzaker, G., Ramoni-Perazzi, P., et al. (1996). Heart rate responses to intravenous serotonin in rats with acute chagasic myocarditis. *Braz J. Med. Biol. Res.* 29 (6), 817–822.

Trendelenburg, U. (1960). The action of histamine and 5-hydroxytryptamine on isolated mammalian atria. *J. Pharmacol. Exp. Ther.* 130, 450–460. PMID: 13777992.

Uthaug, M. V., Lancelotta, R., van Oorsouw, K., Kuypers, K. P. C., Mason, N., Rak, J., et al. (2019). A single inhalation of vapor from dried toad secretion containing 5-methoxy-N,N-dimethyltryptamine (5-MeO-DMT) in a naturalistic setting is related to sustained enhancement of satisfaction with life, mindfulness-related capacities, and a decrement of psychopathological symptoms. *Psychopharmacol. Berl.* 236 (9), 2653–2666. doi:10.1007/s00213-019-05236-w

van den Broek, R. W., Bhalla, P., VanDenBrink, A. M., de Vries, R., Sharma, H. S., and Saxena, P. R. (2002). Characterization of sumatriptan-induced contractions in human isolated blood vessels using selective 5-HT(1B) and 5-HT(1D) receptor antagonists and *in situ* hybridization. *Cephalalgia* 22 (2), 83–93. doi:10.1046/j.1468-2982.2002.00295.x

Villalón, C. M., den Boer, M. O., Heiligers, J. P., and Saxena, P. R. (1990). Mediation of 5-hydroxytryptamine-induced tachycardia in the pig by the putative 5-HT4 receptor. *Br. J. Pharmacol.* 100 (4), 665–667. doi:10.1111/j.1476-5381.1990.tb14073.x

Wacker, D., Wang, S., McCorvy, J. D., Betz, R. M., Venkatakrishnan, A. J., Levit, A., et al. (2017). Crystal structure of an LSD-bound human serotonin receptor. *Cell* 168 (3), 377–389. e12. doi:10.1016/j.cell.2016.12.033

Wieland, H., Konz, W., and Mittasch, H. (1934). Die Konstitution von Bufotenin und Bufotenidin. *Über Giftst. VII. Justus Liebigs Ann. Chem.* 513, 1–15. doi:10.1002/jlac.19345130102

Winstock, A. R., Kaar, S., and Borschmann, R. (2014). Dimethyltryptamine (DMT): prevalence, user characteristics and abuse liability in a large global sample. *J. Psychopharmacol.* 28 (1), 49–54. doi:10.1177/0269881113513852

Wolf, H. (2000). Preclinical and clinical pharmacology of the 5-HT3 receptor antagonists. *Scand. J. Rheumatol. Suppl.* 113, 37–45. doi:10.1080/030097400446625

World Health Organization (2021). *World Health Organization model list of essential medicines: 22nd list*. Geneva: World Health Organization. hdl:10665/345533. WHO/MHP/HPS/EML/2021.02.

frontiers | Frontiers in Pharmacology

TYPE Review
PUBLISHED 01 March 2024
DOI 10.3389/fphar.2024.1336102

OPEN ACCESS

EDITED BY
Yan Sanders,
Eastern Virginia Medical School, United States

REVIEWED BY
Dongze Qin,
Albert Einstein College of Medicine, United States
Scott M. MacDonnell,
Regeneron Pharmaceuticals, Inc., United States

*CORRESPONDENCE
Qiang Ye,
art006023@yeah.net
Yanfei Du,
dyfswmu0304@swmu.edu.cn

†These authors have contributed equally to this work

RECEIVED 10 November 2023
ACCEPTED 18 January 2024
PUBLISHED 01 March 2024

CITATION
Jiang H, Yang J, Li T, Wang X, Fan Z, Ye Q and Du Y (2024), JAK/STAT3 signaling in cardiac fibrosis: a promising therapeutic target. *Front. Pharmacol.* 15:1336102. doi: 10.3389/fphar.2024.1336102

JAK/STAT3 signaling in cardiac fibrosis: a promising therapeutic target

Heng Jiang[1†], Junjie Yang[1†], Tao Li[2], Xinyu Wang[2], Zhongcai Fan[1], Qiang Ye[1*] and Yanfei Du[1,2*]

[1]Department of Cardiology, The Affiliated Hospital of Southwest Medical University, Luzhou, Sichuan, China, [2]Key Laboratory of Medical Electrophysiology, Ministry of Education and Medical Electrophysiological Key Laboratory of Sichuan Province, Institute of Cardiovascular Research, Southwest Medical University, Luzhou, China

Cardiac fibrosis is a serious health problem because it is a common pathological change in almost all forms of cardiovascular diseases. Cardiac fibrosis is characterized by the transdifferentiation of cardiac fibroblasts (CFs) into cardiac myofibroblasts and the excessive deposition of extracellular matrix (ECM) components produced by activated myofibroblasts, which leads to fibrotic scar formation and subsequent cardiac dysfunction. However, there are currently few effective therapeutic strategies protecting against fibrogenesis. This lack is largely because the molecular mechanisms of cardiac fibrosis remain unclear despite extensive research. The Janus kinase/signal transducer and activator of transcription (JAK/STAT) signaling cascade is an extensively present intracellular signal transduction pathway and can regulate a wide range of biological processes, including cell proliferation, migration, differentiation, apoptosis, and immune response. Various upstream mediators such as cytokines, growth factors and hormones can initiate signal transmission via this pathway and play corresponding regulatory roles. STAT3 is a crucial player of the JAK/STAT pathway and its activation is related to inflammation, malignant tumors and autoimmune illnesses. Recently, the JAK/STAT3 signaling has been in the spotlight for its role in the occurrence and development of cardiac fibrosis and its activation can promote the proliferation and activation of CFs and the production of ECM proteins, thus leading to cardiac fibrosis. In this manuscript, we discuss the structure, transactivation and regulation of the JAK/STAT3 signaling pathway and review recent progress on the role of this pathway in cardiac fibrosis. Moreover, we summarize the current challenges and opportunities of targeting the JAK/STAT3 signaling for the treatment of fibrosis. In summary, the information presented in this article is critical for comprehending the role of the JAK/STAT3 pathway in cardiac fibrosis, and will also contribute to future research aimed at the development of effective anti-fibrotic therapeutic strategies targeting the JAK/STAT3 signaling.

KEYWORDS

cardiovascular diseases, JAK/STAT3 signaling, cardiac fibrosis, cardiac fibroblast proliferation and activation, signal transduction and regulation, upstream mediators, anti-fibrotic therapies

1 Introduction

Cardiovascular disease is still the major cause of global death despite great progress in treatment methods. Myocardial fibrosis is a common pathology of most cardiovascular diseases at the end stage (Rockey et al., 2015). It can destroy the cardiac structure, impair cardiac excitation-contraction coupling, and impede cardiac function of both contraction and relaxation, thereby promoting the development of cardiovascular disease into heart failure (Gyöngyösi et al., 2017; Nguyen et al., 2017). The order of severity of cardiac fibrosis is related to higher long-term mortality of cardiovascular disease, particularly heart failure (Azevedo et al., 2010; Aoki et al., 2011). Due to the complex and incompletely elucidated mechanisms of fibrosis, there is currently no specific antifibrotic treatment available for cardiac fibrosis.

The Janus kinase/signal transducer and activator of transcription (JAK/STAT) signaling pathway, as a central communication node within cells, plays an essential role in a variety of pathophysiological activities like cell division, differentiation, immune regulation and tumorigenesis (Zhang J. Q. et al., 2022). It has been reported that many upstream mediators can activate this pathway to exert their biological functions, comprising growth factors, hormones, and cytokines (Darnell et al., 1994; Liu J. et al., 2023). The JAK/STAT pathway consists of three parts: ligand-receptor complexes, JAKs, along with transcription factors STATs. Among the STAT protein family, STAT3 is the most well-studied member and its activation can play beneficial or detrimental roles in various diseases. On the one hand, STAT3 shows highly activated in most cancers and cardiac injuries (Xian et al., 2021; Zhuang et al., 2022) and is demonstrated to be a pathogenic regulator (Yu and Jove, 2004). On the other hand, STAT3 is also recognized as a protective molecule, and its activation may confer cardioprotection against several cardiovascular diseases including ischemia and ischemia-reperfusion injury (Negoro et al., 2000; Fuglesteg et al., 2008; Harhous et al., 2019) and cardiac hypertrophy (Enomoto et al., 2015). Recently, accumulating evidence has confirmed a novel profibrotic role of the JAK/STAT3 signaling activation in multiple tissues and organs, including the heart (Bao et al., 2020), liver (Ogata et al., 2006), kidney (Zheng et al., 2019), lung (Celada et al., 2018), and skin (Dees et al., 2020). In this regard, the JAK/STAT3 pathway may emerge as a potential therapeutic target for treating fibrotic diseases (Barry et al., 2007). However, there is a lack of a comprehensive summary on the role of the JAK/STAT3 signaling in mediating cardiac fibrosis. In this review, we discuss the structure, transactivation and regulation of the JAK/STAT3 signaling pathway and review current progress on the role of this pathway in cardiac fibrosis and challenges and opportunities of targeting the JAK/STAT3 signaling for the treatment of fibrosis.

2 The cellular and molecular mechanisms of cardiac fibrosis

Cardiac fibrosis usually occurs when myocardial tissue is suffering from a pathological stimulus such as ischemia, hypoxia, overload, inflammation or other pathogenic factors. It serves a dual role: it protects myocardial tissue integrity as a normal reparative response during injury, yet persistent and excessive scar formation greatly impairs the heart's systolic and diastolic functions (Leask, 2015). Cardiac fibrosis not only increases ventricular stiffness but also induces the secretion of growth factors and cytokines to promote cardiomyocyte hypertrophy, ultimately leading to a decline in myocardial compliance, heart failure, and even sudden death (Mohammed et al., 2015; Francis Stuart et al., 2016).

Cardiac fibrosis is a common pathological feature manifested by multiple cardiovascular diseases, such as heart failure, hypertension, arrhythmia, cardiomyopathy, and myocardial infarction, and also plays a significant role in their onset and progression (Tao et al., 2014; Chen et al., 2015; Chung et al., 2021; Qi et al., 2022). Cardiac fibrosis manifests as the over-proliferation and differentiation of CFs and massive accumulation of extracellular matrix (ECM) components in the myocardium, like fibronectin, type I collagen, and type III collagen (Schafer et al., 2017). Myofibroblasts differentiated from CFs can synthesize contractile proteins like α-smooth muscle actin (α-SMA), leading to the distortion of tissue and cell structure (Hinz, 2007; Hinz, 2010). On the other hand, myofibroblasts can express excessive amounts of ECM proteins, thus leading to the substitution of permanent fibrotic scars for normal tissues, increased cardiac stiffness, and varying degrees of cardiac diastolic and systolic dysfunction (Weber, 1989; Cleutjens et al., 1995; Dobaczewski et al., 2006; Liu et al., 2017; Wang et al., 2022b).

The source of myofibroblasts in fibrotic hearts remains a disputed matter. Although some studies indicate that a significant proportion of myofibroblasts may originate from endothelial cells, epithelial cells or hematopoietic fibroblast progenitors (Möllmann et al., 2006; Zeisberg et al., 2007; Aisagbonhi et al., 2011), prevailing evidence confirms that the primary source of myofibroblasts in fibrotic heart tissue could be the activation of resident CFs (Ali et al., 2014; Moore-Morris et al., 2014; Kanisicak et al., 2016; Shinde and Frangogiannis, 2017; Moore-Morris et al., 2018). Furthermore, it has been suggested that pericytes could potentially serve as a reservoir of myofibroblasts, but the precise mechanism by which they operate remains uncertain, and there may be an overlap between pericytes and resident fibroblast subsets (Humphreys et al., 2010).

Although the molecular mechanisms involved in cardiac fibrosis are complex and variable, the transformation of CFs to myofibroblasts plays a central role in the process of cardiac fibrosis. Acute cardiac injury initiates a robust inflammatory response. This process involves the infiltration of immune cells into the cardiac tissue, which subsequently release inflammatory cytokines such as transforming growth factor (TGF)-β1, tumor necrosis factor-α (TNF-α) and interleukins (ILs) (Bujak and Frangogiannis, 2007; Christia et al., 2013). These cytokines activate CFs and instigate ECM remodeling through diverse signaling cascades. Concurrently, neurohormones within the renin-angiotensin-aldosterone system (RAAS) and the sympathetic nervous system, particularly Angiotensin II (Ang II), aldosterone, and catecholamines, are upregulated (Zou et al., 2004; Ferreira et al., 2016; Azushima et al., 2020). Their activation compels myofibroblasts to ramp up collagen production, culminating in the deposition of fibrotic tissue in the heart, which is a hallmark of cardiac remodeling. Additionally, mechanical stress, often a consequence of increased cardiac afterload in conditions like hypertension or valvular disease, prompts cardiomyocytes and

fibroblasts to adapt by modifying their ECM, which alters their size, shape, and function (Li et al., 2018). Moreover, oxidative stress in the cardiac environment, primarily characterized by the overproduction of reactive oxygen species (ROS), inflicts direct cellular damage and fosters inflammation and apoptosis. These effects collectively trigger signaling pathways that exacerbate myocardial fibrosis (Grosche et al., 2018). Lastly, metabolic imbalances, including the production of advanced glycation end-products (AGEs) and lipotoxicity in cardiomyocytes, along with vascular implications like endothelial dysfunction, significantly contribute to the progression of cardiac fibrosis (Huby et al., 2015; Chen et al., 2016; Marciniec et al., 2017).

Among the aforementioned mediators, TGF-β1 is regarded as a central and potent profibrotic factor and evokes cardiac fibrosis mainly through activation of downstream classic small mother against decapentaplegic (Smad) signaling pathway. This process involves the binding of extracellular TGF-β1 ligand to TGF-β type II receptor (TGF-βRII), which phosphorylates TGF-β type I receptor (TGF-βRI). Activated TGF-βRI then phosphorylates and activates R-Smads (mainly Smad2 and Smad3), which further form a complex with Smad4. The complex moves to the nucleus and interacts with other co-activators to induce the transcription of fibrosis-related genes such as fibronectin, α-SMA and collagens (Shi and Massagué, 2003; Działo et al., 2018; Hu et al., 2018). Additionally, TGF-β1 also leads to cardiac fibrosis through activating several noncanonical (also called Smad-independent) signaling pathways, like phosphatidylinositol 3-kinase/protein kinase B (PI3K/Akt), mitogen-activated protein kinase [MAPK, mainly comprising p38, c-Jun NH_2-terminal kinase (JNK) and extracellular signal-regulated kinase (ERK)] or Rho-like GTPases signaling pathways. In addition to the most common TGF-β signaling, the pathogenesis of cardiac fibrosis also involves a variety of other intracellular molecular pathways, including the JAK/STAT3 signaling (Zhang et al., 2019b), Wnt/β-Catenin signaling (Mizutani et al., 2016), integrin/focal adhesion kinase (FAK) signaling (Zhao et al., 2016; Molkentin et al., 2017), Hippo signaling (Singh et al., 2016), and myocardial related transcription factor (MRTF)/serum response factor (SRF) signaling (Tomasek et al., 2005; Lighthouse and Small, 2016). Therefore, targeting these fibrotic mediators or cascades could provide promising therapeutic approaches for treating fibrotic diseases.

3 Structure, function, transcriptional activity and regulation of the JAK/STAT3 signaling pathway

3.1 Molecular structure of STAT3

In mammals, there are seven proteins belonging to the STAT family, which consists of cytoplasmic transcription factors named STAT1-STAT4, STAT5a, STAT5b, and STAT6 (Hu et al., 2020b). Among these, STAT3 is the most extensively studied and plays pivotal roles in controlling various cellular biological processes. STAT3 was originally discovered in 1994 through a series of studies on cytokine-induced acute responses of target genes. Unlike other family members, global deletion of STAT3 can cause embryonic death. The STAT3 protein consists of 770 amino acid residues and, similar to other members of the STAT family, it can be divided into six distinct functional domains (Figure 1): an NH_2-terminal domain (NTD), a coiled-coil domain (CCD), a DNA binding domain (DBD), a linker domain (LD), an Src homology 2 (SH2) domain, and a COOH-terminal transactivation domain (TAD). Each domain has a specific function (Hu et al., 2021) (Table 1).

STAT3 is expressed widely in different cell types within the heart, such as cardiomyocytes, fibroblasts, immune cells, and endothelial cells. Two isoforms of the STAT3 protein, STAT3α (92 kDa) and STAT3β (83 kDa), are produced through alternative splicing of the identical gene. STAT3β is missing the COOH-terminal 55 amino acids, which are correspondingly replaced by seven distinct amino acid residues (Schaefer et al., 1995; Caldenhoven et al., 1996). Research has shown that while STAT3β is not vital for survival, mice deficient in STAT3α do not survive past birth (Maritano et al., 2004). STAT3α possesses two phosphorylation sites, namely, Tyr705 and Ser727, whereas STAT3β only possesses one phosphorylation site, specifically Tyr705. When either Tyr705 or Ser727 is phosphorylated, STAT3 is activated and exerts its function. STAT3 can be activated by more than 50 extracellular ligands, which are commonly some cytokines, hormones, growth factors, and chemokines, such as ILs, interferons, colony-stimulating factors, epidermal growth factor (EGF), and platelet-derived growth factor (PDGF) (Darnell, 1997; Hu et al., 2021). STAT3's biological functions are complicated and diverse and its main physiological roles under normal conditions are summarized in the following section.

STAT3 is an important intracellular signaling molecule that has multiple functions under normal physiological conditions. These functions include: (1) Regulating the proliferation and differentiation of various cell types by binding to specific DNA sequences and affecting gene expression. For example, STAT3 promotes the proliferation of corneal limbal keratinocytes via a ΔNp63-dependent mechanism, and inhibiting this pathway can increase cell differentiation (Hsueh et al., 2011). STAT3 also mediates megakaryocyte differentiation induced by RAD001 (Su et al., 2013). (2) Regulating the activation, proliferation, and secretion of cytokines by immune cells, which can modulate immune responses and inflammation. For instance, STAT3 inhibition can induce apoptosis and/or activate effective immune responses in colon cancer cells, overcoming cancer-induced immune tolerance (Jahangiri et al., 2020). Likewise, systemic injection of penetrating c-Myc and gp130 peptides can inhibit pancreatic tumor growth and induce anti-tumor immunity (Aftabizadeh et al., 2021). (3) Mediating the expression of inflammation-related genes in response to various cytokines and growth factors. One of the most prominent examples is IL-6, which we will discuss in detail later. (4) Maintaining the self-renewal and differentiation of stem cells by regulating the transcription of target genes. Phosphorylated STAT3 is functionally associated with the expression of self-renewal genes in embryonic stem cells (Bourillot et al., 2009). Moreover, constitutively activated STAT3 can sustain the self-renewal process in the absence of leukemia inhibitory factor (LIF) (Matsuda et al., 1999). (5) Participating in tissue repair and regeneration processes by modulating cell survival and growth. For instance, Transmembrane and ubiquitin like domain containing 1 (Tmub1) inhibits the phosphorylation and activation of STAT3, impairing liver regeneration in mice after partial hepatectomy (Fu et al., 2019). Conversely, Krüppel-like factor 4 (KLF4) deletion *in*

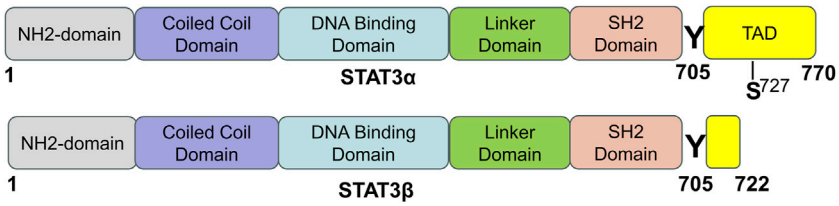

FIGURE 1
The domain structure and phosphorylation sites of STAT3 protein. STAT3 has two splicing isoforms, STAT3α and STAT3β, and they are comprised of 770 and 722 amino acids, respectively. STAT3 contains six different functional domains, including the NH_2-terminal domain, coiled-coil domain, DNA binding domain, linker domain, SH2 domain, and COOH-terminal transactivation domain (TAD). "Y" means a tyrosine phosphorylation site, and "S" means a serine phosphorylation site [adapted from ref. (Hu et al., 2021).

TABLE 1 Function of STAT3 domains.

Domain	Function Kishore and Verma (2012), Haghikia et al. (2014), Harhous et al. (2019), Hu et al. (2021)
NTD	Promoting the formation of STAT3 dimers and regulating nuclear translocation
CCD	Providing binding sites for regulatory factors and participating in regulating nuclear import and export
DBD	Recognizing and binding to specific DNA elements of target genes
LD	Affecting DNA binding stability
SH2	Recognizing phosphotyrosine sites of receptors and contributing to form STAT3 dimers
TAD	Recruiting co-activators and regulating target gene transcription

Abbreviation: NTD, NH_2-terminal domain; CCD, coiled-coiled domain; DBD, DNA-binding domain; LD, linker domain; SH2, Src homology 2 domain; TAD, COOH-terminal transactivation domain.

vivo induces axonal regeneration in adult retinal ganglion cells (RGCs) through the JAK/STAT3 signaling pathway. This regeneration can be further enhanced by removing the endogenous JAK/STAT3 pathway inhibitor SOCS3 (Qin et al., 2013). (6) Regulating the energy metabolism of cells by influencing the expression of mitochondrial oxidative phosphorylation-related genes. For example, icaritin inhibits the survival and glycolysis of glioblastoma (GBM) cells through the IL-6/STAT3 pathway (Li et al., 2019a). Additionally, STAT3 promotes mitochondrial respiration and reduces the production of ROS in neural precursor cells (Su et al., 2020). (7) Playing an essential role in early embryonic development, as embryos with STAT3 gene defects will die in the early stages of development. In humans, LIF and STAT3 are expressed in decidual tissue during early pregnancy. LIF can induce STAT3 phosphorylation in non-decidualized and decidualized human endometrial stromal cells *in vitro*, suggesting that LIF/STAT3 signaling is involved in human embryo implantation and decidualization (Shuya et al., 2011). Furthermore, conditional ablation of STAT3 in the uterus can result in embryo implantation failure (Lee et al., 2013).

3.2 Molecular structure of JAK

In mammals, the JAK family consists of four main members (JAK1-JAK3 and Tyk2), which are non-receptor tyrosine protein kinases (Schindler and Darnell, 1995). JAK1, JAK2, and Tyk2 have broad expression, whereas JAK3 is mainly present in cells of the hematopoietic lineage (Speirs et al., 2018). Upon interaction of cytokines or growth factors with their corresponding receptors, JAK tyrosine kinases are activated, thereby facilitating intracellular signal transduction.

The JAK protein is made up of seven similar regions (JH1-JH7) and includes four functional domains: a domain for tyrosine kinase, a domain for pseudokinase, an SH2 domain, and an NH2-terminal FERM domain (Four-point-one protein, Ezrin, Radixin, Moesin) (Figure 2) (Banerjee et al., 2017). The carboxy-terminal portion of each JAK includes the catalytic kinase domain (JH1) and the pseudokinase domain (JH2). JH1, containing nearly 250 amino acid residues, is the active phosphotransferase domain needed for phosphorylation of cytokine receptors and downstream STAT proteins. JH2 is similar to JH1 in structure, but it is generally considered to have no catalytic activity and can regulate the kinase activity of JH1 (Zhao et al., 2018; Xin et al., 2020). According to reports, the JAK2 protein's JH2 exhibits a minimal level of kinase activity as stated by Ungureanu et al. (2011). The N-terminal region of each JAK contains the SH2 (JH3 with half of JH4) and FERM (JH5-JH7 and one-half of JH4) domains, which collectively facilitate the interaction between JAK proteins and the box1/2 regions of cytokine receptors located near the cell membrane (Saharinen et al., 2000; Wallweber et al., 2014; Hubbard, 2017; Morris et al., 2018; Xin et al., 2020; Raivola et al., 2021).

3.3 Canonical JAK/STAT3 signaling pathway

The JAK/STAT signaling pathway is activated by more than 50 cytokines and growth factors, including hormones, interferons

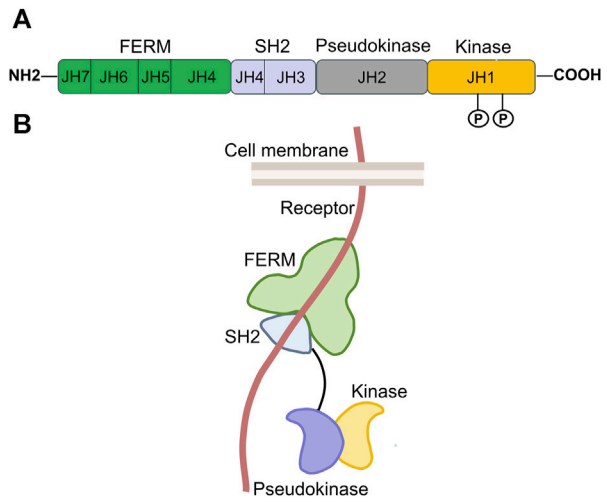

FIGURE 2
Structure of JAK. **(A)**. Domains and conserved phosphorylation sites of the JAK protein. The JAK protein family contains four members, JAK1-3, and TYK2. Each is composed of seven homologous regions, labeled JH1-JH7. These regions make up four distinct functional domains, of which, JH1 corresponds to the kinase domain; JH2 is the pseudokinase domain; JH3 and a portion of JH4 together form the SH2 domain; and the combination of JH5, JH6, JH7, and the rest of JH4 constitutes the FERM domain. "P" represents conserved tyrosine phosphorylation sites of the JAK protein. **(B)**. Three-dimensional spatial structure of JAK in cells [adapted from ref. (Hu et al., 2021).

(IFN), ILs, and colony stimulating factors (Darnell, 1997). These molecules regulate various cellular events, such as hematopoiesis, immune adaptability, tissue repair, inflammation, cell apoptosis, and adipogenesis (Owen et al., 2019). The JAK/STAT3 pathway is activated when these extracellular ligands bind to their dedicated transmembrane receptors (Figure 3). The cytosolic domains of these receptors are constitutively interacting with receptor-related JAK tyrosine kinases. These JAK kinases are nonactivated before the ligand stimulation, while the coupling of the ligand with its receptor results in auto-phosphorylation of JAK kinases (Feng et al., 1997). Upon activation, the JAK molecules phosphorylate the cytoplasmic segment of the receptors at particular tyrosine residues, subsequently serving as binding sites for cytoplasmic STAT3 protein and attracting the recruitment of the STAT3 protein. After docking, STAT3 is phosphorylated by JAK kinase and subsequently associates with itself or other phosphorylated STAT monomers to create homodimers or heterodimers upon separation from the receptor. Ultimately, these dynamic molecular pairs migrate from the cytoplasm to the nucleus, where they attach to target gene promoters and stimulate the expression of target genes (O'Shea et al., 2015; Durham et al., 2019), often causing proliferation, differentiation, and apoptosis.

3.4 Noncanonical JAK/STAT3 signaling pathway

The function of STAT3 is influenced by different post-translational modifications, including phosphorylation, methylation, acetylation, and ubiquitination, occurring at various amino acid sites. In addition to classical signal transduction, JAK/STAT3 may also play a role in nonclassical signal transduction. Research has indicated that STAT3, which is not phosphorylated on Tyr705, has the ability to move from cytoplasm to the nucleus and can activate various STAT3 target genes in the absence of Ser727 phosphorylation (Bharadwaj et al., 2020). Additionally, the process can be facilitated by Lys685 acetylation and NF-kB signaling activation, as suggested by previous studies (Yang et al., 2007; Dasgupta et al., 2014). Besides being activated in the cytosol, all STAT proteins (excluding STAT4) have the ability to localize to the mitochondrion, leading to an enhancement in oxidative phosphorylation and membrane polarization. For example, STAT3 monomers phosphorylated on Ser727 can translocate into the mitochondrion without dimerization to increase membrane polarization and ATP synthesis, and inhibit ROS production and mitochondrial permeability transition pore (MPTP) opening, thus exerting a protective role (Boengler et al., 2010; Garama et al., 2016; Avalle and Poli, 2018). Besides, STAT3 has also been reported to translocate to the endoplasmic reticulum and contribute to reduce oxidative stress-induced apoptosis (Avalle et al., 2019). In the nucleus, certain STAT molecules that are not phosphorylated interact with heterochromatin protein 1 (HP1) located on heterochromatin. Phosphorylation of STAT by JAK or other kinases can cause the detachment of HP1 from heterochromatin, leading to its destabilization. Subsequently, phospho-STAT can interact with particular regions on autosomes and regulate the expression of target genes (Shi et al., 2006; Shi et al., 2008b; Li, 2008). This noncanonical JAK/STAT signaling is critical for sustaining heterochromatin stability. Moreover, increasing evidence has shown that activation of JAK/STAT signaling can cause chromatin remodeling in mammals (Christova et al., 2007; Shi et al., 2008a). Besides being triggered by JAK, STAT3 can also be activated by alternative non-receptor tyrosine kinases or JAK-independent receptors. As an example, the c-Src enzyme is capable of phosphorylating STAT3, which then can promote the expression of oncogenes (Yu et al., 1995). EGF receptor and PDGF receptor can directly activate STAT3 (Ruff-Jamison et al., 1994; Liu et al., 2023a).

3.5 Cross-talk between the STAT3 signaling and other pathways

Besides the prevalent JAK/STAT3 signaling pathway, STAT3 also engages in alternative signaling pathways or establishes communication with these pathways, thereby producing biological impacts. STAT3 is involved in the classic TGF-β/Smad signaling pathway (Pedroza et al., 2018; Chen et al., 2019b; Sun et al., 2022) and Smad-independent TGF-β signaling pathways, such as the ERK-mediated MAPK (Park et al., 2020; Shen et al., 2021), JNK (Park et al., 2020), and PI3K/Akt signaling pathways (Zhu et al., 2018; Lee et al., 2019). In addition to TGF-β-related signaling pathways, STAT3 also participates in many other signaling cascades, such as Fyn (a member of the Src kinase family) (Seo et al., 2016; Zhu et al., 2018; Zhu et al., 2023), peroxisome proliferator-activated receptor (PPAR) (Lo et al., 2017b; Németh et al., 2019), and Notch signaling (Chen et al., 2019c).

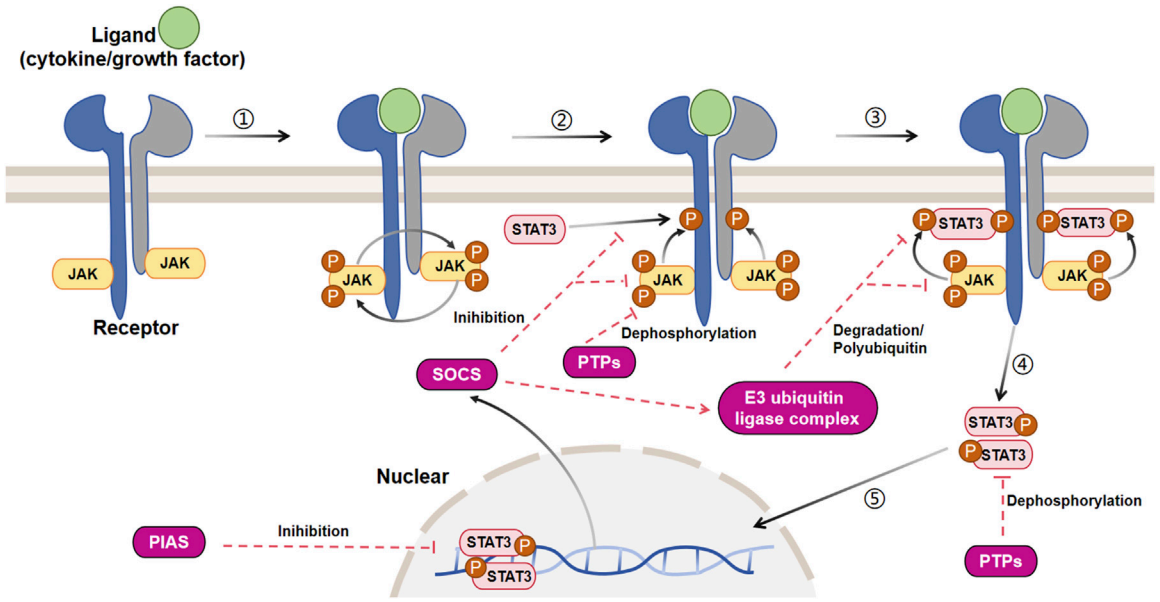

FIGURE 3
Signal transduction and negative regulation of the canonical JAK/STAT3 pathway. The JAK/STAT3 cascade is initiated by the interaction between a ligand and its corresponding receptor. This interaction leads to the auto-phosphorylation of the JAK kinase bound to the receptor. Once activated, JAK phosphorylates a tyrosine residue on the receptor, creating a docking site for cytoplasmic STAT3 and recruiting STAT3. At this docking site, JAK phosphorylates STAT3. The phosphorylated STAT3 then dissociates from the receptor and forms dimers. These STAT3 dimers move to the nucleus, where they bind to promoters and regulate transcription. The JAK/STAT3 cascade is controlled by three primary types of negative regulators: PTPs (protein tyrosine phosphatases), PIAS (protein inhibitor of activated STAT), and CIS/SOCS (suppressor of cytokine signaling). PTPs block the JAK/STAT3 signaling mainly by interacting directly with the STAT3 dimers and JAK to dephosphorylate them. PIAS prevents the JAK/STAT3 signaling principally by inhibiting the binding of STAT3 to DNA. As a common objective caused by the activation of JAK/STAT3, CIS/SOCS mainly hinders the JAK/STAT3 cascade through the following methods: (1) obstructing the recruitment of STAT3 to the phosphorylated receptor; (2) directly interacting with JAK to suppress its kinase function; (3) prompting the creation of an E3 ubiquitin ligase complex that breaks down JAK or prevents STAT3 from binding to the SOCS protein [adapted from refs. (Gurzov et al., 2016; Hu et al., 2021).

3.6 Negative regulation of canonical JAK/STAT3 signaling

The inhibition of canonical JAK/STAT3 signaling involves three primary categories of negative regulators (Figure 3): protein inhibitor of activated STAT (PIAS), protein tyrosine phosphatases (PTPs), and suppressor of cytokine signaling (SOCS/CIS). These regulators, as described by Liongue et al., play a crucial role in preventing the excessive phosphorylation of STAT3 (Liongue et al., 2016; Villarino et al., 2017; Yang et al., 2017).

The process of JAK/STAT signal transduction contains a series of intracellular tyrosine phosphorylation, so PTPs have a key role in regulating this pathway. PTPs can directly dephosphorylate and inactivate the STAT dimers, and block the JAK/STAT cascade. For instance, a receptor tyrosine phosphatase PTPRTR can bind to and dephosphorylate the tyrosine residue at site 705 in STAT3 (Zhang et al., 2007). SHP-2, a significant member of the PTP family and also a target gene for activated STAT3, can decrease the phosphorylation level of STAT3 (Schmitz et al., 2000). In addition, PTPs can dephosphorylate JAK and prevent the JAK/STAT signaling.

The PIAS family comprises four transcription regulatory factors, namely, PIAS1-PIAS4. PIAS was originally identified to be a suppressor of STAT, and PIAS3 can combine with STAT3. PIAS only binds to phosphorylated STAT dimers rather than STAT monomers (Hu et al., 2021). PIAS mainly suppresses the transcriptional activity of STAT by means of three mechanisms. (1) Preventing the DNA-binding activity of STAT and blocking STAT-DNA interactions (Sonnenblick et al., 2004). (2) Recruiting transcriptional co-inhibitory factor such as histone deacetylase (Tussié-Luna et al., 2002). (3) Promoting STAT SUMOylation (Yuan et al., 2015).

SOCS family proteins are considered as major triggers of the JAK/STAT signaling attenuation, and there are eight members in this family: SOCS1-7 and cytokine-inducible SH2 protein (CIS) (Minamoto et al., 1997; Piessevaux et al., 2008; Kazi et al., 2014). Cytokine-stimulated JAK/STAT signaling activation induces the SOCS proteins, which act as negative feedback suppressors to regulate this pathway (Naka et al., 1997; Kershaw et al., 2013b). For example, SOCS3 gene is quickly induced by phosphorylated STAT3 dimers in the nucleus, and in turn SOCS3 protein interacts with activated JAK and its receptor to suppress JAK activity, thus preventing further JAK/STAT3 signaling activation (Babon et al., 2012; Kershaw et al., 2013a). SOCS primarily inhibits the JAK/STAT cascade in the following ways. (1) It competes with STAT for binding to the phosphorylated receptor and prevents STAT recruitment. (2) It forms an E3 ubiquitin ligase complex via the COOH-terminal SOCS box and degrades JAK or STAT that binds to SOCS (Kamran et al., 2013). (3) The SOCS protein has the ability to directly and specifically interact with either JAK or its receptor in order to inhibit the activity of JAK kinase. An example is the presence of a distinct brief pattern known as the kinase inhibitory region (KIR) in SOCS1 and SOCS3. This pattern

enables these two proteins to hinder the catalytic activity of JAK by directly binding to JAK or its receptor (Sasaki et al., 1999; Yasukawa et al., 1999; Alexander, 2002).

3.7 The JAK/STAT3 pathway induces fibrosis

Studies have indicated that the JAK/STAT3 pathway plays a key role in the process of fibrosis. It can be activated by various pro-fibrotic mediators, such as TGF-β1, PDGF, vascular endothelial growth factor (VEGF), IL-6, Ang II, serotonin (5-HT), and endothelin (ET-1), and then leads to fibrogenesis (Rane and Reddy, 2000; Zhang et al., 2015; Roskoski, 2016) (Figure 4A). The JAK/STAT3 pathway is also demonstrated to be a central integrator of multiple pro-fibrotic pathways and its activation can promote the activation of fibroblasts and the expression of fibrosis-related genes, such as α-SMA, collagens, and fibronectin (Zhang et al., 2015; Chakraborty et al., 2017; Dees et al., 2020). In addition, once activated, STAT3 can induce the expression of hypoxia-inducible factor-1α (HIF-1α), a transcription factor that responds to hypoxic conditions and stimulates the production of ECM (Yang et al., 2021) (Figure 4A). Activated STAT3 can also trigger epithelial to mesenchymal transition (EMT), a cellular process that allows epithelial cells to transform into mesenchymal cells with more power in migration and invasion, and facilitates the progression of fibrosis (Montero et al., 2021; Yang et al., 2021) (Figure 4B).

3.8 The effects of the JAK/STAT3 pathway on different types of cardiac injury

The JAK/STAT3 pathway plays a pivotal role in various aspects of cardiac physiology and pathology, exhibiting multifaceted roles in the heart (Figure 5). It mediates protective effects in different stages of ischemia, including ischemia pre-, post-, and remote conditioning (Hattori et al., 2001; You et al., 2011; Gao et al., 2017). Agents such as N-acetylcysteine (NAC) and allopurinol (Wang et al., 2013), and insulin (Fuglesteg et al., 2008) are known to protect against myocardial ischemia-reperfusion injury through activation of the JAK/STAT3 pathway. Their protective mechanism likely involves the reduction of ROS production, decrease in cardiomyocyte apoptosis, promotion of angiogenesis, and delay in MPTP opening. In the context of myocardial infarction, molecular factors like miR-124, IL-10, and growth arrest and DNA damage-inducible α (GADD45A) exert beneficial effects through the STAT3 pathway. Specifically, miR-124 offers anti-apoptotic benefits, IL-10 provides anti-inflammatory effects, and GADD45A enhances VEGF-mediated angiogenesis, collectively improving prognosis (He et al., 2018; Wang et al., 2022a; Tesoro et al., 2022). Conversely, conditional deletion of STAT3 in cardiomyocytes exacerbates cardiac remodeling during the subacute phase of myocardial infarction or under chronic β-adrenergic stimulation (Enomoto et al., 2015; Zhang et al., 2016). Furthermore, cardiomyocyte-specific transgenic expression of SOCS1 inhibits JAK/STAT3 activation in enterovirus-induced myocarditis, but this is associated with increased mortality in mice, highlighting a complex interplay (Yasukawa et al., 2003).

Despite its protective roles, the JAK/STAT3 pathway also has detrimental effects. For instance, in myocarditis, IL-6-triggered increases in liver complement C3 and Th17 cells may exacerbate inflammation (Camporeale et al., 2013; Wang et al., 2020). Additionally, inhibiting the JAK/STAT3 signaling with piceatannol could improve sepsis-induced cardiac dysfunction by relieving cell apoptosis and inflammation in septic mice and H9C2 cardiomyocytes, suggesting a critical role of the JAK/STAT3 pathway in sepsis-related myocardial injury (Xie et al., 2021). This pathway also skews macrophage polarization towards M1 and away from M2, contributing to coxsackievirus B3 (CVB3)-induced myocardial inflammation and injury (Wang et al., 2023). Chronic activation of JAK/STAT3 can induce cardiac hypertrophy, as evidenced by Ang II-induced activation of TLR4 and STAT3, promoting hypertrophy via the IL-6/JAK2/STAT3 pathway (Han et al., 2018). Other activators like Heat-shock transcription factor 1 (HSF1), isoproterenol, and Fibronectin type III domain containing 5 (FNDC5) also trigger this pathway, resulting in increased cardiac inflammation, oxidative stress, and pathological hypertrophy (Zhao et al., 2017; Yuan et al., 2018; Geng et al., 2019). Moreover, JAK/STAT3 is implicated in cardiac arrhythmias. Inhibiting JAK2/STAT3 phosphorylation reduces malignant ventricular arrhythmias post-myocardial infarction by attenuating ventricular remodeling (Gao et al., 2020). Cardiac-specific SOCS3 gene knockout mice exhibit myocardial sarcoplasmic reticulum Ca^{2+} overload and subsequent ventricular arrhythmias because of the activation of cardiac gp130 signaling (Yajima et al., 2011). Additionally, IL-6 overexpression, via the STAT3 pathway, promotes cardiac sympathetic nerve activity, increasing the incidence of ventricular arrhythmias (Peng et al., 2023).

4 Multiple mediators regulate cardiac fibrosis through the STAT3 signaling pathway

4.1 ILs

ILs are a type of cytokine proteins that various cells, mainly immune ones, produce. Cytokines modulate cellular functions such as growth, maturation, movement, adhesion, activation and differentiation (Zhang and An, 2007; Brocker et al., 2010). ILs are a large family of cytokines with more than 60 members, which can be grouped into four categories: IL-1 related, type 1 helical (IL-4 related, γ chain and IL-6/IL-12 related), type 2 helical (IL-10 related and IL-28 related), and IL-17 related (Brocker et al., 2010). ILs regulate homeostasis by influencing the cardiovascular, neuroendocrine and metabolic systems in the human body (Corwin, 2000).

Recent research has demonstrated that ILs contribute to myocardial fibrosis via the STAT3 pathway. Some ILs play proinflammatory and fibrotic roles, and IL-6 is the most representative (Figure 6). In the absence of NF-E2-related factor 2 (Nrf2), IL-6 levels further increase in response to Ang II, thereby activating the IL-6/STAT3 pathway, which causes cardiomegaly and inflammation (Chen et al., 2019a). In addition, Ang II can induce Toll-like receptor phosphorylation of STAT3, increase IL-6 production, and continuously activate the JAK/STAT pathway, thereby providing positive feedback and promoting myocardial hypertrophy, fibrosis, and ventricular remodeling (Chen et al., 2017a; Han et al., 2018; Zhang

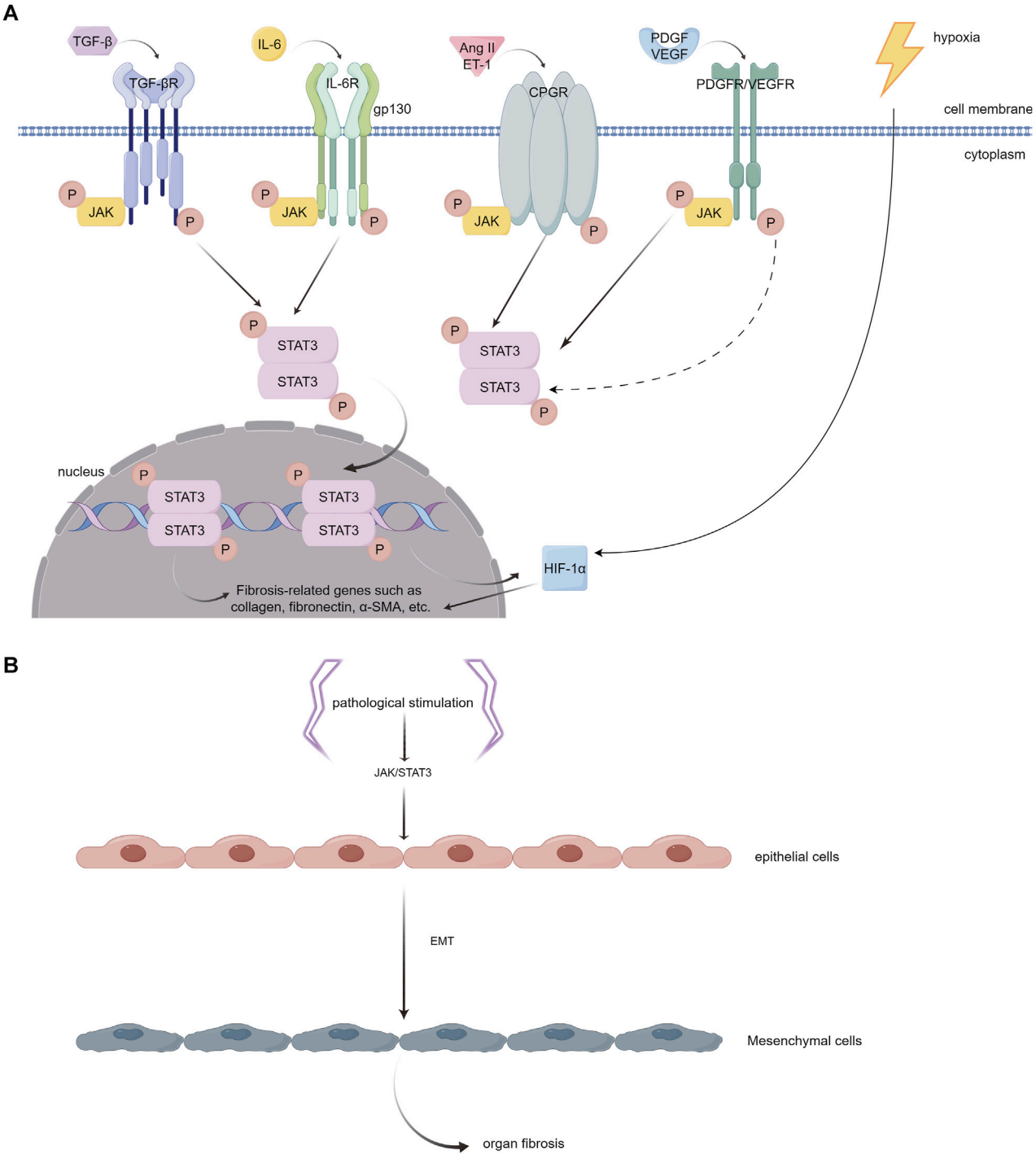

FIGURE 4
(A). Different JAK/STAT3 activators that play important roles in the pathophysiology of myocardial fibrosis. (1) TGF-β interacts with its receptor (TGF-βR) on the cell surface, initiating receptor kinase activity. This activity leads to JAK phosphorylation and subsequent activation of STAT3. However, the precise mechanism underlying this process remains to be fully elucidated. (2) IL-6 binds to its specific receptor, IL-6R, forming a complex. This complex then associates with the membrane protein gp130. Activation of JAKs, which are associated with gp130, is critical for phosphorylating specific tyrosine residues on gp130. These residues act as anchoring points for STAT3. (3) Ang II and ET-1 engage with the GPCR family, triggering the phosphorylation of tyrosine in JAK kinase and consequently activating STAT3. (4) PDGF and VEGF each bind to their respective tyrosine kinase receptors. This binding results in the phosphorylation of tyrosine residues on the receptors, which can indirectly or transactivate JAK, leading to the activation of the STAT3 pathway. Once phosphorylated, STAT3 dimerizes and moves into the nucleus. In the nucleus, these STAT3 dimers attach to specific DNA sequences, enhancing the transcription of genes that are pivotal in driving inflammation and fibrosis, including collagen, fibronectin, α-SMA, etc. In addition, the activation of STAT3 has the capability to stimulate the expression of HIF-1α and enhance the production of ECM in hypoxic environments. **(B)**. Epithelial to mesenchymal transition (EMT). The activation of JAK/STAT3 signaling by pathological stimuli has the potential to induce a phenotypic transition of epithelial cells into mesenchymal cells. These mesenchymal cells exhibit enhanced migration and invasion capabilities. (By Figdraw).

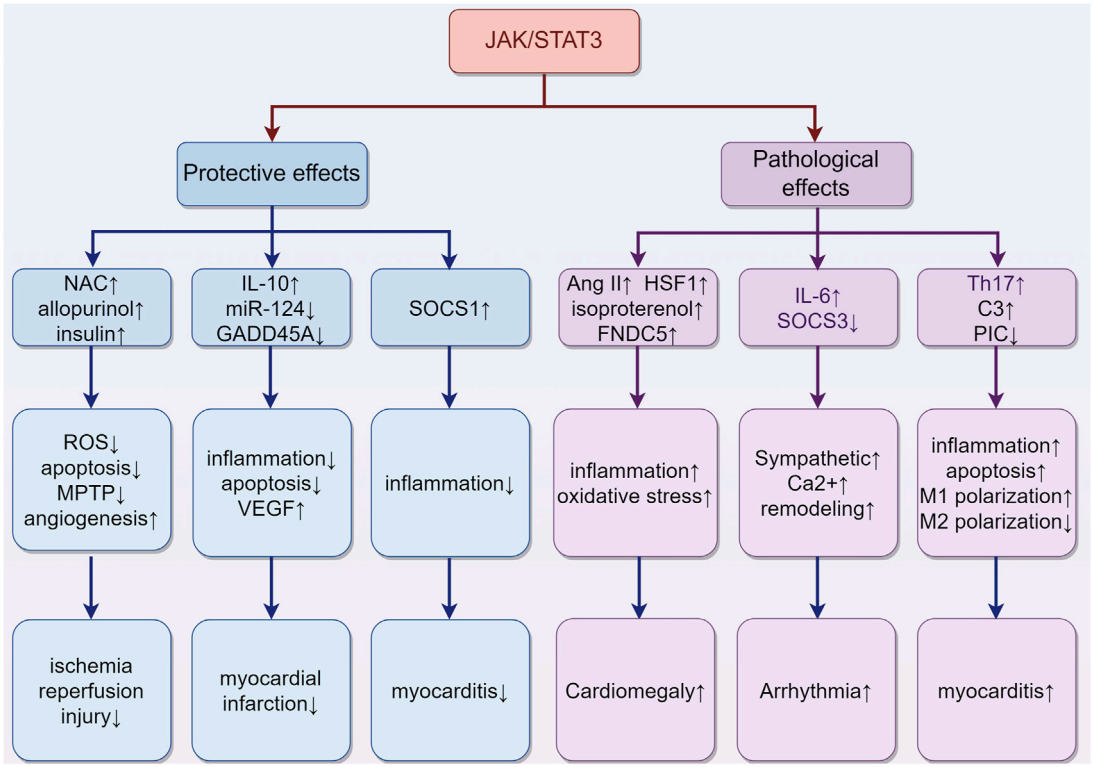

FIGURE 5
The role of activation of the JAK/STAT3 pathway in different types of cardiac damage. (1) In ischemia-reperfusion injury, agents such as NAC, allopurinol, and insulin may confer protective effects. They achieve this by reducing ROS production and cardiomyocyte apoptosis, promoting angiogenesis, and delaying the opening of the MPTP. (2) In the case of myocardial infarction, certain molecular factors like miR-124, IL-10, and GADD45A exert beneficial effects through the STAT3 pathway. These include anti-apoptotic (miR-124), anti-inflammatory (IL-10), and VEGF-mediated angiogenic effects (GADD45A), collectively contributing to improved prognosis. (3) The situation of myocarditis is more complex. The upregulation of SOCS1 can inhibit inflammation. Meanwhile, the upregulation of complement C3 and Th17 cells, along with the downregulation of Piceatannol, may exacerbate inflammation. These findings highlight the multifaceted impact on the progression of myocarditis. (4) Cardiac hypertrophy is influenced by Ang II, HSF1, isoproterenol, and FNDC5, which collaboratively induce hypertrophy through increased oxidative stress and inflammation. (5) Arrhythmias are closely associated with JAK/STAT3 activity, which contributes to myocardial sarcoplasmic reticulum Ca2+ overload, increased cardiac sympathetic nerve activity, and ventricular remodeling. "↑" represents activation, upregulation or exacerbation, and "↓" represents inhibition, downregulation or relief. (By Figdraw).

et al., 2019b). IL-6 enhances STAT3 phosphorylation in cultured CFs, whereas inhibiting STAT3 reduces IL6-induced collagen synthesis and reverses pressure overload-induced cardiac hypertrophy (Mir et al., 2012). In a transverse aortic constriction (TAC)-induced mouse heart failure model, inhibiting IL6/gp130/STAT3 with raloxifene alleviated TAC-induced myocarditis, cardiac remodeling and dysfunction (Huo et al., 2021). In mice with CVB3-induced dilated cardiomyopathy (DCM), IL-6 knockout reduced the phosphorylation level of STAT3 in myocardial tissue, thereby improving myocardial remodeling induced by DCM (Li et al., 2019b).

4.2 TGF-β

The TGF-β and STAT3 signaling pathways have a feedback loop that regulates the acute/chronic stress response in the heart. TGF-β signaling affects STAT3 as an important target in its downstream pathway (Pedroza et al., 2018; Chen et al., 2019b; Sun et al., 2022). Several studies have demonstrated the interaction between TGF-β and STAT3 in cardiac fibrosis. For instance, it has been reported that TGF-β-induced CD44/STAT3 signaling plays a crucial part in atrial fibrosis and fibrillation formation. CD44 is a membrane receptor that modulates fibrosis. Blocking CD44 signaling can reduce TGF-β-induced STAT3 activation and collagen expression in atrial fibroblasts, implicating a potential approach for treating atrial fibrosis and fibrillation (Chang et al., 2017). Moreover, Ephrinb2-mediated myocardial fibrosis involves the activation of the TGF-β/Smad3 and STAT3 pathways. Further study revealed that Ephrinb2 could enhance the interaction of TGF-β/Smad3 and STAT3 signaling to promote cardiac fibrosis (Su et al., 2017). Furthermore, tyrosine mutation at site 705 to glutamic acid constitutively activated STAT3, which could further enhance the interaction between Smad3 and STAT3 (Su et al., 2017). One previous study showed that a high-fat diet could activate the left ventricular renin–angiotensin system (RAS) and JAK1/2-STAT1/3 pathways in rats by increasing ROS and IL-6 production, ultimately causing cardiac fibrosis. This creates a positive feedback loop that activates the TGF-β1/Smad3 fibrotic pathway and enhances left ventricular collagen synthesis (Eid et al., 2019). In cultured CFs, TGF-β1 can activate STAT3 phosphorylation, increasing fibrosis-related protein expression, and relaxin can block STAT3 phosphorylation and reverse TGF-β1-induced fibrosis (Yuan et al., 2017). These results suggest that STAT3 either acts as a separate

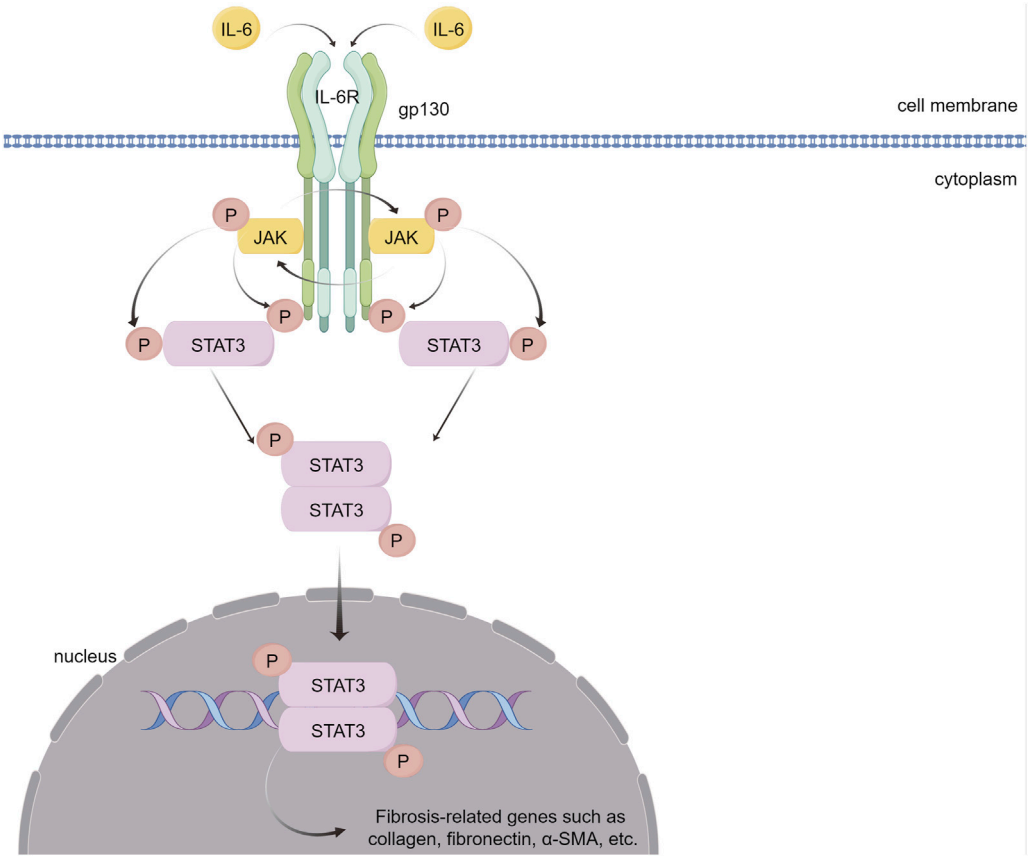

FIGURE 6
IL-6 causes myocardial fibrosis through the JAK/STAT3 signaling pathway. IL-6 binds to its receptor, IL-6R, forming a complex that activates the gp130 receptor. This activation triggers the JAK family of tyrosine kinases. Once activated, these JAKs phosphorylate STAT3, a crucial step in the signaling pathway. Phosphorylated STAT3 dimerizes and translocates into the nucleus. There, STAT3 dimers bind to specific DNA sequences, promoting the transcription of genes that are pivotal in mediating inflammation and fibrosis. (By Figdraw).

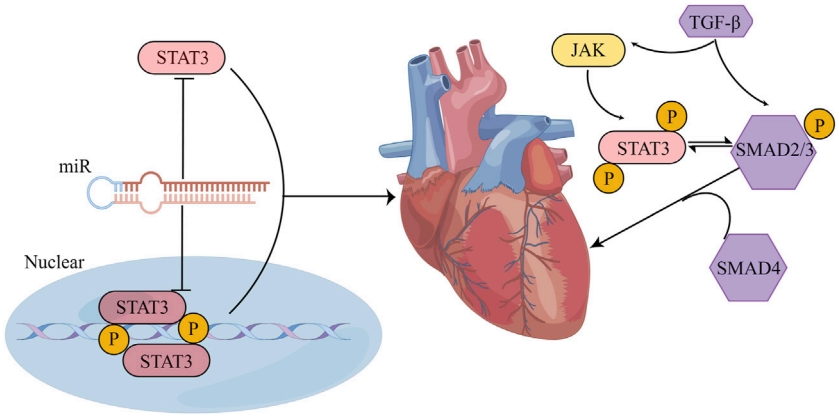

FIGURE 7
STAT3 influences cardiac fibrosis through multiple pathways. (1) The crosstalk between STAT3 and miR manifests in several ways: STAT3 can form either a direct feedback or an indirect feedback loop by binding with miR; it can also mediate the transcription of downstream miR; meanwhile, miR can influence the translation of STAT3 mRNA. (2) Positioned downstream of the TGF-β/SMAD signaling cascade, STAT3 might collaboratively regulate myocardial fibrosis with TGF-β. Their synergistic action could potentially be associated with the phosphorylation of STAT3. (By Figdraw).

signal molecule downstream of TGF-β or interacts with the TGF-β/Smad pathway to regulate cardiac fibrosis (Figure 7).

4.3 MicroRNAs (miRs)

MiRs are a class of endogenous noncoding single-stranded RNAs that are about 19–25 nucleotides long. First, within the nucleus, RNA polymerase II transcribes the gene encoding the miR into the primary transcript (pri-miR). Then, the pri-miR is transported to the cytoplasm under the cooperative action of the Ran-GTP enzyme and transporter Exportin5, and the double-stranded RNA-specific nuclease Dicer enzyme cleaves the pri-miR, which is transported to the cytoplasm to form double-stranded miR of 21–25 nucleotides. The helicase unwinds the double-stranded miR, leading to degradation of one strand and the formation of a mature miR with a hydroxyl group at the 3′-end and a phosphate group at the 5′-end. Finally, the RNA-induced gene silencing complex binds the mature miR, thereby regulating target gene silencing post-transcriptionally (Lu and Rothenberg, 2018). In recent years, the relationship between miRs and pathological fibrosis has been examined, but the specific mechanisms by which miRs regulate fibrosis are still worth exploring. During the development of liver fibrosis induced by viral hepatitis, the levels of miR-16, miR-146a, miR-221, and miR-222 were markedly increased in the serum of patients with chronic hepatitis C (Abdel-Al et al., 2018). In the livers of mice treated with CCl_4, miR-30c and miR-193 were specifically downregulated (Roy et al., 2015). Interestingly, other studies indicated that miR-29 could promote apoptosis in cardiomyocytes by downregulating antiapoptotic genes such as Bcl-2, CDC42 and Tcl-1, while miR-29 could prevent fibrosis by inhibiting the release of collagen from the ECM (Pekarsky et al., 2006; Mott et al., 2007; van Rooij et al., 2008). These results indicate that different miRs may have opposite effects on fibrosis regulation, and the same miR may have significant differences in fibrosis regulation.

STAT3 and miRs have crosstalk that is crucial for maintaining cardiac function under normal and pathological conditions. This STAT3-miR crosstalk can mediate cardiac disease in several ways. First, STAT3 can directly bind to miRs to mediate a feedback regulatory relationship or mediate an indirect feedback regulatory relationship with miRs through a long noncoding RNA (lncRNA)/protein. As an example, in oxygen-glucose deprivation-induced cardiomyocyte injury, lncRNA MIAT, which is associated with myocardial infarction, captures miR-181a-5p and boosts the expression of JAK2. This, in turn, amplifies myocardial inflammation and apoptosis through the JAK2/STAT3 signaling pathway (Tan et al., 2021). In addition, miR-21 activates the STAT3 signaling by targeting tumor suppressor cell adhesion molecule 1 (CADM1) and enhances cardiac fibrosis (Cao et al., 2017). Second, STAT3 can directly mediate the transcription of downstream miRs, and phosphorylated STAT3 can cooperate with other transcription factors to promote or inhibit the transcription of miRs. In diabetic hearts exposed to ischaemia/reperfusion, STAT3 has the ability to attach to the miR-17–92 promoter and stimulate the targeted inhibition of pro-apoptotic prolyl hydroxylase 3 (PHD3) by miR-17/20a, resulting in a decrease in apoptosis (Samidurai et al., 2020). Moreover, phosphorylated STAT3 can interact with NF-κB and inhibit miR-188-3p expression (Kuo et al., 2017; Sp et al., 2018; Masoumi-Dehghi et al., 2020). Third, miRs specifically recognize the 3′UTR of STAT3 mRNA and form incomplete complementary pairing, resulting in the inhibition of STAT3 mRNA translation, thereby blocking STAT3 expression. Following myocardial infarction, the expression of STAT3 mRNA is reduced by miR-17-5p and miR-124, which leads to the deterioration of autophagy, inflammation, myocardial remodeling, and apoptosis. These miRs bind to the 3′UTR of STAT3 mRNA (He et al., 2018; Chen et al., 2022). In summary, multiple miRs can interact with STAT3 through different mechanisms to enhance or inhibit cardiac fibrosis (Figure 7).

4.4 Other mediators impact cardiac fibrosis through the STAT3 signaling pathway

In addition to the above mediators that can affect cardiac fibrosis through the STAT3 signaling pathway, there are other mediators that can affect myocardial fibrosis caused by ischemia/reperfusion, atrial fibrillation, diabetic heart disease, DCM, and hypertensive heart damage through the STAT3 signaling pathway (Table 2).

5 The regulatory role of STAT3 and autophagy in cardiac fibrosis

Autophagy is widely present in eukaryotic organisms and is a process that degrades harmful substances in cells and promotes their recycling through the lysosome pathway. In general, moderate autophagy can maintain the stability of the internal environment, while excessive autophagy can induce cell damage (Kuma et al., 2017). The process is mainly divided into four stages: induction, initiation, elongation, and mature degradation, which are regulated by complex molecular mechanisms (Estrada-Navarrete et al., 2016; Liu et al., 2016; Lin et al., 2019; Kaushal et al., 2020). Autophagy recovers and removes damaged proteins and organelles, playing an important role in maintaining the normal function of myocardial cells (Mialet-Perez and Vindis, 2017). Interestingly, the role of autophagy in fibrosis may vary with fibrosis progression. Zhang et al. found that inhibiting autophagy could improve myocardial fibrosis in mice subjected to TAC surgery (Zhang et al., 2021). At 20 weeks after TAC in mice with endothelial leptin receptor gene knockout, myocardial fibrosis in these mice was improved by autophagy activation (Gogiraju et al., 2019). These research results demonstrate that the activation or inhibition of autophagy may occur during the process of cardiac fibrosis, and the role of autophagy in fibrosis has a dual nature.

Autophagy could potentially be linked to numerous signaling pathways, one of which is the STAT3 signaling pathway that governs the fate of cells, determining whether they survive or perish. Yuan et al.'s research indicates that relaxin attenuates TGF-β1-induced autophagy in primary CFs by suppressing the phosphorylation of STAT3, thereby reducing cardiac fibrosis (Yuan et al., 2017). In septic cardiomyopathy, the reduced expression of miR-125b leads to excessive activation of STAT3/high mobility group box protein 1 (HMGB1), resulting in elevated ROS generation and impaired autophagic flow, ultimately leading to myocardial

TABLE 2 Mediators regulate fibrosis through the STAT3 signaling pathway.

Mediators	Models	Effects and related mechanisms	Reference
SHP-1	SHP-1-overexpressing myocytes and fibroblasts	The use of STAT3 agonist colivelin leads to more ROS generation, ECM deposition, and TGF-β1/SMAD2 activation	Zang et al. (2023)
	Hypoxia/reoxygenation induced cardiomyocytes	Y-box protein 1 knockdown attenuates acute myocardial infarction damage via SHP-1 mediated STAT3 suppression	Cao et al. (2020)
PTEN	Coronary artery ischemia/reperfusion model in Type 1 diabetes rats induced by Streptozotocin	PTEN partially inhibits the post ischemic regulation and post hypoxic regulation of diabetes heart through destroying JAK2/STAT3 signaling pathway	Xue et al. (2016)
βIV spectrin	Cardiac specificity βIV spectrin KO mice	βIV spectrin deficiency in cardiomyocytes causes STAT3 impairment, fibrosis, and impaired cardiac function	Unudurthi et al. (2018)
	Genetic and acquired mouse models of βIV-spectrin deficiency	βIV spectrin protein dysfunction leads to nuclear STAT3 accumulation and activation, which changes gene expression and CF behavior. Fibrosis and cardiac dysfunction in βIV spectrin-deficient mice are abolished by STAT3 inhibition	Patel et al. (2019)
Elabela	Ang II induced myocardial hypertrophy and fibrosis exacerbation in hypertensive mice	By inhibiting the IL-6/STAT3/GPX4 signaling pathway, antagonize the promoting effects of Ang II mediated cardiac microvascular endothelial cells deionization, adverse myocardial remodeling, fibrosis, and cardiac dysfunction	Zhang et al. (2022b)
PPAR	Type 1 diabetes rat model induced by Streptozotocin	PPARδ activation might suppress STAT3 and lower connective tissue growth factor and Fibronectin levels in diabetic rats with cardiac fibrosis	Lo et al. (2017b)
	PPARα knockout mice	PPARα blocks T helper 17 cell differentiation via IL-6/STAT3/RORγT pathway, thus alleviating autoimmune Myocarditis	Chang et al. (2019)
SIRT3	SIRT3 knockout mice	SIRT3 can inhibit the STAT3-NFATc2 signaling pathway, thereby reducing myofibroblast transdifferentiation and preventing cardiac fibrosis	Guo et al. (2017)

Abbreviation: SHP-1, tyrosine phosphatase 1; ECM, extracellular matrix; ROS, active oxygen; TGF-β1, transforming growth factor-β1; SMAD2, small mother against decapentaplegic 2; PTEN, phosphatase and tensin homologue deleted on chromosome 10; CF, cardiac fibroblasts; GPX4, glutathione peroxidase; PPAR, peroxisome proliferator-activated receptor.

dysfunction (Yu et al., 2021). Additionally, the overexpression of Src-associated in mitosis 68 (Sam68) promotes the osteogenic differentiation of human valvular interstitial cells (hVICs) through the STAT3 signaling-mediated autophagy inhibition, thus inducing aortic valve calcification, while knockdown of Sam68 reduces the phosphorylation of TNF-α-activated STAT3 and the expression of downstream genes, thereby affecting autophagic flow in hVICs (Liu et al., 2023b). The activation of STAT3 is crucial for reducing cardiac autophagy and inhibiting cardiac ischemia/reperfusion injury, as demonstrated by the inhibition of soluble receptor for advanced glycation end-products on cardiac ischemia/reperfusion injury (Dang et al., 2019).

6 Challenges and opportunities for targeting the STAT3 signaling pathway for the treatment of fibrosis

Targeting STAT3 for heart disease treatment presents significant challenges. STAT3 is widely recognized for its role in promoting myocardial fibrosis. However, myocardial fibrosis may not always be detrimental in certain heart diseases. Excessive fibrosis, for instance, can lead to adverse remodeling in myocardial infarction patients, potentially resulting in heart failure. Yet, in the early stages of myocardial infarction, fibrosis is crucial in maintaining the structural integrity of the infarcted ventricle (Prabhu and Frangogiannis, 2016). Moreover, STAT3 actively participates in the activation and proliferation of CFs, fostering fibrotic remodeling. In cardiomyocytes, STAT3 exhibits a dual nature. It can offer protective or adverse effects, such as enhancing survival and mitigating oxidative stress or mediating cardiac hypertrophy (Wang et al., 2021; Li et al., 2022). Despite cardiomyocytes not being directly involved in ECM production, they can influence the fibrotic response through paracrine signals (Qu et al., 2017). Additionally, the STAT3 signaling pathway interacts with other pathways, playing varying roles. JAK1, for example, binds to TGF-βR1, while JAKs also associate with gp130 and get activated by TGF-β (Itoh et al., 2018). Previous studies have shown that STAT3 works in tandem with Smad3 to induce connective tissue growth factor, contributing to fibrosis (Liu et al., 2013; Tang et al., 2017). Conversely, overactivated STAT3 signaling in lung fibroblasts diminishes SMAD signaling by reducing Smad3 phosphorylation, potentially due to Smad7 induction, although this theory requires experimental validation (O'Donoghue et al., 2012). Thus, identifying the optimal timing for STAT3 inhibition is crucial for maximizing therapeutic benefits and minimizing side effects. Targeting STAT3 in CFs could effectively reduce fibrosis, but its protective potential in cardiomyocytes warrants consideration. Overall, STAT3's role in cardiac biology is multifaceted. A thorough

TABLE 3 STAT3 inhibitors for treating organ fibrosis.

Classification	Inhibitor name	Target site	Mode of targeting STAT3	Fibrotic organs treated	Reference
Small molecules	Stattic	SH2	Phosphorylation	myocardium, liver, lung, kidney	Celada et al. (2018), Dong et al. (2019), Fu et al. (2019), Park et al. (2022)
	S3I-201	SH2	Dimerization	myocardium, lung, liver	Chen et al. (2017b), Wang et al. (2018), Yuan et al. (2023)
	BP-1–102	SH2	Dimerization	kidney	Zhu et al. (2019)
	STX-0119	NTD	DNA binding	liver, kidney	Choi et al. (2019), Makitani et al. (2020)
	Niclosamide	Unknown	Unknown	liver, lung, kidney	Chen et al. (2021), Cui et al. (2021), Gan et al. (2023)
Natural compounds	Cucurbitacin I	SH2	Phosphorylation	liver	Hu et al. (2020a)
	Cryptotanshinone	SH2	Phosphorylation	myocardium, liver, lung	Lo et al. (2017a), Zhang et al. (2019a), Zhao et al. (2022)

understanding of its function across various cell types and disease stages is essential for developing effective treatments.

Despite the complexities in targeting STAT3 signaling for fibrosis treatment, recent advancements have yielded promising results (Table 3). Presently, methods to directly inhibit STAT3, aimed at targeting fibrosis, are categorized based on various target domains. These include the SH2, DBD, NTD, and TAD. In this section, we highlight key STAT3 inhibitors that specifically target these domains of the STAT3 protein.

6.1 Inhibitors targeting the SH2 domain

STAT3 homodimerization is facilitated by protein-protein interactions between the SH2 domains of the individual monomers, particularly via phosphorylation at Tyr705. This pivotal molecular interaction has been harnessed to develop inhibitors targeting STAT3 directly (Furtek et al., 2016). Inhibiting the SH2 domain not only disrupts STAT3 activation and dimerization but also impedes its subsequent nuclear translocation and the expression of genes regulated by STAT3.

Several small molecule STAT3 inhibitors, notably Stattic, S3I-201, and S3I-201 analogs, play a significant role in mitigating myocardial fibrosis. These inhibitors function by binding to the SH2 domain of STAT3, thereby curtailing its activity. Elevated levels of fibroblast growth factor 23 (FGF23) are reported to induce atrial fibrosis in atrial fibrillation patients through enhancing ROS production and subsequent STAT3 and Smad3 phosphorylation. Stattic has been shown to counteract these effects (Dong et al., 2019). Moreover, administering S3I-201 to mice with myocardial infarction has demonstrated reduced left atrial fibrosis *in vivo* (Chen et al., 2017b).

Another category of inhibitors targeting STAT3's SH2 domain comprises derivatives of natural compounds. Cryptotanshinone, a primary active component extracted from Salvia miltiorrhiza, suppresses the STAT3 pathway to reduce cardiac fibrosis and improve cardiac function in diabetic rats (Lo et al., 2017a). *In vitro* studies reveal that cryptotanshinone significantly curbs Ang II-induced cardiomyocyte hypertrophy and TGF-β-induced myofibroblast activation by impeding STAT3 phosphorylation and nuclear translocation (Li et al., 2023). Additionally, natural compounds like curcumin and resveratrol have been identified to possess properties beneficial in combating atherosclerosis (Zordoky et al., 2015; Ganjali et al., 2017).

These inhibitors are crucial for their anti-inflammatory and anti-atherosclerotic properties, suggesting their potential as therapeutic agents for ameliorating fibrosis. However, these inhibitors are not without drawbacks. A primary issue is that most inhibitors targeting the SH2 domain lack specificity to STAT3, making it challenging to exclude the involvement of other STAT proteins in fibrosis (Szelag et al., 2016). Additionally, STAT3 monomers or unphosphorylated STAT3 proteins can interact with other proteins to transcribe downstream target genes, which limits the efficacy of targeting the SH2 domain. Further complicating matters, activating mutations in the SH domain have been identified in somatic cells. The impact of these somatic mutations on the binding efficiency of SH2 domain inhibitors to STAT3, and consequently on their effectiveness, remains to be fully understood (Qiu and Fan, 2016). Therefore, the precise targeting of STAT3's SH2 domain warrants further research focus.

6.2 Inhibitors targeting the DBD domain

The DBD of STAT3 specifically recognizes and binds to distinct DNA elements in target genes. This selective interaction facilitates the precise induction of target gene expression, characterized by high specificity.

Research has uncovered that platinum compounds, including IS3-295, CPA-1, CPA-7, and platinum tetrachloride (IV), effectively block the DNA-binding activity of STAT3. These compounds can inhibit cell growth and induce apoptosis, while not affecting normal cells and avoiding prolonged STAT3 activation (Beebe et al., 2018). Additionally, Galiellalactone, a natural product, impedes STAT3's DNA-binding activity by interacting with its DBD domain. To enhance its oral bioavailability, N-acetyl L-cysteine methyl ester has been added to the thiol group, resulting in the creation of the prodrug GPA512. However, GPA512's lack of specificity, as it also disrupts other signaling pathways like NF-κB and TGF-β, could pose

challenges in its future development (Don-Doncow et al., 2014; Escobar et al., 2016). InS3-54, discovered through an advanced computer screening method, selectively binds to STAT3's DBD domain *in vitro*, inhibiting its DNA-binding activity. Its analog, InS3-54A18, exhibits improved solubility, specificity, and pharmacological properties, while showing minimal side effects in animal models (Huang et al., 2016).

While virtual screening techniques, including molecular modeling, have demonstrated that certain inhibitors can directly bind to the DBD domain of STAT3, the scarcity of adequate assay systems has limited the identification of small molecule inhibitors in this category. This constraint has significantly impeded the drug development process. Additionally, inhibitors targeting the STAT3 DBD encounter similar challenges to those faced by SH2 domain-targeting inhibitors in terms of therapeutic application.

6.3 Inhibitors targeting NTD and TAD domains

Inhibitors targeting the NTDs and TAD of STAT3 can modulate the binding of STAT3 dimers and regulate DNA transcription, potentially contributing to anti-fibrotic effects. In the study of the selective STAT3 NTD inhibitor ST3-H2A2, Timofeeva et al. observed that this compound robustly activated apoptosis genes, leading to the induction of apoptosis in cancer cells (Timofeeva et al., 2013). Moreover, researchers have successfully identified the allosterically active small molecule K116, which binds to the TAD of STAT3 and effectively inhibits its activity (Huang et al., 2018).

In summary, while numerous STAT3 inhibitors have demonstrated anti-fibrotic properties, identifying inhibitors that are highly efficient, low in toxicity, and have minimal side effects remains a challenge. Additionally, there is a scarcity of extensive animal studies on the pharmacology and toxicology of these inhibitors. Furthermore, only a limited number of these inhibitors have progressed to clinical evaluation. However, the integration of STAT3 inhibitors with other targeted therapeutic agents, particularly in combination with immunotherapy agents, offers promising potential. It is hoped that future research will lead to significant advancements, enabling the broader clinical application of STAT3 inhibitors.

7 Conclusion

Cardiac fibrosis results from the excessive accumulation of ECM in the myocardium and is central to many cardiac pathologies. Since JAK/STAT3 activation can increase fibrotic effector cells and ECM deposition through various pathways, it may be a potential target of antifibrotic therapy. As mentioned previously, we emphasized the promoting effects of various mediators on cardiac fibrosis through activation of the JAK/STAT3 signaling pathway. However, there may be many other mediators that have not yet been identified, and modern proteomics technology and protein identification will speed up the discovery. Regarding fibrosis, the antifibrotic effect of STAT3 inhibitors is receiving attention, but there has been little research on their ability to inhibit myocardial fibrosis. While further research is required to elucidate its role in various types of myocardial fibrosis, the JAK/STAT3 signaling holds promise as a therapeutic target for cardiac fibrosis due to its connection between cardiac inflammation and fibrosis.

Author contributions

HJ: Formal Analysis, Writing–original draft, Writing–review and editing. JY: Data curation, Formal Analysis, Writing–original draft. TL: Formal Analysis, Funding acquisition, Writing–review and editing. XW: Data curation, Writing–review and editing. ZF: Data curation, Visualization, Writing–review and editing. QY: Conceptualization, Software, Writing–review and editing. YD: Conceptualization, Funding acquisition, Writing–original draft, Writing–review and editing.

Funding

The author(s) declare financial support was received for the research, authorship, and/or publication of this article. This work was supported by Grants from the National Natural Science Foundation of China (Grant No. 82200287 to YD), Sichuan Science and Technology Program (Grant Nos. 2023NSFSC1653 to YD and 2022NSFSC0674 to TL), Luzhou Science and Technology Project (Grant No. 2022-JYJ-106 to YD), and Southwest Medical University Science and Technology Project (Grant No. 2021ZKMS034 to TL).

Conflict of interest

The authors declare that the research was conducted in the absence of any commercial or financial relationships that could be construed as a potential conflict of interest.

Publisher's note

References

Abdel-Al, A., El-Ahwany, E., Zoheiry, M., Hassan, M., Ouf, A., Abu-Taleb, H., et al. (2018). miRNA-221 and miRNA-222 are promising biomarkers for progression of liver fibrosis in HCV Egyptian patients. *Virus Res.* 253, 135–139. doi:10.1016/j.virusres.2018.06.007

Aftabizadeh, M., Li, Y. J., Zhao, Q., Zhang, C., Ambaye, N., Song, J., et al. (2021). Potent antitumor effects of cell-penetrating peptides targeting STAT3 axis. *JCI Insight* 6 (2), e136176. doi:10.1172/jci.insight.136176

Aisagbonhi, O., Rai, M., Ryzhov, S., Atria, N., Feoktistov, I., and Hatzopoulos, A. K. (2011). Experimental myocardial infarction triggers canonical Wnt signaling and endothelial-to-mesenchymal transition. *Dis. Model Mech.* 4 (4), 469–483. doi:10.1242/dmm.006510

Alexander, W. S. (2002). Suppressors of cytokine signalling (SOCS) in the immune system. *Nat. Rev. Immunol.* 2 (6), 410–416. doi:10.1038/nri818

Ali, S. R., Ranjbarvaziri, S., Talkhabi, M., Zhao, P., Subat, A., Hojjat, A., et al. (2014). Developmental heterogeneity of cardiac fibroblasts does not predict pathological proliferation and activation. *Circ. Res.* 115 (7), 625–635. doi:10.1161/circresaha.115.303794

Aoki, T., Fukumoto, Y., Sugimura, K., Oikawa, M., Satoh, K., Nakano, M., et al. (2011). Prognostic impact of myocardial interstitial fibrosis in non-ischemic heart failure. -Comparison between preserved and reduced ejection fraction heart failure. *Circ. J.* 75 (11), 2605–2613. doi:10.1253/circj.cj-11-0568

Avalle, L., Camporeale, A., Morciano, G., Caroccia, N., Ghetti, E., Orecchia, V., et al. (2019). STAT3 localizes to the ER, acting as a gatekeeper for ER-mitochondrion Ca(2+) fluxes and apoptotic responses. *Cell Death Differ.* 26 (5), 932–942. doi:10.1038/s41418-018-0171-y

Avalle, L., and Poli, V. (2018). Nucleus, Mitochondrion, or Reticulum? STAT3 à La Carte. *Int. J. Mol. Sci.* 19 (9), 2820. doi:10.3390/ijms19092820

Azevedo, C. F., Nigri, M., Higuchi, M. L., Pomerantzeff, P. M., Spina, G. S., Sampaio, R. O., et al. (2010). Prognostic significance of myocardial fibrosis quantification by histopathology and magnetic resonance imaging in patients with severe aortic valve disease. *J. Am. Coll. Cardiol.* 56 (4), 278–287. doi:10.1016/j.jacc.2009.12.074

Azushima, K., Morisawa, N., Tamura, K., and Nishiyama, A. (2020). Recent research advances in renin-angiotensin-aldosterone system receptors. *Curr. Hypertens. Rep.* 22 (3), 22. doi:10.1007/s11906-020-1028-6

Babon, J. J., Kershaw, N. J., Murphy, J. M., Varghese, L. N., Laktyushin, A., Young, S. N., et al. (2012). Suppression of cytokine signaling by SOCS3: characterization of the mode of inhibition and the basis of its specificity. *Immunity* 36 (2), 239–250. doi:10.1016/j.immuni.2011.12.015

Banerjee, S., Biehl, A., Gadina, M., Hasni, S., and Schwartz, D. M. (2017). JAK-STAT signaling as a target for inflammatory and autoimmune diseases: current and future prospects. *Drugs* 77 (5), 521–546. doi:10.1007/s40265-017-0701-9

Bao, Q., Zhang, B., Suo, Y., Liu, C., Yang, Q., Zhang, K., et al. (2020). Intermittent hypoxia mediated by TSP1 dependent on STAT3 induces cardiac fibroblast activation and cardiac fibrosis. *Elife* 9, e49923. doi:10.7554/eLife.49923

Barry, S. P., Townsend, P. A., Latchman, D. S., and Stephanou, A. (2007). Role of the JAK-STAT pathway in myocardial injury. *Trends Mol. Med.* 13 (2), 82–89. doi:10.1016/j.molmed.2006.12.002

Beebe, J. D., Liu, J. Y., and Zhang, J. T. (2018). Two decades of research in discovery of anticancer drugs targeting STAT3, how close are we? *Pharmacol. Ther.* 191, 74–91. doi:10.1016/j.pharmthera.2018.06.006

Bharadwaj, U., Kasembeli, M. M., Robinson, P., and Tweardy, D. J. (2020). Targeting Janus kinases and signal transducer and activator of transcription 3 to treat inflammation, fibrosis, and cancer: rationale, progress, and caution. *Pharmacol. Rev.* 72 (2), 486–526. doi:10.1124/pr.119.018440

Boengler, K., Hilfiker-Kleiner, D., Heusch, G., and Schulz, R. (2010). Inhibition of permeability transition pore opening by mitochondrial STAT3 and its role in myocardial ischemia/reperfusion. *Basic Res. Cardiol.* 105 (6), 771–785. doi:10.1007/s00395-010-0124-1

Bourillot, P. Y., Aksoy, I., Schreiber, V., Wianny, F., Schulz, H., Hummel, O., et al. (2009). Novel STAT3 target genes exert distinct roles in the inhibition of mesoderm and endoderm differentiation in cooperation with Nanog. *Stem Cells* 27 (8), 1760–1771. doi:10.1002/stem.110

Brocker, C., Thompson, D., Matsumoto, A., Nebert, D. W., and Vasiliou, V. (2010). Evolutionary divergence and functions of the human interleukin (IL) gene family. *Hum. Genomics* 5 (1), 30–55. doi:10.1186/1479-7364-5-1-30

Bujak, M., and Frangogiannis, N. G. (2007). The role of TGF-beta signaling in myocardial infarction and cardiac remodeling. *Cardiovasc Res.* 74 (2), 184–195. doi:10.1016/j.cardiores.2006.10.002

Caldenhoven, E., van Dijk, T. B., Solari, R., Armstrong, J., Raaijmakers, J. A., Lammers, J. W., et al. (1996). STAT3beta, a splice variant of transcription factor STAT3, is a dominant negative regulator of transcription. *J. Biol. Chem.* 271 (22), 13221–13227. doi:10.1074/jbc.271.22.13221

Camporeale, A., Marino, F., Papageorgiou, A., Carai, P., Fornero, S., Fletcher, S., et al. (2013). STAT3 activity is necessary and sufficient for the development of immune-mediated myocarditis in mice and promotes progression to dilated cardiomyopathy. *EMBO Mol. Med.* 5 (4), 572–590. doi:10.1002/emmm.201201876

Cao, W., Shi, P., and Ge, J. J. (2017). miR-21 enhances cardiac fibrotic remodeling and fibroblast proliferation via CADM1/STAT3 pathway. *BMC Cardiovasc Disord.* 17 (1), 88. doi:10.1186/s12872-017-0520-7

Cao, X., Zhu, N., Zhang, Y., Chen, Y., Zhang, J., Li, J., et al. (2020). Y-box protein 1 promotes hypoxia/reoxygenation- or ischemia/reperfusion-induced cardiomyocyte apoptosis via SHP-1-dependent STAT3 inactivation. *J. Cell Physiol.* 235 (11), 8187–8198. doi:10.1002/jcp.29474

Celada, L. J., Kropski, J. A., Herazo-Maya, J. D., Luo, W., Creecy, A., Abad, A. T., et al. (2018). PD-1 up-regulation on CD4+ T cells promotes pulmonary fibrosis through STAT3-mediated IL-17A and TGF-β1 production. *Sci. Transl. Med.* 10 (460), eaar8356. doi:10.1126/scitranslmed.aar8356

Chakraborty, D., Šumová, B., Mallano, T., Chen, C. W., Distler, A., Bergmann, C., et al. (2017). Activation of STAT3 integrates common profibrotic pathways to promote fibroblast activation and tissue fibrosis. *Nat. Commun.* 8 (1), 1130. doi:10.1038/s41467-017-01236-6

Chang, H., Zhao, F., Xie, X., Liao, Y., Song, Y., Liu, C., et al. (2019). PPARα suppresses Th17 cell differentiation through IL-6/STAT3/RORγt pathway in experimental autoimmune myocarditis. *Exp. Cell Res.* 375 (1), 22–30. doi:10.1016/j.yexcr.2018.12.005

Chang, S. H., Yeh, Y. H., Lee, J. L., Hsu, Y. J., Kuo, C. T., and Chen, W. J. (2017). Transforming growth factor-β-mediated CD44/STAT3 signaling contributes to the development of atrial fibrosis and fibrillation. *Basic Res. Cardiol.* 112 (5), 58. doi:10.1007/s00395-017-0647-9

Chen, B., Yang, Y., Wu, J., Song, J., and Lu, J. (2022). microRNA-17-5p downregulation inhibits autophagy and myocardial remodelling after myocardial infarction by targeting STAT3. *Autoimmunity* 55 (1), 43–51. doi:10.1080/08916934.2021.1992754

Chen, D., Li, Z., Bao, P., Chen, M., Zhang, M., Yan, F., et al. (2019a). Nrf2 deficiency aggravates Angiotensin II-induced cardiac injury by increasing hypertrophy and enhancing IL-6/STAT3-dependent inflammation. *Biochim. Biophys. Acta Mol. Basis Dis.* 1865 (6), 1253–1264. doi:10.1016/j.bbadis.2019.01.020

Chen, F., Chen, D., Zhang, Y., Jin, L., Zhang, H., Wan, M., et al. (2017a). Interleukin-6 deficiency attenuates angiotensin II-induced cardiac pathogenesis with increased myocyte hypertrophy. *Biochem. Biophys. Res. Commun.* 494 (3-4), 534–541. doi:10.1016/j.bbrc.2017.10.119

Chen, M., Li, H., Wang, G., Shen, X., Zhao, S., and Su, W. (2016). Atorvastatin prevents advanced glycation end products (AGEs)-induced cardiac fibrosis via activating peroxisome proliferator-activated receptor gamma (PPAR-γ). *Metabolism* 65 (4), 441–453. doi:10.1016/j.metabol.2015.11.007

Chen, Q., Gao, C., Wang, M., Fei, X., and Zhao, N. (2021). TRIM18-Regulated STAT3 signaling pathway via PTP1B promotes renal epithelial-mesenchymal transition, inflammation, and fibrosis in diabetic kidney disease. *Front. Physiol.* 12, 709506. doi:10.3389/fphys.2021.709506

Chen, W., Yuan, H., Cao, W., Wang, T., Chen, W., Yu, H., et al. (2019b). Blocking interleukin-6 trans-signaling protects against renal fibrosis by suppressing STAT3 activation. *Theranostics* 9 (14), 3980–3991. doi:10.7150/thno.32352

Chen, X., Su, J., Feng, J., Cheng, L., Li, Q., Qiu, C., et al. (2019c). TRIM72 contributes to cardiac fibrosis via regulating STAT3/Notch-1 signaling. *J. Cell Physiol.* 234 (10), 17749–17756. doi:10.1002/jcp.28400

Chen, X., Tang, Y., Gao, M., Qin, S., Zhou, J., and Li, X. (2015). Prenatal exposure to lipopolysaccharide results in myocardial fibrosis in rat offspring. *Int. J. Mol. Sci.* 16 (5), 10986–10996. doi:10.3390/ijms160510986

Chen, Y., Surinkaew, S., Naud, P., Qi, X. Y., Gillis, M. A., Shi, Y. F., et al. (2017b). JAK-STAT signalling and the atrial fibrillation promoting fibrotic substrate. *Cardiovasc Res.* 113 (3), 310–320. doi:10.1093/cvr/cvx004

Choi, S., Jung, H. J., Kim, M. W., Kang, J. H., Shin, D., Jang, Y. S., et al. (2019). A novel STAT3 inhibitor, STX-0119, attenuates liver fibrosis by inactivating hepatic stellate cells in mice. *Biochem. Biophys. Res. Commun.* 513 (1), 49–55. doi:10.1016/j.bbrc.2019.03.156

Christia, P., Bujak, M., Gonzalez-Quesada, C., Chen, W., Dobaczewski, M., Reddy, A., et al. (2013). Systematic characterization of myocardial inflammation, repair, and remodeling in a mouse model of reperfused myocardial infarction. *J. Histochem Cytochem* 61 (8), 555–570. doi:10.1369/0022155413493912

Christova, R., Jones, T., Wu, P. J., Bolzer, A., Costa-Pereira, A. P., Watling, D., et al. (2007). P-STAT1 mediates higher-order chromatin remodelling of the human MHC in response to IFNgamma. *J. Cell Sci.* 120 (18), 3262–3270. doi:10.1242/jcs.012328

Chung, H., Kim, Y., Park, C. H., Kim, J. Y., Min, P. K., Yoon, Y. W., et al. (2021). Effect of sarcomere and mitochondria-related mutations on myocardial fibrosis in patients with hypertrophic cardiomyopathy. *J. Cardiovasc Magn. Reson* 23 (1), 18. doi:10.1186/s12968-021-00718-3

Cleutjens, J. P., Verluyten, M. J., Smiths, J. F., and Daemen, M. J. (1995). Collagen remodeling after myocardial infarction in the rat heart. *Am. J. Pathol.* 147 (2), 325–338.

Corwin, E. J. (2000). Understanding cytokines. Part I: physiology and mechanism of action. *Biol. Res. Nurs.* 2 (1), 30–40. doi:10.1177/109980040000200104

Cui, Z. Y., Wang, G., Zhang, J., Song, J., Jiang, Y. C., Dou, J. Y., et al. (2021). Parthenolide, bioactive compound of Chrysanthemum parthenium L., ameliorates fibrogenesis and inflammation in hepatic fibrosis via regulating the crosstalk of TLR4 and STAT3 signaling pathway. *Phytother. Res.* 35 (10), 5680–5693. doi:10.1002/ptr.7214

Dang, M., Zeng, X., Chen, B., Wang, H., Li, H., Liu, Y., et al. (2019). Soluble receptor for advance glycation end-products inhibits ischemia/reperfusion-induced myocardial autophagy via the STAT3 pathway. *Free Radic. Biol. Med.* 130, 107–119. doi:10.1016/j.freeradbiomed.2018.10.437

Darnell, J. E., Jr. (1997). STATs and gene regulation. *Science* 277 (5332), 1630–1635. doi:10.1126/science.277.5332.1630

Darnell, J. E., Jr., Kerr, I. M., and Stark, G. R. (1994). Jak-STAT pathways and transcriptional activation in response to IFNs and other extracellular signaling proteins. *Science* 264 (5164), 1415–1421. doi:10.1126/science.8197455

Dasgupta, M., Unal, H., Willard, B., Yang, J., Karnik, S. S., and Stark, G. R. (2014). Critical role for lysine 685 in gene expression mediated by transcription factor unphosphorylated STAT3. *J. Biol. Chem.* 289 (44), 30763–30771. doi:10.1074/jbc.M114.603894

Dees, C., Pötter, S., Zhang, Y., Bergmann, C., Zhou, X., Luber, M., et al. (2020). TGF-β-induced epigenetic deregulation of SOCS3 facilitates STAT3 signaling to promote fibrosis. *J. Clin. Invest.* 130 (5), 2347–2363. doi:10.1172/jci122462

Dobaczewski, M., Bujak, M., Zymek, P., Ren, G., Entman, M. L., and Frangogiannis, N. G. (2006). Extracellular matrix remodeling in canine and mouse myocardial infarcts. *Cell Tissue Res.* 324 (3), 475–488. doi:10.1007/s00441-005-0144-6

Don-Doncow, N., Escobar, Z., Johansson, M., Kjellström, S., Garcia, V., Munoz, E., et al. (2014). Galiellalactone is a direct inhibitor of the transcription factor STAT3 in prostate cancer cells. *J. Biol. Chem.* 289 (23), 15969–15978. doi:10.1074/jbc.M114.564252

Dong, Q., Li, S., Wang, W., Han, L., Xia, Z., Wu, Y., et al. (2019). FGF23 regulates atrial fibrosis in atrial fibrillation by mediating the STAT3 and SMAD3 pathways. *J. Cell Physiol.* 234 (11), 19502–19510. doi:10.1002/jcp.28548

Durham, G. A., Williams, J. J. L., Nasim, M. T., and Palmer, T. M. (2019). Targeting SOCS proteins to control JAK-STAT signalling in disease. *Trends Pharmacol. Sci.* 40 (5), 298–308. doi:10.1016/j.tips.2019.03.001

Działo, E., Tkacz, K., and Błyszczuk, P. (2018). Crosstalk between the TGF-β and WNT signalling pathways during cardiac fibrogenesis. *Acta Biochim. Pol.* 65 (3), 341–349. doi:10.18388/abp.2018_2635

Eid, R. A., Alkhateeb, M. A., El-Kott, A. F., Eleawa, S. M., Zaki, M. S. A., Alaboodi, S. A., et al. (2019). A high-fat diet rich in corn oil induces cardiac fibrosis in rats by activating JAK2/STAT3 and subsequent activation of ANG II/TGF-1β/Smad3 pathway: the role of ROS and IL-6 trans-signaling. *J. Food Biochem.* 43 (8), e12952. doi:10.1111/jfbc.12952

Enomoto, D., Obana, M., Miyawaki, A., Maeda, M., Nakayama, H., and Fujio, Y. (2015). Cardiac-specific ablation of the STAT3 gene in the subacute phase of myocardial infarction exacerbated cardiac remodeling. *Am. J. Physiol. Heart Circ. Physiol.* 309 (3), H471–H480. doi:10.1152/ajpheart.00730.2014

Escobar, Z., Bjartell, A., Canesin, G., Evans-Axelsson, S., Sterner, O., Hellsten, R., et al. (2016). Preclinical characterization of 3β-(N-acetyl l-cysteine methyl ester)-2aβ,3-dihydrogaliellalactone (GPA512), a prodrug of a direct STAT3 inhibitor for the treatment of prostate cancer. *J. Med. Chem.* 59 (10), 4551–4562. doi:10.1021/acs.jmedchem.5b01814

Estrada-Navarrete, G., Cruz-Mireles, N., Lascano, R., Alvarado-Affantranger, X., Hernández-Barrera, A., Barraza, A., et al. (2016). An autophagy-related kinase is essential for the symbiotic relationship between Phaseolus vulgaris and both rhizobia and arbuscular mycorrhizal fungi. *Plant Cell* 28 (9), 2326–2341. doi:10.1105/tpc.15.01012

Feng, J., Witthuhn, B. A., Matsuda, T., Kohlhuber, F., Kerr, I. M., and Ihle, J. N. (1997). Activation of Jak2 catalytic activity requires phosphorylation of Y1007 in the kinase activation loop. *Mol. Cell Biol.* 17 (5), 2497–2501. doi:10.1128/mcb.17.5.2497

Ferreira, V. M., Marcelino, M., Piechnik, S. K., Marini, C., Karamitsos, T. D., Ntusi, N. A. B., et al. (2016). Pheochromocytoma is characterized by catecholamine-mediated myocarditis, focal and diffuse myocardial fibrosis, and myocardial dysfunction. *J. Am. Coll. Cardiol.* 67 (20), 2364–2374. doi:10.1016/j.jacc.2016.03.543

Francis Stuart, S. D., De Jesus, N. M., Lindsey, M. L., and Ripplinger, C. M. (2016). The crossroads of inflammation, fibrosis, and arrhythmia following myocardial infarction. *J. Mol. Cell Cardiol.* 91, 114–122. doi:10.1016/j.yjmcc.2015.12.024

Fu, H., Dong, R., Zhang, Y., Xu, J., Liu, M., and Chen, P. (2019). Tmub1 negatively regulates liver regeneration via inhibiting STAT3 phosphorylation. *Cell Signal* 55, 65–72. doi:10.1016/j.cellsig.2018.12.013

Fuglesteg, B. N., Suleman, N., Tiron, C., Kanhema, T., Lacerda, L., Andreasen, T. V., et al. (2008). Signal transducer and activator of transcription 3 is involved in the cardioprotective signalling pathway activated by insulin therapy at reperfusion. *Basic Res. Cardiol.* 103 (5), 444–453. doi:10.1007/s00395-008-0728-x

Furtek, S. L., Backos, D. S., Matheson, C. J., and Reigan, P. (2016). Strategies and approaches of targeting STAT3 for cancer treatment. *ACS Chem. Biol.* 11 (2), 308–318. doi:10.1021/acschembio.5b00945

Gan, C., Wang, Y., Xiang, Z., Liu, H., Tan, Z., Xie, Y., et al. (2023). Niclosamide-loaded nanoparticles (Ncl-NPs) reverse pulmonary fibrosis *in vivo* and *in vitro*. *J. Adv. Res.* 51, 109–120. doi:10.1016/j.jare.2022.10.018

Ganjali, S., Blesso, C. N., Banach, M., Pirro, M., Majeed, M., and Sahebkar, A. (2017). Effects of curcumin on HDL functionality. *Pharmacol. Res.* 119, 208–218. doi:10.1016/j.phrs.2017.02.008

Gao, H., Huang, X., Tong, Y., and Jiang, X. (2020). Urolithin B improves cardiac function and reduces susceptibility to ventricular arrhythmias in rats after myocardial infarction. *Eur. J. Pharmacol.* 871, 172936. doi:10.1016/j.ejphar.2020.172936

Gao, S., Zhan, L., Yang, Z., Shi, R., Li, H., Xia, Z., et al. (2017). Remote limb ischaemic postconditioning protects against myocardial ischaemia/reperfusion injury in mice: activation of JAK/STAT3-Mediated nrf2-antioxidant signalling. *Cell Physiol. Biochem.* 43 (3), 1140–1151. doi:10.1159/000481755

Garama, D. J., White, C. L., Balic, J. J., and Gough, D. J. (2016). Mitochondrial STAT3: powering up a potent factor. *Cytokine* 87, 20–25. doi:10.1016/j.cyto.2016.05.019

Geng, Z., Fan, W. Y., Zhou, B., Ye, C., Tong, Y., Zhou, Y. B., et al. (2019). FNDC5 attenuates obesity-induced cardiac hypertrophy by inactivating JAK2/STAT3-associated inflammation and oxidative stress. *J. Transl. Med.* 17 (1), 107. doi:10.1186/s12967-019-1857-8

Gogiraju, R., Hubert, A., Fahrer, J., Straub, B. K., Brandt, M., Wenzel, P., et al. (2019). Endothelial leptin receptor deletion promotes cardiac autophagy and angiogenesis following pressure overload by suppressing akt/mTOR signaling. *Circ. Heart Fail* 12 (1), e005622. doi:10.1161/circheartfailure.118.005622

Grosche, J., Meißner, J., and Eble, J. A. (2018). More than a syllable in fib-ROS-is: the role of ROS on the fibrotic extracellular matrix and on cellular contacts. *Mol. Asp. Med.* 63, 30–46. doi:10.1016/j.mam.2018.03.005

Guo, X., Yan, F., Li, J., Zhang, C., and Bu, P. (2017). SIRT3 attenuates AngII-induced cardiac fibrosis by inhibiting myofibroblasts transdifferentiation via STAT3-NFATc2 pathway. *Am. J. Transl. Res.* 9 (7), 3258–3269.

Gurzov, E. N., Stanley, W. J., Pappas, E. G., Thomas, H. E., and Gough, D. J. (2016). The JAK/STAT pathway in obesity and diabetes. *Febs J.* 283 (16), 3002–3015. doi:10.1111/febs.13709

Gyöngyösi, M., Winkler, J., Ramos, I., Do, Q. T., Firat, H., McDonald, K., et al. (2017). Myocardial fibrosis: biomedical research from bench to bedside. *Eur. J. Heart Fail* 19 (2), 177–191. doi:10.1002/ejhf.696

Haghikia, A., Ricke-Hoch, M., Stapel, B., Gorst, I., and Hilfiker-Kleiner, D. (2014). STAT3, a key regulator of cell-to-cell communication in the heart. *Cardiovasc Res.* 102 (2), 281–289. doi:10.1093/cvr/cvu034

Han, J., Ye, S., Zou, C., Chen, T., Wang, J., Li, J., et al. (2018). Angiotensin II causes biphasic STAT3 activation through TLR4 to initiate cardiac remodeling. *Hypertension* 72 (6), 1301–1311. doi:10.1161/hypertensionaha.118.11860

Harhous, Z., Booz, G. W., Ovize, M., Bidaux, G., and Kurdi, M. (2019). An update on the multifaceted roles of STAT3 in the heart. *Front. Cardiovasc Med.* 6, 150. doi:10.3389/fcvm.2019.00150

Hattori, R., Maulik, N., Otani, H., Zhu, L., Cordis, G., Engelman, R. M., et al. (2001). Role of STAT3 in ischemic preconditioning. *J. Mol. Cell Cardiol.* 33 (11), 1929–1936. doi:10.1006/jmcc.2001.1456

He, F., Liu, H., Guo, J., Yang, D., Yu, Y., Yu, J., et al. (2018). Inhibition of MicroRNA-124 reduces cardiomyocyte apoptosis following myocardial infarction via targeting STAT3. *Cell Physiol. Biochem.* 51 (1), 186–200. doi:10.1159/000495173

Hinz, B. (2007). Formation and function of the myofibroblast during tissue repair. *J. Invest. Dermatol* 127 (3), 526–537. doi:10.1038/sj.jid.5700613

Hinz, B. (2010). The myofibroblast: paradigm for a mechanically active cell. *J. Biomech.* 43 (1), 146–155. doi:10.1016/j.jbiomech.2009.09.020

Hsueh, Y. J., Chen, H. C., Chu, W. K., Cheng, C. C., Kuo, P. C., Lin, L. Y., et al. (2011). STAT3 regulates the proliferation and differentiation of rabbit limbal epithelial cells via a ΔNp63-dependent mechanism. *Invest. Ophthalmol. Vis. Sci.* 52 (7), 4685–4693. doi:10.1167/iovs.10-6103

Hu, H. H., Chen, D. Q., Wang, Y. N., Feng, Y. L., Cao, G., Vaziri, N. D., et al. (2018). New insights into TGF-β/Smad signaling in tissue fibrosis. *Chem. Biol. Interact.* 292, 76–83. doi:10.1016/j.cbi.2018.07.008

Hu, X., Li, J., Fu, M., Zhao, X., and Wang, W. (2021). The JAK/STAT signaling pathway: from bench to clinic. *Signal Transduct. Target Ther.* 6 (1), 402. doi:10.1038/s41392-021-00791-1

Hu, Z. G., Han, Y., Liu, Y., Zhao, Z., Ma, F., Cui, A., et al. (2020a). CREBZF as a key regulator of STAT3 pathway in the control of liver regeneration in mice. *Hepatology* 71 (4), 1421–1436. doi:10.1002/hep.30919

Hu, Z. G., Zhang, S., Chen, Y. B., Cao, W., Zhou, Z. Y., Zhang, J. N., et al. (2020b). DTNA promotes HBV-induced hepatocellular carcinoma progression by activating STAT3 and regulating TGFβ1 and P53 signaling. *Life Sci.* 258, 118029. doi:10.1016/j.lfs.2020.118029

Huang, M., Song, K., Liu, X., Lu, S., Shen, Q., Wang, R., et al. (2018). AlloFinder: a strategy for allosteric modulator discovery and allosterome analyses. *Nucleic Acids Res.* 46 (1), W451–w458. doi:10.1093/nar/gky374

Huang, W., Dong, Z., Chen, Y., Wang, F., Wang, C. J., Peng, H., et al. (2016). Small-molecule inhibitors targeting the DNA-binding domain of STAT3 suppress tumor growth, metastasis and STAT3 target gene expression *in vivo*. *Oncogene* 35 (6), 783–792. doi:10.1038/onc.2015.215

Hubbard, S. R. (2017). Mechanistic insights into regulation of JAK2 tyrosine kinase. *Front. Endocrinol. (Lausanne)* 8, 361. doi:10.3389/fendo.2017.00361

Huby, A. C., Antonova, G., Groenendyk, J., Gomez-Sanchez, C. E., Bollag, W. B., Filosa, J. A., et al. (2015). Adipocyte-Derived hormone leptin is a direct regulator of aldosterone secretion, which promotes endothelial dysfunction and cardiac fibrosis. *Circulation* 132 (22), 2134–2145. doi:10.1161/circulationaha.115.018226

Humphreys, B. D., Lin, S. L., Kobayashi, A., Hudson, T. E., Nowlin, B. T., Bonventre, J. V., et al. (2010). Fate tracing reveals the pericyte and not epithelial origin of myofibroblasts in kidney fibrosis. *Am. J. Pathol.* 176 (1), 85–97. doi:10.2353/ajpath.2010.090517

Huo, S., Shi, W., Ma, H., Yan, D., Luo, P., Guo, J., et al. (2021). Alleviation of inflammation and oxidative stress in pressure overload-induced cardiac remodeling and heart failure via IL-6/STAT3 inhibition by raloxifene. *Oxid. Med. Cell Longev.* 2021, 6699054. doi:10.1155/2021/6699054

Itoh, Y., Saitoh, M., and Miyazawa, K. (2018). Smad3-STAT3 crosstalk in pathophysiological contexts. *Acta Biochim. Biophys. Sin. (Shanghai)* 50 (1), 82–90. doi:10.1093/abbs/gmx118

Jahangiri, A., Dadmanesh, M., and Ghorban, K. (2020). STAT3 inhibition reduced PD-L1 expression and enhanced antitumor immune responses. *J. Cell Physiol.* 235 (12), 9457–9463. doi:10.1002/jcp.29750

Kamran, M. Z., Patil, P., and Gude, R. P. (2013). Role of STAT3 in cancer metastasis and translational advances. *Biomed. Res. Int.* 2013, 421821. doi:10.1155/2013/421821

Kanisicak, O., Khalil, H., Ivey, M. J., Karch, J., Maliken, B. D., Correll, R. N., et al. (2016). Genetic lineage tracing defines myofibroblast origin and function in the injured heart. *Nat. Commun.* 7, 12260. doi:10.1038/ncomms12260

Kaushal, G. P., Chandrashekar, K., Juncos, L. A., and Shah, S. V. (2020). Autophagy function and regulation in kidney disease. *Biomolecules* 10 (1), 100. doi:10.3390/biom10010100

Kazi, J. U., Kabir, N. N., Flores-Morales, A., and Rönnstrand, L. (2014). SOCS proteins in regulation of receptor tyrosine kinase signaling. *Cell Mol. Life Sci.* 71 (17), 3297–3310. doi:10.1007/s00018-014-1619-y

Kershaw, N. J., Murphy, J. M., Liau, N. P., Varghese, L. N., Laktyushin, A., Whitlock, E. L., et al. (2013a). SOCS3 binds specific receptor-JAK complexes to control cytokine signaling by direct kinase inhibition. *Nat. Struct. Mol. Biol.* 20 (4), 469–476. doi:10.1038/nsmb.2519

Kershaw, N. J., Murphy, J. M., Lucet, I. S., Nicola, N. A., and Babon, J. J. (2013b). Regulation of Janus kinases by SOCS proteins. *Biochem. Soc. Trans.* 41 (4), 1042–1047. doi:10.1042/bst20130077

Kishore, R., and Verma, S. K. (2012). Roles of STATs signaling in cardiovascular diseases. *Jakstat* 1 (2), 118–124. doi:10.4161/jkst.20115

Kuma, A., Komatsu, M., and Mizushima, N. (2017). Autophagy-monitoring and autophagy-deficient mice. *Autophagy* 13 (10), 1619–1628. doi:10.1080/15548627.2017.1343770

Kuo, W. Y., Hwu, L., Wu, C. Y., Lee, J. S., Chang, C. W., and Liu, R. S. (2017). STAT3/NF-κB-Regulated lentiviral TK/GCV suicide gene therapy for cisplatin-resistant triple-negative breast cancer. *Theranostics* 7 (3), 647–663. doi:10.7150/thno.16827

Leask, A. (2015). Getting to the heart of the matter: new insights into cardiac fibrosis. *Circ. Res.* 116 (7), 1269–1276. doi:10.1161/circresaha.116.305381

Lee, J. H., Kim, T. H., Oh, S. J., Yoo, J. Y., Akira, S., Ku, B. J., et al. (2013). Signal transducer and activator of transcription-3 (Stat3) plays a critical role in implantation via progesterone receptor in uterus. *Faseb J.* 27 (7), 2553–2563. doi:10.1096/fj.12-225664

Lee, T. M., Harn, H. J., Chiou, T. W., Chuang, M. H., Chen, C. H., Chuang, C. H., et al. (2019). Preconditioned adipose-derived stem cells ameliorate cardiac fibrosis by regulating macrophage polarization in infarcted rat hearts through the PI3K/STAT3 pathway. *Lab. Invest.* 99 (5), 634–647. doi:10.1038/s41374-018-0181-x

Li, H., Liang, Q., and Wang, L. (2019a). Icaritin inhibits glioblastoma cell viability and glycolysis by blocking the IL-6/Stat3 pathway. *J. Cell Biochem.* 120 (5), 7257–7264. doi:10.1002/jcb.28000

Li, Q., Ye, W. X., Huang, Z. J., Zhang, Q., and He, Y. F. (2019b). Effect of IL-6-mediated STAT3 signaling pathway on myocardial apoptosis in mice with dilated cardiomyopathy. *Eur. Rev. Med. Pharmacol. Sci.* 23 (7), 3042–3050. doi:10.26355/eurrev_201904_17586

Li, W., Qu, X., Kang, X., Zhang, H., Zhang, X., Hu, H., et al. (2022). Silibinin eliminates mitochondrial ROS and restores autophagy through IL6ST/JAK2/STAT3 signaling pathway to protect cardiomyocytes from doxorubicin-induced injury. *Eur. J. Pharmacol.* 929, 175153. doi:10.1016/j.ejphar.2022.175153

Li, W. J., Yan, H., Zhou, Z. Y., Zhang, N., Ding, W., Liao, H. H., et al. (2023). Cryptotanshinone attenuated pathological cardiac remodeling *in vivo* and *in vitro* experiments. *Oxid. Med. Cell Longev.* 2023, 4015199. doi:10.1155/2023/4015199

Li, W. X. (2008). Canonical and non-canonical JAK-STAT signaling. *Trends Cell Biol.* 18 (11), 545–551. doi:10.1016/j.tcb.2008.08.008

Li, Y., Zhang, X., Li, L., Wang, X., Chen, Z., Wang, X., et al. (2018). Mechanical stresses induce paracrine β-2 microglobulin from cardiomyocytes to activate cardiac fibroblasts through epidermal growth factor receptor. *Clin. Sci. (Lond)* 132 (16), 1855–1874. doi:10.1042/cs20180486

Lighthouse, J. K., and Small, E. M. (2016). Transcriptional control of cardiac fibroblast plasticity. *J. Mol. Cell Cardiol.* 91, 52–60. doi:10.1016/j.yjmcc.2015.12.016

Lin, T. A., Wu, V. C., and Wang, C. Y. (2019). Autophagy in chronic kidney diseases. *Cells* 8 (1), 61. doi:10.3390/cells8010061

Liongue, C., Taznin, T., and Ward, A. C. (2016). Signaling via the CytoR/JAK/STAT/SOCS pathway: emergence during evolution. *Mol. Immunol.* 71, 166–175. doi:10.1016/j.molimm.2016.02.002

Liu, J., Wang, F., and Luo, F. (2023a). The role of JAK/STAT pathway in fibrotic diseases: molecular and cellular mechanisms. *Biomolecules* 13 (1), 119. doi:10.3390/biom13010119

Liu, N., Shi, Y., and Zhuang, S. (2016). Autophagy in chronic kidney diseases. *Kidney Dis. (Basel)* 2 (1), 37–45. doi:10.1159/000444841

Liu, T., Song, D., Dong, J., Zhu, P., Liu, J., Liu, W., et al. (2017). Current understanding of the pathophysiology of myocardial fibrosis and its quantitative assessment in heart failure. *Front. Physiol.* 8, 238. doi:10.3389/fphys.2017.00238

Liu, X., Zheng, Q., Wang, K., Luo, J., Wang, Z., Li, H., et al. (2023b). Sam68 promotes osteogenic differentiation of aortic valvular interstitial cells by TNF-α/STAT3/autophagy axis. *J. Cell Commun. Signal* 17, 863–879. doi:10.1007/s12079-023-00733-2

Liu, Y., Liu, H., Meyer, C., Li, J., Nadalin, S., Königsrainer, A., et al. (2013). Transforming growth factor-β (TGF-β)-mediated connective tissue growth factor (CTGF) expression in hepatic stellate cells requires Stat3 signaling activation. *J. Biol. Chem.* 288 (42), 30708–30719. doi:10.1074/jbc.M113.478685

Lo, S. H., Hsu, C. T., Niu, H. S., Niu, C. S., Cheng, J. T., and Chen, Z. C. (2017a). Cryptotanshinone inhibits STAT3 signaling to alleviate cardiac fibrosis in type 1-like diabetic rats. *Phytother. Res.* 31 (4), 638–646. doi:10.1002/ptr.5777

Lo, S. H., Hsu, C. T., Niu, H. S., Niu, C. S., Cheng, J. T., and Chen, Z. C. (2017b). Ginsenoside Rh2 improves cardiac fibrosis via pparδ-STAT3 signaling in type 1-like diabetic rats. *Int. J. Mol. Sci.* 18 (7), 1364. doi:10.3390/ijms18071364

Lu, T. X., and Rothenberg, M. E. (2018). MicroRNA. *J. Allergy Clin. Immunol.* 141 (4), 1202–1207. doi:10.1016/j.jaci.2017.08.034

Makitani, K., Ogo, N., and Asai, A. (2020). STX-0119, a novel STAT3 dimerization inhibitor, prevents fibrotic gene expression in a mouse model of kidney fibrosis by regulating Cxcr4 and Ccr1 expression. *Physiol. Rep.* 8 (20), e14627. doi:10.14814/phy2.14627

Marciniec, K., Pawełczak, B., Latocha, M., Skrzypek, L., Maciążek-Jurczyk, M., and Boryczka, S. (2017). Synthesis, anti-breast cancer activity, and molecular docking study of a new group of acetylenic quinolinesulfonamide derivatives. *Molecules* 22 (2), 300. doi:10.3390/molecules22020300

Maritano, D., Sugrue, M. L., Tininini, S., Dewilde, S., Strobl, B., Fu, X., et al. (2004). The STAT3 isoforms alpha and beta have unique and specific functions. *Nat. Immunol.* 5 (4), 401–409. doi:10.1038/ni1052

Masoumi-Dehghi, S., Babashah, S., and Sadeghizadeh, M. (2020). microRNA-141-3p-containing small extracellular vesicles derived from epithelial ovarian cancer cells promote endothelial cell angiogenesis through activating the JAK/STAT3 and NF-κB signaling pathways. *J. Cell Commun. Signal* 14 (2), 233–244. doi:10.1007/s12079-020-00548-5

Matsuda, T., Nakamura, T., Nakao, K., Arai, T., Katsuki, M., Heike, T., et al. (1999). STAT3 activation is sufficient to maintain an undifferentiated state of mouse embryonic stem cells. *Embo J.* 18 (15), 4261–4269. doi:10.1093/emboj/18.15.4261

Mialet-Perez, J., and Vindis, C. (2017). Autophagy in health and disease: focus on the cardiovascular system. *Essays Biochem.* 61 (6), 721–732. doi:10.1042/ebc20170022

Minamoto, S., Ikegame, K., Ueno, K., Narazaki, M., Naka, T., Yamamoto, H., et al. (1997). Cloning and functional analysis of new members of STAT induced STAT inhibitor (SSI) family: SSI-2 and SSI-3. *Biochem. Biophys. Res. Commun.* 237 (1), 79–83. doi:10.1006/bbrc.1997.7080

Mir, S. A., Chatterjee, A., Mitra, A., Pathak, K., Mahata, S. K., and Sarkar, S. (2012). Inhibition of signal transducer and activator of transcription 3 (STAT3) attenuates interleukin-6 (IL-6)-induced collagen synthesis and resultant hypertrophy in rat heart. *J. Biol. Chem.* 287 (4), 2666–2677. doi:10.1074/jbc.M111.246173

Mizutani, M., Wu, J. C., and Nusse, R. (2016). Fibrosis of the neonatal mouse heart after cryoinjury is accompanied by Wnt signaling activation and epicardial-to-mesenchymal transition. *J. Am. Heart Assoc.* 5 (3), e002457. doi:10.1161/jaha.115.002457

Mohammed, S. F., Hussain, S., Mirzoyev, S. A., Edwards, W. D., Maleszewski, J. J., and Redfield, M. M. (2015). Coronary microvascular rarefaction and myocardial fibrosis in heart failure with preserved ejection fraction. *Circulation* 131 (6), 550–559. doi:10.1161/circulationaha.114.009625

Molkentin, J. D., Bugg, D., Ghearing, N., Dorn, L. E., Kim, P., Sargent, M. A., et al. (2017). Fibroblast-specific genetic manipulation of p38 mitogen-activated protein kinase *in vivo* reveals its central regulatory role in fibrosis. *Circulation* 136 (6), 549–561. doi:10.1161/circulationaha.116.026238

Möllmann, H., Nef, H. M., Kostin, S., von Kalle, C., Pilz, I., Weber, M., et al. (2006). Bone marrow-derived cells contribute to infarct remodelling. *Cardiovasc Res.* 71 (4), 661–671. doi:10.1016/j.cardiores.2006.06.013

Montero, P., Milara, J., Roger, I., and Cortijo, J. (2021). Role of JAK/STAT in interstitial lung diseases; molecular and cellular mechanisms. *Int. J. Mol. Sci.* 22 (12), 6211. doi:10.3390/ijms22126211

Moore-Morris, T., Cattaneo, P., Guimarães-Camboa, N., Bogomolovas, J., Cedenilla, M., Banerjee, I., et al. (2018). Infarct fibroblasts do not derive from bone marrow lineages. *Circ. Res.* 122 (4), 583–590. doi:10.1161/circresaha.117.311490

Moore-Morris, T., Guimarães-Camboa, N., Banerjee, I., Zambon, A. C., Kisseleva, T., Velayoudon, A., et al. (2014). Resident fibroblast lineages mediate pressure overload-induced cardiac fibrosis. *J. Clin. Invest.* 124 (7), 2921–2934. doi:10.1172/jci74783

Morris, R., Kershaw, N. J., and Babon, J. J. (2018). The molecular details of cytokine signaling via the JAK/STAT pathway. *Protein Sci.* 27 (12), 1984–2009. doi:10.1002/pro.3519

Mott, J. L., Kobayashi, S., Bronk, S. F., and Gores, G. J. (2007). mir-29 regulates Mcl-1 protein expression and apoptosis. *Oncogene* 26 (42), 6133–6140. doi:10.1038/sj.onc.1210436

Naka, T., Narazaki, M., Hirata, M., Matsumoto, T., Minamoto, S., Aono, A., et al. (1997). Structure and function of a new STAT-induced STAT inhibitor. *Nature* 387 (6636), 924–929. doi:10.1038/43219

Negoro, S., Kunisada, K., Tone, E., Funamoto, M., Oh, H., Kishimoto, T., et al. (2000). Activation of JAK/STAT pathway transduces cytoprotective signal in rat acute myocardial infarction. *Cardiovasc Res.* 47 (4), 797–805. doi:10.1016/s0008-6363(00)00138-3

Németh, Á., Mózes, M. M., Calvier, L., Hansmann, G., and Kökény, G. (2019). The PPARγ agonist pioglitazone prevents TGF-β induced renal fibrosis by repressing EGR-1 and STAT3. *BMC Nephrol.* 20 (1), 245. doi:10.1186/s12882-019-1431-x

Nguyen, M. N., Kiriazis, H., Gao, X. M., and Du, X. J. (2017). Cardiac fibrosis and arrhythmogenesis. *Compr. Physiol.* 7 (3), 1009–1049. doi:10.1002/cphy.c160046

O'Donoghue, R. J., Knight, D. A., Richards, C. D., Prêle, C. M., Lau, H. L., Jarnicki, A. G., et al. (2012). Genetic partitioning of interleukin-6 signalling in mice dissociates Stat3 from Smad3-mediated lung fibrosis. *EMBO Mol. Med.* 4 (9), 939–951. doi:10.1002/emmm.201100604

Ogata, H., Chinen, T., Yoshida, T., Kinjyo, I., Takaesu, G., Shiraishi, H., et al. (2006). Loss of SOCS3 in the liver promotes fibrosis by enhancing STAT3-mediated TGF-beta1 production. *Oncogene* 25 (17), 2520–2530. doi:10.1038/sj.onc.1209281

O'Shea, J. J., Schwartz, D. M., Villarino, A. V., Gadina, M., McInnes, I. B., and Laurence, A. (2015). The JAK-STAT pathway: impact on human disease and therapeutic intervention. *Annu. Rev. Med.* 66, 311–328. doi:10.1146/annurev-med-051113-024537

Owen, K. L., Brockwell, N. K., and Parker, B. S. (2019). JAK-STAT signaling: a double-edged sword of immune regulation and cancer progression. *Cancers (Basel)* 11 (12), 2002. doi:10.3390/cancers11122002

Park, J. Y., Yoo, K. D., Bae, E., Kim, K. H., Lee, J. W., Shin, S. J., et al. (2022). Blockade of STAT3 signaling alleviates the progression of acute kidney injury to chronic kidney disease through antiapoptosis. *Am. J. Physiol. Ren. Physiol.* 322 (5), F553–f572. doi:10.1152/ajprenal.00595.2020

Park, Y. J., Lee, K. H., Jeon, M. S., Lee, Y. H., Ko, Y. J., Pang, C., et al. (2020). Hepatoprotective potency of chrysophanol 8-O-glucoside from rheum palmatum L. Against hepatic fibrosis via regulation of the STAT3 signaling pathway. *Int. J. Mol. Sci.* 21 (23), 9044. doi:10.3390/ijms21239044

Patel, N. J., Nassal, D. M., Greer-Short, A. D., Unudurthi, S. D., Scandling, B. W., Gratz, D., et al. (2019). βIV-Spectrin/STAT3 complex regulates fibroblast phenotype, fibrosis, and cardiac function. *JCI Insight* 4 (20), e131046. doi:10.1172/jci.insight.131046

Pedroza, M., To, S., Assassi, S., Wu, M., Tweardy, D., and Agarwal, S. K. (2018). Role of STAT3 in skin fibrosis and transforming growth factor beta signalling. *Rheumatol. Oxf.* 57 (10), 1838–1850. doi:10.1093/rheumatology/kex347

Pekarsky, Y., Santanam, U., Cimmino, A., Palamarchuk, A., Efanov, A., Maximov, V., et al. (2006). Tcl1 expression in chronic lymphocytic leukemia is regulated by miR-29 and miR-181. *Cancer Res.* 66 (24), 11590–11593. doi:10.1158/0008-5472.Can-06-3613

Peng, C., Lu, Y., Li, R., Zhang, L., Liu, Z., Xu, X., et al. (2023). Neuroimmune modulation mediated by il-6: a potential target for the treatment of ischemia-induced ventricular arrhythmias. *Heart Rhythm.* 1547-5271, 03071. doi:10.1016/j.hrthm.2023.12.020

Piessevaux, J., Lavens, D., Peelman, F., and Tavernier, J. (2008). The many faces of the SOCS box. *Cytokine Growth Factor Rev.* 19 (5-6), 371–381. doi:10.1016/j.cytogfr.2008.08.006

Prabhu, S. D., and Frangogiannis, N. G. (2016). The biological basis for cardiac repair after myocardial infarction: from inflammation to fibrosis. *Circ. Res.* 119 (1), 91–112. doi:10.1161/circresaha.116.303577

Qi, W., Li, X., Ren, Y., Liu, X., Fu, H., Wang, X., et al. (2022). Downregulation of lncRNA Miat contributes to the protective effect of electroacupuncture against myocardial fibrosis. *Chin. Med.* 17 (1), 57. doi:10.1186/s13020-022-00615-6

Qin, S., Zou, Y., and Zhang, C. L. (2013). Cross-talk between KLF4 and STAT3 regulates axon regeneration. *Nat. Commun.* 4, 2633. doi:10.1038/ncomms3633

Qiu, Z. Y., and Fan, Y. (2016). Large granular lymphocytic leukemia and JAK/STAT signaling pathway--review. *Zhongguo Shi Yan Xue Ye Xue Za Zhi* 24 (1), 254–260. doi:10.7534/j.issn.1009-2137.2016.01.049

Qu, H., Wang, Y., Wang, Y., Yang, T., Feng, Z., Qu, Y., et al. (2017). Luhong formula inhibits myocardial fibrosis in a paracrine manner by activating the gp130/JAK2/STAT3 pathway in cardiomyocytes. *J. Ethnopharmacol.* 202, 28–37. doi:10.1016/j.jep.2017.01.033

Raivola, J., Haikarainen, T., Abraham, B. G., and Silvennoinen, O. (2021). Janus kinases in leukemia. *Cancers (Basel)* 13 (4), 800. doi:10.3390/cancers13040800

Rane, S. G., and Reddy, E. P. (2000). Janus kinases: components of multiple signaling pathways. *Oncogene* 19 (49), 5662–5679. doi:10.1038/sj.onc.1203925

Rockey, D. C., Bell, P. D., and Hill, J. A. (2015). Fibrosis--a common pathway to organ injury and failure. *N. Engl. J. Med.* 372 (12), 1138–1149. doi:10.1056/NEJMra1300575

Roskoski, R., Jr. (2016). Janus kinase (JAK) inhibitors in the treatment of inflammatory and neoplastic diseases. *Pharmacol. Res.* 111, 784–803. doi:10.1016/j.phrs.2016.07.038

Roy, S., Benz, F., Vargas Cardenas, D., Vucur, M., Gautheron, J., Schneider, A., et al. (2015). miR-30c and miR-193 are a part of the TGF-β-dependent regulatory network controlling extracellular matrix genes in liver fibrosis. *J. Dig. Dis.* 16 (9), 513–524. doi:10.1111/1751-2980.12266

Ruff-Jamison, S., Zhong, Z., Wen, Z., Chen, K., Darnell, J. E., Jr., and Cohen, S. (1994). Epidermal growth factor and lipopolysaccharide activate Stat3 transcription factor in mouse liver. *J. Biol. Chem.* 269 (35), 21933–21935. doi:10.1016/s0021-9258(17)31735-0

Saharinen, P., Takaluoma, K., and Silvennoinen, O. (2000). Regulation of the Jak2 tyrosine kinase by its pseudokinase domain. *Mol. Cell Biol.* 20 (10), 3387–3395. doi:10.1128/mcb.20.10.3387-3395.2000

Samidurai, A., Roh, S. K., Prakash, M., Durrant, D., Salloum, F. N., Kukreja, R. C., et al. (2020). STAT3-miR-17/20 signalling axis plays a critical role in attenuating myocardial infarction following rapamycin treatment in diabetic mice. *Cardiovasc Res.* 116 (13), 2103–2115. doi:10.1093/cvr/cvz315

Sasaki, A., Yasukawa, H., Suzuki, A., Kamizono, S., Syoda, T., Kinjyo, I., et al. (1999). Cytokine-inducible SH2 protein-3 (CIS3/SOCS3) inhibits Janus tyrosine kinase by binding through the N-terminal kinase inhibitory region as well as SH2 domain. *Genes Cells* 4 (6), 339–351. doi:10.1046/j.1365-2443.1999.00263.x

Schaefer, T. S., Sanders, L. K., and Nathans, D. (1995). Cooperative transcriptional activity of Jun and Stat3 beta, a short form of Stat3. *Proc. Natl. Acad. Sci. U. S. A.* 92 (20), 9097–9101. doi:10.1073/pnas.92.20.9097

Schafer, S., Viswanathan, S., Widjaja, A. A., Lim, W. W., Moreno-Moral, A., DeLaughter, D. M., et al. (2017). IL-11 is a crucial determinant of cardiovascular fibrosis. *Nature* 552 (7683), 110–115. doi:10.1038/nature24676

Schindler, C., and Darnell, J. E., Jr. (1995). Transcriptional responses to polypeptide ligands: the JAK-STAT pathway. *Annu. Rev. Biochem.* 64, 621–651. doi:10.1146/annurev.bi.64.070195.003201

Schmitz, J., Dahmen, H., Grimm, C., Gendo, C., Müller-Newen, G., Heinrich, P. C., et al. (2000). The cytoplasmic tyrosine motifs in full-length glycoprotein 130 have different roles in IL-6 signal transduction. *J. Immunol.* 164 (2), 848–854. doi:10.4049/jimmunol.164.2.848

Seo, H. Y., Jeon, J. H., Jung, Y. A., Jung, G. S., Lee, E. J., Choi, Y. K., et al. (2016). Fyn deficiency attenuates renal fibrosis by inhibition of phospho-STAT3. *Kidney Int.* 90 (6), 1285–1297. doi:10.1016/j.kint.2016.06.038

Shen, K., Li, R., Zhang, X., Qu, G., Li, R., Wang, Y., et al. (2021). Acetyl oxygen benzoate engeletin ester promotes KLF4 degradation leading to the attenuation of pulmonary fibrosis via inhibiting TGFβ1-smad/p38MAPK-lnc865/lnc556-miR-29b-2-5p-STAT3 signal pathway. *Aging (Albany NY)* 13 (10), 13807–13821. doi:10.18632/aging.202975

Shi, M., Lin, T. H., Appell, K. C., and Berg, L. J. (2008a). Janus-kinase-3-dependent signals induce chromatin remodeling at the Ifng locus during T helper 1 cell differentiation. *Immunity* 28 (6), 763–773. doi:10.1016/j.immuni.2008.04.016

Shi, S., Calhoun, H. C., Xia, F., Li, J., Le, L., and Li, W. X. (2006). JAK signaling globally counteracts heterochromatic gene silencing. *Nat. Genet.* 38 (9), 1071–1076. doi:10.1038/ng1860

Shi, S., Larson, K., Guo, D., Lim, S. J., Dutta, P., Yan, S. J., et al. (2008b). Drosophila STAT is required for directly maintaining HP1 localization and heterochromatin stability. *Nat. Cell Biol.* 10 (4), 489–496. doi:10.1038/ncb1713

Shi, Y., and Massagué, J. (2003). Mechanisms of TGF-beta signaling from cell membrane to the nucleus. *Cell* 113 (6), 685–700. doi:10.1016/s0092-8674(03)00432-x

Shinde, A. V., and Frangogiannis, N. G. (2017). Mechanisms of fibroblast activation in the remodeling myocardium. *Curr. Pathobiol. Rep.* 5 (2), 145–152. doi:10.1007/s40139-017-0132-z

Shuya, L. L., Menkhorst, E. M., Yap, J., Li, P., Lane, N., and Dimitriadis, E. (2011). Leukemia inhibitory factor enhances endometrial stromal cell decidualization in humans and mice. *PLoS One* 6 (9), e25288. doi:10.1371/journal.pone.0025288

Singh, A., Ramesh, S., Cibi, D. M., Yun, L. S., Li, J., Li, L., et al. (2016). Hippo signaling mediators yap and taz are required in the epicardium for coronary vasculature development. *Cell Rep.* 15 (7), 1384–1393. doi:10.1016/j.celrep.2016.04.027

Sonnenblick, A., Levy, C., and Razin, E. (2004). Interplay between MITF, PIAS3, and STAT3 in mast cells and melanocytes. *Mol. Cell Biol.* 24 (24), 10584–10592. doi:10.1128/mcb.24.24.10584-10592.2004

Sp, N., Kang, D. Y., Kim, D. H., Park, J. H., Lee, H. G., Kim, H. J., et al. (2018). Nobiletin inhibits CD36-dependent tumor angiogenesis, migration, invasion, and sphere formation through the Cd36/stat3/nf-κb signaling Axis. *Nutrients* 10 (6), 772. doi:10.3390/nu10060772

Speirs, C., Williams, J. J. L., Riches, K., Salt, I. P., and Palmer, T. M. (2018). Linking energy sensing to suppression of JAK-STAT signalling: a potential route for repurposing AMPK activators? *Pharmacol. Res.* 128, 88–100. doi:10.1016/j.phrs.2017.10.001

Su, Y. C., Li, S. C., Peng, H. Y., Ho, Y. H., Chen, L. J., and Liao, H. F. (2013). RAD001-mediated STAT3 upregulation and megakaryocytic differentiation. *Thromb. Haemost.* 109 (3), 540–549. doi:10.1160/th12-10-0734

Su, S. A., Yang, D., Wu, Y., Xie, Y., Zhu, W., Cai, Z., et al. (2017). EphrinB2 regulates cardiac fibrosis through modulating the interaction of Stat3 and TGF-β/smad3 signaling. *Circ. Res.* 121 (6), 617–627. doi:10.1161/circresaha.117.311045

Su, Y., Zhang, W., Patro, C. P. K., Zhao, J., Mu, T., Ma, Z., et al. (2020). STAT3 regulates mouse neural progenitor proliferation and differentiation by promoting mitochondrial metabolism. *Front. Cell Dev. Biol.* 8, 362. doi:10.3389/fcell.2020.00362

Sun, W., Kim, D. H., Byon, C. H., Choi, H. I., Park, J. S., Bae, E. H., et al. (2022). β-Elemene attenuates renal fibrosis in the unilateral ureteral obstruction model by inhibition of STAT3 and Smad3 signaling via suppressing MyD88 expression. *Int. J. Mol. Sci.* 23 (10), 5553. doi:10.3390/ijms23105553

Szelag, M., Piaszyk-Borychowska, A., Plens-Galaska, M., Wesoly, J., and Bluyssen, H. A. (2016). Targeted inhibition of STATs and IRFs as a potential treatment strategy in cardiovascular disease. *Oncotarget* 7 (30), 48788–48812. doi:10.18632/oncotarget.9195

Tan, J. K., Ma, X. F., Wang, G. N., Jiang, C. R., Gong, H. Q., and Liu, H. (2021). LncRNA MIAT knockdown alleviates oxygen-glucose deprivation-induced cardiomyocyte injury by regulating JAK2/STAT3 pathway via miR-181a-5p. *J. Cardiol.* 78 (6), 586–597. doi:10.1016/j.jjcc.2021.08.018

Tang, L. Y., Heller, M., Meng, Z., Yu, L. R., Tang, Y., Zhou, M., et al. (2017). Transforming growth factor-β (TGF-β) directly activates the JAK1-STAT3 Axis to induce hepatic fibrosis in coordination with the SMAD pathway. *J. Biol. Chem.* 292 (10), 4302–4312. doi:10.1074/jbc.M116.773085

Tao, H., Yang, J. J., Shi, K. H., Deng, Z. Y., and Li, J. (2014). DNA methylation in cardiac fibrosis: new advances and perspectives. *Toxicology* 323, 125–129. doi:10.1016/j.tox.2014.07.002

Tesoro, L., Hernández, I., Ramírez-Carracedo, R., Díez-Mata, J., Alcharani, N., Jiménez-Guirado, B., et al. (2022). NIL10: a new IL10-receptor binding nanoparticle that induces cardiac protection in mice and pigs subjected to acute myocardial infarction through STAT3/NF-κB activation. *Pharmaceutics* 14 (10), 2044. doi:10.3390/pharmaceutics14102044

Timofeeva, O. A., Tarasova, N. I., Zhang, X., Chasovskikh, S., Cheema, A. K., Wang, H., et al. (2013). STAT3 suppresses transcription of proapoptotic genes in cancer cells with the involvement of its N-terminal domain. *Proc. Natl. Acad. Sci. U. S. A.* 110 (4), 1267–1272. doi:10.1073/pnas.1211805110

Tomasek, J. J., McRae, J., Owens, G. K., and Haaksma, C. J. (2005). Regulation of alpha-smooth muscle actin expression in granulation tissue myofibroblasts is dependent on the intronic CArG element and the transforming growth factor-beta1 control element. *Am. J. Pathol.* 166 (5), 1343–1351. doi:10.1016/s0002-9440(10)62353-x

Tussié-Luna, M. I., Bayarsaihan, D., Seto, E., Ruddle, F. H., and Roy, A. L. (2002). Physical and functional interactions of histone deacetylase 3 with TFII-I family proteins and PIASxbeta. *Proc. Natl. Acad. Sci. U. S. A.* 99 (20), 12807–12812. doi:10.1073/pnas.192464499

Ungureanu, D., Wu, J., Pekkala, T., Niranjan, Y., Young, C., Jensen, O. N., et al. (2011). The pseudokinase domain of JAK2 is a dual-specificity protein kinase that negatively regulates cytokine signaling. *Nat. Struct. Mol. Biol.* 18 (9), 971–976. doi:10.1038/nsmb.2099

Unudurthi, S. D., Nassal, D., Greer-Short, A., Patel, N., Howard, T., Xu, X., et al. (2018). βIV-Spectrin regulates STAT3 targeting to tune cardiac response to pressure overload. *J. Clin. Invest.* 128 (12), 5561–5572. doi:10.1172/jci99245

van Rooij, E., Sutherland, L. B., Thatcher, J. E., DiMaio, J. M., Naseem, R. H., Marshall, W. S., et al. (2008). Dysregulation of microRNAs after myocardial infarction reveals a role of miR-29 in cardiac fibrosis. *Proc. Natl. Acad. Sci. U. S. A.* 105 (35), 13027–13032. doi:10.1073/pnas.0805038105

Villarino, A. V., Kanno, Y., and O'Shea, J. J. (2017). Mechanisms and consequences of Jak-STAT signaling in the immune system. *Nat. Immunol.* 18 (4), 374–384. doi:10.1038/ni.3691

Wallweber, H. J., Tam, C., Franke, Y., Starovasnik, M. A., and Lupardus, P. J. (2014). Structural basis of recognition of interferon-α receptor by tyrosine kinase 2. *Nat. Struct. Mol. Biol.* 21 (5), 443–448. doi:10.1038/nsmb.2807

Wang, J., Liu, T., Chen, X., Jin, Q., Chen, Y., Zhang, L., et al. (2020). Bazedoxifene regulates Th17 immune response to ameliorate experimental autoimmune myocarditis via inhibition of STAT3 activation. *Front. Pharmacol.* 11, 613160. doi:10.3389/fphar.2020.613160

Wang, M., Li, J., Ding, Y., Cai, S., Li, Z., and Liu, P. (2021). PEX5 prevents cardiomyocyte hypertrophy via suppressing the redox-sensitive signaling pathways MAPKs and STAT3. *Eur. J. Pharmacol.* 906, 174283. doi:10.1016/j.ejphar.2021.174283

Wang, T., Mao, X., Li, H., Qiao, S., Xu, A., Wang, J., et al. (2013). N-Acetylcysteine and allopurinol up-regulated the Jak/STAT3 and PI3K/Akt pathways via adiponectin and attenuated myocardial postischemic injury in diabetes. *Free Radic. Biol. Med.* 63, 291–303. doi:10.1016/j.freeradbiomed.2013.05.043

Wang, Y., Gao, H., Cao, X., Li, Z., Kuang, Y., Ji, Y., et al. (2022a). Role of GADD45A in myocardial ischemia/reperfusion through mediation of the JNK/p38 MAPK and STAT3/VEGF pathways. *Int. J. Mol. Med.* 50 (6), 144. doi:10.3892/ijmm.2022.5200

Wang, Y., Li, M., Chen, J., Yu, Y., Yu, Y., Shi, H., et al. (2023). Macrophage CAPN4 regulates CVB3-induced cardiac inflammation and injury by promoting NLRP3 inflammasome activation and phenotypic transformation to the inflammatory subtype. *Free Radic. Biol. Med.* 208, 430–444. doi:10.1016/j.freeradbiomed.2023.08.032

Wang, Y., Wang, M., Samuel, C. S., and Widdop, R. E. (2022b). Preclinical rodent models of cardiac fibrosis. *Br. J. Pharmacol.* 179 (5), 882–899. doi:10.1111/bph.15450

Wang, Z., Li, J., Xiao, W., Long, J., and Zhang, H. (2018). The STAT3 inhibitor S3I-201 suppresses fibrogenesis and angiogenesis in liver fibrosis. *Lab. Invest.* 98 (12), 1600–1613. doi:10.1038/s41374-018-0127-3

Weber, K. T. (1989). Cardiac interstitium in health and disease: the fibrillar collagen network. *J. Am. Coll. Cardiol.* 13 (7), 1637–1652. doi:10.1016/0735-1097(89)90360-4

Xian, S., Chen, A., Wu, Y., Wen, H., Lu, C., Huang, F., et al. (2021). Interference with the expression of S1PR1 or STAT3 attenuates valvular damage due to rheumatic heart disease. *Int. J. Mol. Med.* 48 (3), 179. doi:10.3892/ijmm.2021.5012

Xie, L., Wu, Y., Zhou, C., Tan, Z., Xu, H., Chen, G., et al. (2021). Piceatannol protects against sepsis-induced myocardial dysfunction via direct inhibition of JAK2. *Int. Immunopharmacol.* 96, 107639. doi:10.1016/j.intimp.2021.107639

Xin, P., Xu, X., Deng, C., Liu, S., Wang, Y., Zhou, X., et al. (2020). The role of JAK/STAT signaling pathway and its inhibitors in diseases. *Int. Immunopharmacol.* 80, 106210. doi:10.1016/j.intimp.2020.106210

Xue, R., Lei, S., Xia, Z. Y., Wu, Y., Meng, Q., Zhan, L., et al. (2016). Selective inhibition of PTEN preserves ischaemic post-conditioning cardioprotection in STZ-induced Type 1 diabetic rats: role of the PI3K/Akt and JAK2/STAT3 pathways. *Clin. Sci. (Lond)* 130 (5), 377–392. doi:10.1042/cs20150496

Yajima, T., Murofushi, Y., Zhou, H., Park, S., Housman, J., Zhong, Z. H., et al. (2011). Absence of SOCS3 in the cardiomyocyte increases mortality in a gp130-dependent manner accompanied by contractile dysfunction and ventricular arrhythmias. *Circulation* 124 (24), 2690–2701. doi:10.1161/circulationaha.111.028498

Yang, J., Liao, X., Agarwal, M. K., Barnes, L., Auron, P. E., and Stark, G. R. (2007). Unphosphorylated STAT3 accumulates in response to IL-6 and activates transcription by binding to NFkappaB. *Genes Dev.* 21 (11), 1396–1408. doi:10.1101/gad.1553707

Yang, X., Bao, M., Fang, Y., Yu, X., Ji, J., and Ding, X. (2021). STAT3/HIF-1α signaling activation mediates peritoneal fibrosis induced by high glucose. *J. Transl. Med.* 19 (1), 283. doi:10.1186/s12967-021-02946-8

Yang, Y., Hu, W., Di, S., Ma, Z., Fan, C., Wang, D., et al. (2017). Tackling myocardial ischemic injury: the signal transducer and activator of transcription 3 (STAT3) at a good site. *Expert Opin. Ther. Targets* 21 (2), 215–228. doi:10.1080/14728222.2017.1275566

Yasukawa, H., Misawa, H., Sakamoto, H., Masuhara, M., Sasaki, A., Wakioka, T., et al. (1999). The JAK-binding protein JAB inhibits Janus tyrosine kinase activity through binding in the activation loop. *Embo J.* 18 (5), 1309–1320. doi:10.1093/emboj/18.5.1309

Yasukawa, H., Yajima, T., Duplain, H., Iwatate, M., Kido, M., Hoshijima, M., et al. (2003). The suppressor of cytokine signaling-1 (SOCS1) is a novel therapeutic target for enterovirus-induced cardiac injury. *J. Clin. Invest.* 111 (4), 469–478. doi:10.1172/jci16491

You, L., Li, L., Xu, Q., Ren, J., and Zhang, F. (2011). Postconditioning reduces infarct size and cardiac myocyte apoptosis via the opioid receptor and JAK-STAT signaling pathway. *Mol. Biol. Rep.* 38 (1), 437–443. doi:10.1007/s11033-010-0126-y

Yu, C. L., Meyer, D. J., Campbell, G. S., Larner, A. C., Carter-Su, C., Schwartz, J., et al. (1995). Enhanced DNA-binding activity of a Stat3-related protein in cells transformed by the Src oncoprotein. *Science* 269 (5220), 81–83. doi:10.1126/science.7541555

Yu, H., and Jove, R. (2004). The STATs of cancer--new molecular targets come of age. *Nat. Rev. Cancer* 4 (2), 97–105. doi:10.1038/nrc1275

Yu, Y., Ou-Yang, W. X., Zhang, H., Jiang, T., Tang, L., Tan, Y. F., et al. (2021). MiR-125b enhances autophagic flux to improve septic cardiomyopathy via targeting STAT3/HMGB1. *Exp. Cell Res.* 409 (2), 112842. doi:10.1016/j.yexcr.2021.112842

Yuan, H. X., Chen, Y. T., Li, Y. Q., Wang, Y. S., Ou, Z. J., Li, Y., et al. (2023). Endothelial extracellular vesicles induce acute lung injury via follistatin-like protein 1. *Sci. China Life Sci.* 22, 1–15. doi:10.1007/s11427-022-2328-x

Yuan, J., Zhang, F., and Niu, R. (2015). Multiple regulation pathways and pivotal biological functions of STAT3 in cancer. *Sci. Rep.* 5, 17663. doi:10.1038/srep17663

Yuan, L., Qiu, L., Ye, Y., Wu, J., Wang, S., Wang, X., et al. (2018). Heat-shock transcription factor 1 is critically involved in the ischaemia-induced cardiac hypertrophy via JAK2/STAT3 pathway. *J. Cell Mol. Med.* 22 (9), 4292–4303. doi:10.1111/jcmm.13713

Yuan, Y., Zhang, Y., Han, X., Li, Y., Zhao, X., Sheng, L., et al. (2017). Relaxin alleviates TGFβ1-induced cardiac fibrosis via inhibition of Stat3-dependent autophagy. *Biochem. Biophys. Res. Commun.* 493 (4), 1601–1607. doi:10.1016/j.bbrc.2017.09.110

Zang, X., Zhao, Z., Chen, K., Song, W., Ma, J., Fu, H., et al. (2023). SHP-1 alleviates atrial fibrosis in atrial fibrillation by modulating STAT3 activation. *Exp. Biol. Med. (Maywood)* 248, 979–990. doi:10.1177/15353702231165717

Zeisberg, E. M., Tarnavski, O., Zeisberg, M., Dorfman, A. L., McMullen, J. R., Gustafsson, E., et al. (2007). Endothelial-to-mesenchymal transition contributes to cardiac fibrosis. *Nat. Med.* 13 (8), 952–961. doi:10.1038/nm1613

Zhang, J. M., and An, J. (2007). Cytokines, inflammation, and pain. *Int. Anesthesiol. Clin.* 45 (2), 27–37. doi:10.1097/AIA.0b013e318034194e

Zhang, J. Q., Li, R., Dong, X. Y., He, N., Yin, R. J., Yang, M. K., et al. (2022a). Design, synthesis and structure-activity relationship studies of meridianin derivatives as novel JAK/STAT3 signaling inhibitors. *Int. J. Mol. Sci.* 23 (4), 2199. doi:10.3390/ijms23042199

Zhang, L., He, J., Wang, J., Liu, J., Chen, Z., Deng, B., et al. (2019). Knockout RAGE alleviates cardiac fibrosis through repressing endothelial-to-mesenchymal transition

(EndMT) mediated by autophagy. *Cell Death Dis.* 12 (5), 470. doi:10.1038/s41419-021-03750-4

Zhang, W., Qu, X., Chen, B., Snyder, M., Wang, M., Li, B., et al. (2016). Critical roles of STAT3 in β-adrenergic functions in the heart. *Circulation* 133 (1), 48–61. doi:10.1161/circulationaha.115.017472

Zhang, X., Guo, A., Yu, J., Possemato, A., Chen, Y., Zheng, W., et al. (2007). Identification of STAT3 as a substrate of receptor protein tyrosine phosphatase T. *Proc. Natl. Acad. Sci. U. S. A.* 104 (10), 4060–4064. doi:10.1073/pnas.0611665104

Zhang, Y., Dees, C., Beyer, C., Lin, N. Y., Distler, A., Zerr, P., et al. (2015). Inhibition of casein kinase II reduces TGFβ induced fibroblast activation and ameliorates experimental fibrosis. *Ann. Rheum. Dis.* 74 (5), 936–943. doi:10.1136/annrheumdis-2013-204256

Zhang, Y., Lu, W., Zhang, X., Lu, J., Xu, S., Chen, S., et al. (2019a). Cryptotanshinone protects against pulmonary fibrosis through inhibiting Smad and STAT3 signaling pathways. *Pharmacol. Res.* 147, 104307. doi:10.1016/j.phrs.2019.104307

Zhang, Y., Zhang, L., Fan, X., Yang, W., Yu, B., Kou, J., et al. (2019b). Captopril attenuates TAC-induced heart failure via inhibiting Wnt3a/β-catenin and Jak2/Stat3 pathways. *Biomed. Pharmacother.* 113, 108780. doi:10.1016/j.biopha.2019.108780

Zhang, Z., Tang, J., Song, J., Xie, M., Liu, Y., Dong, Z., et al. (2022b). Elabela alleviates ferroptosis, myocardial remodeling, fibrosis and heart dysfunction in hypertensive mice by modulating the IL-6/STAT3/GPX4 signaling. *Free Radic. Biol. Med.* 181, 130–142. doi:10.1016/j.freeradbiomed.2022.01.020

Zhao, L., Wu, D., Sang, M., Xu, Y., Liu, Z., and Wu, Q. (2017). Stachydrine ameliorates isoproterenol-induced cardiac hypertrophy and fibrosis by suppressing inflammation and oxidative stress through inhibiting NF-κB and JAK/STAT signaling pathways in rats. *Int. Immunopharmacol.* 48, 102–109. doi:10.1016/j.intimp.2017.05.002

Zhao, Q., Bai, J., Chen, Y., Liu, X., Zhao, S., Ling, G., et al. (2022). An optimized herbal combination for the treatment of liver fibrosis: hub genes, bioactive ingredients, and molecular mechanisms. *J. Ethnopharmacol.* 297, 115567. doi:10.1016/j.jep.2022.115567

Zhao, X. B., Qin, Y., Niu, Y. L., and Yang, J. (2018). Matrine inhibits hypoxia/reoxygenation-induced apoptosis of cardiac microvascular endothelial cells in rats via the JAK2/STAT3 signaling pathway. *Biomed. Pharmacother.* 106, 117–124. doi:10.1016/j.biopha.2018.06.003

Zhao, X. K., Cheng, Y., Liang Cheng, M., Yu, L., Mu, M., Li, H., et al. (2016). Focal adhesion kinase regulates fibroblast migration via integrin beta-1 and plays a central role in fibrosis. *Sci. Rep.* 6, 19276. doi:10.1038/srep19276

Zheng, C., Huang, L., Luo, W., Yu, W., Hu, X., Guan, X., et al. (2019). Inhibition of STAT3 in tubular epithelial cells prevents kidney fibrosis and nephropathy in STZ-induced diabetic mice. *Cell Death Dis.* 10 (11), 848. doi:10.1038/s41419-019-2085-0

Zhu, B., Han, R., Ni, Y., Guo, H., Liu, X., Li, J., et al. (2023). Podocarpusflavone alleviated renal fibrosis in obstructive nephropathy by inhibiting Fyn/Stat3 signaling pathway. *J. Nat. Med.* 77 (3), 464–475. doi:10.1007/s11418-023-01685-y

Zhu, F., Bai, X., Hong, Q., Cui, S., Wang, X., Xiao, F., et al. (2019). STAT3 inhibition partly abolishes IL-33-induced bone marrow-derived monocyte phenotypic transition into fibroblast precursor and alleviates experimental renal interstitial fibrosis. *J. Immunol.* 203 (10), 2644–2654. doi:10.4049/jimmunol.1801273

Zhu, X., Shi, D., Cao, K., Ru, D., Ren, J., Rao, Z., et al. (2018). Sphingosine kinase 2 cooperating with Fyn promotes kidney fibroblast activation and fibrosis via STAT3 and AKT. *Biochim. Biophys. Acta Mol. Basis Dis.* 1864 (11), 3824–3836. doi:10.1016/j.bbadis.2018.09.007

Zhuang, L., Jia, K., Chen, C., Li, Z., Zhao, J., Hu, J., et al. (2022). DYRK1B-STAT3 drives cardiac hypertrophy and heart failure by impairing mitochondrial bioenergetics. *Circulation* 145 (11), 829–846. doi:10.1161/circulationaha.121.055727

Zordoky, B. N., Robertson, I. M., and Dyck, J. R. (2015). Preclinical and clinical evidence for the role of resveratrol in the treatment of cardiovascular diseases. *Biochim. Biophys. Acta* 1852 (6), 1155–1177. doi:10.1016/j.bbadis.2014.10.016

Zou, Y., Akazawa, H., Qin, Y., Sano, M., Takano, H., Minamino, T., et al. (2004). Mechanical stress activates angiotensin II type 1 receptor without the involvement of angiotensin II. *Nat. Cell Biol.* 6 (6), 499–506. doi:10.1038/ncb1137

frontiers | Frontiers in Pharmacology

TYPE Original Research
PUBLISHED 05 April 2024
DOI 10.3389/fphar.2024.1332394

OPEN ACCESS

EDITED BY
Bradley John Roth,
Oakland University, United States

REVIEWED BY
Katy Sanchez-Pozos,
Hospital Juárez de México, Mexico
Elena Kutumova,
Sirius University, Russia

*CORRESPONDENCE
K. Melissa Hallow,
hallowkm@uga.edu

RECEIVED 02 November 2023
ACCEPTED 21 March 2024
PUBLISHED 05 April 2024

CITATION
Yu H, Greasley P, Lambers-Heerspink H, Boulton DW, Hamrén B and Hallow KM (2024), Quantifying the integrated physiological effects of endothelin-1 on cardiovascular and renal function in healthy subjects: a mathematical modeling analysis.
Front. Pharmacol. 15:1332394.
doi: 10.3389/fphar.2024.1332394

Quantifying the integrated physiological effects of endothelin-1 on cardiovascular and renal function in healthy subjects: a mathematical modeling analysis

Hongtao Yu[1], Peter Greasley[2], Hiddo Lambers-Heerspink[3,4], David W. Boulton[1], Bengt Hamrén[5] and K. Melissa Hallow[6,7]*

[1]Clinical Pharmacology and Quantitative Pharmacology, Clinical Pharmacology and Safety Sciences, R&D, AstraZeneca, Gaithersburg, MD, United States, [2]Early Clinical Development, Research, and Early Development, Cardiovascular, Renal and Metabolism, BioPharmaceutical R&D, AstraZeneca, Gothenburg, Sweden, [3]Department of Clinical Pharmacy and Pharmacology, University of Groningen, Groningen, Netherlands, [4]The George Institute for Global Health, Sydney, NSW, Australia, [5]Clinical Pharmacology and Quantitative Pharmacology, Clinical Pharmacology and Safety Sciences, R&D, AstraZeneca, Gothenburg, Sweden, [6]School of Chemical, Materials, and Biomedical Engineering, University of Georgia, Athens, GA, United States, [7]Department of Epidemiology and Biostatistics, University of Georgia, Athens, GA, United States

Endothelin-1 (ET-1) is a potent vasoconstrictor with strong anti-natriuretic and anti-diuretic effects. While many experimental studies have elucidated the mechanisms of ET-1 through its two receptors, ET_A and ET_B, the complexity of responses and sometimes conflicting data make it challenging to understand the effects of ET-1, as well as potential therapeutic antagonism of ET-1 receptors, on human physiology. In this study, we aimed to develop an integrated and quantitative description of ET-1 effects on cardiovascular and renal function in healthy humans by coupling existing experimental data with a mathematical model of ET-1 kinetics and an existing mathematical model of cardiorenal function. Using a novel agnostic and iterative approach to incorporating and testing potential mechanisms, we identified a minimal set of physiological actions of endothelin-1 through ET_A and ET_B receptors by fitting the physiological responses (changes in blood pressure, renal blood flow, glomerular filtration rate (GFR), and sodium/water excretion) to ET-1 infusion, with and without ET_A/ET_B antagonism. The identified mechanisms align with previous experimental studies on ET-1 and offer novel insights into the relative magnitude and significance of endothelin's effects. This model serves as a foundation for further investigating the mechanisms of ET-1 and its antagonists.

KEYWORDS

endothelin-1, natriuresis and diuresis, ET_A receptor antagonist, ET_B receptor antagonist, cardiovascular and renal function, mathematical modeling

1 Introduction

ET-1 is a potent vasoconstrictor, especially in the renal vasculature, and is anti-natriuretic and anti-diuretic. It exerts these effects through its two receptors–ET_A and ET_B. Both receptors have been detected in all tissues with blood supply, indicating their ubiquitous expression (Regard et al., 2008; Davenport et al., 2016). Their relative and absolute densities vary by location and across species. Systemically, saturation binding assays show that resistance vessels express primarily ET_A, while in the kidney, relative expression of ET_B overall is much higher compared to ET_A (Davenport et al., 2016). Within the kidney, though, the relative concentrations of ET_A and ET_B vary. ET_A and ET_B have both been found to be expressed in the preafferent, afferent, efferent, and peritubular capillaries, as well is in the proximal tubule, thick ascending limb, and collecting duct. But preafferent and afferent arterioles have relatively higher expression of ET_A, while efferent and peritubular arterioles have higher expression of ET_B. Both receptor types are also expressed in the tubule. ET_A is found primarily in the proximal tubule. ET_B is found in all segments, but the inner medullary collecting duct has the highest density of ET_B receptors (Kohan et al., 2011).

A large body of experimental studies have provided a great deal of data for understanding of the effects of ET-1 through each receptor by utilizing various approaches, including ET-1 infusion studies, knock-out studies, and perturbation with various receptor agonists/antagonists [for a thorough review, see (Davenport et al., 2016; Kohan et al., 2011)]. However, the complexity of responses and sometimes conflicting data, especially across species, make it challenging to predict effects in human physiology. For instance, while it is well established that ET-1 causes vasoconstriction through ET_A, the effects of ET_B are more complex. Both ET_B agonism and antagonism have been shown to cause vasoconstriction (Haynes et al., 1995; Love et al., 2000). ET_B appears to constrict the afferent arteriole but dilate the efferent arteriole (Inscho et al., 2005). In addition, while ET-1 infusion certainly exerts anti-natriuretic and anti-diuretic effects, under some conditions ET-1 appears to inhibit reabsorption and promote natriuresis/diuresis in the collecting duct (Kohan et al., 2011).

Mathematical modeling can be a tool for integrating knowledge of physiology and various data sets into a consistent quantitative framework in order to better understand a system. In this study, we aimed to utilize existing experimental data to develop an integrated and quantitative description of endothelin effects on cardiovascular and renal function in healthy humans. Using a mathematical model of endothelin kinetics published in a sister paper, coupled to an existing mathematical model of cardiorenal function (Hallow et al., 2014; Hallow and Gebremichael, 2017; Hallow et al., 2018), we aimed to estimate the magnitude of physiological actions of endothelin-1 through ET_A and ET_B receptors by fitting the physiological response to ET-1 infusion, with and without ET_A/ET_B antagonism. Quantitively understanding the physiological effects of ET-1 and ET-1 antagonism in normal subjects is a first step toward better understanding its role in cardiovascular and renal disease, and both the beneficial effects and deleterious fluid retention in previous clinical studies of ET_A antagonists. This knowledge could help harness ET_A antagonists to gain renal benefit while mitigating fluid retention.

2 Materials and methods

2.1 Cardiorenal model

We utilized a previously published cardiorenal model (Hallow et al., 2014; Hallow et al., 2017; Hallow and Gebremichael, 2017; Hallow et al., 2018), summarized schematically in Figures 1A–D. This model describes the key physiological processes of kidney function, Na^+ and water homeostasis, and blood pressure control, including blood flow and pressure through the renal vasculature (Figure 1A); renal filtration, reabsorption, and excretion of sodium, water, and glucose (Figure 1C); whole-body fluid/electrolyte distribution (Figure 1B); and key neurohormonal and intrinsic feedback mechanisms (Figure 1D). Full model equations, parameters, and initial conditions have been published previously.

2.2 Endothelin 1 kinetics model

The development, calibration, and validation of a mathematical model of endothelin-1 kinetics is described in a sister paper (Hallow et al., manuscript in review - Frontiers in Pharmacology), and illustrated schematically in Figure 1E. In brief, Big ET-1 is assumed to be produced at a constant rate; ECE converts Big ET-1 to ET-1 in the tissue compartment; ET-1 is distributed between the tissue and plasma compartments; in each compartment, ET-1 binds to ET_A and ET_B receptors to form receptor-ligand complexes which are then cleared by internalization. The model also describes competitive binding of antagonists to the ET_A and ET_B receptor, and allows specification of selectivity and binding affinities for each receptor. The model was calibrated to the response to infusion of ET-1 or BigET-1 in three studies (Kaasjager et al., 1997; Parker et al., 1999; Hunter et al., 2017), and was validated by reproducing the ET-1 response to ET-1 in a different study (Bohm et al., 2003), as well as the ET-1 response to ET_A antagonist BQ123 and ET_B antagonist BQ788.

2.3 Integration and calibration of endothelin-1 effects in the cardiorenal model

The model of endothelin-1 kinetics and receptor antagonism was incorporated into and mechanistically linked with the cardiorenal model. Specifically, endothelin-1 exerts its physiological effects by binding to ET_A and ET_B receptors. Thus, the concentrations of ET-1 bound to ET_A or ET_B receptors [($ET1R_A$) and ($ET1R_B$), respectively in Figure 1E] were linked to the mechanistic effects of each receptor.

To do this, it was first necessary to identify the primary mechanisms of each receptor, and then to determine the shape and magnitude of the mathematical relationship between each ET1-receptor complex and its mechanisms, as presented in Figure 1F.

Based on the body of available experimental data (Haynes et al., 1995; Love et al., 2000; Inscho et al., 2005; Kohan et al., 2011; Davenport et al., 2016), we postulated possible mechanistic effects of

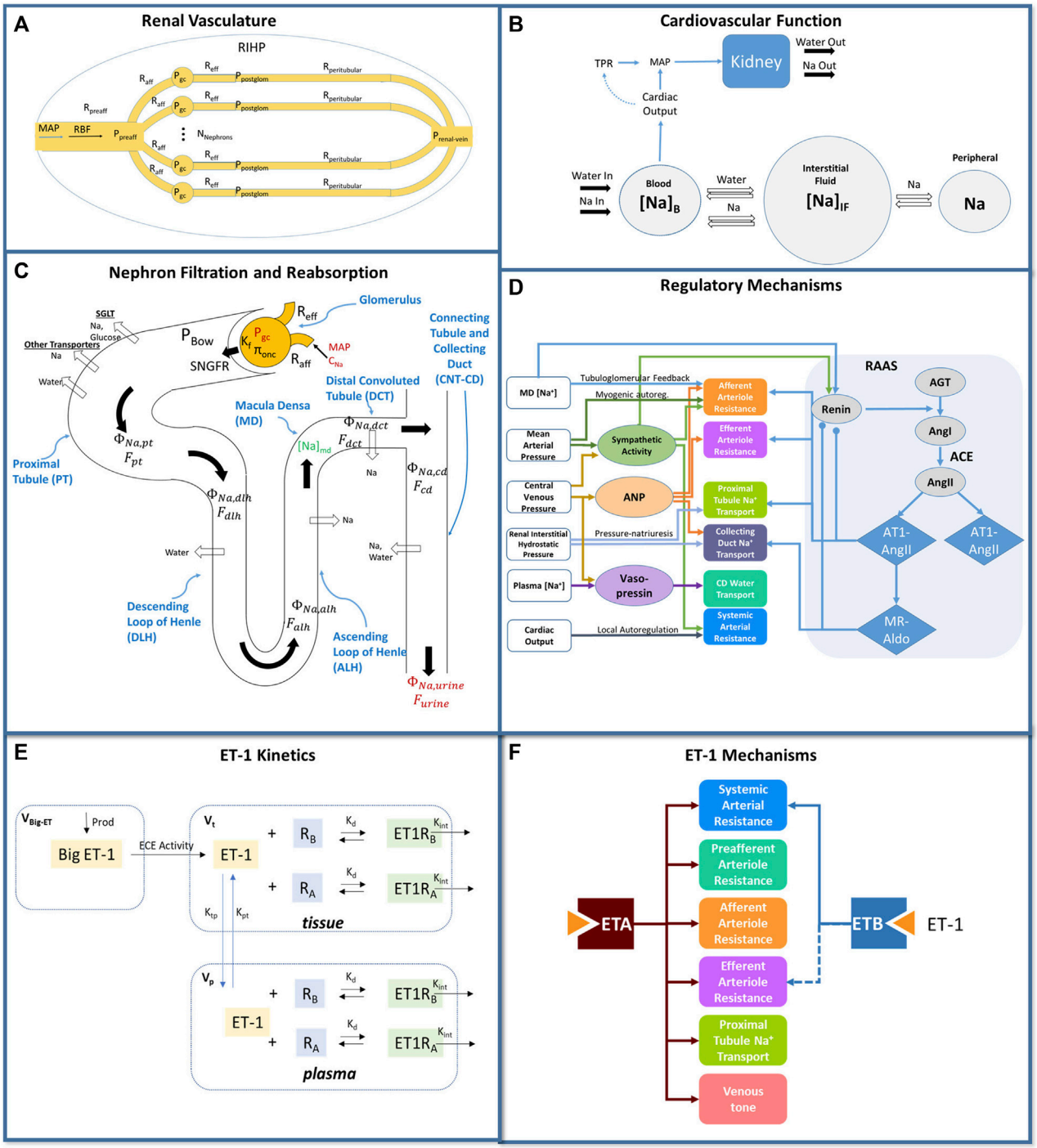

FIGURE 1
Mathematical model of cardiorenal function. **(A)** the renal vasculature is modeled by a single preafferent resistance vessel flowing into N parallel nephrons with an afferent, efferent, and peritubular resistance; RBF and glomerular hydrostatic and oncotic pressures are calculated as a function of MAP, renal venous pressure, and resistances. **(B)** The balance between Na^+ and water excretion and intake determines blood volume and plasma Na^+ concentration. Na^+ and water move between the blood and interstitial fluid according to starling forces, and Na^+ may be sequestered non-osmotically in a peripheral storage compartment. Blood volume and venous compliance and capacitance determines venous return and cardiac output, which together with total peripheral resistance, determine MAP. **(C)** Glomerular filtration is described by the balance of starling forces and the glomerular ultrafiltration coefficient K_f. Na^+, glucose, and water are reabsorbed at different fractional rates in the proximal tubule, loop of Henle, distal convoluted tubule, and connecting tubule/collecting duct. **(D)** Multiple regulatory mechanisms, including the renin-angiotensin-aldosterone system (RAAS), renal sympathetic activity, atrial natriuretic peptide (ANP), and vasopressin, provide feedback on model variables. **(E)** Endothelin-1 kinetics submodel. Big ET-1 is assumed to be produced at a constant rate; ECE converts Big ET-1 to ET-1 in the tissue compartment; ET-1 is distributed between the tissue and plasma compartments; in each compartment, ET-1 binds to ET_A and ET_B receptors to form receptor-ligand complexes which are then cleared by internalization. **(F)** Physiological effects of ET-1 through the ET_A and ET_B receptor, included in the final model. P, pressure; R, resistance; RBF: renal blood flow; MAP, mean arterial pressure; RIHP, renal interstitial hydrostatic pressure; Na, sodium; SNGFR: single nephron glomerular filtration rate; ϕ, mass flow rate; F, volumetric flow rate; C, concentration; MD, macula densa; ANP, atrial natriuretic peptide; RAAS, renin angiotensin aldosterone system; AGT,
(*Continued*)

FIGURE 1 (Continued)
angiotensinogen; Ang, angiotensin; AT1, angiotensin receptor type 1; AT2, angiotensin receptor type 2; MR, mineralocorticoid receptor; aldo, aldosterone; V, volume; k_d, binding affinity; k_{tp} and k_{pt}, intercompartmental transfer rate constants.

ET-1 through the ET_A and ET_B receptor, illustrated in Figure 2A. However, we took an agnostic approach to the existence, magnitude, and functional form of each relationship. Most physiological effects are saturable and thus well described as sigmoidal when considered over the full range of concentrations. However, if the range of concentrations observed physiologically or experimentally do not sufficiently cover the extremes, the saturation may not be detectable. Also, even if saturation occurs, there is not always sufficient data to estimate both the magnitude and steepness of the relationship. In these cases, a linear model, which only requires estimation of the slope m, may be more appropriate. Thus, for each possible mechanism, two possible functional forms were considered: linear (Eq. 1) and sigmoidal (Eq. 2).

$$E_{linear} = \max(1 + m_i([ET1R_i] - [ET1R_{i0}]), 0) \quad (1)$$

$$E_{sig} = 1 + \frac{m_i}{1 + e^{\frac{[ET1R_i]-[ET1R_{i0}]}{b}}} - \frac{m_i}{2} \quad (2)$$

Here, $ET1R_i$ represents the concentration of ET-1 bound to the either the ET_A or ET_B receptor. $ET1R_{i0}$ is the bound concentration under normal conditions. m_i defines the magnitude of the effect, and for the sigmoidal response, b defines the steepness of the sigmoidal function. E is the physiological effect on the target parameter. E is one when $ET1R_i$ is at its normal concentration, and may increase or decrease the target parameter as $ET1R_i$ changes.

2.3.1 Mechanism selection

The possible mechanistic effects of ET-1 through the ET_A and ET_B receptor, illustrated in Figure 2A, were first tested and selected for inclusion in the final model using a forward selection approach followed by a backward elimination step. The mechanism selection process is illustrated in Figure 3. Briefly, the base model, referred to as the NULL model, contained no mechanistic effects of ET-1. An initial objective function (OBJ) was determined by calculating the sum of the square error between the simulation and observed data for two experimental studies, described below. In the first round of selection, each mechanism and functional form was tested individually. For each, the slope m (linear) or slope m and steepness b (sigmoidal) was optimized to the experimental data. The mechanism that produced the greatest OBJ reduction, compared to the NULL model, was kept in the model for the next round. In the second round, each remaining mechanism/shape combination was tested in combination with the mechanism from the first round. The mechanism that produced the greatest reduction in OBJ, compared to the first round OBJ, was kept for the next round. This was repeated until no further improvements in OBJ occurred. At this point, the remaining mechanisms that did not improve OBJ were considered unimportant in explaining the experimental data, and were not included in the model. For the mechanisms identified as important in each of the forward rounds, a backward elimination round was used to confirm the contribution of each included mechanism. For this, first the OBJ with all included mechanisms was calculated. Then the OBJ was calculated after dropping each of the mechanisms individually. If any mechanism did not increase OBJ when dropped, this would indicate that that mechanism was not necessary to explain the data.

2.3.2 Parameter estimation

During the mechanism selection process, unknown model parameters were estimated by simultaneously fitting two experimental studies. These two studies were selected because they were conducted in human subjects and measured both plasma ET-1 and renal and systemic responses over time. The studies provide complementary information for constraining model parameters.

Infusion of increasing doses of ET-1: In (Kaasjager et al., 1997), six healthy subjects were placed on a diet of 200 mmol sodium per day for 5 days. They were then administered an infusion of ET-1 at increasing infusion rates: 0.5 ng/kg/min (0.2 pmol/kg/min) ET-1 for 60 min, followed by 1 ng/kg/min (0.4 pmol/kg/min) for 60 min, followed by a final 2.0 ng/kg/min (0.8 pmol/kg/min) for 60 min. Subjects were given an oral water load of 25 mL/kg body weight before the experiment began, and were asked to drink water matching their urinary output volume to maintain water loading. Plasma ET-1 was measured before infusion and at 75, 125, and 225 min after the start of the infusion. GFR was measured through inulin clearance and estimated renal plasma flow (RPF) was measured through para-aminohippuric acid (PAH). Renal blood flow (RBF) was calculated as RPF*(1-packed cell volume). Mean arterial pressure (MAP) was measured continuously. Renal vascular resistance (RVR) was calculated as MAP/RBF. Urine was collected throughout the study and urine flow rate, sodium excretion rate, fractional excretion of sodium, and fractional excretion of lithium were reported.

ET_A or ET_B inhibition followed by ET-1 infusion: In Bohm et al. (2003), six healthy, male subjects were studied on three different days separated by at least 1 week. Subjects were infused with either 0.9% saline (for 15 min), the ET_A inhibitor BQ123 (2.5–5 nmol/kg/min for 50 min), or the ET_B inhibitor BQ788 (4 nmol/kg/min for 15 min). After 30 min, subjects were also infused with ET-1 (4 pmol/kg/min; 10 ng/kg/min) for 20 min. Plasma ET-1 was measured at 0, 15, 30, 40, and 50 min. RBF was measured through PAH clearance. MAP was measured continuously, and RVR was calculated from RBF and MAP.

Study protocols were simulated as described in each manuscript, including sodium and water loading, doses of ET-1, ET_A, and ET_B

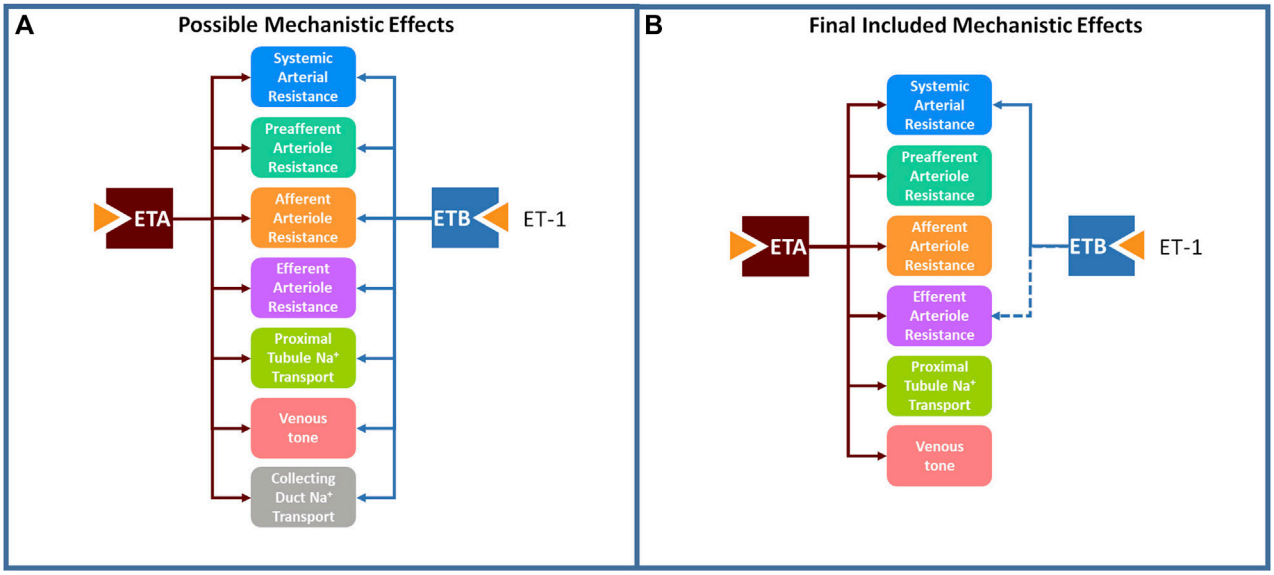

FIGURE 2
A large set of postulated mechanistic effects of ET-1 through ET_A and ET_B tested for inclusion in the model **(A)**, and a subset of these mechanisms, found to be necessary to explain experimental data, were included in the final model **(B)**.

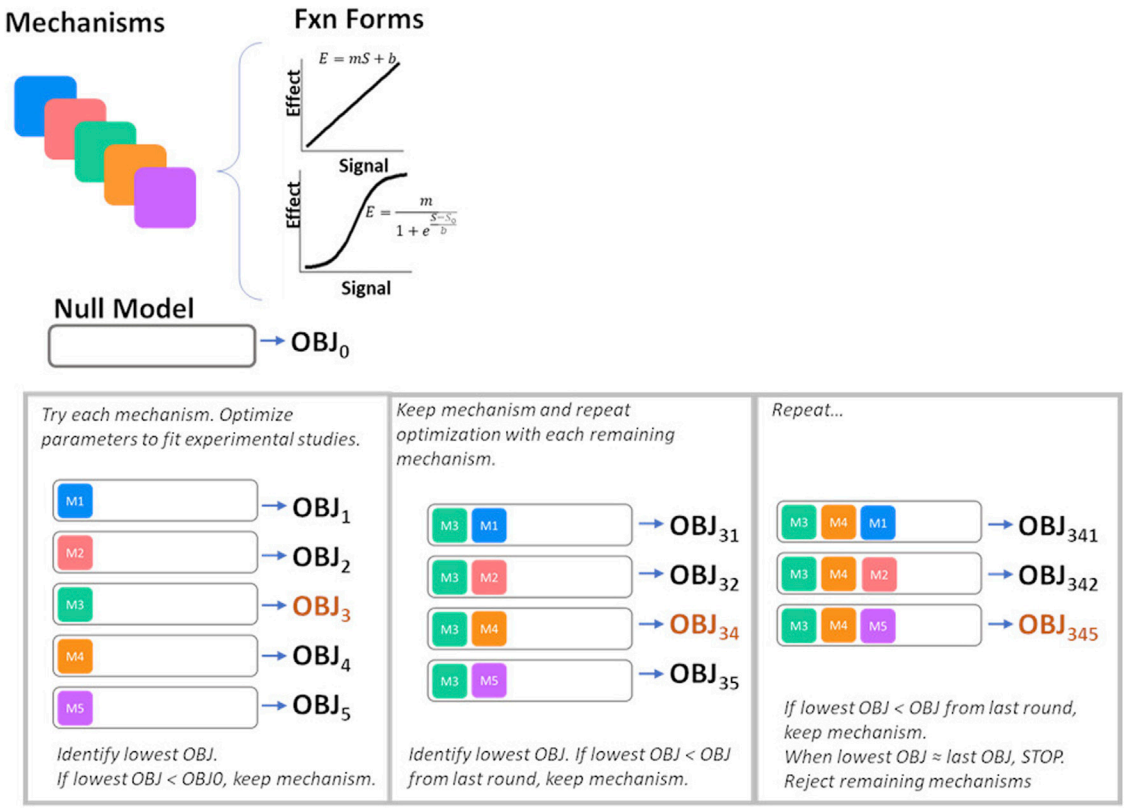

FIGURE 3
Process for mechanism selection and parameter estimation. OBJ, objective function value.

TABLE 1 Estimated slope for each include mechanism, and contribution of mechanism to improvement in objective function.

Signal	Effect	Initial calibration			Refined calibration
		Slope (SE)	OBJ		
			Reduction from NULL (%)	Reduction from previous round (%)	
ET1-ET_A	Preafferent Arteriole Resistance	0.344 (9.1%)	−59	−59	0.288 (8.9%)
	Proximal Tubule Na^+ Reabsorption	0.041 (4.6%)	−18	−45	0.0311 (5.1%)
	Afferent Arteriole Resistance	1.79 (3.6%)	−2.3	−13	1.66 (3.5%)
	Systemic Arterial Resistance	0.068 (3.1%)	−4.2	−19	0.060 (3.5%)
	Efferent Arteriole Resistance	0.086 (12%)	−1.4	−10	0.0635 (14%)
ET1-ET_B	Efferent Arteriole Resistance	−0.008 (19%)	−0.05	−4	−0.0059 (22%)
	Systemic Arterial Resistance	0.013 (5.1%)	−3.1	−19	0.0135 (5.2%)

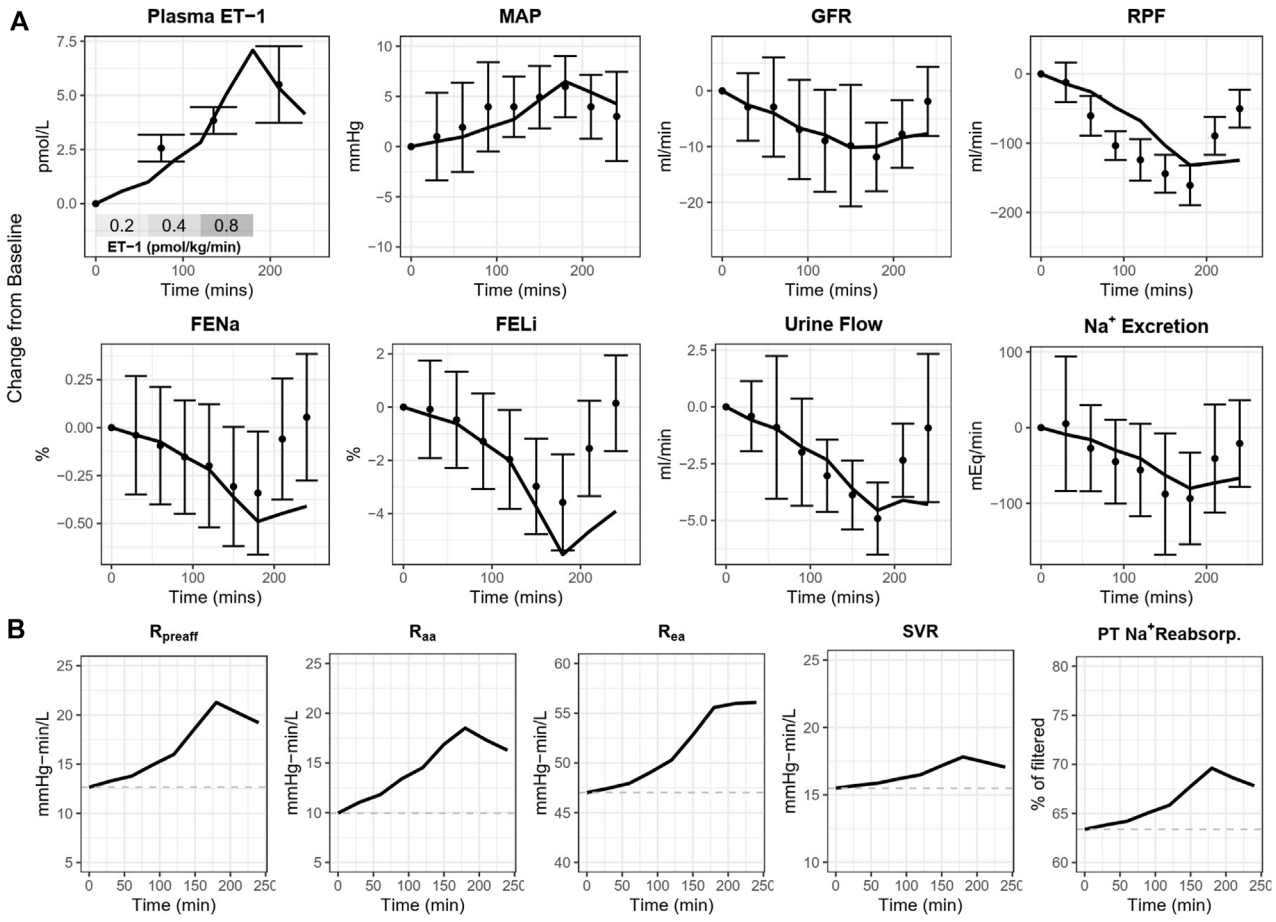

FIGURE 4
(A) Calibrated model reproduces the response of healthy subjects to ET-1 infusion observed in Kaasjager et al. (1997). **(B)** Simulated direct mechanistic effects of ET-1 infusion. MAP, mean arterial pressure; GFR, glomerular filtration rate; RPF, renal plasma flow; FENa, fractional excretion of sodium; FELi, fractional excretion of lithium; R, resistance; aa, afferent arteriole; ea, efferent arteriole; SVR, systemic vascular resistance; PT, proximal tubule.

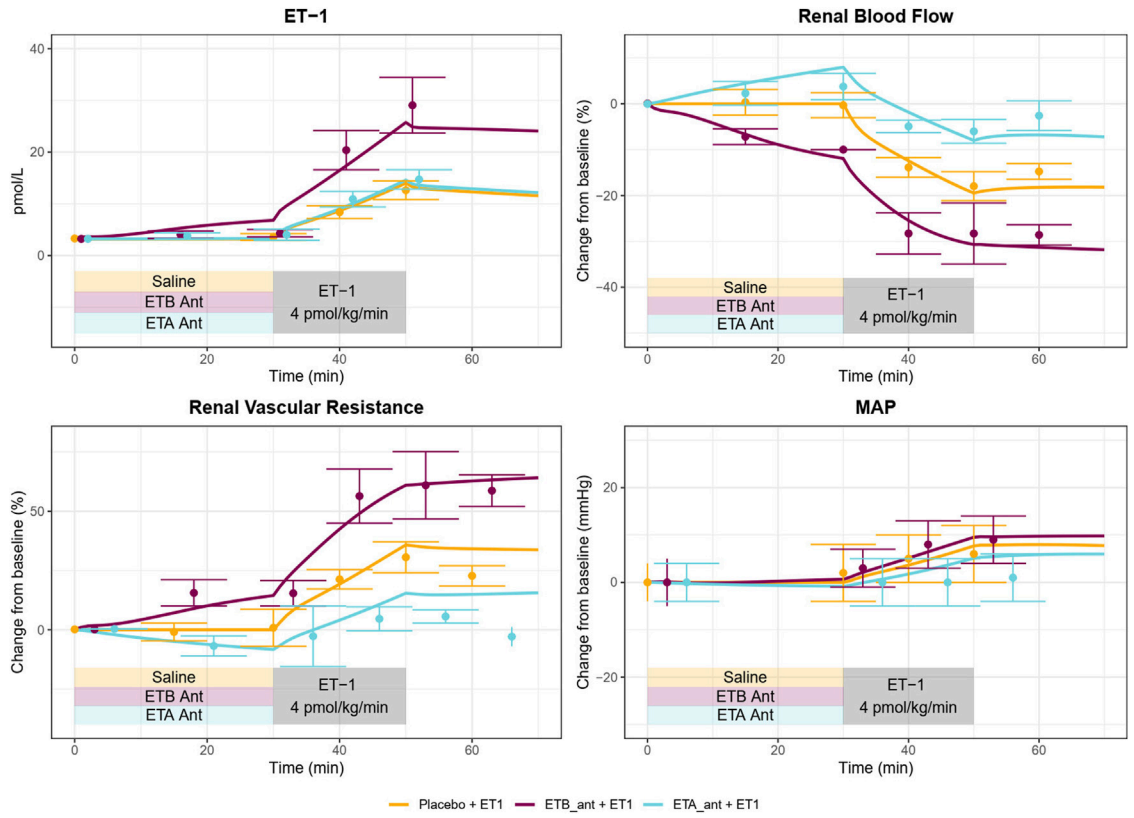

FIGURE 5
A Calibrated model reproduces the response of healthy subjects to ET_A or ET_B antagonism followed by ET-1 infusion observed in Bohm et al. (2003).

antagonist administered, and timing of doses. Parameters were estimated by minimizing the least square error between the observed and model-predicted responses.

2.3.3 Validation

The model was validated by simulating a separate experimental study of ET_A inhibition followed by ET-1 infusion (Vuurmans et al., 2004). In this study, nine healthy, male subjects were studied on four different days separated by at least 1 week, in randomized order. To maintain diuresis, subjects were infused with a 5% glucose solution, and then were instructed to consume water matching urinary output. Subjects then received either 0.9% saline (for 15 min) or the ET_A inhibitor VML588 at a dose of 0.05, 0.2, or 0.4 mg/kg/hr through the remainder of the study. Ninety minutes after the start of the study, subjects were also infused with ET-1 (1 pmol/kg/min) for 20 min. GFR was measured through inulin clearance and estimated renal plasma flow (RPF) was measured through para-aminohippuric acid (PAH). Renal blood flow (RBF) was calculated as RPF*(1- packed cell volume). Mean arterial pressure (MAP) was measured continuously. Renal vascular resistance (RVR) was calculated as MAP/RBF. Urine was collected at 30 min intervals and sodium excretion rate was reported.

2.3.4 Technical implementation

The model was implemented in R v4.1.2 using the RxODE package (Wang et al., 2016). Optimization was performed using the L-BFGS-B method in the optim package. Model code is available at https://bitbucket.org/cardiorenalmodel/endothelin-dynamics.

3 Results and discussion

3.1 Model calibration and mechanism selection

Figure 2B shows the final mechanisms selected for inclusion in the model. Estimated parameter values are given in Table 1. For all mechanisms, a linear form was found to be sufficient, and use of a sigmoidal function did not improve the objective function. This should not be interpreted to mean that the relationships are not saturable - only that they are reasonably approximated as linear over the range of the available experimental data. There certainly must be saturation of effects at high concentrations. It may be that the concentrations in the experimental studies do not reach concentrations sufficient to saturate the response, or that the data is not sufficiently granular to detect nonlinearity.

As shown in Figures 4A, 5, the calibrated model reasonably reproduced the observed magnitude and time course of changes in physiological variables in both experimental studies used for model calibration. The model was able to describe all of the key features of the response to ET-1 infusion (Figures 4A, 5—yellow), as well as the differing effects of ET_A and ET_B antagonism (Figures 5 – blue and purple). As observed in the experimental data, each antagonist alone had a minimal effect on RBF, RVR, and MAP, but blunted (ET_A antagonist) or exacerbated (ET_B antagonist) the response to ET-1.

Because the model parameters were optimized to fit both studies simultaneously, some aspects of the experimental data are fit less

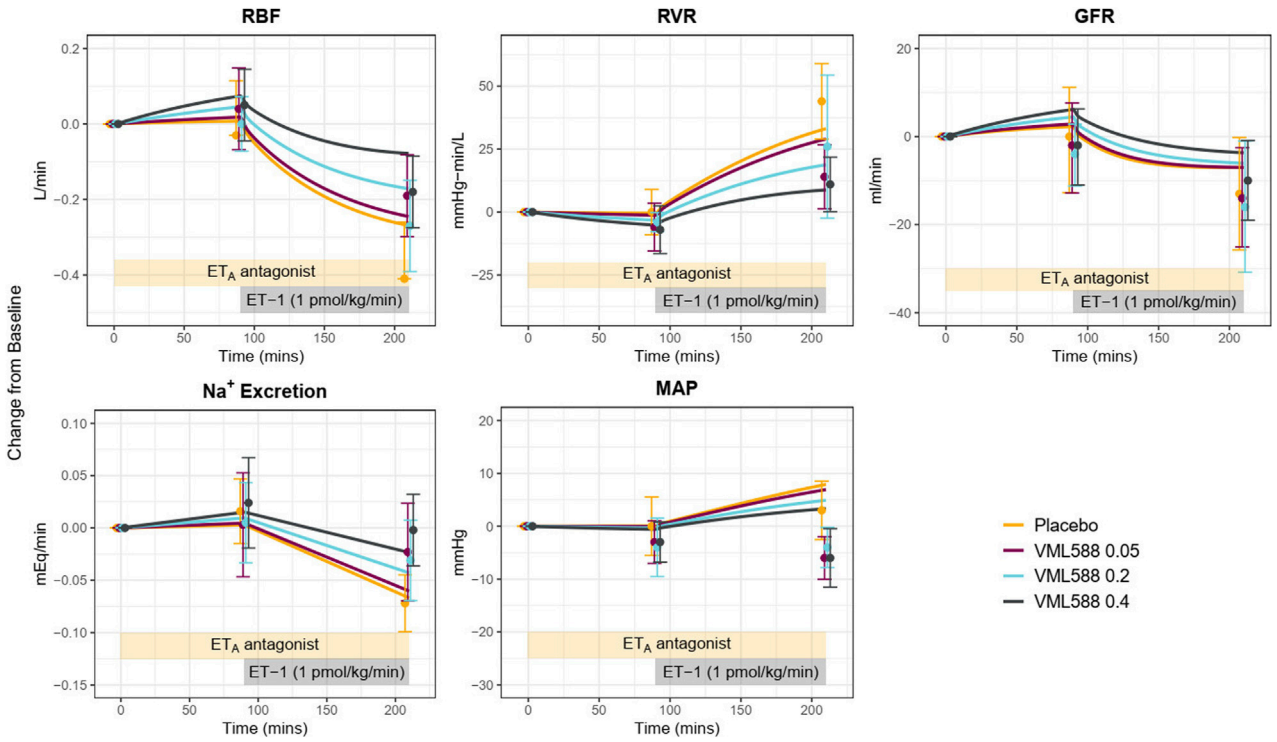

FIGURE 6
Model validation: Using identified mechanisms and calibrated parameters, the model reasonably reproduces the response to ET_A antagonism (VML588) and ET-1 infusion in a separate clinical study in healthy subjects (Vuurmans et al., 2004). RBF, renal blood flow; RVR, renal vascular resistance; GFR, glomerular filtration rate; MAP, mean arterial pressure.

than perfectly. The optimization process makes tradeoffs between individual study and variable fits to find the set of parameters that best fits the data overall. For instance, the observed RBF response to ET-1 infusion in (Figure 4A) was stronger than the observed response to ET-1 infusion in (Figure 5 - yellow), even though the increase in plasma ET-1 was slightly higher in Bohm et al. Thus, the optimization produced a simulated change in RBF that was slightly weaker than observed in the first study and slightly stronger than observed in the second study. The mechanistic effects of ET-1 infusion, adjusted to reproduce the outcomes observed in Kaasjager et al. (1997) are depicted in Figure 4B.

Using the calibrated parameters, the model reasonably predicted the response to the ET_A antagonist VML588, as shown in Figure 6. To simulate this study, only the plasma concentrations of VMK 588 were adjusted–all other parameters were fixed to their estimated values in Table 1. The model reproduced observed changes in GFR and Na^+ excretion in response to ET_A inhibition well, alone and with ET-1 infusion. It also reproduced the changes in RBF and RVR, although the predicted response was on the low end of the standard error of the measured value. For MAP, the model reproduced the lack of change with ET_A inhibition alone (at 90 min), and the simulated rise in MAP with ET-1 infusion at 210 min fell within the standard error of the measured value, although it was on the high end.

However, while it reproduced the trend of a reduction in MAP with ET_A antagonism relative to placebo during ET-1 infusion, the simulated absolute MAP at 210 min fell above the observed values in the ET_A antagonist arms. This is likely due to differences in the observed MAP response to ET_A antagonism between the calibration study (Bohm et al., 2003) and the experimental study used for validation. In MAP remained unchanged during ET-1 infusion following ET_A antagonism (Figures 5 blue), while in MAP fell below baseline during ET-1 infusion and ET_A antagonism. Increasing the simulated concentration of VML588 (and thus the degree of ET_A inhibition) could improve the MAP response but worsened the response of other variables (not shown).

This validation step demonstrated that the calibrated model and mechanisms identified can reasonably predict the key trends and behaviors in a new study. But this new study also provides further information for further constraining the model parameters. Therefore, the model parameters were estimated again, this time including the data from Vuurmans et al. (2004) in the objective function. The parameter estimates from the initial and refined calibration are given in Table 1. Parameter values shifted slightly from the initial calibration, but there were no major changes in values.

3.2 ET-1 mechanisms

3.2.1 Renal vascular effects

The strongest and most important mechanism of ET-1 identified was a vasoconstrictive effect through ET_A on the renal preglomerular vasculature (preafferent and afferent arterioles). This effect was identified in the first round of optimization and greatly reduced the objective function relative to the NULL model, and to a

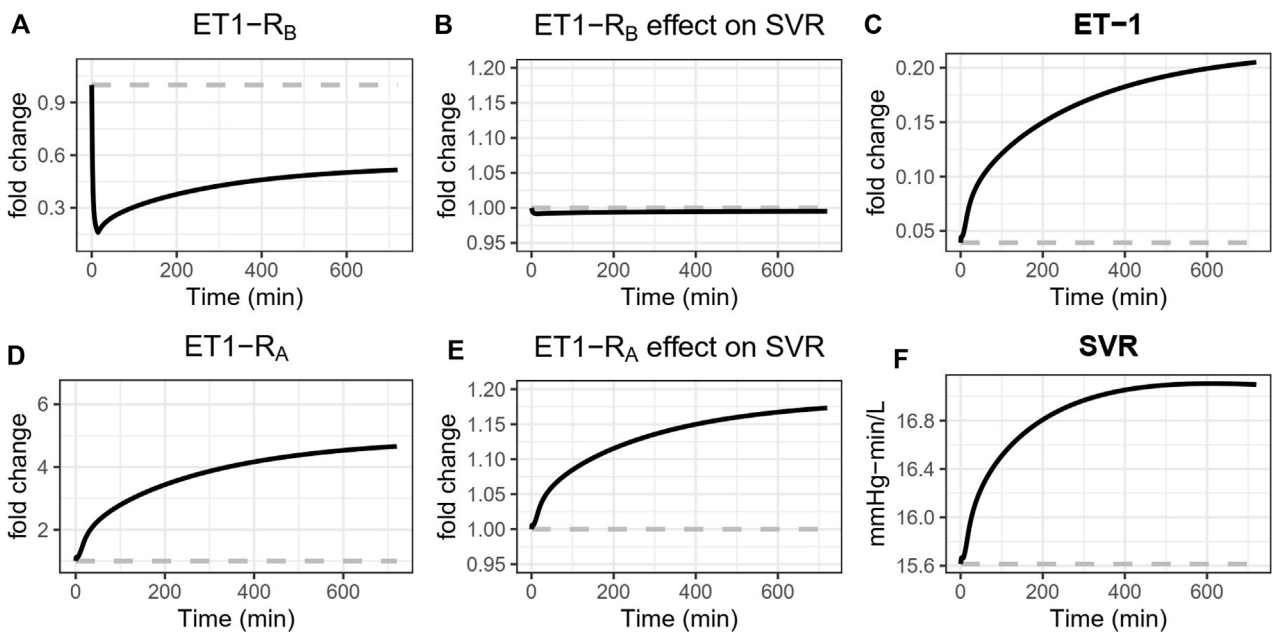

FIGURE 7
Simulated effects of ETB antagonism with BQ788 on systemic vascular resistance (SVR). ET_B antagonism reduces ET-1 binding to ET_B **(A)**, sending a weak vasodilatory signal to SVR **(B)**. But because ET_B is the main clearance receptor for ET-1, ET_B antagonism also causes ET-1 to rise **(C)**, thus increasing its binding to the ET_A receptor **(D)**. Because the vasoconstrictive effect of ET_A is much stronger than that of ET_B, the vasoconstrictive effect through ET_A dominates **(E)**, causing SVR to rise **(F)**.

vastly greater extent than other mechanisms tested. After including this mechanism, though, other mechanisms provided substantial further improvements in the model. On the efferent arteriole, a weak vasoconstrictive effect of ET-1 through ET_A and a vasodilatory effect through ET_B were found to be important, but these effects were much weaker than the preglomerular effect of ET_A. No effect of ET_B on the afferent arteriole was necessary to explain the data.

These findings are generally consistent with the experimental literature. The renal vasoconstrictive effects of ET-1 are well-established (Kohan et al., 2011), and ET_A expression has been found in all parts of the renal vasculature (Davenport et al., 1994; Endlich et al., 1996; Wendel et al., 2006). However, it is expressed relatively higher in the preglomerular vasculature (Wendel et al., 2006; Kohan et al., 2011; Davenport et al., 2016). Studies have shown that ET_A antagonists reduce vasoconstriction of the preafferent and afferent arterioles with ET-1 infusion (Endlich et al., 1996; Inscho et al., 2005), and the maximum vasoconstrictive effect of ET-1 on the afferent is greater than on efferent (Edwards et al., 1990). Thus, the finding of a strong vasoconstrictive effect of ET_A on the afferent and weaker effect on the efferent is consistent with these studies.

Studies in the hydronephrotic rat kidney have reported that ET_A antagonists block preglomerular constriction with ET-1, but have little effect on efferent tone (Endlich et al., 1996). Experiments in blood-perfused juxtaglomerular nephron preparations found that ET_B constricts the afferent arteriole but dilates the efferent arteriole. In this study, the vasodilatory effect of ET_B on efferent resistance was detected, although it was the least necessary to explain the data. An effect of ET_B on afferent resistance was not detected. This does not necessarily conflict with the experiments by (Inscho et al., 2005)—but it suggests that the data used in building this model was not sufficient to detect this mechanism, and suggests that this effect is less important in determining the response to ET-1 infusion as ET_A/ET_B agonists under the conditions in the calibration experiments.

3.2.2 Systemic arterial vasoconstriction

A vasoconstrictive effect of both ET_A and ET_B on the systemic vasculature was identified, and the effect through ET_A was about four times stronger than the effect through ET_B. The vasoconstrictive effect of ET-1 through ET_A on a wide range of blood vessel types is well established (Davenport et al., 2016). However, the data regarding ET_B is conflicting. Of particular interest, while studies have found that ET_B antagonists induce constriction (Love et al., 2000), studies of the ET_B agonist sarafotoxin have found that it also induces constriction (Haynes et al., 1995). These results at first seem in conflict, but the model is actually consistent with both of these results and offers an explanation as well. This is illustrated in Figure 7, which shows the simulated changes in systemic vascular resistance (SVR), [ET-1], [ET1-RA], [ET1-RB], and their respective effects on vascular resistance during ET_B antagonism. Because ET_B stimulates vasoconstriction, ET_B antagonism reduces ET-1 binding to ET_B, sending a weak vasodilatory signal to SVR. But because ET_B is the main clearance receptor for ET-1, ET_B antagonism also causes ET-1 to rise, thus increasing its binding to the ET_A receptor. Because the vasoconstrictive effect of ET_A is much stronger than that of ET_B, the vasoconstrictive effect through ET_A dominates, causing SVR to rise. A similar effect occurs to renal vascular resistance.

3.2.3 Sodium transport

The second most important effect in explaining the experimental data, after the ET_A vasoconstriction of the preglomerular vasculature, was an effect of ET-1 on sodium retention in the proximal tubule through ET_A. ET_A is expressed in the proximal nephron, and studies that have measured lithium clearance (a measure of proximal sodium reabsorption) with ET-1 infusion have consistently found a decrease in lithium clearance or fractional excretion of lithium, indicating an increase in proximal Na + reabsorption (Rabelink et al., 1994; Sorensen et al., 1994; Kaasjager et al., 1997; Vuurmans et al., 2004). However, studies of ET-1 control of sodium excretion are complex and difficult to study at the organ level, and results across studies are conflicting (Kohan et al., 2011). Garcia and Garvin found increased PT fluid reabsorption at low ET-1 concentrations (0.1–1 p.m.) and decreased reabsorption at high concentrations (~1,000 p.m.) (Garcia and Garvin, 1994). ET-1 concentrations in the experimental studies used in fitting the model ranges from 1 to 50 p.m., closer to the low-concentration range used by Garcia and Garvin, and thus consistent with sodium retention.

Effects of ET_B on sodium transport, in either the proximal tubule or the collecting duct, were found to be unnecessary to explain the experimental data. This does not mean that this effect does not exist–experimental studies have demonstrated a role of ET_B in collecting duct natriuresis (Kohan et al., 2011). However, it indicates that this effect cannot be detected in the data used for calibration, and that this mechanism is not necessary to explain the responses observed in the experimental studies considered. In (Kaasjager et al., 1997), the decrease in fractional excretion of lithium parallels the changes in Na + excretion, and the effects of ET-1 on proximal tubule reabsorption are sufficient to produce the observed Na + excretion rates in this study, as well as in the validation study by (Vuurmans et al., 2004).

3.2.4 Venous constriction/reduced venous capacitance

The model was insensitive to effects of ET-1 on venous capacitance or venous compliance. Including this effect tended to shift other parameters, but did not improve or worsen the objective function. This indicates that the measured data does not hold sufficient information to identify and quantify venous effects. However, the effects of ET-1 on venous tone through ET-1 have been clearly demonstrated experimentally. ET-1 caused both venous and arterial contractions in both human and canine vessels, with significantly lower EC50 in veins compared to arteries (Cocks et al., 1989). Maximum contraction in veins was 100% that of max contraction with K+ depolarization, while in arteries it ranges from 25% to 80%. In small arteries and veins, ET_A antagonists blocked this effect, but ET_B antagonists and agonists had no effect, indicating that it is mediated by ET_A (Riezebos et al., 1994). Therefore, further investigating and additional data is needed to better inform this mechanism in the model going forward.

3.2.5 The role of ET_B

ET_B antagonism induces renal vasoconstriction and reduced renal blood flow (see Figure 5), but interestingly, the only identified direct effects of ET_B were weak systemic vasoconstriction and weak efferent vasodilation. The model suggests that the effects of ET_B antagonists are primarily the consequence of reduced clearance of ET-1 through ET_B when it is blocked, resulting in higher plasma and renal ET-1 and increased binding to the ET_A receptor (Figure 7). In the context of ET_A antagonist selectivity, this suggests that as selectivity decreases and the potential for ET_B binding increases, the primary consequence is likely to be reduced ET-1 clearance, increased ET-1 concentrations, more ET-1 available to bind to any open ET_A receptors, thus effectively reducing the degree of ET_A antagonism.

3.2.6 Limitations

There are a number of limitations of this study. As noted, the ability to detect ET-1 mechanisms is limited by the data used to inform the model. Lack of identification of an effect does not mean an effect does not exist. It only means that the effect is not necessary to explain the observed data, and mechanisms not detected in this study may emerge as important if additional variables were measured. For example, effects on venous capacitance were not needed o explain the current data, but this could be because the data utilized included only measures that strongly reflect arterial function (e.g., cardiac output and blood pressure). Inclusion of additional variables such as venous pressure or cardiac filling pressure may be necessary to identify a venous effect, but these variables are unfortunately much more difficult to obtain clinically.

This model provides a starting point for continuous testing and integration of additional data sets going forward, which may allow detection and quantification of further mechanisms, especially in the collecting duct and venous circulation. Also, inclusion of additional data sets may allow identification of nonlinear effects, which could not be detected in this study.

All experimental studies used in this analysis were conducted in men. Therefore, this model represents the male response to ET-1. The response could look distinctly different in females, and studies conducted in females should be incorporated into the model in the future.

4 Conclusion

In this study, we updated our previously published cardiorenal model to account for the pathophysiological mechanism of ET1 and its complexes of ET1A and ET1B. The physiologic mechanisms of ET-1 through each of its receptors in the systemic and renal vasculature and renal tubules was rigorously evaluated and calibrated using clinical observations of acute vascular and renal response to ET-1 infusion and ET_A/ET_B antagonists in healthy subjects. The model is capable of reproducing changes in blood pressure, renal blood flow, GFR, and sodium/water excretion with ET_A or ET_B antagonism. The mechanisms identified are consistent with the larger body of experimental studies on ET-1, and provide novel insights into the relative magnitude and importance of endothelin's effects. The preglomerular vasoconstrictive effect of ET-1 through ET_A was found to be much stronger than either its efferent vasoconstrictive effect through ET_A or its efferent vasodilatory effect through ET_B. This analysis suggests that the vasoconstrictive and fluid retention responses to ET_B antagonists are more likely explained by reduced ET-1 clearance by ET_B, resulting in increased binding to ET_A, rather than direct effects through ET_B. However, finding that a mechanism was not necessary

to explain the data in this analysis, which in included arterial and renal function measures, does not negate its existence. For instance, an effect on venous capacitance was not detected, but this could be due to lack of information on venous function in the variables measured. This model provides a tool for understanding and predicting clinical responses to therapeutics that targeting the endothelin system. For example, this model is currently being utilized to aid in the clinical development of the highly selective ET_A antagonist zibotentan by predicting the renal hemodynamics and fluid status alone and in combination with a sodium glucose cotransporter 2 (SGLT2 inhibitor).

Data availability statement

The original contributions presented in the study are included in the article/Supplementary Material, further inquiries can be directed to the corresponding author.

Ethics statement

Ethical approval was not required for the study involving humans in accordance with the local legislation and institutional requirements. Written informed consent to participate in this study was not required from the participants or the participants' legal guardians/next of kin in accordance with the national legislation and the institutional requirements.

Author contributions

HY: Conceptualization, Formal Analysis, Investigation, Methodology, Software, Validation, Visualization, Writing–original draft. PG: Conceptualization, Project administration, Supervision, Validation, Writing–review and editing. HL-H: Conceptualization, Investigation, Validation, Writing–review and editing. DB: Conceptualization, Funding acquisition, Project administration, Resources, Supervision, Writing–review and editing. BH: Conceptualization, Project administration, Supervision, Writing–review and editing. KH: Conceptualization, Formal Analysis, Funding acquisition, Investigation, Methodology, Project administration, Software, Supervision, Validation, Visualization, Writing–original draft.

Funding

The author(s) declare that financial support was received for the research, authorship, and/or publication of this article.

Conflict of interest

This study received funding from AstraZeneca Pharmaceuticals. The funder had the following involvement in the study: Employees of AstraZeneca are co-authors on this manuscript and were involved in conceptualization, project administration, supervision, formal analysis, investigation, methodology, validation, review and editing. HY, PG, DB, and BH are employees of AstraZeneca and own AstraZeneca stock or stock options. HL-H is a consultant for and received honoraria from AbbVie, Astellas, Astra Zeneca, Boehringer Ingelheim, Fresenius, Janssen and Merck. He has a policy that all honoraria are paid to his employer. KH has received research funding from AstraZeneca in the last 3 years.

Publisher's note

References

Bohm, F., Pernow, J., Lindström, J., and Ahlborg, G. (2003). ETA receptors mediate vasoconstriction, whereas ETB receptors clear endothelin-1 in the splanchnic and renal circulation of healthy men. *Clin. Sci. (Lond)* 104 (2), 143–151. doi:10.1042/CS20020192

Cocks, T. M., Faulkner, N. L., Sudhir, K., and Angus, J. (1989). Reactivity of endothelin-1 on human and canine large veins compared with large arteries *in vitro*. *Eur. J. Pharmacol.* 171 (1), 17–24. doi:10.1016/0014-2999(89)90425-1

Davenport, A. P., Hyndman, K. A., Dhaun, N., Southan, C., Kohan, D. E., Pollock, J. S., et al. (2016). Endothelin. *Pharmacol. Rev.* 68 (2), 357–418. doi:10.1124/pr.115.011833

Davenport, A. P., Kuc, R. E., Hoskins, S. L., Karet, F. E., and Fitzgerald, F. (1994). [125I]-PD151242: a selective ligand for endothelin ETA receptors in human kidney which localizes to renal vasculature. *Br. J. Pharmacol.* 113 (4), 1303–1310. doi:10.1111/j.1476-5381.1994.tb17140.x

Edwards, R. M., Trizna, W., and Ohlstein, E. H. (1990). Renal microvascular effects of endothelin. *Am. J. Physiol.* 259 (2), F217–F221. doi:10.1152/ajprenal.1990.259.2.F217

Endlich, K., Hoffend, J., and Steinhausen, M. (1996). Localization of endothelin ETA and ETB receptor-mediated constriction in the renal microcirculation of rats. *J. Physiol.* 497 (1), 211–218. doi:10.1113/jphysiol.1996.sp021761

Garcia, N. H., and Garvin, J. L. (1994). Endothelin's biphasic effect on fluid absorption in the proximal straight tubule and its inhibitory cascade. *J. Clin. Invest.* 93 (6), 2572–2577. doi:10.1172/JCI117268

Hallow, K. M., Beh, J., Rodrigo, M., Ermakov, S., and Friedman, S. (2014). A model-based approach to investigating the pathophysiological mechanisms of hypertension and response to antihypertensive therapies: extending the Guyton model. *Am. J. Physiol. Regul. Integr. Comp. Physiol.* 306 (9), R647–R662. doi:10.1152/ajpregu.00039.2013

Hallow, K. M., and Gebremichael, Y. (2017). A quantitative systems physiology model of renal function and blood pressure regulation: model description. *CPT Pharmacometrics Syst. Pharmacol.* 6 (6), 383–392. doi:10.1002/psp4.12178

Hallow, K. M., Gebremichael, Y., Helmlinger, G., and Vallon, V. (2017). Primary proximal tubule hyperreabsorption and impaired tubular transport counterregulation determine glomerular hyperfiltration in diabetes: a modeling analysis. *Am. J. Physiol. Ren. Physiol.* 312 (5), F819–F835. doi:10.1152/ajprenal.00497.2016

Hallow, K. M., Greasley, P. J., Helmlinger, G., Chu, L., Heerspink, H. J., and Boulton, D. W. (2018). Evaluation of renal and cardiovascular protection mechanisms of SGLT2 inhibitors: model-based analysis of clinical data. *Am. J. Physiol. Ren. Physiol.* 315 (5), F1295–F1306. doi:10.1152/ajprenal.00202.2018

Haynes, W. G., Strachan, F. E., and Webb, D. J. (1995). Endothelin ETA and ETB receptors cause vasoconstriction of human resistance and capacitance vessels *in vivo*. *Circulation* 92 (3), 357–363. doi:10.1161/01.cir.92.3.357

Hunter, R. W., Moorhouse, R., Farrah, T. E., MacIntyre, I. M., Asai, T., Gallacher, P. J., et al. (2017). First-in-Man demonstration of direct endothelin-mediated natriuresis and diuresis. *Hypertension* 70 (1), 192–200. doi:10.1161/HYPERTENSIONAHA.116.08832

Inscho, E. W., Imig, J. D., Cook, A. K., and Pollock, D. M. (2005). ETA and ETB receptors differentially modulate afferent and efferent arteriolar responses to endothelin. *Br. J. Pharmacol.* 146 (7), 1019–1026. doi:10.1038/sj.bjp.0706412

Kaasjager, K. A., Shaw, S., Koomans, H. A., and Rabelink, T. J. (1997). Role of endothelin receptor subtypes in the systemic and renal responses to endothelin-1 in humans. *J. Am. Soc. Nephrol.* 8 (1), 32–39. doi:10.1681/ASN.V8132

Kohan, D. E., Inscho, E. W., Wesson, D., and Pollock, D. M. (2011). Physiology of endothelin and the kidney. *Compr. Physiol.* 1 (2), 883–919. doi:10.1002/cphy.c100039

Love, M. P., Ferro, C. J., Haynes, W. G., Plumpton, C., Davenport, A. P., Webb, D. J., et al. (2000). Endothelin receptor antagonism in patients with chronic heart failure. *Cardiovasc Res.* 47 (1), 166–172. doi:10.1016/s0008-6363(00)00081-x

Parker, J. D., Thiessen, J. J., Reilly, R., Tong, J. H., Stewart, D. J., and Pandey, A. S. (1999). Human endothelin-1 clearance kinetics revealed by a radiotracer technique. *J. Pharmacol. Exp. Ther.* 289 (1), 261–265.

Rabelink, T. J., Kaasjager, K. A., Boer, P., Stroes, E. G., Braam, B., and Koomans, H. A. (1994). Effects of endothelin-1 on renal function in humans: implications for physiology and Pathophysiology. *Kidney Int.* 46 (2), 376–381. doi:10.1038/ki.1994.284

Regard, J. B., Sato, I. T., and Coughlin, S. R. (2008). Anatomical profiling of G protein-coupled receptor expression. *Cell* 135 (3), 561–571. doi:10.1016/j.cell.2008.08.040

Riezebos, J., Watts, I. S., and Vallance, P. J. (1994). Endothelin receptors mediating functional responses in human small arteries and veins. *Br. J. Pharmacol.* 111 (2), 609–615. doi:10.1111/j.1476-5381.1994.tb14780.x

Sorensen, S. S., Madsen, J. K., and Pedersen, E. B. (1994). Systemic and renal effect of intravenous infusion of endothelin-1 in healthy human volunteers. *Am. J. Physiol.* 266 (3), F411–F418. doi:10.1152/ajprenal.1994.266.3.F411

Vuurmans, J. L., Boer, P., and Koomans, H. A. (2004). Effects of endothelin-1 and endothelin-1-receptor blockade on renal function in humans. *Nephrol. Dial. Transpl.* 19 (11), 2742–2746. doi:10.1093/ndt/gfh471

Wang, W., Hallow, K. M., and James, D. A. (2016). A tutorial on RxODE: simulating differential equation pharmacometric models in R. *CPT Pharmacometrics Syst. Pharmacol.* 5 (1), 3–10. doi:10.1002/psp4.12052

Wendel, M., Knels, L., Kummer, W., and Koch, T. (2006). Distribution of endothelin receptor subtypes ETA and ETB in the rat kidney. *J. Histochem Cytochem* 54 (11), 1193–1203. doi:10.1369/jhc.5A6888.2006

frontiers | Frontiers in Pharmacology

TYPE Review
PUBLISHED 17 June 2024
DOI 10.3389/fphar.2024.1408679

OPEN ACCESS

EDITED BY
Simon Lebek,
University of Regensburg, Germany

REVIEWED BY
Benjamin Nelson,
University of Texas Southwestern Medical Center, United States
Eleonora Cianflone,
Magna Græcia University, Italy

*CORRESPONDENCE
Rabea Hinkel,
rhinkel@dpz.eu

RECEIVED 28 March 2024
ACCEPTED 21 May 2024
PUBLISHED 17 June 2024

CITATION
von Bibra C and Hinkel R (2024), Non-human primate studies for cardiomyocyte transplantation—ready for translation?
Front. Pharmacol. 15:1408679.
doi: 10.3389/fphar.2024.1408679

Non-human primate studies for cardiomyocyte transplantation—ready for translation?

Constantin von Bibra[1,2,3] and Rabea Hinkel[1,2,3]*

[1]Institute for Animal Hygiene, Animal Welfare and Farm Animal Behavior, Stiftung Tieraerztliche Hochschule Hannover, University of Veterinary Medicine, Hanover, Germany, [2]Laboratory Animal Science Unit, German Primate Center, Leibniz Institute for Primate Research, Goettingen, Germany, [3]DZHK (German Centre of Cardiovascular Research), Partner Site Lower Saxony, Goettingen, Germany

Non-human primates (NHP) are valuable models for late translational pre-clinical studies, often seen as a last step before clinical application. The unique similarity between NHPs and humans is often the subject of ethical concerns. However, it is precisely this analogy in anatomy, physiology, and the immune system that narrows the translational gap to other animal models in the cardiovascular field. Cell and gene therapy approaches are two dominant strategies investigated in the research field of cardiac regeneration. Focusing on the cell therapy approach, several xeno- and allogeneic cell transplantation studies with a translational motivation have been realized in macaque species. This is based on the pressing need for novel therapeutic options for heart failure patients. Stem cell-based remuscularization of the injured heart can be achieved via direct injection of cardiomyocytes (CMs) or patch application. Both CM delivery approaches are in the late preclinical stage, and the first clinical trials have started. However, are we already ready for the clinical area? The present review concentrates on CM transplantation studies conducted in NHPs, discusses the main sources and discoveries, and provides a perspective about human translation.

KEYWORDS

cardiac regeneration, cardiomyocyte transplantation, heart failure, myocardial infarction, large animal models, non-human primates, pluripotent stem cells

1 Introduction

Cardiovascular diseases are the primary cause of death worldwide, and the heart failure rate is still increasing (Khan et al., 2020; Bozkurt et al., 2023). Ischemic heart disease ranks as the most prevalent, which justifies the scientific desire to explore new treatment options for the injured heart. Current pharmacological treatments focus on the remaining myocardium to manage the symptoms by reducing the adverse remodeling process (Azevedo et al., 2016) but not reversing the process. The only curative treatment option for end-stage heart failure patients at the moment is heart transplantation. However, due to a limited donor pool and post-transplant complications, it is only an opportunity for a restricted patient population (Awad et al., 2022). Therefore, cardiac regenerative approaches have been studied intensively over the last decades (Eschenhagen et al., 2022; Garbern and Lee, 2022). Since induced pluripotent stem (iPS) cell-derived cardiomyocytes (CMs) are available in unlimited numbers (Takahashi and Yamanaka, 2006; Yu et al., 2007), one ambitious strategy became realistic: the transplantation of new CMs to the injured heart (Weinberger and Eschenhagen, 2021). Remuscularization of the damaged heart has been successfully

TABLE 1 Key publications of cardiomyocyte replacement therapy in non-human primates.

Study reference	NHP species	Age and weight (kg)	n-number and sex	MI induction method	Tx post MI (weeks)	Delivery approach	Cell source	Immunosuppression	Follow-up (weeks)
Gruh et al. (2024)	*M. fascicularis*	4–8 years, 7–13	n = 14 (15) (1f, 14 m)	Thoracotomy PL	2	Injection	hiCMA	MPred, ABC, and CsA	2, 12
Cheng et al. (2023)	*M. mulatta*	5–18 years, 9–11	n = 11 (m)	PCI or Thoracotomy I/R, 90 min	4	Injection	hiPSC-CM and EC	MPred, ABC, and Tac	4
Li et al. (2021)	*M. mulatta*	4–6 years, 7–14	n = 15 (17) (m)	Thoracotomy I/R, 180 min	0	Injection and i.v. and i.c.	hiPSC-CM	MPred, Tac, and MMF	4, 8, 12
Kashiyama et al. (2019)	*M. fascicularis*	6 years, 4–6	n = 12 (m)	Thoracotomy PL	2	Cardiac sheets	Allogeneic	Pred, Tac, and MMF	12, 24, 36
Liu et al. (2018)	*M. nemestrina*	6–15 years, 5–13	n = 9 (17), (1 m, 8f)	PCI I/R, 180 min	2	Injection	hESC-CM	MPred, CsA, and ABC	4, 12
Shiba et al. (2016)	*M. fascicularis*	4–5 years, 3	n = 10 (f)	Sternotomy I/R, 180 min	2	Injection	Allogeneic	MPred and Tac	12
Chong et al. (2014)	*M. nemestrina*	5–14 years, 9–12	n = 6 (7), (3 m, 3f)	PCI I/R, 90 min	2	Injection	hESC-CM	MPred, CsA, and ABC	2, 4, 12

Abbreviations: NHP, non-human primate; M, *Macaca*; kg, kilogram; m, male; f, female; MI, myocardial infarction; PCI, percutaneous coronary intervention; I/R, ischemia reperfusion injury; PL, permanent ligation; min, minutes; Tx, transplantation; i.v., intravenous; i.c., intracoronary, hiCMA, human-induced pluripotent stem cell-derived cardiomyocyte aggregates; hiPSC, human-induced pluripotent stem cells; hESC, human embryonic stem cells; CM, cardiomyocytes; EC, endothelial cells, MPred, methylprednisolone; Pred, prednisolone; CsA, cyclosporine A; ABC, abatacept; Tac, tacrolimus; MMF, mycophenolate mofetil.

approached in several small animal studies. Large grafts combined with beneficial functional outcomes were achieved with direct CM injection (Caspi et al., 2007; Laflamme et al., 2007; Shiba et al., 2012) and CM-containing patches (Zimmermann et al., 2006; Weinberger et al., 2016; Querdel et al., 2021). These promising results encouraged the field to move forward toward translation. Therefore, as a next step, large animal models are deemed indispensable for this therapeutic strategy prior to clinical translation (Dixon and Spinale, 2009; Chong and Murry, 2014). First, first-in-human clinical trials with healthy volunteers are not applicable for this kind of therapeutic approach. Second, the heart weight to cell number/patch size and the different routes of application cannot be addressed sufficiently in rodents. In addition, large animals better model human disease phenotypes due to their comparable anatomy and physiology (Plews et al., 2012; Hotham and Henson, 2020; Martínez-Falguera et al., 2021). The CM transplantation approach, therefore, has mainly been addressed in pigs and non-human primates (NHPs). The advantages of the pig model are the similar heart size and heart weight-to-body weight ratio, as well as the identical heart rate to humans (Lelovas et al., 2014; Romagnuolo et al., 2019). However, the establishment of a sufficient human transferable immunosuppression to avoid graft rejection seems challenging (Kawamura et al., 2012; Chong and Murry, 2014; Zimmermann, 2017). The other clinically highly relevant large animal model for CM transplantation is the non-human primate. Several groups translated the cardiac remuscularization approach to NHP models (key publications summarized in Table 1).

This review will introduce the utilized NHP models, the applied myocardial infarction (MI) induction methods, the cell sources, and their delivery to the injured heart. Additionally, we will discuss the study designs of transplantation and follow-up timing. Finally, we will sum up the limitations and have a discussion on clinical obstacles and future deliberations.

2 Main

2.1 Non-human primate models

Primates consist of more than 300 species, classified into three major categories: New World monkeys/*Platyrrhini*, Old World monkeys/*Catarrhini*, and others (T. Nakamura et al., 2021). Within the European Union, only non-human primates can be used for preclinical biomedical research due to their close phylogenetic background and similarities to human beings. NHP models still play an important role in translation and applied research, not only in the cardiovascular field. Within the broad variety of NHPs, the following species are the most utilized ones in biomedical research: common marmoset (*Callithrix jacchus*, New World monkey), cynomolgus macaque (*Macaca fascicularis*, Old World monkey), rhesus macaque (*Macaca mulatta*, Old World monkey), and baboons (*Papio* genus, e.g., *anubis* or *hamadryas*, Old World monkey) (Chatfield and Morton, 2018). The latter species are presently used primarily for solid organ or cardiac valve xenotransplantation studies. Their size/large scale is a key value to investigate pig heart to primate transplantation (Bailey, 2009; Längin et al., 2018). Marmosets are not suitable for transplantation purposes due to their small size (300–500 g, adult animals) and hematopoietic chimerism, which complicates the evaluation of the immune reaction (Silva et al., 2017). Non-human primates are conspicuously suitable for exploring MI-based treatment options due to their negligible collateral perfusion, similar to the human coronary network (Buss et al.,

	Callithrix	Macaca	Papio	Human
Life span (years)	16.5	30	25-35	71
Body weight (kg)	0.4	8	10-31	70
Heart weight (g)	3	25	40	350
Heart rate (bpm)	180	100-240	74-200	80

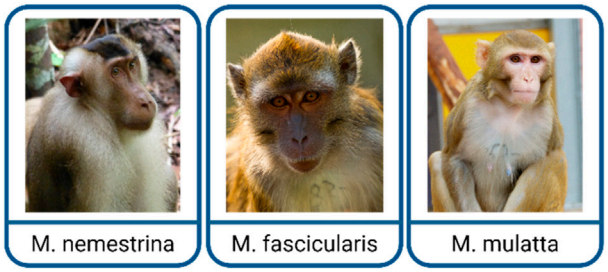

FIGURE 1
Non-human primates as a late preclinical model of cardiac remuscularization. Comparison of the main physiological parameters of NHPs to humans (left). Examples of utilized macaque species (right): *Macaca nemestrina* (pig-tailed macaque), *Macaca fascicularis* (cynomolgus macaque), and *Macaca mulatta* (rhesus macaque). Pictures taken (from left to right) by Carolin Kade, Chris Schloegl, and Margrit Hampe with the permission from the German Primate Center (DPZ).

TABLE 2 Key publications of cardiomyocyte replacement therapy in non-human primates.

Study reference	Cell source	CM preparation	Transfer	Scar size	Input cell number	Graft size	Quantification engrafted CM
Gruh et al. (2024)	hiCMAs	Aggregates	10–12 i.m. injection	n/a	50mio	n/a	n/a
Cheng et al. (2023)	hiPSC-CM (and EC)	Single cells	4 i.m. injections	n/a	500mio CM (+500mio EC)	3%–5% of LV	n/a
Li et al. (2021)	hiPSC-CM	Single cells	10 i.m. injections	n/a	100mio/kg for i.m. application	n/a	n/a
Kashiyama et al. (2019)	Allogeneic	Cardiac sheets	4 epicardial sheets	n/a	4 × 3,6mio (14mio)	n/a	n/a
Liu et al. (2018)	hESC-CM	Single cells	15 i.m. injections	20% of LV	750mio	2% of LV 10% of Scar	22-126mio
Shiba et al. (2016)	Allogeneic	Single cells	10 i.m. injections	9% of LV	400mio	16% of Scar	n/a
Chong et al. (2014)	hESC-CM	Single cells	15 i.m. injections	5% of LV	1000mio	2% of LV	n/a

Abbreviations: hiCMA, human-induced pluripotent stem cell-derived cardiomyocyte aggregate; hiPSC, human-induced pluripotent stem cell; hESC, human embryonic stem cell; CM: cardiomyocyte; EC, endothelial cell; i.m, intramyocardial; LV, left ventricle; mio, million; kg, kilogram; n/a, not applicable.

1983). Considering the size, phylogenetic similarities, and availability for translational, clinically relevant CM transplantation studies, macaques seem to be the best model to use. In addition, they are well-characterized, immunosuppression protocols are established, and a variety of assays and antibodies are available to analyze the heart. To investigate cardiac remuscularization, different macaque species were utilized (Figure 1). Which of the three macaque species was selected for use in the studies normally depends on the availability and experience of the individual institutes with the respective species.

In addition to the model organism (the NHP here), the choice of cell source for iPS cell-derived CMs is of importance for translational studies, as summarized in the question of allo- versus xenotransplantation, both with advantages and disadvantages. Allotransplantation would reflect the human clinical trial situation, because the cell source here is finally used, while using human cells means xenotransplantation, which might need intensified immunosuppression. However, for macaques, as well as for other NHP species, iPS cell-derived CMs are available and would allow for an allogeneic approach (Stauske et al., 2020; Rodriguez-Polo and Behr, 2022). Still, in most translational studies discussed in this review (Tables 1, 2), human iPS cell-derived CMs were used for transplantation; only in two of the studies was the allogeneic transplantation approach utilized (Shiba et al., 2016; Kashiyama et al., 2019). As shown in Table 1, homogeneity within these studies is less stringent as in rodent studies, which is reflected in a wide age range (4–18 years) and in the weight of the used animals. Heart failure is most prevalent among patients over 60 years of age (Bozkurt et al., 2023). However, CM transplantation studies in rodents mainly used young animals; therefore, adult animals (as used in the studies displayed in Table 1) might reflect more of the human situation, even though only animals over 15 years of age would be considered older. Nevertheless, the consequences of cardiac aging and CM senescence (Anderson et al., 2019; Salerno et al., 2022) have not been discussed in the displayed NHP studies. In addition to the age differences, variations in body weight (3–14kg, Table 1) should be emphasized. Body weight correlates with heart weight (Stahl, 1965); therefore, differences in heart size should be considered when discussing cell dosage. Variances of up to 8 kg in body weight within the studies could

impact the calculation of sufficient cell quantities and thereby affect the effect size as well as the immune reaction and off-target effects. A general limitation in studies conducted in macaques is that almost exclusively male animals are used. The rational for this is that mainly male monkeys are available as young males have to be excluded from the breeding groups, while female animals are of utmost importance for the social structure of the breeding groups and therefore are rarely obtainable. It is, therefore, gratifying that female animals were included in more than one study. Although not specifically addressed in these studies, it is known from the field of cell transplantation that sex (mis)matches between the donor and recipient can affect the outcome (Kim et al., 2016; Ali et al., 2019). Therefore, when translating this to clinical trials, the sex of the donor versus recipient, in addition to the human leukocyte antigen (HLA) match, should be taken into account.

2.2 Methods to induce myocardial infarction

Several procedures have been established to induce myocardial infarction (MI) in animal models (Martin et al., 2022). In comparison to ablation methods (e.g., cryoinjury), direct interventions on coronary arteries, such as the left anterior descending coronary artery (LAD), are thought to be the more clinically relevant model, reflecting MI in patients. In general, two models are used in this context: total occlusion of a coronary vessel and ischemia/reperfusion (I/R) injury, which is only a timely occlusion of the coronary artery. The later reflects more of the clinical situation since in patients, revascularization is the first choice of treatment. However, iPS cell-derived CM-transplantation seeks more treatment in the chronic phase (development of or reversal of heart failure) after myocardial infarction than the acute phase; therefore, we do not discuss the two different models and their impact on inflammation, scarring, and remodeling in the review. The different approaches of infarct induction in biomedical research are described as follows: induction of vessel occlusion can be achieved either surgically in an open-chest approach (via lateral thoracotomy or sternotomy) or via interventional catheter approaches (percutaneous transluminal coronary angioplasty, PTCA), both of which were used in the studies discussed in this review. The open-chest approach allows for either I/R or permanent occlusion via ligation, a procedure that has been studied in NHP for nearly a hundred years (de Waart et al., 1936). The advantage of a surgical approach is the direct visualization of the coronary artery to identify the correct position of the ligature and have a visually controlled target area of infarction after vessel occlusion (Shin et al., 2021). However, the surgical exposure of the heart is an invasive, painful procedure that includes a serious risk of infection. Tissue damage, especially the pericardial incision, leads to inflammation and epicardial fibrosis and thereby complicating re-operation for CM application in the surgical approach. Therefore, another access possibility could be considered: transluminal access is used to generate ischemic events through balloon inflation. The deflation of the balloon after a specific time (up to 180 min in NHPs, Table 1) results in a reperfusion. The catheter-based I/R is a minimally invasive strategy that circumvents the open chest. However, the identification of the desired occlusion location is more challenging, and anticoagulant and antiarrhythmic therapy is needed (Camacho et al., 2016). Furthermore, equipment needed for the catheter-based approach, an angiography system, is not available in all animal facilities, while the surgical approach does not require a specific equipment setup. From the perspective of animal welfare, the catheter-based, minimally invasive access seems to be advantageous since it is associated with less tissue damage and therefore less painful. The Murry group used the catheter-based approach, starting with an ischemic time of 90 min of the distal LAD in their first NHP study (Chong et al., 2014). However, the duration and position were insufficient to induce substantial damage, and only a minimal decline in global myocardial function was described (Liu et al., 2018). Therefore, in the second study, they chose a more extended period of ischemia (180 min) and occluded the coronary artery more proximal (mid-LAD) (Liu et al., 2018). The results demonstrated larger, transmural infarct scars with a clear decline in global myocardial function. Surprisingly, the increase in ischemic time did not lead to increased trop-out of animals in the second published study. The latest study by Cheng et al. generated functional impairment after 90 min occlusion time of the mid-LAD. Since interventional revascularization (percutaneous coronary intervention, PCI) has become a standard procedure for hospitalized patients with acute MI, the I/R model closely resembles their history. Nevertheless, there are still up to 30% of MI patients where no timely reperfusion is achievable (Cohen et al., 2010; Gharacholou et al., 2010), which is better reflected by the permanent ligation model. A further clinically relevant aspect is that the reperfusion itself causes additional damage (I/R injury) through a complex array of immune responses (Dorweiler et al., 2007; Yellon and Hausenloy, 2007). The differences in the subsequent inflammation and remodeling processes caused by these two different MI induction methods and the time point of transplantation after MI could influence the engraftment of the iPS cell-derived CMs; however, this has not been part of the investigations in NHPs so far. The induction techniques of permanent ligation and the I/R approach model the acute change from normal perfusion to complete vessel occlusion, mimicking therefore thrombotic, embolic or vasospastic etiologies. However, these causes are less common in humans than ischemia due to slowly progressing coronary atherosclerosis and stenosis, which can then be exacerbated by acute thrombotic occlusion or plaque rupture (DeWood et al., 1980; Burke and Virmani, 2007; Herrington et al., 2016; Severino et al., 2020). Both the permanent occlusion and the reperfusion approach (Figure 2) are clinically relevant.

However, since the used animals are rather young and healthy, no additional cardiovascular risk factors or co-morbidities were involved, and the occlusion occured suddenly. This only partially reflects the patient's situation, and the results (especially functional improvement) need to be interpreted cautiously.

2.3 Cardiomyocyte delivery and engraftment

In addition to the variation in ischemia duration and the kind of approach, the CM delivery is a second important technical aspect

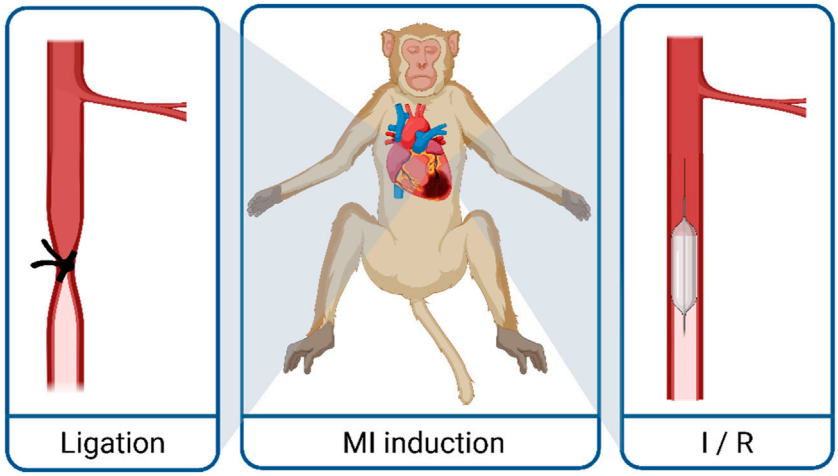

FIGURE 2
Techniques to generate myocardial infarction in macaques. MI, myocardial infarction; I/R, ischemia reperfusion.

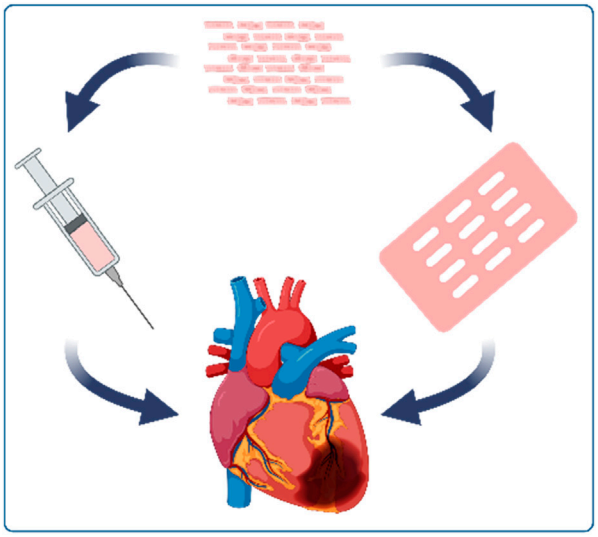

FIGURE 3
Main delivery approaches of cardiomyocyte (CM) transfer to the injured heart: intramyocardial CM injection and epicardial patch application.

that needs to be taken into account. The major goal of the CM transplantation is to implant an effective number of cells at the site of interest with a good integration and survival of the transplanted cells. When reviewing methods to introduce new CMs to the heart, two main delivery routes have been accomplished: transplantation via intramyocardial (or intra-scar) injection (as single-cell solution or small aggregates) and the epicardial application of preformed 3D-constructs (Figure 3).

Both approaches carry their advantages and drawbacks (Feric and Radisic, 2016; Kadota and Shiba, 2019). Although efficacy was repeatedly proven in small animal models for both delivery approaches, the CM injection strategy has been mainly tested in NHP models (Tables 1, 2). This is thought to be more convenient for patient application because it can be performed minimally invasively via a catheter-based transluminal approach and does not necessarily require an open-chest approach. The study of Kashiyama et al. is the only publication that reported epicardial CM delivery via cell sheets in NHPs. The other remuscularization studies realized in NHPs focused on CM injection (Chong et al., 2014; Shiba et al., 2016; Liu et al., 2018; Cheng et al., 2023; Gruh et al., 2024). A recent project tested additional CM delivery approaches in cynomolgus monkeys (Li et al., 2021). Li et al. compared intracoronary, intravenous, and intramyocardial application of CMs and concluded that among the tested delivery strategies, intramyocardial injection is the most efficient delivery route for clinical purposes.

The CM transplantation studies followed the hypothesis that functional recovery is based on repopulated force-generating CMs. This implies that a substantial remuscularization must be achieved to validate their therapeutic potential. As mentioned previously, sufficient immunosuppression is required to afford cell engraftment in the xeno- and allogeneic approach. Based on clinical organ transplant treatment, different combinations of immunosuppression drugs (Table 1) have been successfully applied in terms of CM survival. Graft size also depends on the input cell number (Querdel et al., 2021). The tested CM numbers per macaque heart ranged from 50 million to one billion cells via 4 to 15 injections per heart (Table 2).

Kashiyama et al. applied 14 million cells spread over four cardiac sheets. These publications reported the graft-related repopulation of CMs. Evaluation of the graft size was only performed in some macaque studies (Chong et al., 2014; Shiba et al., 2016; Liu et al., 2018) and exhibited that CM injection resulted in a remuscularization of up to 5% of the left ventricle, which is comparable with the achievements in small animal studies (Eschenhagen et al., 2022). However, most studies lack a quantification of cell mass and number at the end of the experiments (Table 2) to better investigate cell survival and the engraftment of different approaches. In further studies, the focus should be not only on safety and functional improvement but also

on cell survival, gain of myocardial mass, and coupling/engraftment of the cells in the host myocardium.

2.4 Cell sources

In addition to the delivery method, the cell source is an important aspect in terms of an adequate engraftment and potential side effects of different cell types. The cell-based field of cardiac regeneration tested already different cell sources. In addition to differentiated CMs, iPS cells have also been applied for transplantation in small animals. Beneficial effects were observed when iPS cells were delivered via injection and with a patch approach (Nelson et al., 2009; Dai et al., 2011). To reduce the teratogenic risk of iPS cells, cardiovascular progenitor cells (CVPCs) were also part of the investigations (Vicinanza et al., 2017; Wang et al., 2017; Monsanto et al., 2020). However, the only study which addressed CVPC in NHPs reported a lack of remuscularization (Zhu et al., 2018). Herein, we focus on the cell type of this review: the widely used stem cell-derived cardiomyocytes. The first CM transplantation study described in NHPs used human embryonic stem cell (hESC)-derived CMs (Chong et al., 2014). In order to overcome legal, political, and ethical concerns associated with human embryos, the field has evolved in the direction of human iPS cells as a basis for CM generation (Aboul-Soud et al., 2021). The best exogenously cell source to avoid immunological cell rejection would be individual patient-derived (=autologous) CMs. Currently, the autologous approach does not seem applicable for a broad clinical use. High costs, the time-consuming process of cell-line generation, and regulatory hurdles limit it since an individual cell line would be counted as ATMP (advanced therapy medicinal product) and therefore has to fulfill all safety and functionality requirements. From a clinical perspective, it is comprehensible that CMs of human origin were generated and tested for transplantation purposes. Most preclinical studies are based on the xenogenic background, where human cells were transplanted. Nevertheless, this might require more intense immunosuppression and does not reflect the clinical situation. However, as an equivalent to the clinical phase I trial, an allogeneic approach was used in two studies, where CMs derived from macaque iPS cells were used. Shiba and coworkers demonstrated that allogeneic major histocompatibility complex (MHC)-matched CM transplantation is feasible with immunosuppression, and the engrafted CM survived the observation period (12 weeks). The second study, which addressed the allogeneic approach via cardiac sheet application, described cell survival for both MHC-matched and mismatched recipients. Unfortunately, no more transplanted CMs were detectable in the group with the most extended follow-up period of 6 months (Kashiyama et al., 2019). Regardless of the cell origin (xeno- or allogeneic), the studies displayed that immunosuppression still seems unavoidable.

2.5 Study designs: timing of transplantation and follow-up

Previous studies in small animals mainly transplanted CMs in the early stage after injury and were analyzed after a short follow-up period (Zimmermann et al., 2006; Laflamme et al., 2007; Caspi et al., 2007; Shiba et al., 2012; Funakoshi et al., 2016; Weinberger et al., 2016; W. Zhu et al., 2018; Munarin et al., 2020; Sun et al., 2020; Jabbour et al., 2021; Querdel et al., 2021). In this setting, promising results were obtained: partial scar remuscularization resulted in functional improvement. For a more basic research approach, these proof-of-principal studies with early cell transplantation were sufficient to address the fundamental questions of cell survival and functional benefit after (sub-)acute myocardial infarction. However, since the widespread access to reperfusion therapy, more and more patients survive an acute MI event and develop heart failure over time (Heusch et al., 2014; Heusch and Gersh, 2017). The transplantation early after MI does not resemble well the most likely clinical application for these regenerative approaches (Eschenhagen et al., 2022). To narrow the gap to the clinical scenario of patients with advanced heart failure, transplantation was performed in the chronic stage after injury in selected rodent studies (Fernandes et al., 2010; Shiba et al., 2014; Riegler et al., 2015; von Bibra et al., 2022). Irrespective of the CM delivery route (injection and patch application), the outcomes were almost identical: transplantation is less efficient than that in the subacute injury models. Grafts were smaller, and no significant increase in functional parameters was observed. In the proof-of-concept studies performed in NHPs, where the goal should be to represent the potential human application as effectively as possible, it was surprising that, apart from one study (Cheng et al., 4 weeks), only the early injury (0 days and 2 weeks) was again the subject of investigation. This does not reflect the anticipated CM therapy as a last resort for patients with chronic ischemic heart failure (Kadota et al., 2020; Silver et al., 2021). To phrase it more provocatively, it is understandable that the subacute transplantation setting was used again because better results can be expected here. However, the contribution to narrowing the translational gap is debatable in this acute to subacute phase after MI. Inflammation, remodeling, and the development of heart failure are still ongoing and might influence engraftment, cell survival, and partly masks the beneficial effects of the transplanted CMs. In regard to investigating long-term survival of the transplanted CMs, some NHP studies included extended follow-up periods (Table 1). Animals treated with injected CMs were observed for up to 3 months, and cells survived with an efficient immunosuppression regimen. The transplantation of cardiac sheets was monitored for up to half a year, with the less encouraging observation of chronic rejection.

3 NHP study achievements and translational impediments

The preclinical investigations of cardiac remuscularization therapy advanced considerably since NHP models entered the validation process. Since 2014, several publications evaluated the transplantation of *in vitro*-generated CM in injured macaque hearts. The key benefit of these studies is undoubtedly the translational value due to the proximity to humans. Central achievements were gained in the clinically predictive, human-like NHP model. The *in vitro* generation of iPSC-derived CMs is at an advanced technological level (Lyra-Leite et al., 2022). Application in NHPs demonstrated that clinically scalable amounts of CMs with a high

purity can be produced and applied to the injured heart. Induction of myocardial infarction was created via permanent or transient LAD occlusion, mimicking the human's MI scenario and simulating closely clinical reality. Substantial damage of the heart with functional impairment was generated and therefore opened a therapeutic window. Sufficient immunosuppression regimen, in clinically relevant doses, enabled xeno- and allogeneic transplanted cells to survive over months. Safety was demonstrated over the post-transplant observation period, and no teratoma or abnormal cell growth has been reported.

To summarize it with a more global picture, CM transplantation resulted in a substantial remuscularization of the injured macaque hearts, and an amelioration of function was repeatedly demonstrated. These findings can be considered encouraging for the translational field and led to clinical translation. Now, more than five clinical trials using iPS cell-derived CMs in heart failure patients are ongoing (*ClinicalTrials.gov*).

However, some limitations should be discussed regarding the macaque model.

Limited availability of these animals and ethical and economic conflicts led to studies with small sample sizes (Table 1). This implicates a high standard deviation, with a limited statistical outcome in evaluating efficacy. Both induction methods of MI in the NHP models generated an acute-to-normal rather than an acute-to-chronic vessel occlusion, therefore lacking the ability to mimic the history of atherosclerosis and endothelial dysfunction that is frequently displayed in patients.

NHPs are often regarded as the ideal model of translation. In comparison to other large animal models (e.g., pigs), the macaque species are smaller in size. According to that, the heart has 1/10 of the weight of a human adult heart (Gandolfi et al., 2011; Chong and Murry, 2014). In particular, regarding dose-finding studies, the macaques allow only limited investigations. Calculations to determine an effective cell amount for human application should be carried out carefully (Eschenhagen et al., 2022).

To return to the original question: Is the CM transplantation approach ready for clinical application? No, because aside from the translational achievements ascertained in NHP models, relevant clinical impediments need to be discussed, addressed, and resolved first:

Since large animal models have been implemented in the preclinical investigation of cardiac remuscularization, engraftment arrhythmias (EA) were frequently reported (Chong et al., 2014; Shiba et al., 2016; Liu et al., 2018). These observations of post-transplant arrhythmias emphasise the importance of large animal models for preclinical validation, as these studies have additional value to the rodent results. EAs are discussed at the moment as one of the most concerning barrier toward translation (Eschenhagen et al., 2017). This ventricular tachycardia occurred transiently, mainly in the first weeks after CM transplantation. Hence, the immaturity of the implanted CMs seems reasonable to cause this focal automaticity. To suppress these potentially life-threatening EAs, pharmacological treatment has already been investigated in pigs (K. Nakamura et al., 2021). In addition, approaches to enhance CM maturation prior to *in vivo* application could tackle the issue (Karbassi and Murry, 2022).

The consensus in the research community that the allogeneic approach will be most likely applicable in the clinic harbors the immunological dilemma. Even if MHC-matched donors were selected for allogeneic transplantation, therapy with immunosuppressants is still necessary to avoid graft rejection (Shiba et al., 2016; Kashiyama et al., 2019). Further investigations in evaluating concentrations and ideal combinations are important due to the fact that the long-term treatment of gravely ill heart failure patients can result in severe side effects, and the immunosuppression itself could have an impact on the MI disease pathway (Ruiz and Kirk, 2015; Diehl et al., 2016; Demkes et al., 2021). A more elegant way of avoiding immune rejection has emerged with the generation of hypoimmunogenic cell lines (Deuse et al., 2019). The application of gene-edited CMs that can evade the immune system is a highly desirable alternative to immunocompromising agents (Lanza et al., 2019; Sung et al., 2023).

An additional issue is still the poor cell survival and the low engraftment rate (Robey et al., 2008). One approach to improve cell retention after injection has recently been demonstrated in cynomolgus monkeys. The co-transplantation of endothelial cells substantially enlarged graft size (Cheng et al., 2023). Cell survival can also be limited by the application route. Macaque studies mainly addressed the CM injection, where a major discussed drawback is the direct cell washout after injection (Chong and Murry, 2014; Martens et al., 2014). Patch approaches are often discussed as the delivery alternative to prevent a high cell loss after injection (Huang et al., 2020; Li et al., 2021; Yu et al., 2023). A cell survival comparison with patch-based CM application is, due to the sparse publication record, not possible in NHPs so far. To overcome the limitations of each delivery approach and to synergize their benefits, one stimulating idea would be to combine both strategies.

The so-called intramyocardial injection of CMs is frequently displayed in NHP studies. Nevertheless, the global idea is to remuscularize the damaged part (scar) of the heart and not to create hyperplasia in the viable myocardium. For most of the studies, the intramyocardial injection is indeed the correct term because the presented grafts are frequently surrounded by the vital myocardium. The neologistic term of intrascar injection would better reflect the aim of the approach, which is remuscularization, not hypermuscularization. Unfortunately, inadequate application to the infarct area was not only a limitation of the tiny hearts of small mammals, it was also evident or apparent in large animal NHP studies. In future projects, technical approaches that result in injecting the CMs primarily in the scar (and of course in the border zone) rather than generating additional myocardium in the viable zone should be addressed.

As mentioned previously, most of the NHP studies transplanted CMs in an early (sub-)acute stage of injury. Therefore, the translational question, of how successful will the engraftment be when targeting chronically injured hearts in patients, is still open. For future perspective, one idea to improve the transplantation success in the chronic setting could be to identify beneficial pathways present in the subacute injury. Identified targets could be included in the patch or injection medium or eventually used to pretreat the injured heart prior to transplantation. The chronically injured heart is more hostile for CM transplantation because of the absence of inflammatory cells and the stiff collagenous scar with a low vascular density (von Bibra et al., 2022). In other words, the

subacute setting could be more likely because of the ongoing remodeling process with inflammation and neoangiogenesis. Targets of these pathways could be used to improve the transplantation success in the clinically relevant chronic setting. For a clinical application, the long-term graft maintenance is essential. The only study that included a follow-up observation of 6 months reported chronic rejection. Longer follow-up studies are also needed to scrutinize the risk of tumor growth.

In spite of the advanced translational progress gained with the NHP studies, numerous demands remain and need further investigation. However, cardiac remuscularization is currently at an exciting stage; the intensive preclinical work has already led to the first clinical trials. According to ClinicalTrials.gov, more than five clinical trials are running at the moment to evaluate the therapeutic potential of CM transplantation. Even though the studies conducted in NHPs mainly investigated the CM injection, a variety of delivery strategies are approached in the clinical trials. The HEAL-CHF trial (NTC03763136) from China is set up to test the intramyocardial injection of CMs during coronary artery bypass grafting. In addition to the epicardial injection, the same group is testing an alternative access for intramyocardial injection. Via a catheter-based endocardial application, different CM doses are injected (NTC04982081). The German BioVAT-HF trial (NCT04396899) used engineered heart muscles as an epicardial patch approach. The collagen-based tissue contains, in addition to iPS cell-derived CMs, stromal cells. The Japanese LAPiS trial (NTC04645018) evaluated the safety of CM spheroid. In addition, a case report from Japan (#jRCT205319008) described recently the successful transplantation of CM-containing patches (Miyagawa et al., 2022). Fortunately, no adverse events (e.g., arrhythmias and tumor growth) were detected. However, immunosuppression was suspended 3 months after transplantation.

In summary, first steps toward clinical application are done in iPS cell-derived CM transplantation. However, these are all early clinical trials, with low patient numbers, and only a few centers participating in these trials. Therefore, larger clinical trials have to be performed before bringing this approach to a broad clinical application. The field, however, is, in our view, moving in the right direction, and late translation seems to be possible.

Author contributions

CB: writing–original draft. RH: writing–review and editing.

Funding

The authors declare that no financial support was received for the research, authorship, and/or publication of this article.

Acknowledgments

We acknowledge financial support by the Open Access Publication Fund of the University of Veterinary Medicine Hannover, Foundation. Illustrations in Figures 1–3 were created with biorender.com.

Conflict of interest

The authors declare that the research was conducted in the absence of any commercial or financial relationships that could be construed as a potential conflict of interest.

Publisher's note

References

Aboul-Soud, M. A. M., Alzahrani, A. J., and Mahmoud, A. (2021). Induced pluripotent stem cells (iPSCs)—roles in regenerative therapies, disease modelling and drug screening. *Cells* 10 (9), 2319. doi:10.3390/CELLS10092319

Ali, N., Ullah, H., Shaikh, M. U., and Adil, S. N. (2019). Outcome of donor and recipient sex match versus mismatch in stem cell transplant procedure. *Int. J. Hematol. Oncol.* 8 (4), IJH21. doi:10.2217/IJH-2019-0006

Anderson, R., Lagnado, A., Maggiorani, D., Walaszczyk, A., Dookun, E., Chapman, J., et al. (2019). Length-independent telomere damage drives post-mitotic cardiomyocyte senescence. *EMBO J.* 38 (5), e100492. doi:10.15252/embj.2018100492

Awad, M. A., Shah, A., and Griffith, B. P. (2022). Current status and outcomes in heart transplantation: a narrative review. *Rev. Cardiovasc. Med.* 23 (1), 11. doi:10.31083/J.RCM2301011

Azevedo, P. S., Polegato, B. F., Minicucci, M. F., Paiva, S. A. R., and Zornoff, L. A. M. (2016). Cardiac remodeling: concepts, clinical impact, pathophysiological mechanisms and pharmacologic treatment. *Arq. Bras. Cardiol.* 106 (1), 62–69. doi:10.5935/ABC.20160005

Bailey, L. L. (2009). The baboon in xenotransplant research. *Baboon Biomed. Res.*, 371–380. doi:10.1007/978-0-387-75991-3_19

Bozkurt, B., Ahmad, T., Alexander, K. M., Baker, W. L., Bosak, K., Breathett, K., et al. (2023). Heart failure epidemiology and outcomes statistics: a report of the heart failure society of America. *J. Cardiac Fail.* 29 (10), 1412–1451. doi:10.1016/J.CARDFAIL.2023.07.006

Burke, A. P., and Virmani, R. (2007). Pathophysiology of acute myocardial infarction. *Med. Clin. N. Am.* 91 (4), 553–572. doi:10.1016/J.MCNA.2007.03.005

Buss, D. D., Hyde, D. M., and Steffey, E. P. (1983). Coronary collateral development in the rhesus monkey (*Macaca mulatta*). *Basic Res. Cardiol.* 78 (5), 510–517. doi:10.1007/BF01906462

Camacho, P., Fan, H., Liu, Z., and He, J. Q. (2016). Large mammalian animal models of heart disease. *J. Cardiovasc. Dev. Dis.* 3 (4), 30. doi:10.3390/jcdd3040030

Caspi, O., Huber, I., Kehat, I., Habib, M., Arbel, G., Gepstein, A., et al. (2007). Transplantation of human embryonic stem cell-derived cardiomyocytes improves myocardial performance in infarcted rat hearts. *J. Am. Coll. Cardiol.* 50 (19), 1884–1893. doi:10.1016/J.JACC.2007.07.054

Chatfield, K., and Morton, D. (2018). *The use of non-human primates in research*, 81–90. doi:10.1007/978-3-319-64731-9_10

Cheng, Y. C., Hsieh, M. L., Lin, C. J., Chang, C. M. C., Huang, C. Y., Puntney, R., et al. (2023). Combined treatment of human induced pluripotent stem cell-derived cardiomyocytes and endothelial cells regenerate the infarcted heart in mice and non-human primates. *Circulation* 148 (18), 1395–1409. doi:10.1161/CIRCULATIONAHA.122.061736

Chong, J. J. H., and Murry, C. E. (2014). Cardiac regeneration using pluripotent stem cells—progression to large animal models. *Stem Cell. Res.* 13 (3), 654–665. doi:10.1016/J.SCR.2014.06.005

Chong, J. J. H., Yang, X., Don, C. W., Minami, E., Liu, Y. W., Weyers, J. J., et al. (2014). Human embryonic-stem-cell-derived cardiomyocytes regenerate non-human primate hearts. *Nature* 510 (7504), 273–277. doi:10.1038/NATURE13233

Cohen, M., Boiangiu, C., and Abidi, M. (2010). Therapy for ST-segment elevation myocardial infarction patients who present late or are ineligible for reperfusion therapy. *J. Am. Coll. Cardiol.* 55 (18), 1895–1906. doi:10.1016/J.JACC.2009.11.087

Dai, B., Huang, W., Xu, M., Millard, R. W., Gao, M. H., Hammond, H. K., et al. (2011). Reduced collagen deposition in infarcted myocardium facilitates induced pluripotent stem cell engraftment and angiomyogenesis for improvement of left ventricular function. *J. Am. Coll. Cardiol.* 58 (20), 2118–2127. doi:10.1016/j.jacc.2011.06.062

Demkes, E. J., Rijken, S., Szymanski, M. K., Hoefer, I. E., Sluijter, J. P. G., and de Jager, S. C. A. (2021). Requirements for proper immunosuppressive regimens to limit translational failure of cardiac cell therapy in preclinical large animal models. *J. Cardiovasc. Transl. Res.* 14 (1), 88–99. doi:10.1007/s12265-020-10035-2

Deuse, T., Hu, X., Gravina, A., Wang, D., Tediashvili, G., De, C., et al. (2019). Hypoimmunogenic derivatives of induced pluripotent stem cells evade immune rejection in fully immunocompetent allogeneic recipients. *Nat. Biotechnol.* 37 (3), 252–258. doi:10.1038/s41587-019-0016-3

de Waart, A., Storm, C. J., and Koumans, A. K. J. (1936). Ligation of the coronary arteries in Javanese monkeys: I. Introduction, general experimental results, especially the changes in the ventricular electrocardiogram. *Am. Heart J.* 11 (6), 676–704. doi:10.1016/S0002-8703(36)90495-7

DeWood, M. A., Spores, J., Notske, R., Mouser, L. T., Burroughs, R., Golden, M. S., et al. (1980). Prevalence of total coronary occlusion during the early hours of transmural myocardial infarction. *N. Engl. J. Med.* 303 (16), 897–902. doi:10.1056/NEJM198010163031601

Diehl, R., Ferrara, F., Müller, C., Dreyer, A. Y., McLeod, D. D., Fricke, S., et al. (2016). Immunosuppression for *in vivo* research: state-of-the-art protocols and experimental approaches. *Cell. Mol. Immunol.* 14 (2), 146–179. doi:10.1038/cmi.2016.39

Dixon, J. A., and Spinale, F. G. (2009). Large animal models of heart failure: a critical link in the translation of basic science to clinical practice. *Circ. Heart Fail.* 2 (3), 262–271. doi:10.1161/CIRCHEARTFAILURE.108.814459

Dorweiler, B., Pruefer, D., Andrasi, T. B., Maksan, S. M., Schmiedt, W., Neufang, A., et al. (2007). Ischemia-reperfusion injury: pathophysiology and clinical implications. *Eur. J. Trauma Emerg. Surg.* 33 (6), 600–612. doi:10.1007/s00068-007-7152-z

Eschenhagen, T., Bolli, R., Braun, T., Field, L. J., Fleischmann, B. K., Frisén, J., et al. (2017). Cardiomyocyte regeneration: a consensus statement. *Circulation* 136 (7), 680–686. doi:10.1161/CIRCULATIONAHA.117.029343

Eschenhagen, T., Ridders, K., and Weinberger, F. (2022). How to repair a broken heart with pluripotent stem cell-derived cardiomyocytes. *J. Mol. Cell. Cardiol.* 163, 106–117. doi:10.1016/j.yjmcc.2021.10.005

Feric, N. T., and Radisic, M. (2016). Strategies and challenges to myocardial replacement therapy. *Stem Cells Transl. Med.* 5 (4), 410–416. doi:10.5966/SCTM.2015-0288

Fernandes, S., Naumova, A. V., Zhu, W. Z., Laflamme, M. A., Gold, J., and Murry, C. E. (2010). Human embryonic stem cell-derived cardiomyocytes engraft but do not alter cardiac remodeling after chronic infarction in rats. *J. Mol. Cell. Cardiol.* 49 (6), 941–949. doi:10.1016/j.yjmcc.2010.09.008

Funakoshi, S., Miki, K., Takaki, T., Okubo, C., Hatani, T., Chonabayashi, K., et al. (2016). Enhanced engraftment, proliferation, and therapeutic potential in heart using optimized human iPSC-derived cardiomyocytes. *Sci. Rep.* 6, 19111. doi:10.1038/SREP19111

Gandolfi, F., Vanelli, A., Pennarossa, G., Rahaman, M., Acocella, F., and Brevini, T. A. L. (2011). Large animal models for cardiac stem cell therapies. *Theriogenology* 75 (8), 1416–1425. doi:10.1016/J.THERIOGENOLOGY.2011.01.026

Garbern, J. C., and Lee, R. T. (2022). Heart regeneration: 20 years of progress and renewed optimism. *Dev. Cell.* 57 (4), 424–439. doi:10.1016/J.DEVCEL.2022.01.012

Gharacholou, S. M., Alexander, K. P., Chen, A. Y., Wang, T. Y., Melloni, C., Gibler, W. B., et al. (2010). Implications and reasons for the lack of use of reperfusion therapy in patients with ST-segment elevation myocardial infarction: findings from the CRUSADE initiative. *Am. Heart J.* 159 (5), 757–763. doi:10.1016/J.AHJ.2010.02.009

Gruh, I., Martens, A., Cebotari, S., Schrod, A., Haase, A., Halloin, C., et al. (2023). *Cell therapy with human iPSC-derived cardiomyocyte aggregates leads to efficient engraftment and functional recovery after myocardial infarction in non-human primates*. doi:10.1101/2023.12.31.573775

Herrington, W., Lacey, B., Sherliker, P., Armitage, J., and Lewington, S. (2016). Epidemiology of atherosclerosis and the potential to reduce the global burden of atherothrombotic disease. *Circulation Res.* 118 (4), 535–546. doi:10.1161/CIRCRESAHA.115.307611

Heusch, G., and Gersh, B. J. (2017). The pathophysiology of acute myocardial infarction and strategies of protection beyond reperfusion: a continual challenge. *Eur. heart J.* 38 (11), 774–784. doi:10.1093/EURHEARTJ/EHW224

Heusch, G., Libby, P., Gersh, B., Yellon, D., Böhm, M., Lopaschuk, G., et al. (2014). Cardiovascular remodelling in coronary artery disease and heart failure. *Lancet* 383 (9932), 1933–1943. doi:10.1016/S0140-6736(14)60107-0

Home (2024). *ClinicalTrials.gov*. Available at: https://clinicaltrials.gov/ (Accessed: March 28, 2024).

Hotham, W. E., and Henson, F. M. D. (2020). The use of large animals to facilitate the process of MSC going from laboratory to patient—"bench to bedside". *Cell. Biol. Toxicol.* 36 (2), 103–114. doi:10.1007/S10565-020-09521-9

Huang, K., Ozpinar, E. W., Su, T., Tang, J., Shen, D., Qiao, L., et al. (2020). An off-the-shelf artificial cardiac patch improves cardiac repair after myocardial infarction in rats and pigs. *Sci. Transl. Med.* 12 (538), 9683. doi:10.1126/scitranslmed.aat9683

Jabbour, R. J., Owen, T. J., Pandey, P., Reinsch, M., Wang, B., King, O., et al. (2021). *In vivo* grafting of large engineered heart tissue patches for cardiac repair. *JCI Insight* 6 (15), e144068. doi:10.1172/JCI.INSIGHT.144068

Kadota, S., and Shiba, Y. (2019). Pluripotent stem cell-derived cardiomyocyte transplantation for heart disease treatment. *Curr. Cardiol. Rep.* 21 (8), 73–77. doi:10.1007/s11886-019-1171-3

Kadota, S., Tanaka, Y., and Shiba, Y. (2020). Heart regeneration using pluripotent stem cells. *J. Cardiol.* 76 (5), 459–463. doi:10.1016/j.jjcc.2020.03.013

Karbassi, E., and Murry, C. E. (2022). Flexing their muscles: maturation of stem cell-derived cardiomyocytes on elastomeric substrates to enhance cardiac repair. *Circulation* 145 (18), 1427–1430. doi:10.1161/CIRCULATIONAHA.122.059079

Kashiyama, N., Miyagawa, S., Fukushima, S., Kawamura, T., Kawamura, A., Yoshida, S., et al. (2019). MHC-Mismatched allotransplantation of induced pluripotent stem cell-derived cardiomyocyte sheets to improve cardiac function in a primate ischemic cardiomyopathy model. *Transplantation* 103 (8), 1582–1590. doi:10.1097/TP.0000000000002765

Kawamura, M., Miyagawa, S., Miki, K., Saito, A., Fukushima, S., Higuchi, T., et al. (2012). Feasibility, safety, and therapeutic efficacy of human induced pluripotent stem cell-derived cardiomyocyte sheets in a porcine ischemic cardiomyopathy model. *Circulation* 126 (11 Suppl. 1), S29–S37. doi:10.1161/CIRCULATIONAHA.111.084343

Khan, M. A., Hashim, M. J., Mustafa, H., Baniyas, M. Y., Al Suwaidi, S. K. B. M., AlKatheeri, R., et al. (2020). Global epidemiology of ischemic heart disease: results from the global burden of disease study. *Cureus* 12 (7), e9349. doi:10.7759/cureus.9349

Kim, H. T., Zhang, M. J., Woolfrey, A. E., St Martin, A., Chen, J., Saber, W., et al. (2016). Donor and recipient sex in allogeneic stem cell transplantation: what really matters. *Haematologica* 101 (10), 1260–1266. doi:10.3324/HAEMATOL.2016.147645

Laflamme, M. A., Chen, K. Y., Naumova, A. V., Muskheli, V., Fugate, J. A., Dupras, S. K., et al. (2007). Cardiomyocytes derived from human embryonic stem cells in pro-survival factors enhance function of infarcted rat hearts. *Nat. Biotechnol.* 25 (9), 1015–1024. doi:10.1038/nbt1327

Längin, M., Mayr, T., Reichart, B., Michel, S., Buchholz, S., Guethoff, S., et al. (2018). Consistent success in life-supporting porcine cardiac xenotransplantation. *Nature* 564 (7736), 430–433. doi:10.1038/S41586-018-0765-Z

Lanza, R., Russell, D. W., and Nagy, A. (2019). Engineering universal cells that evade immune detection. *Nat. Rev. Immunol.* 19 (12), 723–733. doi:10.1038/s41577-019-0200-1

Lelovas, P. P., Kostomitsopoulos, N. G., and Xanthos, T. T. (2014). A comparative anatomic and physiologic overview of the porcine heart. *J. Am. Assoc. Lab. Animal Sci.* 53 (5), 432–438.

Li, H., Wang, T., Feng, Y. Y., Sun, K., Huang, G. R., Cao, Y. L., et al. (2023). Optimal transplantation strategy using human induced pluripotent stem cell-derived cardiomyocytes for acute myocardial infarction in nonhuman primates. *MedComm* 4 (3), e289. doi:10.1002/MCO2.289

Li, J., Hu, S., Zhu, D., Huang, K., Mei, X., López de Juan Abad, B., et al. (2021). All roads lead to Rome (the heart): cell retention and outcomes from various delivery routes of cell therapy products to the heart. *J. Am. Heart Assoc.* 10 (8), e020402. doi:10.1161/JAHA.120.020402

Liu, Y. W., Chen, B., Yang, X., Fugate, J. A., Kalucki, F. A., Futakuchi-Tsuchida, A., et al. (2018). Human embryonic stem cell-derived cardiomyocytes restore function in infarcted hearts of non-human primates. *Nat. Biotechnol.* 36 (7), 597–605. doi:10.1038/nbt.4162

Lyra-Leite, D. M., Gutiérrez-Gutiérrez, Ó., Wang, M., Zhou, Y., Cyganek, L., and Burridge, P. W. (2022). A review of protocols for human iPSC culture, cardiac differentiation, subtype-specification, maturation, and direct reprogramming. *Star. Protoc.* 3 (3), 101560. doi:10.1016/J.XPRO.2022.101560

Martens, A., Rojas, S. V., Baraki, H., Rathert, C., Schecker, N., Zweigerdt, R., et al. (2014). Substantial early loss of induced pluripotent stem cells following transplantation in myocardial infarction. *Artif. Organs* 38 (11), 978–984. doi:10.1111/AOR.12268

Martin, T. P., MacDonald, E. A., Elbassioni, A. A. M., O'Toole, D., Zaeri, A. A. I., Nicklin, S. A., et al. (2022). Preclinical models of myocardial infarction: from mechanism to translation. *Br. J. Pharmacol.* 179 (5), 770–791. doi:10.1111/BPH.15595

Martínez-Falguera, D., Iborra-Egea, O., and Gálvez-Montón, C. (2021). iPSC therapy for myocardial infarction in large animal models: land of hope and dreams. *Biomedicines* 9 (12), 1836. doi:10.3390/BIOMEDICINES9121836

Miyagawa, S., Kainuma, S., Kawamura, T., Suzuki, K., Ito, Y., Iseoka, H., et al. (2022). Case report: transplantation of human induced pluripotent stem cell-derived

cardiomyocyte patches for ischemic cardiomyopathy. *Front. Cardiovasc. Med.* 9, 950829. doi:10.3389/fcvm.2022.950829

Monsanto, M. M., Wang, B. J., Ehrenberg, Z. R., Echeagaray, O., White, K. S., Alvarez, R., et al. (2020). Enhancing myocardial repair with CardioClusters. *Nat. Commun.* 11 (1), 3955. doi:10.1038/S41467-020-17742-Z

Munarin, F., Kant, R. J., Rupert, C. E., Khoo, A., and Coulombe, K. L. K. (2020). Engineered human myocardium with local release of angiogenic proteins improves vascularization and cardiac function in injured rat hearts. *Biomaterials* 251, 120033. doi:10.1016/J.BIOMATERIALS.2020.120033

Nakamura, K., Neidig, L. E., Yang, X., Weber, G. J., El-Nachef, D., Tsuchida, H., et al. (2021). Pharmacologic therapy for engraftment arrhythmia induced by transplantation of human cardiomyocytes. *Stem Cell. Rep.* 16, 2473–2487. doi:10.1016/J.STEMCR.2021.08.005

Nakamura, T., Fujiwara, K., Saitou, M., and Tsukiyama, T. (2021). Non-human primates as a model for human development. *Stem Cell. Rep.* 16 (5), 1093–1103. doi:10.1016/j.stemcr.2021.03.021

Nelson, T. J., Martinez-Fernandez, A., Yamada, S., Perez-Terzic, C., Ikeda, Y., and Terzic, A. (2009). Repair of acute myocardial infarction by human stemness factors induced pluripotent stem cells. *Circulation* 120 (5), 408–416. doi:10.1161/CIRCULATIONAHA.109.865154

Plews, J. R., Gu, M., Longaker, M. T., and Wu, J. C. (2012). Large animal induced pluripotent stem cells as pre-clinical models for studying human disease. *J. Cell. Mol. Med.* 16 (6), 1196–1202. doi:10.1111/J.1582-4934.2012.01521.X

Querdel, E., Reinsch, M., Castro, L., Köse, D., Bähr, A., Reich, S., et al. (2021). Human engineered heart tissue patches remuscularize the injured heart in a dose-dependent manner. *Circulation* 143, 1991–2006. doi:10.1161/CIRCULATIONAHA.120.047904

Riegler, J., Tiburcy, M., Ebert, A., Tzatzalos, E., Raaz, U., Abilez, O. J., et al. (2015). Human engineered heart muscles engraft and survive long term in a rodent myocardial infarction model. *Circulation Res.* 117 (8), 720–730. doi:10.1161/CIRCRESAHA.115.306985

Robey, T. E., Saiget, M. K., Reinecke, H., and Murry, C. E. (2008). Systems approaches to preventing transplanted cell death in cardiac repair. *J. Mol. Cell. Cardiol.* 45 (4), 567–581. doi:10.1016/J.YJMCC.2008.03.009

Rodriguez-Polo, I., and Behr, R. (2022). Non-human primate pluripotent stem cells for the preclinical testing of regenerative therapies. *Neural Regen. Res.* 17 (9), 1867–1874. doi:10.4103/1673-5374.335689

Romagnuolo, R., Masoudpour, H., Porta-Sánchez, A., Qiang, B., Barry, J., Laskary, A., et al. (2019). Human embryonic stem cell-derived cardiomyocytes regenerate the infarcted pig heart but induce ventricular tachyarrhythmias. *Stem Cell. Rep.* 12 (5), 967–981. doi:10.1016/J.STEMCR.2019.04.005

Ruiz, R., and Kirk, A. D. (2015). Long-term toxicity of immunosuppressive therapy. *Transplant. Liver*, 1354–1363. doi:10.1016/B978-1-4557-0268-8.00097-X

Salerno, N., Marino, F., Scalise, M., Salerno, L., Molinaro, C., Filardo, A., et al. (2022). Pharmacological clearance of senescent cells improves cardiac remodeling and function after myocardial infarction in female aged mice. *Mech. Ageing Dev.* 208, 111740. doi:10.1016/J.MAD.2022.111740

Severino, P., D'Amato, A., Pucci, M., Infusino, F., Adamo, F., Birtolo, L. I., et al. (2020). Ischemic heart disease pathophysiology paradigms overview: from plaque activation to microvascular dysfunction. *Int. J. Mol. Sci.* 21 (21), 8118. doi:10.3390/IJMS21218118

Shiba, Y., Fernandes, S., Zhu, W. Z., Filice, D., Muskheli, V., Kim, J., et al. (2012). Human ES-cell-derived cardiomyocytes electrically couple and suppress arrhythmias in injured hearts. *Nature* 489 (7415), 322–325. doi:10.1038/nature11317

Shiba, Y., Filice, D., Fernandes, S., Minami, E., Dupras, S. K., Biber, B. V., et al. (2014). Electrical integration of human embryonic stem cell-derived cardiomyocytes in a Guinea pig chronic infarct model. *J. Cardiovasc. Pharmacol. Ther.* 19 (4), 368–381. doi:10.1177/1074248413520344

Shiba, Y., Gomibuchi, T., Seto, T., Wada, Y., Ichimura, H., Tanaka, Y., et al. (2016). Allogeneic transplantation of iPS cell-derived cardiomyocytes regenerates primate hearts. *Nature* 538 (7625), 388–391. doi:10.1038/nature19815

Shin, H. S., Shin, H. H., and Shudo, Y. (2021). Current status and limitations of myocardial infarction large animal models in cardiovascular translational research. *Front. Bioeng. Biotechnol.* 9, 673683. doi:10.3389/FBIOE.2021.673683

Silva, M. O. M., Armada, J. L. A. D., Verona, C. E. S., Heliodoro, G., and Nogueira, D. M. (2017). Cytogenetics and molecular genetic analysis of chimerism in marmosets (*Callithrix*: primates). *An. Acad. Bras. Ciências* 89 (4), 2793–2804. doi:10.1590/0001-3765201720170484

Silver, S. E., Barrs, R. W., and Mei, Y. (2021). Transplantation of human pluripotent stem cell-derived cardiomyocytes for cardiac regenerative therapy. *Front. Cardiovasc. Med.* 8, 707890. doi:10.3389/fcvm.2021.707890

Stahl, W. R. (1965). Organ weights in primates and other mammals. *Science* 150 (699), 1039–1042. doi:10.1126/SCIENCE.150.3699.1039

Stauske, M., Rodriguez Polo, I., Haas, W., Knorr, D. Y., Borchert, T., Streckfuss-Bömeke, K., et al. (2020). Non-human primate iPSC generation, cultivation, and cardiac differentiation under chemically defined conditions. *Cells* 9 (6), 1349. doi:10.3390/CELLS9061349

Sun, X., Wu, J., Qiang, B., Romagnuolo, R., Gagliardi, M., Keller, G., et al. (2020). Transplanted microvessels improve pluripotent stem cell-derived cardiomyocyte engraftment and cardiac function after infarction in rats. *Sci. Transl. Med.* 12 (562), eaax2992. doi:10.1126/SCITRANSLMED.AAX2992

Sung, T. C., Maitiruze, K., Pan, J., Gong, J., Bai, Y., Pan, X., et al. (2023). Universal and hypoimmunogenic pluripotent stem cells for clinical usage. *Prog. Mol. Biol. Transl. Sci.* 199, 271–296. doi:10.1016/BS.PMBTS.2023.02.014

Takahashi, K., and Yamanaka, S. (2006). Induction of pluripotent stem cells from mouse embryonic and adult fibroblast cultures by defined factors. *Cell.* 126 (4), 663–676. doi:10.1016/j.cell.2006.07.024

Vicinanza, C., Aquila, I., Scalise, M., Cristiano, F., Marino, F., Cianflone, E., et al. (2017). Adult cardiac stem cells are multipotent and robustly myogenic: c-kit expression is necessary but not sufficient for their identification. *Cell. death Differ.* 24 (12), 2101–2116. doi:10.1038/CDD.2017.130

von Bibra, C., Shibamiya, A., Geertz, B., Querdel, E., Köhne, M., Stüdemann, T., et al. (2022). Human engineered heart tissue transplantation in a Guinea pig chronic injury model. *J. Mol. Cell. Cardiol.* 166, 1–10. doi:10.1016/j.yjmcc.2022.01.007

Wang, L., Meier, E. M., Tian, S., Lei, I., Liu, L., Xian, S., et al. (2017). Transplantation of Isl1+ cardiac progenitor cells in small intestinal submucosa improves infarcted heart function. *Stem Cell. Res. Ther.* 8 (1), 230. doi:10.1186/S13287-017-0675-2

Weinberger, F., Breckwoldt, K., Pecha, S., Kelly, A., Geertz, B., Starbatty, J., et al. (2016). Cardiac repair in Guinea pigs with human engineered heart tissue from induced pluripotent stem cells. *Sci. Transl. Med.* 8 (363), 363ra148. doi:10.1126/scitranslmed.aaf8781

Weinberger, F., and Eschenhagen, T. (2021). Cardiac regeneration: new hope for an Old dream. *Annu. Rev. Physiology* 83 (1), 59–81. doi:10.1146/annurev-physiol-031120-103629

Yellon, D. M., and Hausenloy, D. J. (2007). Myocardial reperfusion injury. *Injury* 357 (11), 1121–1135. doi:10.1056/NEJMRA071667

Yu, J., Vodyanik, M. A., Smuga-Otto, K., Antosiewicz-Bourget, J., Frane, J. L., Tian, S., et al. (2007). Induced pluripotent stem cell lines derived from human somatic cells. *Science* 318 (5858), 1917–1920. doi:10.1126/science.1151526

Yu, Y., Tham, S. K., Roslan, F. F., Shaharuddin, B., Yong, Y. K., Guo, Z., et al. (2023). Large animal models for cardiac remuscularization studies: a methodological review. *Front. Cardiovasc. Med.* 10, 1011880. doi:10.3389/FCVM.2023.1011880

Zhu, K., Wu, Q., Ni, C., Zhang, P., Zhong, Z., Wu, Y., et al. (2018). Lack of remuscularization following transplantation of human embryonic stem cell-derived cardiovascular progenitor cells in infarcted nonhuman primates. *Circ. Res.* 122 (7), 958–969. doi:10.1161/CIRCRESAHA.117.311578

Zhu, W., Zhao, M., Mattapally, S., Chen, S., and Zhang, J. (2018). CCND2 overexpression enhances the regenerative potency of human induced pluripotent stem cell-derived cardiomyocytes: remuscularization of injured ventricle. *Circulation Res.* 122 (1), 88–96. doi:10.1161/CIRCRESAHA.117.311504

Zimmermann, W. H. (2017). Translating myocardial remuscularization. *Circulation Res.* 120 (2), 278–281. doi:10.1161/CIRCRESAHA.116.310194

Zimmermann, W.-H., Melnychenko, I., Wasmeier, G., Didié, M., Naito, H., Nixdorff, U., et al. (2006). Engineered heart tissue grafts improve systolic and diastolic function in infarcted rat hearts. *Nat. Med.* 12 (4), 452–458. doi:10.1038/nm1394

frontiers | Frontiers in Pharmacology

TYPE Original Research
PUBLISHED 20 June 2024
DOI 10.3389/fphar.2024.1411822

OPEN ACCESS

EDITED BY
Felix Wiedmann,
Heidelberg University Hospital, Germany

REVIEWED BY
Jordi Heijman,
Medical University of Graz, Austria
Jan Sebastian Schulte,
University of Münster, Germany

*CORRESPONDENCE
Simon Lebek,
Simon.Lebek@ukr.de
Stefan Wagner,
Stefan.Wagner@ukr.de

†These authors have contributed equally to this work and share last authorship

RECEIVED 03 April 2024
ACCEPTED 16 May 2024
PUBLISHED 20 June 2024

CITATION
Hegner P, Ofner F, Schaner B, Gugg M, Trum M, Lauerer A-M, Maier LS, Arzt M, Lebek S and Wagner S (2024), CaMKIIδ-dependent dysregulation of atrial Na^+ homeostasis promotes pro-arrhythmic activity in an obstructive sleep apnea mouse model. *Front. Pharmacol.* 15:1411822. doi: 10.3389/fphar.2024.1411822

CaMKIIδ-dependent dysregulation of atrial Na^+ homeostasis promotes pro-arrhythmic activity in an obstructive sleep apnea mouse model

Philipp Hegner[1], Florian Ofner[1], Benedikt Schaner[1,2], Mathias Gugg[1], Maximilian Trum[1], Anna-Maria Lauerer[1], Lars Siegfried Maier[1], Michael Arzt[1], Simon Lebek[1*†] and Stefan Wagner[1*†]

[1]Department of Internal Medicine II, University Hospital Regensburg, Regensburg, Germany, [2]Department of Neurology and Clinical Neurophysiology, University Hospital Augsburg, Augsburg, Germany

Background: Obstructive sleep apnea (OSA) has been linked to various pathologies, including arrhythmias such as atrial fibrillation. Specific treatment options for OSA are mainly limited to symptomatic approaches. We previously showed that increased production of reactive oxygen species (ROS) stimulates late sodium current through the voltage-dependent Na^+ channels via Ca^{2+}/calmodulin-dependent protein kinase IIδ (CaMKIIδ), thereby increasing the propensity for arrhythmias. However, the impact on atrial intracellular Na^+ homeostasis has never been demonstrated. Moreover, the patients often exhibit a broad range of comorbidities, making it difficult to ascertain the effects of OSA alone.

Objective: We analyzed the effects of OSA on ROS production, cytosolic Na^+ level, and rate of spontaneous arrhythmia in atrial cardiomyocytes isolated from an OSA mouse model free from comorbidities.

Methods: OSA was induced in C57BL/6 wild-type and CaMKIIδ-knockout mice by polytetrafluorethylene (PTFE) injection into the tongue. After 8 weeks, their atrial cardiomyocytes were analyzed for cytosolic and mitochondrial ROS production via laser-scanning confocal microscopy. Quantifications of the cytosolic Na^+ concentration and arrhythmia were performed by epifluorescence microscopy.

Results: PTFE treatment resulted in increased cytosolic and mitochondrial ROS production. Importantly, the cytosolic Na^+ concentration was dramatically increased at various stimulation frequencies in the PTFE-treated mice, while the CaMKIIδ-knockout mice were protected.

Accordingly, the rate of spontaneous Ca^{2+} release events increased in the wild-type PTFE mice while being impeded in the CaMKIIδ-knockout mice.

Conclusion: Atrial Na^+ concentration and propensity for spontaneous Ca^{2+} release events were higher in an OSA mouse model in a CaMKIIδ-dependent manner, which could have therapeutic implications.

KEYWORDS

sleep-disordered breathing, reactive oxygen species, CaMKIIδ, Na^+ homeostasis, cardiac arrhythmias, obstructive sleep apnea

1 Introduction

Over the past few decades, sleep-disordered breathing (SDB) has emerged as a highly prevalent disease that currently affects about one billion patients worldwide (Benjafield et al., 2019). SDB is frequently associated with various cardiovascular disorders, such as hypertension (Pengo et al., 2020), heart failure with reduced or preserved ejection fractions (HFrEF/HFpEF) (Arzt et al., 2016; Lebek et al., 2021; Wester et al., 2023; Hegner et al., 2024), and arrhythmias like atrial fibrillation (Gami et al., 2004; Hegner et al., 2021a; Hegner et al., 2021b; Mehra et al., 2022), which may lead to subsequent strokes (Arzt et al., 2005). The interactions between SDB and these cardiovascular disorders can substantially contribute to patient morbidity and mortality while also posing economic challenges (Gami et al., 2004; Arzt et al., 2005; Arzt et al., 2016; Benjafield et al., 2019; Pengo et al., 2020; Lebek et al., 2021; Mehra et al., 2022; Wester et al., 2023). The current therapeutic strategies for SDB are mainly based on lifestyle interventions (e.g., weight loss, reduced alcohol intake, sports, and exercise) and continuous positive airway pressure (CPAP) therapy (Aurora et al., 2012; Randerath et al., 2017; Patil et al., 2019). However, patient compliance with these measures are often quite low, and adaptive servo-ventilation therapy has even been shown to increase mortality in HFrEF patients with central sleep apnea (Cowie et al., 2015; McEvoy et al., 2016). Thus, new and advanced therapeutic strategies are urgently needed for patients with SDB, which in turn requires detailed understanding of the pathological mechanisms involved.

We previously found increased production levels of reactive oxygen species (ROS) in human atrial biopsies of patients with SDB (Lebek et al., 2020b). This increase was shown to result in increased Ca^{2+}/calmodulin-dependent protein kinase II (CaMKII) activation and enhanced CaMKII-dependent late Na^+ current in the biopsies of patients with SDB (Lebek et al., 2020b; Lebek et al., 2022). Notably, the enhanced late Na^+ current is an important trigger for early afterdepolarizations (EADs) and subsequent arrhythmias (Wagner et al., 2006; Sossalla et al., 2010; Glynn et al., 2015; Lebek et al., 2020b; Lebek et al., 2022). Indeed, we demonstrated an increased frequency of multicellular arrhythmias in the isolated trabeculae of patients with SDB that could be blocked with CaMKII inhibition as well as late Na^+ current inhibition (Lebek et al., 2020b; Lebek et al., 2022). However, these studies were limited by patient heterogeneity and their various comorbidities that impacted myocardial Na^+ homeostasis (Lebek et al., 2020b; Lebek et al., 2022). It is also unclear whether myocardial Na^+ concentration is actually affected by the altered Na^+ currents in SDB. Recently, we demonstrated for the first time that intracellular Na^+ entry and Na^+ concentration were higher in the atrial myocytes of patients with heart failure and preserved ejection fraction—conditions in which SDB is very common (Trum et al., 2024).

Therefore, we developed a mouse model of obstructive sleep apnea (OSA) by injecting polytetrafluorethylene (PTFE) into the murine tongue (Lebek et al., 2020a; Hegner et al., 2023); these mice developed diastolic and mild systolic left-ventricular dysfunctions after 8 weeks (Lebek et al., 2020a; Hegner et al., 2023). Importantly, this approach allows analysis of OSA mice without the confounding comorbidities that are frequently exhibited by patients. PTFE is an inert substance that permanently increases the murine tongue volume, thereby leading to increased frequency of apneas, inspiratory flow limitations (hypopneas), and subsequent hypoxemia (Lebek et al., 2020a; Hegner et al., 2023). Notably, these OSA events occur spontaneously in PTFE-injected mice and preferentially during the murine sleeping period, making this mouse model a suitable tool for investigating OSA-dependent effects in the absence of any potentially confounding comorbidities (Lebek et al., 2020a; Hegner et al., 2023). The objective of the current work was to explore whether atrial ROS production increased in the OSA mice that could subsequently lead to CaMKIIδ-dependent pro-arrhythmic dysregulation of atrial Na^+ homeostasis.

2 Materials and methods

All experiments involving mice were in compliance with the directive 2010/63/EU of the European Parliament, Guide for the Care and Use of Laboratory Animals published by the US National Institutes of Health (NIH Publication No. 85–23, revised 1985), and local institutional guidelines. The government of Unterfranken, Bavaria, Germany also approved the animal protocol for this study (protocol number: 55.2-2532-2-512).

2.1 OSA induction by PTFE injection

OSA was induced in the study mice as described previously (Lebek et al., 2020a; Hegner et al., 2023). CaMKIIδ knockout ($^{-/-}$) and C57BL/6 wild-type mice were randomly assigned to either the control (CTRL) or OSA induction by PTFE injection (PTFE) groups (Figure 1). The PTFE (35 µm particle size, Sigma-Aldrich) was injected into the tongues of the male mice at the age of 8–12 weeks (Lebek et al., 2020a). For optimal analgesia, the mice were treated with buprenorphine (0.1 mg/kg bodyweight intraperitoneal) 1 h before PTFE injection. Anesthesia was

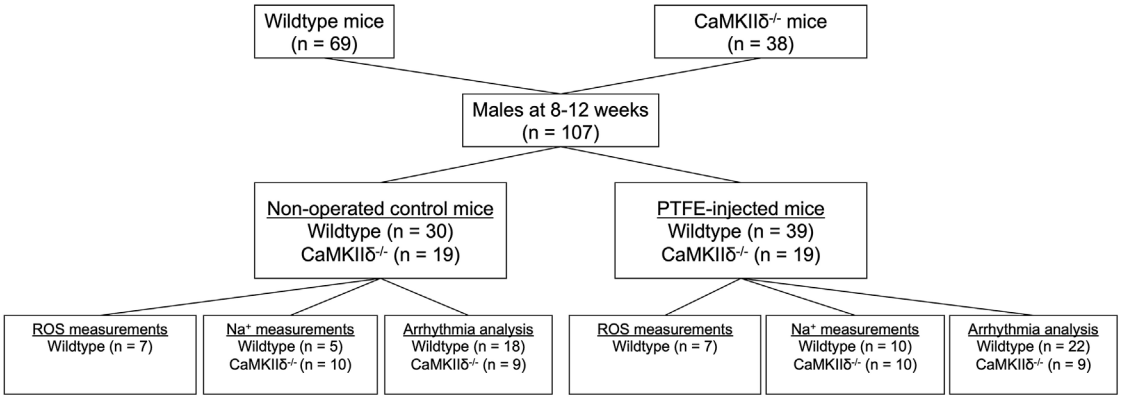

FIGURE 1
Experimental study flowchart.

established using intraperitoneal injections of fentanyl (0.05 mg/kg bodyweight), medetomidine (0.5 mg/kg), and midazolam (5 mg/kg). Thereafter, the mice were placed on a heating plate in the supine position. The anesthesia was continuously monitored by recording the respiration and ECG, and the body temperature was monitored using a rectal probe. In total, 100 µL of diluted PTFE (50% w/v in glycerol, Sigma-Aldrich) was injected into multiple sites at the base of the tongue using a 27-gauge cannula. Ultrasound imaging was used to confirm successful PTFE injection into the tongue (Vevo3100 system, VisualSonics). Once the procedure was completed, the anesthesia was reversed using intraperitoneal injections of atipamezole (2.5 mg/kg), flumazenil (0.5 mg/kg), and buprenorphine (0.1 mg/kg bodyweight). The surgeries were performed by an experienced investigator who was blinded to the genotype of the mice. To reduce the stress on the animals, we refrained from revalidating the OSA severity resulting from PTFE injection as this was previously investigated in detail (Lebek et al., 2020a).

2.2 Isolation of atrial cardiomyocytes

The mouse atrial cardiomyocytes were isolated as described previously (Hegner et al., 2023). In brief, the explanted hearts were mounted on a Langendorff perfusion apparatus and retrogradely perfused with 113 mmol/L of NaCl, 4.7 mmol/L of KCl, 0.6 mmol/L of KH_2PO_4, 0.6 mmol/L of $Na_2HPO_4 \times 2$ mmol/L of H_2O, 1.2 mmol/L of $MgSO_4 \times 7$ mmol/L of H_2O, 12 mmol/L of $NaHCO_3$, 10 mmol/L of $KHCO_3$, 10 mmol/L of HEPES, 30 mmol/L of taurine, 10 mmol/L of 2,3-butanedione monoxime, and 5.5 mmol/L of glucose for 4 min at 37°C (pH 7.4). Next, trypsin 0.6%, 7.5 mg/mL of liberase TM (Roche), and 0.125 mmol/L of $CaCl_2$ were added while maintaining perfusion until the heart became flaccid. Then, the murine atrium was collected in a perfusion buffer supplemented with 5% bovine calf serum. The tissue was sliced into small pieces and disintegrated by pipetting. Stepwise Ca^{2+} reintroduction was then performed by increasing $[Ca^{2+}]$ from 0.1 to 1.0 mmol/L. Owing to the limited number of atrial cardiomyocytes obtained from the cell isolation, only one of the following methods could be performed per subject.

2.3 Measurements of atrial ROS production

Isolated atrial cardiomyocytes were plated on laminin-coated recording chambers and loaded with either 5 µmol/L of CellRox™ Orange (Thermo Fisher Scientific) or 5 µmol/L of MitoSox™ Red (Thermo Fisher Scientific) in the presence of 0.04% (w/v) pluronic acid (Invitrogen; 15 min incubation at 37°C). The chambers were then placed on a laser-scanning confocal microscope (Zeiss LSM 700), and measurements were performed in Tyrode's solution containing 140 mmol/L of NaCl, 4 mmol/L of KCl, 5 mmol/L of HEPES, 1 mmol/L of $MgCl_2$, 10 mmol/L of glucose, and 1 mmol/L of $CaCl_2$ (pH 7.4 at room temperature with NaOH). The frame scans (CellRox™ Orange: 555 nm excitation, LP 560 nm emission; MitoSox™ Red: 488 nm excitation, LP 490 nm emission) were acquired once every minute for 10 min upon electrical field stimulation (1 Hz). The CellRox™ Orange and MitoSox™ Red fluorescence (F) values were then normalized with respect to the background fluorescence (F/F_0). The slope of increase in F/F_0 over time was used as the measure of cellular (CellRox™ Orange) and mitochondrial (MitoSox™ Red) ROS productions.

2.4 Epifluorescence microscopy

Intracellular Na^+ was determined by epifluorescence microscopy using the Na^+-sensitive sodium-binding benzofuran isophthalate-AM (SBFI-AM) dye (Thermo Fisher Scientific). The isolated atrial cardiomyocytes were plated on laminin-coated measurement chambers and loaded with 10 µmol/L of SBFI-AM for 90 min at room temperature according to manufacturer instructions. The loaded chambers were then placed on the stage of an inverted microscope (Nikon Eclipse TE2000-U) and superfused with Tyrode's solution containing 140 mmol/L of NaCl, 4 mmol/L of KCl, 5 mmol/L of HEPES, 1 mmol/L of $MgCl_2$, 10 mmol/L of glucose, and 1 mmol/L of $CaCl_2$ (pH 7.4 at 37°C with NaOH). Regular electrical stimulation was then performed by field stimulation (1, 2, and 4 Hz with 20 V for 4 ms) in a sequential manner for 5 min per frequency. The emissions were obtained using a fluorescence detection system (IonOptix), and the SBFI fluorescence emission ratio was measured by alternating

excitations at 340 nm and 380 nm. Then, steady-state measurements averaged over 10 s with ongoing stimulation were analyzed. For some experiments, calibration of the $F_{340\ nm/380\ nm}$ fluorescence ratio for fixed Na^+ concentrations (0, 10, and 20 mmol/L) was performed. To achieve this, a K^+-free solution containing 30 mmol/L of NaCl, 115 mmol/L of Na-gluconate, 10 mmol/L of HEPES, 2 mmol/L of EGTA, and 10 mmol/L of glucose (pH 7.2 at 37°C with TRIS) was mixed with an Na^+-free solution containing 30 mmol/L of KCl, 115 mmol/L of K-gluconate, 10 mmol/L of HEPES, 2 mmol/L of EGTA, and 10 mmol/L of glucose (pH 7.2 at 37°C with TRIS) in an appropriate proportion to achieve the desired Na^+ concentration. For all Na^+ calibration solutions, the ionophore Gramicidin D (10 µmol/L, Sigma-Aldrich) was added to achieve cell permeabilization. For the 10 and 20 mmol/L Na^+ calibration solutions, an additional 100 µmol/L of the Na^+/K^+-ATPase inhibitor strophanthidin (Sigma-Aldrich) was added. Continuous electrical stimulation was then performed at 1 Hz as described above, and the steady-state fluorescence ratio was recorded after 20 min for each step in the calibration process (with Tyrode's solution for 0, 10, and 20 mmol/L of Na^+).

The spontaneous Ca^{2+} release events were analyzed by epifluorescence microscopy as described previously (Hegner et al., 2023). In short, the atrial cardiomyocytes were loaded with the Ca^{2+}-sensitive dye Fura-2-AM (5 µmol/L, Thermo Fisher Scientific) and subjected to regular electrical field stimulation at 1, 2, and 4 Hz for 5 min per frequency. Deviations from the diastolic Ca^{2+} baseline between two stimulated transients were defined as the spontaneous Ca^{2+} release events and counted by one investigator blinded to the genotype and intervention.

2.5 Statistical analysis

The experiments were performed and analyzed after being blinded to the genotype (wild-type vs CaMKII$\delta^{-/-}$) and treatment (CTRL vs PTFE) of the mice, and the results were presented as mean values per mouse ±standard error of the mean (SEM) for three significant digits. The normal distribution was assessed via the Shapiro–Wilk normality test, and student's t-test was used to compare two normally distributed continuous variables. One-way ANOVA with Holm–Sidak's *post hoc* correction was performed for comparisons of more than two normally distributed groups. GraphPad PRISM 10 was used to test for differences between the linear regression slopes. Two-sided *p*-values below 0.05 were considered to be statistically significant.

3 Results

3.1 ROS production is increased in atrial cardiomyocytes of OSA mice

Previously, we demonstrated increased ROS production in the myocardium of patients with SDB (Arzt et al., 2022). Additionally, we were able to show increased ROS production in the ventricular cardiomyocytes of the PTFE-treated mice (Hegner et al., 2023). Since high-risk cardiovascular patients often have various comorbidities, such as diabetes, heart failure, and coronary artery disease, it is difficult to determine the independent effect of SDB on ROS production. Therefore, in this study, we analyzed the effect of specific OSA induction by PTFE treatment in mouse atrial cardiomyocytes.

Eight weeks after the PTFE injections, the cytosolic ROS production in the experimental mice increased compared to those of the control animals (1.63e-2 ± 2.2e-3 in PTFE vs 7.95e-3 ± 1.3e-3 ($\Delta F/F_0$*min^{-1}) in control, $p = 0.006$, n = 7 vs 7, Figures 2A–C). Moreover, the time-dependent cytosolic ROS production estimated by linear regression analysis was elevated in the PTFE-treated mice compared to the controls ($r^2 = 0.666$, $p < 0.001$, n = 7 in PTFE vs $r^2 = 0.327$, $p < 0.001$, n = 7 in control, and $p < 0.001$ for difference in slopes, Figure 2B).

Similarly, mitochondrial ROS production quantified by MitoSox™ Red was higher in the PTFE-treated mice than the controls (2.68e-2 ± 4.4e-3 in PTFE vs 1.51e-2 ± 1.7e-3 in control, $p = 0.030$, n = 7 vs 7, Figures 2D–F). Congruently, the time-dependent mitochondrial ROS production estimated by linear regression analysis was elevated in the PTFE mice compared to the controls ($r^2 = 0.578$, $p < 0.001$, n = 7 in PTFE vs $r^2 = 0.540$, $p < 0.001$, n = 7 in control, $p < 0.001$ for difference in slopes, Figure 2E).

3.2 CaMKII-dependent dysregulation of atrial Na^+ homeostasis

The atrial cardiomyocyte Na^+ concentration was assessed by epifluorescence microscopy using the Na^+-sensitive SBFI-AM fluorescence dye. The cardiomyocytes underwent continuous electrical stimulation at 1, 2, and 4 Hz to account for differences between the physiological human and murine heart rates. The SBFI $F_{340}/_{380}$ ratio was analyzed at steady-state levels (Figure 3A). In the wild-type PTFE mice, the SBFI ratio increased to 1.26 ± 8.2e-3 as compared to 1.17 ± 1.2e-2 in the control mice ($p < 0.001$, Figure 3B), while the CaMKII$\delta^{-/-}$ PTFE mice remained protected ($p < 0.001$, Figure 3B). Importantly, the SBFI $F_{340}/_{380}$ ratio increased similarly across all frequencies, including 2 and 4 Hz, in the wild-type PTFE mice while remaining at healthy control levels in the CaMKII$\delta^{-/-}$ PTFE mice (Figures 3C, D).

Calibration experiments were conducted to convert the ratiometric SBFI fluorescence values to Na^+ concentrations (mmol/L) (Figure 4A). The SBFI fluorescence ratios were plotted for fixed Na^+ concentrations (0, 10, and 20 mmol/L, Figure 4B). The SBFI $F_{340}/_{380}$ ratio was converted to intracellular Na^+ concentration (mmol/L) using the resulting calibration curve. The atrial cardiomyocyte Na^+ concentration at 1 Hz increased in the wild-type PTFE mice to 20.0 ± 0.65 from 12.6 ± 0.94 mmol/L in the wild-type control ($p < 0.001$, Figure 4C) but remained at the control level (13.5 ± 0.74 mmol/L) in the CaMKII$\delta^{-/-}$ PTFE mice ($p < 0.001$ vs wild-type PTFE, Figure 4C). At 2 Hz stimulation, the Na^+ concentration increased to 20.6 ± 0.53 mmol/L in the wild-type PTFE mice from 14.1 ± 0.96 mmol/L in the wild-type control ($p < 0.001$). During 4 Hz stimulation, the intracellular Na^+ concentration increased further to 21.6 ± 0.62 mmol/L in the wild-type PTFE mice from 15.7 ± 1.2 mmol/L in the control ($p = 0.002$). Moreover, at 2 and 4 Hz, Na^+ concentrations in the

10.3389/fphar.2024.1411822

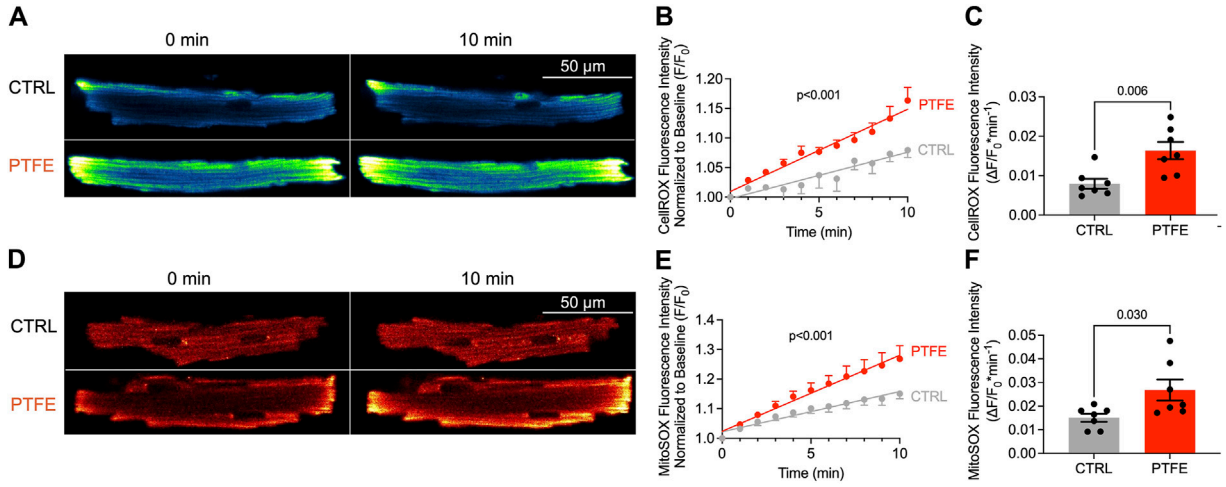

FIGURE 2
ROS production is increased in the atrial cardiomyocytes of PTFE mice: **(A)** original laser-scanning confocal microscopy images of atrial cardiomyocytes loaded with the CellRox™ Orange dye (artificial coloring of monochrome image with Blue_Yellow LUT); **(B)** linear regression analysis of the cytosolic ROS production over time (n = 15/7 control (CTRL) vs n = 14/7 PTFE); **(C)** mean slope of cytosolic ROS production over time (n = 15/7 CTRL vs n = 14/7 PTFE); **(D)** original laser scanning confocal microscopy images of atrial cardiomyocytes loaded with the MitoSox™ Red dye (artificial coloring of monochrome image with Red_Hot LUT); **(E)** linear regression analysis of the mitochondrial ROS production over time (n = 15/7 CTRL vs n = 13/7 PTFE); **(F)** mean slope of mitochondrial ROS production over time (n = 15/7 CTRL vs n = 13/7 PTFE). N indicates the number of cells/number of mice. The comparisons are based on student's t-test and linear regression analysis as appropriate.

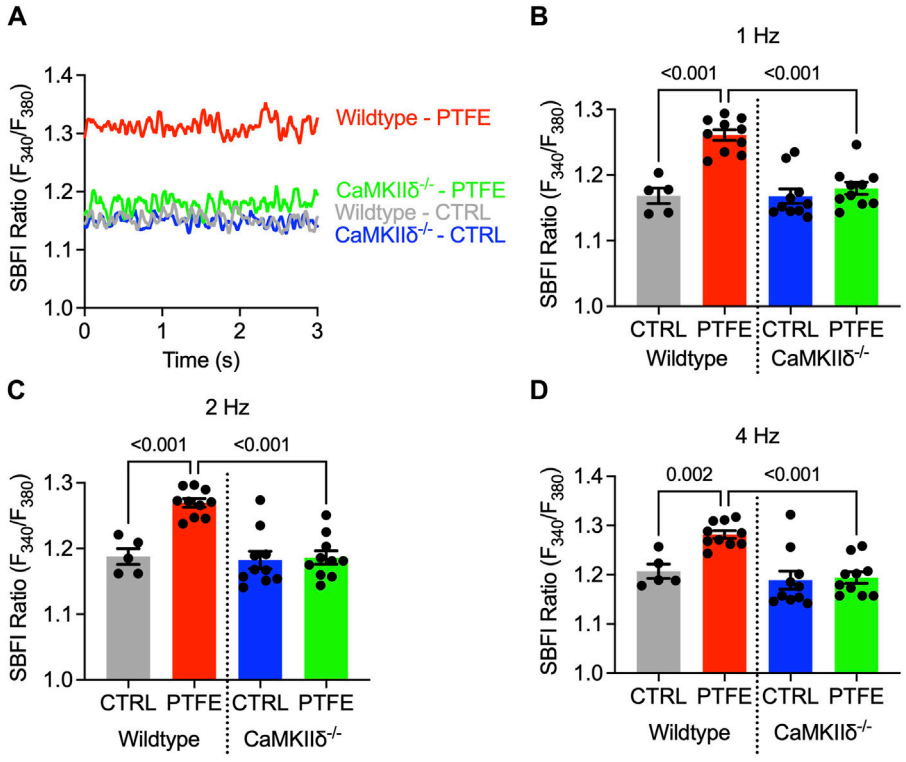

FIGURE 3
Cytosolic Na^+ is elevated only in the atrial cardiomyocytes of wild-type PTFE mice: **(A)** original traces of the SBFI ratio (F_{340}/F_{380}) in the atrial cardiomyocytes; mean SBFI ratios at **(B)** 1 Hz, **(C)** 2 Hz, and **(D)** 4 Hz electrical stimulation (n = 19/5 wild-type control (CTRL), n = 38/10 wild-type PTFE, n = 32/10 CaMKIIδ$^{-/-}$ CTRL, and n = 36/10 CaMKIIδ$^{-/-}$ PTFE). N indicates the number of cells/number of mice. The comparisons are based on one-way ANOVA with Holm–Sidak's *post hoc* correction.

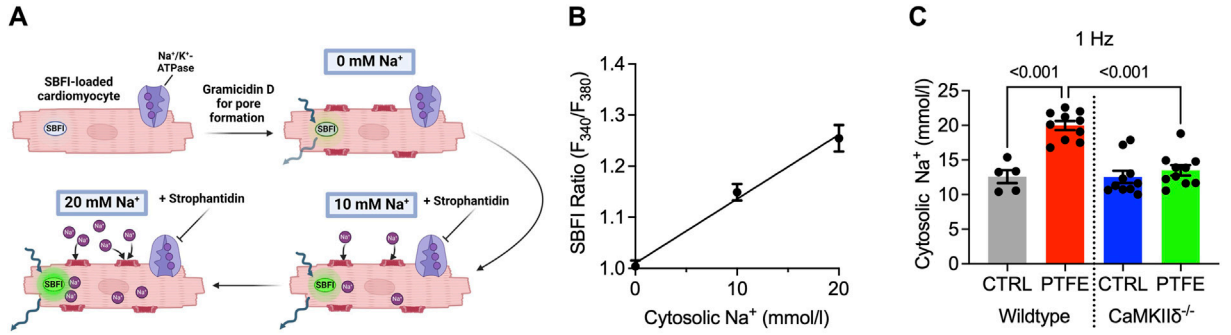

FIGURE 4
Measurement of Na^+ concentration and calibration procedure: **(A)** protocol for SBFI-AM calibration to Na^+ concentration performed in the atrial cardiomyocytes; **(B)** mean SBFI ratios (F_{340}/F_{380}) at 0, 10, and 20 mmol/L of Na^+ with linear regression (n = 14 cells); mean intracellular Na^+ concentration at **(C)** 1 Hz electrical stimulation (n = 19/5 wild-type control (CTRL), n = 38/10 wild-type PTFE, n = 32/10 CaMKIIδ$^{-/-}$ CTRL, and n = 36/10 CaMKIIδ$^{-/-}$ PTFE). N indicates the number of cells/number of mice. The comparisons are based on one-way ANOVA with Holm–Sidak's *post hoc* correction or linear regression analysis as appropriate.

CaMKIIδ$^{-/-}$ PTFE mice were similar to those of the wild-type control mice (2 Hz: 14.0 ± 0.82 mmol/L, $p < 0.001$ vs wild-type PTFE; 4 Hz: 14.6 ± 0.93 mmol/L, $p < 0.001$ vs wild-type PTFE).

3.3 CaMKII-dependent arrhythmias in isolated atrial myocytes of OSA mice

Spontaneous Ca^{2+} release events were assessed in isolated atrial cardiomyocytes loaded with the Ca^{2+}-sensitive Fura-2-AM dye during regular electrical stimulation. Non-stimulated pro-arrhythmic events could be observed in the myocytes from the wild-type PTFE mice (Figure 5A, indicated by red arrows), while the Ca^{2+} transient characteristics remained unaltered in the PTFE mice (Figures 5B–D). At 1 Hz stimulation, the incidence of spontaneous Ca^{2+} release events increased in the wild-type PTFE mice by more than two-fold to 5.85e-2 ± 7.9e-3 (s^{-1}) from 2.11e-2 ± 3.5e-3 in the wild-type control mice ($p < 0.001$, Figure 5E). Atrial cardiomyocytes from the CaMKIIδ$^{-/-}$ PTFE mice were protected from such an increase in the rate of arrhythmias (2.65e-2 ± 7.8e-3, $p = 0.007$ vs wild-type PTFE, Figure 5E). Similar effects were also observed at 2 Hz stimulation, with the rate of pro-arrhythmic non-stimulated events increasing to 9.86e-2 ± 1.4e-2 in the wild-type PTFE mice from 4.11e-2 ± 8.0e-3 in the wild-type control mice ($p < 0.001$, Figure 5F), whilst the CaMKIIδ$^{-/-}$ PTFE mice exhibited no increase in the frequency of spontaneous Ca^{2+} release events (3.20e-2 ± 7.4e-3, $p < 0.001$ vs wild-type PTFE, Figure 5F). At a stimulation rate of 4 Hz, which is closer to the physiological murine heart rate (Li et al., 1999), the rate of atrial pro-arrhythmic events remained elevated by more than two-fold in the wild-type PTFE mice compared to the control (1.29e-1 ± 1.7e-2 vs 5.24e-2 ± 6.8e-3, $p < 0.001$, Figure 5G). Once again, atrial cardiomyocytes from the CaMKIIδ$^{-/-}$ PTFE mice exhibited arrhythmia frequencies comparable to those of the healthy controls (4.34e-2 ± 1.1e-2, $p < 0.001$ vs wild-type PTFE, Figure 5G). Additionally, no significant differences were observed between the CaMKIIδ$^{-/-}$ control and PTFE mice (Figures 5E–G).

4 Discussion

In the present study, we show increased ROS production, Na^+ overload, and more frequent spontaneous Ca^{2+} release events in the atrial cardiomyocytes of OSA mice. The current therapeutic strategies for SDB are mostly limited to lifestyle interventions and CPAP therapy (Aurora et al., 2012; Randerath et al., 2017; Patil et al., 2019). However, patient compliance is often low in such cases, and interventions such as adaptive servo-ventilation therapy may even be detrimental in certain patients (Cowie et al., 2015; McEvoy et al., 2016). Although SDB is associated with increased incidence of atrial fibrillation and lower sustained success of cardioversion or pulmonary vein isolation (Gami et al., 2004; Gami et al., 2007; Linz et al., 2018), CPAP therapy has failed to reduce the arrhythmia burden and incidence of adverse cardiovascular events (Peker et al., 2016; Traaen et al., 2021). Additionally, SDB patients have been reported to frequently suffer from heart failure, especially HFpEF (Lebek et al., 2021; Levy et al., 2022; Wester et al., 2023). These aspects highlight the urgent need for more targeted and effective therapies for SDB patients.

Recently, we showed for the first time that intracellular Na^+ entry and Na^+ concentration are higher in the atrial myocytes of patients with HFpEF, a condition in which SDB is very common, which could contribute to atrial contractile dysfunction and arrhythmias (Trum et al., 2024). Interestingly, we also showed that patients with SDB have increased late Na^+ current in their remodeled atria, which could contribute to intracellular Na^+ overload (Lebek et al., 2022). However, because these patients could also have various comorbidities, it is very difficult to determine the standalone effects of OSA.

The SDB mouse model utilized in this study is ideal for exploration of the pathological mechanisms and novel therapeutic targets as it is devoid of the confounding comorbidities frequently exhibited by patients; the mouse model is also more widely available than SDB patient biomaterial (Lebek et al., 2020a; Hegner et al., 2023). It is noted that these mice developed diastolic and mild systolic left-ventricular dysfunctions, which also resulted in increased heart and lung weights (Lebek et al.,

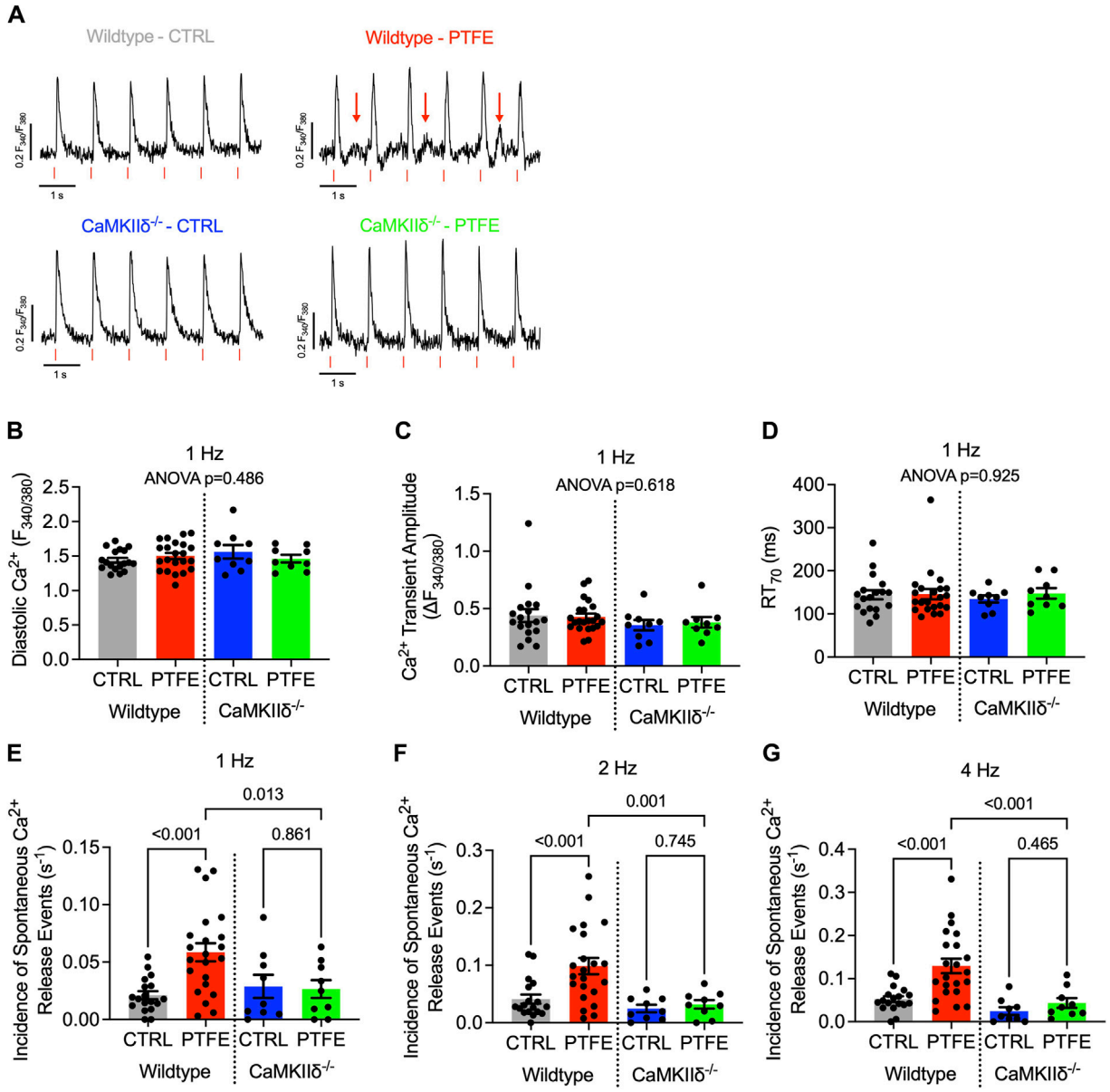

FIGURE 5
CaMKIIδ$^{-/-}$ mice are protected from spontaneous Ca^{2+} release events: **(A)** original recordings of Ca^{2+} transients (Fura-2 ratio, F_{340}/F_{380}) in the atrial cardiomyocytes, where the spontaneous Ca^{2+} release events are indicated by red arrows in the wild-type PTFE mice; **(B)** mean diastolic Ca^{2+}, **(C)** Ca^{2+} transient amplitude, and **(D)** relaxation time to 70% of baseline at 1 Hz with ANOVA; p = n.s. Incidence of spontaneous Ca^{2+} release events at **(E)** 1 Hz, **(F)** 2 Hz, and **(G)** 4 Hz electrical stimulation. N = 57/18 wild-type control (CTRL), n = 66/22 wild-type PTFE, n = 27/9 CaMKIIδ$^{-/-}$ CTRL, and n = 26/9 CaMKIIδ$^{-/-}$ PTFE. N indicates the number of cells/number of mice. The comparisons are based on one-way ANOVA with Holm–Sidak's *post hoc* correction.

2020a; Hegner et al., 2023). It is therefore possible that the effects observed in the ventricles may contribute to changes in the atria.

4.1 SDB-dependent pathological mechanisms promoting arrhythmias

The frequently discussed pro-arrhythmic mechanisms that could facilitate atrial fibrillation in SDB include intrathoracic pressure changes (Linz et al., 2011), autonomous imbalance and beta-adrenergic stimulation during nocturnal awakening periods (Abboud and Kumar, 2014), increased arterial blood pressure (Hetzenecker et al., 2013), structural remodeling (Anter et al., 2017), conduction abnormalities (Anter et al., 2017; Hegner et al., 2021b), ion-channel dysfunction and triggered activity (Lebek et al., 2020b; Lebek et al., 2022), and intermittent hypoxia/desaturation (Tkacova et al., 1998; Iwasaki et al., 2014). The latter is also a strong inductor of oxidative stress and ROS production (Gozal and Kheirandish-Gozal, 2008). Indeed, we previously observed increased production of cytosolic ROS in human atrial tissues of SDB patients (Lebek et al., 2020b). In agreement with these observations, in this study, we report

increased cytosolic and mitochondrial ROS production in the atrial myocytes of OSA mice without comorbidities.

ROS have been shown to oxidize many ion channels and transporters. Indeed, direct oxidation of the ryanodine type-2 receptors (RyR2) can promote increased diastolic sarcoplasmic reticulum Ca^{2+} release and subsequent arrhythmias (Huang et al., 2021). On the other hand, CaMKIIδ is a kinase central to myocardial Na^+ and Ca^{2+} homeostasis that can also be directly oxidized at methionine-281 and -282, thereby releasing the catalytic domain leading to increased enzyme activation (Erickson et al., 2008; Lebek et al., 2023b; Lebek et al., 2024).

Our group previously established that cardiac CaMKIIδ activity is pathologically increased in SDB patients and also in SDB mice in the model used in this study (Lebek et al., 2020a; Lebek et al., 2020b; Arzt et al., 2022; Hegner et al., 2023). In the present study, we present data from isolated atrial cardiomyocytes, but the limited amount of tissue precluded further protein target analysis, which is a potential limitation of this study. There are several important downstream targets of CaMKIIδ, including voltage-gated Na^+ channels $Na_V1.5$ and $Na_V1.8$, RyR2, phospholamban, L-type Ca^{2+} channels, and Na^+/Ca^{2+} exchangers, which have been shown to be involved in arrhythmogenesis (Bers, 2002; Fischer et al., 2013; Bengel et al., 2021). CaMKIIδ overactivation in SDB can lead to disturbed Ca^{2+} homeostasis, including increased sarcoplasmic reticulum Ca^{2+} leakage, pro-arrhythmic non-stimulated events in humans and mice, and multicellular arrhythmias in the patient trabeculae (Lebek et al., 2020b; Arzt et al., 2022; Hegner et al., 2023). These pro-arrhythmic events could serve as triggers of atrial fibrillation (Nattel et al., 2020).

4.2 Disturbance of atrial Na^+ homeostasis as a novel pathological mechanism in SDB

Increased CaMKIIδ activation can facilitate intracellular Na^+ level overload (Wagner et al., 2006; Wagner et al., 2011), and recent studies have highlighted the interactions between CaMKIIδ and increased Na^+ influx in heart failure (Bengel et al., 2021), resulting in increased myocyte Na^+ concentration (Despa, 2018). One of the proposed mechanisms is increased late Na^+ current (late I_{Na}), which was detected in the atrial myocytes of patients with SDB (Lebek et al., 2020b; Lebek et al., 2022). However, data regarding Na^+ in the mouse atrial myocytes is scarce as the biomaterial is limited by the small murine atrium and methodological challenges (Garber et al., 2022). Garber et al. (2017, 2022) recommend calibrating each myocyte individually, which we did not perform for every cell in this study with the aim of increasing the yield. Consequently, the converted Na^+ concentrations may be more general estimates. The quiescent murine atrial myocyte Na^+ concentrations were previously reported at ~8 mmol/L with an increase to 11–12 mmol/L at 1 Hz stimulation. Since the Na^+ concentration increases in a frequency-dependent manner (Despa et al., 2002; Pieske et al., 2002), we conducted measurements at multiple frequencies (1, 2, and 4 Hz) to account for the increased rates that are commonly seen in human atrial arrhythmias (Lu and Chen, 2021). In addition, this allowed us to take into account the physiologically different heart rates of humans and mice to offer a more comprehensive translational perspective. Our data are in direct agreement with the findings of previously published literature as we estimated the atrial myocyte Na^+ concentration to be ~12 mmol/L at 1 Hz stimulation in healthy wild-type mice.

Importantly, at all the tested frequencies, the Na^+ concentrations in the atrial cardiomyocytes were profoundly higher in the OSA mice in excess of Δ+5 mmol/L. Owing to the selected calibration range of 0–20 mmol/L Na^+ (Figure 4B), any reported concentrations above 20 mmol/L may even be underestimated. An increase in the intracellular Na^+ by this margin impairs Na^+/Ca^{2+} exchanger (NCX) function owing to reduced transmembrane Na^+ gradients in a manner similar to that observed in heart failure (Despa et al., 2002; Pieske et al., 2002; Hegner et al., 2022). Impaired NCX function may further increase the cellular Ca^{2+} levels by reduced Ca^{2+} export, which could further increase CaMKIIδ activation in a Ca^{2+}-dependent fashion, thereby exacerbating Na^+ increase (Sapia et al., 2010; Bengel et al., 2021). Moreover, increased Na^+ influx is linked to initiation of atrial fibrillation (Sossalla et al., 2010; Wan et al., 2016). Cellular Na^+ overload is also known to increase cytosolic and mitochondrial ROS productions (Kohlhaas et al., 2010). Indeed, we measured increased intracellular and mitochondrial ROS productions in the cardiomyocytes of OSA mice. In turn, this could promote a vicious cycle by leading to further Na^+ increase via CaMKIIδ activation. Importantly, we did not observe any increase in atrial Na^+ concentrations in the cardiomyocytes of CaMKIIδ$^{-/-}$ SDB mice at any of the evaluated frequencies.

In line with the disturbed Na^+ homeostasis, we also observed more than two-fold increase in pro-arrhythmic events in the atrial cardiomyocytes of the wild-type SDB mice at all stimulation frequencies (1, 2, and 4 Hz), which was almost similar to the levels of healthy controls in the CaMKIIδ$^{-/-}$ SDB mice. Moreover, production of ROS has been linked to arrhythmogenesis in cardiomyocytes (Liu et al., 2022). Importantly, ROS production and NADPH oxidase activity are higher in SDB (Gozal and Kheirandish-Gozal, 2008), whereas the other Ca^{2+} transient characteristics remain unaltered in the PTFE mice. This may be attributed to compensatory effects on the sarcoplasmic reticulum Ca^{2+} content, as observed in patients with paroxysmal atrial fibrillation (Voigt et al., 2014). We previously reported a reduced Ca^{2+} transient amplitude in the ventricular cardiomyocytes of SDB mice (Hegner et al., 2023), which we did not observe in the atrial cardiomyocytes in the present study.

Our data suggest that modulation of CaMKIIδ activity could be a promising antiarrhythmic approach in SDB. Even as pharmacological inhibition of CaMKIIδ is being investigated (Pellicena and Schulman, 2014; Lebek et al., 2018), CRISPR-Cas9 gene editing of *CAMK2D* could be an advanced strategy to overcome the previous limitations, as this technology has been used with >2,000-fold increased specificity toward *CAMK2D* compared to other isoforms (Lebek et al., 2023a). Additionally, pharmacological inhibition and genetic ablation of (oxidative) activation of CaMKIIδ have been shown to protect from pro-arrhythmic activities (Lebek et al., 2018; Lebek et al., 2023a; Lebek et al., 2023b; Hegner et al., 2023).

5 Conclusion

Patients with SDB are at increased risk of developing atrial fibrillation and have demonstrated lower efficacy for currently available anti-arrhythmic therapies. In fact, targeted anti-arrhythmic

therapies are completely lacking in SDB. In the present study, we demonstrated that in an SDB mouse model devoid of comorbidities, the production of cytosolic and mitochondrial ROS increased in the atrial cardiomyocytes. ROS are known to facilitate persistent overactivation of Ca^{2+}/calmodulin-dependent protein kinase IIδ (CaMKIIδ), which results in disruption of the cellular Na^+ and Ca^{2+} homeostasis. Herein, we describe elevated Na^+ concentrations at multiple stimulation frequencies associated with higher chances of spontaneous Ca^{2+} release events in SDB mice. Importantly, the CaMKIIδ$^{-/-}$ mice were protected from such effects. Therefore, inhibition of CaMKIIδ in SDB may reduce Na^+ overload and protect against arrhythmias, which could have therapeutic implications in the future.

Data availability statement

The original contributions presented in the study are included in the article/Supplementary material; further inquiries can be directed to the corresponding authors.

Ethics statement

All experiments involving mice were in compliance with the directive 2010/63/EU of the European Parliament, Guide for the Care and Use of Laboratory Animals published by the US National Institutes of Health (NIH Publication No. 85–23, revised 1985), and local institutional guidelines. The government of Unterfranken, Bavaria, Germany, gave approval for the animal protocol (no.: 55.2-2532-2-512). The study was conducted in accordance with the local legislation and institutional requirements.

Author contributions

PH: conceptualization, formal analysis, funding acquisition, investigation, visualization, writing–original draft, and writing–review and editing. FO: formal analysis, investigation, and writing–review and editing. BS: formal analysis, investigation, writing–review and editing. MG: formal analysis, investigation, and writing–review and editing. MT: formal analysis, visualization, and writing–review and editing. A-ML: formal analysis, visualization, and writing–review and editing. LM: funding acquisition, resources, and writing–review and editing. MA: funding acquisition, resources, and writing–review and editing. SL: conceptualization, funding acquisition, investigation, writing–original draft, and writing–review and editing. SW: conceptualization, funding acquisition, methodology, project administration, supervision, and writing–review and editing.

Funding

The author(s) declare that financial support was received for the research, authorship, and/or publication of this article. PH was funded by a clinician scientist research grant from the German Cardiac Society (DGK) and by the Medical Faculty at the University of Regensburg (ReForM A). MT was funded by the Else Kröner-Fresenius-Stiftung (EKFS). LSM was funded by the EU Horizon grant STRATIFY-HF (no. 101080905). LSM and SW were funded by the German Research Foundation (DFG; TRR 374 grant, no. 509149993, TPA6). MA was funded by the EKFS (no. 2018_A159) and German Federal Ministry of Education and Research (BMBF; no. 01ZZ2324C). SL was funded by research grants from the DGK and EKFS, a DFG research grant (LE 5009/3-1, no. 528297116), and the DFG Heisenberg professorship (LE 5009/2-1, no. 528296867). SW was funded by the DFG (no. WA 2539/8-1) and the EKFS.

Acknowledgments

The authors appreciate the expert technical assistances of Gabriela Pietrzyk, Thomas Sowa, and Dr. Susanne Klatt. Figure 4A was created with biorender.com.

Conflict of interest

The authors declare that the research was conducted in the absence of any commercial or financial relationships that could be construed as a potential conflict of interest.

The handling editor FW declared a past co-authorship with the author(s) PH, LM.

Publisher's note

References

Abboud, F., and Kumar, R. (2014). Obstructive sleep apnea and insight into mechanisms of sympathetic overactivity. *J. Clin. Investig.* 124 (4), 1454–1457. doi:10.1172/JCI70420

Anter, E., Di Biase, L., Contreras-Valdes, F. M., Gianni, C., Mohanty, S., Tschabrunn, C. M., et al. (2017). Atrial substrate and triggers of paroxysmal atrial fibrillation in patients with obstructive sleep apnea. *Circ. Arrhythm. Electrophysiol.* 10 (11), e005407. doi:10.1161/CIRCEP.117.005407

Arzt, M., Drzymalski, M. A., Ripfel, S., Meindl, S., Biedermann, A., Durczok, M., et al. (2022). Enhanced cardiac CaMKII oxidation and CaMKII-dependent SR Ca leak in patients with sleep-disordered breathing. *Antioxidants (Basel)* 11 (2), 331. doi:10.3390/antiox11020331

Arzt, M., Woehrle, H., Oldenburg, O., Graml, A., Suling, A., Erdmann, E., et al. (2016). Prevalence and predictors of sleep-disordered breathing in patients with stable chronic heart failure: the SchlaHF registry. *JACC Heart Fail* 4 (2), 116–125. doi:10.1016/j.jchf.2015.09.014

Arzt, M., Young, T., Finn, L., Skatrud, J. B., and Bradley, T. D. (2005). Association of sleep-disordered breathing and the occurrence of stroke. *Am. J. Respir. Crit. Care Med.* 172 (11), 1447–1451. doi:10.1164/rccm.200505-702OC

Aurora, R. N., Chowdhuri, S., Ramar, K., Bista, S. R., Casey, K. R., Lamm, C. I., et al. (2012). The treatment of central sleep apnea syndromes in adults: practice parameters with an evidence-based literature review and meta-analyses. *Sleep* 35 (1), 17–40. doi:10.5665/sleep.1580

Bengel, P., Dybkova, N., Tirilomis, P., Ahmad, S., Hartmann, N., B, A. M., et al. (2021). Detrimental proarrhythmogenic interaction of Ca(2+)/calmodulin-dependent protein kinase II and NaV1.8 in heart failure. *Nat. Commun.* 12 (1), 6586. doi:10.1038/s41467-021-26690-1

Benjafield, A. V., Ayas, N. T., Eastwood, P. R., Heinzer, R., Ip, M. S. M., Morrell, M. J., et al. (2019). Estimation of the global prevalence and burden of obstructive sleep apnoea: a literature-based analysis. *Lancet Respir. Med.* 7 (8), 687–698. doi:10.1016/S2213-2600(19)30198-5

Bers, D. M. (2002). Cardiac excitation-contraction coupling. *Nature* 415 (6868), 198–205. doi:10.1038/415198a

Cowie, M. R., Woehrle, H., Wegscheider, K., Angermann, C., d'Ortho, M. P., Erdmann, E., et al. (2015). Adaptive servo-ventilation for central sleep apnea in systolic heart failure. *N. Engl. J. Med.* 373 (12), 1095–1105. doi:10.1056/NEJMoa1506459

Despa, S. (2018). Myocyte [Na(+)](i) dysregulation in heart failure and diabetic cardiomyopathy. *Front. Physiol.* 9, 1303. doi:10.3389/fphys.2018.01303

Despa, S., Islam, M. A., Weber, C. R., Pogwizd, S. M., and Bers, D. M. (2002). Intracellular Na(+) concentration is elevated in heart failure but Na/K pump function is unchanged. *Circulation* 105 (21), 2543–2548. doi:10.1161/01.cir.0000016701.85760.97

Erickson, J. R., Joiner, M. L., Guan, X., Kutschke, W., Yang, J., Oddis, C. V., et al. (2008). A dynamic pathway for calcium-independent activation of CaMKII by methionine oxidation. *Cell.* 133 (3), 462–474. doi:10.1016/j.cell.2008.02.048

Fischer, T. H., Neef, S., and Maier, L. S. (2013). The Ca-calmodulin dependent kinase II: a promising target for future antiarrhythmic therapies? *J. Mol. Cell. Cardiol.* 58, 182–187. doi:10.1016/j.yjmcc.2012.11.003

Gami, A. S., Hodge, D. O., Herges, R. M., Olson, E. J., Nykodym, J., Kara, T., et al. (2007). Obstructive sleep apnea, obesity, and the risk of incident atrial fibrillation. *J. Am. Coll. Cardiol.* 49 (5), 565–571. doi:10.1016/j.jacc.2006.08.060

Gami, A. S., Pressman, G., Caples, S. M., Kanagala, R., Gard, J. J., Davison, D. E., et al. (2004). Association of atrial fibrillation and obstructive sleep apnea. *Circulation* 110 (4), 364–367. doi:10.1161/01.CIR.0000136587.68725.8E

Garber, L., Joca, H. C., Coleman, A. K., Boyman, L., Lederer, W. J., and Greiser, M. (2022). Camera-based measurements of intracellular [Na+] in murine atrial myocytes. *J. Vis. Exp.* 183. doi:10.3791/59600

Garber, L., Lederer, W. J., and Greiser, M. (2017). Characterization of intracellular sodium homeostasis in murine atrial myocytes. *Biophysical J.* 112 (3), 96a. doi:10.1016/j.bpj.2016.11.557

Glynn, P., Musa, H., Wu, X., Unudurthi, S. D., Little, S., Qian, L., et al. (2015). Voltage-gated sodium channel phosphorylation at Ser571 regulates late current, arrhythmia, and cardiac function *in vivo*. *Circulation* 132 (7), 567–577. doi:10.1161/CIRCULATIONAHA.114.015218

Gozal, D., and Kheirandish-Gozal, L. (2008). Cardiovascular morbidity in obstructive sleep apnea: oxidative stress, inflammation, and much more. *Am. J. Respir. Crit. Care Med.* 177 (4), 369–375. doi:10.1164/rccm.200608-1190PP

Hegner, P., Drzymalski, M., Biedermann, A., Memmel, B., Durczok, M., Wester, M., et al. (2022). SAR296968, a novel selective Na(+)/Ca(2+) exchanger inhibitor, improves Ca(2+) handling and contractile function in human atrial cardiomyocytes. *Biomedicines* 10 (8), 1932. doi:10.3390/biomedicines10081932

Hegner, P., Lebek, S., Maier, L. S., Arzt, M., and Wagner, S. (2021a). The effect of gender and sex hormones on cardiovascular disease, heart failure, diabetes, and atrial fibrillation in sleep apnea. *Front. Physiol.* 12, 741896. doi:10.3389/fphys.2021.741896

Hegner, P., Lebek, S., Schaner, B., Ofner, F., Gugg, M., Maier, L. S., et al. (2023). CaMKII-dependent contractile dysfunction and pro-arrhythmic activity in a mouse model of obstructive sleep apnea. *Antioxidants (Basel)* 12 (2), 315. doi:10.3390/antiox12020315

Hegner, P., Lebek, S., Tafelmeier, M., Camboni, D., Schopka, S., Schmid, C., et al. (2021b). Sleep-disordered breathing is independently associated with reduced atrial connexin 43 expression. *Heart rhythm.* 18 (12), 2187–2194. doi:10.1016/j.hrthm.2021.09.009

Hegner, P., Wester, M., Tafelmeier, M., Provaznik, Z., Klatt, S., Schmid, C., et al. (2024). Systemic inflammation predicts diastolic dysfunction in patients with sleep-disordered breathing. *Eur. Respir. J.*, 2400579. doi:10.1183/13993003.00579-2024

Hetzenecker, A., Buchner, S., Greimel, T., Satzl, A., Luchner, A., Debl, K., et al. (2013). Cardiac workload in patients with sleep-disordered breathing early after acute myocardial infarction. *Chest* 143 (5), 1294–1301. doi:10.1378/chest.12-1930

Huang, Y., Lei, C., Xie, W., Yan, L., Wang, Y., Yuan, S., et al. (2021). Oxidation of ryanodine receptors promotes Ca(2+) leakage and contributes to right ventricular dysfunction in pulmonary hypertension. *Hypertension* 77 (1), 59–71. doi:10.1161/HYPERTENSIONAHA.120.15561

Iwasaki, Y. K., Kato, T., Xiong, F., Shi, Y. F., Naud, P., Maguy, A., et al. (2014). Atrial fibrillation promotion with long-term repetitive obstructive sleep apnea in a rat model. *J. Am. Coll. Cardiol.* 64 (19), 2013–2023. doi:10.1016/j.jacc.2014.05.077

Kohlhaas, M., Liu, T., Knopp, A., Zeller, T., Ong, M. F., Bohm, M., et al. (2010). Elevated cytosolic Na+ increases mitochondrial formation of reactive oxygen species in failing cardiac myocytes. *Circulation* 121 (14), 1606–1613. doi:10.1161/CIRCULATIONAHA.109.914911

Lebek, S., Caravia, X. M., Chemello, F., Tan, W., McAnally, J. R., Chen, K., et al. (2023a). Elimination of CaMKIIδ autophosphorylation by CRISPR-cas9 base editing improves survival and cardiac function in heart failure in mice. *Circulation* 148 (19), 1490–1504. doi:10.1161/CIRCULATIONAHA.123.065117

Lebek, S., Caravia, X. M., Straub, L. G., Alzhanov, D., Tan, W., Li, H., et al. (2024). CRISPR-Cas9 base editing of pathogenic CaMKIIδ improves cardiac function in a humanized mouse model. *J. Clin. Investig.* 134 (1), e175164. doi:10.1172/JCI175164

Lebek, S., Chemello, F., Caravia, X. M., Tan, W., Li, H., Chen, K., et al. (2023b). Ablation of CaMKIIδ oxidation by CRISPR-Cas9 base editing as a therapy for cardiac disease. *Science* 379 (6628), 179–185. doi:10.1126/science.ade1105

Lebek, S., Hegner, P., Hultsch, R., Rohde, J., Rupprecht, L., Schmid, C., et al. (2022). Voltage-gated sodium channel $Na_V1.8$ dysregulates Na and Ca, leading to arrhythmias in patients with sleep-disordered breathing. *Am. J. Respir. Crit. Care Med.* 206 (11), 1428–1431. doi:10.1164/rccm.202205-0981LE

Lebek, S., Hegner, P., Schach, C., Reuthner, K., Tafelmeier, M., Maier, L. S., et al. (2020a). A novel mouse model of obstructive sleep apnea by bulking agent-induced tongue enlargement results in left ventricular contractile dysfunction. *PLoS One* 15 (12), e0243844. doi:10.1371/journal.pone.0243844

Lebek, S., Hegner, P., Tafelmeier, M., Rupprecht, L., Schmid, C., Maier, L. S., et al. (2021). Female patients with sleep-disordered breathing display more frequently heart failure with preserved ejection fraction. *Front. Med. (Lausanne)* 8, 675987. doi:10.3389/fmed.2021.675987

Lebek, S., Pichler, K., Reuthner, K., Trum, M., Tafelmeier, M., Mustroph, J., et al. (2020b). Enhanced CaMKII-dependent late INa induces atrial proarrhythmic activity in patients with sleep-disordered breathing. *Circ. Res.* 126 (5), 603–615. doi:10.1161/CIRCRESAHA.119.315755

Lebek, S., Plossl, A., Baier, M., Mustroph, J., Tarnowski, D., Lucht, C. M., et al. (2018). The novel CaMKII inhibitor GS-680 reduces diastolic SR Ca leak and prevents CaMKII-dependent pro-arrhythmic activity. *J. Mol. Cell. Cardiol.* 118, 159–168. doi:10.1016/j.yjmcc.2018.03.020

Levy, P., Naughton, M. T., Tamisier, R., Cowie, M. R., and Bradley, T. D. (2022). Sleep apnoea and heart failure. *Eur. Respir. J.* 59 (5), 2101640. doi:10.1183/13993003.01640-2021

Li, P., Sur, S. H., Mistlberger, R. E., and Morris, M. (1999). Circadian blood pressure and heart rate rhythms in mice. *Am. J. Physiol.* 276 (2), R500–R504. doi:10.1152/ajpregu.1999.276.2.R500

Linz, D., McEvoy, R. D., Cowie, M. R., Somers, V. K., Nattel, S., Levy, P., et al. (2018). Associations of obstructive sleep apnea with atrial fibrillation and continuous positive airway pressure treatment: a review. *JAMA Cardiol.* 3 (6), 532–540. doi:10.1001/jamacardio.2018.0095

Linz, D., Schotten, U., Neuberger, H. R., Bohm, M., and Wirth, K. (2011). Negative tracheal pressure during obstructive respiratory events promotes atrial fibrillation by vagal activation. *Heart rhythm.* 8 (9), 1436–1443. doi:10.1016/j.hrthm.2011.03.053

Liu, C., Ma, N., Guo, Z., Zhang, Y., Zhang, J., Yang, F., et al. (2022). Relevance of mitochondrial oxidative stress to arrhythmias: innovative concepts to target treatments. *Pharmacol. Res.* 175, 106027. doi:10.1016/j.phrs.2021.106027

Lu, W. D., and Chen, J. Y. (2021). Atrial high-rate episodes and risk of major adverse cardiovascular events in patients with dual chamber permanent pacemakers: a retrospective study. *Sci. Rep.* 11 (1), 5753. doi:10.1038/s41598-021-85301-7

McEvoy, R. D., Antic, N. A., Heeley, E., Luo, Y., Ou, Q., Zhang, X., et al. (2016). CPAP for prevention of cardiovascular events in obstructive sleep apnea. *N. Engl. J. Med.* 375 (10), 919–931. doi:10.1056/NEJMoa1606599

Mehra, R., Chung, M. K., Olshansky, B., Dobrev, D., Jackson, C. L., Kundel, V., et al. (2022). Sleep-disordered breathing and cardiac arrhythmias in adults: mechanistic insights and clinical implications: a scientific statement from the American heart association. *Circulation* 146 (9), e119–e136. doi:10.1161/CIR.0000000000001082

Nattel, S., Heijman, J., Zhou, L., and Dobrev, D. (2020). Molecular basis of atrial fibrillation pathophysiology and therapy: a translational perspective. *Circ. Res.* 127 (1), 51–72. doi:10.1161/CIRCRESAHA.120.316363

Patil, S. P., Ayappa, I. A., Caples, S. M., Kimoff, R. J., Patel, S. R., and Harrod, C. G. (2019). Treatment of adult obstructive sleep apnea with positive airway pressure: an American academy of sleep medicine clinical practice guideline. *J. Clin. Sleep. Med.* 15 (2), 335–343. doi:10.5664/jcsm.7640

Peker, Y., Glantz, H., Eulenburg, C., Wegscheider, K., Herlitz, J., and Thunstrom, E. (2016). Effect of positive airway pressure on cardiovascular outcomes in coronary artery disease patients with nonsleepy obstructive sleep apnea. The RICCADSA randomized controlled trial. *Am. J. Respir. Crit. Care Med.* 194 (5), 613–620. doi:10.1164/rccm.201601-0088OC

Pellicena, P., and Schulman, H. (2014). CaMKII inhibitors: from research tools to therapeutic agents. *Front. Pharmacol.* 5, 21. doi:10.3389/fphar.2014.00021

Pengo, M. F., Soranna, D., Giontella, A., Perger, E., Mattaliano, P., Schwarz, E. I., et al. (2020). Obstructive sleep apnoea treatment and blood pressure: which phenotypes predict a response? A systematic review and meta-analysis. *Eur. Respir. J.* 55 (5), 1901945. doi:10.1183/13993003.01945-2019

Pieske, B., Maier, L. S., Piacentino, V., Weisser, J., Hasenfuss, G., and Houser, S. (2002). Rate dependence of [Na+]i and contractility in nonfailing and failing human myocardium. *Circulation* 106 (4), 447–453. doi:10.1161/01.cir.0000023042.50192.f4

Randerath, W., Verbraecken, J., Andreas, S., Arzt, M., Bloch, K. E., Brack, T., et al. (2017). Definition, discrimination, diagnosis and treatment of central breathing disturbances during sleep. *Eur. Respir. J.* 49 (1), 1600959. doi:10.1183/13993003.00959-2016

Sapia, L., Palomeque, J., Mattiazzi, A., and Petroff, M. V. (2010). Na+/K+-ATPase inhibition by ouabain induces CaMKII-dependent apoptosis in adult rat cardiac myocytes. *J. Mol. Cell. Cardiol.* 49 (3), 459–468. doi:10.1016/j.yjmcc.2010.04.013

Sossalla, S., Kallmeyer, B., Wagner, S., Mazur, M., Maurer, U., Toischer, K., et al. (2010). Altered Na(+) currents in atrial fibrillation effects of ranolazine on arrhythmias and contractility in human atrial myocardium. *J. Am. Coll. Cardiol.* 55 (21), 2330–2342. doi:10.1016/j.jacc.2009.12.055

Tkacova, R., Rankin, F., Fitzgerald, F. S., Floras, J. S., and Bradley, T. D. (1998). Effects of continuous positive airway pressure on obstructive sleep apnea and left ventricular afterload in patients with heart failure. *Circulation* 98 (21), 2269–2275. doi:10.1161/01.cir.98.21.2269

Traaen, G. M., Aakeroy, L., Hunt, T. E., Overland, B., Bendz, C., Sande, L. O., et al. (2021). Effect of continuous positive airway pressure on arrhythmia in atrial fibrillation and sleep apnea: a randomized controlled trial. *Am. J. Respir. Crit. Care Med.* 204 (5), 573–582. doi:10.1164/rccm.202011-4133OC

Trum, M., Riechel, J., Schollmeier, E., Lebek, S., Hegner, P., Reuthner, K., et al. (2024). Empagliflozin inhibits increased Na influx in atrial cardiomyocytes of patients with HFpEF. *Cardiovasc Res.*, cvae095. doi:10.1093/cvr/cvae095

Voigt, N., Heijman, J., Wang, Q., Chiang, D. Y., Li, N., Karck, M., et al. (2014). Cellular and molecular mechanisms of atrial arrhythmogenesis in patients with paroxysmal atrial fibrillation. *Circulation* 129 (2), 145–156. doi:10.1161/CIRCULATIONAHA.113.006641

Wagner, S., Dybkova, N., Rasenack, E. C., Jacobshagen, C., Fabritz, L., Kirchhof, P., et al. (2006). Ca2+/calmodulin-dependent protein kinase II regulates cardiac Na+ channels. *J. Clin. Investig.* 116 (12), 3127–3138. doi:10.1172/JCI26620

Wagner, S., Ruff, H. M., Weber, S. L., Bellmann, S., Sowa, T., Schulte, T., et al. (2011). Reactive oxygen species-activated Ca/calmodulin kinase IIδ is required for late I(Na) augmentation leading to cellular Na and Ca overload. *Circ. Res.* 108 (5), 555–565. doi:10.1161/CIRCRESAHA.110.221911

Wan, E., Abrams, J., Weinberg, R. L., Katchman, A. N., Bayne, J., Zakharov, S. I., et al. (2016). Aberrant sodium influx causes cardiomyopathy and atrial fibrillation in mice. *J. Clin. Investig.* 126 (1), 112–122. doi:10.1172/JCI84669

Wester, M., Arzt, M., Sinha, F., Maier, L. S., and Lebek, S. (2023). Insights into the interaction of heart failure with preserved ejection fraction and sleep-disordered breathing. *Biomedicines* 11 (11), 3038. doi:10.3390/biomedicines11113038

frontiers | Frontiers in Pharmacology

TYPE Original Research
PUBLISHED 12 July 2024
DOI 10.3389/fphar.2024.1409321

OPEN ACCESS

EDITED BY
Simon Lebek,
University of Regensburg, Germany

REVIEWED BY
Amit Kumar,
Virginia Commonwealth University, United States
Ana Fernanda Castillo,
University of Buenos Aires, Argentina

*CORRESPONDENCE
Xiaofeng Ye,
xiaofengye@hotmail.com
Qiang Zhao,
zq11607@rjh.com.cn

†These authors take responsibility for all aspects of reliability and freedom from bias of the data presented and their discussed interpretation

RECEIVED 29 March 2024
ACCEPTED 07 June 2024
PUBLISHED 12 July 2024

CITATION
He X, Long Q, Zhong Y, Zhang Y, Qian B, Huang S, Chang L, Qi Z, Li L, Wang X, Yang X, Dong Gao W, Ye X and Zhao Q (2024), Short-chain fatty acids regulate erastin-induced cardiomyocyte ferroptosis and ferroptosis-related genes.
Front. Pharmacol. 15:1409321.
doi: 10.3389/fphar.2024.1409321

Short-chain fatty acids regulate erastin-induced cardiomyocyte ferroptosis and ferroptosis-related genes

Xiaojun He[1†], Qiang Long[1], Yiming Zhong[1], Yecen Zhang[1], Bei Qian[1], Shixing Huang[1], Lan Chang[1], Zhaoxi Qi[1], Lihui Li[1], Xinming Wang[1], Xiaomei Yang[2,3,4], Wei Dong Gao[5], Xiaofeng Ye[1*] and Qiang Zhao[1*†]

[1]Department of Cardiovascular Surgery, Ruijin Hospital, Shanghai Jiaotong University School of Medicine, Shanghai, China, [2]Department of Anesthesiology, Qilu Hospital, Cheeloo College of Medicine, Shandong University, Jinan, China, [3]School of Medicine, Cheeloo College of Medicine, Shandong University, Jinan, China, [4]Department of Cardiology, Johns Hopkins School of Medicine, Baltimore, MD, United States, [5]Department of Anesthesiology and Critical Care Medicine, Johns Hopkins University School of Medicine, Baltimore, MD, United States

Background: Ferroptosis has been proven to contribute to the progression of myocardial ischemia/reperfusion (I/R) injury and can be inhibited or promoted by ATF3. Short-chain fatty acids (SCFAs) have shown benefits in various cardiovascular diseases with anti-inflammatory and antioxidant effects. However, the impact of SCFAs on ferroptosis in ischemic-stimulated cardiomyocytes remains unknown. This study aimed to investigate the effect of SCFAs on cardiomyocyte ferroptosis, the expression of ATF3, and its potential upstream regulators.

Methods and results: The expression of ATF3, ferroptosis pathway geneset (*FPG*), and geneset of potential regulators for ATF3 (*GPRA*, predicted by the PROMO database) was explored in the public human myocardial infarction single-cell RNA-seq (sma) dataset. Cardiomyocyte data was extracted from the dataset and re-clustered to explore the FPG, ATF3, and GPRA expression patterns in cardiomyocyte subclusters. A dose-dependent toxic experiment was run to detect the suitable dose for SCFA treatment. The erastin-induced ferroptosis model and hypoxia-reoxygenation (H/R) model (10 h of hypoxia followed by 6 h of reoxygenation) were adopted to assess the effect of SCFAs via the CCK8 assay. Gene expression was examined via RT-PCR and western blot. Ferroptosis markers, including lipid peroxides and Fe^{2+}, were detected using the liperfluo and ferroOrange probes, respectively. In the sma dataset, upregulated ferroptosis pathway genes were mainly found in the infarction-stimulated cardiac cells (border zone and fibrotic zone), particularly the cardiomyocytes and adipocytes. The ATF3 and some of its potential transcription factors (*VDR, EGR3*, *PAX5*, and *SP1*) can be regulated by SCFA. SCFA can attenuate erastin-induced lipid peroxidation in cardiomyocytes. SCFA treatment can also reverse erastin-induced Fe^{2+} increase but may strengthen the Fe^{2+} in the H/R model. We also precisely defined a ferroptosis subcluster of cardiomyocytes (CM09) that highly expressed *FPG*, ATF3, and *GPRA*.

Conclusion: The ATF3 and the ferroptosis pathway are elevated in cardiomyocytes of injury-related cardiac regions (border zone, ischemic zone,

and fibrotic zone). SCFA can attenuate cardiomyocyte ferroptosis and regulate the expression of ATF3. Our study offers novel insights into the potential targets of SCFAs in the cardiovascular system.

KEYWORDS

short-chain fatty acids, cardiomyocytes, ferroptosis, ischemia/reperfusion injury, ATF3

Introduction

Cardiovascular disease remains the leading cause disease of death worldwide annually. Despite progress in acute treatment, the effectiveness of therapies aimed at reducing the progress of heart failure has been limited due to an incomplete understanding of remodeling processes (Niccoli et al., 2019). Over the last 10 years, ferroptosis, an iron- and lipid-dependent form of regulated cell death, has been recognized as an important process involved in numerous cardiovascular diseases (Fang et al., 2023). The inhibition of ferroptosis and chelation of iron during acute and chronic myocardial ischemia/reperfusion (I/R) injury can result in cardioprotection, highlighting ferroptosis as a potential therapeutic target in myocardial I/R injury (Conrad and Proneth, 2019; Fang et al., 2019; Han et al., 2023). Therefore, thoroughly understanding the mechanisms involved in regulating ferroptosis in cardiomyocytes might improve disease management.

The gene *ATF3* (Activating Transcription Factor 3) has been upregulated in cardiomyocyte subtypes activated by myocardial infarction (MI) stimulation (Kuppe et al., 2022). Studies have indicated that ATF3 can function as a cardioprotective molecule, (Ke et al., 2023), elevated at the early stage of cardiac reperfusion, and inhibit cardiomyocyte ferroptosis triggered by erastin and RSL3 (Liu H. et al., 2022). However, ATF3 also has the ability to promote ferroptosis, (Wang et al., 2020; Fu et al., 2021), indicating its complex role as a ferroptosis regulator.

Short-chain fatty acids (SCFAs) are the main product of fiber fermentation by the gut microbiota and have been shown to protect against myocardial ischemia and I/R injury, (Yu et al., 2021; Zhou et al., 2021), but the underlying mechanisms remain to be elucidated. SCFAs can be absorbed into the bloodstream and play important roles in various physiological processes, such as metabolism, gut barrier function, immune regulation, and inflammation (Yang et al., 2020). The glutathione (GSH) synthesis plays an important role in regulating ferroptosis (Kang et al., 2023). Studies have shown that sodium acetate can reverse the increased level of plasma GSH induced by nicotine in rats, (Dangana et al., 2020) and sodium butyrate was reported to aggravate lipid peroxidation in a high-fat diet (HFD)-fed rats, (Oyabambi and Olaniyi, 2023) both of which indicate the impact of SCFAs on ferroptosis. Butyrate has been reported to ameliorate ferroptosis in ulcerative colitis by modulating the Nrf2/GPX4 signal pathway (Chen et al., 2024). However, whether SCFAs benefit against myocardial ischemia and I/R injury was mediated by the regulation of ferroptosis remains unknown.

Given the emerging evidence of a link between ferroptosis and cardiomyocyte injury, there is a need to investigate the impact of SCFAs on ATF3 expression, as well as its potential regulators, and their role in modulating ferroptosis in cardiomyocytes. This study aims to address this knowledge gap and provide further insights into the therapeutic potential of SCFAs in attenuating cardiomyocyte injury and regulating the occurrence of ferroptosis. We provide expression patterns of ferroptosis pathway genes at single-cell resolution based on public human myocardial infarction. Besides, the effects of SCFA on ferroptosis and ATF3 mRNA levels in cardiomyocytes were explored.

Methods

Analysis of single-nucleus RNA sequencing (snRNA-seq) data

The processed spatial multi-omic atlas data (sma) "All-snRNA-Spatial multi-omic map of human Myocardial infarction" was downloaded from the cellxgene database (https://cellxgene.cziscience.com/collections/8191c283-0816-424b-9b61-c3e1d6258a77), and was analyzed by the Seurat (v4.3.0) R package. Cardiomyocyte data was extracted and normalized, followed by principal component analysis (PCA) reduction, batch effect correction with the harmony package, and clustering using Seurat's FindNeighbors and FindClusters function. The Unified Manifold Approximation and Projection (UMAP) was created via Seurat's RunUMAP function. The weighted correlation network analysis (WGCNA) was taken by the hdwgcna R package (Morabito et al., 2021; Morabito et al., 2023). Pseudotime trajectory analysis was taken by the Monocle2 R package (Trapnell et al., 2014; Qiu et al., 2017a; Qiu et al., 2017b). The cell-cell communication was analyzed by the cellchat R package (Jin et al., 2021/02).

The ferroptosis-related genes in KEGG hsa04216 (https://www.kegg.jp/dbget-bin/www_bget?hsa04216) and wikipathways WP4313 (https://www.wikipathways.org/pathways/WP4313.html) were combined as a single geneset. We then calculated the z score (Amrute et al., 2023) of this ferroptosis pathway geneset across cardiac regions and cell types in the sma datasets. The heterogeneity distribution of the ferroptosis pathway geneset was observed.

Potential transcription factors of *ATF3* were predicted by the PROMO database (http://alggen.lsi.upc.es/cgi-bin/promo_v3/promo/promoinit.cgi?dirDB=TF_8.3) with species restricted to humans. The promoter region of *ATF3* was defined as the 2000 upstream bases and 100 downstream bases of the ATF3 gene sequence (hg38_knownGene_ENST00000341491.9, range = chr1:212606761-212620875) and acquired from the UCSC database (https://genome.ucsc.edu/) (Table 1).

The R language code used for single-cell data analysis and the ferroptosis pathway geneset were available in GitHub repositories (https://github.com/Xiao851213/SCFA_Ferroptosis_new/blob/main/20240329).

TABLE 1 ATF3 promoter sequence used for transcription factor prediction.

ATF3 promoter sequence
>hg38_knownGene_ENST00000341491.9 range = chr1:212606761-212620875 5'pad = 0 3'pad = 0 strand = + repeatMasking = none GAGATAACAAATAACTTCATTCAAATGCAAACACTCCTCCACCTAATCCCGCCCGGTGTCCGCCGGGCTGCTCCGACACGCCCGGGGTTTACCTGCGCGCA CTCCAGCGGGAGGGCGGGTTGTGGAGGTGTGCTGAGCGGCGCGCGGGGGTGAGGGCGTGGAAGCGGAGGGTGGGGCCCGGAGAGCCGTTACCAGGGCGA AAAGTAAAGCGAAAACACCCGCCCTGCACTTCCCGCGCGACGCCGCTGGAAATCGGTTCAGGTCCAGAGCAGGATCTCGGAGGATCCCGCGTGGAACTCCAG GGCTCCCGGGTCCGCCGGGGCGCAAAGACTTCCGAGGCCGCCCTCCGCGTGTTCCCAGGCCCGTGGAGAGGTGGGTGGTCTGAGTGAGGTCGGGCTTGGCG GCGAGGAACCCCGGTGGGGGGAACTGGGGACTTCAAGTGAGACCCAGGCTCCAGACACCTCTAGTTTCTACCCCAAATTACCAAACTGTGACCTTCGGCCGC CTCTCTCCCAGAGGCAGGTGGAAAGGAGCAGGTGTTTCTGCCCTTCACCGTGCCCCCACACCCTGCGGCCGCGCAGGTCTCCCTCCCAGGCAGGTGCGAAAG TCCCAGGCCACACTTGTGTCTACAAATAGTCATCCACGGGCAGTCAAGAAGGTTCCTTGGTTCTGCCGCTCTCTGAGCAGAAATTGTTGGGGTCGGGGAATAA GAACCAGGAAATCGTTTTTAAGGTTCAAACCCAGTTCTGCTGAGGTCTCAGCTCGAATCTCGGACCACGGGGCCCCGCCTTTCCCGCCACCCTGGCTTGAGG GCAGAGGGGATTTCTGCTGCGGGTTCCGCCTGTGGTCATTGCGTCCCCATTCCGGGCCGTCCGGTCCCAGTCCAATCGGCTCTGGGAGCAGAAGAACACGTG AAAGCTGAACATGGGTTTTCCCTAAATATTGCCTGAGAGCGGGGCGACCCCCAGGCCTGGGCAGGTTCGCGGACCCCAAAGCACCTTCTCTTTCCCCCTCCTC CTGGCCGCTGGCTTCCGCCCCCTCCTACCCTCCCACCGGGTTGCCTCTGATTCCTCCTGGACTCCGATCTTTTCACGCTCTTGTTGGTTTCACTGACATGTTC TTGTCAATTTCAAACGCTTTGTGATTGTAAAAAAAAAAAAATCGAACCGATACGGTCCTACCACTCGCCCTAGTTTCGGAGCCCGGAGCTGTCCTGCGTGTGC GTCCATGTGGAGTGTCCGGGGCTGCGGGCTCGGGCGCACGGTGCCAGCCGAGGGCTGCCCTCCGCTTTTGTGTTAACCGGCGGGCTTCTCGCGGTCCCCGCC GCAGAGGTCACACCCGGCGGGTAACGGCGTGGATACACCGAAGGGTGACTTTGGACACCTTCCCCACACCACAGACTAACGCTTCTGCCCCTACTCCGCCCCT GCTAGAGAAGTAGGAGGCCAGTGGGGGAGGGGGTATTTTCCTGAAGCTCCAGAAAATGACCACGCATTTTAGAGAAAGGTCGTGCCCGCTTCCCAGCCTCAC CTAGTCTGGGCTGGGGCCGGGACCCGCCTCCCCACCTTCCCCGCCCCCCCCCGCTCTTCAACCTAGCGGAGGGACAGATGCCAGCGCGGTGGAGTCATGCCGC TGGCTTGGGCACCATTGGTCATGCCTGGAACACGCAGCAGCGAGTACGCACATCTGGCGGCTATCCCGGGCGGCTCCGGTCCTGATATGGAGAGAGAGGGC GGGCTGGTGTGTGTCTCAGTGAGCGAGGCTGGGGGAACGCGCCTGGGCTGGCTCCTCCCCGAACTTGCATCACCAGTGCCCCCTCTCTCCACCCGCCTTCGG CCCCGCCTTGGCCCCTCCTCCACCCCCCTTCCTCCGCTCCGTTCGGCCGGTTCTCCCGGGAAGCTATTAATAGCATTACGTCAGCCTGGGACTGGCAACACGG AGTAAACGACCGCGCCGCCAGCCTGAGGGCTATAAAAGGGGTGATGCAACGCTCTCCAAGCCCATGTGTTGTGCTGGTTTCTGTTCATTTAAATCTGTCGGTT GCTGAGACCTAGCGATTCCCTGCCTTTCCCTCCCCATTATGGGGGGTGCCTAGCTTTAA

Cell culture

The human AC16 cardiomyocytes (cat. #C1360, WHELAB, China) and murine HL1 cardiomyocytes (cat. #C2173, WHELAB, China) were cultured in a humidified incubator (5% CO2, 37°C) with the Dulbecco's modified Eagle's (DMEM)/F12 1:1 medium (cat. #CB003, Shanghai Epizyme Biomedical Technology Co., Ltd, Shanghai, China) supplemented with 12.5% fetal bovine serum (FBS, cat. #S711-001S, the Lonsera) and penicillin/streptomycin (100 U/mL, 100 U/mL, cat. #CB010, Shanghai Epizyme Biomedical Technology Co., Ltd., Shanghai, China). Cells at 70%–80% confluence were used for subsequent experiments.

Hypoxia-reoxygenation injury model

The hypoxia-reoxygenation (H/R) model was induced using the AnaeroPack™ (anaerobic cultivation set) with an airtight container (a 2.5 L rectangle jar, Mitsubishi gas chemical, Japanese) (Wen et al., 2021). In detail, cells cultured for 1 day were washed twice with phosphate-buffered saline (PBS), cultured in sugar and serum-free DMEM, and then placed into a sealed airtight container that contains an AnaeroPack, the oxygen concentration decreased to <0.1% within 1 hour, and the carbon dioxide concentration was maintained at about 5%. Hypoxia was continued for 10 h and terminated by removing the culture bottle from the airtight container and replacing it with a standard culture medium in a CO_2 incubator at 37°C for 6 h.

SCFA exposure

To assess the impact of SCFAs on the viability of cardiomyocytes *in vitro*, AC16 cells were seeded in 96-well plates for 24 h with DMEM/F12 containing 12.5% FBS. The cells were then treated with either sodium acetate (NaAc, cat. #S116319, Aladdin, Shang, China), sodium butyrate (NaBu, cat. #S102954, Aladdin, Shanghai, China), sodium propionate (NaPr, cat. #S100121, Aladdin, Shanghai, China), or a SCFA mixture (NaAc: NaPr: NaBu ≈ 30:2:1) for 24 h.

The detectable physiological levels of SCFA are in the range of (acetate 0–410 μM; propionate 0–18.3 μM; butyrate 0–81 μM, including blood, cerebrospinal fluid (CSF), breast milk, and urine; Human Metabolome Database, http://www.hmdb.ca/) and the relative levels of the three SCFAs correspond to approximately 30:2:1 for acetate: propionate: butyrate (Yang et al., 2020). The physical and upper physiological levels of concentrations were adopted to obtain a dose-dependent curve. The concentrations of the SCFAs are presented in Table 2.

Ferroptosis model induction and assessment

The ferroptosis model was induced by erastin (cat. #S7242, Selleck), a typical ferroptosis inducer (Yan et al., 2022). Erastin was diluted to a 10 mM working stock solution with dimethylsulfoxide (DMSO). AC16 cells were seeded in 96-well plates for 24 h with DMEM/F12 containing 12.5% FBS, followed by exposure to 10 μM erastin for 24 h (Wu et al., 2023).

A Liperfluo probe (cat. #L248, Dojindo Molecular Technologies, Inc.) was used to evaluate cellular lipid peroxidation. Cells after the indicated treatments were washed with serum-free DMEM and incubated with 5 μM Liperfluo for 30 min at 37°C (Nakamura et al., 2023). The intracellular Fe^{2+} was detected by the FerroOrange probe (cat. #F374, Dojindo Molecular Technologies, Inc.). Cells were incubated with 1 μM FerroOrange for 30 min at 37°C (Tian et al., 2021). Stained cells were observed using confocal scanning microscopy. The fluorescence of each group was evaluated using ImageJ software.

CCK-8 assay

Cell viability was assessed using the cell counting kit-8 (CCK-8, cat. #CX001S, Shanghai Epizyme Biomedical Technology Co., Ltd,

TABLE 2 Short-chain fatty acid concentrations used in this study.

SCFA concentration	C0	C1	C2	C3	C4	C5	C6	C7
Mixture	0	NaAc (3 μM) + NaPr (0.2 μM) + NaBu (0.1 μM)	NaAc (30 μM) + NaPr (2 μM) + NaBu (1 μM)	NaAc (300 μM) + NaPr (20 μM) + NaBu (10 μM)	NaAc (3 mM) + NaPr (0.2 mM) + NaBu (0.1 mM)	NaAc (30 mM) + NaPr (2 mM) + NaBu (1 mM)	NaAc (300 mM) + NaPr (2 mM) + NaBu (1 mM)	NaAc (3 M) + NaPr (0.2 M) + NaBu (0.1 M)
NaAc	0	3 μM	30 μM	300 μM	3 mM	30 mM	300 mM	3 M
NaPr	0	0.2 μM	2 μM	20 μM	200 μM	2 mM	20 mM	200 mM
NaBu	0	0.1 μM	1 μM	10 μM	100 μM	1 mM	10 mM	100 mM

The mixture consists of sodium acetate (NaAc), sodium propionate (NaPr), and sodium butyrate (NaBu) with concentrations in the same column of the table; for example, the C1 mixture = NaAc (3 μM): NaPr (0.2 μM): NaBu (0.1 μM).

Shanghai, China). Briefly, cells were incubated with fresh medium (containing 10% CCK-8 reagent) for 2 h. The optical density at 450 nm (OD450) was determined by a microplate reader (BioTek, United States) and normalized to blank wells (cell-free medium with CCK-8 reagent).

Quantification of mRNA levels

Total RNA was acquired using a TRIzol reagent (cat. #R0016, Beyotime, Shanghai, China) and an RNA extraction kit (cat. #A2010A0402, BioTNT, Shanghai, China). The concentration was analyzed with a Nanodrop 8000 spectrophotometer (Thermo Fischer Scientific), with concentration at 50–120 ng/μL and A260/A280 of 1.8–2.1 for all samples. RNA was converted into cDNA using a reverse transcription kit (Wuhan servicebio Technology CO., LTD, Wuhan, China). Then, RT-PCR was performed using SYBR Green qPCR Master Mix (Wuhan servicebio Technology CO., Ltd., Wuhan, China); expression was detected using a fast real-time PCR system (CFX Connect, Bio-rad, CA, United States). Cycle counts for mRNA quantification were normalized to GAPDH. Relative expression (ΔCt) and quantification (RQ = $2^{-\Delta\Delta C}$) for each mRNA were calculated using the ΔΔCt method. All reactions were performed according to the manufacturer's instructions. All primers were verified for producing a single specific PCR product via melting curve analysis. The primers used in the study are presented in Table 3.

Western blot

Total cellular proteins were extracted using RIPA lysis buffer (cat. #FD008, HANGZHOU FUDE BIOLOGICAL TECHNOLOGY CO. LTD., China), ultrasonic lysis machine (cat. #VCX130, Sonics & Materials, INC. United States), and metal bath (cat. #HB120-S, DragonLab DWB, China). Proteins were separated via electrophoresis on a 4%–20% SDS gel (cat. #36250ES10, YEASEN, China) and transferred to PVDF membranes (cat. #IPVH00010, Millipore, Germany). After blocking with 5% bovine serum albumin (BSA, cat. #V908933, Merk, Germany) for 1 h, The PVDF membranes were incubated with primary antibodies, including anti-GAPDH (1:5000, cat. #A19056, ABclonal, China) (Bian et al., 2024), anti-ATF3 (1:1000, cat. #A13469, Abclonal, China) (Li et al., 2023; Liu et al., 2023), and anti-GPX4 (1:1000, cat. #CL488-67763, PTG, China) (Wang L. et al., 2022) antibodies at 4°C for >10 h. Subsequently, the membranes were incubated with the HRP-conjugated Goat anti-Rabbit/Mouse IgG (H + L) (cat. #AS014 & AS003, Abclonal, China) for 1 hour at room temperature. The protein bands were visualized with a Fdbio-Dural ECL Chemiluminescence Kit (cat. #FD8020, HANGZHOU FUDE BIOLOGICAL TECHNOLOGY CO. LTD., China) and imaged.

Results

The relationship between ATF3 and ferroptosis pathway in ischemic heart

Our research delves into the crucial topic of the ferroptosis pathway genes and the pivotal role of ferroptosis regulator ATF3 in myocardial infarction. To create a comprehensive ferroptosis pathway geneset (FPG), we combined the genes in KEGG hsa04216 and wikipathways WP431. We then calculated the z score of this ferroptosis pathway geneset across cardiac regions and cell types in the published spatial multi-omic atlas dataset (the sma dataset) (Kuppe et al., 2022). This dataset provides an integrative high-resolution map of human cardiac remodeling after myocardial infarction using single-nucleus RNA sequencing (snRNA-seq), single-nucleus chromatin accessibility, and spatial transcriptomic profiling method. The dataset includes 31 samples from 23 individuals, including four non-transplanted donor hearts as controls (CTRL), and samples from tissues with necrotic areas (ischaemic zone (IZ) and border zone (BZ)) and the unaffected left ventricular myocardium (remote zone (RZ)) of patients with acute myocardial infarction. Nine human heart specimens at later stages after myocardial infarction that exhibited ischaemic heart disease were defined as fibrotic zone (FZ) samples. The snRNA-seq part of the sma dataset (191,795 cells included) was extracted for analysis in this study. Figure 1A illustrates the whole cells, identified cell types, and region sources of the sma snRNA-seq dataset. Potential regulators of ATF3 were predicted via the PROMO database (Supplementary Figure S1A) and combined as a geneset of potential regulators for ATF3 (*GPRA*).

In the sma snRNA-seq dataset, BZ samples have the largest proportion of cells with upregulated *FPG* (Figure 1B). When divided

by cell types, *FPG* was enriched in adipocytes, myeloid, cardiomyocytes, and mast cells (Figure 1C). The FZ tissue has the most significant proportion of ATF3$^+$ cells (Figure 1D). Elevated expression of ATF3 was also observed in IZ cells (Figure 1E). The relative enrichment of *FPG*, ATF3, and *GPRA* for different cell types differed among region groups (Supplementary Figure S2). In the BZ, there was the same elevation trend of *FPG*, ATF3, and *GPRA* in cardiomyocytes, adipocytes, and cycling cells [a cluster with enriched cell-cycle marker gene MKI67 and showed a high score of cell-cycle G2/M and S phases (Kuppe et al., 2022)]. This indicates the involvement of ATF3 and its potential transcription factors in the ferroptosis of cardiomyocytes, adipocytes, and cycling cells during post-MI cardiac remodeling.

In cardiomyocytes, *FPG* was upregulated in injury-related cells (BZ and FZ), while ATF3 and GPRA were mostly enriched in FZ (Figure 1F). The elevation of ATF3 was also found in IZ cardiomyocytes (Figure 1G). To identify the cardiomyocyte subpopulation that is critical to ferroptosis, we extracted cardiomyocyte data from the sma snRNA-seq dataset, corrected the batch effect (Supplementary Figure S3A, B), and re-clustered according to cell density on the Uniform manifold approximation and projection (UMAP) plot to recognize the subclusters of each region (Supplementary Figure S3C). Cardiomyocytes were clustered into 14 subpopulations, which are CM0-CM13 (Figure 1H; Supplementary Figure S4). The *FPG* was enriched in the FZ cluster CM09 (top marker genes: *ABRA*, *DDIT3*, and *OTUD1*) and the BZ cluster CM02 (top marker genes: UBASH3B, C4orf54, NRXN3). The co-enrichment of FPG, ATF3, and GPRA were also observed in cardiomyocytes' CM09 and CM02 clusters (Figure 1I; Supplementary Figure S4B). In conclusion, ATF3 may involved but partially regulates ferroptosis pathway genes in myocardial infarction.

SCFA regulates ferroptosis in the physiological and pathophysiological condition

We then adopted human (AC16 cell line) and murine (HL1 cell line) cardiomyocytes to study the effect of SCFAs on ferroptosis and ATF3 expression at physiological conditions, 1 h-hypoxia exposure, hypoxia-reoxygenation (H/R) model, and erastin-induced ferroptosis model. A dose-dependent toxic experiment was run to detect the suitable dose for SCFA treatment. The concentration of acetate, propionate, butyrate, and SCFA mixture was divided into seven levels (Table 2). The 24-h treatment of SCFAs with the C6 and C7 concentrations decreased cell viability (Supplementary Figure S5). In the 1-h hypoxia model, SCFAs (sodium propionate (NaPr), sodium butyrate (NaBu), and mixture) significantly and consistently decrease cardiomyocyte viability (Supplementary Figure S5B). The C5 level concentration (the maximum dose that does not reduce cell viability) was adopted for the following experiments.

SCFA treatment can promote the mRNA expression level of *ATF3*, either in mice (normal and 1h-hypoxia model, Figure 2A) or human cardiomyocyte cell line (normal, 1h-hypoxia exposure), H/R exposure (10-h hypoxia plus 6-h re-oxygen), and erastin-induced ferroptosis model, Figure 2B). The potential promoters of ATF3 (*VDR, EGR3*, *PAX5*, and *SP1*) were also affected by 24-h SCFA exposure. In the murine cardiomyocyte cell line, NaPr and NaBu upregulated *VDR* under both normal and hypoxic conditions, while hypoxia attenuated the *VDR* upregulation by NaPr. *EGR3* was upregulated by either a single or a mixture of SCFA. The effect of sodium acetate (NaAc) and the SCFA mixture on *EGR3* was attenuated by 1-h hypoxia exposure (Figure 2A). In the human cardiomyocyte cell line, VDR and SP1 were upregulated by SCFA mixture in 1-h hypoxia exposure and H/R model (Figure 2B, upper & middle panel). SCFA mixture promotes the expression of PAX5 in the H/R model but not the 1-h hypoxia model (Figure 2B, upper & middle panel). In the erastin-induced ferroptosis model, *VDR* and *EGR3* were increased under SCFA mixture stimulation (Figure 2B, lower panel).

We also detected the effect of SCFA on the ATF3 protein level. The results were totally opposite to those of the mRNA level. SCFA decreased the ATF3 protein in nearly all cases except the 1 h-hypoxia model of the human cardiomyocyte AC16 cell line (Figure 2C). The protein expression of anti-ferroptosis markers, glutathione peroxidase 4 (GPX4), was inhibited by the SCFA mixture except in the 1h-hypoxia model of the mouse cardiomyocyte HL1 cell line.

SCFA treatment can increase the cell viability of AC16 cardiomyocytes in H/R exposure ($p < 0.0001$) but not the erastin-induced ferroptosis model ($p = 0.9984$) (Figure 2D). To confirm the occurrence of ferroptosis, we performed Liperfluo staining and FerroOrange staining in the H/R model and erastin-induced ferroptosis model with or without SCFA rescue (Figures 2E, F). Liperfluo staining showed obvious lipid peroxidation in response to H/R or erastin stimulation. This effect in the erastin stimulation model was rescued by SCFA treatment. In the H/R model, a decrease in lipid peroxides was observed in the SCFA-managed group but without statistical significance. The fluorescence intensity of FerroOrange, a Fe^{2+}-specific probe, increased sharply upon erastin stimulation. SCFA treatment can reverse erastin-induced Fe^{2+} increase but may strengthen the Fe^{2+} in the H/R model.

TABLE 3 Primers for RT-PCR

Genes	Primers
GAPDH	5′-CCTCGTCCCGTAGACAAAATG-3′, 5′-TGAGGTCAATGAAGGGGTCGT-3′
ATF3	5′-CGCTGGAGTCAGTTACCGTCAA-3′, 5′-TTCCGGTGTCCGTCCATTC-3′
VDR	5′-CTGCCTGACCCTGGTGACTT-3′, 5′- CTTGGTGATGCGGCAATCT-3′
EGR3	5′-ACTACAACCTGTACCACCATCCCA-3′, 5′-TGATGGTCTCCAGTGGGGTAAT-3′
PAX5	5′-CATCAAGCCAGAACAGACCACA-3′, 5′-TGACAATAGGGTAGGACTGTGGG-3′
SP1	5′-AAGATGTTGGTGGCAATAATGGG-3′, 5′-GTTGTTGCTGTTCTCATTGGGTG-3′

10.3389/fphar.2024.1409321

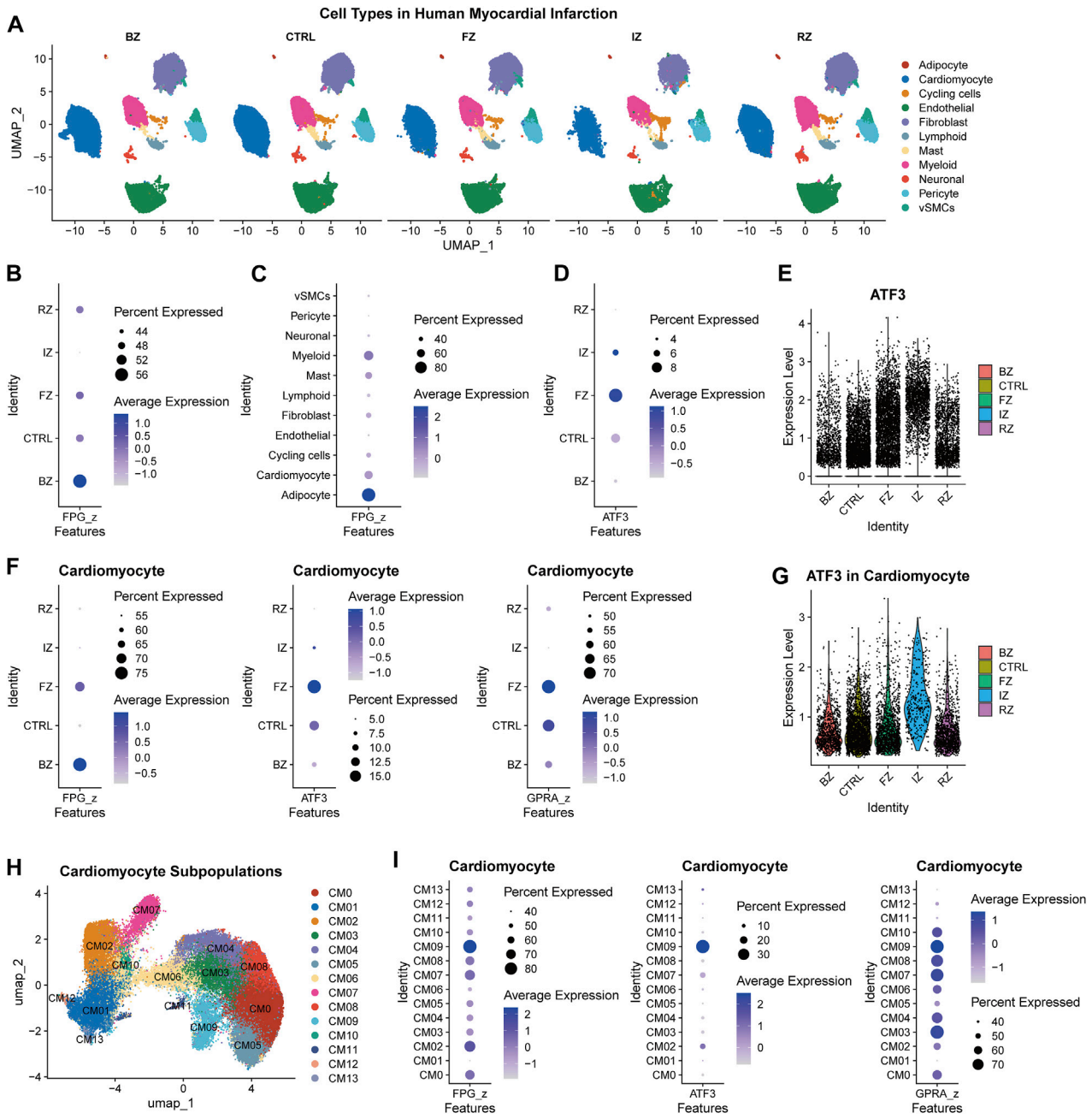

FIGURE 1
The relationship between ATF3 and ferroptosis pathway in ischemic heart **(A)**, Uniform manifold approximation and projection (UMAP) embedding of the single-nuclear RNA-seq data of myocardial infarction heart tissue derived from the spatial multi-omic atlas (sma) study, titled "Spatial multi-omic map of human myocardial infarction" (Christoph Kuppe et al.). Cell types were illustrated in different cardiac regions (BZ, border zone; CTRL, control samples; FZ, fibrotic zone; IZ, ischaemic zone; RZ, remote zone) **(B,C)**, Dot plot illustrating the expression of ferroptosis pathway geneset (*FPG*) among myocardial infarction regions **(B)** and cell types **(C)** **(D)**, The expression of ATF3 among myocardial infarction regions **(E)**, Violin plot of ATF3 expression level across myocardial infarction regions **(F)**, The expression of ferroptosis pathway geneset (*FPG*), ATF3, and geneset of potential regulators for ATF3 (*GPRA*) in different regions of cardiomyocytes **(G)**, Violin plot of ATF3 expression in different regions of cardiomyocytes **(H)**, UMAP of 64,510 cardiomyocytes derived from the sma study **(I)**, The FPG, ATF3, and GPRA expression across cardiomyocyte subclusters.

Discussion

In this study, we found the upregulation of the ferroptosis pathway geneset (derived from the KEGG hsa04216 and wikipathways WP4313) and ATF3 in infarction-stimulated cardiac cells (border zone, ischemic zone, and fibrotic zone), particularly the cardiomyocytes. The ATF3 and some of its potential transcription factors (*VDR*, *EGR3*, *PAX5*, and *SP1*) can be regulated by SCFA. SCFA can attenuate ischemia-reperfusion cell death and erastin-induced lipid peroxidation cardiomyocytes. SCFA treatment can also reverse erastin-induced Fe^{2+} increase but may strengthen the Fe^{2+} in the H/R model. We also precisely defined a

10.3389/fphar.2024.1409321

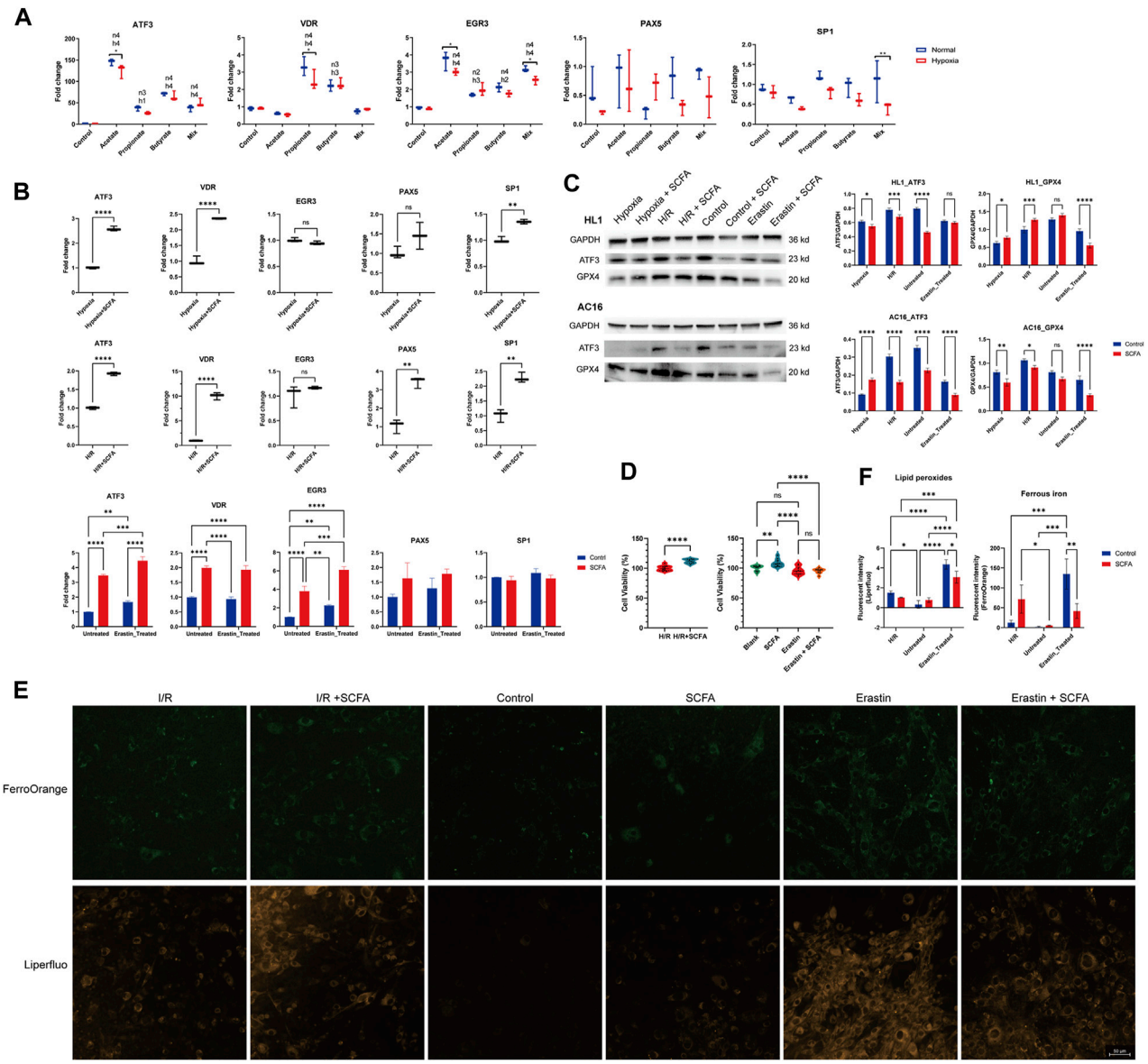

FIGURE 2
Short-chain fatty acids (SCFAs) regulate ferroptosis and ferroptosis-related genes **(A)**, Murine HL1 cardiomyocytes were treated for 24 h with SCFAs and either 1-h hypoxia stimulation or normoxic conditions. Acetate: 30 mM, propionate: 2 mM, butyrate: 1 mM, SCFA mixture: 30 mM acetate, 2 mM propionate, and 1 mM butyrate. *$p < 0.05$ and **$p < 0.01$ for comparisons between the hypoxia and normal conditions groups. h1: $p < 0.05$, h2: $p < 0.01$, h3: $p < 0.001$, h4: $p < 0.0001$, hypoxia group gene expression fold change compared to control. n1: $p < 0.05$, n2: $p < 0.01$, n3: $p < 0.001$, n4: $p < 0.0001$, normal condition group gene expression fold change compared to control **(B)**, Human AC16 cardiomyocytes were treated for 24 h with SCFA (a mixture containing 30 mM acetate, 2 mM propionate, and 1 mM butyrate) and either 1-h hypoxia stimulation (upper panel), H/R (10-h hypoxia plus 6-h re-oxygen, middle panel), or erastin-induced ferroptosis model (10 μM erastin for 24 h, lower panel) **(C)**, HL1 (upper panel) and AC16 cells (lower panel) treated for 24 h with SCFA (a mixture containing 30 mM acetate, 2 mM propionate, and 1 mM butyrate) followed by 1-h hypoxia stimulation, H/R (10-hour hypoxia plus 6-hour re-oxygen), or erastin-induced ferroptosis model (10 μM erastin for 24 h). The ATF3 and GPX4 protein levels were detected via western blot. The density of the plot was quantitated via the ImageJ software. **(D)**, The effect of SCFA on cell viability was tested using the CCK8 method in H/R (10-h hypoxia plus 6-h re-oxygen) and the erastin-induced ferroptosis (10 μM erastin for 24 h) model **(E)**, Effect of SCFA on ferroptosis index in H/R (10-hour hypoxia plus 6-hour re-oxygen) and the erastin-induced (10 μM erastin for 24 h) ferroptosis. Representative Liperfluo and FerroOrange staining images are presented (scale bar: 50 μm) **(F)**, Semiquantitative analysis of the fluorescence intensity of lipid peroxides (detected by Liperfluo) and ferrous iron (detected by FerroOrange). For **(A–D,F)**, Data are expressed as the mean ± SD. Ns, no significance, *$p < 0.05$, **$p < 0.01$, ***$p < 0.001$, ****$p < 0.0001$, calculated by either t-test or two-way ANOVA with Tukey's post hoc test via the GraphPad software. $n = 3$ (3 independent experiments).

ferroptosis subcluster of cardiomyocytes (ABRA$^+$DDIT3$^+$OTUD1$^+$ CM09).

The ATF3, a member of the activator protein 1 (AP-1) transcription factor family, plays a crucial role in various cellular processes, including cell differentiation, apoptosis, proliferation, inflammation, and responses to cellular stress (Hai and Hartman, 2001). It has been noted that ATF3 promotes ferroptosis9, 10 and improves pathological cardiac fibrosis (Wang B. et al., 2022). However, it has also been implicated that ATF3 expression in cardiomyocytes

preserves homeostasis in the heart and controls peripheral glucose tolerance (Kalfon et al., 2017). Otherwise, elevated ATF3 can inhibit cardiomyocyte ferroptosis triggered by erastin and RSL3 (Liu H. et al., 2022). In our study, SCFA may inhibit cardiomyocyte ferroptosis via the regulation of ATF3 expression in either H/R injury or erastin-induced ferroptosis.

The upregulation of these genes in response to SCFAs suggests that SCFAs can potentially influence various downstream cellular processes such as ferroptosis. Ferroptosis is closely linked to specific molecular pathways associated with lipid peroxidation, which can be triggered by intracellular iron supplementation and inhibition of the synthesis of GSH (Kang et al., 2023). Previous research has indicated that NaAc can reverse the nicotine-induced elevation of plasma GSH levels, (Dangana et al., 2020), while NaBu has been shown to exacerbate lipid peroxidation (Oyabambi and Olaniyi, 2023). Consequently, SCFAs have the potential to either promote cell ferroptosis via the GSH inhibition effect or attenuate ferroptosis via the anti-inflammatory and anti-oxidative stress effect. Butyrate could ameliorate ferroptosis in ulcerative colitis by modulating the Nrf2/GPX4 signal pathway and improving the intestinal barrier (Chen et al., 2024).

In our study, SCFA has nearly the opposite effect on the mRNA and protein levels of ATF3 and GPX4. This indicates the post-translational regulation function of SCFA, which is consistent with a previously published article that butyrate could reduce the expression of inflammatory genes via the inhibition of mRNA-stabilizing proteins (Torun et al., 2019). SCFA presented with the attenuation of H/R-induced cell death and erastin-induced cardiomyocyte ferroptosis, proved by the change of cell viability, ferrous iron, and lipid peroxides. While no effect is observed in Supplementary Figure S5A; Figure 2D (right graph) shows that SCFAs increase viability. However, the differences in cell viability between control and SCFA-treated groups are minimal, indicating the limited effect in our studied models and heterogeneity among different experiments.

Our previous study demonstrated that SCFAs exert a negative cardiac inotropic effect both *in vitro* and *in vivo*, providing evidence of their direct impact on cardiac tissue (Poll et al., 2021). NaBu has been reported to offer protection against cardiac I/R injury and induce changes in gene expression within the cardiac tissue. Specifically, these gene expression alterations were observed in pathways related to "signaling molecules and interaction," "immune system," "cell growth and death," and "global and overview maps," including pathways associated with antigen processing and presentation (Yu et al., 2021). Another study published in 2016 demonstrated that NaBu can protect against oxidative stress in HepG2 cells (Xing et al., 2016). These findings strengthen the stability of our study.

The unique elevated ferroptosis level in adipocytes of cardiac tissue was observed in this study, which was not reported before. However, it has been reported that high-altitude hypoxia exposure can induce iron overload and ferroptosis in adipose tissue (Zhang et al., 2022). Since the adipose tissue is a crucial regulator secreting various bioactive factors signaling to myocardial cells, (Liu X. et al., 2022), ferroptosis pathway dysregulation in cardiac adipocytes may play critical roles in responding to cardiac ischemic and I/R injury.

There were some limitations in this study. First, whether SCFA attenuated cardiomyocyte H/R injury via inhibition of ferroptosis still needs to be explored. Second, whether the effects of SCFA on I/R injury and ferroptosis rely on ATF3 regulation remains unknown. On the other hand, there are two direct receptors of SCFA, G-protein coupled receptor 41 (GPR41) and GPR43. The role of GPR41/43 in SCFA benefits has not been studied. These issues will be investigated in future research.

Conclusion

In the heart of myocardial infarction, the ferroptosis pathway is elevated in cardiomyocytes and adipocytes injury-related cardiac regions (border zone, ischemic zone, and fibrotic zone), as well as the ATF3. SCFA can regulate lipid peroxidation and ferrous iron induced by either hypoxia-reoxygenation or erastin. SCFA can promote the stress-responsive and ferroptosis gene ATF3 at the mRNA level but inhibit the protein level. We also identified a distinct subcluster of cardiomyocytes exhibiting a high ferroptosis pathway expression level. These findings shed light on potential targets of SCFAs involved in ferroptosis and their role in conferring protection against cardiac ischemic injury.

Data availability statement

Publicly available datasets were analyzed in this study. This data can be found here: https://cellxgene.cziscience.com/collections/8191c283-0816-424b-9b61-c3e1d6258a77.

Ethics statement

Ethical approval was not required for the studies on humans in accordance with the local legislation and institutional requirements because only commercially available established cell lines were used. Ethical approval was not required for the studies on animals in accordance with the local legislation and institutional requirements because only commercially available established cell lines were used.

Author contributions

XH: Conceptualization, Data curation, Formal Analysis, Funding acquisition, Investigation, Methodology, Project administration, Resources, Software, Validation, Visualization, Writing–original draft, Writing–review and editing. QL: Data curation, Formal Analysis, Methodology, Writing–review and editing. YiZ: Investigation, Methodology, Project administration, Writing–review and editing. YeZ: Data curation, Resources, Writing–review and editing. BQ: Formal Analysis, Software, Writing–review and editing. SH: Data curation, Investigation, Software, Writing–review and editing. LC: Formal Analysis, Resources, Writing–review and editing. ZQ: Conceptualization, Supervision, Writing–review and editing. LL: Formal Analysis, Writing–review and editing. XW: Data curation, Software,

Validation, Visualization, Writing–review and editing. XYa: Formal Analysis, Methodology, Writing–review and editing. WD: Conceptualization, Methodology, Writing–review and editing. XYe: Conceptualization, Validation, Writing–review and editing. QZ: Conceptualization, Methodology, Supervision, Validation, Writing–review and editing.

Funding

The author(s) declare that financial support was received for the research, authorship, and/or publication of this article. This study was funded by the Youth Cultivation Program of Ruijin Hospital Affiliated with Shanghai Jiao Tong University School of Medicine (KY20230221).

Conflict of interest

The authors declare that the research was conducted in the absence of any commercial or financial relationships that could be construed as a potential conflict of interest.

Publisher's note

All claims expressed in this article are solely those of the authors and do not necessarily represent those of their affiliated organizations, or those of the publisher, the editors and the reviewers. Any product that may be evaluated in this article, or claim that may be made by its manufacturer, is not guaranteed or endorsed by the publisher.

Supplementary material

The Supplementary Material for this article can be found online at: https://www.frontiersin.org/articles/10.3389/fphar.2024.1409321/full#supplementary-material

SUPPLEMENTARY FIGURE S1
The screening process to identify transcription factors (TFs) associated with ATF3 **(A)**, Identification of the TFs predicted to associate with the promoter of ATF3, as determined by PROMO software. A total of 83 transcription factors were identified **(B)**, The binding site of VDR, EGR3, PAX5, and SP1 on the promoter region of ATF3.

SUPPLEMENTARY FIGURE S2
The heterogeneity of ferroptosis pathway genes, ATF3, and its promoters geneset **(A)**, Cell types heterogeneity of ferroptosis pathway genes (FPG) in different cardiac regions of the sma dataset **(B)**, Cell types heterogeneity of ATF3 in different cardiac regions of the sma dataset **(C)**, The geneset of potential regulators for ATF3 (*GPRA*) in different cardiac regions of the sma dataset.

SUPPLEMENTARY FIGURE S3
The cardiomyocyte in the published sma dataset **(A)**, The sma single-nuclear cardiomyocytes data before batch correction **(B)**, The sma single-nuclear cardiomyocytes data after batch correction **(C)**, Density estimation of the number of cardiomyocyte nuclei split by the cardiac zone.

SUPPLEMENTARY FIGURE S4
The cardiomyocyte subclusters of human myocardial infarction tissue **(A)**, UMAP of cardiomyocyte subclusters in different zones of the human heart. RZ, remote zone; BZ, border zone; IZ, ischemic zone; FZ, fibrotic zone **(B)**, Top marker genes of the cardiomyocyte subclusters **(C,D)**, Distribution of cardiomyocyte subclusters in different groups **(C)** and samples **(D)**.

SUPPLEMENTARY FIGURE S5
Dose-dependent effect of SCFAs on cardiomyocyte viability. Cell viability of AC16 cells treated with different concentrations of SCFAs (24 h) at normal condition **(A)** or with 1-h hypoxia exposure **(B)**. N = 3. Data are expressed as the mean ± SD. Significance was calculated using one-way ANOVA with Tukey's post hoc test or the t-test. *p*-values < 0.05 were considered statistically significant. **p* < 0.05, ***p* < 0.01, ****p* < 0.001, *****p* < 0.0001, compared to C0 concentration. SCFA concentration (C0–C7) is presented in Table 2.

References

Amrute, J. M., Lai, L., Ma, P., Koenig, A. L., Kamimoto, K., Bredemeyer, A., et al. (2023). Defining cardiac functional recovery in end-stage heart failure at single-cell resolution. *Nat. Cardiovasc Res.* 2 (4), 399–416. doi:10.1038/s44161-023-00260-8

Bian, Z., Yang, F., Xu, P., Gao, G., Yang, C., Cao, Y., et al. (2024). LINC01852 inhibits the tumorigenesis and chemoresistance in colorectal cancer by suppressing SRSF5-mediated alternative splicing of PKM. *Mol. Cancer* 23 (1), 23. doi:10.1186/s12943-024-01939-7

Chen, H., Qian, Y., Jiang, C., Tang, L., Yu, J., Zhang, L., et al. (2024). Butyrate ameliorated ferroptosis in ulcerative colitis through modulating Nrf2/GPX4 signal pathway and improving intestinal barrier. *Biochim. Biophys. Acta Mol. Basis Dis.* 1870 (2), 166984. doi:10.1016/j.bbadis.2023.166984

Conrad, M., and Proneth, B. (2019). Broken hearts: iron overload, ferroptosis and cardiomyopathy. *Cell Res.* 29 (4), 263–264. doi:10.1038/s41422-019-0150-y

Dangana, E. O., Omolekulo, T. E., Areola, E. D., Olaniyi, K. S., Soladoye, A. O., and Olatunji, L. A. (2020). Sodium acetate protects against nicotine-induced excess hepatic lipid in male rats by suppressing xanthine oxidase activity. *Chem. Biol. Interact.* 316, 108929. doi:10.1016/j.cbi.2019.108929

Fang, X., Ardehali, H., Min, J., and Wang, F. (2023). The molecular and metabolic landscape of iron and ferroptosis in cardiovascular disease. *Nat. Rev. Cardiol.* 20 (1), 7–23. doi:10.1038/s41569-022-00735-4

Fang, X., Wang, H., Han, D., Xie, E., Yang, X., Wei, J., et al. (2019). Ferroptosis as a target for protection against cardiomyopathy. *Proc. Natl. Acad. Sci. U S A.* 116 (7), 2672–2680. doi:10.1073/pnas.1821022116

Fu, D., Wang, C., Yu, L., and Yu, R. (2021). Induction of ferroptosis by ATF3 elevation alleviates cisplatin resistance in gastric cancer by restraining Nrf2/Keap1/xCT signaling. *Cell Mol. Biol. Lett.* 26 (1), 26. doi:10.1186/s11658-021-00271-y

Hai, T., and Hartman, M. G. (2001). The molecular biology and nomenclature of the activating transcription factor/cAMP responsive element binding family of transcription factors: activating transcription factor proteins and homeostasis. *Gene* 273 (1), 1–11. doi:10.1016/s0378-1119(01)00551-0

Han, X., Zhang, J., Liu, J., Wang, H., Du, F., Zeng, X., et al. (2023). Targeting ferroptosis: a novel insight against myocardial infarction and ischemia-reperfusion injuries. *Apoptosis* 28 (1-2), 108–123. doi:10.1007/s10495-022-01785-2

Jin, S., Guerrero-Juarez, C. F., Zhang, L., Chang, I., Ramos, R., Kuan, C. H., et al. (2021/02/17 2021). Inference and analysis of cell-cell communication using CellChat. *Nat. Commun.* 12 (1), 1088. doi:10.1038/s41467-021-21246-9

Kalfon, R., Koren, L., Aviram, S., Schwartz, O., Hai, T., and Aronheim, A. (2017). ATF3 expression in cardiomyocytes preserves homeostasis in the heart and controls peripheral glucose tolerance. *Cardiovasc Res.* 113 (2), 134–146. doi:10.1093/cvr/cvw228

Kang, N., Son, S., Min, S., Hong, H., Kim, C., An, J., et al. (2023). Stimuli-responsive ferroptosis for cancer therapy. *Chem. Soc. Rev.* 52 (12), 3955–3972. doi:10.1039/d3cs00001j

Ke, H., Chen, Z., Zhao, X., Yang, C., Luo, T., Ou, W., et al. (2023). Research progress on activation transcription factor 3: a promising cardioprotective molecule. *Life Sci.* 328, 121869. doi:10.1016/j.lfs.2023.121869

Kuppe, C., Ramirez Flores, R. O., Li, Z., Hayat, S., Levinson, R. T., Liao, X., et al. (2022). Spatial multi-omic map of human myocardial infarction. *Nature* 608 (7924), 766–777. doi:10.1038/s41586-022-05060-x

Li, H., Zhang, M., Zhao, Q., Zhao, W., Zhuang, Y., Wang, J., et al. (2023). Self-recruited neutrophils trigger over-activated innate immune response and phenotypic change of cardiomyocytes in fulminant viral myocarditis. *Cell Discov.* 9 (1), 103. doi:10.1038/s41421-023-00593-5

Liu, H., Mo, H., Yang, C., Mei, X., Song, X., Lu, W., et al. (2022a). A novel function of ATF3 in suppression of ferroptosis in mouse heart suffered ischemia/reperfusion. *Free Radic. Biol. Med.* 189, 122–135. doi:10.1016/j.freeradbiomed.2022.07.006

Liu, X., Liu, L., Zhao, J., Wang, H., and Li, Y. (2022b). Mechanotransduction regulates inflammation responses of epicardial adipocytes in cardiovascular diseases. *Front. Endocrinol (Lausanne)* 13, 1080383. doi:10.3389/fendo.2022.1080383

Liu, Y., Cao, Y., Liu, P., Zhai, S., Liu, Y., Tang, X., et al. (2023). ATF3-induced activation of NF-κB pathway results in acquired PARP inhibitor resistance in pancreatic adenocarcinoma. *Cell Oncol (Dordr)*. doi:10.1007/s13402-023-00907-5

Morabito, S., Miyoshi, E., Michael, N., Shahin, S., Martini, A. C., Head, E., et al. (2021). Single-nucleus chromatin accessibility and transcriptomic characterization of Alzheimer's disease. *Nat. Genet.* 53 (8), 1143–1155. doi:10.1038/s41588-021-00894-z

Morabito, S., Reese, F., Rahimzadeh, N., Miyoshi, E., and Swarup, V. (2023). hdWGCNA identifies co-expression networks in high-dimensional transcriptomics data. *Cell Rep. Methods* 3 (6), 100498. doi:10.1016/j.crmeth.2023.100498

Nakamura, T., Hipp, C., Santos Dias Mourão, A., Borggräfe, J., Aldrovandi, M., Henkelmann, B., et al. (2023). Phase separation of FSP1 promotes ferroptosis. *Nature* 619 (7969), 371–377. doi:10.1038/s41586-023-06255-6

Niccoli, G., Montone, R. A., Ibanez, B., Thiele, H., Crea, F., Heusch, G., et al. (2019). Optimized treatment of ST-elevation myocardial infarction. *Circ. Res.* 125 (2), 245–258. doi:10.1161/circresaha.119.315344

Oyabambi, A. O., and Olaniyi, K. S. (2023). Sodium butyrate aggravates glucose dysregulation and dyslipidemia in high fat-fed Wistar rats. *Metabol. Open* 17, 100226. doi:10.1016/j.metop.2022.100226

Poll, B. G., Xu, J., Jun, S., Sanchez, J., Zaidman, N. A., He, X., et al. (2021). Acetate, a short-chain fatty acid, acutely lowers heart rate and cardiac contractility along with blood pressure. *J. Pharmacol. Exp. Ther.* 377 (1), 39–50. doi:10.1124/jpet.120.000187

Qiu, X., Hill, A., Packer, J., Lin, D., Ma, Y. A., and Trapnell, C. (2017b). Single-cell mRNA quantification and differential analysis with Census. *Nat. Methods* 14 (3), 309–315. doi:10.1038/nmeth.4150

Qiu, X., Mao, Q., Tang, Y., Wang, L., Chawla, R., Pliner, H. A., et al. (2017a). Reversed graph embedding resolves complex single-cell trajectories. *Nat. Methods* 14 (10), 979–982. doi:10.1038/nmeth.4402

Tian, R., Abarientos, A., Hong, J., Hashemi, S. H., Yan, R., Dräger, N., et al. (2021). Genome-wide CRISPRi/a screens in human neurons link lysosomal failure to ferroptosis. *Nat. Neurosci.* 24 (7), 1020–1034. doi:10.1038/s41593-021-00862-0

Torun, A., Enayat, S., Sheraj, I., Tunçer, S., Ülgen, D. H., and Banerjee, S. (2019). Butyrate mediated regulation of RNA binding proteins in the post-transcriptional regulation of inflammatory gene expression. *Cell Signal* 64, 109410. doi:10.1016/j.cellsig.2019.109410

Trapnell, C., Cacchiarelli, D., Grimsby, J., Pokharel, P., Li, S., Morse, M., et al. (2014). The dynamics and regulators of cell fate decisions are revealed by pseudotemporal ordering of single cells. *Nat. Biotechnol.* 32 (4), 381–386. doi:10.1038/nbt.2859

Wang, B., Tan, Y., Zhang, Y., Zhang, S., Duan, X., Jiang, Y., et al. (2022b). Loss of KDM5B ameliorates pathological cardiac fibrosis and dysfunction by epigenetically enhancing ATF3 expression. *Exp. Mol. Med.* 54 (12), 2175–2187. doi:10.1038/s12276-022-00904-y

Wang, L., An, H., Yu, F., Yang, J., Ding, H., Bao, Y., et al. (2022a). The neuroprotective effects of paeoniflorin against MPP(+)-induced damage to dopaminergic neurons via the Akt/Nrf2/GPX4 pathway. *J. Chem. Neuroanat.* 122, 102103. doi:10.1016/j.jchemneu.2022.102103

Wang, L., Liu, Y., Du, T., Yang, H., Lei, L., Guo, M., et al. (2020). ATF3 promotes erastin-induced ferroptosis by suppressing system Xc. *Cell Death Differ.* 27 (2), 662–675. doi:10.1038/s41418-019-0380-z

Wen, J., Wang, D., Cheng, L., Wu, D., Qiu, L., Li, M., et al. (2021). The optimization conditions of establishing an H9c2 cardiomyocyte hypoxia/reoxygenation injury model based on an AnaeroPack System. *Cell Biol. Int.* 45 (4), 757–765. doi:10.1002/cbin.11513

Wu, Y. T., Zhang, G. Y., Hua, Y., Fan, H. J., Han, X., Xu, H. L., et al. (2023). Ferrostatin-1 suppresses cardiomyocyte ferroptosis after myocardial infarction by activating Nrf2 signaling. *J. Pharm. Pharmacol.* 75 (11), 1467–1477. doi:10.1093/jpp/rgad080

Xing, X., Jiang, Z., Tang, X., Wang, P., Li, Y., Sun, Y., et al. (2016). Sodium butyrate protects against oxidative stress in HepG2 cells through modulating Nrf2 pathway and mitochondrial function. *J. Physiol. Biochem.* 73 (3), 405–414. doi:10.1007/s13105-017-0568-y

Yan, R., Xie, E., Li, Y., Li, J., Zhang, Y., Chi, X., et al. (2022). The structure of erastin-bound xCT-4F2hc complex reveals molecular mechanisms underlying erastin-induced ferroptosis. *Cell Res.* 32 (7), 687–690. doi:10.1038/s41422-022-00642-w

Yang, L. L., Millischer, V., Rodin, S., MacFabe, D. F., Villaescusa, J. C., and Lavebratt, C. (2020). Enteric short-chain fatty acids promote proliferation of human neural progenitor cells. *J. Neurochem.* 154 (6), 635–646. doi:10.1111/jnc.14928

Yu, Z., Han, J., Chen, H., Wang, Y., Zhou, L., Wang, M., et al. (2021). Oral supplementation with butyrate improves myocardial ischemia/reperfusion injury via a gut-brain neural circuit. *Front. Cardiovasc Med.* 8, 718674. doi:10.3389/fcvm.2021.718674

Zhang, Y., Fang, J., Dong, Y., Ding, H., Cheng, Q., Liu, H., et al. (2022). High-altitude hypoxia exposure induces iron overload and ferroptosis in adipose tissue. *Antioxidants (Basel)* 11 (12), 2367. doi:10.3390/antiox11122367

Zhou, M., Li, D., Xie, K., Xu, L., Kong, B., Wang, X., et al. (2021). The short-chain fatty acid propionate improved ventricular electrical remodeling in a rat model with myocardial infarction. *Food Funct.* 12 (24), 12580–12593. doi:10.1039/d1fo02040d

frontiers | Frontiers in Pharmacology

TYPE Review
PUBLISHED 30 July 2024
DOI 10.3389/fphar.2024.1413123

OPEN ACCESS

EDITED BY
Rhys David Evans,
University of Oxford, United Kingdom

REVIEWED BY
Evangelia Zvintzou,
University of Patras, Greece
Aldo Grefhorst,
Amsterdam University Medical Center,
Netherlands

*CORRESPONDENCE
Xiaoyu Yang,
yangxy1900@zzu.edu.cn

†These authors have contributed equally to this work

RECEIVED 06 April 2024
ACCEPTED 08 July 2024
PUBLISHED 30 July 2024

CITATION
Lu F, Li E and Yang X (2024), Proprotein convertase subtilisin/kexin type 9 deficiency in extrahepatic tissues: emerging considerations. *Front. Pharmacol.* 15:1413123. doi: 10.3389/fphar.2024.1413123

Proprotein convertase subtilisin/kexin type 9 deficiency in extrahepatic tissues: emerging considerations

Fengyuan Lu[1†], En Li[1†] and Xiaoyu Yang [1,2*]

[1]The Second Affiliated Hospital, Zhengzhou University, Zhengzhou, China, [2]School of Basic Medical Sciences, Zhengzhou University, Zhengzhou, China

Proprotein convertase subtilisin/kexin type 9 (PCSK9) is primarily secreted by hepatocytes. PCSK9 is critical in liver low-density lipoprotein receptors (LDLRs) metabolism. In addition to its hepatocellular presence, PCSK9 has also been detected in cardiac, cerebral, islet, renal, adipose, and other tissues. Once perceived primarily as a "harmful factor," PCSK9 has been a focal point for the targeted inhibition of both systemic circulation and localized tissues to treat diseases. However, PCSK9 also contributes to the maintenance of normal physiological functions in numerous extrahepatic tissues, encompassing both LDLR-dependent and -independent pathways. Consequently, PCSK9 deficiency may harm extrahepatic tissues in close association with several pathophysiological processes, such as lipid accumulation, mitochondrial impairment, insulin resistance, and abnormal neural differentiation. This review encapsulates the beneficial effects of PCSK9 on the physiological processes and potential disorders arising from PCSK9 deficiency in extrahepatic tissues. This review also provides a comprehensive analysis of the disparities between experimental and clinical research findings regarding the potential harm associated with PCSK9 deficiency. The aim is to improve the current understanding of the diverse effects of PCSK9 inhibition.

KEYWORDS

PCSK9, PCSK9 deficiency, PCSK9 inhibition, PCSK9 monoclonal antibody, low-density lipoprotein receptors

1 Introduction

Proprotein convertase subtilisin/kexin type 9 (PCSK9) was originally termed neural apoptosis-regulated convertase 1 because of its robust expression in the telencephalons of embryonic mice (Seidah et al., 2003). The expression of PCSK9 correlates with neural progenitor cell differentiation into more abundant neuronal lineages (Seidah et al., 2003). Subsequently identified as the third pathogenic gene associated with familial hypercholesterolemia, along with low-density lipoprotein receptors (LDLRs) and apolipoprotein B (ApoB) genes, PCSK9 has been extensively studied concerning its interplay with lipid homeostasis (Abifadel et al., 2003). The modulation of lipid levels by PCSK9 occurs mainly through the downregulation of LDLRs on the hepatocyte membrane surface, which inhibits the degradation of low-density lipoprotein cholesterol (LDL-C) in circulation (Rudenko et al., 2002; Lagace et al., 2006). Mechanistically, PCSK9 lacks proteolytic activity. Instead, it binds to the epidermal growth factor fragment of LDLR through its catalytic domain, facilitating delivery of LDLR to the

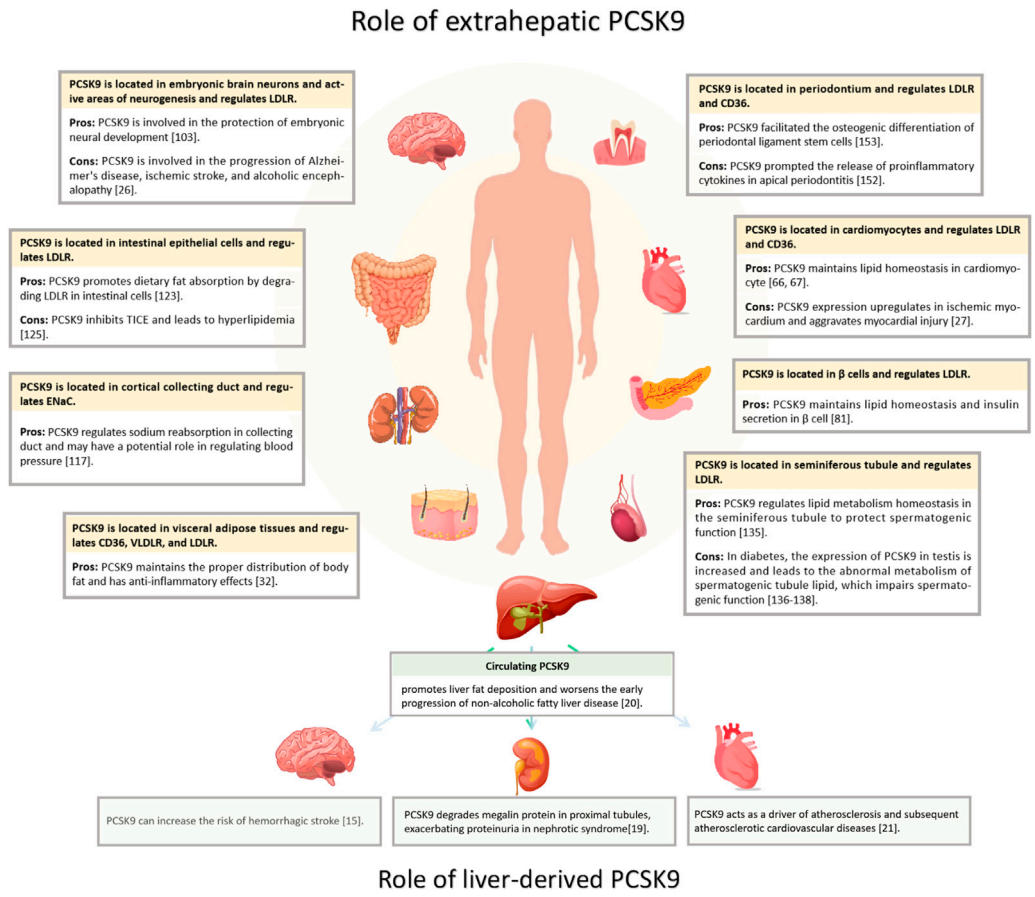

FIGURE 1
Distribution of PCSK9 expression and effects. PCSK9 is located in various extrahepatic organs, including heart, brain, islets, kidney, intestine, testis, and periodontium, and in adipose tissue. The yellow segments indicate PCSK9 locations; Pros, the protective impact of PCSK9; Cons, detrimental effects.

endosome-lysosome for degradation. For example, when Gypenoside LVI is used to inhibit the expression of PCSK9 in HepG2 cells, an increase in the density of LDLR on the HepG2 cell membrane can be detected, along with an observed increase in red fluorescently labeled LDL in the cytoplasm (Wang et al., 2021). Subsequently, PCSK9 re-circulates to the cellular outer membrane to initiate further LDLR interactions (Bottomley et al., 2009; Cui et al., 2015). PCSK9 also orchestrates the degradation of membrane receptors, such as low-density lipoprotein receptor-related protein 1 (LRP1/ApoER) (Fu et al., 2017), low-density lipoprotein receptor-related protein 8 (LRP8/ApoER2) (Poirier et al., 2008), cluster of differentiation 36 (CD36) (Demers et al., 2015), cluster of differentiation 81 (CD81) (Le et al., 2015), very-low-density lipoprotein receptor (VLDLR) (Poirier et al., 2008), and epithelial sodium channel (ENaC) (Sharotri et al., 2012) through a similar pathway. The role of PCSK9 as a predictor of the risk of atherosclerosis is evident from its gain-of-function mutation, which correlates with the occurrence of conditions, such as coronary heart disease (CAD), abdominal aortic aneurysm, peripheral artery disease, and stroke (Ferreira et al., 2020; Qin et al., 2021; Sawada et al., 2022). In contrast, individuals with loss-of-function (LOF) mutations in the PCSK9 gene have lower serum LDL-C levels, which reduces the risk of coronary heart disease and stroke (Kent et al., 2017). These insights substantiate the potential of PCSK9 inhibition as a strategy to lower LDL-C levels. Currently, PCSK9 monoclonal antibodies are the most extensively employed inhibitors. These antibodies reduce serum LDL-C levels by 60%–70% and deliver sustained benefits to individuals with established CAD (ODonoghue et al., 2022).

Hepatic PCSK9 is abundantly expressed and is the primary source of serum PCSK9 (Zaid et al., 2008). Extrahepatic tissues, such as the heart, brain, intestine, kidney, and pancreas, also secrete PCSK9 (Figure 1) (Qin et al., 2021; Momtazi-Borojeni et al., 2022; Boutari et al., 2023; Skeby et al., 2023). PCSK9 operates in an autocrine manner in these tissues and does not constitute circulating PCSK9 (Levy et al., 2013; Barisione et al., 2021; Lin et al., 2021). In the heart, PCSK9 acts as an inflammatory mediator expressed in ischemic myocardial cells, fostering local inflammation and cell death (Wang et al., 2020). In the brain, PCSK9 binds to LRP1 and impedes β-amyloid protein clearance, and interacts with various inflammatory factors, underpinning neurodegenerative conditions like Alzheimer's disease (AD) (Mazura et al., 2022). Therefore, in addition to affecting LDL-C levels, PCSK9 has several other functions, and its inhibition offers a novel therapeutic avenue for extrahepatic organ diseases, such as acute myocardial infarction (AMI) and AD (Abuelezz and Hendawy, 2021).

Although studies have focused on targeted PCSK9 inhibition for disease treatment, it is crucial to acknowledge its role in maintaining normal physiological functions in multiple tissues (Şener and Tokgözoğlu, 2023). The inhibition of PCSK9 increases various lipoprotein receptors, such as LDLR, VLDLR, and CD36, significantly enhancing the ability of cells to absorb lipids (Poirier et al., 2008; Bottomley et al., 2009; Cui et al., 2015; Demers et al., 2015). Unlike the liver, many extrahepatic tissues struggle to manage excessive lipid uptake by redirecting excess cholesterol into the liver through *high-density lipoprotein* packaging (Lewis and Rader, 2005). Thus, PCSK9 deficiency disrupts lipid homeostasis in extrahepatic cells by fostering excessive cholesterol uptake over metabolism, impairing damage to cells (Paul et al., 2016), while also contributing to various physiological activities, including brain nerve development, renal blood pressure regulation, and body fat distribution (Poirier et al., 2006; Baragetti et al., 2017).

This review summarizes the pleiotropic biological functions of PCSK9 and the potential physiological consequences of its deficiency, offering insights into the rationale for the widespread use of PCSK9 inhibitors.

2 PCSK9 gene transcriptional regulation

In vitro, both sterol regulatory element-binding protein 1-c (SREBP1-c) and sterol regulatory element-binding protein 2 (SREBP2) bind to the sterol regulator element (SRE) within the PCSK9 gene promoter, leading to the upregulation of PCSK9 expression (Jeong et al., 2008). However, *in vivo*, the primary regulator of PCSK9 is SREBP2 (Jeong et al., 2008). The expression of SREBP2 can be induced by low sterol concentrations and statin usage (Eberlé et al., 2004; Davignon and Dubuc, 2009). Positioned upstream of the SRE is histone nuclear factor P, which enhances PCSK9 expression by facilitating the acetylation of the PCSK9 promoter histone H4. This process greatly intensifies the transcriptional activity of SREBP2 in PCSK9 (Li and Liu, 2012). As a cholesterol-sensitive transcription factor of PCSK9, E2F transcription factor 1 directly elevates its transcriptional activity or enhances PCSK9 expression by activating SREBP1-c under insulin stimulation (Denechaud et al., 2016; Lai et al., 2017).

The binding sequence for hepatocyte nuclear factor 1-α (HNF1-α), situated 28bp upstream of SRE, is also important in upregulating PCSK9 expression. Mutations in this sequence disrupt the SRE sequence promoter (Li et al., 2009). Forkhead box class O 3a (FoxO3a) acts as an inhibitory transcription factor for PCSK9 and is activated by epigallocatechin gallate derived from green tea. The expression of FoxO3a potentially competes with the action of HNF1-α, inhibiting its effect (Cui et al., 2020). Notably, in a patient with drug-resistant hypercholesterolemia, serum PCSK9 concentrations surged by 15-fold, coinciding with the detection of HNF4-α overexpression, indicating that HNF4-α might also play a role in PCSK9 regulation (Lau et al., 2020). An association between PCSK9 and HNF4-α was also observed in a rat model with partial fat resection (Dettlaff-Pokora et al., 2019).

Further upstream of the SRE, the specificity protein 1 (sp1) binding site is believed to mediate PCSK9 transcription. Mutations at this site lead to significant changes in PCSK9 expression (Blesa et al., 2008; Jeong et al., 2008). The PCSK9 promoter region also features a binding site for carbohydrate-responsive element-binding protein (ChREBP). Metformin acts in a glucose-dependent manner and suppresses PCSK9 expression by inhibiting ChREBP (Hu et al., 2021). A comprehensive overview of the regulatory factors that influence PCSK9 expression is shown in Figure 2 (Costet et al., 2006; Cariou et al., 2010; Chen et al., 2014; Ooi et al., 2015; Levenson et al., 2017; Sponder et al., 2017; Guo WJ. et al., 2021; Sadik et al., 2022).

3 PCSK9 protects lipid metabolism in myocardium

3.1 Cardiomyocyte and lipid toxicity

Cardiomyocytes have substantial energy requirements and exhibit a distinct approach to energy metabolism. Remarkably, 60% of this energy is derived from fatty acid (FA) oxidation, primarily esterified FAs from circulation coupled with *de novo* FA synthesis (Razani et al., 2011). The precise composition of FAs is crucial, because they affect the physiological performance of the heart. Notably, FAs contribute to membrane phospholipids and cardiolipin, which are essential components of both cell and mitochondrial membranes (Chen et al., 2021). Additionally, certain entities, such as prostaglandin E2 (PGE2), PGD2, PGI2, linoleic acid, n-3 polyunsaturated FAs, and their metabolites exhibit cardiovascular safeguarding effects and improve ischemia-reperfusion injury (Moriyama et al., 2022). However, when the supply of FAs surpasses the capacity of β oxidation and storage as triacylglycerol, excessive accumulation of FAs leads to lipotoxicity (Lopaschuk et al., 2021). Clinically, lipotoxicity has been identified as a precursor of myocardial remodeling in cardiomyocytes of patients with diabetes, potentially driving ventricular remodeling and cardiac dysfunction (Ernande et al., 2010; Salvatore et al., 2021). Mechanistically, excessive intake of FAs by cardiomyocytes culminates in the accumulation of detrimental lipid metabolites, such as ceramide and diacylglycerol (DSouza et al., 2016). Concurrently, excessive FA intake disrupts the mitochondrial respiratory chain function and uncouples oxidative phosphorylation, impairing mitochondrial integrity and energy metabolism in cardiomyocytes (Goldberg et al., 2012).

3.2 PCSK9 deficiency in myocardium is associated with heart failure

Heart failure with preserved ejection fraction (HFpEF) is defined as heart failure with an ejection fraction ≥50%. HFpEF is frequently accompanied by metabolic risk factors that include type 2 diabetes mellitus (T2DM), obesity, and hypertension (Schiattarella et al., 2019). At a molecular level, these patients often exhibit cardiomyocyte lipid overload (Schiattarella et al., 2019). Excessive lipid uptake by cardiomyocytes is a pivotal factor in HFpEF (Leggat et al., 2021). Studies have revealed the significance of cardiomyocyte lipoprotein receptors (CD36, LDLR, and VLDLR) as conduits for the uptake and transport of FAs, which are strongly associated with progression of heart failure (Sung et al., 2011). In middle-aged wild

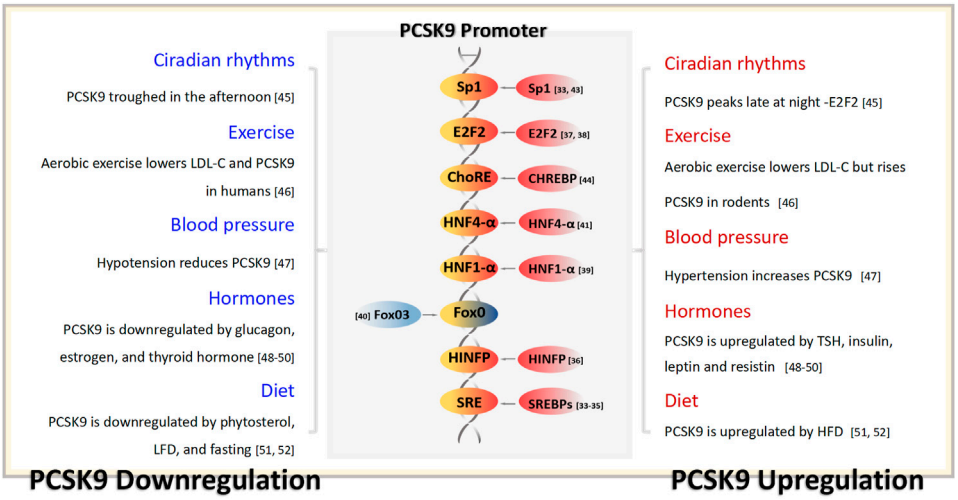

FIGURE 2
PCSK9 transcriptional regulation and the physiological factors capable of influencing the serum concentration of PCSK9. TSH, thyrotropin; LFD, low-fat diets; HFD, low-fat diets.

type (WT) mice fed on a high-fat diet, increased CD36 expression reportedly causes cardiomyocyte hypertrophy (Sung et al., 2011). Patients with diabetes and HFpEF show elevated LDLR expression in the myocardium (Patel et al., 2020). In WT mouse models, VLDLR exacerbates the cardiomyocyte lipid burden and hastens the progression of heart failure (Perman et al., 2011).

Previous studies have confirmed that PCSK9 regulates the degradation of lipid uptake receptors, such as LDLR, CD36, and VLDLR (Poirier et al., 2008; Bottomley et al., 2009; Cui et al., 2015; Demers et al., 2015). Whether PCSK9 deficiency leads to enrichment of these receptors in the cardiomyocyte membrane, and also leads to HEpEF has garnered attention (Da Dalt et al., 2021). Da Dalt et al. first established that PCSK9 knockdown in mice resulted in HFpEF, as evidenced by increased left ventricular posterior wall thickness and reduced exercise capacity (Da Dalt et al., 2021). Cardiomyocytes from PCSK9 knockout mice exhibited elevated LDLR and CD36 levels, accompanied by substantial lipid droplet accumulation around the mitochondria (Da Dalt et al., 2021). The authors also described that, remarkably, liver-specific PCSK9 knockout mice displayed none of these changes, suggesting that myocardial autocrine PCSK9 plays a cardioprotective and lipid regulatory role (Da Dalt et al., 2021). This was further validated in a cardiomyocyte-specific PCSK9 knockout model by Laudette et al. (2023). Reduced PCSK9 expression in the myocardium resulted in signs of heart failure, left ventricular dilatation, myocardial interstitial fibrosis, and pulmonary congestion in middle-aged mice (28 weeks old), ultimately leading to mortality within 8 weeks (Laudette et al., 2023). The authors also described that *in vitro* cultured cardiomyocytes with silenced PCSK9 exhibited changes in mitochondrial membrane lipid components, increased levels of free FAs, decreased electron transfer chain activity, and mitochondrial distortion and breakage (Laudette et al., 2023).

Individuals harboring p.R46L variants accumulate epicardial fat and have an increased left ventricular mass index, despite maintaining a normal left ventricular ejection fraction, underscoring the significance of PCSK9 in cardiomyocyte lipid uptake balance (Baragetti et al., 2017; Da Dalt et al., 2021). However, in another extensive nested case-control study, PCSK9 LOF carriers displayed left ventricular size, ejection fraction, and heart failure prevalence comparable to those in normal individuals (Trudsø et al., 2023).

In summary, PCSK9 is released from the myocardium, rather than from circulation, and actively preserves myocardial lipid homeostasis. The absence of PCSK9 within the myocardium leads to disruption of lipid metabolism, myocardial dysfunction, and potential heart failure. However, PCSK9 LOF carriers in the general population do not exhibit the same degree of myocardial damage as that observed in PCSK9 knockout animals and *in vitro* models. Possible explanations, which remain to be comprehensively examined, include the partial retention of lipid regulatory effects in low-expressing PCSK9 myocardium compared to knockout models or enhanced compensatory mechanisms in human cardiomyocytes against PCSK9 deficiency.

4 PCSK9 protects lipid metabolism in β-cells

4.1 β-cells and lipid toxicity

The American Diabetes Association characterizes T2DM as progressive insulin insufficiency coupled with insulin resistance (2, 2022). Central to T2DM pathology is the demise of islet β-cells, driven by factors like lipid toxicity, glucotoxicity, and amyloid formation (Stumvoll et al., 2005; Eizirik et al., 2020). Excessive cholesterol accumulation within islet cells fosters lipid toxicity, impeding insulin secretion, and inducing β-cell death (Perego et al., 2019; Tricò et al., 2022). The lipid buildup curtails ATP production by inhibiting glycolysis, depletes calcium stores that are necessary for insulin secretion, and alters insulin particle formation, all damaging the release process of β-cells (Cnop et al., 2002; Lu

et al., 2011; Bogan et al., 2012). Additionally, the accumulation of cholesterol on mitochondrial membranes impairs mitochondrial function, accumulation on endoplasmic reticulum triggers endoplasmic reticulum stress, and accumulation on cytoplasmic membranes triggers apoptosis proteins, leading to β-cell death (Lu et al., 2011; Paul et al., 2016; Lytrivi et al., 2020). Notably, β-cell lipotoxicity is primarily driven by the accumulation of LDL-C, while HDL-C averts β-cell apoptosis (Rütti et al., 2009). In LDLR knockout mice, LDLR is essential for β-cell LDL-C uptake, mediating lipotoxicity (Kruit et al., 2010).

4.2 Deficiency of PCSK9 in β-cells and association with diabetes

PCSK9 is detectable in islets and regulates the abundance of LDLR on the surface of β-cells (Tchéoubi et al., 2022). While many studies suggest an autocrine function of β-cells, a paracrine role of PCSK9 from δ-cells impacting β-cells cannot be excluded (Mbikay et al., 2010; Da Dalt et al., 2019). In PCSK9 knockout mice, pancreatic islets displayed anomalous contours, inflammatory cell infiltration, and early β-cell apoptosis (Mbikay et al., 2010). High glucose levels and relative insulin deficiencies were evident in the blood (Mbikay et al., 2010). Subsequent investigations indicated that PCSK9 knockout boosted LDLR density on β-cell surfaces, with a large presence of lipid droplets and immature insulin secretion particles within cells, despite low plasma insulin levels (Mbikay et al., 2015; Da Dalt et al., 2019). These findings imply that PCSK9 deficiency-driven lipid accumulation does not affect insulin synthesis but does impair β-cell secretory function. Remarkably, in PCSK9 knockout models, females displayed relatively normal glucose disposal compared to glucose-intolerant males, who manifested impaired plasma glucose and glucose-stimulated insulin secretion (Mbikay et al., 2015; Roubtsova et al., 2015). Ovariectomies in females mirrored the islet damage observed in males, and estrogen treatment reversed this effect (Roubtsova et al., 2015). The ability of estrogen to protect against apoptosis through its interaction with estrogen receptors on β-cells suggests an islet-protective role in the absence of PCSK9 (Babiloni-Chust et al., 2022; Sharma and Prossnitz, 2022). Notably, β-cell lipotoxicity induced by PCSK9 deficiency was reversed in PCSK9 and LDLR double-knockout mice, implying that LDLR-based lipid uptake pathways underlie this damage (Da Dalt et al., 2019). Furthermore, liver-specific PCSK9 knockout prevented lipid accumulation and restored islet β-cell secretory function, suggesting that localized islet PCSK9 regulates LDLR degradation, rather than serum PCSK9 levels (Da Dalt et al., 2019). Conversely, pancreatic-specific PCSK9 knockout boosted LDLR on β-cell surfaces, despite normal serum PCSK9 levels, leading to insufficient insulin secretion (Marku et al., 2022). Surprisingly, PCSK9 deficiency appears to trigger a protective strategy against lipid accumulation in β-cells (Marku et al., 2022). Enhanced expression of ATP-binding cassette transporter A1 (ABCA1), ATP-binding cassette transporter G1, and liver X receptor has been noted in β-cells, suggesting heightened lipid efflux to combat lipid buildup (Brunham et al., 2007; Kruit et al., 2012). Moreover, proteins responsible for cholesterol esterification, including acetyl coenzyme A acetyltransferase 1, and sterol O-acyltransferase 1, are reportedly significantly upregulated (Da Dalt et al., 2019; Marku et al., 2022). As key players in cholesterol esterification, their increased levels aid cholesterol consumption (Chang et al., 2006).

The islet-protective effects of PCSK9 have also been reported in humans. A meta-analysis linking PCSK9 LOF variants and diabetes risk demonstrated the correlation between decreased LDL-C and increased risk of diabetes, with an odds ratio of 1.19 (95% confidence interval 1.02–1.38) for each 1 mmol/L decrease in LDL-C (Lotta et al., 2016). This trend is consistent with a higher diabetes risk in individuals harboring PCSK9 LOF variants with impaired fasting glucose at baseline, despite a reduced risk of CAD (Ference et al., 2016). In a Mendelian randomized study, PCSK9 LOF mutations causing low LDL-C levels were associated with elevated fasting glucose, body weight, and an increased risk of new-onset diabetes (Schmidt et al., 2017). Nonetheless, several studies have reported that PCSK9 LOF variants do not alter fasting blood glucose or insulin levels and are not linked to diabetes development (Bonnefond et al., 2015; Chikowore et al., 2019). This discrepancy could be explained by the observation that PCSK9 levels in humans are typically reduced by approximately 15% in LOF variants, which is significantly lower than that in PCSK9 knockout animal models. Hence, human PCSK9 deficiency effects might be compensated for more effectively (Humphries et al., 2009).

Notably, merely knocking out PCSK9 may not impair β-cell insulin secretion function, despite the observed substantial upregulation of LDLR on β-cell surfaces (Langhi et al., 2009). In a specific knockout mouse model focused on β-cells, no irregularities in diabetes-related markers were observed, and islet function remained unaffected (Peyot et al., 2021). However, mRNA levels of LDLR and 3-hydroxy-3-methylglutaryl-coenzyme A reductase decreased by 32% and 29%, respectively, indicating that β-cells might curb endogenous cholesterol synthesis to forestall excessive lipid buildup (Peyot et al., 2021). Examination of human β-cells cultured *in vitro* demonstrated that both secreted and exogenous PCSK9 could influence LDLR density, yet the absence of PCSK9 from either source did not disrupt insulin secretion (Ramin-Mangata et al., 2021). Notably, serum PCSK9 does not appear to degrade β-cell LDLR (Da Dalt et al., 2019; Marku et al., 2022).

To summarize, the impact of the lack of PCSK9 secreted by β-cells on islet function remains contentious. The reported reduction in LDLR degradation due to PCSK9 autocrine absence heightens lipid uptake by β-cells. Conversely, islet β-cells appear to exhibit a compensatory capacity against lipid accumulation. This manifests as diminished lipoprotein receptor synthesis, reduced *de novo* cholesterol synthesis, increased receptor excretion of surplus lipids, and augmented cholesterol esterification (Table 1). Furthermore, research has indicated that glucagon secreted by pancreatic α-cells can inhibit PCSK9 expression. Given that many diabetic patients have increased glucagon production and decreased insulin production, could this lead to β-cell lipotoxicity related to islet PCSK9 deficiency? These questions warrant further investigation (Folli et al., 2018; Spolitu et al., 2019). Insulin upregulates liver PCSK9 via the SREBP1-c pathway (Costet et al., 2006), indicating the possibility that insulin promotes autocrine PCSK9 expression as a mechanism for regulating β-cell lipid homeostasis.

TABLE 1 Effects of islet autocrine PCSK9 deficiency on islet β cell function and diabetes risk.

Authors	Study models	Lipoprotein receptors on β cells	Effects on islet	Diabetes risk	Ref.
Langhi, C. et al. 2009	PCSK9 knockout mice	LDLR protein↑	PCSK9 autocrine deficiency did not change the content and composition of cholesterol in islets	PCSK9 autocrine deficiency did not affect fasting glucose levels, insulin levels, or GSIS	Langhi et al. (2009)
Mbikay, M. et al. 2010	PCSK9 knockout mice	LDLR mRNA↑ LDLR protein↑	PCSK9 autocrine deficiency induced abnormal islet morphology, inflammatory cell infiltration, islet cells apoptosis, and less insulin in the islet	PCSK9 autocrine deficiency induced hyperglyce- mia, hypoinsulinemia, and glucose intolerance developed in mice	Mbikay et al. (2010)
Da Dalt, L. et al. 2019	PCSK9 knockout mice; liver-specific PCSK9 knockout mice	LDLR, ACAT1 mRNA↑ HMGCR mRNA↓ LDLR protein↑	PCSK9 autocrine deficiency resulted in enlarged islets, insulin accumulation in beta cells, and the accumulation of mitochondria -related lipid droplets	PCSK9 autocrine deficiency induced impaired glucose tolerance, without insulin resistance and hyperglycemia	Da Dalt et al. (2019)
Peyot, M. L. et al. 2021	PCSK9 knockout mice; pancreas -specific PCSK9 knockout mice	LDLR, HMGCR mRNA↓ LDLR protein↑	PCSK9 knockout mice had normal insulin levels in the islets. Pancreas-specific PCSK9 knockout mice had higher insulin content in islets due to active basal protein secretion	PCSK9-deficient mice showed normal glucose tolerance and insulin sensitivity despite in- creased basal insulin secretion	Peyot et al. (2021)
Ramin-Mangata, S. et al. 2021	Human pancreatic β cell	LDLR protein↑	Although PCSK9 affected LDLR concentration and LDL-C uptake in β cells, neither endoge- nous nor exogenous PCSK9 deficiency affected insulin secretion	PCSK9 autocrine deficiency did not affect GSIS	Ramin-Mangata et al. (2021)
Marku, A. et al. 2022	Pancreas-specific PCSK9 knockout mice	LDLR, ABCA1, ABCG1, LXR, SOAT1 protein↑	PCSK9 autocrine deficiency leads to increased lipid uptake by β cells and intracellular accumulation of cholesterol and insulin	Pancreas-specific PCSK9 knockout mice had normal circulating cholesterol levels but had glucose intolerance and hypoinsulinemia	Marku et al. (2022)
Bonnefond, A. et al. 2015	PCSK9 p.R46L genetic variant	—	—	PCSK9 LOF was not associated with glucose homeostasis (FPG, HbA1c, HOMA-IR), fasting insulin levels and diabetes incidence but was associated with elevated fasting glucose levels	Bonnefond et al. (2015)
Ference, B. A. et al. 2016	PCSK9 variants	—	—	PCSK9 LOF mutations increased the incidence of diabetes, but only in individuals with impaired fasting glucose and on an order of magnitude less than the protection of the cardiovascular system	Ference et al. (2016)
Lotta, L. A. et al. 2016	PCSK9 variants	—	—	A decrease in serum LDL-C concentration is associated with an increased risk of new-onset diabetes	Lotta et al. (2016)
Lotta, L. A. et al. 2016	PCSK9 variants	—	—	A decrease in serum LDL-C concentration is associated with an increased risk of new-onset diabetes	Kleinewietfeld and Hafler (2013)
Chikowore, T. et al. 2019	PCSK9 variants	—	—	PCSK9 LOF is associated with lower fasting blood glucose levels during adolescence	Chikowore et al. (2019)

5 Neuroprotective effect of PCSK9 in the brain

In rodent studies, no alteration in brain LDLR levels was observed following adenovirus-mediated overexpression of PCSK9 in the liver or by injection of recombinant PCSK9. These findings indicate that serum PCSK9 cannot breach the blood-brain barrier (Schmidt et al., 2008). This assertion is further supported by the substantial disparity between PCSK9 concentrations in cerebrospinal fluid and serum PCSK9 levels, along with the lack of circadian rhythm synchronization between the two (Chen et al., 2014). These observations collectively underscore the significance of brain-derived autocrine PCSK9, rather than hepatic PCSK9 within the brain.

The expression of PCSK9 in the brain exhibits regional specificity. During embryonic development of zebrafish, PCSK9 is highly expressed in the notochord, cerebral cortex, cerebellar granulosa cell precursors, and other neural-forming regions

TABLE 2 Clinical trials.

Trail	Number	Duration	Target population	Intervention	Primary endpoints	Secondary endpoints	Significant outcomes	Reference
ATHEROREMO-IVUS study	581	—	Patients who underwent coronary angiography for acute coronary syndrome (ACS) or stable angina	—	—	—	Circulating PCSK9 levels are positively correlated with the volume of the plaque necrotic core tissue	Cheng et al. (2016)
GLAGOV randomized clinical trial	968	76 weeks	Patients with coronary artery disease taking statins	Evolocumab 420 mg monthly	The nominal change in percent atheroma volume	Percentage of patients demonstrating plaque regression	Evolocumab significantly reduces the volume of atherosclerotic plaques	Nicholls et al. (2016)
PACMAN-AMI randomized clinical trial	300	52 weeks	Patients undergoing percutaneous coronary intervention for acute myocardial infarction	Alirocumab 150 mg biweekly	The change in percent atheroma volume of non-infarct-related coronary arteries	Changes in maximum lipid core burden index and minimal fibrous cap thickness	Alirocumab significantly improves the regression of plaques in non-infarct-related coronary arteries	Räber et al. (2022)
ARCHITECT study	104	78 weeks	Patients with familial hypercholesterolemia without clinical ASCVD	Alirocumab 150 mg biweekly	Coronary plaque burden	Atherosclerotic Plaque Volume, Architecture and Composition	Alirocumab reduces plaque burden, increases the volume of calcified/fibrotic plaques, and reduces necrotic tissue volume	Pérez de Isla et al. (2023)
FOURIER trial	27,564	2.2 years	Patients with ASCVD and LDL-C ≥1.8 mmol/L	Evolocumab 420 mg monthly/140 mg biweekly	Composite of cardiovascular death, myocardial infarction (MI), stroke, hospitalization for unstable angina, or coronary revascularization	Composite of cardiovascular death, myocardial infarction, or stroke.	Evolocumab significantly lowers the risk of primary and secondary endpoint events	Sabatine et al. (2017)
ORION-9, -10 and –11 study	3,655	18 months	Patients with heterozygous familial hypercholesterolaemia, ASCVD, or ASCVD risk equivalent on maximally tolerated statin-therapy	Inclisiran 284 mg On days 1, 90, and 6-monthly	Non-adjudicated CV death, cardiac arrest, non-fatal MI, and fatal and non-fatal stroke	Total fatal and non-fatal MI, and stroke	Inclisiran significantly reduced composite MACE, but not fatal/non-fatal MIs or fatal/non-fatal stroke	Ray et al. (2023a)
PC-SCA-9 prospective study	174	—	Patients hospitalized for ACS	—	—	—	Serum PCSK9 levels are positively associated with severity of coronary artery lesions in ACS	Cariou et al. (2017)
ODYSSEY program	985	3.2 years	Patients diagnosed with heterozygous familial hypercholesterolemia	Alirocumab 75/150 mg biweekly	The long-term safety of alirocumab (treatment-emergent adverse events, laboratory data, and vital signs)	Efficacy of alirocumab on lipid parameters and the long-term immunogenicity of alirocumab	No long-term safety issues were observed with alirocumab	Farnier et al. (2018)
ORION-3 trial	382	4 years	Patients with prevalent ASCVD or high-risk primary prevention and elevated LDL cholesterol despite maximally tolerated statins or other LDL-lowering treatments	Inclisiran 300 mg 6-monthly	The percentage change in LDL-C	Changes in serum LDL-C and PCSK9 levels	The 4-year averaged mean reduction of LDL-C cholesterol was 44.2%, with reductions in PCSK9 ranging from 62·2% to 77·8%.	Ray et al. (2023b)
ORION-1 trial	501	240 days	Patients at high risk for cardiovascular disease who had elevated LDL cholesterol levels	Inclisiran 100, 200, or 300 mg at days 1 and 90	The change from baseline in LDL cholesterol level	Adverse event incidence rate	Patients who received inclisiran had dose-dependent reductions in PCSK9 and LDL--C levels	Liu et al. (2019)

10.3389/fphar.2024.1413123

(Poirier et al., 2006). Prominent PCSK9 expression in the frontal cortex of mouse embryos has been described (Rousselet et al., 2011). In contrast, the adult mouse brain has significantly lower PCSK9 expression than its fetal counterpart, with a prevalence in regions of sustained neurogenesis, such as the outer granular layer and rostral extension of the cerebellar olfactory peduncle (Seidah et al., 2003). Collectively, these observations strongly hint at a role of PCSK9 in neurodevelopment. In zebrafish embryos injected with PCSK9 mRNA inhibitors, abnormal neurogenesis was observed 24 h post-fertilization, as evidenced by cerebellar neuron disarray, deletion of the parietal cap and posterior brain, and disappearance of the posterior midbrain boundary. The peak mortality rate was observed at 48–96 h post-fertilization (Poirier et al., 2006). During retinoic acid-induced differentiation of mouse embryonic pluripotent cells, PCSK9 mRNA levels peaked on the 2nd day. Simultaneously, SREBP2 mRNA and LDLR protein levels exhibited negligible changes, indicating that the influence of PCSK9 on neurogenesis was independent of LDLR (Poirier et al., 2006). Similarly, PCSK9 deficiency in adult mice did not affect LDLR levels within the olfactory bulb (Rousselet et al., 2011). In rodent models, PCSK9 levels were notably diminished in both neural centers and the placenta of fetal mice with neural tube defects (An et al., 2015). This suggests that PCSK9 plays a pivotal role in fetal neural development and serves as a potential biomarker for the diagnosis of prenatal neural tube defect (An et al., 2015). Notably, although PCSK9 is essential for brain survival in certain species, its importance does not seem to extend to mammals. Experiments with PCSK9 knockout mouse embryos showed that the integrity of the telencephalon tissue remained intact, suggesting that PCSK9 is not particularly critical for mouse brain development (Rousselet et al., 2011). Furthermore, there were no indications of disorders in the stratification of the cerebral cortex or cerebellar structures in adult mice lacking PCSK9 (Rashid et al., 2005).

A long-term study involving African American individuals with PCSK9 LOF variants found no link between prolonged exposure to low PCSK9 levels and neurocognitive impairment or cognitive decline (Mefford et al., 2018). Similarly, a randomized controlled study involving European participants revealed no significant differences in neurocognitive function, intelligence, memory, or brain gray or white matter volumes between PCSK9 LOF variant carriers and controls (Ghouse et al., 2022). Even in cases of complete PCSK9 LOF mutations, in which serum PCSK9 is undetectable, individuals exhibit normal survival and fertility (Zhao et al., 2006; Hooper et al., 2007). Considering the potential positive effect of PCSK9 on neurodevelopment, several studies have explored the association between PCSK9 monoclonal antibodies and neurocognitive diseases. Analysis of pooled data from 14 trials indicated no notable increase in overall adverse events, including neurological disorders, associated with the use of PCSK9 inhibitors (Robinson et al., 2017).

In summary, although PCSK9 deficiency negatively affects neurodevelopment in experimental models, this effect seems to be less severe in humans. This can be explained from three perspectives. First, the complexity of the lipid metabolism pathway in the mammalian brain compared with that in fish may enable compensatory mechanisms that mitigate the effects of PCSK9 deficiency. Second, owing to the challenge of lipoprotein penetration through the blood-brain barrier, the brain predominantly relies on neurons and glial cells for *de novo* cholesterol synthesis, which maintains the stability of the cholesterol pool (Orth and Bellosta, 2012). Third, the passage of PCSK9 monoclonal antibodies into the brain via the blood-brain barrier is challenging.

6 PCSK9 regulates sodium reabsorption in the kidney

The Epithelial Sodium Channel (ENaC) non-voltage-gated ion channel protein is widely expressed in the kidneys, lungs, distal colon, sebaceous glands, eccrine glands, and other tissues, facilitating the transcellular absorption of sodium ions (Hanukoglu et al., 2017). In the kidney, ENaC resides in the luminal membrane of the distal tubules and collecting ducts of the distal nephrons. Its activity is influenced by salt intake and mineralocorticoid secretion (Zhang et al., 2022). Given its role in sodium absorption and blood volume maintenance, gain-of-function and deletion mutations in ENaC can lead to severe salt-sensitive hypertension and hypotension, respectively (Bonny and Hummler, 2000; Furuhashi et al., 2005). PCSK9 is notably abundant in the distal renal collecting duct, making it the second-largest source of PCSK9 after the liver (Seidah et al., 2003; Liu and Vaziri, 2014). Unlike LDLR endocytosis, PCSK9 orchestrates ENaC degradation via the proteasomal pathway. This action curtails the intracellular ENaC pool, suppresses ENaC exocytosis, and reduces ENaC density on the cell membrane surfaces (Sharotri et al., 2012). In a PCSK9 knockout mouse model, renal ENaC expression increased by nearly one-third, but blood pressure and sodium homeostasis remained unaffected (Berger et al., 2015). Post-amiloride ENaC inhibition and urinary sodium excretion increased comparably in wild-type and PCSK9 knockout mice, further underscoring the lack of physiological impact of PCSK9 deficiency on ENaC function (Berger et al., 2015).

Consequently, there is a discordance in the link between PCSK9 deficiency and blood pressure in humans. Among Caucasians, p.R46L variants do not increase the risk of hypertension compared to controls (Zhao et al., 2006). In an exploration of the association between PCSK9 genetic variants and blood pressure in African Americans, the PCSK9 variant was found to have a modest influence on diastolic blood pressure (Tran et al., 2015). However, in a male population of Asian descent, the PCSK9 p.R46L group demonstrated markedly higher blood pressure than non-carriers (Jeenduang et al., 2015). In one unique case, an individual bearing a PCSK9 LOF mutation barely expressed PCSK9 and did not manifest hypertension (Cariou et al., 2009). Furthermore, examination of patients with hypertension showed no correlation between blood pressure and serum PCSK9 levels (Yang et al., 2016).

In summary, there are disparities in research findings regarding the link between PCSK9 deficiency and salt-sensitive hypertension among Asian and African American groups. Thus, there may be racial disparities in the effects of PCSK9 deficiency on blood pressure. However, due to the scarcity of research data, the extent to which renal PCSK9 deficiency influences blood pressure regulation remains unclear. The establishment of additional animal models, such as specific renal collecting duct PCSK9 knockout

models, is imperative to more precisely determine the regulatory effects of PCSK9 on ENaC and blood pressure.

7 PCSK9 is involved in intestinal lipid absorption

The efficient excretion of cholesterol through the intestine is important for maintaining optimal plasma cholesterol levels. In addition to the conventional hepatobiliary route, recent studies have revealed a novel mechanism termed transintestinal cholesterol efflux (TICE), which is particularly active in the proximal intestine (van der Velde et al., 2007). The efficacy of TICE hinges on multiple factors. One factor is the role of ApoB-48 in basolateral membrane binding to chylomicrons, facilitating their reuptake via LDLR presentation. PCSK9 influences this reuptake by modulating LDLR density (Le May et al., 2009). Another factor is the complementary cooperation between the ATP-binding cassette transporter G5/G8 and ABCB1 proteins in the apical intestinal epithelial membrane, which orchestrates cholesterol transport from the lumen to the interior (Hui et al., 2008; Le May et al., 2013; Dugardin et al., 2017). In rodents, approximately one-third of the total fecal cholesterol discharge occurs through TICE, doubling the amount via bile pathways, underscoring the dominant role of TICE in cholesterol elimination (van der Veen et al., 2009). TICE can be activated by food and medications that include phytosterols, bile acids, fasting, liver X receptor agonists, peroxisome proliferator-activated receptor agonists, ezetimibe, and statins (Tanaka and Kamisako, 2021; Garçon et al., 2022). In humans, TICE is also an important component of the body's reverse cholesterol transport (RCT) process. It is estimated that 35% of fecal cholesterol is produced through the TICE pathway (Garçon et al., 2022). In humans, TICE is also inducible, clinical studies have found that treatment with 10 mg/day of the lipid-lowering drug ezetimibe for 4 weeks can enhance TICE by fourfold (Jakulj et al., 2016). These findings has spurred research aimed at lipid reduction. Compared with hepatobiliary stimulation, TICE activation has fewer adverse effects, making it a promising avenue for further investigation (Garçon et al., 2022).

Within the gastrointestinal tract of rodents, abundant PCSK9 and LDLR expression spans the small intestine to the colon. The PCSK9 and LDLR levels are harmoniously distributed along the cephalocaudal axis of the intestine (Le May et al., 2009). Immunofluorescence staining has revealed that PCSK9 primarily resides within the intestinal epithelium, including goblet cells and enterocytes, and is prominently situated on both the basolateral and apical facets (Le May et al., 2009). However, whether PCSK9 produced by the intestinal cells can enter the bloodstream remains debatable. In the early stages of differentiation of the Caco-2 colon cancer cell line, PCSK9 secretion from the basolateral compartment was observed (Levy et al., 2013; Moreau et al., 2021). However, after the differentiation and maturation of Caco-2 cells, PCSK9 secretion reportedly became negligible (Moreau et al., 2021). Despite significant PCSK9 protein detection in human and rodent intestinal tissues, *in vitro* cultivation of these intestinal tissues did not reveal PCSK9 secretion, suggesting a predominantly autocrine role for PCSK9 expressed by intestinal cells (Moreau et al., 2021).

PCSK9 knockout upregulates TICE *in vivo* and *in vitro* (Le May et al., 2013). Studies involving rodents have indicated that increased chylomicron clearance in PCSK9 knockout mice leads to a significant postprandial reduction in triglyceride (Le May et al., 2009). However, while PCSK9 knockout results in decreased ApoB secretion in intestinal cells, which logically leads to a decrease in the number of triglyceride-rich chylomicrons, there is a compensatory increase in the volume of these structures (Le May et al., 2009). Subsequent investigations revealed that PCSK9 knockout can trigger a notable increase in intestinal LDLR levels (Le May et al., 2009). Considering that the clearance of chylomicrons remnants relies largely on the LDLR-ApoB pathway, it is plausible to speculate that a deficiency in intestinal PCSK9 promotes the reuptake of chylomicrons by increasing intestinal LDLR levels, thereby reducing postprandial plasma LDL-C and triglyceride levels (Le May et al., 2009). These findings pave the way for potential lipid regulation treatments centered on the intestinal PCSK9/LDLR axis. Dietary therapy involving the acute intragastric administration of plant sterols in rodents resulted in a five-fold increase in intestinal LDLR expression, greatly enhancing TICE (De Smet et al., 2015). Similarly, exercise training in rodents leads to elevated LDLR levels in the basolateral membrane of the intestinal canal, further boosting TICE (Farahnak et al., 2018). Interventions involving a rodent diet and exercise have also yielded interesting results, such as significant upregulation of intestinal PCSK9 expression. This could be partially explained by the upregulation of SREBP2 expression in the intestine, whereas hepatic PCSK9 expression was inhibited. However, this phenomenon warrants further investigation to provide a more comprehensive explanation (De Smet et al., 2015; Farahnak et al., 2018).

Although preliminary studies in animal and *in vitro* models have revealed the impact of PCSK9 on TICE, relevant clinical research on the impact of PCSK9 on TICE in humans is still lacking. Future clinical research is needed to observe changes in TICE among individuals with PCSK9 LOF mutations and patients using PCSK9 inhibitors.

8 Protective effect of PCSK9 in other tissues

8.1 PCSK9 protects lipid metabolism in seminiferous tubules

The testes are partitioned into two cellular compartments by the blood-testosterone barrier: the interstitium, which is primarily responsible for lipid metabolism and androgen synthesis, and the seminiferous tubule, which is responsible for germ cell growth and development. Within seminiferous tubules, LDLR-mediated lipid transport plays a crucial role in maintaining high lipid levels and providing essential nutrients necessary for spermatogonial division and differentiation (Schenk and Hoeger, 2010). Although PCSK9 mRNA has been detected in the testis, its length (2.2 kb) differs from that in other tissues (2.8 kb) (Seidah et al., 2003). PCSK9 has been identified in the adipose tissue of the epididymis, interstitial tissue of the testis, sperm tubules, in rodents (Pelletier et al., 2022). Recent research has highlighted the role of PCSK9 in regulating lipid metabolism to maintain seminiferous tubule

function. In PCSK9 knockout mice, cholesterol accumulation and immune cell infiltration were observed in the seminiferous tubules, accompanied by increased LDLR levels and the presence of the inflammatory factor interleukin-17 (Pelletier et al., 2022). This cytokine, secreted mainly by highly infiltrating γδT cells in the testis, has been linked to macrophage polarization and autoimmune responses in experimental orchitis models (Park et al., 2005; Kleinewietfeld and Hafler, 2013; Wilharm et al., 2021). Excessive cholesterol accumulation promotes expression of this interleukin and creates an inflammatory environment that contributes to seminiferous tubule dysfunction (Wang et al., 2015; Varshney et al., 2016; Kim et al., 2019).

8.2 PCSK9 prevents abnormal distribution of adipose tissue and local inflammation

PCSK9 is expressed in visceral adipose tissue and is regulated by natriuretic peptides and insulin (Bordicchia et al., 2019). Within adipose tissue, the primary influences of PCSK9 appear to be on CD36 and VLDLR, involving the intake and accumulation of FAs, rather than on LDLR (Roubtsova et al., 2011; Christiaens et al., 2012; Demers et al., 2015). Among these receptors, CD36 governs the differentiation of pre-adipocytes into mature adipocytes, and the absence of CD36 significantly diminishes the subcutaneous and gonadal fat content in mice (Christiaens et al., 2012). *In vitro* experiments involving adipocytes have revealed a three-fold increase in CD36 expression and uptake of oxidized LDL following PCSK9 knockout. This genetic alteration leads to ectopic fat accumulation in the visceral organs of mice (Baragetti et al., 2017).

In individuals carrying PCSK9 LOF variants, heightened visceral fat thickness, including central obesity, liver steatosis, and epicardial fat, has been detected. These changes appear to be tied to adipocyte hypertrophy and inflammatory responses (Baragetti et al., 2017; Hay et al., 2022). Given these findings, it is reasonable to infer that the presence of PCSK9 in adipose tissue contributes to the balanced distribution of body fat through the regulation of adipocyte metabolism.

Although LDLR is not typically regarded as the primary pathway for lipid uptake in adipose tissue, particularly in white adipose tissue, including epicardial adipose tissue, low levels of PCSK9 can trigger upregulated LDLR expression within adipocytes (Dozio et al., 2020), consequently prompting additional uptake of LDL-C (Dozio et al., 2020). The accumulation of excess LDL-C in adipocytes can initiate localized inflammation and insulin resistance by activating the NOD-like receptor thermal protein domain-associated protein 3 (NLRP3) inflammatory corpuscles. These activated inflammatory corpuscles induce mitochondrial dysfunction and insulin resistance by activating macrophages infiltrated within adipose tissue (Dozio et al., 2020; Javaid et al., 2023). Notably, among obese individuals with low serum PCSK9 concentrations, the surface expression of LDLR and CD36 increased by 81% and 36%, respectively, on white adipose tissue cells (Cyr et al., 2021). This led to a corresponding elevation in the activation level of NLRP3 inflammatory corpuscles and increased susceptibility to diabetes mellitus, surpassing that observed in other subjects (Cyr et al., 2021). The fact that PCSK9 exhibits an anti-inflammatory effect within adipose tissue is intriguing, given that it is typically considered a pro-inflammatory factor (Ding et al., 2020; Punch et al., 2022). This implies that PCSK9 has dual functions in inflammatory reactions, exerting both anti- and pro-inflammatory effects. This novel hypothesis requires validation in various tissue types other than adipose tissue.

8.3 PCSK9 deficiency aggravates apical periodontitis

PCSK9 deficiency significantly influences apical periodontitis. Gram-negative bacteria mainly drive this chronic inflammatory ailment, particularly *Porphyromonas gingivalis*, which infiltrates periodontal support tissue (Ye et al., 2023). The expression of PCSK9 was increased in a mouse model of apical periodontitis induced by *P. gingivalis* and in the gingival tissues of patients with periodontitis (Sun et al., 2018). Although PCSK9 can promote the release of pro-inflammatory cytokines and exacerbates the inflammatory response, it can also facilitate the osteogenic differentiation of periodontal ligament stem cells (Sun et al., 2018). However, in cases of PCSK9 deficiency, LDLR expression within periodontal tissue increases, intensifying the differentiation of bone marrow macrophages to osteoclasts and amplifying cementum loss (Huang et al., 2022). This cascade of events hinges on LDLR dependence, as evidenced by experiments involving LDLR knockout, which reportedly arrested the worsened progression of apical periodontitis in a state of PCSK9 deficiency (Huang et al., 2022).

9 Advancements in the clinical benefits and safety of PCSK9 inhibition therapy

9.1 PCSK9 and vasculature

Within the vasculature, PCSK9 serves as a pivotal regulator of LDL-C levels and acts as a driver of atherosclerosis and subsequent atherosclerotic cardiovascular diseases (ASCVD) (Boutari et al., 2023). This effect is manifest through the promotion of chronic vascular inflammation, formation of atherosclerotic plaques, and initiation of thrombosis (Boutari et al., 2023; Hummelgaard et al., 2023). In macrophages, the secretion of PCSK9 is triggered by oxidized LDL, leading to macrophage polarization via the Toll-like receptor 4/nuclear factor kappa B signaling pathway (Wang et al., 2022). PCSK9 is also secreted by vascular smooth muscle cells, which exhibit enhanced proliferation, migration, and foam cell formation induced by oxidized LDL, thus aggravating atherosclerosis (Liu et al., 2023). The influence of PCSK9 extends to platelets; PCSK9 secretion stimulates platelet activation, intensifies platelet-dependent thrombosis, and fosters thrombotic inflammatory reactions (Petersen-Uribe et al., 2021). In clinical practice, a noteworthy correlation has been established between the serum concentration of PCSK9 and the presence and proportion of atherosclerotic necrotic core tissues, as demonstrated by intramural ultrasound virtual histological imaging (Cheng et al., 2016). The focus of recent research has shifted to the impact of PCSK9 inhibition therapy on coronary plaque (Nicholls et al., 2016). In a double-blind randomized controlled trial involving patients

with AMI, serial multimodal intracoronary imaging was performed (Räber et al., 2022). The percent atheroma volume in non-infarct related coronary arteries showed a more significant reduction in patients treated with PCSK9 monoclonal antibodies in combination with statins for 52 weeks compared to those treated with statins alone (−2.13% vs. −1.21%) (Räber et al., 2022). Furthermore, in an open-label, single-arm clinical trial involving patients with familial hypercholesterolemia but without clinical ASCVD, 78 weeks of PCSK9 monoclonal antibody alirocumab treatment led to a decrease in the coronary plaque burden from 34.6% to 30.4% (Pérez de Isla et al., 2023). Notably, there are changes in the characteristics of coronary artery plaques, with an increase in the proportion of calcified and mainly fibrous plaques, along with a decrease in necrotic and fibrous fatty plaques (Pérez de Isla et al., 2023). The collective findings indicate the benefits of PCSK9 inhibition therapy on the volume, composition, and phenotype of coronary plaque (Räber et al., 2022; Pérez de Isla et al., 2023).

PCSK9 LOF variants associated with congenital PCSK9 deficiency reportedly exhibited a 14% reduction in plasma LDL-C levels and a 21% decrease in TG levels compared with non-carriers (Ooi et al., 2017). A comprehensive meta-analysis of nine studies on PCSK9 LOF variants further revealed variations in plasma LDL-C levels among black and white populations, with reductions of 35 and 13 mg/dL, respectively. Importantly, both groups exhibited a lower risk of CAD than non-carriers (Kent et al., 2017). Thus, PCSK9 LOF mutations provide substantial vascular protection in clinical settings.

9.2 PCSK9 inhibition and clinical cardiovascular benefits

PCSK9 inhibitors have promising potential in the treatment of ASCVD (Hummelgaard et al., 2023). Beyond well-established monoclonal antibodies such as evolocumab and alirocumab, which target the PCSK9 protein, and small interfering RNA (siRNA) therapies, such as inclisiran targeting PCSK9 mRNA, various innovative approaches, including gene editing, vaccines, and peptides, have been explored (Hummelgaard et al., 2023). In a randomized, double-blind, prospective controlled trial involving patients with ASCVD, the incidence of the primary endpoint (9.8% vs. 11.3%) and critical secondary endpoint (5.9% vs. 7.4%) after 48 weeks of treatment with a PCSK9 monoclonal antibody was significantly lower than that in the control group (Sabatine et al., 2017). Similarly, a comprehensive analysis of multiple Phase III trials found that after 90 days of treatment with PCSK9 siRNA, the incidence of composite major adverse cardiovascular events (MACE) was notably reduced (7.1% vs. 9.4%) compared with the placebo group (Ray et al., 2023a). Patients who undergo percutaneous coronary intervention (PCI) usually face a heightened risk of MACE (Furtado et al., 2022). In a randomized controlled study with a median follow-up period of 2.2 years, patients with a history of PCI were treated with PCSK9 monoclonal antibodies, resulting in a significant reduction in the incidence of MACE (11.2% vs. 13.2%) and risk of vascular remodeling (7.2% vs. 9.3%), as reported previously (Furtado et al., 2022).

Furthermore, beyond their primary and secondary preventive applications in ASCVD, the clinical use of PCSK9 inhibitors has been increasing. Recent research has shifted its focus toward the feasibility of applying PCSK9 inhibition therapy to patients with acute coronary syndrome (ACS) as soon as possible, as both serum and ischemic myocardial PCSK9 levels surge rapidly during ACS, potentially contributing to acute inflammatory reactions (Cariou et al., 2017; Ding et al., 2018; Ferri et al., 2022). In a placebo-controlled trial in patients with AMI, the PCSK9 monoclonal antibody treatment group was treated with alirocumab within 24 h of emergency PCI (Räber et al., 2022). After 52 weeks, the alirocumab treatment group exhibited a significantly lower incidence of adverse events (70.7% vs. 72.8%) and coronary revascularization (8.2% vs. 18.5%) than the placebo group (Räber et al., 2022). In another prospective randomized controlled study among extremely high-risk ACS patients, patients were randomly assigned to the evolocumab group or placebo group at a ratio of 1:1, and the first medication was administered within 48 h after PCI (Hao et al., 2022). During the 3 months follow-up period, MACE incidences were significantly lower in the evolocumab group than in the placebo group (8.82% vs. 24.59%). In summary, PCSK9 inhibition therapy has significant cardiovascular benefits in patients with ACSVD (Hao et al., 2022).

9.3 Advances in clinical studies on the safety of PCSK9 inhibition

While PCSK9 inhibition therapy has become increasingly pivotal in lipid reduction and cardiovascular event management, concerns regarding its safety have arisen given the vital role of PCSK9 in overall physiological metabolism and organ function. In the ODYSSEY open-label extension study, spanning an average observation period of 2.5 years, no significant increase in sudden adverse events was observed in patients with familial hypercholesterolemia undergoing PCSK9 monoclonal antibody treatment (Farnier et al., 2018). Similarly, a more extended FOURIER-OLE study with a median follow-up time of 5 years concluded that PCSK9 inhibitor use did not significantly increase the incidence of serious adverse events, including neurocognitive impairment or new-onset diabetes mellitus in patients with ASCVD (ODonoghue et al., 2022). Additionally, an open-label extension study assessing the safety of inclisiran reported a mere 1% incidence of serious safety adverse events after 4 years of drug intervention, equivalent to that in the control group (Ray et al., 2023b). Recognizing the potential negative effects of statins on neurocognitive function, multiple studies have investigated the relationship between PCSK9 inhibitors and neurocognitive function (Shahid et al., 2022). A systematic review of seven studies found no association between the use of PCSK9 monoclonal antibodies and neurocognitive events (Shahid et al., 2022). While statins can slightly elevate the risk of new-onset diabetes mellitus, mainly by reducing sensitivity to blood sugar fluctuations via inhibiting islet β-cell glucose transporter-2 and insulin receptors in tissues, current clinical evidence suggests that PCSK9 monoclonal antibodies are sufficiently safe (McNamara et al., 2009; Gotoh and Negishi, 2015). Although PCSK9 inhibition therapy may lead to a slight increase in

hyperglycemia, this increase is not significant enough to induce new-onset diabetes mellitus (Guo Y. et al., 2021; Carugo et al., 2022). Furthermore, there remains a notable gap in clinical research regarding the potential adverse effects of PCSK9 silencing in extrahepatic organs. The clinical trials mentioned in this chapter are summarized in Table 2.

The collective findings suggest that PCSK9 deficiency in clinical practice may not carry the same degree of harm as that observed in experimental models. However, in individuals with PCSK9 loss-of-function mutations and patients using PCSK9 inhibitors, PCSK9 levels are only partially reduced, far from the extent of PCSK9 knockout observed in experimental animal and *in vitro* models. Therefore, the potential negative consequences of a PCSK9 deficiency should not be ignored. Moreover, current research on the safety of PCSK9 inhibitors is limited by relatively short observation periods, making it challenging to ensure the long-term safety of continuous PCSK9 inhibition therapy, especially in high-risk patients who may require lifelong treatment. Extensive prospective studies are needed to ascertain whether such therapies can harm extrahepatic tissues. Currently, there are some shortcomings in the research on the safety of PCSK9 inhibitors, notably in proving their potential benefits or risks across different patient groups, particularly in high-risk patients with specific conditions. Additionally, when patients were administered PCSK9 inhibitors, there were substantial individual variations in PCSK9 and LDL-C levels. To assess whether PCSK9 inhibition poses a risk to extrahepatic organs, it is crucial to closely monitor individuals with significantly reduced levels of PCSK9 and LDL-C levels when using PCSK9 inhibitors. Monoclonal antibodies are the most widely used PCSK9 inhibitors in clinical practice. While such antibodies primarily counteract circulating PCSK9, it is essential to consider their potential impact on PCSK9 levels in extrahepatic tissues. The emergence of PCSK9 gene silencing therapies has further emphasized this concern. In contrast to monoclonal antibodies, PCSK9 siRNA and PCSK9 gene editing techniques that do not target the liver are more likely to interfere with PCSK9 synthesis in extrahepatic tissues.

10 Discussion

To date, despite the vigorous development of PCSK9 inhibitors, the understanding of the diverse physiological functions of PCSK9 in extrahepatic tissues remains incomplete. The lack of PCSK9 in mouse myocardium has been shown to affect myocardial contractility. However, these results are limited to animal knockout models. The impact of clinical use of PCSK9 inhibitors on myocardial contractility requires long-term clinical observation and rigorous clinical studies.

The relationship between PCSK9 and diabetes is complex. A deficiency of autocrine PCSK9 in the islets may impair β-cell function, leading to diabetes (Da Dalt et al., 2019). However, serum PCSK9 levels are generally elevated in diabetic patients (Ibarretxe et al., 2016). This suggests that the roles of islet-derived PCSK9 and liver-derived PCSK9 in diabetes may differ, necessitating more research to uncover the underlying mechanisms.

Existing evidence indicates that the function of PCSK9 in the brain may be independent of LDLR (Poirier et al., 2006). Future research should clarify whether the neuroprotective effects of PCSK9 depend on lipoprotein receptors other than LDLR or on specific non-lipid-related effects, and further elucidate the molecular mechanisms involved. Additionally, when exploring the effects of PCSK9 on the brain, special attention should be paid to differences in research conclusions due to species variations in experimental animals.

Current studies suggest that PCSK9 deficiency does not significantly affect blood pressure (Berger et al., 2015). However, given that PCSK9 does regulate renal ENaC, there is a clinical need to gather long-term follow-up data on the blood pressure of patients using PCSK9 inhibitors. Research on the impact of PCSK9 on TICE in the intestine is limited to laboratory findings. Clinical studies are needed to verify whether PCSK9 inhibitors can significantly stimulate TICE, similar to ezetimibe (Jakulj et al., 2016).

Generally, future research should aim to construct more tissue-specific PCSK9 knockout animal models and conduct more clinical studies, preclinical experiments, and interdisciplinary collaborations to better understand the roles of PCSK9 in extrahepatic tissues.

In human, studies indicate that, on average, the plasma PCSK9 level in PCSK9 LOF mutants is only reduced by 15%–20% compared to the normal population, with significant variability among individuals (Humphries et al., 2009; Lakoski et al., 2009; Wanneh et al., 2017). Future research should focus on comparing PCSK9-deficient mutant populations exhibiting the lowest PCSK9 expression with the normal population to ascertain any potential link between PCSK9 deficiency and associated diseases. Furthermore, clinical usage of PCSK9 inhibitors has not demonstrated an increased risk of serious safety adverse events, such as neurocognitive impairment or NODM. However, it is crucial not to overlook the substantial reduction of over 90% in serum PCSK9 levels observed within hours of clinical application of PCSK9 monoclonal antibodies, and this effect can last for 15 days (Gibbs et al., 2017; Liu et al., 2019). Inclisiran, another PCSK9 inhibitor, reduces serum PCSK9 levels by over 70% within 30 days and maintains this reduction for 180 days (Ray et al., 2017; Ray et al., 2019; Ray et al., 2023b). According to the frequency of use of these drugs, patients will be in a state of low PCSK9 level for a long time. Moreover, studies demonstrate that CRISPR base editing of PCSK9 can remarkably reduce PCSK9 expression in nonhuman primates by 90% (Musunuru et al., 2021). These findings highlight a more significant reduction of PCSK9 level in individuals using PCSK9 inhibitors long-term compared to PCSK9 LOF mutants. Consequently, the potential consequences of prolonged PCSK9 deficiency may be more severe in PCSK9 inhibitor users. It remains imperative to conduct comprehensive, long-term clinical monitoring to assess the safety and efficacy of PCSK9 inhibition therapy in different patient populations, especially those at high risk for extrahepatic tissue-related complications. In conclusion, while the clinical significance of PCSK9 circulation and localized inhibition is apparent, our understanding of the role(s) of PCSK9 in extrahepatic tissue remains limited. Circulating PCSK9 originates from the liver and primarily acts on the liver. All the effects of extrahepatic PCSK9 are autocrine and generally do not increase circulating PCSK9 levels. This may suggest that PCSK9 could have both intracellular and extracellular effects on these tissues. Although existing data show that the possibility of serious safety problems due to the application of PCSK9 inhibitors is low, long-term follow-up of their possible negative effects cannot be

ignored when PCSK9 inhibitors are used clinically. This is the first review to delve into the pathophysiological interplay between PCSK9 deficiency and diverse extrahepatic tissue diseases. We hope that this review helps galvanize future research efforts toward unraveling protective contributions of PCSK9 in extrahepatic tissue.

Author contributions

FL: Writing–original draft. EL: Writing–review and editing. XY: Funding acquisition, Investigation, Project administration, Supervision, Writing–review and editing.

Funding

The authors declare that financial support was received for the research, authorship, and/or publication of this article. Startup Research Fund of the Second Affiliated Hospital, Zhengzhou University (Grant number, 202004047).

Conflict of interest

The authors declare that the research was conducted in the absence of any commercial or financial relationships that could be construed as a potential conflict of interest.

Publisher's note

References

2 (2022). 2. Classification and diagnosis of diabetes: standards of medical care in diabetes-2022. *Diabetes Care* 45, S17–s38. doi:10.2337/dc22-S002

Abifadel, M., Varret, M., Rabès, J. P., Allard, D., Ouguerram, K., Devillers, M., et al. (2003). Mutations in PCSK9 cause autosomal dominant hypercholesterolemia. *Nat. Genet.* 34, 154–156. doi:10.1038/ng1161

Abuelezz, S. A., and Hendawy, N. (2021). HMGB1/RAGE/TLR4 axis and glutamate as novel targets for PCSK9 inhibitor in high fat cholesterol diet induced cognitive impairment and amyloidosis. *Life Sci.* 273, 119310. doi:10.1016/j.lfs.2021.119310

An, D., Wei, X., Li, H., Gu, H., Huang, T., Zhao, G., et al. (2015). Identification of PCSK9 as a novel serum biomarker for the prenatal diagnosis of neural tube defects using iTRAQ quantitative proteomics. *Sci. Rep.* 5, 17559. doi:10.1038/srep17559

Babiloni-Chust, I., Dos Santos, R. S., Medina-Gali, R. M., Perez-Serna, A. A., Encinar, J. A., Martinez-Pinna, J., et al. (2022). G protein-coupled estrogen receptor activation by bisphenol-A disrupts the protection from apoptosis conferred by the estrogen receptors ERα and ERβ in pancreatic beta cells. *Environ. Int.* 164, 107250. doi:10.1016/j.envint.2022.107250

Baragetti, A., Balzarotti, G., Grigore, L., Pellegatta, F., Guerrini, U., Pisano, G., et al. (2017). PCSK9 deficiency results in increased ectopic fat accumulation in experimental models and in humans. *Eur. J. Prev. Cardiol.* 24, 1870–1877. doi:10.1177/2047487317724342

Barisione, C., Verzola, D., Garibaldi, S., Ferrari, P. F., Garibotto, G., Ameri, P., et al. (2021). Renal ischemia/reperfusion early induces myostatin and PCSK9 expression in rat kidneys and HK-2 cells. *Int. J. Mol. Sci.* 22, 9884. doi:10.3390/ijms22189884

Berger, J. M., Vaillant, N., Le May, C., Calderon, C., Brégeon, J., Prieur, X., et al. (2015). PCSK9-deficiency does not alter blood pressure and sodium balance in mouse models of hypertension. *Atherosclerosis* 239, 252–259. doi:10.1016/j.atherosclerosis.2015.01.012

Blesa, S., Vernia, S., Garcia-Garcia, A. B., Martinez-Hervas, S., Ivorra, C., Gonzalez-Albert, V., et al. (2008). A new PCSK9 gene promoter variant affects gene expression and causes autosomal dominant hypercholesterolemia. *J. Clin. Endocrinol. Metab.* 93, 3577–3583. doi:10.1210/jc.2008-0269

Bogan, J. S., Xu, Y., and Hao, M. (2012). Cholesterol accumulation increases insulin granule size and impairs membrane trafficking. *Traffic* 13, 1466–1480. doi:10.1111/j.1600-0854.2012.01407.x

Bonnefond, A., Yengo, L., Le May, C., Fumeron, F., Marre, M., Balkau, B., et al. (2015). The loss-of-function PCSK9 p.R46L genetic variant does not alter glucose homeostasis. *Diabetologia* 58, 2051–2055. doi:10.1007/s00125-015-3659-8

Bonny, O., and Hummler, E. (2000). Dysfunction of epithelial sodium transport: from human to mouse. *Kidney Int.* 57, 1313–1318. doi:10.1046/j.1523-1755.2000.00968.x

Bordicchia, M., Spannella, F., Ferretti, G., Bacchetti, T., Vignini, A., Di Pentima, C., et al. (2019). PCSK9 is expressed in human visceral adipose tissue and regulated by insulin and cardiac natriuretic peptides. *Int. J. Mol. Sci.* 20, 245. doi:10.3390/ijms20020245

Bottomley, M. J., Cirillo, A., Orsatti, L., Ruggeri, L., Fisher, T. S., Santoro, J. C., et al. (2009). Structural and biochemical characterization of the wild type PCSK9-EGF(AB) complex and natural familial hypercholesterolemia mutants. *J. Biol. Chem.* 284, 1313–1323. doi:10.1074/jbc.M808363200

Boutari, C., Hill, M. A., Procaccini, C., Matarese, G., and Mantzoros, C. S. (2023). The key role of inflammation in the pathogenesis and management of obesity and CVD. *Metabolism* 145, 155627. doi:10.1016/j.metabol.2023.155627

Brunham, L. R., Kruit, J. K., Pape, T. D., Timmins, J. M., Reuwer, A. Q., Vasanji, Z., et al. (2007). Beta-cell ABCA1 influences insulin secretion, glucose homeostasis and response to thiazolidinedione treatment. *Nat. Med.* 13, 340–347. doi:10.1038/nm1546

Cariou, B., Guérin, P., Le May, C., Letocart, V., Arnaud, L., Guyomarch, B., et al. (2017). Circulating PCSK9 levels in acute coronary syndrome: results from the PC-SCA-9 prospective study. *Diabetes Metab.* 43, 529–535. doi:10.1016/j.diabet.2017.07.009

Cariou, B., Le Bras, M., Langhi, C., Le May, C., Guyomarc'h-Delasalle, B., Krempf, M., et al. (2010). Association between plasma PCSK9 and gamma-glutamyl transferase levels in diabetic patients. *Atherosclerosis* 211, 700–702. doi:10.1016/j.atherosclerosis.2010.04.015

Cariou, B., Ouguerram, K., Zaïr, Y., Guerois, R., Langhi, C., Kourimate, S., et al. (2009). PCSK9 dominant negative mutant results in increased LDL catabolic rate and familial hypobetalipoproteinemia. *Arterioscler. Thromb. Vasc. Biol.* 29, 2191–2197. doi:10.1161/ATVBAHA.109.194191

Carugo, S., Sirtori, C. R., Corsini, A., Tokgozoglu, L., and Ruscica, M. (2022). PCSK9 inhibition and risk of diabetes: should we worry? *Curr. Atheroscler. Rep.* 24, 995–1004. doi:10.1007/s11883-022-01074-y

Chang, T. Y., Chang, C. C., Ohgami, N., and Yamauchi, Y. (2006). Cholesterol sensing, trafficking, and esterification. *Annu. Rev. Cell. Dev. Biol.* 22, 129–157. doi:10.1146/annurev.cellbio.22.010305.104656

Chen, Y. Q., Troutt, J. S., and Konrad, R. J. (2014). PCSK9 is present in human cerebrospinal fluid and is maintained at remarkably constant concentrations throughout the course of the day. *Lipids* 49, 445–455. doi:10.1007/s11745-014-3895-6

Chen, Z., Zhu, S., Wang, H., Wang, L., Zhang, J., Gu, Y., et al. (2021). PTPMT1 is required for embryonic cardiac cardiolipin biosynthesis to regulate mitochondrial morphogenesis and heart development. *Circulation* 144, 403–406. doi:10.1161/CIRCULATIONAHA.121.054768

Cheng, J. M., Oemrawsingh, R. M., Garcia-Garcia, H. M., Boersma, E., van Geuns, R. J., Serruys, P. W., et al. (2016). PCSK9 in relation to coronary plaque inflammation: results of the ATHEROREMO-IVUS study. *Atherosclerosis* 248, 117–122. doi:10.1016/j.atherosclerosis.2016.03.010

Chikowore, T., Sahibdeen, V., Hendry, L. M., Norris, S. A., Goedecke, J. H., Micklesfield, L. K., et al. (2019). C679X loss-of-function PCSK9 variant is associated with lower fasting glucose in black South African adolescents: birth to Twenty Plus Cohort. *J. Clin. Transl. Endocrinol.* 16, 100186. doi:10.1016/j.jcte.2019.100186

Christiaens, V., Van Hul, M., Lijnen, H. R., and Scroyen, I. (2012). CD36 promotes adipocyte differentiation and adipogenesis. *Biochim. Biophys. Acta* 1820, 949–956. doi:10.1016/j.bbagen.2012.04.001

Cnop, M., Hannaert, J. C., Grupping, A. Y., and Pipeleers, D. G. (2002). Low density lipoprotein can cause death of islet beta-cells by its cellular uptake and oxidative modification. *Endocrinology* 143, 3449–3453. doi:10.1210/en.2002-220273

Costet, P., Cariou, B., Lambert, G., Lalanne, F., Lardeux, B., Jarnoux, A. L., et al. (2006). Hepatic PCSK9 expression is regulated by nutritional status via insulin and sterol regulatory element-binding protein 1c. *J. Biol. Chem.* 281, 6211–6218. doi:10.1074/jbc.M508582200

Cui, C. J., Jin, J. L., Guo, L. N., Sun, J., Wu, N. Q., Guo, Y. L., et al. (2020). Beneficial impact of epigallocatechingallate on LDL-C through PCSK9/LDLR pathway by blocking HNF1α and activating FoxO3a. *J. Transl. Med.* 18, 195. doi:10.1186/s12967-020-02362-4

Cui, C. J., Li, S., and Li, J. J. (2015). PCSK9 and its modulation. *Clin. Chim. Acta* 440, 79–86. doi:10.1016/j.cca.2014.10.044

Cyr, Y., Lamantia, V., Bissonnette, S., Burnette, M., Besse-Patin, A., Demers, A., et al. (2021). Lower plasma PCSK9 in normocholesterolemic subjects is associated with upregulated adipose tissue surface-expression of LDLR and CD36 and NLRP3 inflammasome. *Physiol. Rep.* 9, e14721. doi:10.14814/phy2.14721

Da Dalt, L., Castiglioni, L., Baragetti, A., Audano, M., Svecla, M., Bonacina, F., et al. (2021). PCSK9 deficiency rewires heart metabolism and drives heart failure with preserved ejection fraction. *Eur. Heart J.* 42, 3078–3090. doi:10.1093/eurheartj/ehab431

Da Dalt, L., Ruscica, M., Bonacina, F., Balzarotti, G., Dhyani, A., Di Cairano, E., et al. (2019). PCSK9 deficiency reduces insulin secretion and promotes glucose intolerance: the role of the low-density lipoprotein receptor. *Eur. Heart J.* 40, 357–368. doi:10.1093/eurheartj/ehy357

Davignon, J., and Dubuc, G. (2009). Statins and ezetimibe modulate plasma proprotein convertase subtilisin kexin-9 (PCSK9) levels. *Trans. Am. Clin. Climatol. Assoc.* 120, 163–173.

Demers, A., Samami, S., Lauzier, B., Des Rosiers, C., Ngo, S. E. T., Ong, H., et al. (2015). PCSK9 induces CD36 degradation and affects long-chain fatty acid uptake and triglyceride metabolism in adipocytes and in mouse liver. *Arterioscler. Thromb. Vasc. Biol.* 35, 2517–2525. doi:10.1161/ATVBAHA.115.306032

Denechaud, P. D., Lopez-Mejia, I. C., Giralt, A., Lai, Q., Blanchet, E., Delacuisine, B., et al. (2016). E2F1 mediates sustained lipogenesis and contributes to hepatic steatosis. *J. Clin. Investig.* 126, 137–150. doi:10.1172/JCI81542

De Smet, E., Mensink, R. P., Konings, M., Brufau, G., Groen, A. K., Havinga, R., et al. (2015). Acute intake of plant stanol esters induces changes in lipid and lipoprotein metabolism-related gene expression in the liver and intestines of mice. *Lipids* 50, 529–541. doi:10.1007/s11745-015-4020-1

Dettlaff-Pokora, A., Sucajtys-Szulc, E., and Sledzinski, T. (2019). Up-regulation of PCSK9 gene expression and diminished level of LDL-receptor in rat liver as a potential cause of post-lipectomy hypercholesterolemia. *Mol. Cell. Biochem.* 455, 207–217. doi:10.1007/s11010-018-3484-8

Ding, Z., Pothineni, N. V. K., Goel, A., Lüscher, T. F., and Mehta, J. L. (2020). PCSK9 and inflammation: role of shear stress, pro-inflammatory cytokines, and LOX-1. *Cardiovasc Res.* 116, 908–915. doi:10.1093/cvr/cvz313

Ding, Z., Wang, X., Liu, S., Shahanawaz, J., Theus, S., Fan, Y., et al. (2018). PCSK9 expression in the ischaemic heart and its relationship to infarct size, cardiac function, and development of autophagy. *Cardiovasc Res.* 114, 1738–1751. doi:10.1093/cvr/cvy128

Dozio, E., Ruscica, M., Vianello, E., Macchi, C., Sitzia, C., Schmitz, G., et al. (2020). PCSK9 expression in epicardial adipose tissue: molecular association with local tissue inflammation. *Mediat. Inflamm.* 2020, 1348913. doi:10.1155/2020/1348913

DSouza, K., Nzirorera, C., and Kienesberger, P. C. (2016). Lipid metabolism and signaling in cardiac lipotoxicity. *Biochim. Biophys. Acta* 1861, 1513–1524. doi:10.1016/j.bbalip.2016.02.016

Dugardin, C., Briand, O., Touche, V., Schonewille, M., Moreau, F., Le May, C., et al. (2017). Retrograde cholesterol transport in the human Caco-2/TC7 cell line: a model to study trans-intestinal cholesterol excretion in atherogenic and diabetic dyslipidemia. *Acta Diabetol.* 54, 191–199. doi:10.1007/s00592-016-0936-z

Eberlé, D., Hegarty, B., Bossard, P., Ferré, P., and Foufelle, F. (2004). SREBP transcription factors: master regulators of lipid homeostasis. *Biochimie* 86, 839–848. doi:10.1016/j.biochi.2004.09.018

Eizirik, D. L., Pasquali, L., and Cnop, M. (2020). Pancreatic β-cells in type 1 and type 2 diabetes mellitus: different pathways to failure. *Nat. Rev. Endocrinol.* 16, 349–362. doi:10.1038/s41574-020-0355-7

Ernande, L., Rietzschel, E. R., Bergerot, C., De Buyzere, M. L., Schnell, F., Groisne, L., et al. (2010). Impaired myocardial radial function in asymptomatic patients with type 2 diabetes mellitus: a speckle-tracking imaging study. *J. Am. Soc. Echocardiogr.* 23, 1266–1272. doi:10.1016/j.echo.2010.09.007

Farahnak, Z., Chapados, N., and Lavoie, J. M. (2018). Exercise training increased gene expression of LDL-R and PCSK9 in intestine: link to transintestinal cholesterol excretion. *Gen. Physiol. Biophys.* 37, 309–317. doi:10.4149/gpb_2017047

Farnier, M., Hovingh, G. K., Langslet, G., Dufour, R., Baccara-Dinet, M. T., Din-Bell, C., et al. (2018). Long-term safety and efficacy of alirocumab in patients with heterozygous familial hypercholesterolemia: an open-label extension of the ODYSSEY program. *Atherosclerosis* 278, 307–314. doi:10.1016/j.atherosclerosis.2018.08.036

Ference, B. A., Robinson, J. G., Brook, R. D., Catapano, A. L., Chapman, M. J., Neff, D. R., et al. (2016). Variation in PCSK9 and HMGCR and risk of cardiovascular disease and diabetes. *N. Engl. J. Med.* 375, 2144–2153. doi:10.1056/NEJMoa1604304

Ferreira, J. P., Xhaard, C., Lamiral, Z., Borges-Canha, M., Neves, J. S., Dandine-Roulland, C., et al. (2020). PCSK9 protein and rs562556 polymorphism are associated with arterial plaques in healthy middle-aged population: the STANISLAS cohort. *J. Am. Heart Assoc.* 9, e014758. doi:10.1161/JAHA.119.014758

Ferri, N., Ruscica, M., Lupo, M. G., Vicenzi, M., Sirtori, C. R., and Corsini, A. (2022). Pharmacological rationale for the very early treatment of acute coronary syndrome with monoclonal antibodies anti-PCSK9. *Pharmacol. Res.* 184, 106439. doi:10.1016/j.phrs.2022.106439

Folli, F., La Rosa, S., Finzi, G., Davalli, A. M., Galli, A., Dick, E. J., Jr., et al. (2018). Pancreatic islet of Langerhans' cytoarchitecture and ultrastructure in normal glucose tolerance and in type 2 diabetes mellitus. *Diabetes Obes. Metab.* 20 (Suppl. 2), 137–144. doi:10.1111/dom.13380

Fu, T., Guan, Y., Xu, J., and Wang, Y. (2017). APP, APLP2 and LRP1 interact with PCSK9 but are not required for PCSK9-mediated degradation of the LDLR *in vivo*. *Biochim. Biophys. Acta Mol. Cell. Biol. Lipids* 1862, 883–889. doi:10.1016/j.bbalip.2017.05.002

Furtado, R. H. M., Fagundes, A. A., Jr., Oyama, K., Zelniker, T. A., Tang, M., Kuder, J. F., et al. (2022). Effect of evolocumab in patients with prior percutaneous coronary intervention. *Circ. Cardiovasc Interv.* 15, e011382. doi:10.1161/CIRCINTERVENTIONS.121.011382

Furuhashi, M., Kitamura, K., Adachi, M., Miyoshi, T., Wakida, N., Ura, N., et al. (2005). Liddle's syndrome caused by a novel mutation in the proline-rich PY motif of the epithelial sodium channel beta-subunit. *J. Clin. Endocrinol. Metab.* 90, 340–344. doi:10.1210/jc.2004-1027

Garçon, D., Berger, J. M., Cariou, B., and Le May, C. (2022). Transintestinal cholesterol excretion in health and disease. *Curr. Atheroscler. Rep.* 24, 153–160. doi:10.1007/s11883-022-00995-y

Ghouse, J., Ahlberg, G., Bundgaard, H., and Olesen, M. S. (2022). Effect of loss-of-function genetic variants in PCSK9 on glycemic traits, neurocognitive impairment, and hepatobiliary function. *Diabetes Care* 45, 251–254. doi:10.2337/dc21-0955

Gibbs, J. P., Doshi, S., Kuchimanchi, M., Grover, A., Emery, M. G., Dodds, M. G., et al. (2017). Impact of target-mediated elimination on the dose and regimen of evolocumab, a human monoclonal antibody against proprotein convertase subtilisin/kexin type 9 (PCSK9). *J. Clin. Pharmacol.* 57, 616–626. doi:10.1002/jcph.840

Goldberg, I. J., Trent, C. M., and Schulze, P. C. (2012). Lipid metabolism and toxicity in the heart. *Cell. Metab.* 15, 805–812. doi:10.1016/j.cmet.2012.04.006

Gotoh, S., and Negishi, M. (2015). Statin-activated nuclear receptor PXR promotes SGK2 dephosphorylation by scaffolding PP2C to induce hepatic gluconeogenesis. *Sci. Rep.* 5, 14076. doi:10.1038/srep14076

Guo, W. J., Wang, Y. C., Ma, Y. D., Cui, Z. H., Zhang, L. X., Nie, L., et al. (2021a). Contribution of high-fat diet-induced PCSK9 upregulation to a mouse model of PCOS is mediated partly by SREBP2. *Reproduction* 162, 397–410. doi:10.1530/REP-21-0164

Guo, Y., Yan, B., Gui, Y., Tang, Z., Tai, S., Zhou, S., et al. (2021b). Physiology and role of PCSK9 in vascular disease: potential impact of localized PCSK9 in vascular wall. *J. Cell. Physiol.* 236, 2333–2351. doi:10.1002/jcp.30025

Hanukoglu, I., Boggula, V. R., Vaknine, H., Sharma, S., Kleyman, T., and Hanukoglu, A. (2017). Expression of epithelial sodium channel (ENaC) and CFTR in the human epidermis and epidermal appendages. *Histochem Cell. Biol.* 147, 733–748. doi:10.1007/s00418-016-1535-3

Hao, Y., Yang, Y. L., Wang, Y. C., and Li, J. (2022). Effect of the early application of evolocumab on blood lipid profile and cardiovascular prognosis in patients with extremely high-risk acute coronary syndrome. *Int. Heart J.* 63, 669–677. doi:10.1536/ihj.22-052

Hay, R., Cullen, B., Graham, N., Lyall, D. M., Aman, A., Pell, J. P., et al. (2022). Genetic analysis of the PCSK9 locus in psychological, psychiatric, metabolic and cardiovascular traits in UK Biobank. *Eur. J. Hum. Genet.* 30, 1380–1390. doi:10.1038/s41431-022-01107-9

Hooper, A. J., Marais, A. D., Tanyanyiwa, D. M., and Burnett, J. R. (2007). The C679X mutation in PCSK9 is present and lowers blood cholesterol in a Southern African population. *Atherosclerosis* 193, 445–448. doi:10.1016/j.atherosclerosis.2006.08.039

Hu, D., Guo, Y., Wu, R., Shao, T., Long, J., Yu, B., et al. (2021). New insight into metformin-induced cholesterol-lowering effect crosstalk between glucose and cholesterol homeostasis via ChREBP (Carbohydrate-Responsive element-binding protein)-mediated PCSK9 (proprotein convertase subtilisin/kexin type 9) regulation. *Arterioscler. Thromb. Vasc. Biol.* 41, e208–e223. doi:10.1161/ATVBAHA.120.315708

Huang, L., Wu, H., Wu, Y., Song, F., Zhang, L., Li, Z., et al. (2022). Pcsk9 knockout aggravated experimental apical periodontitis via LDLR. *J. Dent. Res.* 101, 83–92. doi:10.1177/00220345211015128

Hui, D. Y., Labonté, E. D., and Howles, P. N. (2008). Development and physiological regulation of intestinal lipid absorption. III. Intestinal transporters and cholesterol absorption. *Am. J. Physiol. Gastrointest. Liver Physiol.* 294, G839–G843. doi:10.1152/ajpgi.00061.2008

Hummelgaard, S., Vilstrup, J. P., Gustafsen, C., Glerup, S., and Weyer, K. (2023). Targeting PCSK9 to tackle cardiovascular disease. *Pharmacol. Ther.* 249, 108480. doi:10.1016/j.pharmthera.2023.108480

Humphries, S. E., Neely, R. D., Whittall, R. A., Troutt, J. S., Konrad, R. J., Scartezini, M., et al. (2009). Healthy individuals carrying the PCSK9 p.R46L variant and familial hypercholesterolemia patients carrying PCSK9 p.D374Y exhibit lower plasma concentrations of PCSK9. *Clin. Chem.* 55, 2153–2161. doi:10.1373/clinchem.2009.129759

Ibarretxe, D., Girona, J., Plana, N., Cabré, A., Ferré, R., Amigó, N., et al. (2016). Circulating PCSK9 in patients with type 2 diabetes and related metabolic disorders. *Clin. Investig. Arterioscler.* 28, 71–78. doi:10.1016/j.arteri.2015.11.001

Jakulj, L., van Dijk, T. H., de Boer, J. F., Kootte, R. S., Schonewille, M., Paalvast, Y., et al. (2016). Transintestinal cholesterol transport is active in mice and humans and controls ezetimibe-induced fecal neutral sterol excretion. *Cell. Metab.* 24, 783–794. doi:10.1016/j.cmet.2016.10.001

Javaid, H. M. A., Ko, E., Joo, E. J., Kwon, S. H., Park, J. H., Shin, S., et al. (2023). TNFα-induced NLRP3 inflammasome mediates adipocyte dysfunction and activates macrophages through adipocyte-derived lipocalin 2. *Metabolism* 142, 155527. doi:10.1016/j.metabol.2023.155527

Jeenduang, N., Porntadavity, S., and Wanmasae, S. (2015). Combined PCSK9 and APOE polymorphisms are genetic risk factors associated with elevated plasma lipid levels in a Thai population. *Lipids* 50, 543–553. doi:10.1007/s11745-015-4017-9

Jeong, H. J., Lee, H. S., Kim, K. S., Kim, Y. K., Yoon, D., and Park, S. W. (2008). Sterol-dependent regulation of proprotein convertase subtilisin/kexin type 9 expression by sterol-regulatory element binding protein-2. *J. Lipid Res.* 49, 399–409. doi:10.1194/jlr.M700443-JLR200

Kent, S. T., Rosenson, R. S., Avery, C. L., Chen, Y. I., Correa, A., Cummings, S. R., et al. (2017). PCSK9 loss-of-function variants, low-density lipoprotein cholesterol, and risk of coronary heart disease and stroke: data from 9 studies of blacks and whites. *Circ. Cardiovasc Genet.* 10, e001632. doi:10.1161/CIRCGENETICS.116.001632

Kim, Y. U., Kee, P., Danila, D., and Teng, B. B. (2019). A critical role of PCSK9 in mediating IL-17-producing T cell responses in hyperlipidemia. *Immune Netw.* 19, e41. doi:10.4110/in.2019.19.e41

Kleinewietfeld, M., and Hafler, D. A. (2013). The plasticity of human Treg and Th17 cells and its role in autoimmunity. *Semin. Immunol.* 25, 305–312. doi:10.1016/j.smim.2013.10.009

Kruit, J. K., Kremer, P. H., Dai, L., Tang, R., Ruddle, P., de Haan, W., et al. (2010). Cholesterol efflux via ATP-binding cassette transporter A1 (ABCA1) and cholesterol uptake via the LDL receptor influences cholesterol-induced impairment of beta cell function in mice. *Diabetologia* 53, 1110–1119. doi:10.1007/s00125-010-1691-2

Kruit, J. K., Wijesekara, N., Westwell-Roper, C., Vanmierlo, T., de Haan, W., Bhattacharjee, A., et al. (2012). Loss of both ABCA1 and ABCG1 results in increased disturbances in islet sterol homeostasis, inflammation, and impaired β-cell function. *Diabetes* 61, 659–664. doi:10.2337/db11-1341

Lagace, T. A., Curtis, D. E., Garuti, R., McNutt, M. C., Park, S. W., Prather, H. B., et al. (2006). Secreted PCSK9 decreases the number of LDL receptors in hepatocytes and in livers of parabiotic mice. *J. Clin. Investig.* 116, 2995–3005. doi:10.1172/JCI29383

Lai, Q., Giralt, A., Le May, C., Zhang, L., Cariou, B., Denechaud, P. D., et al. (2017). E2F1 inhibits circulating cholesterol clearance by regulating Pcsk9 expression in the liver. *JCI Insight* 2, e89729. doi:10.1172/jci.insight.89729

Lakoski, S. G., Lagace, T. A., Cohen, J. C., Horton, J. D., and Hobbs, H. H. (2009). Genetic and metabolic determinants of plasma PCSK9 levels. *J. Clin. Endocrinol. Metab.* 94, 2537–2543. doi:10.1210/jc.2009-0141

Langhi, C., Le May, C., Gmyr, V., Vandewalle, B., Kerr-Conte, J., Krempf, M., et al. (2009). PCSK9 is expressed in pancreatic delta-cells and does not alter insulin secretion. *Biochem. Biophys. Res. Commun.* 390, 1288–1293. doi:10.1016/j.bbrc.2009.10.138

Lau, P., Soubeyrand, S., Hegele, R. A., Lagace, T. A., and McPherson, R. (2020). Molecular mechanism linking a novel PCSK9 copy number variant to severe hypercholesterolemia. *Atherosclerosis* 304, 39–43. doi:10.1016/j.atherosclerosis.2020.05.013

Laudette, M., Lindbom, M., Arif, M., Cinato, M., Ruiz, M., Doran, S., et al. (2023). Cardiomyocyte-specific PCSK9 deficiency compromises mitochondrial bioenergetics and heart function. *Cardiovasc Res.* 119, 1537–1552. doi:10.1093/cvr/cvad041

Le, Q. T., Blanchet, M., Seidah, N. G., and Labonté, P. (2015). Plasma membrane tetraspanin CD81 complexes with proprotein convertase subtilisin/kexin type 9 (PCSK9) and low density lipoprotein receptor (LDLR), and its levels are reduced by PCSK9. *J. Biol. Chem.* 290, 23385–23400. doi:10.1074/jbc.M115.642991

Leggat, J., Bidault, G., and Vidal-Puig, A. (2021). Lipotoxicity: a driver of heart failure with preserved ejection fraction? *Clin. Sci. (Lond)* 135, 2265–2283. doi:10.1042/CS20210127

Le May, C., Berger, J. M., Lespine, A., Pillot, B., Prieur, X., Letessier, E., et al. (2013). Transintestinal cholesterol excretion is an active metabolic process modulated by PCSK9 and statin involving ABCB1. *Arterioscler. Thromb. Vasc. Biol.* 33, 1484–1493. doi:10.1161/ATVBAHA.112.300263

Le May, C., Kourimate, S., Langhi, C., Chétiveaux, M., Jarry, A., Comera, C., et al. (2009). Proprotein convertase subtilisin kexin type 9 null mice are protected from postprandial triglyceridemia. *Arterioscler. Thromb. Vasc. Biol.* 29, 684–690. doi:10.1161/ATVBAHA.108.181586

Levenson, A. E., Milliren, C. E., Biddinger, S. B., Ebbeling, C. B., Feldman, H. A., Ludwig, D. S., et al. (2017). Calorically restricted diets decrease PCSK9 in overweight adolescents. *Nutr. Metab. Cardiovasc Dis.* 27, 342–349. doi:10.1016/j.numecd.2016.12.010

Levy, E., Ben Djoudi Ouadda, A., Spahis, S., Sane, A. T., Garofalo, C., Grenier, É., et al. (2013). PCSK9 plays a significant role in cholesterol homeostasis and lipid transport in intestinal epithelial cells. *Atherosclerosis* 227, 297–306. doi:10.1016/j.atherosclerosis.2013.01.023

Lewis, G. F., and Rader, D. J. (2005). New insights into the regulation of HDL metabolism and reverse cholesterol transport. *Circ. Res.* 96, 1221–1232. doi:10.1161/01.RES.0000170946.56981.5c

Li, H., Dong, B., Park, S. W., Lee, H. S., Chen, W., and Liu, J. (2009). Hepatocyte nuclear factor 1alpha plays a critical role in PCSK9 gene transcription and regulation by the natural hypocholesterolemic compound berberine. *J. Biol. Chem.* 284, 28885–28895. doi:10.1074/jbc.M109.052407

Li, H., and Liu, J. (2012). The novel function of HINFP as a co-activator in sterol-regulated transcription of PCSK9 in HepG2 cells. *Biochem. J.* 443, 757–768. doi:10.1042/BJ20111645

Lin, Y. K., Yeh, C. T., Kuo, K. T., Yadav, V. K., Fong, I. H., Kounis, N. G., et al. (2021). Pterostilbene increases LDL metabolism in HL-1 cardiomyocytes by modulating the PCSK9/HNF1α/SREBP2/LDLR signaling cascade, upregulating epigenetic hsa-miR-335 and hsa-miR-6825, and LDL receptor expression. *Antioxidants (Basel)* 10, 1280. doi:10.3390/antiox10081280

Liu, C., Lu, H., Yuan, F., Chen, W. L., Xu, H. R., Li, H., et al. (2019). A phase 1, randomized, double-blind, single-dose, placebo-controlled safety, tolerability, and pharmacokinetic/pharmacodynamic study of evolocumab in healthy Chinese subjects. *Clin. Pharmacol.* 11, 145–153. doi:10.2147/CPAA.S208033

Liu, S., and Vaziri, N. D. (2014). Role of PCSK9 and IDOL in the pathogenesis of acquired LDL receptor deficiency and hypercholesterolemia in nephrotic syndrome. *Nephrol. Dial. Transpl.* 29, 538–543. doi:10.1093/ndt/gft439

Liu, Y., Zhao, Y., Feng, P., and Jiang, H. (2023). PCSK9 inhibitor attenuates atherosclerosis by regulating SNHG16/EZH2/TRAF5-mediated VSMC proliferation, migration, and foam cell formation. *Cell. Biol. Int.* 47, 1267–1280. doi:10.1002/cbin.12018

Lopaschuk, G. D., Karwi, Q. G., Tian, R., Wende, A. R., and Abel, E. D. (2021). Cardiac energy metabolism in heart failure. *Circ. Res.* 128, 1487–1513. doi:10.1161/CIRCRESAHA.121.318241

Lotta, L. A., Sharp, S. J., Burgess, S., Perry, J. R. B., Stewart, I. D., Willems, S. M., et al. (2016). Association between low-density lipoprotein cholesterol-lowering genetic variants and risk of type 2 diabetes: a meta-analysis. *JAMA* 316, 1383–1391. doi:10.1001/jama.2016.14568

Lu, X., Liu, J., Hou, F., Liu, Z., Cao, X., Seo, H., et al. (2011). Cholesterol induces pancreatic β cell apoptosis through oxidative stress pathway. *Cell. Stress Chaperones* 16, 539–548. doi:10.1007/s12192-011-0265-7

Lytrivi, M., Castell, A. L., Poitout, V., and Cnop, M. (2020). Recent insights into mechanisms of β-cell lipo- and glucolipotoxicity in type 2 diabetes. *J. Mol. Biol.* 432, 1514–1534. doi:10.1016/j.jmb.2019.09.016

Marku, A., Da Dalt, L., Galli, A., Dule, N., Corsetto, P., Rizzo, A. M., et al. (2022). Pancreatic PCSK9 controls the organization of the β-cell secretory pathway via LDLR-cholesterol axis. *Metabolism* 136, 155291. doi:10.1016/j.metabol.2022.155291

Mazura, A. D., Ohler, A., Storck, S. E., Kurtyka, M., Scharfenberg, F., Weggen, S., et al. (2022). PCSK9 acts as a key regulator of Aβ clearance across the blood-brain barrier. *Cell. Mol. Life Sci.* 79, 212. doi:10.1007/s00018-022-04237-x

Mbikay, M., Sirois, F., Gyamera-Acheampong, C., Wang, G. S., Rippstein, P., Chen, A., et al. (2015). Variable effects of gender and Western diet on lipid and glucose homeostasis in aged PCSK9-deficient C57BL/6 mice CSK9PC57BL/6. *J. Diabetes* 7, 74–84. doi:10.1111/1753-0407.12139

Mbikay, M., Sirois, F., Mayne, J., Wang, G. S., Chen, A., Dewpura, T., et al. (2010). PCSK9-deficient mice exhibit impaired glucose tolerance and pancreatic islet abnormalities. *FEBS Lett.* 584, 701–706. doi:10.1016/j.febslet.2009.12.018

McNamara, D. B., Murthy, S. N., Fonseca, A. N., Desouza, C. V., Kadowitz, P. J., and Fonseca, V. A. (2009). Animal models of catheter-induced intimal hyperplasia in type 1 and type 2 diabetes and the effects of pharmacologic intervention. *Can. J. Physiol. Pharmacol.* 87, 37–50. doi:10.1139/Y08-098

Mefford, M. T., Rosenson, R. S., Cushman, M., Farkouh, M. E., McClure, L. A., Wadley, V. G., et al. (2018). PCSK9 variants, low-density lipoprotein cholesterol, and neurocognitive impairment: reasons for geographic and racial differences in stroke study (REGARDS). *Circulation* 137, 1260–1269. doi:10.1161/CIRCULATIONAHA.117.029785

Momtazi-Borojeni, A. A., Banach, M., Ruscica, M., and Sahebkar, A. (2022). The role of PCSK9 in NAFLD/NASH and therapeutic implications of PCSK9 inhibition. *Expert Rev. Clin. Pharmacol.* 15, 1199–1208. doi:10.1080/17512433.2022.2132229

Moreau, F., Thédrez, A., Garçon, D., Ayer, A., Sotin, T., Dijk, W., et al. (2021). PCSK9 is not secreted from mature differentiated intestinal cells. *J. Lipid Res.* 62, 100096. doi:10.1016/j.jlr.2021.100096

Moriyama, H., Endo, J., Ikura, H., Kitakata, H., Momoi, M., Shinya, Y., et al. (2022). Qualitative and quantitative effects of fatty acids involved in heart diseases. *Metabolites* 12, 210. doi:10.3390/metabo12030210

Musunuru, K., Chadwick, A. C., Mizoguchi, T., Garcia, S. P., DeNizio, J. E., Reiss, C. W., et al. (2021). *In vivo* CRISPR base editing of PCSK9 durably lowers cholesterol in primates. *Nature* 593, 429–434. doi:10.1038/s41586-021-03534-y

Nicholls, S. J., Puri, R., Anderson, T., Ballantyne, C. M., Cho, L., Kastelein, J. J., et al. (2016). Effect of evolocumab on progression of coronary disease in statin-treated patients: the GLAGOV randomized clinical trial. *Jama* 316, 2373–2384. doi:10.1001/jama.2016.16951

ODonoghue, M. L., Giugliano, R. P., Wiviott, S. D., Atar, D., Keech, A., Kuder, J. F., et al. (2022). Long-term evolocumab in patients with established atherosclerotic cardiovascular disease. *Circulation* 146, 1109–1119. doi:10.1161/CIRCULATIONAHA.122.061620

Ooi, T. C., Krysa, J. A., Chaker, S., Abujrad, H., Mayne, J., Henry, K., et al. (2017). The effect of PCSK9 loss-of-function variants on the postprandial lipid and ApoB-lipoprotein response. *J. Clin. Endocrinol. Metab.* 102, 3452–3460. doi:10.1210/jc.2017-00684

Ooi, T. C., Raymond, A., Cousins, M., Favreau, C., Taljaard, M., Gavin, C., et al. (2015). Relationship between testosterone, estradiol and circulating PCSK9: cross-sectional and interventional studies in humans. *Clin. Chim. Acta* 446, 97–104. doi:10.1016/j.cca.2015.03.036

Orth, M., and Bellosta, S. (2012). Cholesterol: its regulation and role in central nervous system disorders. *Cholesterol* 2012, 292598. doi:10.1155/2012/292598

Park, H., Li, Z., Yang, X. O., Chang, S. H., Nurieva, R., Wang, Y. H., et al. (2005). A distinct lineage of CD4 T cells regulates tissue inflammation by producing interleukin 17. *Nat. Immunol.* 6, 1133–1141. doi:10.1038/ni1261

Patel, M., Rodriguez, D., Yousefi, K., John-Williams, K., Mendez, A. J., Goldberg, R. B., et al. (2020). Osteopontin and LDLR are upregulated in hearts of sudden cardiac death victims with heart failure with preserved ejection fraction and diabetes mellitus. *Front. Cardiovasc Med.* 7, 610282. doi:10.3389/fcvm.2020.610282

Paul, R., Choudhury, A., Choudhury, S., Mazumder, M. K., and Borah, A. (2016). Cholesterol in pancreatic β-cell death and dysfunction: underlying mechanisms and pathological implications. *Pancreas* 45, 317–324. doi:10.1097/MPA.0000000000000486

Pelletier, R. M., Layeghkhavidaki, H., Seidah, N. G., Prat, A., and Vitale, M. L. (2022). PCSK9 contributes to the cholesterol, glucose, and Insulin2 homeostasis in seminiferous tubules and maintenance of immunotolerance in testis. *Front. Cell. Dev. Biol.* 10, 889972. doi:10.3389/fcell.2022.889972

Perego, C., Da Dalt, L., Pirillo, A., Galli, A., and Catapano, A. L. (2019). Norata GD: cholesterol metabolism, pancreatic β-cell function and diabetes. *Biochim. Biophys. Acta Mol. Basis Dis.* 1865, 2149–2156. doi:10.1016/j.bbadis.2019.04.012

Pérez de Isla, L., Díaz-Díaz, J. L., Romero, M. J., Muñiz-Grijalvo, O., Mediavilla, J. D., Argüeso, R., et al. (2023). Alirocumab and coronary atherosclerosis in asymptomatic patients with familial hypercholesterolemia: the ARCHITECT study. *Circulation* 147, 1436–1443. doi:10.1161/CIRCULATIONAHA.122.062557

Perman, J. C., Boström, P., Lindbom, M., Lidberg, U., StÅhlman, M., Hägg, D., et al. (2011). The VLDL receptor promotes lipotoxicity and increases mortality in mice following an acute myocardial infarction. *J. Clin. Investig.* 121, 2625–2640. doi:10.1172/JCI43068

Petersen-Uribe, Á., Kremser, M., Rohlfing, A. K., Castor, T., Kolb, K., Dicenta, V., et al. (2021). Platelet-derived PCSK9 is associated with LDL metabolism and modulates atherothrombotic mechanisms in coronary artery disease. *Int. J. Mol. Sci.* 22, 11179. doi:10.3390/ijms222011179

Peyot, M. L., Roubtsova, A., Lussier, R., Chamberland, A., Essalmani, R., Murthy Madiraju, S. R., et al. (2021). Substantial PCSK9 inactivation in β-cells does not modify glucose homeostasis or insulin secretion in mice. *Biochim. Biophys. Acta Mol. Cell. Biol. Lipids* 1866, 158968. doi:10.1016/j.bbalip.2021.158968

Poirier, S., Mayer, G., Benjannet, S., Bergeron, E., Marcinkiewicz, J., Nassoury, N., et al. (2008). The proprotein convertase PCSK9 induces the degradation of low density lipoprotein receptor (LDLR) and its closest family members VLDLR and ApoER2. *J. Biol. Chem.* 283, 2363–2372. doi:10.1074/jbc.M708098200

Poirier, S., Prat, A., Marcinkiewicz, E., Paquin, J., Chitramuthu, B. P., Baranowski, D., et al. (2006). Implication of the proprotein convertase NARC-1/PCSK9 in the development of the nervous system. *J. Neurochem.* 98, 838–850. doi:10.1111/j.1471-4159.2006.03928.x

Punch, E., Klein, J., Diaba-Nuhoho, P., Morawietz, H., and Garelnabi, M. (2022). Effects of PCSK9 targeting: alleviating oxidation, inflammation, and atherosclerosis. *J. Am. Heart Assoc.* 11, e023328. doi:10.1161/JAHA.121.023328

Qin, J., Liu, L., Su, X. D., Wang, B. B., Fu, B. S., Cui, J. Z., et al. (2021). The effect of PCSK9 inhibitors on brain stroke prevention: a systematic review and meta-analysis. *Nutr. Metab. Cardiovasc Dis.* 31, 2234–2243. doi:10.1016/j.numecd.2021.03.026

Räber, L., Ueki, Y., Otsuka, T., Losdat, S., Häner, J. D., Lonborg, J., et al. (2022). Effect of alirocumab added to high-intensity statin therapy on coronary atherosclerosis in patients with acute myocardial infarction: the PACMAN-AMI randomized clinical trial. *Jama* 327, 1771–1781. doi:10.1001/jama.2022.5218

Ramin-Mangata, S., Thedrez, A., Nativel, B., Diotel, N., Blanchard, V., Wargny, M., et al. (2021). Effects of proprotein convertase subtilisin kexin type 9 modulation in human pancreatic beta cells function. *Atherosclerosis* 326, 47–55. doi:10.1016/j.atherosclerosis.2021.03.044

Rashid, S., Curtis, D. E., Garuti, R., Anderson, N. N., Bashmakov, Y., Ho, Y. K., et al. (2005). Decreased plasma cholesterol and hypersensitivity to statins in mice lacking Pcsk9. *Proc. Natl. Acad. Sci. U. S. A.* 102, 5374–5379. doi:10.1073/pnas.0501652102

Ray, K. K., Landmesser, U., Leiter, L. A., Kallend, D., Dufour, R., Karakas, M., et al. (2017). Inclisiran in patients at high cardiovascular risk with elevated LDL cholesterol. *N. Engl. J. Med.* 376, 1430–1440. doi:10.1056/NEJMoa1615758

Ray, K. K., Raal, F. J., Kallend, D. G., Jaros, M. J., Koenig, W., Leiter, L. A., et al. (2023a). Inclisiran and cardiovascular events: a patient-level analysis of phase III trials. *Eur. Heart J.* 44, 129–138. doi:10.1093/eurheartj/ehac594

Ray, K. K., Stoekenbroek, R. M., Kallend, D., Nishikido, T., Leiter, L. A., Landmesser, U., et al. (2019). Effect of 1 or 2 doses of inclisiran on low-density lipoprotein cholesterol levels: one-year follow-up of the ORION-1 randomized clinical trial. *JAMA Cardiol.* 4, 1067–1075. doi:10.1001/jamacardio.2019.3502

Ray, K. K., Troquay, R. P. T., Visseren, F. L. J., Leiter, L. A., Scott Wright, R., Vikarunnessa, S., et al. (2023b). Long-term efficacy and safety of inclisiran in patients with high cardiovascular risk and elevated LDL cholesterol (ORION-3): results from the 4-year open-label extension of the ORION-1 trial. *Lancet Diabetes Endocrinol.* 11, 109–119. doi:10.1016/S2213-8587(22)00353-9

Razani, B., Zhang, H., Schulze, P. C., Schilling, J. D., Verbsky, J., Lodhi, I. J., et al. (2011). Fatty acid synthase modulates homeostatic responses to myocardial stress. *J. Biol. Chem.* 286, 30949–30961. doi:10.1074/jbc.M111.230508

Robinson, J. G., Rosenson, R. S., Farnier, M., Chaudhari, U., Sasiela, W. J., Merlet, L., et al. (2017). Safety of very low low-density lipoprotein cholesterol levels with alirocumab: pooled data from randomized trials. *J. Am. Coll. Cardiol.* 69, 471–482. doi:10.1016/j.jacc.2016.11.037

Roubtsova, A., Chamberland, A., Marcinkiewicz, J., Essalmani, R., Fazel, A., Bergeron, J. J., et al. (2015). PCSK9 deficiency unmasks a sex- and tissue-specific subcellular distribution of the LDL and VLDL receptors in mice. *J. Lipid Res.* 56, 2133–2142. doi:10.1194/jlr.M061952

Roubtsova, A., Munkonda, M. N., Awan, Z., Marcinkiewicz, J., Chamberland, A., Lazure, C., et al. (2011). Circulating proprotein convertase subtilisin/kexin 9 (PCSK9) regulates VLDLR protein and triglyceride accumulation in visceral adipose tissue. *Arterioscler. Thromb. Vasc. Biol.* 31, 785–791. doi:10.1161/ATVBAHA.110.220988

Rousselet, E., Marcinkiewicz, J., Kriz, J., Zhou, A., Hatten, M. E., Prat, A., et al. (2011). PCSK9 reduces the protein levels of the LDL receptor in mouse brain during development and after ischemic stroke. *J. Lipid Res.* 52, 1383–1391. doi:10.1194/jlr.M014118

Rudenko, G., Henry, L., Henderson, K., Ichtchenko, K., Brown, M. S., Goldstein, J. L., et al. (2002). Structure of the LDL receptor extracellular domain at endosomal pH. *Science* 298, 2353–2358. doi:10.1126/science.1078124

Rütti, S., Ehses, J. A., Sibler, R. A., Prazak, R., Rohrer, L., Georgopoulos, S., et al. (2009). Low- and high-density lipoproteins modulate function, apoptosis, and proliferation of primary human and murine pancreatic beta-cells. *Endocrinology* 150, 4521–4530. doi:10.1210/en.2009-0252

Sabatine, M. S., Giugliano, R. P., Keech, A. C., Honarpour, N., Wiviott, S. D., Murphy, S. A., et al. (2017). Evolocumab and clinical outcomes in patients with cardiovascular disease. *N. Engl. J. Med.* 376, 1713–1722. doi:10.1056/NEJMoa1615664

Sadik, N. A., Rashed, L. A., and El-Sawy, S. S. (2022). The relationship of circulating proprotein convertase subtilisin/kexin type 9 with TSH and lipid profile in newly diagnosed patients with subclinical and overt hypothyroidism. *Clin. Med. Insights Endocrinol. Diabetes* 15, 11795514221093317. doi:10.1177/11795514221093317

Salvatore, T., Pafundi, P. C., Galiero, R., Albanese, G., Di Martino, A., Caturano, A., et al. (2021). The diabetic cardiomyopathy: the contributing pathophysiological mechanisms. *Front. Med. (Lausanne)* 8, 695792. doi:10.3389/fmed.2021.695792

Sawada, H., Daugherty, A., and Lu, H. S. (2022). Expression of a PCSK9 gain-of-function mutation in C57bl/6J mice to facilitate angiotensin II-induced AAAs. *Biomolecules* 12, 915. doi:10.3390/biom12070915

Schenk, S., and Hoeger, U. (2010). Lipid accumulation and metabolism in polychaete spermatogenesis: role of the large discoidal lipoprotein. *Mol. Reprod. Dev.* 77, 710–719. doi:10.1002/mrd.21208

Schiattarella, G. G., Altamirano, F., Tong, D., French, K. M., Villalobos, E., Kim, S. Y., et al. (2019). Nitrosative stress drives heart failure with preserved ejection fraction. *Nature* 568, 351–356. doi:10.1038/s41586-019-1100-z

Schmidt, A. F., Swerdlow, D. I., Holmes, M. V., Patel, R. S., Fairhurst-Hunter, Z., Lyall, D. M., et al. (2017). PCSK9 genetic variants and risk of type 2 diabetes: a mendelian randomisation study. *Lancet Diabetes Endocrinol.* 5, 97–105. doi:10.1016/S2213-8587(16)30396-5

Schmidt, R. J., Beyer, T. P., Bensch, W. R., Qian, Y. W., Lin, A., Kowala, M., et al. (2008). Secreted proprotein convertase subtilisin/kexin type 9 reduces both hepatic and extrahepatic low-density lipoprotein receptors *in vivo*. *Biochem. Biophys. Res. Commun.* 370, 634–640. doi:10.1016/j.bbrc.2008.04.004

Seidah, N. G., Benjannet, S., Wickham, L., Marcinkiewicz, J., Jasmin, S. B., Stifani, S., et al. (2003). The secretory proprotein convertase neural apoptosis-regulated convertase 1 (NARC-1): liver regeneration and neuronal differentiation. *Proc. Natl. Acad. Sci. U. S. A.* 100, 928–933. doi:10.1073/pnas.0335507100

Şener, Y. Z., and Tokgözoğlu, L. (2023). Pleiotropy of PCSK9: functions in extrahepatic tissues. *Curr. Cardiol. Rep.* 25, 979–985. doi:10.1007/s11886-023-01918-2

Shahid, R., Naik, S. S., Ramphall, S., Rijal, S., Prakash, V., Ekladios, H., et al. (2022). Neurocognitive impairment in cardiovascular disease patients taking statins versus proprotein convertase subtilisin/kexin type 9 (PCSK9) inhibitors: a systematic review. *Cureus* 14, e30942. doi:10.7759/cureus.30942

Sharma, G., and Prossnitz, E. R. (2022). Assessment of metabolic regulation by estrogen receptors. *Methods Mol. Biol.* 2418, 383–404. doi:10.1007/978-1-0716-1920-9_21

Sharotri, V., Collier, D. M., Olson, D. R., Zhou, R., and Snyder, P. M. (2012). Regulation of epithelial sodium channel trafficking by proprotein convertase subtilisin/kexin type 9 (PCSK9). *J. Biol. Chem.* 287, 19266–19274. doi:10.1074/jbc.M112.363382

Skeby, C. K., Hummelgaard, S., Gustafsen, C., Petrillo, F., Frederiksen, K. P., Olsen, D., et al. (2023). Proprotein convertase subtilisin/kexin type 9 targets megalin in the kidney proximal tubule and aggravates proteinuria in nephrotic syndrome. *Kidney Int.* 104, 754–768. doi:10.1016/j.kint.2023.06.024

Spolitu, S., Okamoto, H., Dai, W., Zadroga, J. A., Wittchen, E. S., Gromada, J., et al. (2019). Hepatic glucagon signaling regulates PCSK9 and low-density lipoprotein cholesterol. *Circ. Res.* 124, 38–51. doi:10.1161/CIRCRESAHA.118.313648

Sponder, M., Campean, I. A., Dalos, D., Emich, M., Fritzer-Szekeres, M., Litschauer, B., et al. (2017). Effect of long-term physical activity on PCSK9, high- and low-density lipoprotein cholesterol, and lipoprotein(a) levels: a prospective observational trial. *Pol. Arch. Intern Med.* 127, 506–511. doi:10.20452/pamw.4044

Stumvoll, M., Goldstein, B. J., and van Haeften, T. W. (2005). Type 2 diabetes: principles of pathogenesis and therapy. *Lancet* 365, 1333–1346. doi:10.1016/S0140-6736(05)61032-X

Sun, H. L., Wu, Y. R., Song, F. F., Gan, J., Huang, L. Y., Zhang, L., et al. (2018). Role of PCSK9 in the development of mouse periodontitis before and after treatment: a double-edged sword. *J. Infect. Dis.* 217, 667–680. doi:10.1093/infdis/jix574

Sung, M. M., Koonen, D. P., Soltys, C. L., Jacobs, R. L., Febbraio, M., and Dyck, J. R. (2011). Increased CD36 expression in middle-aged mice contributes to obesity-related cardiac hypertrophy in the absence of cardiac dysfunction. *J. Mol. Med. Berl.* 89, 459–469. doi:10.1007/s00109-010-0720-4

Tanaka, Y., and Kamisako, T. (2021). Regulation of the expression of cholesterol transporters by lipid-lowering drugs ezetimibe and pemafibrate in rat liver and intestine. *Biochim. Biophys. Acta Mol. Basis Dis.* 1867, 166215. doi:10.1016/j.bbadis.2021.166215

Tchéoubi, S. E. R., Akpovi, C. D., Coppée, F., Declèves, A. E., Laurent, S., Agbangla, C., et al. (2022). Molecular and cellular biology of PCSK9: impact on glucose homeostasis. *J. Drug Target* 30, 948–960. doi:10.1080/1061186X.2022.2092622

Tran, N. T., Aslibekyan, S., Tiwari, H. K., Zhi, D., Sung, Y. J., Hunt, S. C., et al. (2015). PCSK9 variation and association with blood pressure in African Americans: preliminary findings from the HyperGEN and REGARDS studies. *Front. Genet.* 6, 136. doi:10.3389/fgene.2015.00136

Tricò, D., Mengozzi, A., Baldi, S., Bizzotto, R., Olaniru, O., Toczyska, K., et al. (2022). Lipid-induced glucose intolerance is driven by impaired glucose kinetics and insulin metabolism in healthy individuals. *Metabolism* 134, 155247. doi:10.1016/j.metabol.2022.155247

Trudsø, L. C., Ghouse, J., Ahlberg, G., Bundgaard, H., and Olesen, M. S. (2023). Association of PCSK9 loss-of-function variants with risk of heart failure. *JAMA Cardiol.* 8, 159–166. doi:10.1001/jamacardio.2022.4798

van der Veen, J. N., van Dijk, T. H., Vrins, C. L., van Meer, H., Havinga, R., Bijsterveld, K., et al. (2009). Activation of the liver X receptor stimulates trans-intestinal excretion of plasma cholesterol. *J. Biol. Chem.* 284, 19211–19219. doi:10.1074/jbc.M109.014860

van der Velde, A. E., Vrins, C. L., van den Oever, K., Kunne, C., Oude Elferink, R. P., Kuipers, F., et al. (2007). Direct intestinal cholesterol secretion contributes significantly to total fecal neutral sterol excretion in mice. *Gastroenterology* 133, 967–975. doi:10.1053/j.gastro.2007.06.019

Varshney, P., Narasimhan, A., Mittal, S., Malik, G., Sardana, K., and Saini, N. (2016). Transcriptome profiling unveils the role of cholesterol in IL-17A signaling in psoriasis. *Sci. Rep.* 6, 19295. doi:10.1038/srep19295

Wang, C., Yosef, N., Gaublomme, J., Wu, C., Lee, Y., Clish, C. B., et al. (2015). CD5L/AIM regulates lipid biosynthesis and restrains Th17 cell pathogenicity. *Cell.* 163, 1413–1427. doi:10.1016/j.cell.2015.10.068

Wang, F., Li, M., Zhang, A., Li, H., Jiang, C., and Guo, J. (2022). PCSK9 modulates macrophage polarization-mediated ventricular remodeling after myocardial infarction. *J. Immunol. Res.* 2022, 7685796. doi:10.1155/2022/7685796

Wang, J., Wang, Y. S., Huang, Y. P., Jiang, C. H., Gao, M., Zheng, X., et al. (2021). Gypenoside LVI improves hepatic LDL uptake by decreasing PCSK9 and upregulating LDLR expression. *Phytomedicine* 91, 153688. doi:10.1016/j.phymed.2021.153688

Wang, X., Li, X., Liu, S., Brickell, A. N., Zhang, J., Wu, Z., et al. (2020). PCSK9 regulates pyroptosis via mtDNA damage in chronic myocardial ischemia. *Basic Res. Cardiol.* 115, 66. doi:10.1007/s00395-020-00832-w

Wanneh, E., Luna, G., Dufour, R., and Baass, A. (2017). Predicting proprotein convertase subtilisin kexin type-9 loss of function mutations using plasma PCSK9 concentration. *J. Clin. Lipidol.* 11, 55–60. doi:10.1016/j.jacl.2016.09.015

Wilharm, A., Brigas, H. C., Sandrock, I., Ribeiro, M., Amado, T., Reinhardt, A., et al. (2021). Microbiota-dependent expansion of testicular IL-17-producing Vγ6(+) γδ T cells upon puberty promotes local tissue immune surveillance. *Mucosal Immunol.* 14, 242–252. doi:10.1038/s41385-020-0330-6

Yang, S. H., Du, Y., Li, S., Zhang, Y., Xu, R. X., Zhu, C. G., et al. (2016). Plasma PCSK9 level is unrelated to blood pressure and not associated independently with carotid intima-media thickness in hypertensives. *Hypertens. Res.* 39, 598–605. doi:10.1038/hr.2016.38

Ye, L., Cao, L., Song, W., Yang, C., Tang, Q., and Yuan, Z. (2023). Interaction between apical periodontitis and systemic disease (Review). *Int. J. Mol. Med.* 52, 60. doi:10.3892/ijmm.2023.5263

Zaid, A., Roubtsova, A., Essalmani, R., Marcinkiewicz, J., Chamberland, A., Hamelin, J., et al. (2008). Proprotein convertase subtilisin/kexin type 9 (PCSK9): hepatocyte-specific low-density lipoprotein receptor degradation and critical role in mouse liver regeneration. *Hepatology* 48, 646–654. doi:10.1002/hep.22354

Zhang, L., Yang, Y., Aroor, A. R., Jia, G., Sun, Z., Parrish, A., et al. (2022). Endothelial sodium channel activation mediates DOCA-salt-induced endothelial cell and arterial stiffening. *Metabolism* 130, 155165. doi:10.1016/j.metabol.2022.155165

Zhao, Z., Tuakli-Wosornu, Y., Lagace, T. A., Kinch, L., Grishin, N. V., Horton, J. D., et al. (2006). Molecular characterization of loss-of-function mutations in PCSK9 and identification of a compound heterozygote. *Am. J. Hum. Genet.* 79, 514–523. doi:10.1086/507488

frontiers | Frontiers in Pharmacology

TYPE Original Research
PUBLISHED 31 July 2024
DOI 10.3389/fphar.2024.1399248

OPEN ACCESS

EDITED BY
Eliot Ohlstein,
Drexel University, United States

REVIEWED BY
Bidhan C. Bandyopadhyay,
United States Department of Veterans Affairs, United States
Xu Teng,
Hebei Medical University, China

*CORRESPONDENCE
Viktória Jeney,
jeney.viktoria@med.unideb.hu

RECEIVED 11 March 2024
ACCEPTED 17 July 2024
PUBLISHED 31 July 2024

CITATION
Tóth A, Lente G, Csiki DM, Balogh E, Szöőr Á, Nagy B Jr. and Jeney V (2024), Activation of PERK/eIF2α/ATF4/CHOP branch of endoplasmic reticulum stress response and cooperation between HIF-1α and ATF4 promotes Daprodustat-induced vascular calcification.
Front. Pharmacol. 15:1399248.
doi: 10.3389/fphar.2024.1399248

Activation of PERK/eIF2α/ATF4/CHOP branch of endoplasmic reticulum stress response and cooperation between HIF-1α and ATF4 promotes Daprodustat-induced vascular calcification

Andrea Tóth[1], Gréta Lente[1,2], Dávid Máté Csiki[1], Enikő Balogh[1], Árpád Szöőr[3], Béla Nagy Jr.[4] and Viktória Jeney[1]*

[1]MTA-DE Lendület Vascular Pathophysiology Research Group, Research Centre for Molecular Medicine, Faculty of Medicine, University of Debrecen, Debrecen, Hungary, [2]Doctoral School of Molecular Cell and Immune Biology, Faculty of Medicine, University of Debrecen, Debrecen, Hungary, [3]Department of Biophysics and Cell Biology, Faculty of Medicine, University of Debrecen, Debrecen, Hungary, [4]Department of Laboratory Medicine, Faculty of Medicine, University of Debrecen, Debrecen, Hungary

Introduction: Vascular calcification is accelerated in patients with chronic kidney disease (CKD) and increases the risk of cardiovascular events. CKD is frequently associated with anemia. Daprodustat (DPD) is a prolyl hydroxylase inhibitor for the treatment of CKD-associated anemia that enhances erythropoiesis through the activation of the hypoxia-inducible factor 1 (HIF-1) pathway. Studies showed that DPD promotes osteogenic differentiation of human aortic smooth muscle cells (HAoSMCs) and increases aorta calcification in mice with CKD. HIF-1 activation has been linked with endoplasmic reticulum (ER) stress; therefore, here we investigated the potential contribution of ER stress, particularly activating transcription factor 4 (ATF4), to the pro-calcification effect of DPD.

Methods: Here, we used an adenine-induced CKD mouse model and HAoSMCs as an *in vitro* vascular calcification model to study the effect of DPD.

Results: DPD treatment (15 mg/kg/day) corrects anemia but increases the expression of hypoxia (Glut1, VEGFA), ER stress (ATF4, CHOP, and GRP78), and osteo-/chondrogenic (Runx2, Sox9, BMP2, and Msx2) markers and accelerates aorta and kidney calcification in CKD mice. DPD activates the PERK/eIF2α/ATF4/CHOP pathway and promotes high phosphate-induced osteo-/chondrogenic differentiation of HAoSMCs. Inhibition of ER stress with 4-PBA or silencing of ATF4 attenuates HAoSMC calcification. DPD-induced ATF4 expression is abolished in the absence of HIF-1α; however, knockdown of ATF4 does not affect HIF-1α expression.

Conclusion: We concluded that DPD induces ER stress *in vitro* and *in vivo*, in which ATF4 serves as a downstream effector of HIF-1 activation. Targeting ATF4 could be a potential therapeutic approach to attenuate the pro-calcific effect of DPD.

KEYWORDS

chronic kidney disease (CKD), vascular calcification, prolyl hydroxylase inhibitor, hypoxia-inducible factor 1, endoplasmic reticulum stress, ATF4, Daprodustat

1 Introduction

CKD is frequently associated with cardiovascular calcification, mainly driven by hyperphosphatemia, a well-characterized calcification inducer (Giachelli, 2009; Ogata et al., 2024). CKD-associated calcification participates in disease progression and the development of cardiovascular complications, which are the major causes of death in CKD patients (Mizobuchi et al., 2009; Zoccali et al., 2023).

Anemia is common and contributes to the increased mortality and morbidity of CKD patients (Hanna et al., 2021; Atkinson and Warady, 2018; Kovesdy et al., 2023). The current standard of anemia treatment is intravenous iron supplementation together with the administration of erythropoiesis-stimulating agents (ESAs) (Hanna et al., 2021). Unfortunately, studies showed that ESAs increase the probability of major cardiovascular events (MACE) in CKD patients (Babitt and Lin, 2012; Portolés et al., 2021). Prolyl hydroxylase domain-containing (PHD) enzyme inhibitors represent a new concept in treating CKD-associated anemia through the activation of the hypoxia-inducible factor (HIF) pathway and subsequent erythropoiesis (Mima, 2021).

Numerous clinical trials have been completed with three different PHD inhibitors Roxadustat, Vadadustat, and Daprodustat (DPD) concluding that these orally administrable compounds are effective and safe alternatives to ESAs for anemia treatment in CKD patients. All of the compounds are approved for marketing in Japan, Roxadustat is approved in China and DPD is the only one approved by the United States Food and Drug Administration (FDA) for anemia management in CKD patients. On the other hand, according to the ASCEND-D trial, DPD is not a safer alternative in comparison to ESAs for the occurrence of MACE in CKD patients (Singh et al., 2021). Previously, we showed that DPD promotes CKD-associated vascular and aortic valve calcification via the activation of the HIF pathway (Tóth et al., 2022; Csiki et al., 2023). However, the involvement of other molecular mechanisms by which DPD could contribute to MACE in CKD patients remained unclear.

The endoplasmic reticulum (ER) is a multifunctional organelle that plays important roles in protein folding, assembly, secretion, lipid synthesis, and calcium homeostasis (Lin et al., 2008; Walter and Ron, 2011). Various types of stress, e.g., starvation, hypoxia, certain drugs, toxins, etc., can trigger disruption of ER homeostasis (Lin et al., 2008; Walter and Ron, 2011). Cells respond to ER stress by activating a complex signal transduction pathway known as the unfolded protein response (UPR) through three stress sensor proteins, i.e., protein kinase RNA-like ER kinase (PERK), inositol-requiring protein 1α (IRE1α), and activating transcription factor 6 (ATF6) (Ron and Walter, 2007; Hetz, 2012). UPR can trigger adaptive responses, or if ER stress is sustained, it can lead to apoptosis. PERK phosphorylates the alpha subunit of eukaryotic initiation factor 2 (eIF2α), leading to a nearly global translational arrest and selective translation of activating transcription factor 4 (ATF4). Transcriptional factor C/EBP homologous protein (CHOP) is an important target of ATF4, which promotes ER stress-induced apoptosis when restoration of ER homeostasis fails (Ron and Walter, 2007; Hetz, 2012). ATF4 is an essential transcription factor that mediates not only ER stress but also the terminal differentiation of osteoblasts by regulating osteoblast-specific gene expressions (Yang et al., 2004; Karsenty, 2008). Additionally, ATF4 actively participates in the phenotype switch of vascular smooth muscle cells (VSMCs) into osteoblast-like cells and subsequent vascular calcification, which notion is supported by the attenuation of CKD-driven aortic calcification in vascular smooth muscle cell-specific ATF4-deficient mice (Masuda et al., 2016; Rao et al., 2022).

It has been shown that ATF4 is translationally induced by hypoxia and the PHD inhibitor dimethyloxalylglycine (Köditz et al., 2007). We previously reported that DPD accelerates high phosphate-induced calcification of human aortic smooth muscle cells (HAoSMCs) and valve interstitial cells that causes an increase in aortic and valve calcification respectively, in mice with adenine-induced CKD (Tóth et al., 2022; Csiki et al., 2023).

Thus, we postulated that DPD-induced vascular calcification involves the activation of ER stress. In this study, we investigated whether 1) DPD induces ER stress and hypoxia in adenine-induced CKD mice, 2) DPD upregulates osteogenic markers and promotes calcification in adenine-induced CKD mice, 3) DPD induces PERK phosphorylation, ATF4, glucose-regulated protein 78 (GRP78), and CHOP expression in HAoSMCs, 4) DPD promotes calcification and osteogenic differentiation of HAoSMCs in an ER-stress and ATF4-dependent manner, and 5) there is a hierarchy between DPD-induced HIF-1α and ATF4 responses.

2 Materials and methods

2.1 Materials

The detailed list of materials (company name, catalog number, sequences, etc.) can be found in the "Resources table" in the Supplementary Material.

2.2 Cell culture and treatments

HAoSMCs were maintained in Dulbecco's Modified Eagle Medium (DMEM) supplemented with 10% fetal bovine serum (FBS), antibiotic antimycotic solution, sodium pyruvate, and L-glutamine. Cells were maintained at 37°C in a humidified

atmosphere with 5% CO2. Cells were grown to ~90% confluency and used between passages five and 8. To induce calcification, HAoSMCs were exposed to an osteogenic medium (OM) that was obtained by supplementing the growth medium with inorganic phosphate (Pi) (NaH_2PO_4-Na_2HPO_4, 1–2.5 mmol/L, pH 7.4). DPD was utilized at concentrations ranging from 1 to 100 μmol/L after being dissolved in dimethyl sulfoxide (DMSO) to create a stock solution (25 mmol/L). In some experiments, we used sodium-4-phenylbutyrate (4-PBA, stock solution: 50 mmol/L in DMSO, working concentration: 250 μmol/L) to inhibit ER stress.

2.3 Alizarin red (AR) staining and quantification

After washing with Dulbecco's phosphate buffered saline (DPBS), the cells were fixed in 4% paraformaldehyde for 20 min and rinsed with distilled water. Cells were stained with Alizarin Red S solution (2%, pH 4.2) for 10 min at room temperature. Excessive dye was removed by several washes in distilled water. To quantify AR staining, we added 100 μL of hexadecyl-pyridinium chloride solution (100 mmol/L) to each well and measured optical density (OD), using a microplate reader at 560 nm.

2.4 Quantification of Ca deposition

Cells grown on 96-well plates were washed twice with DPBS and decalcified with HCl (0.6 mol/L) for 30 min. The Ca content of the HCl supernatants was determined by the QuantiChrome Calcium Assay Kit. Following decalcification, cells were washed with DPBS and solubilized with a solution of NaOH (0.1 mol/L) and sodium dodecyl sulfate (0.1%), and the protein content of the samples was measured with the BCA protein assay kit. The Ca content of the cells was normalized to protein content and expressed as μg/mg protein.

2.5 Osteocalcin (OCN) detection

Cells grown on 6-well plates were washed twice with DPBS and decalcified with 100 μL of EDTA (0.5 mol/L, pH 6.9) for 30 min. OCN content of the EDTA-solubilized ECM samples was quantified by an enzyme-linked immunosorbent assay according to the manufacturer's protocol.

2.6 *Ex vivo* aorta organ culture model and quantification of aortic ca

C57BL/6 mice (8–12-week-old male, n = 18) were exterminated by CO_2 inhalation and perfused with 5 mL of sterile DPBS. The entire aorta was harvested and cleaned under aseptic conditions, and cut into pieces. Aorta rings were maintained in control, high Pi + DPD (25 μmol/L), and high Pi+4-PBA (250 μmol/L) in DMEM supplemented with 10% FBS, antibiotic antimycotic solution, sodium pyruvate, L-glutamine, and 2.5 μg/mL Fungizone. After 7 days, the aorta pieces were washed in phosphate-balanced saline (PBS), opened longitudinally, and decalcified in 25 μL of 0.6 mmol/L HCl overnight. Ca content was determined by the QuantiChrom Ca-assay kit, as described previously.

2.7 CKD induction, DPD treatment and near-infrared imaging and quantification of aortic calcification in mice

Animal care and experimental procedures were performed following the institutional and national guidelines and were approved by the Institutional Ethics Committee of the University of Debrecen under registration number 10/2021/DEMÁB. Animal studies were reported in compliance with the ARRIVE guidelines. All the mice were housed in a temperature- (22°C) and light-controlled (12-h light/12-h dark) room, in cages with standard beddings and unlimited access to food and water. C57BL/6 mice (10 weeks old, male, n = 30) were randomly divided into three groups: control (Ctrl), CKD, and CKD + DPD (CKDD) (10 mice/group). CKD was induced by a two-phase diet, as described previously (Tani et al., 2017). In the first 6 weeks, the mice received a diet containing 0.2% adenine and 0.7% phosphate, followed by a diet containing 0.2% adenine and 1.8% phosphate for 3 weeks. Ctrl mice received a normal chow diet. DPD was suspended in 1% methylcellulose and administered orally at a dose of 15 mg/kg/day from week 7. Following the 9-week diet five mice/group were anesthetized with isoflurane and injected retro-orbitally with 2 nmol of OsteoSense dye that was dissolved in 100 μL of PBS. Twenty-4 hours later, mice were euthanized by CO_2 inhalation and blood was taken by heart puncture into K3-EDTA-containing tubes. Then mice were perfused with 5 mL of ice-cold PBS. Kidneys and aortas were isolated and analyzed immediately *ex vivo* by an IVIS Spectrum *In Vivo* Imaging System. We took kidney and aorta tissues out from the remaining 15 mice (5 mice/group), snap freeze them in liquid nitrogen and kept at −80°C for further analysis.

2.8 Laboratory analysis of renal function and anemia in CKD mice

Serum urea, creatinine, phosphate and calcium levels were determined in mice by kinetic assays on a Cobas® c501 instrument. K3-EDTA anticoagulated whole blood murine samples were analyzed by a Siemens Advia-2120i hematology analyzer with the 800 Mouse C57BL program of Multi-Species software. Hemoglobin concentration was measured by a cyanide-free colorimetric method. Hematocrit values were determined as a calculated parameter derived from red blood cell count (RBC in T/L) and mean cell volume (MCV in fL).

2.9 Real-time quantitative polymerase chain reaction (qPCR)

Total RNA was extracted from the kidney and aorta of C57BL/6 mice using Tri Reagent following the manufacturer's protocol. RNA was reverse transcribed using a High-Capacity cDNA Reverse Transcription Kit. The qPCR reactions were carried out according to the protocol of the iTaq universal SYBR® Green Supermix reagent,

10.3389/fphar.2024.1399248

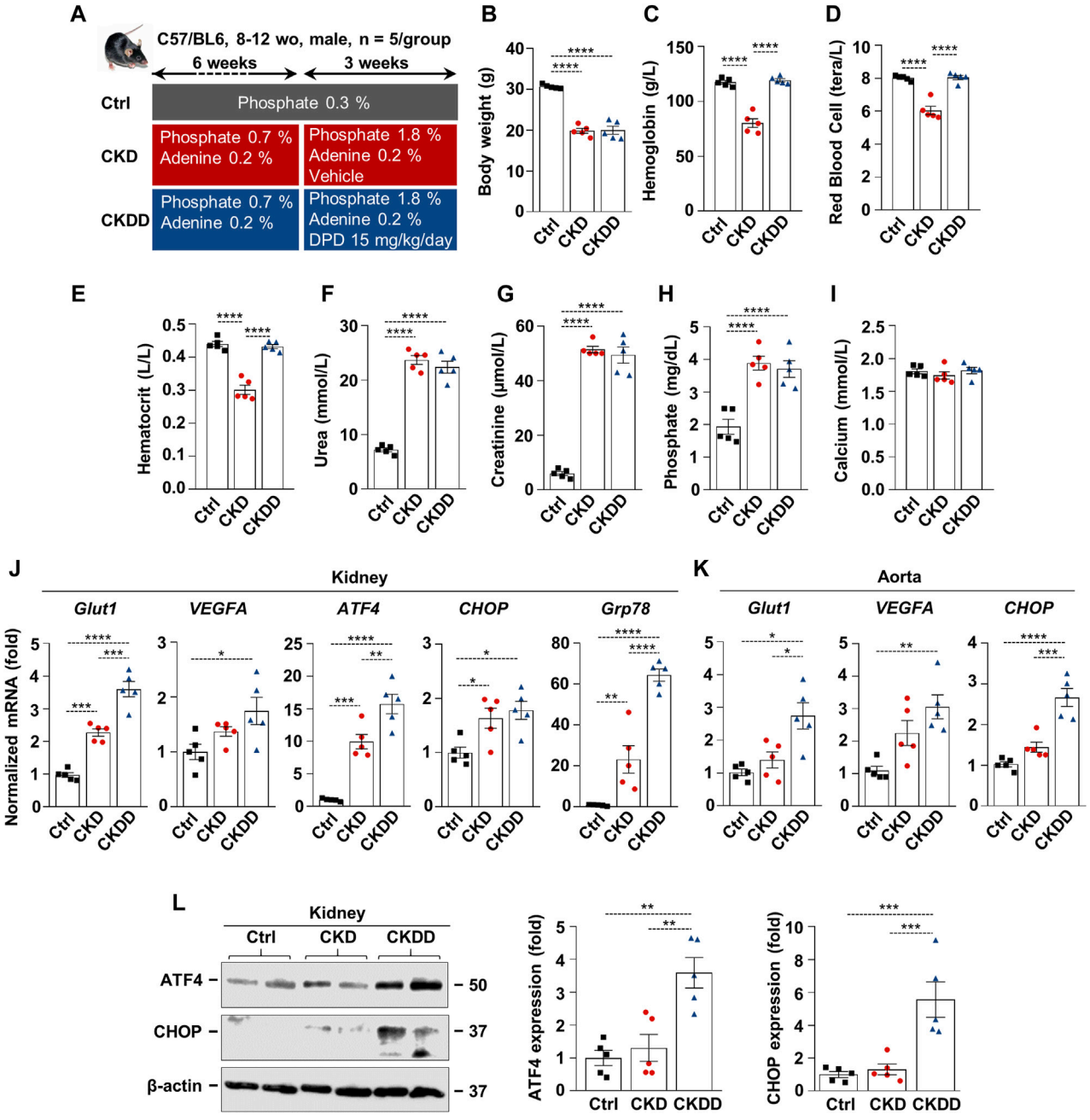

FIGURE 1
DPD promotes HIF pathway activation and ER stress in kidney and aorta in C57BL/6 mice fed with an adenine + high Pi diet. **(A)** Scheme of the experimental protocol. **(B)** Body weight; **(C)** hemoglobin; **(D)** red blood cell count; **(E)** hematocrit; **(F)** plasma urea; **(G)** creatinine; **(H)** phosphate; and **(I)** calcium level. **(J and K)** mRNA levels of hypoxia and ER stress markers in **(J)** kidney and **(K)** aorta samples. **(L)** Protein expressions of ATF4 and CHOP in kidney lysates. Membranes were reprobed for β-actin. Representative Western blots and analyses (n = 3). Data are expressed as mean ± SD, n = 5. Ordinary one-way ANOVA followed by Tukey's multiple comparison test was used to calculate *p* values. **p* < 0.05, ***p* < 0.01, ****p* < 0.005, *****p* < 0.001.p

using primers listed in the "Resources table." PCR was performed using a real-time PCR machine.

2.10 Western blot analysis

HAoSMCs were lysed in Laemmli lysis buffer. Proteins were resolved by SDS-PAGE (7.5% and 10%) and transferred onto nitrocellulose membranes. Western blotting was performed with the use of the primary antibodies listed in the "Resources table." Following the primary antibody binding, membranes were incubated with horseradish peroxidase-linked rabbit and mouse IgG. Antigen-antibody complexes were visualized with the enhanced chemiluminescence system Clarity Western ECL. Chemiluminescent signals were detected conventionally on an X-ray film or digitally with the use of a C-Digit Blot Scanner.

After detection, the membranes were stripped and reprobed for β-actin. Blots were quantified by using the built-in software on the C-Digit Blot Scanner.

2.11 RNA silencing

To knockdown ATF4 gene expressions, we used Silencer® select siRNA constructs targeting HIF-1α and ATF4. As a control, we used the negative control #1 construct. Lipofectamine® RNAiMAX reagent was used to transfect HAoSMCs according to the manufacturer's protocol.

2.12 Statistical analysis

Results are expressed as mean ± SD. At least three independent experiments were performed for all *in vitro* studies. Statistical analyses were performed with GraphPad Prism 8.0.1 software. Comparisons between more than two groups were carried out by a one-way ANOVA followed by Tukey's multiple-comparisons test. To compare each of several treatment groups with a single control group, we performed a one-way ANOVA followed by Dunnett's *post hoc* test. A value of $p < 0.05$ was considered significant.

3 Results

3.1 DPD promotes HIF pathway activation and ER stress in the kidney and aorta of CKD mice

Fifteen C57BL/6 mice (8–12 weeks old, male) were randomized into three groups (n = 5/group): control (Ctrl), CKD, and CKD treated with DPD (CKDD). CKD was induced with a 9-week-long, two-phase adenine- and high-phosphate-containing diet, as detailed in Figure 1A. DPD was administered orally at a dose of 15 mg/kg/day in the last 3 weeks of the experiment (Figure 1A). Ctrl mice received a normal chow diet. Hematological parameters, body weight, and kidney function were evaluated at the end of the experiment. Both CKD and CKDD mice lost approximately one-third of their initial weight during the experiment (Figure 1B). DPD completely corrected CKD-induced anemia revealed by similar hemoglobin, RBC count, and hematocrit values in Ctrl and CKDD mice (Figures 1C,E). Elevated plasma urea, creatinine, and phosphate levels indicated that the kidney function of the CKDD mice had declined to the same degree as that of the CKD mice (Figures 1F–I). CKD treatment did not change plasma calcium levels (Figure 1I).

CKD was associated with increased renal mRNA expression of specific hypoxia and ER stress markers, such as glucose transporter 1 (Glut1), ATF4, CHOP, and glucose-regulated protein 78 (GRP78) (Figure 1J). DPD treatment further exacerbated CKD-induced activation of HIF-1 target genes and ER stress markers in the kidneys (Figure 1J). In comparison to Ctrl, CKDD treatment triggered a 3-fold increase in Glut1, vascular endothelial growth factor A (VEGFA), and CHOP mRNA expressions in the aorta (Figure 1K). We observed marked upregulation of the protein expressions of ER stress markers ATF4 and CHOP in the kidneys of CKDD mice (Figure 1L).

3.2 DPD upregulates markers of osteo-/chondrogenic differentiation and increases kidney and aorta calcification in CKD mice

Osteosense staining was performed to evaluate soft tissue calcification in Ctrl, CKD, and CKDD mice. CKD was associated with increased kidney and aorta calcification, which was further exacerbated by DPD treatment (Figures 2A–D). Aorta calcium measurement supported the pro-calcifying effect of DPD in CKD animals (Figure 2E). Calcification is a highly regulated process, similar to bone formation; therefore, next, we investigated the expression of osteo-/chondrogenic markers in kidney and aorta samples. Compared to Ctrl, Runt-related transcription factor 2 (Runx2), SRY-box transcription factor 9 (Sox9), bone morphogenetic protein 2 (BMP2), and Msh Homeobox 2 (Msx2) mRNA levels were higher in the kidneys of CKD mice. Furthermore, we noticed that CKDD mice had higher Sox9 and Msx2 mRNA levels than CKD animals had (Figure 2F). In the aorta, CKD triggered an increase in BMP2 mRNA expression compared to Ctrl, whereas CKDD induced marked elevations of Sox9, BMP2, and Msx2 mRNA levels (Figure 2G). Overall, these results show that DPD treatment induces hypoxia response and ER stress, increases osteo-/chondrogenic marker expressions, and promotes hydroxyapatite deposition in the kidney and aorta of CKD mice.

3.3 DPD induces HIF-1 activation and the PERK-eIF2α-ATF4 pathway and promotes high Pi-induced calcification in HAoSMCs

The stress signal network between hypoxia and ER stress is implicated in the progression of CKD; therefore, we further examined the effect of DPD on these pathways using an *in vitro* calcification model. Exposition of HAoSMCs to DPD (1–100 μmol/L) induced stabilization of HIF-1α and subsequent activation of the HIF-1 pathway, as revealed by a dose-dependent increase in Glut-1 protein expression (Figure 3A). We could not detect changes in HIF-1α mRNA levels in DPD-treated HAoSMCs, suggesting that DPD regulates HIF-1α in a post-transcriptional manner (Figure 3B). Hypoxia is a pathophysiological condition that induces ER stress through PERK; therefore, next, we investigated PERK activation in HAoSMCs in response to high Pi (2.5 mmol/L) with or without DPD (10 μmol/L). Pi-induced PERK phosphorylation was further exacerbated by DPD (Figure 3C). Furthermore, compared to control, the levels of phosphorylated eIF2α (P-eIF2α) were elevated by Pi and Pi + DPD (Figure 3C). The activation of the PERK pathway by Pi + DPD induced a massive upregulation of ATF4 mRNA and protein expressions (Figures 3D,E) as well as CHOP, and Grp78 (Figure 3F). Sustained ER stress can induce apoptosis, therefore next we investigated whether DPD influences cell viability. We performed MTT assay, and found that DPD (10 μmol/L) decreased cell viability in both normal and high Pi conditions (Figure 3G). Then, we addressed the pro-calcifying effect of DPD in HAoSMCs. As revealed by Alizarin red staining, DPD (10 μmol/L) largely intensified Pi-induced

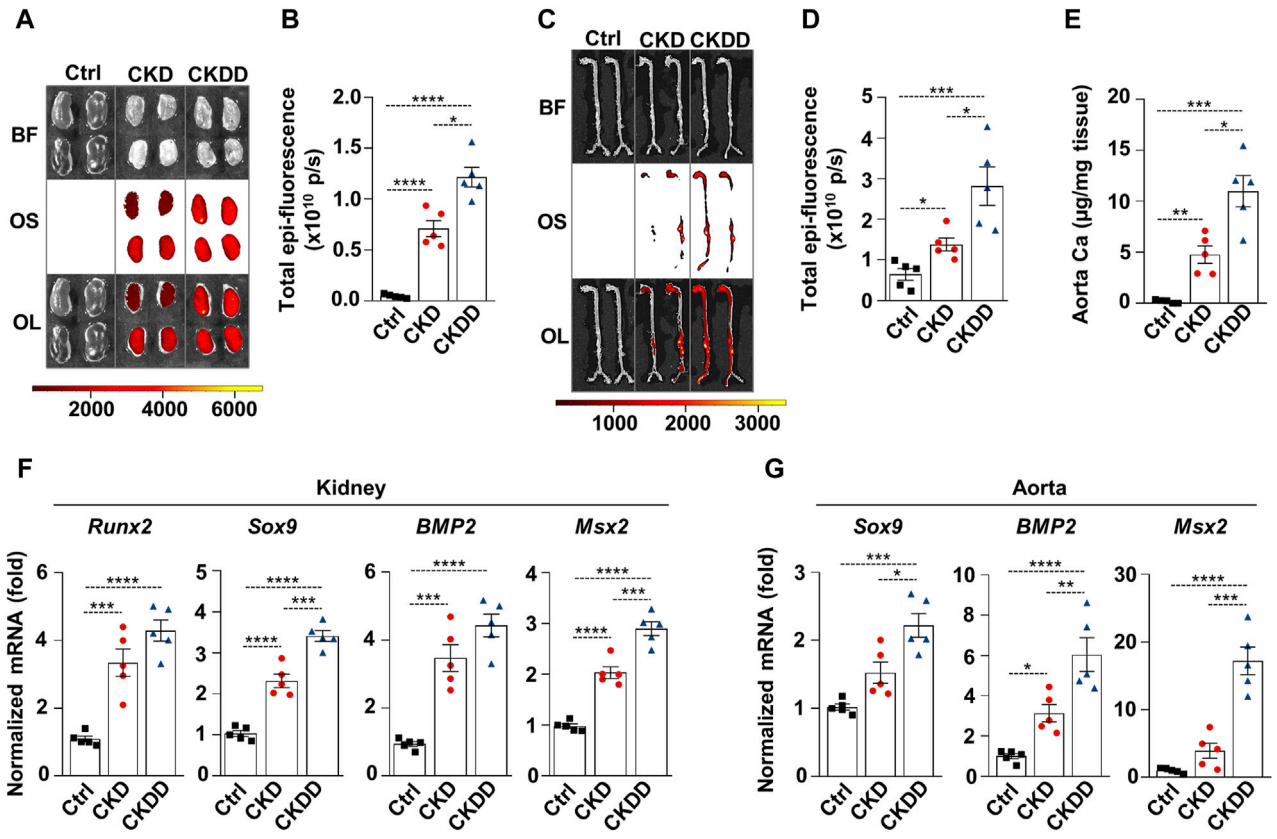

FIGURE 2
DPD increases soft tissue calcification in the kidney and aorta of CKD mice. Mice were treated as shown in Figure 1A. **(A–D)** Brightfield and macroscopic fluorescence reflectance imaging of **(A)** kidney and **(C)** aorta; **(B and D)** quantification of OsteosenseTM staining. **(E)** Ca content of aortas normalized to protein level. **(F)** mRNA levels of osteogenic markers in kidney and **(G)** aorta samples. Data are expressed as mean ± SD, n = 5. Ordinary one-way ANOVA followed by Tukey's multiple comparison test was used to calculate *p* values. **p* < 0.05, ***p* < 0.01, ****p* < 0.005, *****p* < 0.001.

calcification (Figure 3H). The ECM of HAoSMCs treated with Pi + DPD had approximately 2.4 times more calcium deposition than the ECM of Pi-treated cells (Figure 3I). Moreover, OCN accumulation in the ECM of Pi + DPD-treated HAoSMCs was about 4-times higher compared to Pi-treated cells (Figure 3J).

3.4 The pro-calcification effect of DPD is dependent on ER stress activation and ATF4

After establishing that DPD induces ER stress and accelerates high Pi-induced calcification, we investigated whether ER stress plays a causative role in HAoSMC calcification triggered by Pi + DPD. First, we tested the effect of an ER stress inhibitor, 4-phenylbutyrate (4-PBA), on HAoSMC calcification. AR staining revealed that 4-PBA inhibited Pi + DPD-induced calcification of HAoSMCs (Figure 4A). Additionally, 4-PBA inhibited the accumulation of Ca and OCN in the ECM of Pi + DPD-treated HAoSMCs and attenuated *ex vivo* aorta calcification (Figures 4B–D). Furthermore, the knockdown of ATF4 by siRNA decreased Pi + DPD-induced calcification of HAoSMCs as evaluated by AR staining, as well as Ca and OCN measurements from the ECM (Figures 4E–H). These results show that DPD induces ER stress, particularly ATF4, which plays a crucial role in Pi + DPD-induced HAoSMC calcification.

3.5 HIF-1α is required for DPD-induced upregulation of ATF4

After showing that both the HIF-1 pathway and ATF4 activation play essential roles in Pi + DPD-induced HAoSMC calcification, we wanted to understand whether there is a cross-communication between these two pathways. To this end, we applied HIF-1α targeted siRNA and examined the protein expression of HIF-1α and ATF4 in response to Pi (2.5 mmol/L), DPD (10 µmol/L), and Pi + DPD (Figure 5A). Western blot results revealed that the HIF-1α knock-down approach was successful and that in the absence of HIF-1α, DPD fails to upregulate ATF4 expression (Figure 5A). On the other hand, DPD induced HIF-1α expression regardless of the presence of ATF4 (Figure 5B). These results suggest a hierarchy between HIF-1α and ATF4 upon DPD treatment, in which HIF-1α is upstream of ATF4.

4 Discussion

The pathomechanism of vascular calcification in CKD is extremely complex and influenced by many factors and molecular pathways (Tóth et al., 2020). Growing evidence suggests that ER stress is a major contributor to vascular

10.3389/fphar.2024.1399248

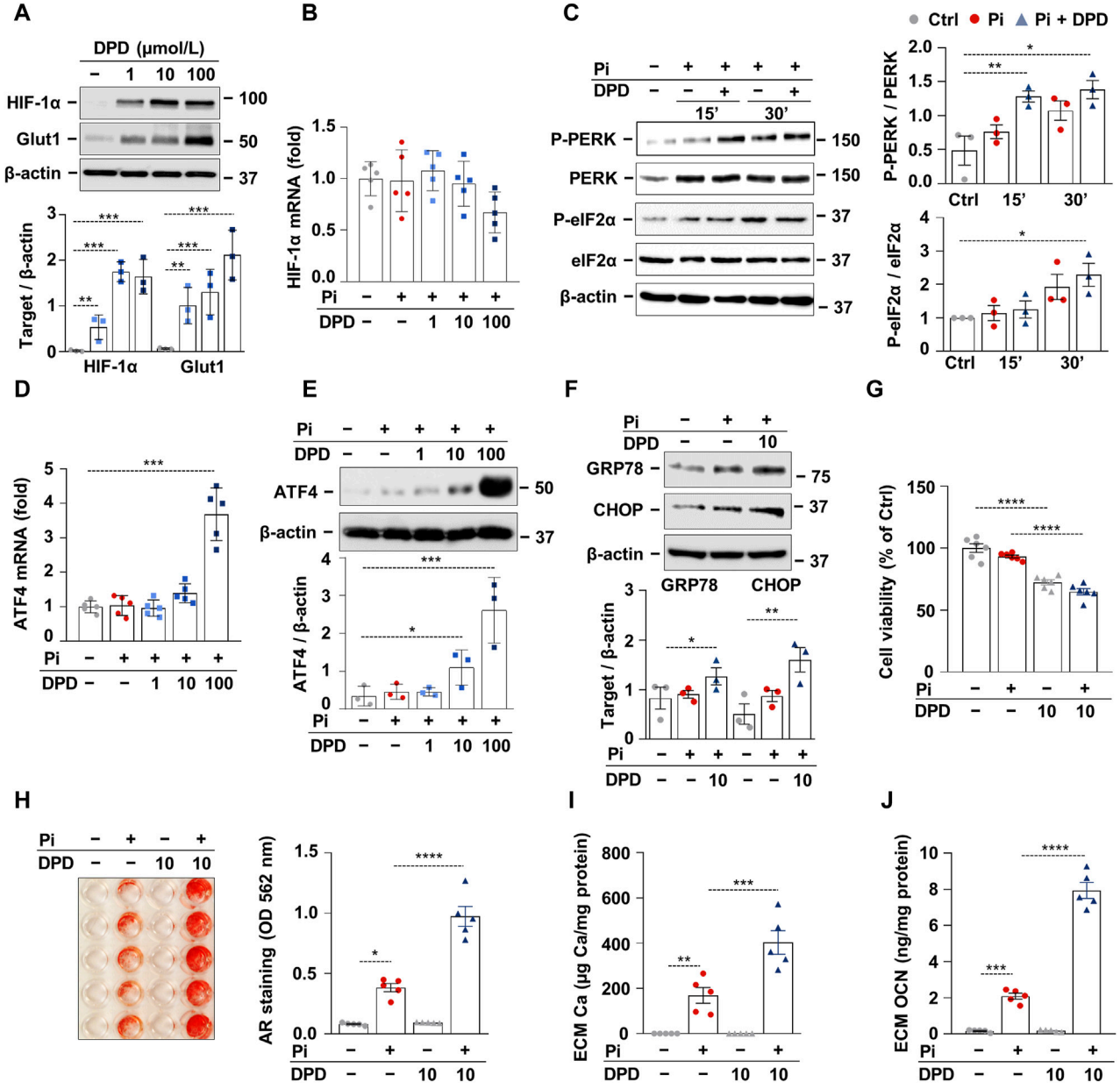

FIGURE 3
DPD induces hypoxia signaling and endoplasmic reticulum stress and promotes Pi-induced calcification of HAoSMCs. **(A, B)** HAoSMCs were cultured in the presence of DPD (1–100 μmol/L). **(A)** Protein expression of HIF-1α and Glut1 in whole cell lysates was evaluated after 24 h of treatment. Membranes were reprobed for β-actin. Representative Western blots and densitometry analyses on the relative expression of HIF-1α and Glut1 (n = 3). **(B)** mRNA level of HIF-1α after 12 h of treatment. **(C)** HAoSMCs were cultured in the presence or absence of Pi (2 mmol/L) and DPD (10 μmol/L). Protein expression of phospho-PERK (P-PERK), PERK, phospho-eIF2α (P-eIF2α), and eIF2α was measured in whole cell lysates (15 min, 30 min). Membranes were reprobed for β-actin. Representative Western blots and relative expression of P-PERK normalized to PERK and P-eIF2α normalized to eIF2α (n = 3). **(D–F)** HAoSMCs were cultured in the presence of DPD (1–100 μmol/L). **(D)** ATF4 mRNA and **(E–F)** protein expression of ATF4, CHOP, and GRP78 in whole cell lysates (6 h). Membranes were reprobed for β-actin. Representative Western blots and densitometry analyses on the relative expression of ATF4, CHOP, and GRP78 (n = 3). **(H–J)** HAoSMCs were cultured in an osteogenic medium supplemented with phosphate (2 mmol/L Pi) in the presence or absence of DPD (10 μmol/L). **(H)** Representative Alizarin Red staining (day 4) and quantification (n = 5). **(I)** Ca content of HCl-solubilized ECM samples. **(J)** OCN level in EDTA-solubilized ECM samples (day 8). Data are expressed as mean ± SD. Ordinary one-way ANOVA followed by Tukey's multiple comparison test was used to calculate *p* values. **p* < 0.05, ***p* < 0.01, ****p* < 0.005, *****p* < 0.001.p

calcification (Duan et al., 2009; Liberman et al., 2011; Masuda et al., 2012; Masuda et al., 2013; Shanahan and Furmanik, 2017; Furmanik et al., 2021). In the present study, we found that DPD promotes vascular calcification through the coordinated activation of the HIF-1 pathway and the PERK–eIF2α–ATF4–CHOP axis.

The first important observation of this study is that DPD increases HIF activation, generates ER stress, and promotes kidney and aorta calcification in CKD mice (Figures 1, 2). In this work, we used a non-invasive, well-characterized CKD model in which we induced tubular damage by an adenine-containing diet

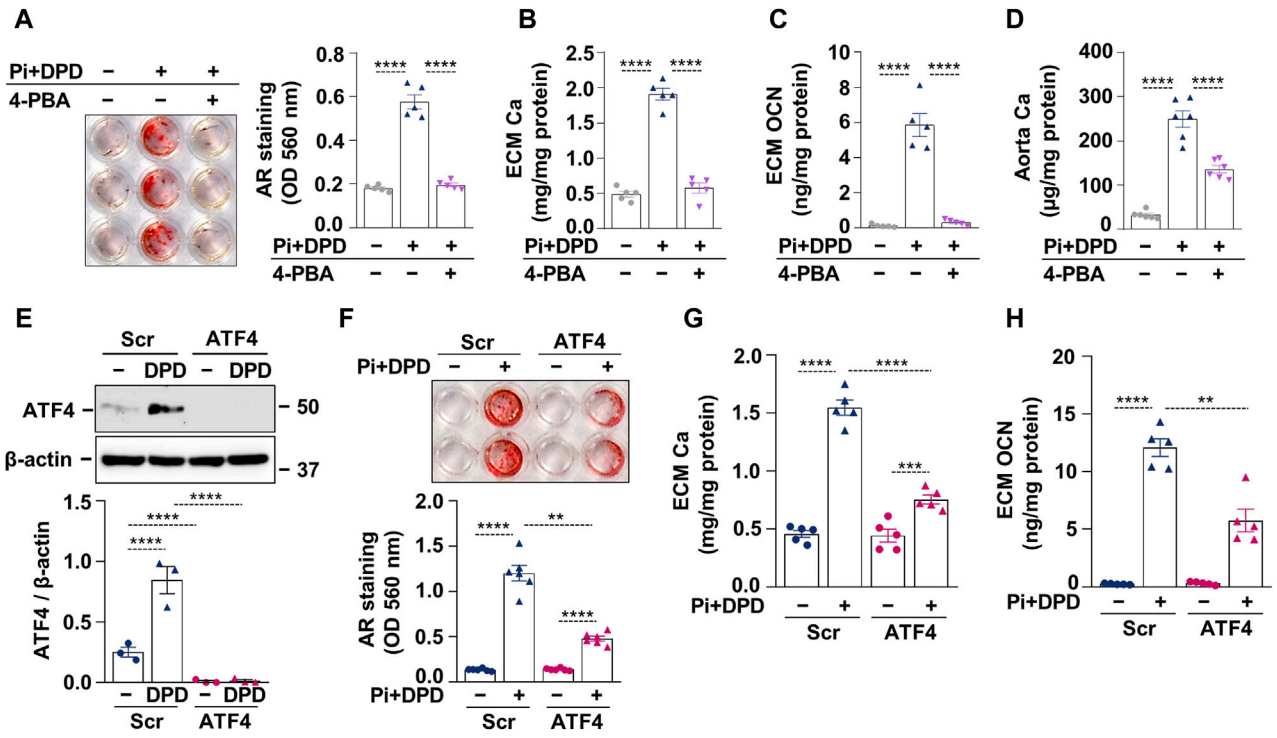

FIGURE 4
DPD increases the calcification of HAoSMCs through ER stress and ATF4 activation. **(A–C)** HAoSMCs were exposed to high Pi (2 mmol/L) and DPD (10 µmol/L) in the presence or absence of 4-PBA (250 µmol/L). **(A)** Representative AR staining (day 4) and quantification. **(B)** Ca content of HCl-solubilized ECM (day 4). **(C)** OCN level in EDTA-solubilized ECM samples (day 10). **(D)** Aortic rings of C57BL/6 mice were cultured in control, high Pi + DPD (25 µmol/L), and high Pi + DPD+4-PBA conditions. Ca content of aorta rings normalized to protein level (day 7). **(E–H)** HAoSMCs were exposed to Pi (2 mmol/L) and DPD (10 µmol/L) in the presence of ATF4 or scrambled siRNA. **(E)** Protein expression of ATF4 in whole cell lysates (6 h). Membranes were reprobed for β-actin. Representative Western blots and relative expression of ATF4 normalized to β-actin. **(F)** Representative AR staining (day 4) and quantification. **(G)** Ca content of HCl-solubilized ECM (day 4). **(H)** OCN level in EDTA-solubilized ECM samples (day 8). Data are expressed as mean ± SD, n = 3–6. Ordinary one-way ANOVA followed by Tukey's multiple comparison test was used to calculate *p* values. $^{**}p < 0.01$, $^{***}p < 0.005$, $^{****}p < 0.001$.

(Tani et al., 2017). Previously, we showed that these CKD mice are anemic and titrated out the dose of DPD that corrects CKD-induced anemia in this model (Tóth et al., 2022; Csiki et al., 2023). Using the minimal anemia-correcting dose of DPD, we observed an elevation of the mRNA level of the HIF target genes Glut1 and VEGFA in both the kidney and the aorta (Figure 1). This is in agreement with our previous *in vitro* results, in which we showed that PHD inhibitors, including DPD, stabilize HIF-α subunits, activate HIF signaling, and upregulate Glut1 and VEGFA in HAoSMCs and valve interstitial cells (Tóth et al., 2022; Csiki et al., 2023).

A growing body of evidence suggests that hypoxia and ER stress signaling are interconnected and implicated in the pathogenesis of various diseases, including CKD (Maekawa and Inagi, 2017; Díaz-Bulnes et al., 2020). Hypoxia and the PHD inhibitor $CoCl_2$ activate PERK and phosphorylate eIF2α in embryonic fibroblasts (Koumenis et al., 2002). It is interesting to note that PHD inhibition attenuates post-ischemic myocardial damage in hearts challenged by ischemia/reperfusion by inducing ER stress proteins including ATF4 and GRP78 while also lowering the level of pro-apoptotic component CHOP (Pereira et al., 2014). The interplay between HIF and ER stress pathways is well-known in tumor biology and serves as an important adaptation mechanism (Lin et al., 2024).

Our results revealed that mRNA levels of ER stress markers (ATF4, CHOP, and GRP78) are elevated in the kidneys of CKD mice, and DPD triggers further increases in these markers. Additionally, we showed that DPD treatment upregulates protein expression of ATF4 and CHOP in the kidneys of CKDD mice (Figure 1). Vascular calcification is a common feature of CKD and contributes to the increased morbidity and mortality of CKD patients. Here we found that HIF activation and ER stress observed in CKDD mice are accompanied by increased kidney and aorta calcification and elevation of mRNA markers of osteo-/chondrogenic differentiation (Runx2, Sox9, BMP2, and Msx2) as compared to CKD mice (Figure 2).

An additional noteworthy finding of this investigation is that DPD stimulates the PERK–eIF2α–ATF4–CHOP axis, hence facilitating high Pi-induced calcification *in vitro* in HAoSMCs (Figure 3). In agreement with our results, previous studies showed that PHD inhibitors are capable of activating the PERK–eIF2α branch of UPR; as such, $CoCl_2$ triggers PERK and eIF2α activation in embryonic fibroblasts, and dimethyloxalylglycine stabilizes ATF4 in HeLa cells (Koumenis et al., 2002; Köditz et al., 2007).

Failure of ER stress resolution via UPR may lead to the activation of pro-apoptotic mechanisms. A recent study showed that activation of the PERK-eIF2α-ATF4-CHOP pathway is involved in Arnicolide D-induced oncosis in hepatocellular carcinoma cells (Lin et al.,

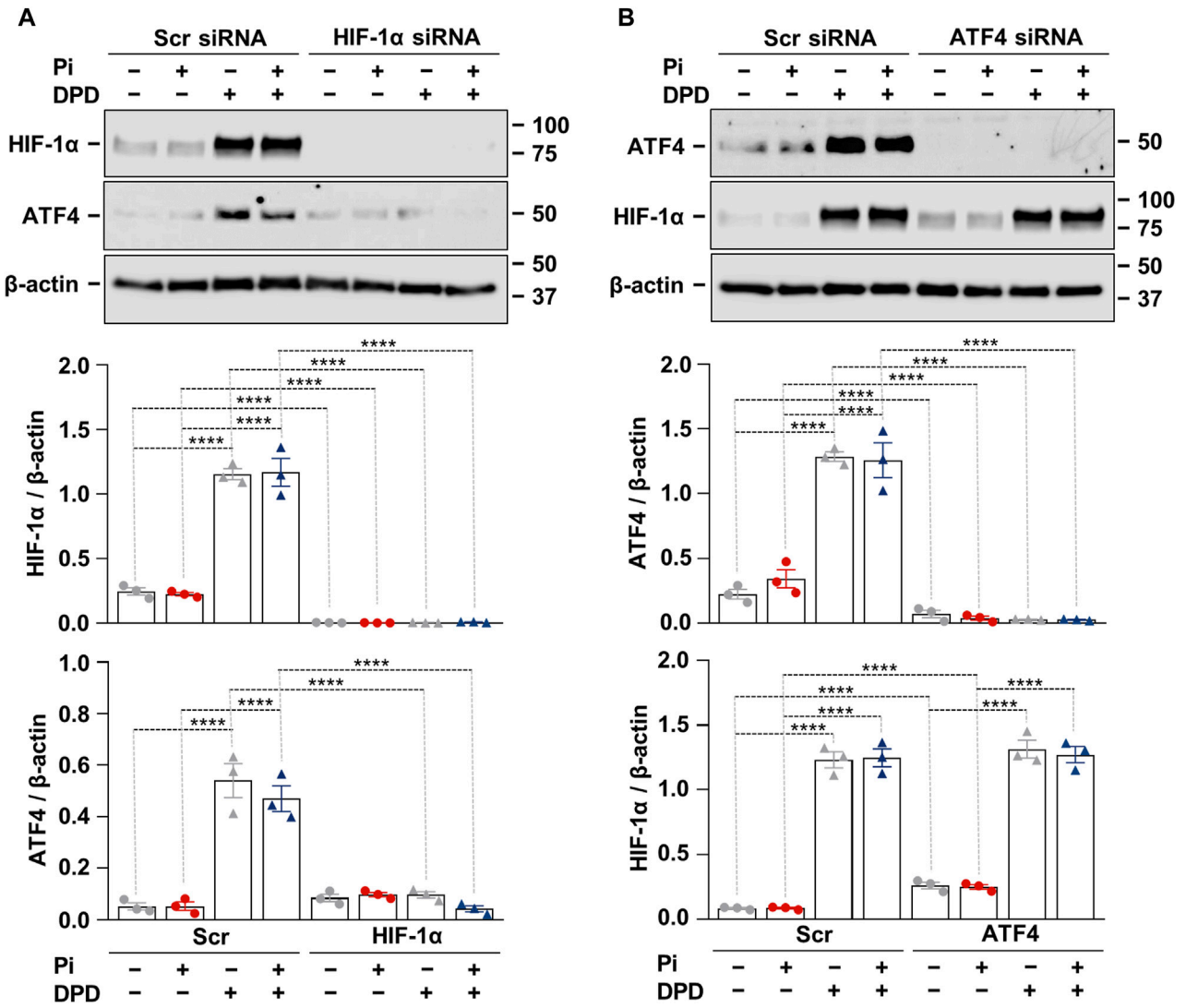

FIGURE 5
Crosstalk between hypoxia signaling and ER stress in Pi + DPD-induced HIF-1α and ATF4 responses in HAoSMCs. **(A,B)** Cells were exposed to Pi (2 mmol/L) and DPD (10 μmol/L) in the presence of HIF-1α, ATF4, and scrambled siRNA. Protein expression of HIF-1α and ATF4 in whole cell lysates (24 h). Membranes were reprobed for β-actin. Representative Western blots and relative expression of HIF-1α and ATF4 normalized to β-actin. Data are expressed as mean ± SD, n = 3. Ordinary one-way ANOVA followed by Tukey's multiple comparison test was used to calculate *p* values. $^{**}p < 0.01$, $^{****}p < 0.001$.

2024). Here we showed that DPD decreases the viability of HAoSMCs but further investigation is needed to clarify the type of DPD-induced cell death and the potential involvement of the PERK-eIF2α-ATF4-CHOP pathway.

Accumulating evidence suggests the critical involvement of ER stress activation in the transition of smooth muscle cells to a calcifying osteoblast-like phenotype. Diverse molecules such as BMP2, stearate, tumor necrosis factor α, high glucose, saturated fatty acids, parathyroid hormone, and C5a-C5aR1 have been shown to promote the osteogenic transition of VSMCs through ER stress induction (Liberman et al., 2011; Masuda et al., 2012; Masuda et al., 2013; Zhu et al., 2015; Shanahan and Furmanik, 2017; Shiozaki et al., 2018; Furmanik et al., 2021; Duang et al., 2022; Liu et al., 2023). Here we showed that the ER stress inhibitor 4-PBA prevents DPD-induced HAoSMCs and *ex vivo* aorta ring calcification (Figure 4), which observations prove that ER stress plays a key role in the pro-calcification effect of DPD.

ATF4 is an ER stress-induced pro-osteogenic transcriptional activator that has been identified as a central mediator of the ER stress-induced osteogenic transition of VSMCs and vascular calcification by several studies (Masuda et al., 2012; Masuda et al., 2013; Masuda et al., 2016; Furmanik and Shanahan, 2018). The most important proof of this notion is Masuda et al.'s study, which showed calcification attenuation in smooth muscle cell-specific ATF4 knock-out mice (Masuda et al., 2016). Our results also revealed that knockdown of ATF4 inhibits DPD-induced promotion of HAoSMC calcification (Figure 4). Therefore, the third key finding of this work is that ER stress and particularly ATF4 play a critical causative role in the pro-calcification effect of DPD.

DPD is a PHD inhibitor that initiates HIF signaling by stabilizing HIF alpha subunits of the HIF complex. Recent studies demonstrated that HIF activation, mediated either by hypoxia or PHD inhibition, promotes the phenotype switch of VSMCs into osteoblast-like cells under both normal and high phosphate conditions in a HIF-1α-dependent manner (Mokas et al., 2016; Balogh et al., 2019; Tóth et al., 2022; Csiki et al., 2023; Negri, 2023).

DPD induces both HIF-1α and ATF4 expressions in HAoSMCs. Growing evidence suggests bidirectional cooperation between HIF-1α and ATF4 in regulating diverse processes. For example, a single-allele deletion of HIF-1α is associated with lower CHOP expression and smaller infarct size in a mouse model of chronic intermittent hypoxia-mediated myocardial injury (Moulin et al., 2020). Here, using the siRNA approach to knockdown HIF-1α and ATF4, we found that HIF-1α is involved in DPD-induced upregulation of ATF4, but ATF4 does not control HIF-1α expression under these circumstances (Figure 5). Contradictory with this Chee et al. found that ATF4 regulates HIF-1α expression, but HIF-1α is not required for hypoxia-induced upregulation of ATF4 in pancreatic cancer cells (Chee et al., 2023). One explanation for this discrepancy could be that Chee et al. used 0.2% O_2 to induce HIF-1α, while we used a prolyl hydroxylase inhibitor. Also, pancreatic cancer cells exist in a hypoxic environment while HAoSMCs live in a relatively well-oxygenated niche, which can lead to differences in their hypoxia responses. Nevertheless, further studies are needed to deepen our understanding of this phenomenon.

PHIs represent novel oral drug options for anemia management in patients with CKD. The use of PHIs is expected to rise, warranting further research to investigate the potential off-target effects of these drugs. In line with this notion, previously we have shown that DPD enhances vascular calcification in a mice model of CKD (Tóth et al., 2022), and here we described that DPD-induced activation of the PERK-eIF2α-ATF4-CHOP axis of ER stress contributes to the pro-calcification effect of DPD. The limitation of our study is that we focused our work on DPD and have not tested the other PHIs; Roxadustat and Vadadustat. Another limitation of our work is that we performed our experiments exclusively in male C57BL/6 mice. Other mice strains and female mice should also be tested in the future. Nevertheless, to our knowledge, this is the first study showing that DPD induces ER stress *in vitro* and *in vivo*. ER stress is a key vascular calcification mechanism, therefore we strongly believe that this research can initiate further development to fine-tune PHIs for better and safer anemia management in CKD patients.

Data availability statement

The data that support the findings of this study are available from the corresponding author upon reasonable request.

Ethics statement

Ethical approval was not required for the studies on humans in accordance with the local legislation and institutional requirements because only commercially available established cell lines were used. The animal study was approved by Institutional Ethics Committee of the University of Debrecen University of Debrecen. The study was conducted in accordance with the local legislation and institutional requirements.

Author contributions

AT: Conceptualization, Investigation, Project administration, Writing–original draft, Writing–review and editing. GL: Investigation, Writing–review and editing. DC: Investigation, Writing–review and editing. EB: Investigation, Writing–review and editing. AS: Investigation, Writing–review and editing, Methodology. BN: Investigation, Methodology, Writing–review and editing. VJ: Investigation, Writing–review and editing, Conceptualization, Data curation, Formal Analysis, Funding acquisition, Resources, Supervision, Validation, Writing–original draft.

Funding

The author(s) declare that financial support was received for the research, authorship, and/or publication of this article. This work was funded by the Hungarian National Research, Development and Innovation Office (NKFIH) [K146669 to VJ] and the Hungarian Academy of Sciences [MTA-DE Lendület Vascular Pathophysiology Research Group, grant number 96050 to VJ]. EB was supported by the János Bolyai Research Scholarship of the Hungarian Academy of Sciences (BO/00443/21) and by ÚNKP-23-5-DE-499 New Excellence Program of the Ministry for Culture and Innovation from the Source of the National Research, Development and Innovation Fund.

Conflict of interest

The authors declare that the research was conducted in the absence of any commercial or financial relationships that could be construed as a potential conflict of interest.

Publisher's note

Supplementary material

The Supplementary Material for this article can be found online at: https://www.frontiersin.org/articles/10.3389/fphar.2024.1399248/full#supplementary-material

References

Atkinson, M. A., and Warady, B. A. (2018). Anemia in chronic kidney disease. 33, 227–238. doi:10.1007/s00467-017-3663-y

Babitt, J. L., and Lin, H. Y. (2012). Mechanisms of anemia in CKD. *J. Am. Soc. Nephrol.* 23, 1631–1634. doi:10.1681/ASN.2011111078

Balogh, E., Tóth, A., Méhes, G., Trencsényi, G., Paragh, G., and Jeney, V. (2019). Hypoxia triggers osteochondrogenic differentiation of vascular smooth muscle cells in an HIF-1 (Hypoxia-Inducible factor 1)-dependent and reactive oxygen species-dependent manner. *Arterioscler. Thromb. Vasc. Biol.* 39, 1088–1099. doi:10.1161/ATVBAHA.119.312509

Chee, N. T., Carriere, C. H., Miller, Z., Welford, S., and Brothers, S. P. (2023). Activating transcription factor 4 regulates hypoxia inducible factor 1α in chronic hypoxia in pancreatic cancer cells. *Oncol. Rep.* 49, 14. doi:10.3892/or.2022.8451

Csiki, D. M., Ababneh, H., Tóth, A., Lente, G., Szöőr, Á., Tóth, A., et al. (2023). Hypoxia-inducible factor activation promotes osteogenic transition of valve interstitial cells and accelerates aortic valve calcification in a mice model of chronic kidney disease. *Front. Cardiovasc. Med.* 10, 1168339. doi:10.3389/fcvm.2023.1168339

Díaz-Bulnes, P., Saiz, M. L., López-Larrea, C., and Rodríguez, R. M. (2020). Crosstalk between hypoxia and ER stress response: a key regulator of macrophage polarization. *Front. Immunol.* 10, 2951–3016. doi:10.3389/fimmu.2019.02951

Duan, X., Zhou, Y., Teng, X., Tang, C., and Qi, Y. (2009). Endoplasmic reticulum stress-mediated apoptosis is activated in vascular calcification. *Biochem. Biophys. Res. Commun.* 387, 694–699. doi:10.1016/j.bbrc.2009.07.085

Duang, S., Zhang, M., Liu, C., and Dong, Q. (2022). Parathyroid hormone-induced vascular smooth muscle cells calcification by endoplasmic reticulum stress. *J. Physiol. Pharmacol. Off. J. Pol. Physiol. Soc.* 73. doi:10.26402/jpp.2022.5.03

Furmanik, M., and Shanahan, C. M. (2018). ER stress regulates alkaline phosphatase gene expression in vascular smooth muscle cells via an ATF4-dependent mechanism. *BMC Res. Notes* 11, 483. doi:10.1186/s13104-018-3582-4

Furmanik, M., van Gorp, R., Whitehead, M., Ahmad, S., Bordoloi, J., Kapustin, A., et al. (2021). Endoplasmic reticulum stress mediates vascular smooth muscle cell calcification via increased release of Grp78 (Glucose-Regulated protein, 78 kDa)-Loaded extracellular vesicles. *Arterioscler. Thromb. Vasc. Biol.* 41, 898–914. doi:10.1161/atvbaha.120.315506

Giachelli, C. M. (2009). The emerging role of phosphate in vascular calcification. *Kidney Int.* 75, 890–897. doi:10.1038/ki.2008.644

Hanna, R. M., Streja, E., and Kalantar-Zadeh, K. (2021). Burden of anemia in chronic kidney disease: beyond erythropoietin. *Adv. Ther.* 38, 52–75. doi:10.1007/s12325-020-01524-6

Hetz, C. (2012). The unfolded protein response: controlling cell fate decisions under ER stress and beyond. *Nat. Rev. Mol. Cell Biol.* 132 (13), 89–102. doi:10.1038/nrm3270

Karsenty, G. (2008). Transcriptional control of skeletogenesis. *Annu. Rev. Genomics Hum. Genet.* 9, 183–196. doi:10.1146/annurev.genom.9.081307.164437

Köditz, J., Nesper, J., Wottawa, M., Stiehl, D. P., Camenisch, G., Franke, C., et al. (2007). Oxygen-dependent ATF-4 stability is mediated by the PHD3 oxygen sensor. *Blood* 110, 3610–3617. doi:10.1182/blood-2007-06-094441

Koumenis, C., Naczki, C., Koritzinsky, M., Rastani, S., Diehl, A., Sonenberg, N., et al. (2002). Regulation of protein synthesis by hypoxia via activation of the endoplasmic reticulum kinase PERK and phosphorylation of the translation initiation factor eIF2alpha. *Mol. Cell. Biol.* 22, 7405–7416. doi:10.1128/MCB.22.21.7405-7416.2002

Kovesdy, C. P., Davis, J. R., Duling, I., and Little, D. J. (2023). Prevalence of anaemia in adults with chronic kidney disease in a representative sample of the United States population: analysis of the 1999–2018 National Health and Nutrition Examination Survey. *Clin. Kidney J.* 16, 303–311. doi:10.1093/ckj/sfac240

Liberman, M., Johnson, R. C., Handy, D. E., Loscalzo, J., and Leopold, J. A. (2011). Bone morphogenetic protein-2 activates NADPH oxidase to increase endoplasmic reticulum stress and human coronary artery smooth muscle cell calcification. *Biochem. Biophys. Res. Commun.* 413, 436–441. doi:10.1016/j.bbrc.2011.08.114

Lin, J. H., Walter, P., and Yen, T. S. B. (2008). Endoplasmic reticulum stress in disease pathogenesis. *Annu. Rev. Pathol.* 3, 399–425. doi:10.1146/annurev.pathmechdis.3.121806.151434

Lin, Y. S., Sun, Z., Shen, L. S., Gong, R. H., Chen, J. W., Xu, Y., et al. (2024). Arnicolide D induces endoplasmic reticulum stress-mediated oncosis via ATF4 and CHOP in hepatocellular carcinoma cells. *Cell Death Discov.* 10 (1), 134. doi:10.1038/s41420-024-01911-w

Liu, A., Chen, Z., Li, X., Xie, C., Chen, Y., Su, X., et al. (2023). C5a-C5aR1 induces endoplasmic reticulum stress to accelerate vascular calcification via PERK-eIF2α-ATF4-CREB3L1 pathway. *Cardiovasc. Res.* 119, 2563–2578. doi:10.1093/cvr/cvad133

Maekawa, H., and Inagi, R. (2017). Stress signal network between hypoxia and ER stress in chronic kidney disease. *Front. Physiol.* 8, 74. doi:10.3389/FPHYS.2017.00074

Masuda, M., Miyazaki-Anzai, S., Keenan, A. L., Shiozaki, Y., Okamura, K., Chick, W. S., et al. (2016). Activating transcription factor-4 promotes mineralization in vascular smooth muscle cells. *JCI Insight* 1, e88646. doi:10.1172/jci.insight.88646

Masuda, M., Miyazaki-Anzai, S., Levi, M., Ting, T. C., and Miyazaki, M. (2013). PERK-eIF2α-ATF4-CHOP signaling contributes to TNFα-induced vascular calcification. *J. Am. Heart Assoc.* 2, e000238. doi:10.1161/JAHA.113.000238

Masuda, M., Ting, T. C., Levi, M., Saunders, S. J., Miyazaki-Anzai, S., and Miyazaki, M. (2012). Activating transcription factor 4 regulates stearate-induced vascular calcification. *J. Lipid Res.* 53, 1543–1552. doi:10.1194/jlr.M025981

Mima, A. (2021). Hypoxia-inducible factor-prolyl hydroxylase inhibitors for renal anemia in chronic kidney disease: advantages and disadvantages. *Eur. J. Pharmacol.* 912, 174583. doi:10.1016/j.ejphar.2021.174583

Mizobuchi, M., Towler, D., and Slatopolsky, E. (2009). Vascular calcification: the killer of patients with chronic kidney disease. *J. Am. Soc. Nephrol.* 20, 1453–1464. doi:10.1681/ASN.2008070692

Mokas, S., Larivière, R., Lamalice, L., Gobeil, S., Cornfield, D. N., Agharazii, M., et al. (2016). Hypoxia-inducible factor-1 plays a role in phosphate-induced vascular smooth muscle cell calcification. *Kidney Int.* 90, 598–609. doi:10.1016/j.kint.2016.05.020

Moulin, S., Thomas, A., Arnaud, C., Arzt, M., Wagner, S., Maier, L. S., et al. (2020). Cooperation between hypoxia-inducible factor 1α and activating transcription factor 4 in sleep apnea-mediated myocardial injury. *Can. J. Cardiol.* 36, 936–940. doi:10.1016/j.cjca.2020.04.002

Negri, A. L. (2023). Role of prolyl hydroxylase/HIF-1 signaling in vascular calcification. *Clin. Kidney J.* 16, 205–209. doi:10.1093/ckj/sfac224

Ogata, H., Sugawara, H., Yamamoto, M., and Ito, H. (2024). Phosphate and coronary artery disease in patients with chronic kidney disease. *J. Atheroscler. Thromb.* 31, 1–14. doi:10.5551/jat.RV22012

Pereira, E. R., Frudd, K., Awad, W., and Hendershot, L. M. (2014). Endoplasmic reticulum (ER) stress and hypoxia response pathways interact to potentiate hypoxia-inducible factor 1 (HIF-1) transcriptional activity on targets like vascular endothelial growth factor (VEGF). *J. Biol. Chem.* 289, 3352–3364. doi:10.1074/jbc.M113.507194

Portolés, J., Martín, L., Broseta, J. J., and Cases, A. (2021). Anemia in chronic kidney disease: from Pathophysiology and current treatments, to future agents. *Front. Med.* 8, 642296. doi:10.3389/fmed.2021.642296

Rao, Z., Zheng, Y., Xu, L., Wang, Z., Zhou, Y., Chen, M., et al. (2022). Endoplasmic reticulum stress and pathogenesis of vascular calcification. *Front. Cardiovasc. Med.* 9, 918056. doi:10.3389/fcvm.2022.918056

Ron, D., and Walter, P. (2007). Signal integration in the endoplasmic reticulum unfolded protein response. *Nat. Rev. Mol. Cell Biol.* 8, 519–529. doi:10.1038/nrm2199

Shanahan, C. M., and Furmanik, M. (2017). Endoplasmic reticulum stress in arterial smooth muscle cells: a novel regulator of vascular disease. *Curr. Cardiol. Rev.* 13, 94–105. doi:10.2174/1573403X12666161014094738

Shiozaki, Y., Okamura, K., Kohno, S., Keenan, A. L., Williams, K., Zhao, X., et al. (2018). The CDK9-cyclin T1 complex mediates saturated fatty acid-induced vascular calcification by inducing expression of the transcription factor CHOP. *J. Biol. Chem.* 293, 17008–17020. doi:10.1074/jbc.RA118.004706

Singh, A. K., Carroll, K., Perkovic, V., Solomon, S., Jha, V., Johansen, K. L., et al. (2021). Daprodustat for the treatment of anemia in patients undergoing dialysis. *N. Engl. J. Med.* 385, 2325–2335. doi:10.1056/nejmoa2113379

Tani, T., Orimo, H., Shimizu, A., and Tsuruoka, S. (2017). Development of a novel chronic kidney disease mouse model to evaluate the progression of hyperphosphatemia and associated mineral bone disease. *Sci. Rep.* 7, 2233. doi:10.1038/s41598-017-02351-6

Tóth, A., Balogh, E., and Jeney, V. (2020). Regulation of vascular calcification by reactive oxygen species. *Antioxidants (Basel, Switzerland)* 9, 963–1024. doi:10.3390/ANTIOX9100963

Tóth, A., Csiki, D. M., Nagy, B., Balogh, E., Lente, G., Ababneh, H., et al. (2022). Daprodustat accelerates high phosphate-induced calcification through the activation of HIF-1 signaling. *Front. Pharmacol.* 13, 798053. doi:10.3389/FPHAR.2022.798053

Walter, P., and Ron, D. (2011). The unfolded protein response: from stress pathway to homeostatic regulation. *Science* 334, 1081–1086. doi:10.1126/science.1209038

Yang, X., Matsuda, K., Bialek, P., Jacquot, S., Masuoka, H. C., Schinke, T., et al. (2004). ATF4 is a substrate of RSK2 and an essential regulator of osteoblast biology; implication for Coffin-Lowry Syndrome. *Cell* 117, 387–398. doi:10.1016/s0092-8674(04)00344-7

Zhu, Q., Guo, R., Liu, C., Fu, D., Liu, F., Hu, J., et al. (2015). Endoplasmic reticulum stress-mediated apoptosis contributing to high glucose-induced vascular smooth muscle cell calcification. *J. Vasc. Res.* 52, 291–298. doi:10.1159/000442980

Zoccali, C., Mallamaci, F., Adamczak, M., de Oliveira, R. B., Massy, Z. A., Sarafidis, P., et al. (2023). Cardiovascular complications in chronic kidney disease: a review from the European renal and cardiovascular medicine working group of the European renal association. *Cardiovasc. Res.* 119, 2017–2032. doi:10.1093/cvr/cvad083

Glossary

AR	alizarin red
ATF4	activating transcription factor 4
ATF6	activating transcription factor 6
BMP2	bone morphogenetic protein 2
CHOP	transcriptional factor C/EBP homologous protein
CKD	chronic kidney disease
CKDD	CKD treated with DPD
Ctrl	Control
DMEM	Dublecco's modified eagle medium
DMSO	dimethyl sulphoxide
DPBS	Dulbecco's phosphate-buffered saline
DPD	Daprodustat
ECM	extracellular matrix
EDTA	ethylenediamine-tetraacetic acid
ER	endoplasmic reticulum
ESAs	erythropoiesis-stimulating agents
eIF2α	eukaryotic initiation factor 2 alpha
FBS	fetal bovine serum
FDA	U.S. Food and Drug Administration
Glut1	glucose transporter 1
GM	growth medium
GRP78	glucose-regulated protein 78
HAoSMC	human aortic smooth muscle cell
HIF	hypoxia-inducible factor
IRE1α	inositol-requiring protein 1α
MACE	major cardiovascular event
OCN	Osteocalcin
OD	optical density
OM	osteogenic medium
PBS	phosphate-buffered saline
P-eIF2α	phospho-eIF2α
PHD	prolyl hydroxylase domain-containing
PERK	protein kinase RNA-like ER kinase
Pi	inorganic phosphate
P-PERK	phospho-PERK
Runx2	runt-related transcription factor 2
4-PBA	sodium-4-phenylbutyrate
qPCR	quantitative polymerase chain reaction
Sox9	SRY-box transcription factor 9
VEGFA	vascular endothelial growth factor A
VSMCs	vascular smooth muscle cells
UPR	unfolded protein response

frontiers | Frontiers in Pharmacology

TYPE Original Research
PUBLISHED 14 November 2024
DOI 10.3389/fphar.2024.1398630

OPEN ACCESS

EDITED BY
Tamer M. Mohamed,
University of Louisville, United States

REVIEWED BY
Sarah Lydia Pedretti,
University of Cape Town, South Africa
Mona Fouad Mahmoud,
Zagazig University, Egypt

*CORRESPONDENCE
Aishah Al-Jarallah,
aishah.aljarallah@ku.edu.kw

RECEIVED 10 March 2024
ACCEPTED 29 October 2024
PUBLISHED 14 November 2024

CITATION
Al-Othman R, Al-Jarallah A and Babiker F (2024) High-density lipoprotein protects normotensive and hypertensive rats against ischemia-reperfusion injury through differential regulation of mTORC1 and mTORC2 signaling. *Front. Pharmacol.* 15:1398630. doi: 10.3389/fphar.2024.1398630

High-density lipoprotein protects normotensive and hypertensive rats against ischemia-reperfusion injury through differential regulation of mTORC1 and mTORC2 signaling

Reham Al-Othman[1], Aishah Al-Jarallah[1]* and Fawzi Babiker[2]

[1]Department of Biochemistry, Faculty of Medicine, Kuwait University, Kuwait City, Kuwait, [2]Department of Physiology, College of Medicine, Kuwait University, Kuwait City, Kuwait

Background: High-density lipoprotein (HDL) protects against myocardial ischemia-reperfusion (I/R) injury. Mammalian target of rapamycin complexes 1 and 2 (mTORC1 and mTORC2) play opposing roles in protecting against I/R injury, whereby mTORC1 appears to be detrimental while mTORC2 is protective. However, the role of HDL and mTORC signaling in protecting against I/R in hypertensive rodents is not clearly understood. In this study, we investigated the involvement of mTORC1 and mTORC2 in HDL-mediated protection against myocardial I/R injury in normotensive Wistar Kyoto (WKY) rats and spontaneously hypertensive rats (SHR).

Methods: Hearts from WKY and SHR were subjected to I/R injury using a modified Langendorff system. Hemodynamics data were collected, and infarct size was measured. Rapamycin and JR-AB2-011 were used to test the role of mTORC1 and mTORC2, respectively. MK-2206 was used to test the role of Akt in HDL-mediated cardiac protection. The expression levels and the activation states of mediators of mTORC1 and mTORC2 signaling and myocardial apoptosis were measured by immunoblotting and/or enzyme-linked immunosorbent assay (ELISA).

Results: HDL protected hearts from WKY and SHR against I/R injury as indicated by significant improvements in cardiac hemodynamics and reduction in infarct size. HDL induced greater protection in WKY compared to SHR. HDL treatment attenuated mTORC1 signaling in WKY by reducing the phosphorylation of P70S6K (mTORC1 substrate). In SHR however, HDL attenuated mTORC1 signaling by reducing the levels of phospho-mTORC1, Rag C (mTORC1 activator), and phospho-PRAS40 (mTORC1 inhibitor). HDL increased the phosphorylation of mTORC2 substrate Akt, specifically the Akt2 isoform in SHR and to a greater extent in WKY. HDL-induced protection was abolished in the presence of Akt antagonist and involved attenuation of GSK, caspases 7 and 8 activation, and cytochrome C release.

Conclusion: HDL mediates cardiac protection via attenuation of mTORC1, activation of mTORC2-Akt2, and inhibition of myocardial apoptosis. HDL regulates mTORC1 and mTORC2 signaling via distinct mechanisms in

normotensive and hypertensive rats. HDL attenuation of mTORC1 and activation of mTORC2-Akt2 signaling could be a mechanism by which HDL protects against myocardial I/R injury in hypertension.

KEYWORDS

HDL, mTOR, Akt, ischemia/reperfusion injury, hypertension, apoptosis

Introduction

Hypertension continues to be a key risk factor in the development of cardiovascular diseases (Khan et al., 2020). Hypertension-induced cardiovascular complications involve functional and structural changes in the myocardium and coronary arteries including, but not limited, to increased workload, left ventricular hypertrophy (Yildiz et al., 2020), endothelial dysfunction (Gallo et al., 2021), and enhanced atherosclerotic plaque development (Ruilope and Schmieder, 2008; Li and Chen, 2005) resulting in ischemic heart disease (IHD). Hearts from hypertensive rodents demonstrated a notable resistance to the protection offered by ischemic postconditioning (Wagner et al., 2013; Babiker et al., 2019), erythropoietin (Yano et al., 2011), helium (Oei et al., 2012), and captopril (Penna et al., 2010). We have recently reported that acute and chronic treatment with high-density lipoprotein (HDL) protects hearts from spontaneously hypertensive rats (SHR) against myocardial ischemia-reperfusion (I/R) injury (Al-Jarallah and Babiker, 2022; Al-Jarallah and Babiker, 2024). The cardioprotective effects of HDL in hypertension are however not clearly understood.

Mammalian target of rapamycin complex 1 (mTORC1) and complex 2 (mTORC2) regulate cellular responses to stress conditions including ischemia (Laplante and Sabatini, 2012). mTORC1 inhibition with rapamycin protected against myocardial I/R injury and reduced cardiomyocyte apoptosis (Filippone et al., 2017; Das et al., 2015; Samidurai et al., 2020) suggesting a detrimental role of mTORC1 in mediating myocardial I/R injury. mTORC2 on the other hand, via the activation of protein kinase B (Akt), appears to be cardioprotective (Filippone et al., 2017; Samidurai et al., 2020; Yano et al., 2014). Interestingly, rapamycin-mediated inhibition of mTORC1 reduced blood pressure, albumin secretion and renal inflammatory cell infiltration in Dahl salt-sensitive rats (Kumar et al., 2017). HDL activated phosphatidylinositol-3-kinase (PI3K)/AKt/mTORC signaling and protected against oxidative stress-induced cardiomyocyte apoptosis (Nagao et al., 2017). Nonetheless, the effect of HDL on mTORC1 and mTORC2 in the protection against I/R injury in hypertensive rodents is not clearly understood. We hypothesize that HDL protects against I/R injury by inhibiting mTORC1 and activating mTORC2 in spontaneously hypertensive rats (SHR). We report that mTORC1 and mTORC2 exhibit contrasting functions in mediating myocardial I/R injury. Moreover, we demonstrate that HDL offers protection against I/R injury in normotensive and hypertensive rats to varying degrees. HDL inhibited mTORC1 in normotensive and hypertensive rats via different mechanisms. HDL, however, activated mTORC2 in both genotypes. HDL-mediated protection against I/R injury in WKY and SHR involved attenuation of myocardial apoptosis.

Materials and methods

Materials

All materials were purchased from Sigma Aldrich (Germany, Steinheim) unless stated otherwise.

Animals and instrumentation

Twelve to fourteen-week-old male Wistar Kyoto (WKY) rats and spontaneously hypertensive rats (SHR) were randomized and used in the study (n = 4–9 rats per treatment). The SHR model was chosen because it is a well-established model for studying essential hypertension and hypertension-related physiological and biochemical changes (Al-Jarallah and Babiker, 2024; Dodd et al., 2012). SHR are characterized by elevated blood pressure, autonomic nervous system imbalances cardiovascular and renal complications, making it a valuable tool for understanding the pathophysiology of hypertension and testing potential treatments (Jama et al., 2022; Zhou and Frohlich, 2007). Animals were kept under internationally accepted conditions in the Animal Resource Center, Faculty of Medicine, Kuwait University. All animals were maintained under controlled temperature (21–24 C), 12 h light/dark cycle (light 7 a.m.–7 p.m.) and 50% humidity. The rats were housed in plastic cages (2 rats/cage) with unrestricted access to tap water and food. All procedures were approved by the Health Sciences Research Ethics Committee (ID:3640). Blood pressure was measured using the CODA-4 channel system (Kent Scientific Corporation, United States). Normotensive and hypertensive rats were defined by systolic blood pressure (SBP) cutoff values of ≤120 mmHg and ≥160 mmHg, respectively.

Experimental procedures and protocols

Heart cannulation and perfusion were performed using a modified Langendorff system as previously described in (Juggi et al., 2011). Briefly, the heart was carefully isolated and immersed in cold (4°C) Krebs-Hensleit (KH) solution. The isolated hearts were perfused retrogradely with a freshly prepared KH buffer mmol/L: NaCl 117.86, KCl 5.59, $CaCl_2.H_2O$ 2.4, $NaHCO_3$ 20, KH_2PO_4 1.19, $MgCl_2.6H_2O$ 1.2, Glucose 12.11. The buffer was gazed with a mixture of O_2 (95%) and CO_2 (5%), pH (7.35–7.45) at 37°C. After stabilization (20 min), regional ischemia was induced by occluding the left anterior descending (LAD) coronary artery for 30 min. The success of ischemia induction was evaluated at the onset of ischemia by an immediate drop in the coronary flow. Preload was kept constant at 6 mmHg under basal controlled conditions and perfusion pressure (PP) at 50 mmHg was maintained throughout

the experimental procedure. A water-filled latex balloon was placed and secured in the left ventricular (LV) cavity. The balloon was attached to a pressure transducer and a "DC-Bridge amplifier (DC-BA)" with a pressure module (DC-BA type 660, Hugo-Sachs Electronik, Germany) and interfaced to a personal computer for monitoring LV developed pressure (DPmax). LV developed pressure was derived from acquisition of LV end systolic pressure (LVESP) using Max-Min module (Number MMM type 668, Hugo Sachs Elektronik-Harvard Apparatus GmbH, Germany) which converts the output from DC bridge amplifier to DPmax by subtracting LV end diastolic pressure (LVEDP) from the LVESP. All hearts were subjected to ischemia produced by LAD coronary artery occlusion by a snare at ~0.5 cm below the atrioventricular groove, and a small rigid plastic tube was positioned between the heart and the snare to ensure complete occlusion of the coronary artery.

Hearts were subjected to I/R injury without any treatments (untreated controls, Supplementary Figure S1, group A) or treated with mTORC1 antagonist, rapamycin (100 nM) (Das et al., 2015), mTORC2 specific antagonist JR-AB2-011 (5 μM) (Benavides-Serrato et al., 2017) or Akt antagonist, MK-2206 (5 μM) (Chen et al., 2018) infused at 25 min of ischemia and continued until 10 min of reperfusion (Supplementary Figure S1, group B). Alternatively, hearts were treated with HDL (400 μg) (Lee BioSolutions, United States) (Al-Jarallah and Babiker, 2024) administered 5 min before reperfusion and continued for an additional 10 min (Supplementary Figure S1, group C). In the fourth group, hearts were pretreated with MK-2206 (5 μM) infused 5 min prior to the addition of HDL (400 μg) and continued during the first 10 min of reperfusion (Supplementary Figure S1, group D). At the end of each experiment, hearts were collected, snap-frozen in liquid nitrogen, and stored at −80 °C for further analysis.

Data collection and processing

Left ventricular function was evaluated by the assessment of LV end diastolic pressure (LVEDP) and DPmax, cardiac contractility was monitored by heart contractility index values (±dp/dt), while coronary-vascular dynamics were evaluated by the coronary flow, measured using an electromagnetic flow probe attached to the inflow of the aortic cannula interfaced to a personal computer. The coronary flow (CF) (mL/min) was continuously monitored using a software developed specifically for this purpose and was manually verified by the timed collection of coronary effluent. The coronary vascular resistance (CVR) and hemodynamics data were determined every 10 s using an online data acquisition program (Isoheart software V 1.524-S, Hugo-Sachs Electronik, Germany).

Evaluation of infarct size by triphenyltetrazolium chloride staining

Hearts (n = 3) were sliced transversely into 4–6 pieces from apex to base. The slices were incubated in 1% triphenyltetrazolium chloride (TTC) solution in isotonic (pH 7.40) phosphate buffer and fixed in 4% formaldehyde for 24 h. Infarct size was measured blindly using Scion ImageJ (ImageJ, Wayne Rasb and National Institute of Health, United States). The infarcted area of the LV was expressed as a percentage of the total LV area.

Tissue homogenization and protein extraction

Hearts were homogenized using a polytron homogenizer (Ultra-Turrax: T 25 basic: IKA®-Werk, Germany) in ice cold buffer containing: 0.2x PBS, 0.1% triton-x100, 1x protease inhibitor cocktail, 1x phosphatase inhibitor cocktail, pH (7.40). The hearts were subjected to four homogenization cycles, 30 s each, with 60 s cooling in between. Homogenates were centrifuged at 6,000 rpm for 15 min at 4°C in a benchtop centrifuge (Beckman J2-MI, United States). The supernatant was collected, aliquoted, and stored at −80°C for further analysis. Protein concentration was estimated using a BCA assay kit (Thermo Fisher Scientific, MA, United States) following manufacturer instructions. Absorbance readings were measured at 562 nm (BMG LabTech ClarioStar, Germany).

Immunoblotting

Protein expression was detected using sodium dodecyl sulfate-polyacrylamide gel electrophoresis (SDS-PAGE) followed by immunoblotting against target proteins. Samples (50 μg protein) mixed with the loading buffer were boiled for 5 min and loaded into 4%–20% gradient Tris-glycine polyacrylamide gels (BioRad, United States). Proteins were then transferred to polyvinylidene difluoride (PVDF) membranes. Membranes were blocked with 5% nonfat dairy milk (NFDM) or 5% bovine serum albumin (BSA) in Tris-buffered saline, 0.1% Tween (TBS-T) for 1 h at room temperature. Membranes were blotted with primary antibodies against phospho-mTOR (Ser2448), total mTOR, phosphorylated-40 kDa proline-rich AKT substrate (PRAS40) (Thr246), total PRAS40, phosphorylated-ribosomal protein S6 kinase beta-1 (P70S6K) (Thr 389), total P70S6K, phosphorylated-eukaryotic translation initiation factor 4E (eIF4E)-binding protein (4E-BP1) (Thr37/46) and total 4E-BP1, Ras-related GTP-binding protein C (RagC), phospho-Akt (Ser473), total Akt, phosphorylated-Akt1 (Ser473), total Akt1, phosphorylated-Akt2 (Ser474), total Akt2, phosphorylated-glycogen synthase kinase (GSK)-3β (Ser9), total GSK-3β, caspase-7, GAPDH (Cell Signaling, MA, United States) or caspase-8 (Santacruz, United States), overnight at 4°C, followed by horseradish peroxidase (HRP)-conjugated donkey anti-rabbit or donkey anti-mouse antibodies (Jackson ImmunoResearch, United States). Bands were developed using enhanced chemiluminescence (ECL) reagent (Bio-Rad, United States) and detected using Bio-Rad Chemidoc (Bio-Rad chemi-Doc™ MP Imaging System, United States). Bands were quantified using Image Lab software (Bio-Rad, United States).

Measurements of cytochrome C release

Cytochrome c release was measured in heart homogenates using a commercially available kit from Abcam (ab210575) following the

TABLE 1 Heart and body weights of WKY and SHR, and CODA 4-channel high throughput non-invasive blood pressure measurement data.

	WKY	SHR
Body weight (g)	324.7 ± 6.090	279.5 ± 3.832****
Heart Weight (g)	1.667 ± 0.02619	1.551 ± 0.02530**
Heart weight/Body weight	5.23E-03 ± 1.10E-04	5.59E-03 ± 9.18E-05*
Systolic Blood Pressure (mmHg)	113.8 ± 1.277	180.0 ± 1.368****
Diastolic Blood Pressure (mmHg)	74.05 ± 1.013	122.2 ± 1.663****
Mean	86.95 ± 1.079	141.1 ± 1.538****
Rate (Plus/min)	167.8 ± 4.871	291.3 ± 4.572****
Flow (μL/min)	5.787 ± 0.4262	9.023 ± 0.3133****
Volume (μL)	32.36 ± 2.472	62.24 ± 2.058****

*P vs. WKY (P < 0.05).
**P vs. WKY (P < 0.01).
****P vs. WKY (P < 0.0001).

manufacturer's protocol. Briefly, heart homogenates were diluted (200 x), added to wells precoated with cytochrome c antibody cocktail, and incubated for 1 h at room temperature on a plate shaker. The reaction was then developed by the addition of a substrate solution for 10 min followed by the addition of the stop solution. Cytochrome c levels were determined by measuring the absorbance at 450 nm (BMG LabTech ClarioStar, Germany) and plotting the obtained values against the cytochrome c standard provided with the kit.

Statistical analysis

Data are presented as means ± *standard error* of the *mean (SEM)*. A two-way analysis of variance (ANOVA) followed by *post hoc* analysis using Bonferroni test was used to test the difference between the means of multiple groups (GraphPad Prism 10.0.2). The two-tailed unpaired student t-test was used to test the significance between two groups that followed a normal distribution while the Mann–Whitney *U* test was used to compare two groups that failed to follow the normal distribution. Differences were considered statically significant at $P < 0.05$.

Results

mTORC1 and mTORC2 play opposing roles in mediating myocardial I/R injury in normotensive and hypertensive rats

Hearts from SHR demonstrated signs of cardiac enlargement (Table 1). SHR had significantly higher ($P < 0.01$) SBP and diastolic blood pressure (DBP) relative to WKY. In addition, SHR exhibited significantly ($P < 0.01$) higher heart rate, blood flow, and volume relative to WKY (Table 1).

Inhibition of mTORC1 with rapamycin protected rodents against myocardial I/R injury (Filippone et al., 2017). Hearts from hypertensive rodents were shown to be resistant to protection induced by pharmacological agents proven, otherwise, to be protective in normotensive rodents (Babiker et al., 2019). The involvement of mTORC1 in mediating I/R injury in SHR has not been previously investigated, we therefore tested if mTORC1 inhibition with rapamycin can protect hypertensive rats from myocardial I/R injury. Rapamycin treatment significantly ($P < 0.05$) improved LVEDP and Pmax (Figures 1A,B) compared to the respective ischemic period and untreated controls in WKY and SHR. On the other hand, infusion of JR-AB2-011 significantly ($P < 0.05$) increased LVEDP in SHR and decreased Pmax in WKY and SHR. Moreover, rapamycin significantly ($P < 0.05$) increased the contractility index ± dP/dt (Table 2) and CF and decreased CVR compared to the respective ischemic period and untreated controls (Figures 1C,D) in WKY and SHR. In addition, rapamycin treatment reduced infarct size in normotensive and hypertensive rats (Figure 1E). This data suggests that mTORC1 plays a detrimental role in mediating I/R injury and inhibition of mTORC1 is protective in normotensive and hypertensive rats. To test the role of mTORC2 we used mTORC2 specific antagonist JR-AB2-011 (Benavides-Serrato et al., 2017; Guenzle et al., 2020). Administration of JR-AB2-011 (5 μM) did not improve cardiac functions in WKY and SHR evident by the persistent deterioration in LV function (Figures 1A,B), cardiac contractility, (Table 2), and coronary vascular dynamics, (Figures 1C,D), compared to the respective ischemic period and untreated control, neither it reduced the infarct size (Figure 1E) suggesting that mTORC2 plays a protective role in WKY and SHR. Collectively this data suggest that mTORC1 and mTORC2 play opposing roles in mediating myocardial I/R injury in normotensive and hypertensive rats.

HDL protects against myocardial I/R injury by selectively inhibiting mTORC1 and activating mTORC2 signaling

We tested the effect of HDL on I/R-induced myocardial injury in hearts isolated from WKY and SHR. HDL administration, 5 minutes before reperfusion, protected hearts from WKY and SHR from myocardial I/R injury (Figure 2). This was evident by the significant ($P < 0.05$) improvements in LV functions (LVEDP, Pmax) (Figures 2A,B) cardiac contractility (±dp/dt), (Table 2), and coronary hemodynamics (CF, CVR) (Figures 2C,D) relative to ischemia and relative to untreated controls. Interestingly, HDL induced significantly ($P < 0.05$) greater protection in WKY relative to SHR, possibly suggesting differences in HDL-mediated signaling between WKY and SHR. Consistent with the protection observed in the physiological parameters we tested, HDL reduced the infarct size in both genotypes (Figure 2E).

To test the effects of HDL on the mTORC1 signaling pathway we measured the activation state of mTORC1, mTORC1 substrates, P70S6K, 4E-BP1, and mTORC1 inhibitor, PRAS40. In addition, we examined the expression levels of mTORC1 activator, Rag C in heart homogenates from WKY and SHR treated with or without HDL. SHR demonstrated significantly ($P < 0.05$) higher basal levels of mTOR phosphorylation at Ser2448, a site predominantly phosphorylated in mTORC1 (Copp et al., 2009)

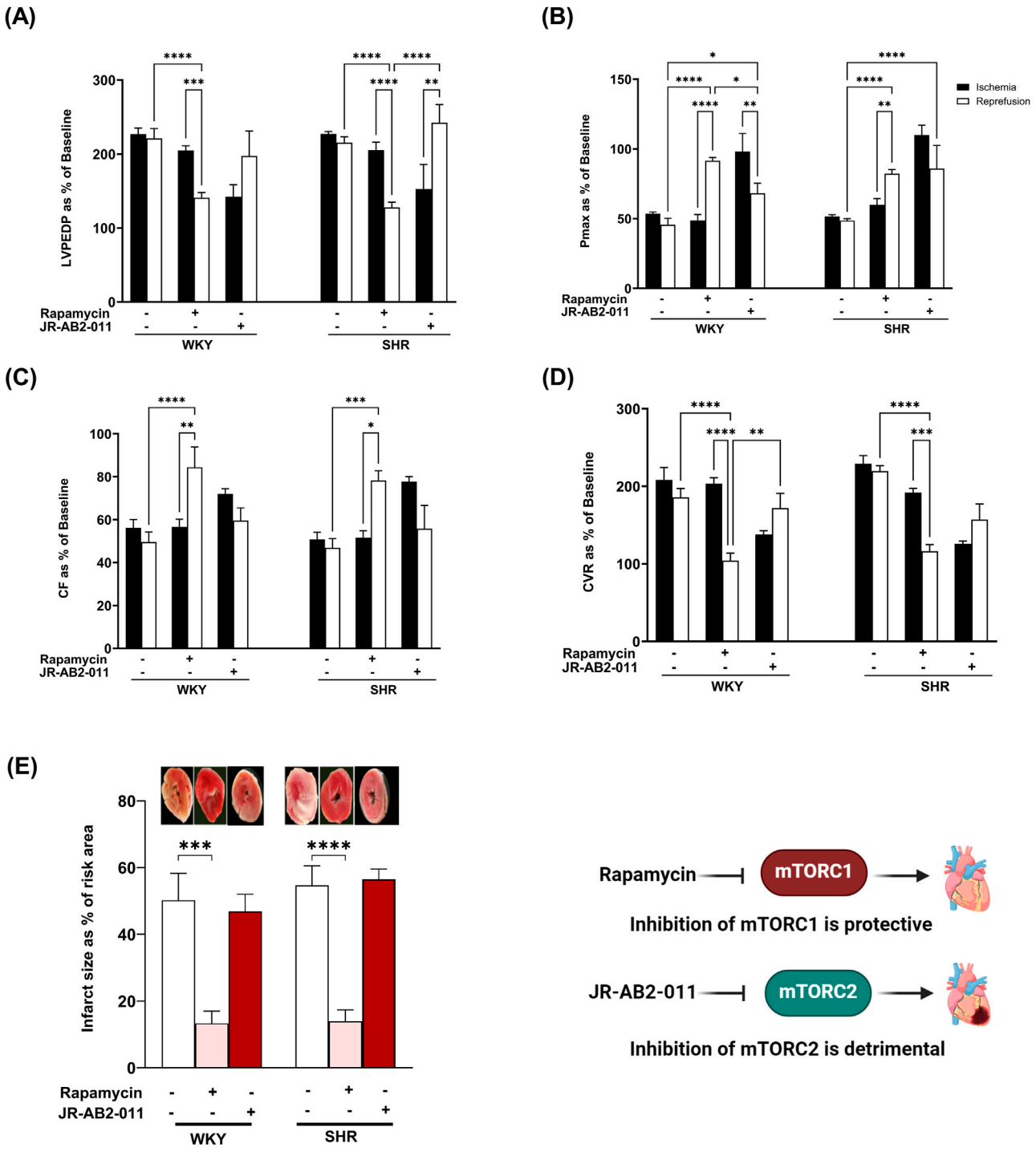

FIGURE 1
The role of mTORC1 and mTORC2 in mediating I/R injury in WKY and SHR. Post-ischemic recovery parameters of cardiac functions including left ventricular functions (LVPEDP **(A)**, Pmax **(B)**) and coronary hemodynamic (CF **(C)**, CVR **(D)**). Data were computed at 30 min of reperfusion and presented as means ± SEM of n = 4–9 rats per group. Infarct size determination by TTC staining on (n = 3) rats per group **(E)**. *P < 0.05, **P< 0.01, ***P< 0.001, ****P< 0.0001, LVEDP, left ventricular end diastolic pressure; Pmax, maximum developed pressure; CF, coronary flow; CVR, coronary vascular resistance.

(Figure 3A). HDL treatment significantly (P < 0.05) reduced Ser2448 phosphorylation in SHR but did not have any significant effects in WKY (Figure 3A). This data suggests enhanced basal activation of mTORC1 in SHR that is significantly reduced by HDL treatment.

The binding of PRAS40 to mTORC1 results in complex inhibition (Oshiro et al., 2007). The phosphorylation of PRAS40 by Akt, however, results in its dissociation from the complex and alleviation of inhibition (Sancak et al., 2007; Wang et al., 2007). SHR expressed significantly (P < 0.05) higher basal

TABLE 2 Cardiac contractility in normotensive and hypertensive rats subjected to different treatments.

Treatment	WKY				SHR			
	+dp/dt		-dp/dt		+dp/dt		-dp/dt	
	Ischemia	Reperfusion	Ischemia	Reperfusion	Ischemia	Reperfusion	Ischemia	Reperfusion
Control	51.5 ± 2.3	53.5 ± 6.5	52.3 ± 2.95	49.7 ± 4.3	50.5 ± 1.7	46.2 ± 2.6	51.6 ± 1.8	49.3 ± 1.4
Rapamycin	52.0 ± 6.1	90.7 ± 7.4$^{\$\$\$\$\#\#\#\#}$	50.9 ± 5.1	86.7 ± 7.7$^{\$\$\$\#\#\#\#}$	67.9 ± 3.7	95.9 ± 4.1$^{\$\#\#\#\#}$	64.8 ± 7.6	91.3 ± 9.1$^{\$\#\#\#\#}$
JR-AB-011	101.2 ± 6.1	94.2 ± 12.7$^{\#\#\#}$	96.8 ± 8.6	79.6 ± 9.0$^{\#}$	106.3 ± 10.4	86.5 ± 13.1$^{\#\#}$	104.5 ± 8.7	89.0 ± 9.2$^{\#\#}$
HDL	60.9 ± 6.4	95.2 ± 5.3$^{\$\$\$\$\#\#\#\#}$	55.4 ± 4.1	96.8 ± 8.2$^{\$\$\$\$\#\#\#\#}$	48.3 ± 2.2	71.4 ± 3.9$^{\$\#\#*}$	48.7 ± 2.0	68.5 ± 1.1$^{\$\#\#***}$
MK-0226	65.4 ± 4.1	42.1 ± 6.6	53.0 ± 3.9	39.5 ± 5.7	57.3 ± 3.9	51.7 ± 4.1	41.0 ± 3.1	46.6 ± 1.7
MK-0226+HDL	54.3 ± 4.8	51.2 ± 7.9	42.1 ± 4.8	32.6 ± 4.6$^{\bullet\bullet\bullet\bullet}$	45.8 ± 3.3	50.2 ± 4.8	42.7 ± 7.3	36.5 ± 7.3$^{\bullet\bullet\bullet}$

$p vs. Ischemia ($P < 0.05$).
$^{\$\$\$}$p vs. Ischemia ($P < 0.001$).
$^{\$\$\$\$}$p vs. Ischemia ($P < 0.0001$).
#P vs. Control ($P < 0.05$).
$^{\#\#}$P vs. Control ($P < 0.01$).
$^{\#\#\#}$P vs. Control ($P < 0.001$).
$^{\#\#\#\#}$P vs. Control ($P < 0.0001$).
*P vs. the same treatment in WKY ($P < 0.05$).
***P vs. the same treatment in WKY ($P < 0.001$).
$^{\bullet\bullet\bullet}$P vs. HDL, in the same genotype ($P < 0.001$).
$^{\bullet\bullet\bullet\bullet}$P vs. HDL, in the same genotype ($P < 0.0001$).

10.3389/fphar.2024.1398630

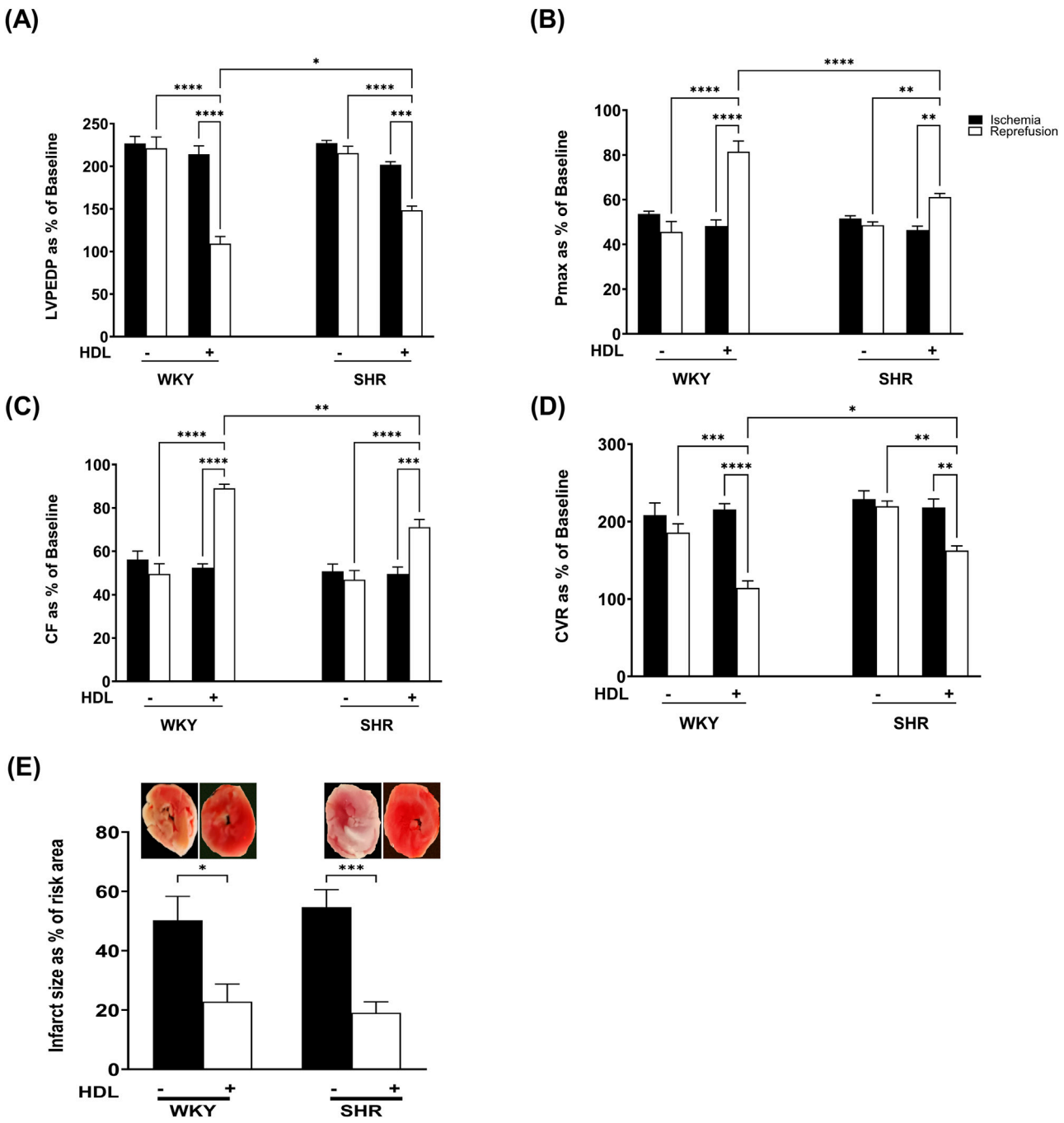

FIGURE 2
HDL protects WKY and SHR against myocardial I/R injury. Post-ischemic recovery parameters of cardiac functions including left ventricular functions (LVPEDP **(A)**, Pmax **(B)**) and coronary hemodynamic (CF **(C)**, CVR **(D)**). Data were computed at 30 min of reperfusion and presented as means ± SEM of n = 9 rats per group. Infarct size determination by TTC staining (n = 3) rats per group **(E)**. *P < 0.05, **P< 0.01, ***P< 0.001, ****P< 0.0001, LVEDP, left ventricular end diastolic pressure; Pmax, maximum developed pressure; CF, coronary flow; CVR, coronary vascular resistance.

levels of phospho-PRAS40 compared to WKY (Figure 3C), indicating the presence of increased levels of active mTORC1-PRAS40-free in SHR. HDL treatment significantly ($P < 0.05$) reduced PRAS40 phosphorylation in SHR, however, it did not change the phosphorylation state of PRAS40 in WKY (Figure 3C). Moreover, HDL treatment did not affect total PRAS40 expression in WKY and SHR (Figure 3D). Similar levels of total-PRAS40 were detected in hearts from normotensive and hypertensive rats. Furthermore, we examined the protein levels of mTORC1 activator, Rag C (Figure 3E). Basal protein levels of Rag C were not significantly ($P < 0.05$) different between WKY, and SHR. HDL did not affect Rag C protein levels in WKY, yet it significantly ($P < 0.05$) reduced Rag C expression in SHR (Figure 3E). Finally, we tested the effect of HDL on the activation state of the mTORC1 substrate, P70S6K. (Figure 3F). WKY expressed significantly ($P < 0.05$) higher basal levels of phospho-P70S6K

10.3389/fphar.2024.1398630

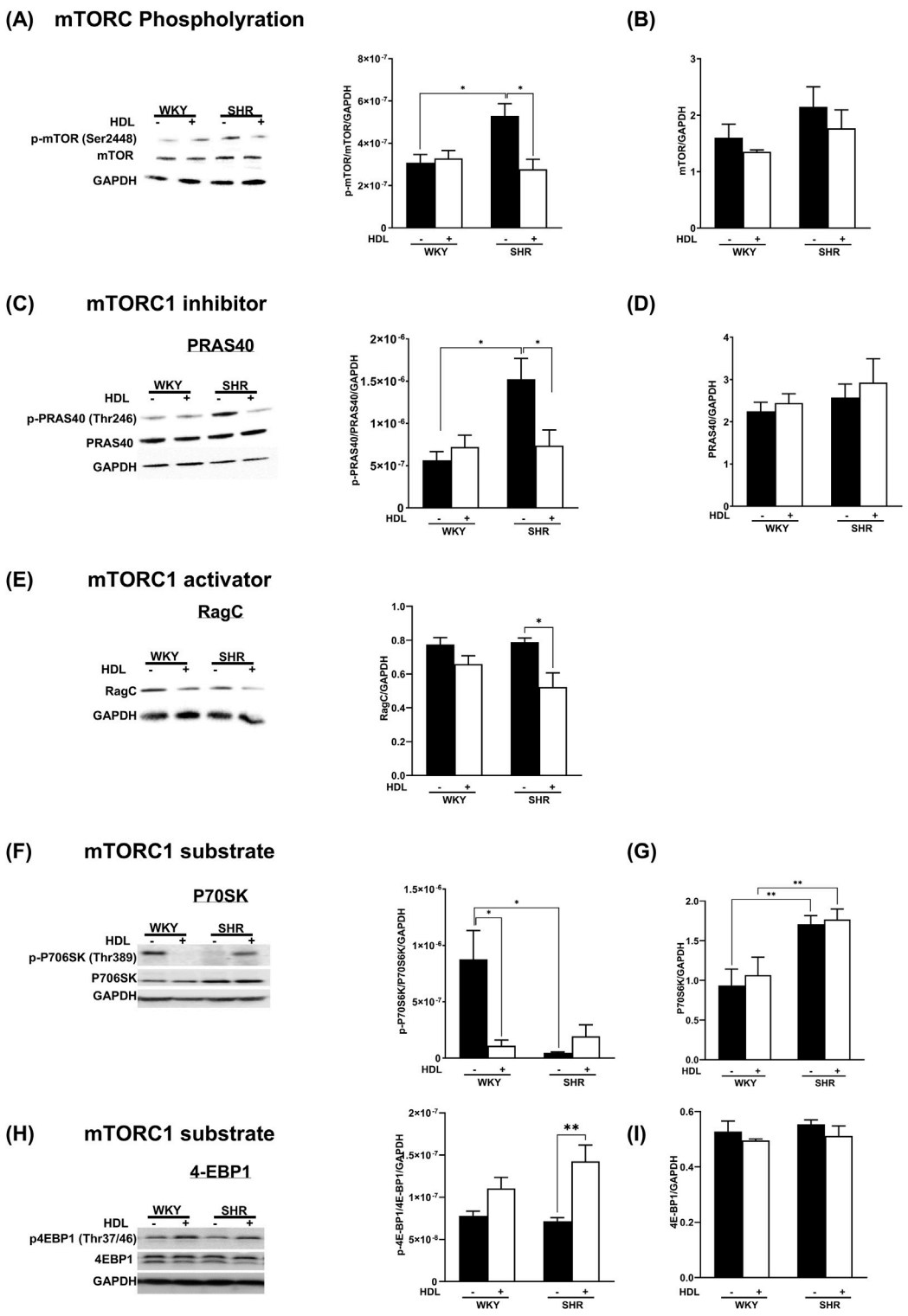

FIGURE 3
HDL inhibits mTORC1 signaling in WKY and SHR. Hearts from WKY and SHR subjected to I/R injury in the presence or absence of HDL were immunoblotted against mediators of mTORC1 signaling cascade: phospho-mTOR **(A)**, total mTORC **(B)**, phospho-PRAS40 **(C)**, total PRAS40 **(D)**, Rag C **(E)**, phospho-P70S6K **(F)**, total P70S6K **(G)**, phospho-4EBP1 **(H)**, total 4EBP1 **(I)**, and GAPDH as a loading control. Data are means ± SEM. *P < 0.05, **P< 0.01, ***P< 0.001, ****P< 0.0001, n = 3-6.

compared to SHR (Figure 3F). HDL treatment significantly (P < 0.05) reduced P70S6K phosphorylation in WKY. Total P70S6K protein levels were significantly (P < 0.05) higher in SHR than in WKY (Figure 3G). HDL treatment, however, did not affect total P70S6K levels in WKY or SHR (Figure 3G). The HDL treatment significantly (P < 0.05) increased levels of phospho-4E-BP1 in SHR

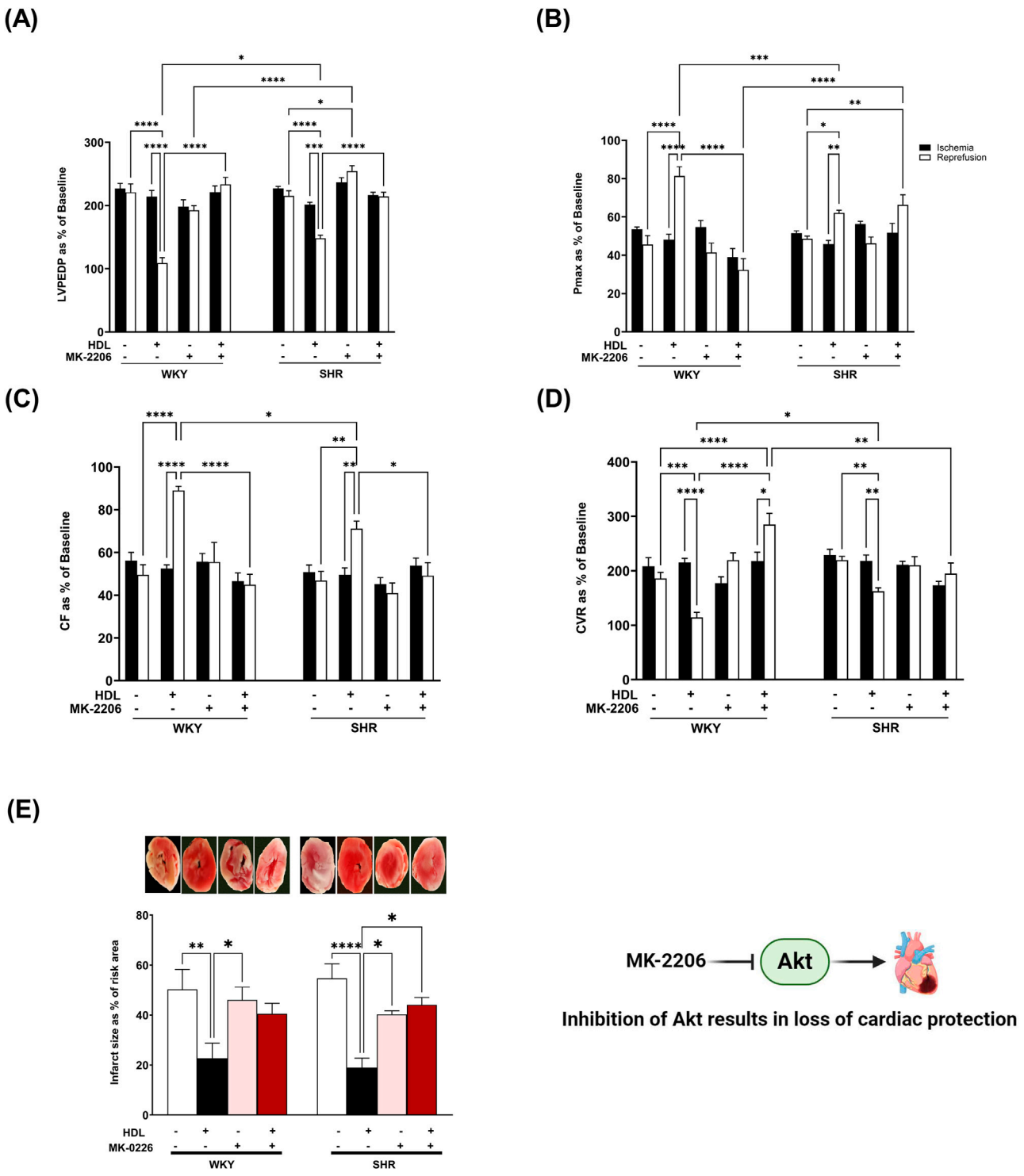

FIGURE 4
HDL-mediated cardiac protection requires Akt. Post-ischemic recovery parameters of cardiac functions including left ventricular functions (LVPEDP **(A)**, Pmax **(B)**) and coronary hemodynamic (CF **(C)**, CVR **(D)**). Data were computed at 30 min of reperfusion and presented as means ± SEM of n = 9 rats per group. Infarct size determination by TTC staining (n = 3) rats per group **(E)**. *P < 0.05, **P< 0.01, ***P< 0.001, ****P< 0.0001, LVEDP, left ventricular end diastolic pressure; Pmax, maximum developed pressure; CF, coronary flow; CVR, coronary vascular resistance.

but not in WKY (Figure 3H). To summarize, immunoblotting experiments revealed that HDL has an inhibitory effect on mTORC1 signaling in WKY and SHR. The mechanism of HDL-mediated inhibition of mTORC1 appears to be different between normotensive and hypertensive rats. In WKY, HDL reduced the levels of phospho-P70S6K. In SHR however, HDL decreased PRAS40 phosphorylation and Rag C protein levels (Figures 3A–G). Together this suggests that HDL-mediated inhibition of

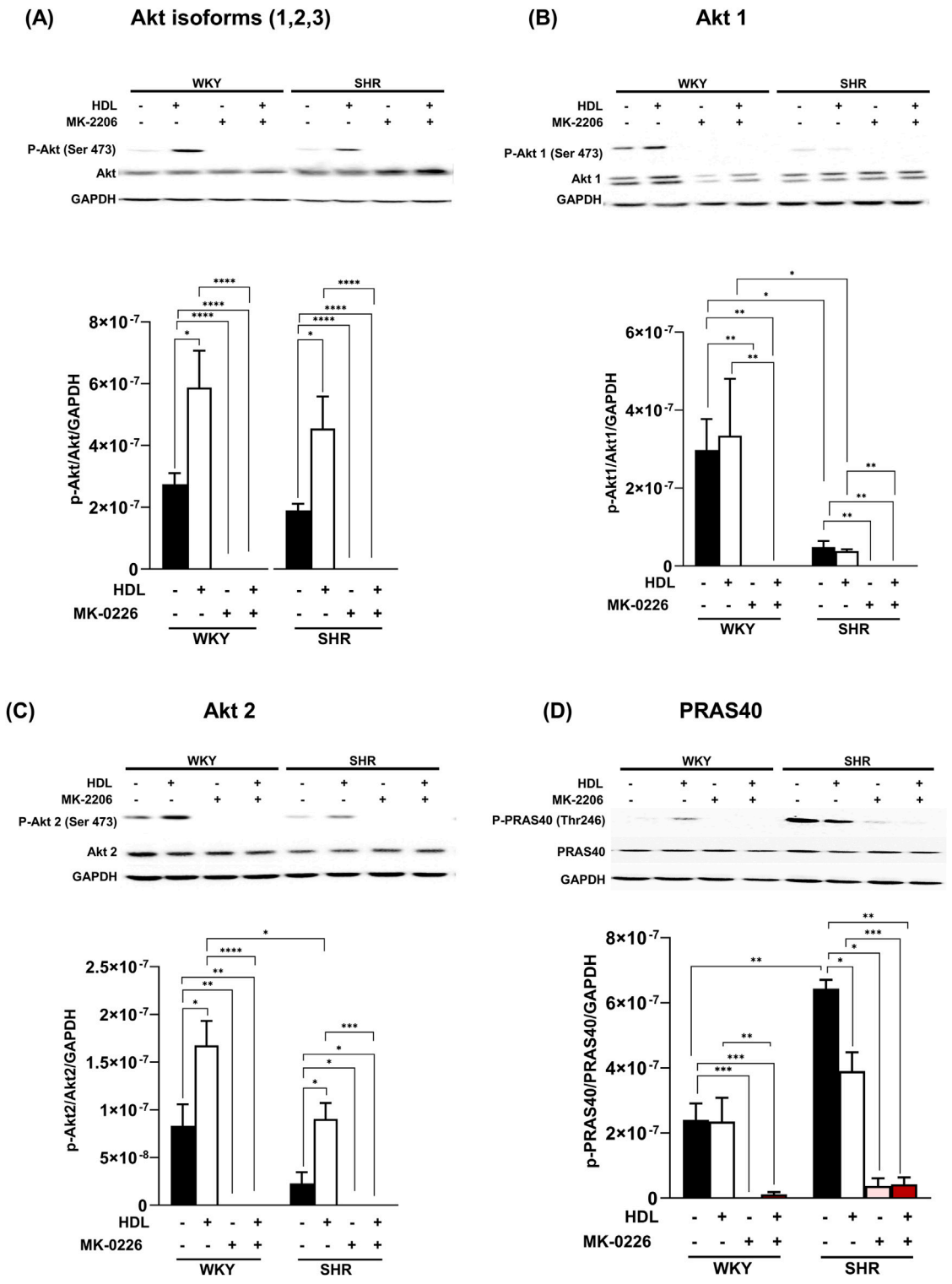

FIGURE 5
HDL induces the activation of Akt2 isoform. Heart homogenates from WKY and SHR subjected to I/R injury, treated with MK-2206 in the presence or absence of HDL, were subjected to immunoblotting against phospho-Akt, phospho-Akt1 or phospho-Akt2, total Akt, total Akt1, or total Akt2 **(A–C)** or phosphorylated and total PRAS40 **(D)** and GAPDH as a loading control. Data are means ± SEM, *P < 0.05, **P< 0.01, ***P< 0.001, ****P< 0.0001, n = 3–6.

mTORC1 could be one mechanism by which HDL protects against I/R injury in WKY and SHR. Nonetheless, HDL appears to differentially regulate mediators of mTORC1 signaling in WKY and SHR.

Protein kinase B (Akt) is a downstream target of mTORC2 (Oh and Jacinto, 2011). To test the effect of HDL on mTORC2 signaling we used Akt specific antagonist MK-2206 (Chen et al., 2018; Akhtar and Jabeen, 2018) and examined the phosphorylation state of

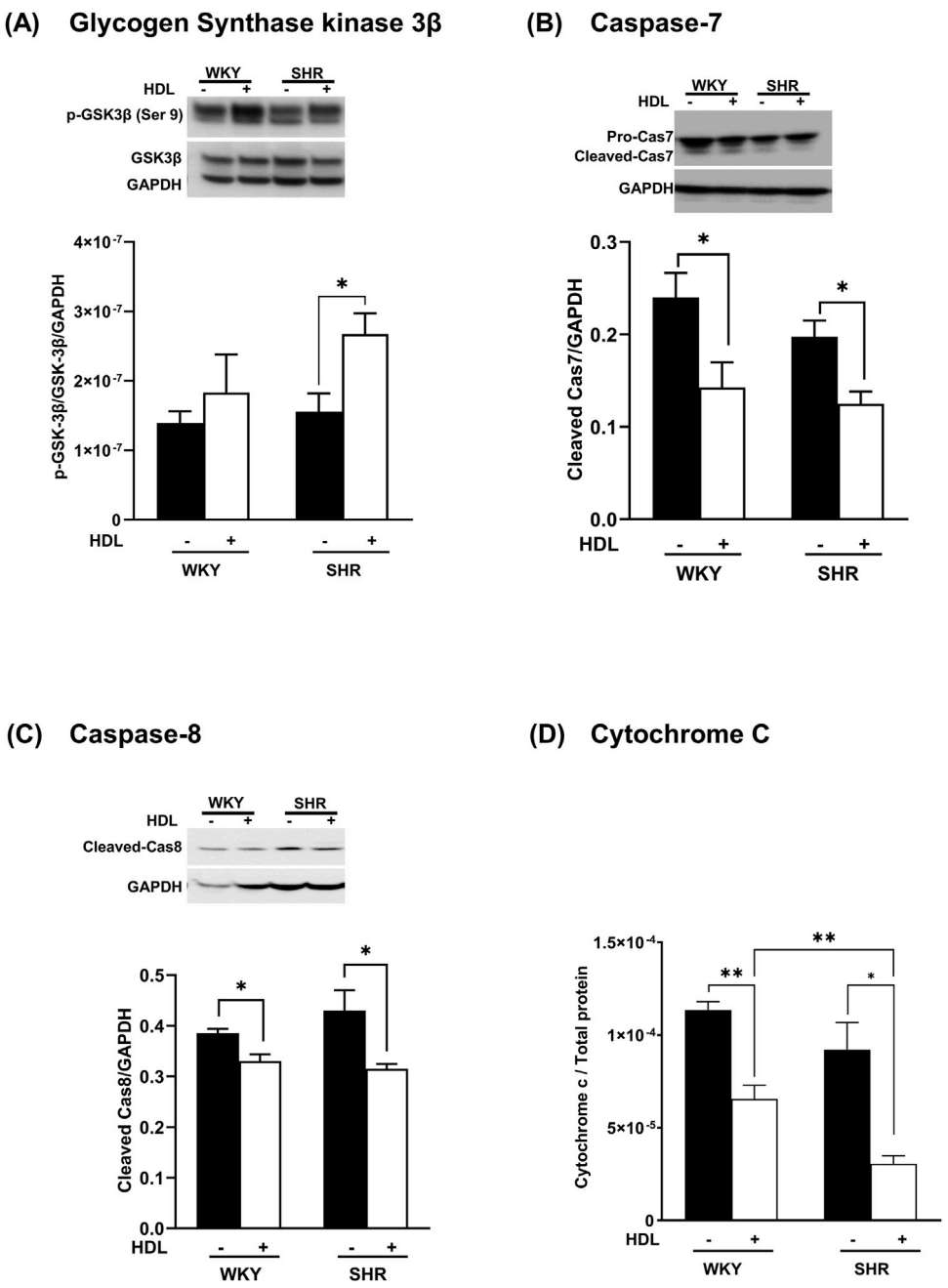

FIGURE 6
HDL reduces markers of myocardial apoptosis. Heart homogenates from WKY and SHR, subjected to I/R injury in the presence or absence of HDL, were subjected to immunoblotting against, phospho-GSK-3β (Ser9), and total GSK-3β **(A)**, procaspase –7, cleaved caspase 7 **(B)**, cleaved caspase 8 **(C)** and GAPDH as a loading control, and were subjected to ELISA against cytochrome c **(D)**. Data are means ± SEM, *P < 0.05, **P< 0.01, ***P< 0.001, ****P< 0.0001, n = 3-6.

specific Akt isoforms in response to HDL treatment. MK-2206 infusion did not protect the heart against I/R injury in WKY and SHR as indicated by impaired LV function (Figures 4A,B), cardiac contractility (Table 2), and coronary vascular dynamics (Figures 4C,D) and the lack of change in infarct size (Figure 4E) relative to the control. MK-2206 treatment however, abolished the protective effects of HDL in WKY and SHR (Figure 4). This was consistent with the infarct size data whereby HDL did not reduce the infarct size in MK-2206 treated WKY or SHR (Figure 4E).

Three Akt isoforms have been identified (Kumar and Madison, 2005; Yu et al., 2015), of which Akt1 and Akt2 are predominantly expressed in the myocardium (Abeyrathna and Su, 2015; Muslin, 2011). We examined the effect of HDL on the phosphorylation of these isoforms. HDL treatment significantly increased ($P < 0.05$) total Akt phosphorylation at Ser473 in WKY and SHR which was completely abolished in the presence of Akt antagonist (Figure 5A). Interestingly, HDL treatment did not increase Akt1 phosphorylation (Figure 5B), yet it significantly ($P < 0.05$) increased

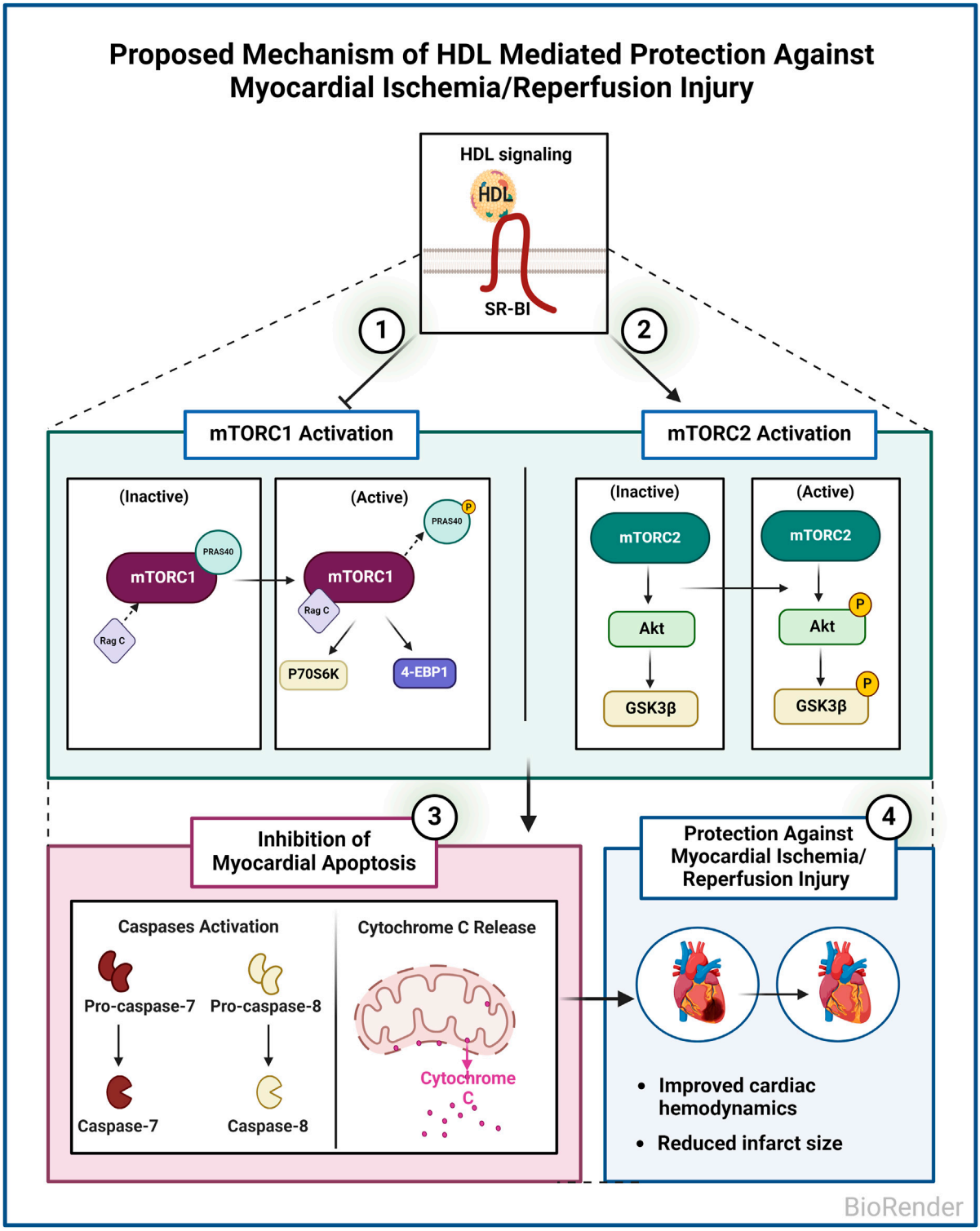

FIGURE 7
Proposed Mechanism of HDL mediated protection against myocardial I/R injury in WKY and SHR. HDL inhibits mTORC1, activates mTORC2, and inhibits myocardial apoptosis in WKY and SHR. HDL-mediated inhibition of myocardial apoptosis could be one mechanism by which HDL protects against I/R injury in normotensive and hypertensive rats.

Akt2 phosphorylation in WKY and SHR (Figure 5C). Furthermore, HDL induced significantly ($P < 0.05$) greater activation of Akt2 in WKY relative to SHR. Treatment with Akt inhibitor abolished total, non-isoform specific, Akt (Figure 5A), Akt1 (Figure 5B), and Akt2 (Figure 5C) phosphorylation in the presence or absence of HDL. Moreover, Akt inhibition reduced the phosphorylation of Akt substrate, PRAS40 (Figure 5D) in WKY and SHR by 100% and 94.3%, respectively. Akt inhibition reduced PRAS40 phosphorylation

by 95.4% and 93.3% in HDL-treated WKY and SHR, respectively (Figure 5D). Together this data suggests that Akt is an essential signaling mediator downstream of HDL that is involved in HDL-mediated cardiac protection. HDL specifically induced Akt2 activation in a magnitude that was proportional to the level of HDL-mediated cardiac protection in normotensive and hypertensive rats. Enhanced HDL-induced activation of Akt2, and enhanced HDL mediated cardiac protection were observed in WKY relative to SHR. Moreover, our data suggest that PRAS40 is a downstream target of Akt in WKY and SHR. HDL appears to phosphorylate PRAS40 through Akt dependent (major) and independent (minor) mechanisms in SHR.

HDL protects against I/R injury by inhibiting myocardial apoptosis

The phosphorylation of Akt inhibits GSK-3β and attenuates myocardial apoptosis (Liu et al., 2020; Huang et al., 2016; Murphy and Steenbergen, 2005). We demonstrate that HDL treatment significantly enhanced GSK-3β phosphorylation (Figure 6A) in SHR with a trend towards an increase in WKY. Furthermore, HDL administration reduced the levels of caspase 7 (Figure 6B) and caspase 8 (Figure 6C) and significantly reduced cytochrome c release (Figure 6D) in heart homogenates from normotensive and hypertensive rats. Together these data suggest that HDL attenuates pathways involved in cardiomyocyte apoptosis. HDL attenuation of cardiomyocyte apoptosis could be one mechanism by which HDL protects against myocardial I/R injury in normotensive and hypertensive rats.

Discussion

In this study, we investigated the involvement of mTORC1 and mTORC2 signaling in HDL-mediated cardiac protection in normotensive and hypertensive rats. We demonstrate that mTORC1 and mTORC2 play opposing roles in mediating myocardial I/R injury. Furthermore, we show that HDL protects against I/R injury in normotensive and hypertensive rats to different extents. HDL inhibits mTORC1 and activates mTORC2 signaling and attenuates myocardial apoptosis following I/R injury (Figure 7).

Mammalian target of rapamycin (mTOR) is present in two complexes, the rapamycin-sensitive mTORC1 and the rapamycin-insensitive mTORC2 (Loewith et al., 2002). mTORC1 regulates protein synthesis, cellular growth, proliferation, ribosomal and mitochondrial biogenesis, autophagy, and metabolism (Johnson et al., 2013; Wullschleger et al., 2006). mTORC1 form a complex with mammalian lethal with SEC13 protein 8 (mLST8), DEP domain-containing mTOR-interacting protein (deptor), PRAS40, tti1/tel2 and regulatory-associated protein of regulatory-associated protein of mammalian target of rapamycin (raptor) (Sciarretta et al., 2014). PRAS40 inhibits complex activity, however, upon phosphorylation it dissociates resulting in the alleviation of the complex (Oshiro et al., 2007; Nascimento and Ouwens, 2009). On the other hand, mTORC1 is activated by Rag GTPases. Rag GTPases form heterodimers whereby Rag A or Rag B interact with Rag C or Rag D (Kim et al., 2008). Active mTORC1 phosphorylates and activates p70S6K which then phosphorylates ribosomal protein S6 and inhibits the binding of 4E-BP1 to eIF4E (Choo et al., 2008; Pullen and Thomas, 1997). mTORC2 however, is composed of the following subunits: SEC13 protein 8, deptor, sin 1, tti1/tel2 and rapamycin-insensitive companion of mTOR (rictor). mTORC2 activates Akt (Sarbassov et al., 2005) and inhibits apoptosis (Filippone et al., 2017). Our data suggests that mTORC1 plays a detrimental role while mTORC2 plays a protective role in mediating myocardial I/R injury in WKY and SHR (Figure 1; Table 2). In addition, hearts from normotensive and hypertensive rats expressed significantly different basal levels of mTORC1 signaling mediators. SHR expressed significantly higher basal levels of phosphorylated-mTOR, phosphorylated-PRAS40, and total-P70S6K, while WKY expressed significantly higher basal levels of phosphorylated-P70S6K (Figure 3). WKY and SHR also expressed significantly different levels of mTORC2 substrates, Akt1 and Akt2. These differences in the basal expression level or activation states of mTORC1 and mTORC2 signaling mediators may suggest differences in the function and/or contribution of these cascades between WKY and SHR which awaits further investigations.

We demonstrate that short-term treatment of HDL protects against myocardial I/R injury in normotensive and hypertensive rats as indicated by improvements in cardiac functions, coronary hemodynamics, and reduction in infarct size (Figure 2; Table 2). Consistent with our previously reported data (Al-Jarallah and Babiker, 2022), HDL was more protective in WKY than it was in SHR (Figure 2; Table 2). The finding that HDL is protective when administered at reperfusion suggests that HDL may represent a promising target for the treatment of ischemic heart disease in normotensive and hypertensive patients. Our findings align with previous reports demonstrating the cardioprotective effects of HDL against ischemic injury (Calabresi et al., 2003; Frias et al., 2013; Gomaraschi et al., 2016). However, the protective mechanisms of HDL against myocardial I/R injury appear to be complex and multifaceted (Durham et al., 2018; Pedretti et al., 2019; White et al., 2016).

We report that HDL inhibited mTORC1 signaling in WKY and SHR (Figure 3). Nonetheless, the mechanism of HDL-mediated inhibition of mTORC1 appears to be different between normotensive and hypertensive rats (Figure 3). In WKY, HDL significantly reduced the level of phospho-P70S6K but did not affect the activation state of mTORC or PRAS40, neither it affected the expression of Rag C. HDL-mediated reduction in P70S6K phosphorylation implicates a reduction in mTORC1 activity in response to HDL, despite of the lack of change in the phosphorylation state of mTORC at Ser2448. HDL treatment in SHR however, reduced the levels of phospho-mTORC, phospho-PRAS40 (inactive inhibitor of mTORC1), and Rag C (mTORC1 activator). To our surprise, HDL did not affect the levels of phospho-P70S6K in hearts from hypertensive rats, possibly suggesting the involvement of other substrates downstream of mTORC1 in response to HDL treatment in these rats. In addition to P70S6K, mTORC1 directly phosphorylates 4E-BP1 (Kazi et al., 2011). HDL treatment increased 4E-BP1 phosphorylation (Figure 3H). Nonetheless, this could be due to mTORC1-indenpendent signaling (Qin et al., 2016). To conclude, in WKY P70S6K appears to be a key downstream substrate of

mTORC1, and HDL inhibited mTORC1 by reducing the levels of phosphorylated P70S6K. In SHR however, P70S6K activation seemed to be less significant, despite the increase in basal total levels of P70S6K. Moreover, the mechanism of HDL-mediated inhibition of mTORC1 in SHR involved modulation of mTORC1 activator (Rag C) and inhibitor (PRAS40) suggesting the existence of different mechanisms by which HDL inhibited mTORC1 in WKY and SHR.

In addition, HDL-mediated cardiac protection involved the activation of mTORC2 signaling as indicated by enhanced phosphorylation of mTORC2 substrate, Akt (Oh and Jacinto, 2011; Jacinto et al., 2006), in normotensive and hypertensive rats (Figure 5). This is consistent with the previously reported effect of reconstituted HDL on the activation of mTORC2 in angiogenic cells (Guo et al., 2011). Furthermore, our data is consistent with HDL-mediated activation of Akt in protecting against oxidative damage induced cardiomyocyte necrosis (Durham et al., 2018). Together this suggests that HDL-mediated inhibition of mTORC1 and activation of mTORC2 signaling could be one mechanism by which HDL protects against I/R injury in WKY and SHR.

We further examined the requirement of Akt in HDL-mediated cardiac protection using Akt antagonist, MK-2206. Treatment with MK-2206 abolished HDL-induced improvements in cardiac functions, coronary vascular dynamics (Figures 4A–D; Table 2), and reduction in infarct size (Figure 4E) in WKY and SHR suggesting the requirement of Akt in HDL-induced cardiac protection.

Three Akt isoforms exist of which, Akt1 and Akt2 are the predominant isoforms expressed in the myocardium (Matsui and Rosenzweig, 2005). The lack of Akt1 on an apolipoprotein E knockout background induced features of plaque vulnerability and cardiac dysfunction (Fernandez-Hernando et al., 2009). Moreover, Akt1 played an essential role in mediating physiological cardiac growth and attenuated pathological cardiac hypertrophy (DeBosch et al., 2006a). Akt2 however, was dispensable in maintaining cardiac phenotype (Cho et al., 2001). Nonetheless, Akt2 regulated cardiac glucose metabolism and survival (DeBosch et al., 2006b).

A considerable amount of interaction between mTORC1 and mTORC2 has been reported. For instance, mTORC1-induced activation of P70S6K suppresses mTORC2 (Fu and Hall, 2020; Harrington et al., 2004). In addition, Akt mediates a positive activation loop between mTORC1 and mTORC2 whereby mTORC2 activates Akt (Abeyrathna and Su, 2015), which then alleviates mTORC1 inhibition by phosphorylating PRAS40 (Wang et al., 2007). Treatment with Akt antagonist, MK-2206, abolished the phosphorylation of total, non-isoform specific, Akt, Akt1, and Akt2 and Akt target, PRAS40 (Figure 5). This is consistent with the finding that phosphorylation of PRAS40 at Thr-246 is mediated by Akt in response to insulin (Kovacina et al., 2003; Nascimento et al., 2010). The presence of Akt independent phosphorylation of PRAS40 has also been reported (Lv et al., 2017; Sanchez Canedo et al., 2010). The finding that MK-2206 treatment blocked the cardioprotective effect of HDL and completely abolished Akt phosphorylation in HDL-treated WKY and SHR indicates the requirement of Akt in HDL-mediated cardiac protection. In addition, the reduction in PRAS40 phosphorylation in the presence of Akt antagonist indicates that PRAS40 is a downstream target of Akt. The presence of residual 5.7% phosphorylated PRAS40 in the presence of MK-2206 suggests the presence of, a minor, Akt-independent phosphorylation of PRAS40 in SHR (Figure 5D).

Interestingly, our data indicate that HDL activates Akt2 but not Akt1 in WKY and SHR (Figures 5B,C). Moreover, the magnitude of HDL-induced activation of Akt2 was consistent with the magnitude of HDL-mediated cardiac protection against I/R injury in WKY and SHR. HDL was more potent in activating Akt2 in WKY and resulted in greater protection from I/R injury in these rats. HDL treatment, however, did not affect PRAS40 phosphorylation in hearts from normotensive rats. The finding that HDL specifically activated Akt2 isoform yet did not induce PRAS40 phosphorylation, could possibly suggest that PRAS40 phosphorylation is likely to be mediated by Akt1 or Akt3 isoforms in WKY. In line with this observation, the lack of Akt2 did not affect the phosphorylation state of PRAS40 (Lv et al., 2017). Moreover, slicing Akt3 but not Akt1 or Akt2 blocked PRAS40 phosphorylation (Sun et al., 2020), indicating the involvement of Akt3 in PPRAS40 phosphorylation. In addition, the role of Akt3 in mediating PRAS40 phosphorylation was reported in malignant melanoma (Madhunapantula et al., 2007). A lack of HDL-induced activation of Akt1 (our data), or possibly Akt3 (remains to be tested), may therefore explain the lack of HDL-induced PRAS40 phosphorylation in WKY. The finding that HDL activated Akt2 isoform and reduced the phosphorylation of PRAS40 in hearts from SHR further supports the notion that Akt2 isoform does not play a significant role in the phosphorylation of PRAS40. HDL-mediated reduction in PRAS40 phosphorylation in SHR could alternatively be due to HDL-induced activation of phospho-protein phosphatases. Perturbation of plasma membrane cholesterol has been shown to regulate the activity of PP2A/HePTP phosphatase complex (Wang et al., 2003). PRAS40 activity is regulated by phospho-protein phosphatases including PTEN and MAPK-phosphatase-7 (MKP7) (Du et al., 2014; Wang et al., 2020). Thus, it's plausible to speculate that HDL-mediated cholesterol efflux (Rosenson et al., 2012) may enhance the activity of these phosphatases resulting in reduced PRAS40 phosphorylation. These possibilities, however, remain to be directly tested. To conclude, Akt plays a non-dispensable role in mediating the phosphorylation of PRAS40 in WKY and SHR. HDL appears to differentially regulate PRAS40 in WKY and SHR. In WKY HDL did not affect PRAS40 phosphorylation, in SHR however, HDL attenuated PRAS40 phosphorylation. HDL-mediated reduction in PRAS40 phosphorylation in SHR indicates the enhanced association of un-phosphorylated PRAS40 (active inhibitor) with mTORC1 and subsequent complex inhibition which could possibly be required to suppress the enhanced mTORC1 activity in SHR (Figures 3C, 5D). It has been reported that mTORC1 phosphorylates PRAS40 at Ser-183, Ser-212, and Ser-221 and alleviates PRAS40 induced substrate competition (Wang et al., 2008). The effect of HDL on PRAS40 phosphorylation on other sites remains however to be investigated. The finding that HDL specifically activated Akt2 suggests a novel role of Akt2 in HDL-mediated cardiac protection in normotensive and hypertensive rats. In contrast however, HDL mediated activation of Akt1 and Akt2 has been implicated in HDL-

mediated protection against doxorubicin induced apoptosis (Durham et al., 2018). The lack of involvement of Akt1 in HDL-mediated protection against I/R injury could be due to species (WKY and SHR vs C57BL6 mice), model (*ex-vivo* vs *in vitro*), or pathway (I/R injury vs doxorubicin induced apoptosis) related differences. Apoptosis can be initiated through the extrinsic pathway that involves caspase 8, initiator caspase, (Tummers and Green, 2017), or via the intrinsic mitochondrial pathway, which involves mPTP opening, cytochrome c release, and caspase 7, executioner caspase, activation (Lakhani et al., 2006; Riedl and Salvesen, 2007). Akt phosphorylates and inactivates mediators of cellular apoptosis including inhibits mPTP opening, cytochrome c release, and activation of caspases (Tsang et al., 2004). HDL inactivated GSK and reduced cytochrome c release, caspases 7 and 8 activation (Figure 6).

Our data are consistent with the previously reported data on the anti-apoptotic effects of HDL (Frias et al., 2013; White et al., 2016). In addition to its anti-apoptotic effects, HDL could protect against I/R injury by virtue of its antioxidant (Calabresi et al., 2003; Fogelman et al., 2013; Mineo et al., 2006) and anti-inflammatory (Al-Jarallah and Babiker, 2022; Barter et al., 2004; Gomaraschi et al., 2008) effects. The cardioprotective anti-inflammatory, and antioxidant effects of HDL were not investigated in this study, nonetheless, they cannot be excluded.

To our knowledge, this is the first study to demonstrate the role of HDL in regulating mTORC1 and mTORC2 signaling in protecting against myocardial I/R injury in normotensive and hypertensive rats. HDL inhibited mTORC1 in normotensive and hypertensive rats yet, via different mechanisms. HDL activated mTORC2, indicated by increased Akt2 phosphorylation in WKY and SHR. HDL-mediated inhibition of mTORC1, activation of mTORC2, and inhibition of myocardial apoptosis could explain HDL-mediated cardiac protection from I/R injury in normotensive and hypertensive rats.

Our study, however, has some limitations including the rat's age, gender, and dosage of HDL treatment used. Additional studies in female rats are required to demonstrate if HDL is equally protective in both genders. It also will be interesting to test if HDL can protect hearts from older rats, with marked hypertension-induced deterioration in cardiac functions from I/R injury or if different concentrations and/or routes of HDL administration protect to different extents.

Data availability statement

The original contributions presented in the study are included in the article/Supplementary Material, further inquiries can be directed to the corresponding author.

Ethics statement

The animal study was approved by Health Sciences Research Ethics Committee, Health Sciences Center, Kuwait University. ID3640. The study was conducted in accordance with the local legislation and institutional requirements.

Author contributions

RA-O: Conceptualization, Formal Analysis, Investigation, Writing–original draft. AA-J: Conceptualization, Data curation, Funding acquisition, Investigation, Methodology, Project administration, Resources, Software, Supervision, Validation, Visualization, Writing–review and editing. FB: Conceptualization, Investigation, Methodology, Software, Supervision, Validation, Writing–review and editing.

Funding

The author(s) declare that financial support was received for the research, authorship, and/or publication of this article. We would like to acknowledge the Research Sector (Grant No. YM04/18) and the School of Graduate Studies at Kuwait University, for funding the project.

Acknowledgments

We acknowledge the technical support of Mona Rostum, Godwin Budadasari, Lilly Verges, and Anju Devassy.

Conflict of interest

The authors declare that the research was conducted in the absence of any commercial or financial relationships that could be construed as a potential conflict of interest.

Publisher's note

Supplementary material

The Supplementary Material for this article can be found online at: https://www.frontiersin.org/articles/10.3389/fphar.2024.1398630/full#supplementary-material

SUPPLEMENTARY FIGURE 1
Hearts were isolated and divided into four groups (n=4-9 rat/group from each genotype). Group-A (untreated controls) was subjected to 30 min of ischemia followed by 30 min of reperfusion. Group-B (antagonist) was infused 5 min before reperfusion and continued for an additional 10 min of reperfusion. In group-C (HDL) was subjected to 30 min of ischemia in which HDL was added 5 min before the beginning of reperfusion. HDL administration was continued during the first 10 min of reperfusion. In Group-D (antagonist + HDL) hearts were subjected to ischemia in the presence of MK-2206 (5 μM) infused at 20 min of ischemia followed by the addition of HDL (400 μg) 5 min before reperfusion. HDL and antagonist administration continued during the first 10 min of reperfusion.

References

Abeyrathna, P., and Su, Y. (2015). The critical role of Akt in cardiovascular function. *Vasc. Pharmacol.* 74, 38–48. PubMed PMID: 26025205; PubMed Central PMCID: PMCPMC4659756. doi:10.1016/j.vph.2015.05.008

Akhtar, N., and Jabeen, I. (2018). Pharmacoinformatic approaches to design novel inhibitors of protein kinase B pathways in cancer. *Curr. Cancer Drug Targets* 18 (9), 830–846. doi:10.2174/1568009617666170623104540

Al-Jarallah, A., and Babiker, F. (2022). High density lipoprotein reduces blood pressure and protects spontaneously hypertensive rats against myocardial ischemia-reperfusion injury in an SR-BI dependent manner. *Front. Cardiovasc Med.* 9, 825310. PubMed PMID: 35387446; PubMed Central PMCID: PMCPMC8977778. doi:10.3389/fcvm.2022.825310

Al-Jarallah, A., and Babiker, F. A. (2024). High-density lipoprotein signaling via sphingosine-1-phosphate receptors safeguards spontaneously hypertensive rats against myocardial ischemia/reperfusion injury. *Pharmaceutics* 16 (4), 497. PubMed PMID: 38675158; PubMed Central PMCID: PMCPMC11054943. doi:10.3390/pharmaceutics16040497

Babiker, F., Al-Jarallah, A., and Al-Awadi, M. (2019). Effects of cardiac hypertrophy, diabetes, aging, and pregnancy on the cardioprotective effects of postconditioning in male and female rats. *Cardiol. Res. Pract.* 2019, 3403959. PubMed PMID: 31198607; PubMed Central PMCID: PMCPMC6526533. doi:10.1155/2019/3403959

Barter, P. J., Nicholls, S., Rye, K. A., Anantharamaiah, G. M., Navab, M., and Fogelman, A. M. (2004). Antiinflammatory properties of HDL. *Circ. Res.* 95 (8), 764–772. PubMed PMID: 15486323. doi:10.1161/01.RES.0000146094.59640.13

Benavides-Serrato, A., Lee, J., Holmes, B., Landon, K. A., Bashir, T., Jung, M. E., et al. (2017). Specific blockade of Rictor-mTOR association inhibits mTORC2 activity and is cytotoxic in glioblastoma. *PLoS One* 12 (4), e0176599. PubMed PMID: 28453552; PubMed Central PMCID: PMCPMC5409528. doi:10.1371/journal.pone.0176599

Calabresi, L., Rossoni, G., Gomaraschi, M., Sisto, F., Berti, F., and Franceschini, G. (2003). High-density lipoproteins protect isolated rat hearts from ischemia-reperfusion injury by reducing cardiac tumor necrosis factor-alpha content and enhancing prostaglandin release. *Circ. Res.* 92 (3), 330–337. PubMed PMID: 12595346. doi:10.1161/01.res.0000054201.60308.1a

Chen, X., Cui, D., Bi, Y., Shu, J., Xiong, X., and Zhao, Y. (2018). AKT inhibitor MK-2206 sensitizes breast cancer cells to MLN4924, a first-in-class NEDD8-activating enzyme (NAE) inhibitor. *Cell Cycle* 17 (16), 2069–2079. PubMed PMID: 30198810; PubMed Central PMCID: PMCPMC6224269. doi:10.1080/15384101.2018.1515550

Cho, H., Mu, J., Kim, J. K., Thorvaldsen, J. L., Chu, Q., Crenshaw, E. B., 3rd, et al. (2001). Insulin resistance and a diabetes mellitus-like syndrome in mice lacking the protein kinase Akt2 (PKB beta). *Science* 292 (5522), 1728–1731. PubMed PMID: 11387480. doi:10.1126/science.292.5522.1728

Choo, A. Y., Yoon, S. O., Kim, S. G., Roux, P. P., and Blenis, J. (2008). Rapamycin differentially inhibits S6Ks and 4E-BP1 to mediate cell-type-specific repression of mRNA translation. *Proc. Natl. Acad. Sci. U. S. A.* 105 (45), 17414–17419. PubMed PMID: 18955708; PubMed Central PMCID: PMCPMC2582304. doi:10.1073/pnas.0809136105

Copp, J., Manning, G., and Hunter, T. (2009). TORC-specific phosphorylation of mammalian target of rapamycin (mTOR): phospho-Ser2481 is a marker for intact mTOR signaling complex 2. *Cancer Res.* 69 (5), 1821–1827. PubMed PMID: 19244117; PubMed Central PMCID: PMCPMC2652681. doi:10.1158/0008-5472.CAN-08-3014

Das, A., Salloum, F. N., Filippone, S. M., Durrant, D. E., Rokosh, G., Bolli, R., et al. (2015). Inhibition of mammalian target of rapamycin protects against reperfusion injury in diabetic heart through STAT3 signaling. *Basic Res. Cardiol.* 110 (3), 31. PubMed PMID: 25911189; PubMed Central PMCID: PMCPMC8554777. doi:10.1007/s00395-015-0486-5

DeBosch, B., Sambandam, N., Weinheimer, C., Courtois, M., and Muslin, A. J. (2006b). Akt2 regulates cardiac metabolism and cardiomyocyte survival. *J. Biol. Chem.* 281 (43), 32841–32851. PubMed PMID: 16950770; PubMed Central PMCID: PMCPMC2724003. doi:10.1074/jbc.M513087200

DeBosch, B., Treskov, I., Lupu, T. S., Weinheimer, C., Kovacs, A., Courtois, M., et al. (2006a). Akt1 is required for physiological cardiac growth. *Circulation* 113 (17), 2097–2104. PubMed PMID: 16636172. doi:10.1161/CIRCULATIONAHA.105.595231

Dodd, M. S., Ball, D. R., Schroeder, M. A., Le Page, L. M., Atherton, H. J., Heather, L. C., et al. (2012). *In vivo* alterations in cardiac metabolism and function in the spontaneously hypertensive rat heart. *Cardiovasc Res.* 95 (1), 69–76. PubMed PMID: 22593200; PubMed Central PMCID: PMCPMC4617603. doi:10.1093/cvr/cvs164

Du, W. W., Yang, W., Fang, L., Xuan, J., Li, H., Khorshidi, A., et al. (2014). miR-17 extends mouse lifespan by inhibiting senescence signaling mediated by MKP7. *Cell Death Dis.* 5, e1355. PubMed PMID: 25077541; PubMed Central PMCID: PMCPMC4123096. doi:10.1038/cddis.2014.305

Durham, K. K., Chathely, K. M., and Trigatti, B. L. (2018). High-density lipoprotein protects cardiomyocytes against necrosis induced by oxygen and glucose deprivation through SR-B1, PI3K, and AKT1 and 2. *Biochem. J.* 475 (7), 1253–1265. PubMed PMID: 29523748; PubMed Central PMCID: PMCPMC5887020. doi:10.1042/BCJ20170703

Fernandez-Hernando, C., Jozsef, L., Jenkins, D., Di Lorenzo, A., and Sessa, W. C. (2009). Absence of Akt1 reduces vascular smooth muscle cell migration and survival and induces features of plaque vulnerability and cardiac dysfunction during atherosclerosis. *Arterioscler. Thromb. Vasc. Biol.* 29 (12), 2033–2040. PubMed PMID: 19762778; PubMed Central PMCID: PMCPMC2796372. doi:10.1161/ATVBAHA.109.196394

Filippone, S. M., Samidurai, A., Roh, S. K., Cain, C. K., He, J., Salloum, F. N., et al. (2017). Reperfusion therapy with rapamycin attenuates myocardial infarction through activation of AKT and ERK. *Oxid. Med. Cell Longev.* 2017, 4619720. PubMed PMID: 28373901; PubMed Central PMCID: PMCPMC5360974 conflict of interests. doi:10.1155/2017/4619720

Fogelman, A. M., Reddy, S. T., and Navab, M. (2013). Protection against ischemia/reperfusion injury by high-density lipoprotein and its components. *Circ. Res.* 113 (12), 1281–1282. PubMed PMID: 24311615. doi:10.1161/CIRCRESAHA.113.302943

Frias, M. A., Pedretti, S., Hacking, D., Somers, S., Lacerda, L., Opie, L. H., et al. (2013). HDL protects against ischemia reperfusion injury by preserving mitochondrial integrity. *Atherosclerosis* 228 (1), 110–116. PubMed PMID: 23497785. doi:10.1016/j.atherosclerosis.2013.02.003

Fu, W., and Hall, M. N. (2020). Regulation of mTORC2 signaling. *Genes (Basel)* 11 (9), 1045. PubMed PMID: 32899613; PubMed Central PMCID: PMCPMC7564249. doi:10.3390/genes11091045

Gallo, G., Volpe, M., and Savoia, C. (2021). Endothelial dysfunction in hypertension: current concepts and clinical implications. *Front. Med. (Lausanne)* 8, 798958. PubMed PMID: 35127755; PubMed Central PMCID: PMCPMC8811286. doi:10.3389/fmed.2021.798958

Gomaraschi, M., Calabresi, L., and Franceschini, G. (2016). Protective effects of HDL against ischemia/reperfusion injury. *Front. Pharmacol.* 7, 2. PubMed PMID: 26834639; PubMed Central PMCID: PMCPMC4725188. doi:10.3389/fphar.2016.00002

Gomaraschi, M., Calabresi, L., Rossoni, G., Iametti, S., Franceschini, G., Stonik, J. A., et al. (2008). Anti-inflammatory and cardioprotective activities of synthetic high-density lipoprotein containing apolipoprotein A-I mimetic peptides. *J. Pharmacol. Exp. Ther.* 324 (2), 776–783. PubMed PMID: 18042829. doi:10.1124/jpet.107.129411

Guenzle, J., Akasaka, H., Joechle, K., Reichardt, W., Venkatasamy, A., Hoeppner, J., et al. (2020). Pharmacological inhibition of mTORC2 reduces migration and metastasis in melanoma. *Int. J. Mol. Sci.* 22 (1), 30. PubMed PMID: 33375117; PubMed Central PMCID: PMCPMC7792954. doi:10.3390/ijms22010030

Guo, X., Yu, M., Kang, X., and Yin, H. (2011). mTOR complex 2 activation by reconstituted high-density lipoprotein prevents senescence in circulating angiogenic cells. *Arterioscler. Thromb. Vasc. Biol.* 31 (6), 1421–1429. PubMed PMID: 21415389. doi:10.1161/ATVBAHA.111.224089

Harrington, L. S., Findlay, G. M., Gray, A., Tolkacheva, T., Wigfield, S., Rebholz, H., et al. (2004). The TSC1-2 tumor suppressor controls insulin-PI3K signaling via regulation of IRS proteins. *J. Cell Biol.* 166 (2), 213–223. PubMed PMID: 15249583; PubMed Central PMCID: PMCPMC2172316. doi:10.1083/jcb.200403069

Huang, X., Zuo, L., Lv, Y., Chen, C., Yang, Y., Xin, H., et al. (2016). Asiatic acid attenuates myocardial ischemia/reperfusion injury via akt/GSK-3β/HIF-1α signaling in rat H9c2 cardiomyocytes. *Molecules* 21 (9), 1248. doi:10.3390/molecules21091248

Jacinto, E., Facchinetti, V., Liu, D., Soto, N., Wei, S., Jung, S. Y., et al. (2006). SIN1/MIP1 maintains rictor-mTOR complex integrity and regulates Akt phosphorylation and substrate specificity. *Cell* 127 (1), 125–137. PubMed PMID: 16962653. doi:10.1016/j.cell.2006.08.033

Jama, H. A., Muralitharan, R. R., Xu, C., O'Donnell, J. A., Bertagnolli, M., Broughton, B. R. S., et al. (2022). Rodent models of hypertension. *Br. J. Pharmacol.* 179 (5), 918–937. PubMed PMID: 34363610. doi:10.1111/bph.15650

Johnson, S. C., Rabinovitch, P. S., and Kaeberlein, M. (2013). mTOR is a key modulator of ageing and age-related disease. *Nature* 493 (7432), 338–345. PubMed PMID: 23325216; PubMed Central PMCID: PMCPMC3687363. doi:10.1038/nature11861

Juggi, J. S., Hoteit, L. J., Babiker, F. A., Joseph, S., and Mustafa, A. S. (2011). Protective role of normothermic, hyperthermic and estrogen preconditioning and pretreatment on tumour necrosis factor-alpha-induced damage. *Exp. Clin. Cardiol.* 16 (2), e5–e10. Epub 2011/07/13. PubMed PMID: 21747660; PubMed Central PMCID: PMCPMC3126688.

Kazi, A. A., Pruznak, A. M., Frost, R. A., and Lang, C. H. (2011). Sepsis-induced alterations in protein-protein interactions within mTOR complex 1 and the modulating effect of leucine on muscle protein synthesis. *Shock* 35 (2), 117–125. PubMed PMID: 20577146; PubMed Central PMCID: PMCPMC2995824. doi:10.1097/SHK.0b013e3181ecb57c

Khan, M. A., Hashim, M. J., Mustafa, H., Baniyas, M. Y., Al Suwaidi, S., AlKatheeri, R., et al. (2020). Global epidemiology of ischemic heart disease: results from the global burden of disease study. *Cureus* 12 (7), e9349. PubMed PMID: 32742886; PubMed Central PMCID: PMCPMC7384703. doi:10.7759/cureus.9349

Kim, E., Goraksha-Hicks, P., Li, L., Neufeld, T. P., and Guan, K. L. (2008). Regulation of TORC1 by Rag GTPases in nutrient response. *Nat. Cell Biol.* 10 (8), 935–945.

PubMed PMID: 18604198; PubMed Central PMCID: PMCPMC2711503. doi:10.1038/ncb1753

Kovacina, K. S., Park, G. Y., Bae, S. S., Guzzetta, A. W., Schaefer, E., Birnbaum, M. J., et al. (2003). Identification of a proline-rich Akt substrate as a 14-3-3 binding partner. *J. Biol. Chem.* 278 (12), 10189–10194. PubMed PMID: 12524439. doi:10.1074/jbc.M210837200

Kumar, C. C., and Madison, V. (2005). AKT crystal structure and AKT-specific inhibitors. *Oncogene* 24 (50), 7493–7501. PubMed PMID: 16288296. doi:10.1038/sj.onc.1209087

Kumar, V., Wollner, C., Kurth, T., Bukowy, J. D., and Cowley, A. W., Jr (2017). Inhibition of mammalian target of rapamycin complex 1 attenuates salt-induced hypertension and kidney injury in Dahl salt-sensitive rats. *Hypertension* 70 (4), 813–821. PubMed PMID: 28827472; PubMed Central PMCID: PMCPMC5599353. doi:10.1161/HYPERTENSIONAHA.117.09456

Lakhani, S. A., Masud, A., Kuida, K., Porter, G. A., Jr., Booth, C. J., Mehal, W. Z., et al. (2006). Caspases 3 and 7: key mediators of mitochondrial events of apoptosis. *Science* 311 (5762), 847–851. PubMed PMID: 16469926; PubMed Central PMCID: PMCPMC3738210. doi:10.1126/science.1115035

Laplante, M., and Sabatini, D. M. (2012). mTOR signaling in growth control and disease. *Cell* 149 (2), 274–293. PubMed PMID: 22500797; PubMed Central PMCID: PMCPMC3331679. doi:10.1016/j.cell.2012.03.017

Li, J. J., and Chen, J. L. (2005). Inflammation may be a bridge connecting hypertension and atherosclerosis. *Med. Hypotheses* 64 (5), 925–929. PubMed PMID: 15780486. doi:10.1016/j.mehy.2004.10.016

Liu, M., Huang, X., Tian, Y., Yan, X., Wang, F., Chen, J., et al. (2020). Phosphorylated GSK-3β protects stress-induced apoptosis of myoblasts via the PI3K/Akt signaling pathway. *Mol. Med. Rep.* 22 (1), 317–327. PubMed PMID: 32377749; PubMed Central PMCID: PMCPMC7248528. doi:10.3892/mmr.2020.11105

Loewith, R., Jacinto, E., Wullschleger, S., Lorberg, A., Crespo, J. L., Bonenfant, D., et al. (2002). Two TOR complexes, only one of which is rapamycin sensitive, have distinct roles in cell growth control. *Mol. Cell* 10 (3), 457–468. PubMed PMID: 12408816. doi:10.1016/s1097-2765(02)00636-6

Lv, D., Guo, L., Zhang, T., and Huang, L. (2017). PRAS40 signaling in tumor. *Oncotarget* 8 (40), 69076–69085. PubMed PMID: 28978182; PubMed Central PMCID: PMCPMC5620322. doi:10.18632/oncotarget.17299

Madhunapantula, S. V., Sharma, A., and Robertson, G. P. (2007). PRAS40 deregulates apoptosis in malignant melanoma. *Cancer Res.* 67 (8), 3626–3636. PubMed PMID: 17440074. doi:10.1158/0008-5472.CAN-06-4234

Matsui, T., and Rosenzweig, A. (2005). Convergent signal transduction pathways controlling cardiomyocyte survival and function: the role of PI 3-kinase and Akt. *J. Mol. Cell Cardiol.* 38 (1), 63–71. PubMed PMID: 15623422. doi:10.1016/j.yjmcc.2004.11.005

Mineo, C., Deguchi, H., Griffin, J. H., and Shaul, P. W. (2006). Endothelial and antithrombotic actions of HDL. *Circ. Res.* 98 (11), 1352–1364. PubMed PMID: 16763172. doi:10.1161/01.RES.0000225982.01988.93

Murphy, E., and Steenbergen, C. (2005). Inhibition of GSK-3beta as a target for cardioprotection: the importance of timing, location, duration and degree of inhibition. *Expert Opin. Ther. Targets* 9 (3), 447–456. PubMed PMID: 15948666. doi:10.1517/14728222.9.3.447

Muslin, A. J. (2011). Akt2: a critical regulator of cardiomyocyte survival and metabolism. *Pediatr. Cardiol.* 32 (3), 317–322. PubMed PMID: 21279637. doi:10.1007/s00246-010-9879-2

Nagao, M., Toh, R., Irino, Y., Nakajima, H., Oshita, T., Tsuda, S., et al. (2017). High-density lipoprotein protects cardiomyocytes from oxidative stress via the PI3K/mTOR signaling pathway. *FEBS Open Bio* 7 (9), 1402–1409. PubMed PMID: 28904868; PubMed Central PMCID: PMCPMC5586351. doi:10.1002/2211-5463.12279

Nascimento, E. B., and Ouwens, D. M. (2009). PRAS40: target or modulator of mTORC1 signalling and insulin action? *Arch. Physiol. Biochem.* 115 (4), 163–175. PubMed PMID: 19480563. doi:10.1080/13813450902988580

Nascimento, E. B., Snel, M., Guigas, B., van der Zon, G. C., Kriek, J., Maassen, J. A., et al. (2010). Phosphorylation of PRAS40 on Thr246 by PKB/AKT facilitates efficient phosphorylation of Ser183 by mTORC1. *Cell Signal* 22 (6), 961–967. PubMed PMID: 20138985. doi:10.1016/j.cellsig.2010.02.002

Oei, G. T., Huhn, R., Heinen, A., Hollmann, M. W., Schlack, W. S., Preckel, B., et al. (2012). Helium-induced cardioprotection of healthy and hypertensive rat myocardium *in vivo*. *Eur. J. Pharmacol.* 684 (1-3), 125–131. PubMed PMID: 22497999. doi:10.1016/j.ejphar.2012.03.045

Oh, W. J., and Jacinto, E. (2011). mTOR complex 2 signaling and functions. *Cell Cycle* 10 (14), 2305–2316. PubMed PMID: 21670596; PubMed Central PMCID: PMCPMC3322468. doi:10.4161/cc.10.14.16586

Oshiro, N., Takahashi, R., Yoshino, K., Tanimura, K., Nakashima, A., Eguchi, S., et al. (2007). The proline-rich Akt substrate of 40 kDa (PRAS40) is a physiological substrate of mammalian target of rapamycin complex 1. *J. Biol. Chem.* 282 (28), 20329–20339. PubMed PMID: 17517883; PubMed Central PMCID: PMCPMC3199301. doi:10.1074/jbc.M702636200

Pedretti, S., Brulhart-Meynet, M. C., Montecucco, F., Lecour, S., James, R. W., and Frias, M. A. (2019). HDL protects against myocardial ischemia reperfusion injury via miR-34b and miR-337 expression which requires STAT3. *PLoS One* 14 (6), e0218432. PubMed PMID: 31220137; PubMed Central PMCID: PMCPMC6586303. doi:10.1371/journal.pone.0218432

Penna, C., Tullio, F., Moro, F., Folino, A., Merlino, A., and Pagliaro, P. (2010). Effects of a protocol of ischemic postconditioning and/or captopril in hearts of normotensive and hypertensive rats. *Basic Res. Cardiol.* 105 (2), 181–192. PubMed PMID: 20012872. doi:10.1007/s00395-009-0075-6

Pullen, N., and Thomas, G. (1997). The modular phosphorylation and activation of p70s6k. *FEBS Lett.* 410 (1), 78–82. PubMed PMID: 9247127. doi:10.1016/s0014-5793(97)00323-2

Qin, X., Jiang, B., and Zhang, Y. (2016). 4E-BP1, a multifactor regulated multifunctional protein. *Cell Cycle* 15 (6), 781–786. PubMed PMID: 26901143; PubMed Central PMCID: PMCPMC4845917. doi:10.1080/15384101.2016.1151581

Riedl, S. J., and Salvesen, G. S. (2007). The apoptosome: signalling platform of cell death. *Nat. Rev. Mol. Cell Biol.* 8 (5), 405–413. PubMed PMID: 17377525. doi:10.1038/nrm2153

Rosenson, R. S., Brewer, H. B., Jr., Davidson, W. S., Fayad, Z. A., Fuster, V., Goldstein, J., et al. (2012). Cholesterol efflux and atheroprotection: advancing the concept of reverse cholesterol transport. *Circulation* 125 (15), 1905–1919. PubMed PMID: 22508840; PubMed Central PMCID: PMCPMC4159082. doi:10.1161/CIRCULATIONAHA.111.066589

Ruilope, L. M., and Schmieder, R. E. (2008). Left ventricular hypertrophy and clinical outcomes in hypertensive patients. *Am. J. Hypertens.* 21 (5), 500–508. PubMed PMID: 18437140. doi:10.1038/ajh.2008.16

Samidurai, A., Ockaili, R., Cain, C., Roh, S. K., Filippone, S. M., Kraskauskas, D., et al. (2020). Differential regulation of mTOR complexes with miR-302a attenuates myocardial reperfusion injury in diabetes. *iScience* 23 (12), 101863. PubMed PMID: 33319180; PubMed Central PMCID: PMCPMC7725936. doi:10.1016/j.isci.2020.101863

Sancak, Y., Thoreen, C. C., Peterson, T. R., Lindquist, R. A., Kang, S. A., Spooner, E., et al. (2007). PRAS40 is an insulin-regulated inhibitor of the mTORC1 protein kinase. *Mol. Cell* 25 (6), 903–915. PubMed PMID: 17386266. doi:10.1016/j.molcel.2007.03.003

Sanchez Canedo, C., Demeulder, B., Ginion, A., Bayascas, J. R., Balligand, J. L., Alessi, D. R., et al. (2010). Activation of the cardiac mTOR/p70(S6K) pathway by leucine requires PDK1 and correlates with PRAS40 phosphorylation. *Am. J. Physiol. Endocrinol. Metab.* 298 (4), E761–E769. PubMed PMID: 20051528. doi:10.1152/ajpendo.00421.2009

Sarbassov, D. D., Guertin, D. A., Ali, S. M., and Sabatini, D. M. (2005). Phosphorylation and regulation of Akt/PKB by the rictor-mTOR complex. *Science* 307 (5712), 1098–1101. PubMed PMID: 15718470. doi:10.1126/science.1106148

Sciarretta, S., Volpe, M., and Sadoshima, J. (2014). Mammalian target of rapamycin signaling in cardiac physiology and disease. *Circ. Res.* 114 (3), 549–564. PubMed PMID: 24481845; PubMed Central PMCID: PMCPMC3995130. doi:10.1161/CIRCRESAHA.114.302022

Sun, D., Luo, T., Dong, P., Zhang, N., Chen, J., Zhang, S., et al. (2020). M2-polarized tumor-associated macrophages promote epithelial-mesenchymal transition via activation of the AKT3/PRAS40 signaling pathway in intrahepatic cholangiocarcinoma. *J. Cell Biochem.* 121 (4), 2828–2838. PubMed PMID: 31692069. doi:10.1002/jcb.29514

Tsang, A., Hausenloy, D. J., Mocanu, M. M., and Yellon, D. M. (2004). Postconditioning: a form of "modified reperfusion" protects the myocardium by activating the phosphatidylinositol 3-kinase-Akt pathway. *Circ. Res.* 95 (3), 230–232. PubMed PMID: 15242972. doi:10.1161/01.RES.0000138303.76488.fe

Tummers, B., and Green, D. R. (2017). Caspase-8: regulating life and death. *Immunol. Rev.* 277 (1), 76–89. PubMed PMID: 28462525; PubMed Central PMCID: PMCPMC5417704. doi:10.1111/imr.12541

Wagner, C., Ebner, B., Tillack, D., Strasser, R. H., and Weinbrenner, C. (2013). Cardioprotection by ischemic postconditioning is abrogated in hypertrophied myocardium of spontaneously hypertensive rats. *J. Cardiovasc Pharmacol.* 61 (1), 35–41. PubMed PMID: 23052031. doi:10.1097/FJC.0b013e3182760c4d

Wang, L., Harris, T. E., and Lawrence, J. C., Jr (2008). Regulation of proline-rich Akt substrate of 40 kDa (PRAS40) function by mammalian target of rapamycin complex 1 (mTORC1)-mediated phosphorylation. *J. Biol. Chem.* 283 (23), 15619–15627. PubMed PMID: 18372248; PubMed Central PMCID: PMCPMC2414301. doi:10.1074/jbc.M800723200

Wang, L., Harris, T. E., Roth, R. A., and Lawrence, J. C., Jr (2007). PRAS40 regulates mTORC1 kinase activity by functioning as a direct inhibitor of substrate binding. *J. Biol. Chem.* 282 (27), 20036–20044. PubMed PMID: 17510057. doi:10.1074/jbc.M702376200

Wang, P. Y., Liu, P., Weng, J., Sontag, E., and Anderson, R. G. (2003). A cholesterol-regulated PP2A/HePTP complex with dual specificity ERK1/2 phosphatase activity. *EMBO J.* 22 (11), 2658–2667. PubMed PMID: 12773382; PubMed Central PMCID: PMCPMC156752. doi:10.1093/emboj/cdg255

Wang, W., Wang, X., Guo, H., Cai, Y., Zhang, Y., and Li, H. (2020). PTEN inhibitor VO-OHpic suppresses TSC2(-) (/) (-) MEFs proliferation by excessively inhibiting autophagy via the PTEN/PRAS40 pathway. *Exp. Ther. Med.* 19 (6), 3565–3570. PubMed PMID: 32346419; PubMed Central PMCID: PMCPMC7185083. doi:10.3892/etm.2020.8629

White, C. R., Giordano, S., and Anantharamaiah, G. M. (2016). High-density lipoprotein, mitochondrial dysfunction and cell survival mechanisms. *Chem. Phys.*

Lipids 199, 161–169. PubMed PMID: 27150975; PubMed Central PMCID: PMCPMC4972637. doi:10.1016/j.chemphyslip.2016.04.007

Wullschleger, S., Loewith, R., and Hall, M. N. (2006). TOR signaling in growth and metabolism. *Cell* 124 (3), 471–484. PubMed PMID: 16469695. doi:10.1016/j.cell.2006.01.016

Yano, T., Ferlito, M., Aponte, A., Kuno, A., Miura, T., Murphy, E., et al. (2014). Pivotal role of mTORC2 and involvement of ribosomal protein S6 in cardioprotective signaling. *Circ. Res.* 114 (8), 1268–1280. PubMed PMID: 24557881; PubMed Central PMCID: PMCPMC4006628. doi:10.1161/CIRCRESAHA.114.303562

Yano, T., Miki, T., Tanno, M., Kuno, A., Itoh, T., Takada, A., et al. (2011). Hypertensive hypertrophied myocardium is vulnerable to infarction and refractory to erythropoietin-induced protection. *Hypertension* 57 (1), 110–115. PubMed PMID: 21060000. doi:10.1161/hypertensionaha.110.158469

Yildiz, M., Oktay, A. A., Stewart, M. H., Milani, R. V., Ventura, H. O., and Lavie, C. J. (2020). Left ventricular hypertrophy and hypertension. *Prog. Cardiovasc Dis.* 63 (1), 10–21. PubMed PMID: 31759953. doi:10.1016/j.pcad.2019.11.009

Yu, H., Littlewood, T., and Bennett, M. (2015). Akt isoforms in vascular disease. *Vasc. Pharmacol.* 71, 57–64. PubMed PMID: 25929188; PubMed Central PMCID: PMCPMC4728195. doi:10.1016/j.vph.2015.03.003

Zhou, X., and Frohlich, E. D. (2007). Analogy of cardiac and renal complications in essential hypertension and aged SHR or L-NAME/SHR. *Med. Chem.* 3 (1), 61–65. PubMed PMID: 17266625. doi:10.2174/157340607779317634

frontiers | Frontiers in Pharmacology

TYPE Original Research
PUBLISHED 26 November 2024
DOI 10.3389/fphar.2024.1332388

OPEN ACCESS

EDITED BY
Eliot Ohlstein,
Drexel University School of Medicine,
United States

REVIEWED BY
Duuamene Nyimanu,
University of Kansas Medical Center,
United States
Katy Sanchez-Pozos,
Hospital Juárez de México, Mexico

*CORRESPONDENCE
K. Melissa Hallow,
hallowkm@uga.edu

RECEIVED 02 November 2023
ACCEPTED 28 October 2024
PUBLISHED 26 November 2024

CITATION
Hallow KM, Greasley PJ, Heerspink HJL and Yu H (2024) Kinetics of endothelin-1 and effect selective ET_A antagonism on ET_B activation: a mathematical modeling analysis.
Front. Pharmacol. 15:1332388.
doi: 10.3389/fphar.2024.1332388

Kinetics of endothelin-1 and effect selective ET_A antagonism on ET_B activation: a mathematical modeling analysis

K. Melissa Hallow[1,2]*, Peter J. Greasley[3], Hiddo J. L. Heerspink[4,5] and Hongtao Yu[6]

[1]School of Chemical, Materials, and Biomedical Engineering, University of Georgia, Athens, GA, United States, [2]Department of Epidemiology and Biostatistics, University of Georgia, Athens, GA, United States, [3]Early Clinical Development, Research and Early Development, Cardiovascular, Renal and Metabolism (CVRM), Biopharmaceuticals, R&D, AstraZeneca, Gothenburg, Sweden, [4]Department of Clinical Pharmacy and Pharmacology, University of Groningen, Groningen, Netherlands, [5]The George Institute for Global Health, Sydney, Australia, [6]Clinical Pharmacology and Quantitative Pharmacology, Clinical Pharmacology and Safety Sciences, R&D, AstraZeneca, Gaithersburg, MD, United States

Introduction: Endothelin-1 (ET-1) regulates renal and vascular function, but the clinical utility of selective ET_A receptor antagonists has been limited due to associated fluid retention. The mechanisms underlying fluid retention remain poorly understood but could be a consequence of changes in ET-1 binding to the unantagonized ET_B receptor, either through increased ET-1 or non-selective ET_B.

Methods: A mathematical model of ET-1 kinetics was developed to quantify effects of ET_A antagonist exposure and selectivity on concentrations of ET-1 and its complexes with ET_A and ET_B receptors. The model describes ET-1 production, tissue and plasma distribution, ET_A and ET_B receptor binding, and receptor-mediated clearance, and was calibrated and validated with human ET-1 infusion studies.

Results: The model confirmed the significant role of ET_B in ET-1 clearance. By varying both drug ET_A selectivity (K_{ib}/K_{ia}) and concentration over a wide range, simulations predicted that while selective ET_A antagonist (selectivity >1) always decreased [ET1-ET_A], the change in [ET1-ET_B] was more complex. It increased up to 45% as drug concentrations approached and exceeded K_{ia}, but the increase was diminished as drug concentration increased further and fell below baseline at high concentrations. The drug concentration required to cause a decrease in [ET1-ET_B] was lower as ET_A selectivity decreased.

Discussion: This is the first mechanistic mathematical model of ET-1 kinetics that describes receptor-mediated clearance, and the consequence of ET_B blockade on ET-1 concentrations. It provides a useful tool that can coupled with experimental studies to quantitively understand and investigate this complex and dynamic system.

KEYWORDS

endothelin, endothelin receptor antagonist, mathematical modeling, kinetics, ET_A, ET_B

1 Introduction

Endothelin-1 (ET-1) is an autocrine/paracrine regulator of renal and vascular function, and antagonism of ET-1 effects has been pursued as a therapeutic target for cardiovascular diseases. ET-1 antagonists have proven beneficial in treating pulmonary arterial hypertension (PAH) (Correale et al., 2018), and been shown to reduce proteinuria and

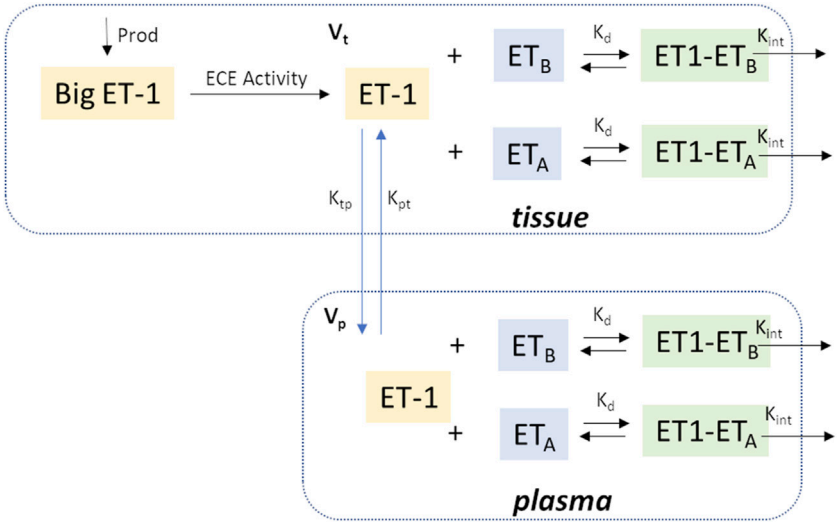

FIGURE 1
Model Schematic. In brief, Big ET-1 is assumed to be produced at a constant rate; ECE converts Big ET-1 to ET-1 in the tissue compartment; ET-1 is distributed between the tissue and plasma compartments; in each compartment, ET-1 binds to ET_A and ET_B receptors to form receptor-ligand complexes which are then cleared by internalization. Vp: Central compartment volume; Vt: Tissue compartment volume.

potentially improve outcomes in patients with diabetic kidney disease (DKD) (de Zeeuw et al., 2014; Heerspink et al., 2019). However, their utility in treating cardiovascular diseases has been limited by adverse events related to fluid retention (Packer et al., 2017; Waijer et al., 2021).The mechanisms underlying this effect have proven difficult to fully understand, in part because of the complex physiology of the endothelin system.

ET-1 is produced primarily in the kidney and lungs by conversion of its precursor Big-ET through endothelin converting enzyme (ECE) in endothelial cells. It elicits its physiological effects by binding to two receptors: ET_A and ET_B. It is also cleared by receptor binding, primarily by ET_B. Binding to ET_A mediates vasoconstriction, while ET_B is thought to mediate vasodilation and natriuresis. See Davenport et al. (2016) for a thorough review of endothelin physiology.

Endothelin receptor antagonists vary in their selectivity for ET_A and ET_B receptors. Inhibiting one receptor can cause ET-1 to increase (since clearance is reduced), and thus may increase binding through the other receptor. Because ET_B is largely responsible for ET-1 clearance, ET_B inhibition in particular may result in a rise in ET-1 binding to ET_A (Kelland et al., 2010).

Fluid retention effects of selective ET_A antagonists have been proposed to be related to non-selective inhibition of ET_B at high doses (Vercauteren et al., 2017; Battistini et al., 2006) or to incompletely understand the pleiotropic effects of ET_A. A better understanding of ET-1 kinetics and dynamics may aid in the identification of optimal dosing of endothelin antagonists that could provide efficacy while minimizing potential risk of adverse effects.

Understanding the physiological response to endothelin antagonists depends on understanding the degree of inhibition and/or activation of each receptor type. In this study, we developed a mechanistic mathematical model of ET-1 kinetics and blockade by selective or non-selective receptor antagonists. We then utilized this model to quantify the effect of endothelin antagonist selectivity on concentrations of ET-1 to the ET_A and ET_B receptors in the plasma and tissue compartments. This is a first step in developing a more quantitative understanding of the mechanisms underlying clinically observed responses to endothelin antagonism.

2 Methods

2.1 Model description

Figure 1 shows a schematic of the ET-1 kinetics model. Big ET-1, the precursor to ET-1, is assumed to be produced endogenously at a constant rate ($Prod_{BigET}$), and is converted to ET-1 through the action of endothelin converting enzyme (ECE).

$$\frac{d([BigET])}{dt} = Prod_{BigET} - \frac{K_{cat}}{K_m}[BigET][ECE] \quad (1)$$

K_{cat}/K_m is the catalytic efficiency of ECE (Schweizer et al., 1997).

ET-1 exhibits saturable, high-affinity binding to ET_A and ET_B receptors, with similar dissociation constant K_d for both receptor types (Bacon et al., 1996). ET-1 is cleared by binding to and internalization of these receptors, with most of the clearance occurring through ET_B. Total ET-1 concentration ($[ET1]_{tot}$) is the sum of concentrations of unbound ET-1 ([ET1]) and ET-1 bound to the ET_A and ET_B receptors ([ET1-ET_A] and [ET1-ET_B],respectively). Because the dissociation constant is similar for both receptors, we lump ET_A and ET_B receptors together as one receptor concentration [ET1-R] for now. Later, we will revisit this and distinguish between binding to the two receptor types.

$$[ET1]_{tot} = [ET1] + [ET1\text{–}ET_A] + [ET1\text{–}ET_B] = [ET1] + [ET1\text{–}R] \quad (2)$$

Similarly, the total receptor concentration ($[R]_{tot}$) is the sum of free ET_A and ET_B receptors concentration ([ET_A] and [ET_B]), and the ligand-receptor complexes ([ET1-ET_A] and [ET1-ET_B]):

$$[R]_{tot} = [ET_A] + [ET1\text{–}ET_A] + [ET_B] + [ET1\text{–}ET_B] = [R] + [ET1\text{–}R] \quad (3)$$

Receptor binding is assumed to occur several orders of magnitude faster than production, distribution, or internalization, so that equilibrium between binding and dissociation is achieved almost instantaneously, and the ligand, receptor, and ligand-receptor complex are assumed to be in quasi-equilibrium (Mager and Krzyzanski, 2005), so that:

$$K_d = \frac{k_{off}}{k_{on}} = \frac{[R]^*[ET1]}{[ET1\text{–}R]} \quad (4)$$

Combining Equations 2–4 gives:

$$K_d = \frac{(R_{tot} - ([ET1]_{tot} - [ET1]))^*[ET1]}{[ET1]_{tot} - [ET1]} \quad (5)$$

Unbound ET-1 can then be solved from Equation 5 in terms of total ET-1 concentration, total receptor concentrations, and K_d, as expressed in Equation 6.

$$[ET] = \left(\frac{1}{2}\right)\left[([ET]_{tot} - [R]_{tot} - K_d) + \sqrt{([ET]_{tot} - [R]_{tot} - K_d)^2 + 4K_d[ET]_{tot}}\right] \quad (6)$$

Combining Equations 2, 4 and rearranging, the receptor-ligand complex concentration [ET1-R] is given by:

$$[ET1\text{–}R] = \frac{[R]_{tot}[ET1]}{K_d + [ET1]} \quad (7)$$

Most ET-1 production occurs in the lung and kidney, where the highest concentrations of ECE are found (Hunter et al., 2017). Studies of radiolabeled ET-1 have also shown that ET-1 is rapidly cleared from the circulation and taken up in the lungs, kidneys, and liver (Fukuroda et al., 1994; Parker et al., 1999). Thus, ET-1 kinetics are modeled with 2 compartments–a plasma and a tissue compartment. ET-1 production is assumed to be much larger in the tissue than plasma compartment, so that plasma ET-1 production is negligible. For each compartment, the rate of change of total ET-1 is the net sum of ET1 production (tissue compartment only), distribution, and internalization by receptor binding. Total ET-1 in each compartment (p denotes plasma and t denotes tissue), is given by:

$$\frac{d([ET1]_{total,t})}{dt} = Prod_{ET-1} - K_{tp}[ET1]_t + K_{pt}[ET1]_p - K_{int}\frac{[R]_{tot,t}[ET1]_t}{K_d + [ET1]_t} \quad (8)$$

$$\frac{d([ET1]_{total,p})}{dt} = K_{tp}[ET1]_t - K_{pt}[ET1]_p - K_{int}\frac{[R]_{tot,p}[ET1]_p}{K_d + [ET1]_p} \quad (9)$$

At steady state, $[ET1]_p$ is the normal plasma ET-1 concentration ($[ET1]_{p0}$). There are 7 unknown parameters: the intercompartmental distribution rates K_{tp} and K_{pt}, the receptor-ligand internalization rate constant K_{int}, the receptor concentrations in each compartment $[R]_{tot,t}$ and $[R]_{tot,p}$, BigET-1 production rate $Prod_{BigET}$, and the concentration of endothelin converting enzyme [ECE].

Endogenous big-ET production is assumed to be constant, and $Prod_{BigET}$ as expressed in Equation 10, can be determined from the steady-state constraint for Equation 1:

$$Prod_{BigET} = \frac{K_{cat}}{K_m}[BigET]_0{}^*[ECE] \quad (10)$$

The steady-state tissue concentration of ET-1 can be determined from Equation 9 at steady-state:

$$[ET1]_{t0} = \frac{K_{pt}[ET1]_{p0} + K_{int}[R]_{tot,p}\frac{[ET1]_{p0}}{K_d + [ET1]_{p0}}}{K_{tp}} \quad (11)$$

Then, the total tissue receptor concentration (Equation 12), which is assumed constant, can be determined from Equation 8 at steady-state and Equation 11.

$$[R]_{tot,t} = \frac{Prod_{ET-1} - K_{tp}[ET1]_{t0} + K_{pt}[ET1]_{p0}}{K_{int}\left(\frac{[ET1]_{p0}}{K_d + [ET1]_{p0}}\right)} \quad (12)$$

This leaves 5 parameters to be estimated by fitting experimental data.

2.2 Parameter estimation

Unknown model parameters were estimated by simultaneously fitting three different experimental studies. Each study provided important pieces of information for parameter estimation.

Radiolabeled ET-1 clearance study: In Parker et al. (1999), 5 healthy human participants were administered a bolus venous infusion of radiolabeled ET-1 over 5 minutes, and radiolabeled plasma ET-1 was measured at 0, 1, 2, 3, 4, 5, 6, 8, 10, 12, 14, 16, 18, 20, 25, 30, 35, 40, 45, 50, 60, 70, 80, 100, 120, 150, 180, 210 and 240 min after the start of the infusion. This study provided information for constraining intercompartmental distribution and receptor internalization rates. However, the ET-1 dose was unknown and assumed tiny relative to plasma ET-1, so only relative concentrations could be fit.

Infusion of increasing doses of ET-1: In Kaasjager et al. (1997), 6 healthy participants were administered an infusion of ET-1 at increasing infusion rates. Participants received 0.5 ng/kg/min ET-1 for 60 min, followed by 1 ng/kg/min for 60 min, followed by a final 2.0 ng/kg/min for 60 min. Plasma ET-1 was measured before infusion and at 75, 125, and 225 min after the start of the infusion. This study provided further information for constraining intercompartmental distribution and receptor internalization rates, and also provided information for constraining receptor concentration and compartment volumes.

Infusion of Big ET-1: In Hunter et al. (2017), 10 healthy human participants were administered an infusion of Big-ET at increasing infusion rates. Participants received 0.75 pmol/min for 30 min, followed by 15 pmol/min for 30 min, followed by 300 pmol/min for another 30 min. Plasma ET-1 was measured at baseline and at 30-min intervals through 150 min. This study provided information for quantifying ECE concentration, and further information for constraining intercompartmental distribution rates, volumes, and receptor concentration.

Fitting these three studies simultaneously provided sufficient information to estimate all model parameters. The study protocol for each study was simulated. Parameters were estimated by minimizing the least square error between the observed and model-predicted plasma ET-1 concentrations.

2.3 Distinguishing ET_A and ET_B binding and internalization

After estimating model parameters with lumped ET_A and ET_B, we then separated out the contributions of $ET1_A$ and $ET1_B$.

Let f_B be the fraction of total receptors that are ET_B receptors. Then the fraction of total receptors that are ET_A receptors, f_A, is 1 – f_B.

Then, the concentration of each receptor (in the absence of an inhibitor) can be determined, as given in Equations 13, 14:

$$[R_B]_{tot} = f_B[R]_{tot} \tag{13}$$

$$[R_A]_{tot} = (1 - f_B)[R]_{tot} \tag{14}$$

And concentration of the bound complex can then be expressed as Equations 15, 16:

$$[ET1\text{–}R_A] = \frac{[R_A]_{tot}[ET1]}{K_d + [ET1]} \tag{15}$$

$$[ET1\text{–}R_B] = \frac{[R_B]_{tot}[ET1]}{K_d + [ET1]} \tag{16}$$

The relative expression of ET_A and ET_B receptors differ across tissues. The density of ET_A is much higher than ET_B in resistance vessels. In the lung, which is the tissue with the highest overall receptor concentration, the fraction of ET_B is around 40%, while in the kidney it is around 70%–80% (Davenport et al., 2016; Kuc et al., 1995). Thus, we allow f_B to be estimated separately for tissue and plasma compartments.

Equations 8, 9 can be rewritten to Equations 17, 18 as:

$$V_t\frac{d([ET1]_{tot,t})}{dt} = Prod_{ET-1} - K_{tp}V_t[ET1]_t + K_{pt}V_p[ET1]_p - K_{int}V_t([R_A]_{tot,t} + [R_B]_{tot,t})\frac{[ET1]_t}{K_d + [ET1]_t} \tag{17}$$

$$V_p\frac{d([ET1]_{tot,p})}{dt} = K_{tp}V_t[ET1]_t - K_{pt}V_p[ET1]_p - K_{int}V_p([R_A]_{tot,p} + [R_B]_{tot,p})\frac{[ET1]_p}{K_d + [ET1]_p} \tag{18}$$

2.4 Modeling competitive ET_A and ET_B inhibition

Endothelin antagonists are competitive inhibitors with varying degrees of selectivity for ET_A or ET_B receptors. Let [I] be the concentration of a competitive endothelin antagonist, with an affinity K_{ia} for ET_A receptors and K_{ib} for ET_B receptors. The concentration of the ligand-receptor complex in the presence of an antagonist can be expressed as Equations 19, 20 (see Supplementary Material for derivation):

$$[ET1\text{–}R_A] = \frac{[R_A]_{tot}[ET1]}{K_d\left(1 + \frac{[I]}{K_{ia}}\right) + [ET1]} \tag{19}$$

$$[ET1\text{–}R_B] = \frac{[R_B]_{tot}[ET1]}{K_d\left(1 + \frac{[I]}{K_{ib}}\right) + [ET1]} \tag{20}$$

It can further be shown that the concentrations of free ET_A and ET_B receptors are:

$$[R_A] = \frac{[R_A]_{tot}}{1 + \frac{[ET1]}{K_d} + \frac{[I]}{K_{ia}}} \tag{21}$$

$$[R_B] = \frac{[R_B]_{tot}}{1 + \frac{[ET1]}{K_d} + \frac{[I]}{K_{ib}}} \tag{22}$$

Substituting Equations 21, 22 into Equation 2 gives $ET1_{tot}$, as expressed in Equation 23.

$$ET1_{tot} = [ET1] + \frac{[ET1]}{K_d}\left(\frac{[R_A]_{tot}}{1 + \frac{[ET1]}{K_d} + \frac{[I]}{K_{ia}}} + \frac{[R_B]_{tot}}{1 + \frac{[ET1]}{K_d} + \frac{[I]}{K_{ib}}}\right) \tag{23}$$

With some additional algebra, the concentration of free [ET1] can be obtained by solving the resulting third order polynomial for [ET1] (see Supplementary Material for full derivation).

2.5 Validation

To validate the model, a separate experimental study, not used in model calibration, was simulated and compared with study results.

Validation Dataset: ET_A or ET_B inhibition followed by ET-1 infusion: In Bohm et al. (2003), 6 healthy, male participants were studied on 3 different days separated by at least 1 week. Participants were infused with either 0.9% saline (for 15 min), the ET_A inhibitor BQ123 (2.5–5 nmol/kg/min for 50 min), or the ET_B inhibitor BQ788 (4 nmol/kg/min for 15 min). After 30 min, participants were also infused with ET-1 (4 pmol/kg/min) for 20 min. Plasma ET-1 was measured at 0, 15, 30, 40, and 50 min.

To model this study, binding affinities and selectivity of the selective ET_A antagonist BQ123 and selective ET_B antagonist BQ788 were set to previously reported values in human tissue (BQ123: K_{ia} = 0.78 nM, K_{ib} = 24.3 μM (Peter and Davenport, 1996); BQ788: K_{ia} = 1 μM, K_{ib} = 9.8 nM (Russell and Davenport, 1996)).

2.6 Sensitivity analysis

To evaluate which parameters contribute most to the uncertainty in the model output, we computed the Sobol indices using the sensobol package in R (Puy et al., 2022), a form of global sensitivity analysis (IM SJMMCE, 1993). Assuming mutual independence among the input parameters, the variance of the output is decomposed into fractions which can be attributed either to a single input parameter (first order Sobol indices) or to a set of parameters (higher order Sobol indices). The total-order index T_i measures the first-order effect of a parameter jointly with its interactions with all the parameters (Homma and Saltelli, 1996).

2.7 Model implementation

The model was implemented in R v4.1.2 using the RxODE package (Wang et al., 2016). Optimization was performed using the

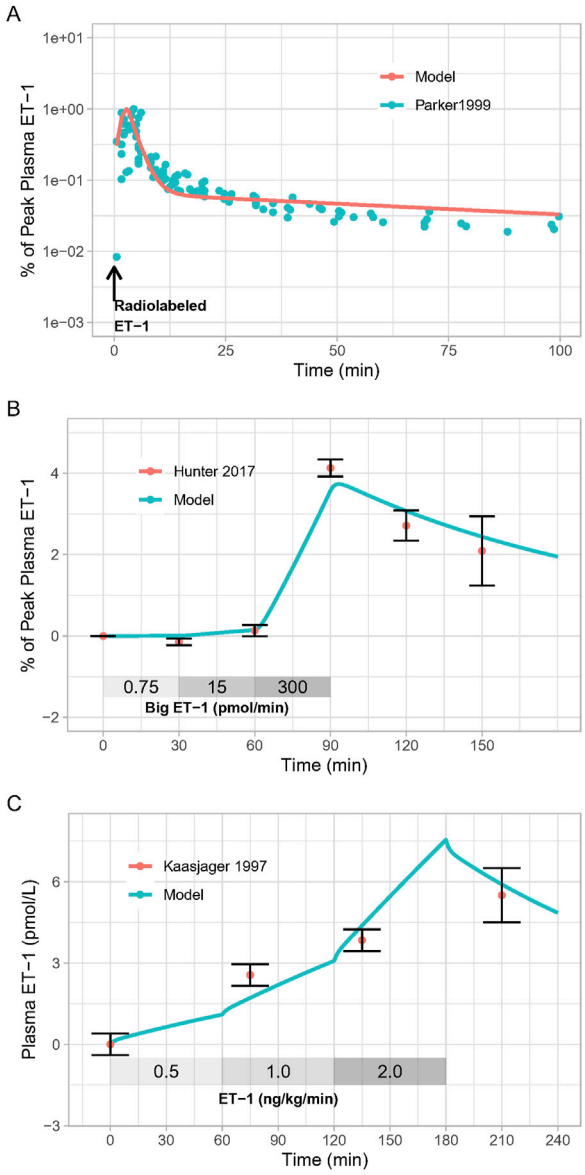

FIGURE 2
Model Calibration: Model parameters were estimated by fitting: **(A)**, the response to radiolabeled ET-1 bolus (Parker et al., 1999); **(B)**, increasing doses of Big ET-1 infusion (Hunter et al., 2017); **(C)**, increasing doses of ET-1 infusion (Kaasjager et al., 1997).

L-BFGS-B method in the optim package. Model code is available at https://bitbucket.org/cardiorenalmodel/endothelin-kinetics.

3 Results and discussion

3.1 Model calibration

As shown in Figure 2, the calibrated model reasonably reproduced the observed magnitude and time-course of changes in ET-1 following an ET-1 bolus (Figure 2A), increasing rates of Big ET-1 infusion (Figure 2B), or increasing rates of ET-1 infusion (Figure 2C). Estimated parameter values are given in Table 1. In order to simultaneously fit all three studies, it was necessary to allow [ECE] to vary for each study. For all other estimated parameters, the same estimated values allowed the model to reasonably fit all studies simultaneously. Simultaneously fitting all studies did require some trade-off in fit: each study could be fit more precisely if parameters were estimated separately for each study. However, the simultaneously fit parameters are more useful than study-specific parameters in providing a general model of ET-1 kinetics, and thus these parameters were used for the rest of this analysis.

3.2 Model Validation

The calibrated model was able to reproduce the changes in plasma ET-1 observed by Bohm et al. (2003) (Figure 3A). First, the model reproduced the change in plasma ET-1 during ET-1 infusion in the placebo arm, demonstrating that the ET-1 model can predict ET-1 kinetics in a new experiment. Secondly, the model reproduced the augmented rises in ET-1 with selective ET_A or ET_B antagonist, resulting from reduced clearance when the receptors are inhibited. Consistent with the experimental data, the rise in ET-1 with ET_B antagonism was much greater than with ET_A antagonism, indicating that the model recapitulates the dominant role of ET_B in ET-1 clearance.

For ET_B antagonism, the model did overpredict the increase in ET-1 during the period of ET_B antagonism alone, prior to the start of ET-1 infusion. While Bohm et al. reported no change in ET-1 during this period, other studies have found that ET-1 does increase with similar doses of BQ788 (Okada and Nishikibe, 2002; Strachan et al., 1999), but this increase is delayed. This could be due to a delay in BQ788 reaching ET_B in peripheral tissues. When a pharmacodynamic delay was introduced, the model came closer to reproducing the observed ET-1 changes. Because other studies have noted a rise in ET-1 with BQ788, we did not want to overfit the model to this single datapoint in this single study, and thus no further changes were made to force fit this point.

3.3 Simulations

3.3.1 Effect of selective ET receptor antagonism on non-antagonized receptor complex

Changes in ET_B activation with selective ET_A antagonists have been proposed as a mechanism for fluid retention with ET_A receptor antagonists. On one hand, inhibition of ET_B at high doses of selective ET_A receptor antagonists has been proposed to cause fluid retention by blocking natriuretic/diuretic effects of ET_B (Battistini et al., 2006; Baltatu et al., 2012). On the other hand, activation of ET_B receptors as a consequence of elevated ET-1 with ET_A antagonism has been proposed to increase vascular permeability and redistribute plasma volume, resulting in edema (Vercauteren et al., 2017). A first step in understanding these possible mechanisms is to quantify how the concentration of a selective antagonist affects plasma ET-1 and the formation of bound complex with the non-antagonized receptor.

TABLE 1 Model parameters.

Parameter	Definition	Value	Units	Source
BigET(0)	Normal plasma Big ET-1 concentration, initial condition	0.93	pmol/L	Miyauchi et al. (2012)
$[ET1]_p(0)$	Normal plasma ET-1 concentration, initial condition	3.2	pmol/L	Kaasjager et al. (1997)
K_{cat}/K_m	ECE catalytic efficiency	2.64e-4	L/min/pmol	Schweizer et al. (1997)
K_d	ET-1 dissociation constant for ET_A and ET_B	400	pmol/L	Bacon et al. (1996)
V_p	Central compartment volume	81.6 (1.1%)	L	estimated
V_t	Tissue compartment volume	2.64 (7%)	L	estimated
[ECE]	Endothelin converting enzyme concentration	Parker: 162.6 (2.5%) Hunter: 98 (4.6%) Kaasjager: 27 (10.7%)	nmol/L	estimated
K_{pt}	ET-1 distribution rate from plasma to tissue	0.87 (18.5%)	/min	estimated
K_{tp}	ET-1 distribution rate from tissue to plasma	0.98 (2.3%)	/min	estimated
K_{int}	Receptor-ligand internalization rate	0.0095 (0.4%)	pmol/min	estimated
$R_{tot,p}$	Total receptor concentration in plasma compartment	460 (1.2%)	pmol/L	estimated
$R_{tot,t}$	Total receptor concentration in tissue compartment	7,738	pmol/L	Calculated from steady-state constraints
$[ET1]_t(0)$	Total (bound and unbound) concentration of ET-1, initial condition	88.3	pmol/L	Calculated from steady-state constraints
$f_{B,t}$	Fraction of total receptors that are ET_B receptors in tissue compartment	0.65 (11%)	—	estimated
$f_{B,c}$	Fraction of total receptors that are ET_B receptors in plasma compartment	0.8 (15%)	—	estimated

We first simulated a perfectly selective ET_A antagonist by setting K_{ia} to 1 and K_{ib} to 10^{20} (to approximate zero ET_B antagonism). The drug concentration was then varied from 0.001 to 1,000X K_{ia}, and steady-state changes in the bound complexes [ET1-ET_A] and [ET1-ET_B] were determined in the plasma and tissue compartments. This was repeated for a perfectly selective ET_B antagonist, with K_{ia} set to 10^{20} (to approximate zero ET_A antagonism)and K_{ib} set to 1, and drug concentration varied from 0.001 to 100,000X K_{ib}.

As shown in Figure 4A, as the concentration of a selective ET_A antagonist was increased relative to K_{ia}, the formation of bound complex [ET1-ET_B] increased up to 33% and 45% in the tissue and plasma compartments, respectively, as bound complex [ET1-ET_A] suppression approached 100%. For selective ET_B antagonism (Figure 4B), as the concentration was increased relative to K_{ib}, the rise in ET1-ET_A complex was quite large, increasing to more than 200% and 500% in the tissue and plasma compartments, respectively, as bound complex [ET1-ET_B] suppression approached 100%.

In both cases, the rise in the complex of ET-1 with the non-inhibited receptor occurred due to a compensatory rise in ET-1 concentration, since inhibiting either receptor reduced ET-1 clearance. Since ET_B is responsible for a larger portion of ET-1 clearance than ET_A, the rise in ET-1 with ET_B antagonism was much larger than with ET_A antagonism. Consequently, the rise in [ET1-ET_A] with ET_B antagonism was also much larger than the rise in ET1-ET_B with ET_A antagonism.

If there were no change in ET-1 concentration, it would be expected that when the drug concentration equals K_i (when log10(conc/K_i) = 1), the complex of ET-1 with the antagonized receptor would be reduced 50%. However, in both cases, the concentration required to produce a 50% reduction was shifted higher as a result of the rise in ET-1 concentration (See Equations 19, 20). This shift was much larger with ET_B antagonism, due to the larger rise in ET-1.

Sobol sensitivity analysis indicated that the uncertainty in predicted changes in ET1-ET_A or ET1-ET_B was nearly completely due to the choice of f_B–fraction of total receptors that are ET_B receptors. To explore the effect of f_B on the model predictions, we repeated the simulations above when f_B is set to 0.5 (a scenario of equal concentrations of ET_A and ET_B receptors, and thus equal clearance through each receptor–inconsistent with (Bohm et al., 2003) and other studies (Fukuroda et al., 1994; Dupuis et al., 1996)), or to 0.999 (a scenario in which ET receptors are 99.9% ET_B and 0.1% ET_A). In the first case, the rise in the non-antagonized receptor complex was equal for selective ET_A and ET_B antagonists (i.e., ET1-ET_B rise with ET_A antagonism was the same as ET1-ET_A rise with ET_B antagonism). The ET-1 concentration also rose equally. At the other extreme, when f_B is set to 0.999, there was no change in ET1-ET_B with ET_A antagonism, but ET1-ET_A increased more than 2000-fold with ET_B antagonism. However, in all cases, the shape of the curves, and thus the dependency on K_i and concentration, remained the same. Only the magnitudes changed (Supplementary Figures S1, S2).

3.3.2 Effect of antagonist selectivity on non-antagonized receptor complex

We then investigated the effect of antagonist receptor selectivity by varying both drug ET_A selectivity (K_{ib}/K_{ia}) and drug

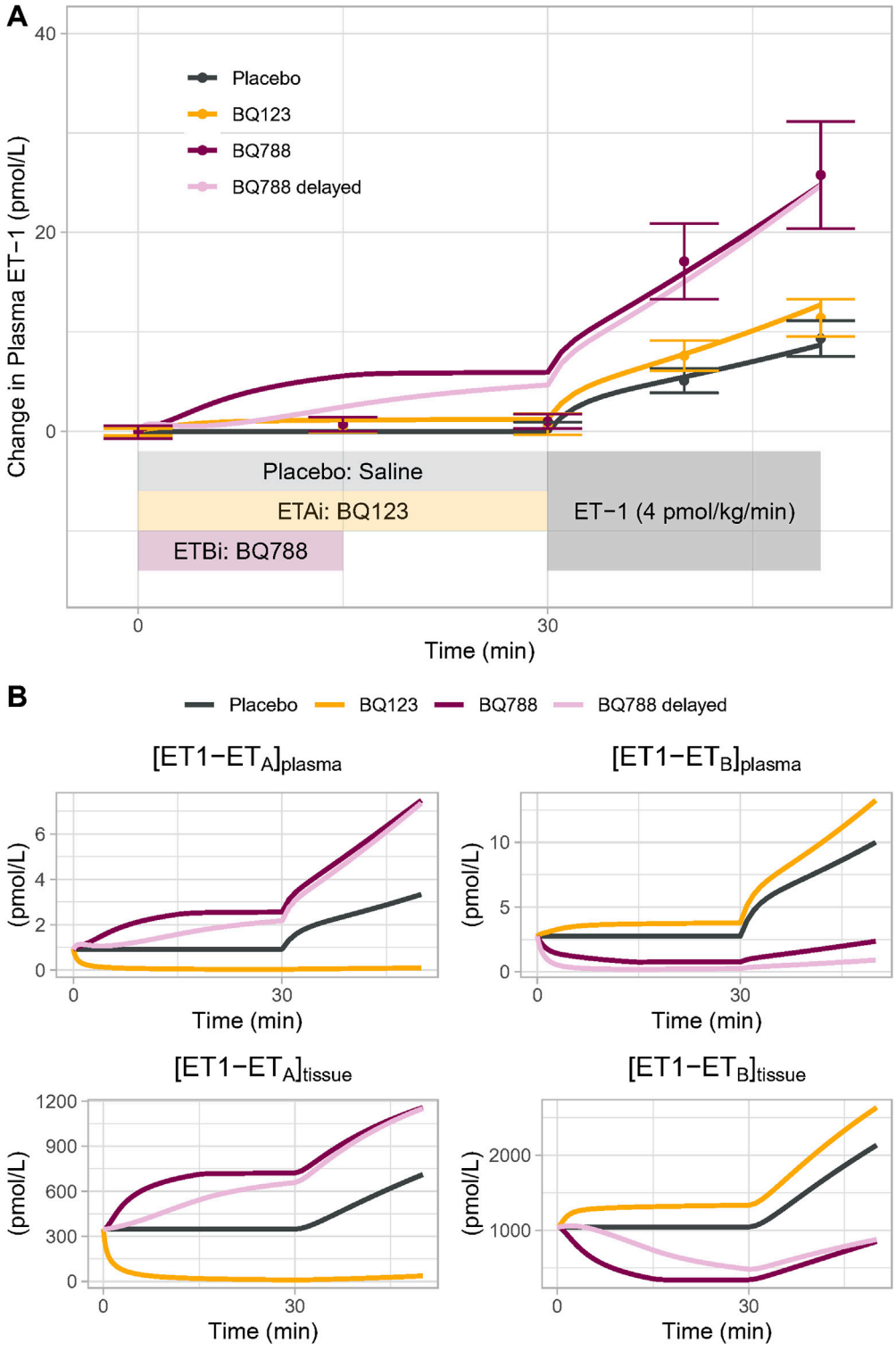

FIGURE 3
(A) Model Validation: The calibrated model reproduced experimentally observed changes in plasma ET-1 observed by Bohm et al. (2003) in response to placebo, BQ123 (ET_A antagonist 4 nmol/kg/min for 50 min), or BQ788 (ET_B antagonist 4 nmol/kg/min for 15 min) followed by ET-1 infusion. Speed of rise in plasma ET-1 with BQ788 is overpredicted; assuming a delay between plasma drug concentration and tissue inhibitory effect on ET_B (light purple) more closely reproduces the data **(B)** Model-predicted changes in the physiologically active bound complexes of ET1 to ET_A or ET_B in the plasma and tissue compartments.

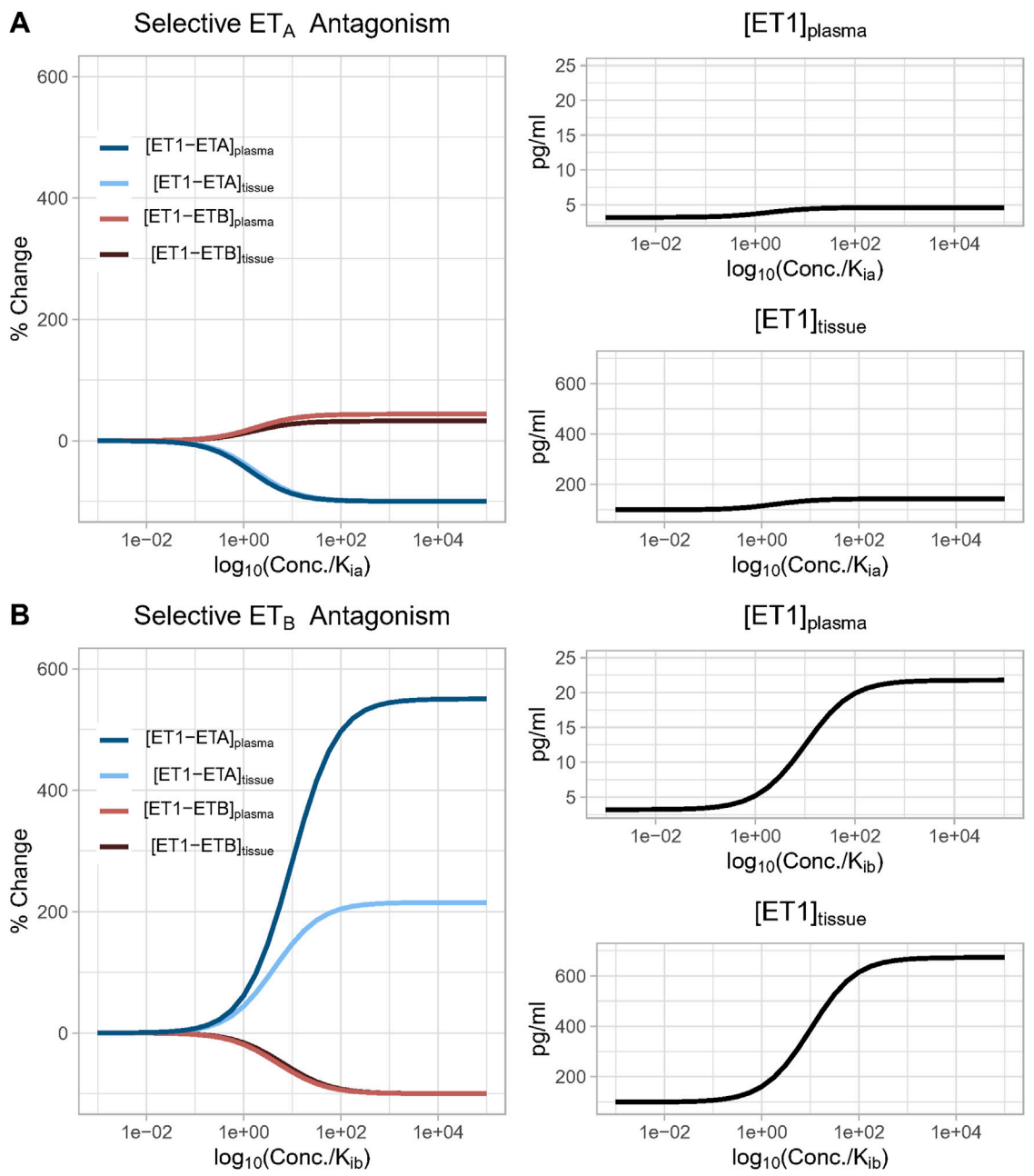

FIGURE 4
(A) Effect of increasing concentration of a perfectly selective ET_A antagonist. Simulation predicts that as the concentration of a selective ET_A antagonist increases, the formation of bound complex [ET1-ET_B] increases up to 33% and 45% in the tissue and plasma compartments, respectively, as bound complex [ET1-ET_A] suppression approaches 100%; **(B)** Effect of increasing concentration of a perfectly selective ET_B antagonist. Simulation predicts that as the concentration of a selective ET_B antagonist increases, the formation of bound complex [ET1-ET_A] increases more than 200% and 500% in the tissue and plasma compartments, respectively, as bound complex [ET1-ET_B] suppression approaches 100%.

concentration over a wide range. In Figure 5, all concentrations are plotted relative to K_{ia} for consistency. [ET-1] increased with increasing concentrations for all selectivity values, but the higher the selectivity for ET_A, the higher the drug concentration (relative to K_{ia}) required to increase ET-1 (Figures 5A, B). Trends were the same but concentrations were much higher in the tissue compared to plasma.

The complex [ET1-ET_A] always decreased with increasing concentration of selective ET_A antagonist (selectivity >1). For ET_B selective antagonism (selectivity <1), [ET1-ET_A] was non-monotonic–for concentrations well below Kia, it increased, and increased faster with increasing. However, as concentrations approached and exceeded K_{ia} (and thus also far exceeded K_{ib}), the rise in [ET1-ET_A] began to become smaller, and [ET1-ET_A] eventually began to decrease at concentrations well above K_{ia} (Figures 5C, D).

The complex [ET1-ET_B] always decreased with increasing concentrations of ET_B-selective antagonists (selectivity <1).

10.3389/fphar.2024.1332388

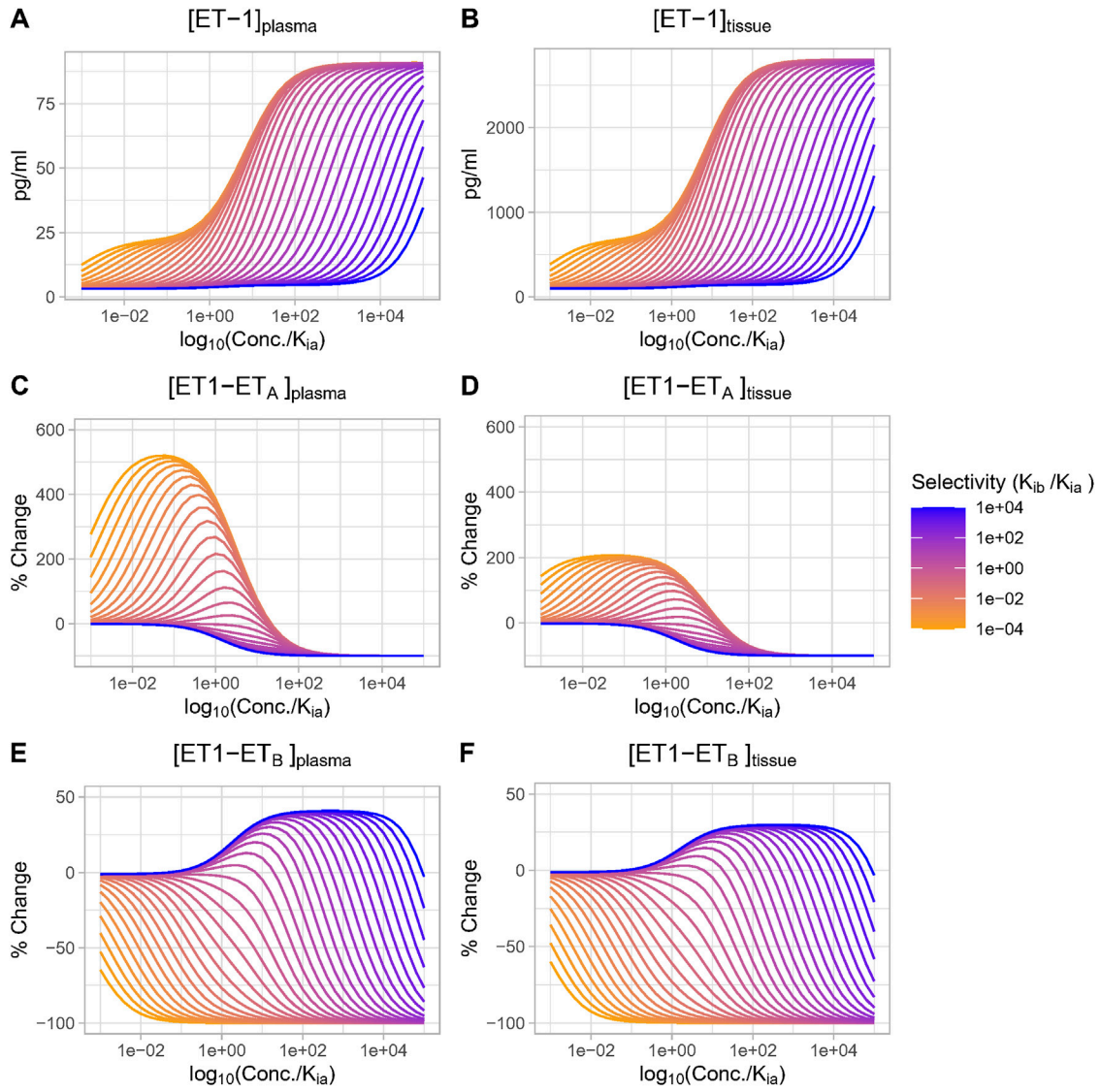

FIGURE 5
Effect of antagonist selectivity on plasma and tissue changes in ET-1 **(A, B)**, ET_A activation by ET-1 **(C, D)**, ET_B activation by ET-1 **(E, F)**. ET_A antagonism: selectivity >1, ET_B antagonism: selectivity <1.

Interestingly, though, for ET_A-selective antagonists, the rise in [ET1-ET_B] was minimal at concentrations less than 0.1X K_{ia}, then became larger as concentrations approached and exceeded K_{ia}. After reaching a maximum increase of around 45% (plasma) or 33% (tissue), further increases in concentration did not further increase [ET1-ET_B]. Instead, as concentrations rose further, [ET1-ET_B] began to fall and quickly became negative. The concentration required to cause a decrease in [ET1-ET_B] was higher as selectivity increased (Figures 5E, F).

Thus, depending on the concentration, ET_A antagonists can increase (at low concentrations) or decrease (at high concentrations) the activation of ET_B. The higher the selectivity for ET_A, the higher the concentration required to cause ET_B to decrease.

Figure 6 shows the change in plasma [ET1-ET_B] for different selective ET_A antagonists, based on their reported selectivities (Davenport et al., 2016). For a relatively non-selective antagonist like bosentan, [ET1-ET_B] rise did not quite reach the maximum before falling, and became negative at concentrations around 100X K_{ia}. However, for more selective ET_A antagonists, the rise in [ET1-ET_B] tended to max out as concentrations rose. There was no difference in the maximum rise between ambrisentan, atrasentan, sitaxentan, and zibotentan. However, while ambrisentan causes [ET1-ET_B] to become negative at concentrations around 1,000x K_{ia}, [ET1-ET_B] remained positive with zibotentan for concentrations up to 100,000xK_{ia}.

Several limitations should be noted. Receptor concentrations of ET_A and ET_B vary across tissues and across species. This analysis assumed a constant relative concentration of receptors, but this could vary by tissue. Receptor concentration may also change due to compensatory upregulation or downregulation due to antagonism, and this was not considered. Nearly all of the experimental data used to develop the model was collected in males, and there are likely sex differences that could impact the model's predictiveness in females. Endogenous ET-1 production

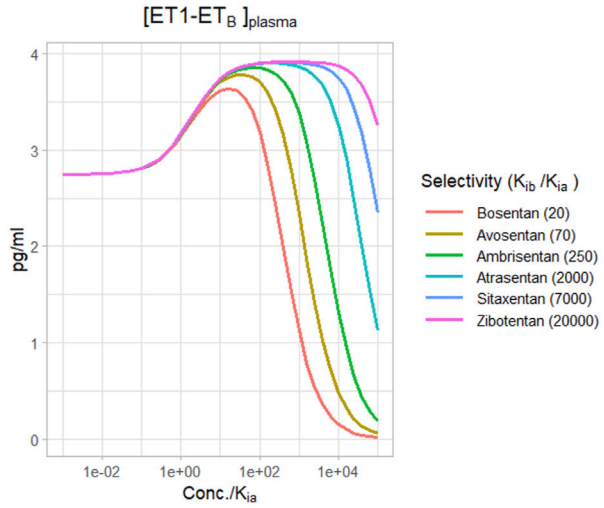

FIGURE 6
Effect of ET_A antagonists with varying degrees of selectivity on ET_B activation by ET1.

was assumed constant, but in reality its secretion changes in response to physiological signals.

4 Conclusion

This is the first mechanistic mathematical model of ET-1 kinetics that describes receptor-mediated clearance, and the consequence of ET_B blockade on ET-1 concentrations. It provides a useful tool that can coupled with experimental studies to quantitively understand and investigate this complex and dynamic system. This analysis quantifies effect of ET_A antagonists on ET_B activation, but does not describe the physiological consequences of changes in ET_A and ET_B binding. This is addressed in our sister paper.

Data availability statement

Publicly available datasets were analyzed in this study. This data can be found here: https://bitbucket.org/cardiorenalmodel/endothelin-kinetics.

Author contributions

KH: Conceptualization, Formal Analysis, Methodology, Project administration, Software, Supervision, Validation, Writing–original draft. PG: Conceptualization, Investigation, Supervision, Writing–review and editing. HH: Conceptualization, Supervision, Writing–review and editing. HY: Conceptualization, Formal Analysis, Methodology, Software, Validation, Visualization, Writing–original draft.

Funding

The author(s) declare financial support was received for the research, authorship, and/or publication of this article.

Conflict of interest

KH has received research funding from AstraZeneca and Eli Lilly in the last 3 years. HY and PG are employees of AstraZeneca and own AstraZeneca stock or stock options. HH is a consultant for and received honoraria from AbbVie, Astellas, Astra Zeneca, Boehringer Ingelheim, Fresenius, Janssen and Merck; he has a policy that all honoraria are paid to his employer.

This study received funding from AstraZeneca Pharmaceuticals. The funder had the following involvement in the study: interpretation of results and writing of the manuscript.

Publisher's note

Supplementary material

The Supplementary Material for this article can be found online at: https://www.frontiersin.org/articles/10.3389/fphar.2024.1332388/full#supplementary-material

References

Bacon, C. R., Cary, N. R. B., and Davenport, A. P. (1996). Endothelin peptide and receptors in human atherosclerotic coronary artery and aorta. *Circulation Res.* 79 (4), 794–801. doi:10.1161/01.res.79.4.794

Baltatu, O. C., Iliescu, R., Zaugg, C. E., Reckelhoff, J. F., Louie, P., Schumacher, C., et al. (2012). Antidiuretic effects of the endothelin receptor antagonist avosentan. *Front. physiology* 3, 103. doi:10.3389/fphys.2012.00103

Battistini, B., Berthiaume, N., Kelland, N. F., Webb, D. J., and Kohan, D. E. (2006). Profile of past and current clinical trials involving endothelin receptor antagonists: the novel "-sentan" class of drug. *Exp. Biol. Med. (Maywood, NJ)* 231 (6), 653–695. doi:10.3181/00379727-231-2310653

Bohm, F., Pernow, J., Lindstrom, J., and Ahlborg, G. (2003). ETA receptors mediate vasoconstriction, whereas ETB receptors clear endothelin-1 in the splanchnic and renal circulation of healthy men. *Clin. Sci. (Lond).* 104 (2), 143–151. doi:10.1042/CS20020192

Correale, M., Ferraretti, A., Monaco, I., Grazioli, D., Di Biase, M., and Brunetti, N. D. (2018). Endothelin-receptor antagonists in the management of pulmonary arterial hypertension: where do we stand? *Vasc. Health Risk Manag.* 14, 253–264. doi:10.2147/VHRM.S133921

Davenport, A. P., Hyndman, K. A., Dhaun, N., Southan, C., Kohan, D. E., Pollock, J. S., et al. (2016). Endothelin. *Pharmacol. Rev.* 68 (2), 357–418. doi:10.1124/pr.115.011833

de Zeeuw, D., Coll, B., Andress, D., Brennan, J. J., Tang, H., Houser, M., et al. (2014). The endothelin antagonist atrasentan lowers residual albuminuria in patients with type 2 diabetic nephropathy. *J. Am. Soc. Nephrol.* 25 (5), 1083–1093. doi:10.1681/ASN.2013080830

Dupuis, J., Goresky, C. A., and Fournier, A. (1996). Pulmonary clearance of circulating endothelin-1 in dogs *in vivo*: exclusive role of ETB receptors. *J. Appl. physiology (Bethesda, Md 1985)* 81 (4), 1510–1515. doi:10.1152/jappl.1996.81.4.1510

Fukuroda, T., Fujikawa, T., Ozaki, S., Ishikawa, K., Yano, M., and Nishikibe, M. (1994). Clearance of circulating endothelin-1 by ETB receptors in rats. *Biochem. Biophys. Res. Commun.* 199 (3), 1461–1465. doi:10.1006/bbrc.1994.1395

Heerspink, H. J. L., Parving, H. H., Andress, D. L., Bakris, G., Correa-Rotter, R., Hou, F. F., et al. (2019). Atrasentan and renal events in patients with type 2 diabetes and chronic kidney disease (SONAR): a double-blind, randomised, placebo-controlled trial. *Lancet London, Engl.* 393 (10184), 1937–1947. doi:10.1016/S0140-6736(19)30772-X

Homma, T., and Saltelli, A. (1996). Importance measures in global sensitivity analysis of nonlinear models. *Reliab. Eng. and Syst. Saf.* 52 (1), 1–17. doi:10.1016/0951-8320(96)00002-6

Hunter, R. W., Moorhouse, R., Farrah, T. E., MacIntyre, I. M., Asai, T., Gallacher, P. J., et al. (2017). First-in-Man demonstration of direct endothelin-mediated natriuresis and diuresis. *Hypertens. (Dallas, Tex 1979)* 70 (1), 192–200. doi:10.1161/HYPERTENSIONAHA.116.08832

IM SJMMCE. (1993). Sensitivity estimates for nonlinear mathematical models. 1(4): 407–414.

Kaasjager, K. A., Shaw, S., Koomans, H. A., and Rabelink, T. J. (1997). Role of endothelin receptor subtypes in the systemic and renal responses to endothelin-1 in humans. *J. Am. Soc. Nephrol.* 8 (1), 32–39. doi:10.1681/ASN.V8132

Kelland, N. F., Kuc, R. E., McLean, D. L., Azfer, A., Bagnall, A. J., Gray, G. A., et al. (2010). Endothelial cell-specific ETB receptor knockout: autoradiographic and histological characterisation and crucial role in the clearance of endothelin-1. *Can. J. physiology Pharmacol.* 88 (6), 644–651. doi:10.1139/Y10-041

Kuc, R. E., Karet, F. E., and Davenport, A. P. (1995). Characterization of peptide and nonpeptide antagonists in human kidney. *J. Cardiovasc Pharmacol.* 26 (Suppl. 3), S373–S375. doi:10.1097/00005344-199506263-00111

Mager, D. E., and Krzyzanski, W. (2005). Quasi-equilibrium pharmacokinetic model for drugs exhibiting target-mediated drug disposition. *Pharm. Res.* 22 (10), 1589–1596. doi:10.1007/s11095-005-6650-0

Miyauchi, Y., Sakai, S., Maeda, S., Shimojo, N., Watanabe, S., Honma, S., et al. (2012). Increased plasma levels of big-endothelin-2 and big-endothelin-3 in patients with end-stage renal disease. *Life Sci.* 91 (13), 729–732. doi:10.1016/j.lfs.2012.08.008

Okada, M., and Nishikibe, M. (2002). BQ-788, A selective endothelin ETB receptor antagonist. *Cardiovasc. Drug Rev.* 20 (1), 53–66. doi:10.1111/j.1527-3466.2002.tb00082.x

Packer, M., McMurray, J. J. V., Krum, H., Kiowski, W., Massie, B. M., Caspi, A., et al. (2017). Long-term effect of endothelin receptor antagonism with bosentan on the morbidity and mortality of patients with severe chronic heart failure: primary results of the ENABLE trials. *JACC Heart Fail.* 5 (5), 317–326. doi:10.1016/j.jchf.2017.02.021

Parker, J. D., Thiessen, J. J., Reilly, R., Tong, J. H., Stewart, D. J., and Pandey, A. S. (1999). Human endothelin-1 clearance kinetics revealed by a radiotracer technique. *J. Pharmacol. Exp. Ther.* 289 (1), 261–265.

Peter, M. G., and Davenport, A. P. (1996). Characterization of the endothelin receptor selective agonist, BQ3020 and antagonists BQ123, FR139317, BQ788, 50235, Ro462005 and bosentan in the heart. *Br. J. Pharmacol.* 117 (3), 455–462. doi:10.1111/j.1476-5381.1996.tb15212.x

Puy, A., Lo, P. S., Saltelli, A., and Levin, S. A. (2022). Sensobol: an R package to compute variance-based sensitivity indices. *J. Stat. Softw.* 102 (5), 1–37. doi:10.18637/jss.v102.i05

Russell, F. D., and Davenport, A. P. (1996). Characterization of the binding of endothelin ETB selective ligands in human and rat heart. *Br. J. Pharmacol.* 119 (4), 631–636. doi:10.1111/j.1476-5381.1996.tb15720.x

Schweizer, A., Valdenaire, O., Nelböck, P., Deuschle, U., Dumas Milne Edwards, J. B., Stumpf, J. G., et al. (1997). Human endothelin-converting enzyme (ECE-1): three isoforms with distinct subcellular localizations. *Biochem. J.* 328 (Pt 3), 871–877. doi:10.1042/bj3280871

Strachan, F. E., Spratt, J. C., Wilkinson, I. B., Johnston, N. R., Gray, G. A., and Webb, D. J. (1999). Systemic blockade of the endothelin-B receptor increases peripheral vascular resistance in healthy men. 33(1):581–585. doi:10.1161/01.hyp.33.1.581

Vercauteren, M., Trensz, F., Pasquali, A., Cattaneo, C., Strasser, D. S., Hess, P., et al. (2017). Endothelin ET_A receptor blockade, by activating ET_B receptors. *Increases Vasc. Permeability Induces Exaggerated Fluid Retent.* 361 (2), 322–333. doi:10.1124/jpet.116.234930

Waijer, S. W., Gansevoort, R. T., Bakris, G. L., Correa-Rotter, R., Hou, F.-F., Kohan, D. E., et al. (2021). The effect of atrasentan on kidney and heart failure outcomes by baseline albuminuria and kidney function: A: *post hoc*: analysis of the SONAR randomized trial. *Clin. J. Am. Soc. Nephrol.* 16 (12), 1824–1832. doi:10.2215/CJN.07340521

Wang, W., Hallow, K., and James, D. (2016). "A tutorial on RxODE: simulating differential equation pharmacometric models in R,". Editor R. CPT, 5, 3–10. doi:10.1002/psp4.12052*pharmacometrics and Syst. pharmacology1*

Frontiers in Pharmacology

Explores the interactions between chemicals and living beings

The most cited journal in its field, which advances access to pharmacological discoveries to prevent and treat human disease.

Discover the latest Research Topics

See more →

Frontiers

Avenue du Tribunal-Fédéral 34
1005 Lausanne, Switzerland
frontiersin.org

Contact us

+41 (0)21 510 17 00
frontiersin.org/about/contact